DESIGN, SYNTHESIS AND STUDY OF PHOTOPHYSICAL/BIOPHYSICAL PROPERTIES OF SMALL MOLECULE SCAFFOLDED PEPTIDES AND FLUORESCENT β-LACTAMS

A Dissertation Submitted to the
Indian Institute of Technology Guwahati
As Partial Fulfillment for the Award of Degree of

Doctor of Philosophy
in Chemistry
by

Afsana Yashmeen
Roll No. 11612202

Department of Chemistry
Indian Institute of Technology Guwahati
Guwahati 781039
October 2017

Dedicated To

My Family

And

Those who have helped me

INDIAN INSTITUTE OF TECHNOLOGY, GUWAHATI
Department of Chemistry

DECLARATION

I do hereby declare that the research work embodied in this thesis entitled "***Design, Synthesis and Study of Photophysical/Biophysical Properties of Small Molecule Scaffolded Peptides and Fluorescent β-Lactams***" has been carried out by me under the supervision of **Dr. Subhendu Sekhar Bag** in the Department of Chemistry, Indian Institute of Technology Guwahati, India.

In keeping with the general practice of reporting scientific observations, due acknowledgements have been made wherever the work described is based on the findings of other investigators.

IIT Guwahati
October, 2017.

Afsana Yashmeen

Dr. Subhendu Sekhar Bag, Ph.D.
Professor
Department of Chemistry
Indian Institute of Technology
Guwahati -781039
Assam, INDIA

Ph: +91-361-258-2324 (O)
Ph: +91-361-258-4324 (R)
Fax: +91-361-258-2349

E-mail: ssbag75@yahoo.co.in
ssbag75@iitg.ernet.in

CERTIFICATE

This is to certify that the research work presented in this thesis entitled "***Design, Synthesis and Study of Photophysical/ Biophysical Properties of Small Molecule Scaffolded Peptides and Fluorescent β-Lactams***" is an authentic record of the results obtained from the research work carried out by **Mrs. Afsana Yashmeen** under my supervision in the Department of Chemistry, Indian Institute of technology Guwahati, India. This work is original and has not been submitted elsewhere for a degree or award.

IIT Guwahati
October, 2017

Dr. Subhendu Sekhar Bag
(Thesis Supervisor)

ACKNOWLODGEMENT

It is with high regards and profound respect that I express a deep sense of sincere gratitude to my supervisor **Prof. Subhendu Sekhar Bag** for his stimulating guidance, precious constructive suggestions and decisive insights during the entire course of my research work.

I would like to thank my Doctoral Committee members, **Prof. Tharmalingam Punniyamurthy** (chairman), **Dr. A.S. Achalkumar** (member) and **Dr. Animes Kr. Golder** (member) for their intellectual input, encouragement, valuable suggestions and comments during the entire course of my research work.

I wish to thank my lab mates Rajen da, Sangita Di, Subhashis Da, Suman, Manoj, Suranjan, and Hiranya for their cooperation, support and pleasant company throughout my research work. Without their help it would have been impossible to complete my research work. I would also like to acknowledge summer trainee students Subhajit, Ashim, Achinta, Raghu, Swapna, Ashim and Sheelbhadra for their help, support and pleasant company in the laboratory during their summer project work.

Sincere thanks go to my other lab mates Zia da, Dipankar Da, Momina Di, Tridip Da, Anindya, Shaad, Abhishek and Gourangi for their cooperation and sharing some happy moments inside and outside the laboratory.

I would like to acknowledge my batch mates Sabera, Nirmali, Dinabandhu, Sameer, Adil, Wajid, Santosh and Sougata for their support and suggestions. Special thanks to Babulal da for his help in collecting XRD data, Suranjan De for recording 2D NMR data and Subhashis Jana and Hiranya Gogoi for recording Life Time data. Thanks to all of my friends, juniors and seniors whom I met during my past five years of life for their help.

My honest regards to all the faculty members of our department for their encouragement and help. I want to express my thanks to Mr. Chandan Borgohain for his help in collecting NMR Spectra data and our technical and official staffs for their help and support.

Finally, I owe success to my parents (Mr. Sheikh Nasiruddin and Mrs. Asma Begum) my in laws (Mr. Md. Nazamuddin and Mrs. Nasima Banu), my husband Mr. Mohsin Jafar and my beautiful sister Ms. Farzana Parveen who have been a constant source of inspiration to

carry out my career. I wish to thank them for giving me the freedom to pursue a career path of my choice and their constant support and encouragement in realizing my dreams.

I want to express my thanks to all the family members for their support.

I would like to acknowledge the Department of Chemistry, IIT Guwahati for giving me the opportunity and fellowship to carry out my research work.

Afsana Yashmeen

Afsana Yashmeen

Present Address:

C/O: Dr. Subhendu Sekhar Bag
Department of Chemistry
Indian Institute of Technology Guwahati
Guwahati – 781039, Assam, India
Phone: +91 361 2582324
E mail: afsana@iitg.ernet.in
afsana.iitd@gmail.com

Permanent Address:

Vill – Rabindrapally
P. O. – Inda
Dist. – Paschim Medinipur
Pin – 721305
West Bengal, India
Mobile**:** +91 8011923692

Area of Interest

Design and synthesis of unnatural fluorescent biomolecules for chemical and biological application.

Education:

2017	**Ph. D.** [Thesis submitted (February)]
2011	**Master of Science** (*in Organic Chemistry*) Vidyasagar University , West Bengal
2009	**Bachelor of Science** *(Chemistry Hons.)* Midnapore College Vidyasagar University

Honors/Awards:

- Junior Research Fellowship and Eligibility for Lectureship (**UGC-JRF-NET**), December–2010 and June–2011 awarded by University Grants Commission, India.
- Graduate Aptitude Test in Engineering (**GATE**) qualified in Year 2010 and 2011.

List of Publications

1. **●Triazolo-β-Aza-ε-Amino Acid and Its Aromatic Analogue as Novel Scaffolds for β-turn Peptidomimetics●** Bag, Subhendu Sekhar*; Jana, Subhashis; **Yashmeen, Afsana**; De, Suranjan● ***Chemical Communication***, **2015**, *51*, 5242.

2. **●Triazolyl-Donor/Acceptor Chromophore Decorated Unnatural Amino Acids and Peptides: FRET Event in β-Turn Conformation●**Bag, Subhendu Sekhar*; Jana, Subhashis; **Yashmeen Afsana**; Senthilkumar, K; Bag, Raghunath● ***Chemical Communications***, **2014**, *50*, 433.

3. **●Synthesis of Functionalized Pyrazoles via Vanadium-Catalyzed C-N Dehydrogenative Cross-Coupling and Fluorescence Switch-On Sensing of BSA Protein●** Sar, Dinabandhu; Bag, Raghunath; **Yashmeen, Afsana**; Bag, Subhendu Sekhar*; Punniyamurthy, Tharmalingam* ● ***Organic Letters***, **2015,** *17***,** 5308.

4. **●Uracil-Amino Acid as a Scaffold for β-Sheet Peptidomimetics: Study of Photophysics and interaction with BSA Protein●** Bag*, Subhendu Sekhar; **Yashmeen, Afsana●** ***Bioorganic & medicinal chemistry letters***, **2017,** *27***,** 5387.

5. **●Signaling the Chemical Cleavage of Fluorescent β-Lactams via FRET/Exciplex or Excimer Emission: A Model Study ●** Bag*, Subhendu Sekhar; **Yashmeen, Afsana●** ***Journal of Photochemistry and Photobiology A: Chemistry***, **2017,** *353***,** 464.

6. **●FRET Relay in an *o,m*-Aromatic Amino Acid Scaffolded Trichromophoric β-Turn Pentapeptide ●** Bag*, Subhendu Sekhar; **Yashmeen, Afsana** (Communicated).

7. **●Distance Dependent Observation of FRET in Aliphatic Triazolo Amino Acid Scaffolded Pentapeptides ●** Bag*, Subhendu Sekhar; **Yashmeen, Afsana** (Communicated).

Article 1, 2 and 3 are not included in the thesis.

List of Conferences/Symposiums

1. **Triazolo-β-aza-ε-amino acid and its aromatic analogue as novel scaffolds for β -turn peptidomimetics**, **ISBOC-2015,** January 11-15, 2015, IISER Pune, Pune, India.

2. **FRET Event among the Terminal Unnatural Triazolyl Fluorescent Amino Acids in a β-Turn Tripeptidomimetic, 17 th CRSI National Symposium in Chemistry-2015**, February 5-8, 2015, CSIR-NCL, Pune, India.

Abstract

Exogeneous natural peptides seldom can be used as therapeutically drug candidates because of the problems associated with their low absorption, rapid metabolism and low oral bioavailability. To harness peptide based therapeutics, researchers are engaged in the design and synthesis of peptidomimetics or peptide like molecules of clinical importance. Introduction of molecular scaffold induces secondary structure in peptides and are also used for the development of pharmacologically useful compounds, artificial receptors and asymmetric catalysts. Thus, a great effort has been paid to design a variety of molecular scaffolds and incorporation of them into peptide backbone to create highly ordered structures of peptides. Furthermore, the molecular scaffold containing hydrogen bonding sites and chiral centers are very useful in this respect which are crucial to their biological activity, protein–protein/protein–peptide interaction and interaction with other biomolecules such as DNA. Therefore, scaffolded peptides are important as potential candidates for medicinal applications.

On the other hand, molecular design that mimic the structure, conformation of proteins or active site of an enzyme are very much effective to show interaction with biomolecules. Thus they have potential to show biological activity and can be utilized as probe of for biophysical studies. A common example in this regard is the bacterial enzyme transpeptidase that recognizes D-Ala–D-Ala peptide sequence for biosynthesis of bacterial cell wall by crosslinking of the peptide side chains of peptidoglycan strands. The β-lactam core is structurally similar to D-Ala–D-Ala terminus of peptidoglycan terminus. Therefore the β-lactam antibiotics such as penicillins are being misrecognized by bacterial transpeptidases for the TPase catalytic reaction which irreversibly inhibit the enzyme and stop the bacterial cell wall synthesis required for survival. The potent antibacterial activity by β-lactams not only controls the spread of life-threatening illness, but have also prevented the onset of opportunistic infections in immune-deficient patients. About 60% of the worldwide sales of antibacterial substances can be allocated to the β-lactam antibiotics and it can be estimated that β-lactam antibiotics account for about 10% of the total sale of drugs. However evaluation of bacterial β-lactamases creates problem of administration of β-lactam antibiotics in clinics. Therefore to combat with β-lactamases, several modified or new β-lactam antibiotics as well as platforms monitoring the β-lactamase activity have been reported. However, these efforts are not sufficient to fulfil the all research need demanding newer methodology to monitor β-lactamases as well as newer design. Now a days, fluorescent β-lactams also serves as an important role in biological and medicinal chemistry. It is demonstrated that fluorescent β-lactams can serve as a sensitive fluorogenic reporter for imaging Tetrahymena ribozyme activity in living cells. Fluorescent labeled β-lactam represents a successful model in the construction of “switch-on” fluorescent biosensor. It also has been explored that fluorescent β-

lactams are used to block bacterial growth by generating reactive oxygen species (ROS).

Therefore, the thesis "**DESIGN, SYNTHESIS AND STUDY OF PHOTOPHYSICAL/ BIOPHYSICAL PROPERTIES OF SMALL MOLECULE SCAFFOLDED PEPTIDES AND FLUORESCENT β-LACTAMS**" contains a total of **5 Chapters**:

1. Application of small molecular scaffold as β-hairpin and β-sheet peptidomimetics. A review.
2. Nucleating β-sheet with uracil-amino acid scaffold: Design synthesis photophysical and biophysical study.
3. *ortho,meta*-aromatic-amino acid scaffold as β-turn inducer: Synthesis of trichromophoric pentapeptide, study of relay FRET process.
4. Studies on the FRET phenomena in fluorescent pentapeptides containing triazolo amino acid scaffold of various spacer lengths.
5. Synthesis of fluorescent β-lactams and study of chemical cleavage fluorimetrically.

On the way to this journey, some natural and fluorescent peptides containing conformationally constrained molecular scaffold were synthesized and their conformation and photophysical properties were evaluated. Furthermore, fluorescent triazolyl β-lactam molecules containing donor and acceptor moiety were synthesized and photophysical property toward discriminating fluorescent β-lactams from their ring opened form was explored by fluorimetry.

The thesis contains a total of **5 Chapters** including one introduction chapter (**Chapter 1**). Each chapter contains individual introduction, experimental and reference sections. **Chapter 1** is a review based on application of small molecular scaffold as β-hairpin and β-sheet peptidomimetics. **Chapter 2** is based on synthesis of uracil-amino acid scaffold and incorporation of it into two fluorescent pentapeptide backbones. Conformational study and exploration of photophysical properties of our synthesized pentapeptide were carried out along with the interaction of BSA molecule. **Chapter 3** demonstrates the synthesis of *ortho, meta*-aromatic-amino acid scaffold and incorporation of it into fluorescent/natural peptide backbone, thereby generating a turn induced β-sheet secondary structure with occurrence of relay FRET process in the synthesized fluorescent peptide. Interaction studies of the fluorescent peptide with BSA protein molecule forms the content of this chapter. **Chapter 4** contains the synthesis of four aliphatic triazolo amino acid scaffolds of varying spacer lengths and incorporation of them into designed fluorescent pentapeptide containing **TMnap** and **TPy** and establishment of distance dependent FRET phenomena into designed fluorescent pentapeptides. **Chapter 5** elaborates on the synthesis of fluorescent triazolyl β-lactams and study of chemical cleavage by fluorimetry.

Chapter 1: Application of Small Molecular Scaffold as β-Hairpin and β-Sheet Peptidomimetics. A Review.

This chapter describes peptidomimetics or peptide-like molecules that induces β-hairpin and β-sheet secondary structure when present in a backbone of a peptide and fined wide applications in peptidomimetic drug design. In peptidomimetics the alternation of some amino acid by rigid molecular scaffold improves its stability and biological activity. Most short chain linear peptides can degrade by enzymatic proteolysis but introducing molecular scaffold on the peptide backbone reduces the rate of degradation. These unnatural peptides provide better binding affinity and selectivity towards the receptor unit reducing unwanted side effects and show highly effective therapeutic activity. Therefore, the unnatural peptide with molecular scaffold and having desired secondary structure draws attention as bioactive agents and pharmacological drug candidates. These peptides are useful in the field of protease inhibition, antimicrobial, anticancer, analgesics, antiviral and antimalarial activities.

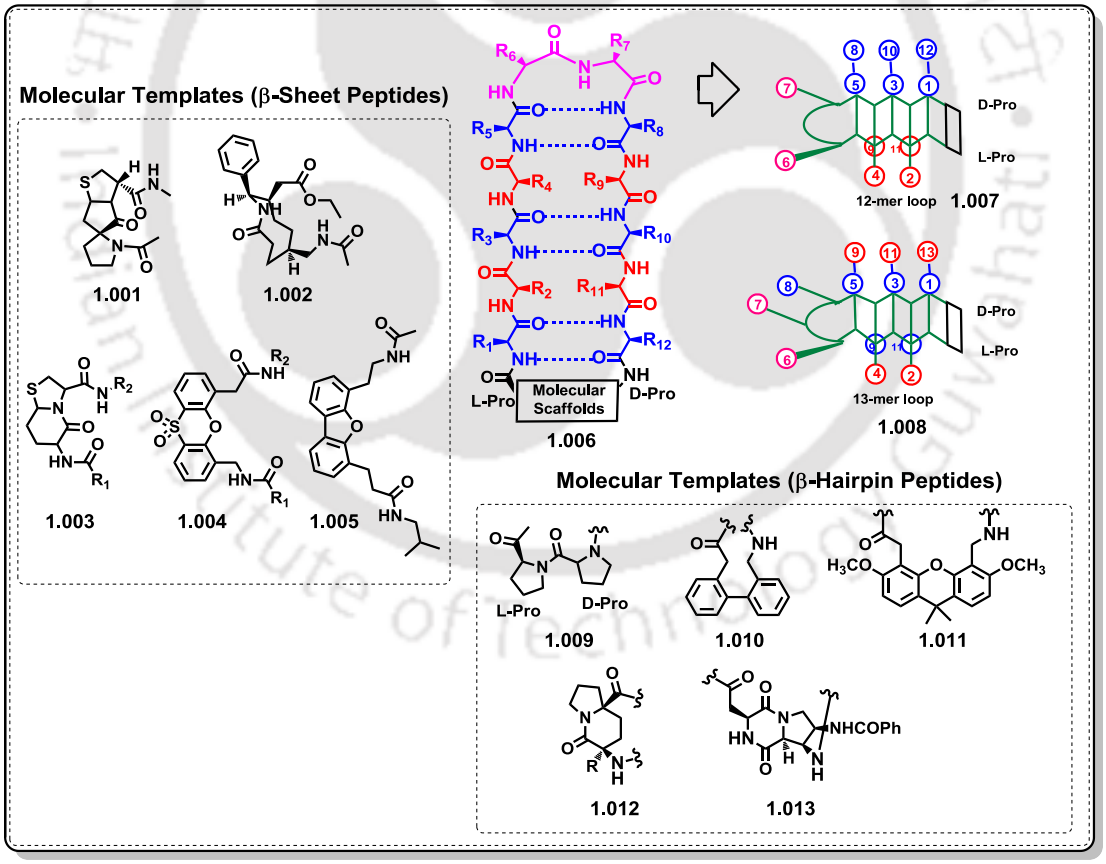

Figure A1: Structures of β-hairpin, β-hairpin and β-sheet templates for mimetics as well as a prototypical template bound 12-mer β-hairpin loop.

Thus, this review chapter contains a critical literature survey of conformationally constrained molecular scaffolds that induce peptide secondary structures like β-hairpin and β-sheet.

Chapter 2: Nucleating β-Sheet with Uracil-Amino Acid Scaffold: Design Synthesis Photophysical and Biophysical Study.

This chapter includes uracil-di-aza-amino acid (**U^{r}AA**) as a new family of molecular scaffold to induce β-hairpin structure with H-bonded β-sheet conformation in a short peptide which is demonstrated in two designed fluorescent pentapeptides. Its application in sensing BSA are also described.

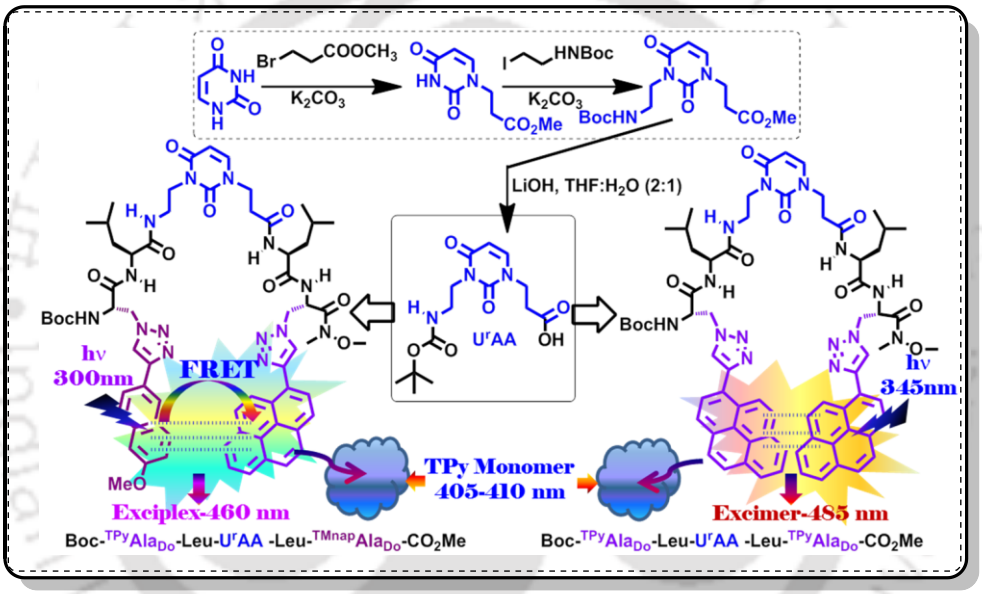

Figure A2: Synthesis of uracil-di-aza-amino acid, **U^{r}AA** as constraint molecular scaffold and structures of designed peptidomimetics with predefined conformation and predicted photophysics.

We successfully synthesised uracil amino acid scaffold (**U^{r}AA**) and incorporated into two short linear fluorescent pentapeptides [**BocNH-^{TMnap}Ala^{Do}-Leu-U^{r}AA-Leu-^{TPy}Ala^{Do}-CONMe(OMe)**] and [**BocNH-^{TPy}Ala^{Do}-Leu-U^{r}AA-Leu-^{TPy}Ala^{Do}-CONMe(OMe)**] and evaluated their conformation and photophysics. The conformational analysis of the two synthesized fluorescent pentapeptides via several spectroscopic techniques like CD spectra, IR, 2D NMR, VT-NMR and molecular dynamics (MD) simulation established β-hairpin structures in both peptides with H-bonded β-sheet conformation. The pentapeptide containing fluorescent triazolyl unnatural amino acids (**^{TMNap}Ala^{Do}/^{TPy}Ala^{Do}**) at the two termini showed dual path entry to exciplex emission-either via FRET or via direct excitation of a FRET acceptor. The other peptide with **^{TPy}Ala^{Do}/ ^{TPy}Ala^{Do}** pair exhibited excimer emission

(**Figure A2**). Both the peptides maintained their fundamental photophysics while interacted with a model protein BSA with fluorescence switch-on response.

All experimental results are presented in this chapter.

Chapter 3: *ortho,meta*-Aromatic-Amino Acid Scaffold as β-Turn Inducer: Synthesis of Trichromophoric Pentapeptide, Study of Relay FRET Process.

This chapter includes the design and synthesis of *ortho,meta*-aromatic triazolo amino acid scaffold and its incorporation into peptide backbone to act as a turn induced β-sheet nucleator. The trichromophoric fluorescent pentapeptide containing *ortho,meta*-aromatic triazolo amino acid scaffold showed relay FRET process and its application for BSA protein sensing are also described in this chapter.

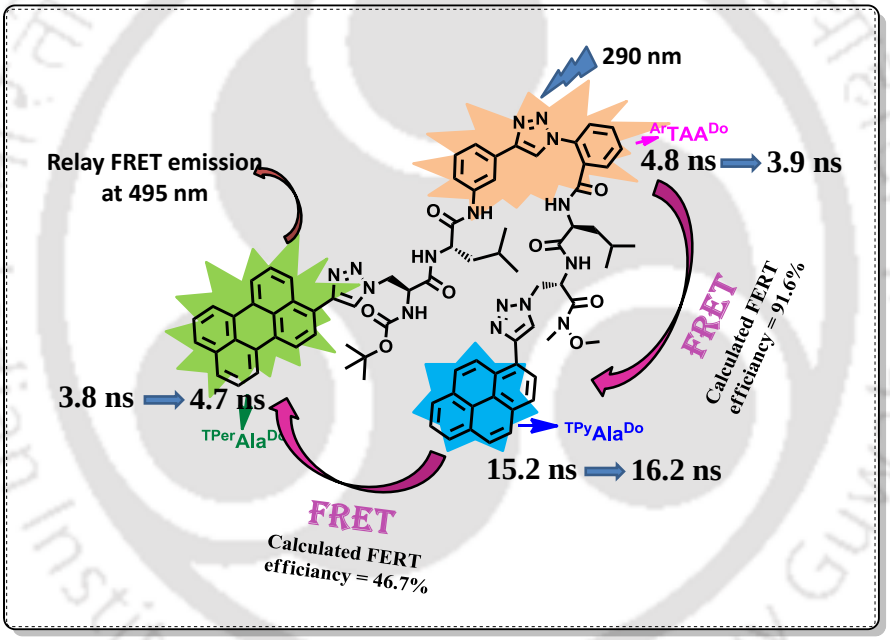

Figure A3: Schematic presentation of ortho meta aromatic triazolyl amino acid scaffold $^{o,m\text{-}Ar}$TAA based relay FRET process in trichromophoric fluorescent pentaptide.

Herein, we demonstrated the synthesis of our desired *ortho,meta*-aromatic triazolo amino acid scaffold (**$^{o,m\text{-}Ar}$TAA**) and its incorporation into a trichromophoric fluorescent pentapeptide [**BocNH–^{TPer}Ala^{Do}–Leu–$^{o,m\text{-}Ar}$TAA–Leu–^{TPy}Ala^{Do}-CONMe(OMe)**] and a natural Leu-enkephalin analogue peptide [**BocNH–Tyr-$^{o,m\text{-}Ar}$TAA–Phe–Leu–COOMe**] (**Figure A3**). The conformation and photophysics of the synthesized peptides were also studied via various spectroscopic methods indicating predominant turn induced β-sheet like structures in both the cases.

Furthermore, we have studied the photophysical property of the fluorescent pentapeptide to test our hypothesis of FRET relay process. Thus, upon excitation at the scaffold we observed three emission bands at 310 nm (negligible) corresponding to the emission of the scaffold, at 365 nm corresponding to **TPy** of ^{TPy}**Ala**^{Do} and at 450 nm corresponding to the emission from **TPer** of ^{TPer}**Ala**^{Do}. The relative intensities and the time resolved spectroscopy suggested a FRET process from the scaffold to **TPy** to **TPer** (**Figure A3**).

This relay FRET peptide probe was also found to act as an effective fluorescence light-up probe for studying protein–peptide interactions in buffer (pH=7.0).

All experimental results are presented in this chapter.

Chapter 4: Studies on the FRET phenomena in fluorescent pentapeptides containing triazolo amino acid scaffold of various spacer lengths.

This chapter describes the synthesis of triazolo aliphatic amino acids with different spacer lengths, incorporation into fluorescent pentapeptide containing triazolyl methoxynaphthalene (^{TMnap}**Ala**^{Do}) and triazolyl pyrene (^{TPy}**Ala**^{Do}) amino acids at the two termini and their conformational analysis. The studies on the spacer length dependent FRET event in these designed peptides are also described (**Figure A4**).

The vast applications of FRET process inspired us to take a challenge of designing scaffold amino acids of arm length differing by 1-2 carbon atoms. For investigating the factors that affect the folding, stability and interactions of β-sheets and proteins, a number of β-turn mimics employing various templates have been developed. Based on our earlier concept of triazolyl aliphatic amino acid as β-turn peptidomimetic scaffolds, we thought that altering the length of amine or acid terminus or both and embedding the same in a peptide backbone could end up with β-turn peptides.

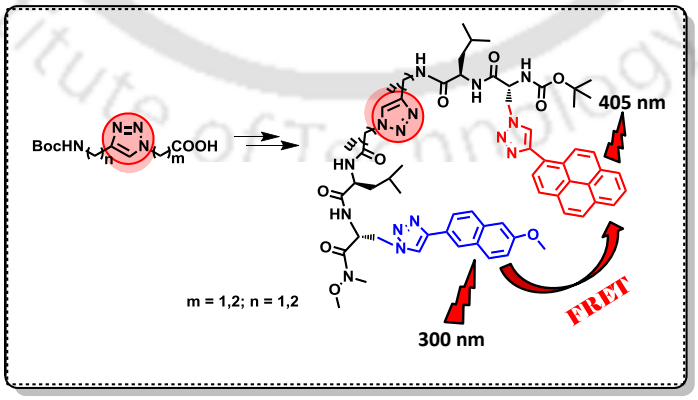

Figure A4: Graphical presentation of aliphatic triazolo amino acid with different spacer lengths and distance dependant FRET phenomena in the designed fluorescent pentapeptide.

Hence, we synthesised four triazolyl amino acids with various spacer lengths via cycloaddition between the corresponding alkynyl ester and azides. These were incorporated into fluorescent pentapeptides wherein two fluorescent amino acids (^{TMnap}**Ala**^{Do} and ^{TPy}**Ala**^{Do}) were placed at the two termini constituting a FRET pair. We studied the conformation with the help of CD, IR, 2D NMR, variable temperature NMR and MD simulation.

As the scaffolds in the backbone induced turn into the peptides, the two termini of the peptides come close together and would show FRET interaction. As the lengths of the spacers of triazolyl amino acid scaffolds were different, the extents of FRET were expected to be different. We observed that with increasing spacer length of the scaffolds the extent of FRET also increased. The peptide with the scaffold containing a C-2/C-2 spacer exhibited the highest FRET efficiency due to its flexibility in bringing the two fluorophoric termini at the shortest distance.

All experimental results are presented in this chapter.

Chapter 5: Synthesis of fluorescent β-lactams and study of chemical cleavage fluorimetrically.

This chapter includes the synthesis of fluorescent triazolyl β-lactams and fluorimetric sensing of chemical cleavage of β-lactam ring. The cleavage of the two β-lactams out of twelve synthesised fluorescent triazolylpenicilines, (^{TMNap}**β-Lac**^{Do} and ^{TPy}**β-Lac**^{Do}) with aminomethylpyrene (**AMePy**) as fluoroscent nucleophile was found to be signaled via the generation of FRET/exciplex and excimer emission respectively (**Figure A5**).

The growing demand of newer β-lactam and β-lactamase assay inspired us to take a project on the generation of fluorescent β-lactams, particularly triazolyl donor/acceptor chromophore decorated fluorescent penicillanic acids. We envisaged that replacing the N-6 acyl unit by triazole would modulate the fluorescence property of the attached donor-acceptor aromatics as well as would electronically stabilize the lactam ring. In our design, the N-5 acyl unit was replaced by triazolyl donor-acceptor aromatics as a source of stability as well as fluorescence property. After synthesizing all the triazolyl donor-acceptor decorated β-lactams the β-lactam ring was cleaved through chemical cleavage. The β-lactam ring was attempted to cleave with fluorogenic amines as nucleophiles. We targeted two fluorescent β-lactams-one with triazolylmethoxynaphthyl (**TMNap**) and other with triazolylpyrene (**TPy**) chromophore for the model ring opening by a fluorogenic nucleophile, namely, aminomethylpyrene (**AMePy**). Thus, upon ring cleavage we observed FRET as well as exciplex and established dual mechanism for exciplex emission in the β-lactams with triazolylmethoxynaphthalene (^{TMNap}**β-Lac**^{Do}) and an excimer emission in

triazolylpyrene (^{TPy}**β-Lac**^{Do}) containg β-lactam. These two systems are important in photophysical outcome and might find applications in future.

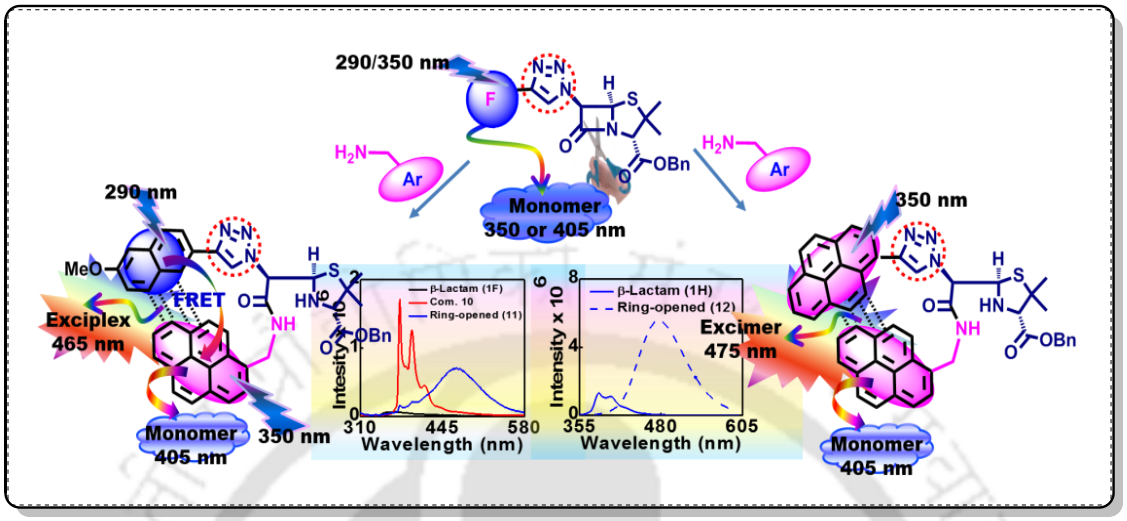

Figure A5. Schematics of fluorescence discrimination of fluorescent triazolyl β-lactam from the ring opened form.

The ring opened ^{TMnap}**β-Lac**^{Do} having **TMNap-AMePy** pair showed dual door entry to exciplex emission due to close proximity and π-π stacking interaction between the **TMNap** and **AMePy** units. On the other hand, in ^{TPy}**β-Lac**^{Do} an excimer formation/ground state complexation in the ring-opened form between the triazolylpyrene (**TPy**) and the aminomethylpyrene (**AMePy**) was observed which would ultimately lead to the generation of excimer emission upon excitation at 350 nm (**Figure A5**).

All experimental results are presented in this chapter.

List of Abbreviations

Aib	α-Amino isobutyric acid
Ala	Alanine
Arg	Arginine
^{Al}TAA	Aliphatic triazolo amino acid
^{Ar}TAA	Aromatic triazolo amino acid
AMePy	1-Aminomethyl Pyrene
Ar	Aryl
Adk	Adenylate kinase
Abs	Absorbance
Bn	Benzyl
BSA	Bovin serum albumin
Cu_2O	Cuprous oxide
CD	Circular Dichrosim
CT	Charge Transfer
Cu	Copper
CuI	Copper iodide
CyHex	Cyclohexane
$CHCl_3$	Chloroform
$CuSO_4$	Copper sulfate
ACN	Acetonitrile
DHFR	Dihydrofolate reductase
Dtc	5,5-Dimethylthiazolidine-4-carboxylic acid
Diox	1,4-Dioxane
DMF	Dimethyl formamide
DMSO	Dimethyl sulfoxide
DMSO-d_6	Deuterated dimethyl sulfoxide

DCE	Dichloroethane
DNA	Deoxyribonucleic acid
DFT	Density functional theory
DCM	Dichloromethane
DIPEA	N,N-Diisopropyl ethyl amine
DMAP	N, N-Dimethylamino pyridine
4-DMAP	4-(*N*,*N*-dimethylamino)-phthalimide
Dnp	Dinitrophenyl
Et_3N	Triethylamine
EtOAc	Ethylacetate
EtOH	Ethanol
eV	Electron volt
EDC.HCl	1-(3-Dimethylaminopropyl)-3-ethylcarbodiimide hydrochloride
Equiv.	Equivalent
Fl	Fluorescence
FRET	Fluorescence Resonance Energy Transfer
HOBT	1-hydroxy-benzotriazole
HRMS	High Resolution Mass Spectrometry
HOMO	Highest Occupied Molecular Orbital
HIV	Human immunodeficiency virus
ICT	Intramolecular Charge Transfer
ITC	Isothermal calorimetry
IR	Infrared Spectroscopy
KOH	Potassium hydroxide
KBr	Potassium bromide
K	Kelvin
Leu	Leucine

LiOH	Lithium hydroxide
LUMO	Lowest Unoccupied Molecular Orbital
MD	Molecular Dynamics
Max	Maxima
MeOH	Methanol
mM	Mili molar
m.p.	Melting point
NaN_3	Sodium azide
$NaHCO_3$	Sodium bicarbonate
Na_2SO_4	Sodium sulphate
NMR	Nuclear Magnetic Resonance
NOESY	Nuclear Overhauser effect spectroscopy
mM	Milimolar
nm	Nanometer
$^{o,m\text{-Ar}}$TAA	*ortho,meta*-Aromatic triazolo amino acid
$^{o,o\text{-Ar}}$TAA	*ortho,ortho*-Aromatic triazolo amino acid
Py	Pyrene
Per	Perylene
PL	Photoluminescence
PNA	Protein nucleic acid
PPh_3	Triphenyl phosphine
Pd	Palladium
Ph	Phenyl
$PdCl_2(PPh_3)_2$	Bis(triphenylphosphine)palladium(II) dichloride
r.t.	Room temperature
RNA	Ribonucleic acid
ROSEY	Rotating frame nuclear Overhauser effect spectroscopy

Ser	Serine
$SOCl_2$	Thionyl Chloride
Trp	Tryptophan
Tyr	Tyrosine
$^{TMnap}\beta$-Lac^{Do}	Triazolyl Methoxynaphthalene β-lactam
$^{TPy}\beta$-Lac^{Do}	Triazolyl Pyrene β-lactam
TPhen	Triazolyl phenanthrene
TCNB	Triazolyl cyanobenzene
TPy	Triazolyl Pyrene
TBAF	Tetrabutylammonium fluoride
TLC	Thin layer chromatography
THF	Tetrahydrofuran
TCSPC	Time correlated single photon counting
TEA	Triethyl amine
TFA	Trifluoroacetic Acid
TMS	Trimethylsilyl
UNAAs	Unnatural Amino Acids
UV	Ultra violate
μM	Micro molar
Val	Valine
VT	Variable Temperature
Φ	Quantum Yield
ε	Molar extinction co-efficient
τ	Decay time
Å	Angstrom (10^{-8}cm)
$\bar{\upsilon}$	Wave Number
λ	Wave Length

ϕ and ψ	Torsion angle
λ_{max}^{abs}	Absorption maxima
λ_{max}^{fl}	Fluorescence maxima
Δf	Solvent polarity parameter

NMR Data

δ	Chemical shift in NMR
s	singlet
d	doublet
t	triplet
q	quartet
m	multiplet
bs	broad singlet
dd	double doublet
dt	doublet of triplet
ddd	doublet of doublet of doublet
J	coupling constant in Hz

CONTENTS **Page No.**

1.1. Introduction:

Exogenous natural peptides are not considered as valued therapeutics because of their low absorption, rapid metabolism and low oral bioavailability. Hence, in order to harness peptide based therapeutics, researchers are engaged in designing and syntheses of peptidomimetics. Use of molecular scaffold is an important strategy in peptidomimetic chemistry to generate scaffolded peptides that are important as potential candidates for medicinal applications.

The term peptidomimetics is used to define peptide like molecule which can be a peptide, a modified peptide or any other biologically active ligands of hormones, cytokines, enzyme substrates or other bio-molecules that mimic a protein's secondary structure. These peptide mimics can stimulate the physiological activity of the natural ligands. Peptides or modified peptides consisting of 14 to 20 amino acids can serve as therapeutically effective agents.[1] Generally peptide mimics are considerably smaller than their parent peptide but they show biological activity similar to the peptide. However, the non-peptide units are structurally different from their parent peptide molecules, thereby lacking flexibility or amide bonds and hence can serve the purpose of a highly selective ligands in both peptide and non-peptide compounds.

A peptidomimetic molecule can be discovered by screening through a large number of compounds or designed as de novo mimetics.[2] This design involves the replacement of the individual peptide bonds by a nonpeptidic moiety or any other spacer group. These may be unnatural amino acids, bond surrogates, cyclic peptide derivatives, isosteric replacements and conformationally constrained molecular scaffolds. These peptidomimetic molecules bridge the gap between completely nonpeptide structures and simple peptide analogs.

1.1.1. Criteria for the Design of Peptidomimetic Molecule with Desired Secondary Structure

The guideline of designing peptidomimetic molecules (both peptide and non-peptide based) has been established and practices since 4-5 decades.[3] The design of peptidomimetics follows the steps bellow (**Figure 1.1**).[4]

1. Replacement of amino acid or peptide unit from large peptide backbone by a nonpeptide framework.
2. Pharmacophoric side chain groups in the main peptides should be similar to the peptidomimetic molecule.
3. Conformational flexibility should be retained in the synthesized peptidomimetic molecule.

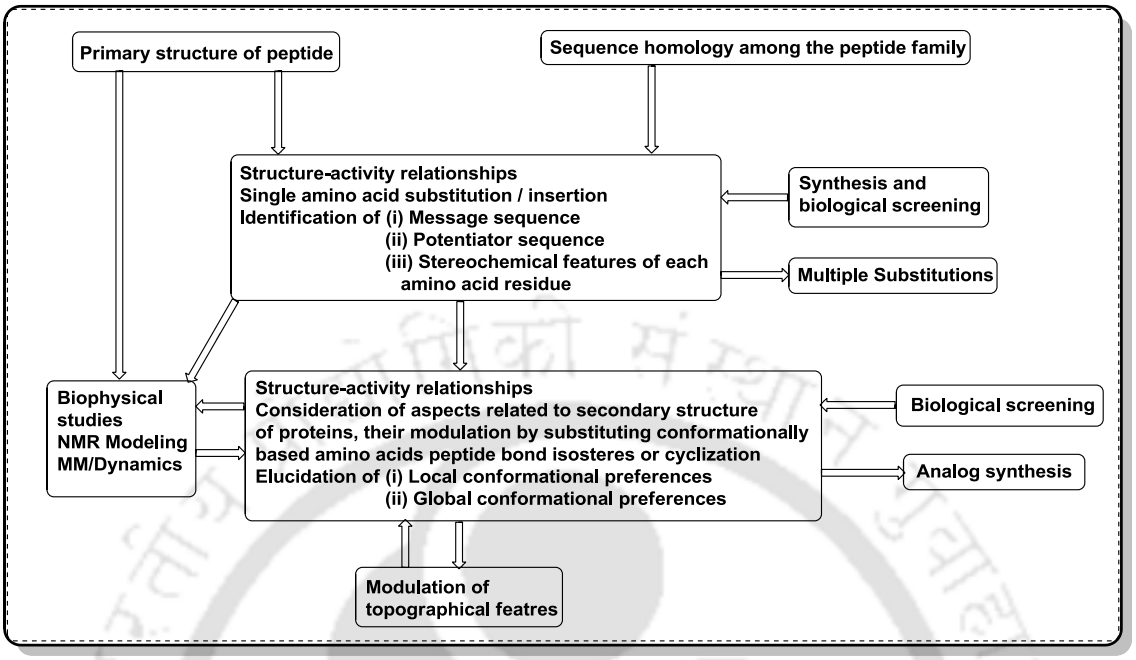

Figure 1.1. Flowchart of the iterative approach to the rational design process of peptidomimetics.[4]

Peptidomimetic molecule with new functionalities exhibits novel and enhanced property such as cell membrane penetration and resistance to enzymatic degradation. Peptidomimetic molecule can fold the protein and give desirable protein secondary structures. Thus a number of compounds have been synthesized that have been utilized to mimic or to induce protein secondary structures such as α-helix, β-turn, and β-sheet. These synthetic molecules with protein like properties may have potential as drug therapeutics. Peptidomimetic molecules are therefore widely used in development of new pharmacologically useful analogues of biologically active peptides.

Conformationally constrained molecular scaffold containing aliphatic/aromatic moiety when introduced into peptide backbone, induce a desirable secondary structure. As for example, aromatic scaffolds (biphenyl system) have been demonstrated to induce β-sheet like structure between two attached peptides.[5] Introduction of molecular scaffold not only induce a particular secondary structure in peptides but also used in development of pharmacologically useful compounds, artificial receptors and asymmetric catalysts.[6] Thus a lot of efforts have been put forth to design a variety of molecular scaffolds and their incorporation into peptide backbone to create highly ordered structures of peptides. The molecular scaffolds, when introduced in the peptide strand generally regulate the strand in appropriate dimensions. In addition to this, the introduction of additional hydrophobic interaction sites permits the further regulation in geometry. Ferrocene containing organometallic

molecular scaffold has been used and reported by Hirao *et al*. for construction of chirality-organized peptide strands via intramolecular hydrogen bonding.[7] Furthermore the molecular scaffold containing hydrogen bonding sites and chiral centers are very useful to create highly ordered peptide secondary structures.[8]

Conformationally constrained small molecular scaffolds/ non-peptide isosteres are attracting much research interest in this regard because they have the ability to induce a peptide to adopt a particular conformation which is the key for showing biological activity by the peptide with high oral viability. Considerable efforts have thus been invested in studying the impact of appended molecular scaffolds in one hand and nucleating β-sheet/β-turn mimics on the other hand, on the conformational preferences of proteins and peptides in solution.

1.2. The Approaches to β-Hairpin Peptidomimetic

The most important secondary structures found in natural proteins are α-helix, β-sheet and β-hairpin. When molecular scaffolds are used as building blocks in peptide backbones, they become preorganized for binding to the target biomolecules through numerous sites for hydrogen bonding.[9]

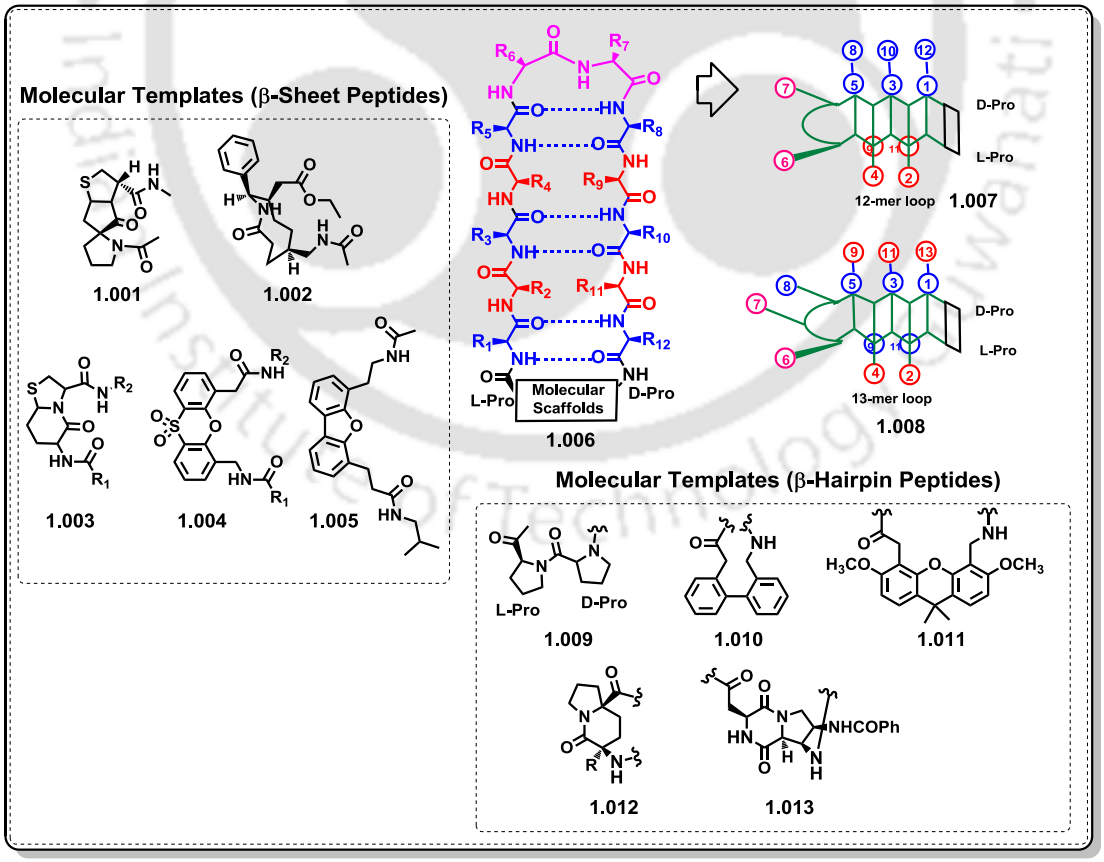

Figure 1.2. Structures of β-hairpin (**1.006**), β-hairpin templates (**1.009-1.013**) for mimetics as well as a prototypical template bound 12/13-mer β-hairpin loop (**1.007-1.008**).[9]

The conformation of β-hairpin structure varies with H-bonding pattern between the strands and loop length. The loop length in general is less than 5 residues (**1.006**, **Figure 1.2**). However, residue 1 and 2 often adopts β-turn structure while residue 3 is a part of left-handed α-helix.[10] The loops with 4 and 5 residues exhibit greater option to adopt cis peptide bonds (**1.007-1.008**, **Figure 1.2**).

The majority of the β-hairpin mimic strands are held together and stabilized dipeptide mimetic that replace i + 1 and i + 2 residues at the corner of the turn. The hairpin mimetics are generally designed in such a way to retain the intramolecular hydrogen bonding network of the neighboring peptide chain (**1.006**, **Figure 1.2**). However, the side chains in the peptides mostly exposed at the surface of the protein are involved in intermolecular interactions with target proteins or receptors. The β-hairpin mimetics should be designed as the original β-turn structure to achieve better binding activity. The structures **1.001-1.005** in **Figure 1.2** represent few small molecular scaffolds utilized for inducing β-sheet and **1.009-1.013** for β-hairpin conformation in peptides while present in peptide backbone.

The turn in β-hairpin can be β-bend, β-loop or reverse turn. This turn plays a crucial role in the recognition events of biological systems. Reverse turn mimetics is very useful to study molecular recognition process and explore structure-function relationships in complex proteins.[11] A great deal of effort has been invested in the design and synthesis of conformationally constrained molecular scaffold with turn structure.

Gellman *et al.* have reported that Pro–Ala or Pro–Gly containing dipeptide can induce β-hairpin in a peptide backbone. The peptide was intramolecularly hydrogen-bonded and shows the enthalpically preferable β-hairpin folding (**1.014-1.015**, **Figure 1.3**).[12]

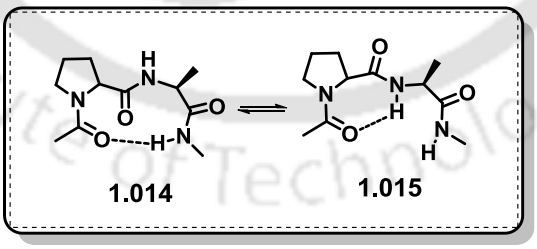

Figure 1.3. The hydrogen bonding of D-Pro–Ala dipeptide (**1.014-1.015**) gives β-turn mimic hairpin structure in peptide backbone. [12]

The successful design of β-hairpin or β-turn exactly would improve the biological activity of the parent peptide. Thus several small molecular scaffolds with turn structure have been synthesized to induce β-sheet or β-hairpin conformation in peptide backbone (**1.016**, **1.017** and **1.018**, **Figure 1.4**).[13]

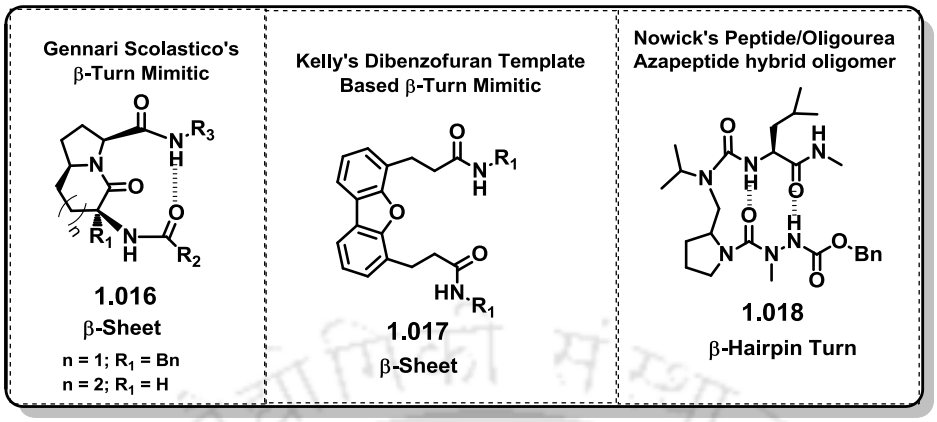

Figure 1.4. β-turn mimic molecular scaffolds (**1.016-1.018**) that nucleate sheet or hairpin structure.[13]

Gellman *et al.* have synthesized trans-5-amino-3,4-dimethylpent-3-enoic acid residue as conformationally constrained molecular scaffold (**1.019-1.021, Figure 1.5**), which is a dipeptide mimic of glycylglycine and its central amide bond is replaced with an E-tetrasubstituted alkene. This isosteric replacement promotes β-hairpin conformational preference. In this trans alkene unit allylic strain is avoided and the backbone is preorganised to adopt the β-hairpin conformation (**1.022-1.024**, **Figure 1.5**). NMR and IR data shows that the di-, tri-, and tetrapeptide analogues containing the ADPA residue aids the formation of β-turn and β-hairpin like folding in methylene chloride solution.[14]

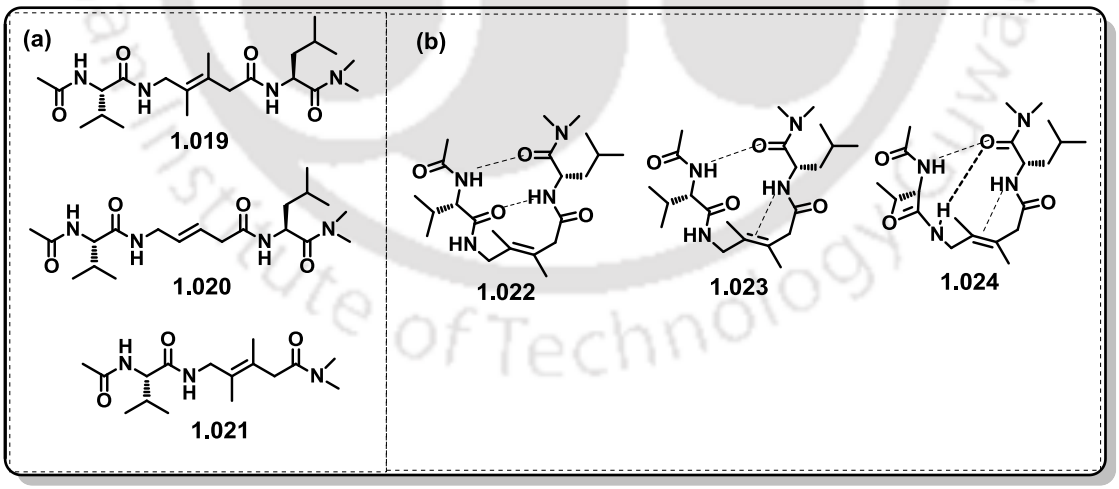

Figure 1.5. (a) General structure of alkene substituted peptides (**1.019-1.021**). (b) Alternative folding patterns for alkene substituted tetrapeptide mimic (**1.022-1.024**).[14]

Nowick and co-workers again reported several examples of turn mimetic molecular scaffolds of β-hairpin secondary structure in peptides.[15] They showed that mirror-image β-turns based upon D-Pro–Gly dipeptide plays a crucial role in

stabilizing the β-hairpin peptidomimetics. The amino acid ornithine can form a good turn structure that can stabilize the β-hairpin peptidomimetics when linked through the δ-amino group.

The peptide that contains unnatural amino acid and linked to the side chain of the amino acid ornithine (Orn) can fold easily and give a sharp β-hairpin secondary structure (**1.025**, **Figure 1.6**) and is comparable to D-Pro–Gly to induce β-hairpin. The ^{1}H NMR chemical shift and NOE studies reveal that [Arg–Trp–Gln–Tyr–Val–$^{\delta}$Orn–Lys–Phe–Thr–Val–Gln–NH_2] generates better β-hairpin folding than D-Pro–Gly folding.[15]

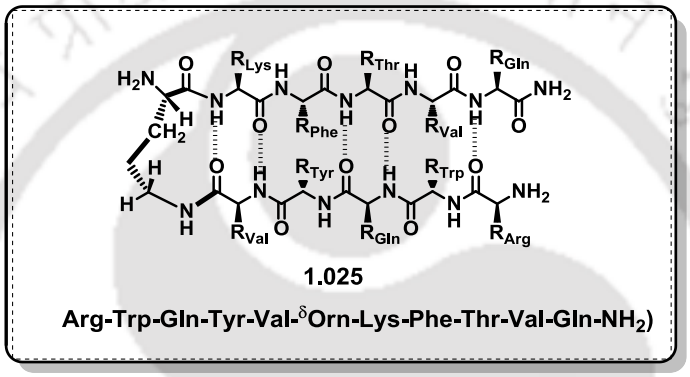

Figure 1.6. Orn-containing peptide **1.025** [Arg–Trp–Gln–Tyr–Val–$^{\delta}$Orn–Lys–Phe–Thr–Val–Gln–NH_2] where $^{\delta}$Orn shows the similar hairpin folding as D-Pro–Gly.[15]

Seebach and coworkers have prepared a 6-residue β-peptide which shows β-hairpin conformation. In this peptide, the ornithine residue acts as a hairpin turn inducer (**1.026**, **Figure 1.7**). The turn of this β-peptide was characterized as 10-membered hydrogen-bonded turn as has been revealed from MD simulation and NMR structure elucidation.[16]

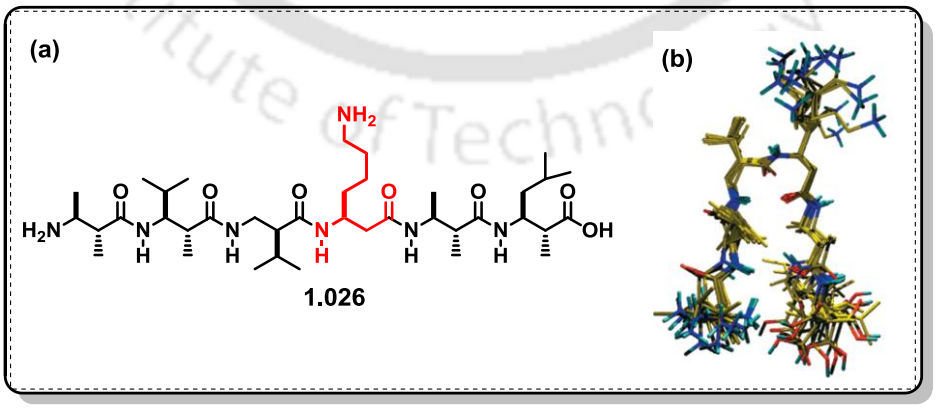

Figure 1.7. (a) The structural formula of the β-hexapeptide **1.026** studied. (b) Macromodel geometry of synthesized β-hexapeptide.[16] Copyright (2001) from American Chemical Society.

Henry B. Lowman and coworkers synthesized a family of β-hairpin peptides containing molecular scaffolds that can bind with FcεRIα. The α-chain of the peptide shows the high-affinity for IgE. This binding results 18-residue peptide-phage clone and related sequence did not look like the fragments of IgE. NMR analysis reveals that the peptide adopts a stable β-hairpin structure in solution phase (**1.028**, **Figure 1.8**). Optimized peptide (**1.027**, **Figure 1.8**) that are with micromolar receptor affinity showed high stability in biological fluids and reserved cellular histamine relief in IgE activity. The hindering of a small epitope on this receptor chain is enough to block IgE activity that was demonstrated by the synthesized peptides. These hairpin structured peptide reveals high potential for treating allergic disease.[17]

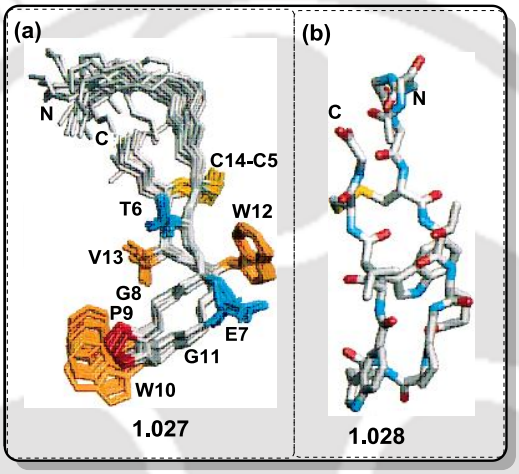

Figure 1.8. (a) Solution structure of Peptide **1.027**. (b) All heavy atoms of the representative structure for Peptide **1.028** are shown, except for the side chains of residues 1-4 and 15, which are not shown for clarity.[17] Copyright (2001) from American Chemical Society.

Gellman *et al.* have synthesized a series of β-amino acid tetramers as conformationally constrained molecular scaffold which show hairpin folding motif (**1.029-1.030**, **Figure 1.9**) they examined the relationship between covalent structure and conformational propensity. They have compared the four possible configurations of the dinipecotic acid segment, (R,S), (S,R), (R,R) and (S,S), and their ability to induce hairpin formation in enantiomerically pure peptide strands. Heterochiral dinipecotic acid segments promote hairpin formation but not homochiral one. It was observed that the hairpin conformations are different in solution and in the solid state.[18]

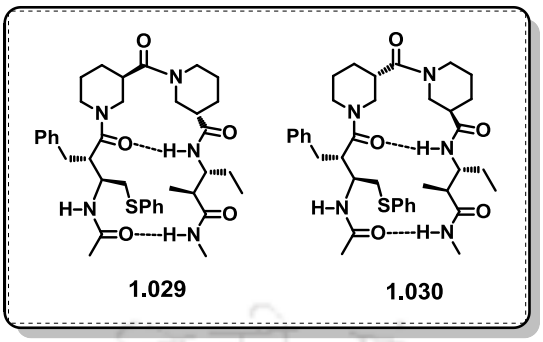

Figure 1.9. Heterochiral dinipecotic acid segments promote hairpin formation in solution phase (**1.029**-**1.030**).[18]

Carlo Scolastico and coworkers have synthesized N-acetylated hexapeptide mimics (**1.031**, **Figure 1.10**). They have also incorporated a bicyclic lactam into the peptide and analyzed its conformation using NMR, IR spectroscopy and computer modeling. The synthesized (5, 6)-bicyclic lactam scaffold containing peptides shows β-hairpin turn ($C{=}O^{3}\cdots H^{6}{-}N$) and are very compact in intramolecularly H-bonded structures (**1.032**-**1.033**, **Figure 1.10**).[19]

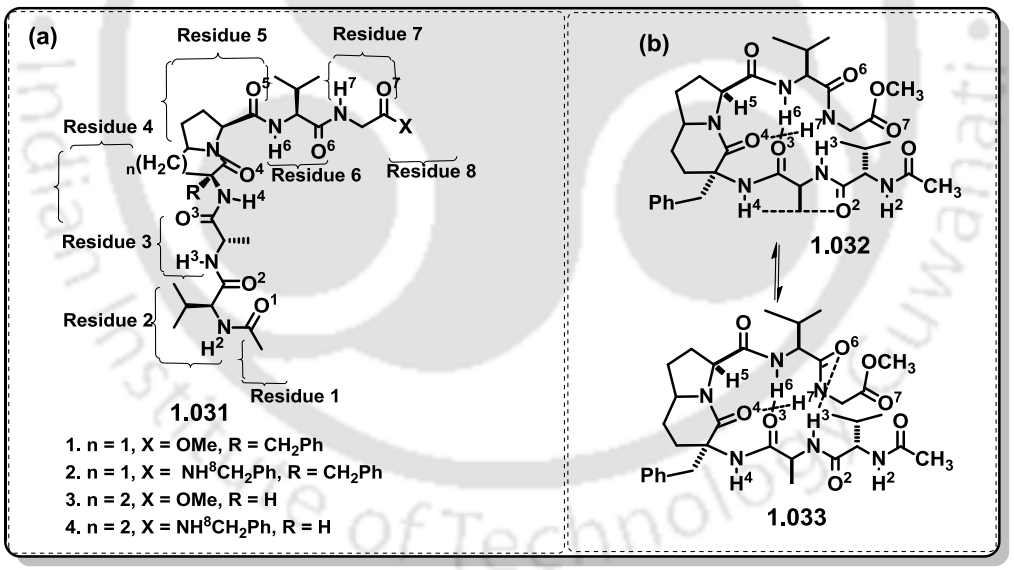

Figure 1.10. (a) N-acetylated hexapeptide mimic design **1.031** and its numbering system (b) Preferred conformation and intramolecular hydrogen-bonding patterns for the *N*-acetylated hexapeptide mimic **1.032**-**1.033**.[19]

Andrea G. Cochran and coworkers synthesized the 10 residue disulfide-constrained β-hairpins and showed that they were suitable to show themselves as a turn inducer (**1.034**-**1.035**, **Figure 1.11**). The disulfide bond was taken as a conformationally constrained molecular scaffold. The tryptophan substituent peptide endorses folding pattern to a good extent. The energies of β-hairpin structure in the

disulfide-cyclized peptides was a good agreement with the result obtained from NMR analysis.[20]

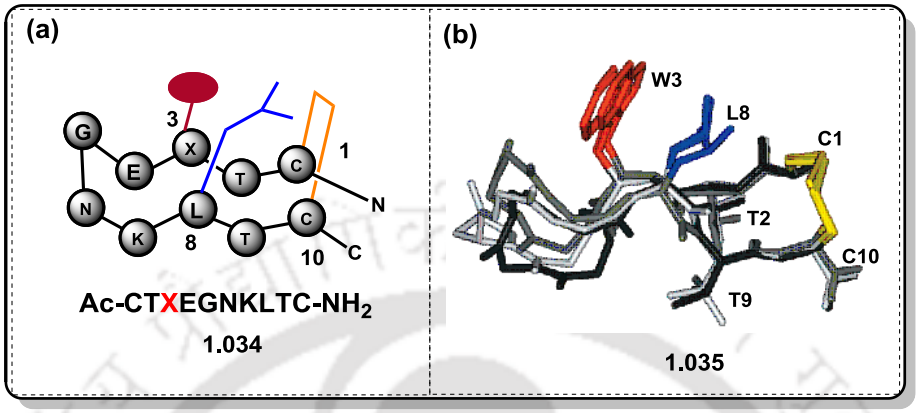

Figure 1.11. Schematic presentation of the model hairpin peptide **1.034**. (b) Minimized mean structures of the tryptophan analogues of peptides **1.035** endorse the β-hairpin folding pattern to a good extent. [20] Copyright (2001) from American Chemical Society

Gellman *et al.* have prepared short and cationic peptide containing a molecular scaffold that show broad-spectrum of antimicrobial activity. This non cysteine containing antimicrobial β-hairpin peptide forms a rigid antiparallel two-stranded β-sheet structure which is stabilized by two disulfide bonds (**1.036**, **Figure 1.12**). The antimicrobial property of the non-disulfide-bonded peptides can associated to the stability of the β-hairpin conformations in aqueous solution.[21]

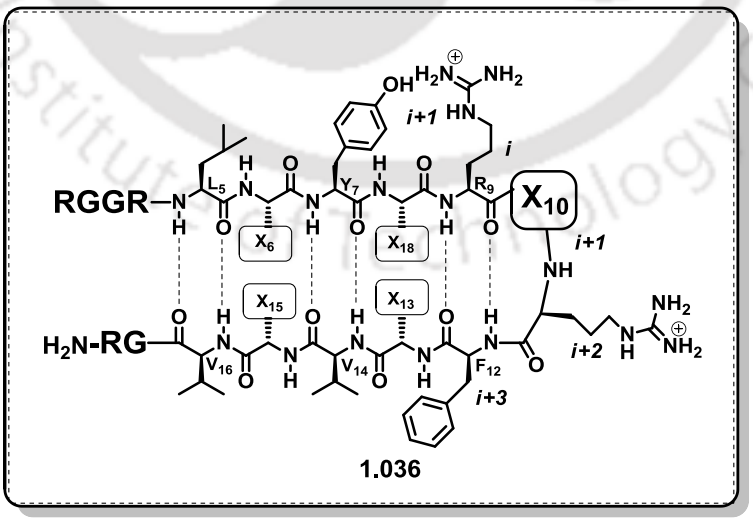

Figure 1.12. General schematic diagrams of peptides in intended of β-hairpin conformation **1.036**. The desired hydrogen-bonding pattern is shown as dotted lines.[21]

DeGrado *et al.* have analyzed the structures of two types of interhelical turns and its sequence preferences when these are connected by a tworesidue linker in an α_L–β conformation (**1.037**, **Figure 1.13**). This analysis reveals that the designed four-helical bundle protein, DF1, does not show an optimal structural context when the turn is introduced. To stabilize the conformation of the two helices in the protein, a longer loop with a β–α_R–β conformation has thus been introduced.[22]

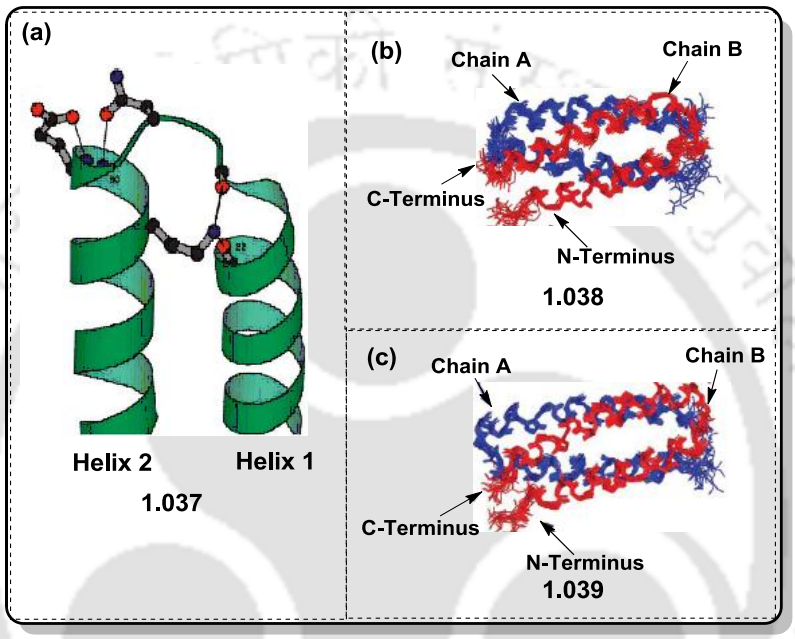

Figure 1.13. (a) The designed helix capping interactions observed in the crystal structure of DF2t **(1.037)**. (b) di–Zn(II)–DF2 **(1.038)** and (c) di–Zn(II)–DF2t **(1.039)**.[22] Copyright (2005) from Elsevier

Gellman *et al.* have synthesized a series of β-peptide hexamers which gives an idea about the relationship between sequence and hairpin folding (**1.040**, **Figure 1.14**). In those synthesized hexamers (**1.041-1.044, Figure 1.14**), reverse turn segments are compared at the central two positions. NMR analysis reveals that predicted reverse turn and side chain pairing arrangements in the peptides are well-matched with antiparallel β-sheet peptide.[23]

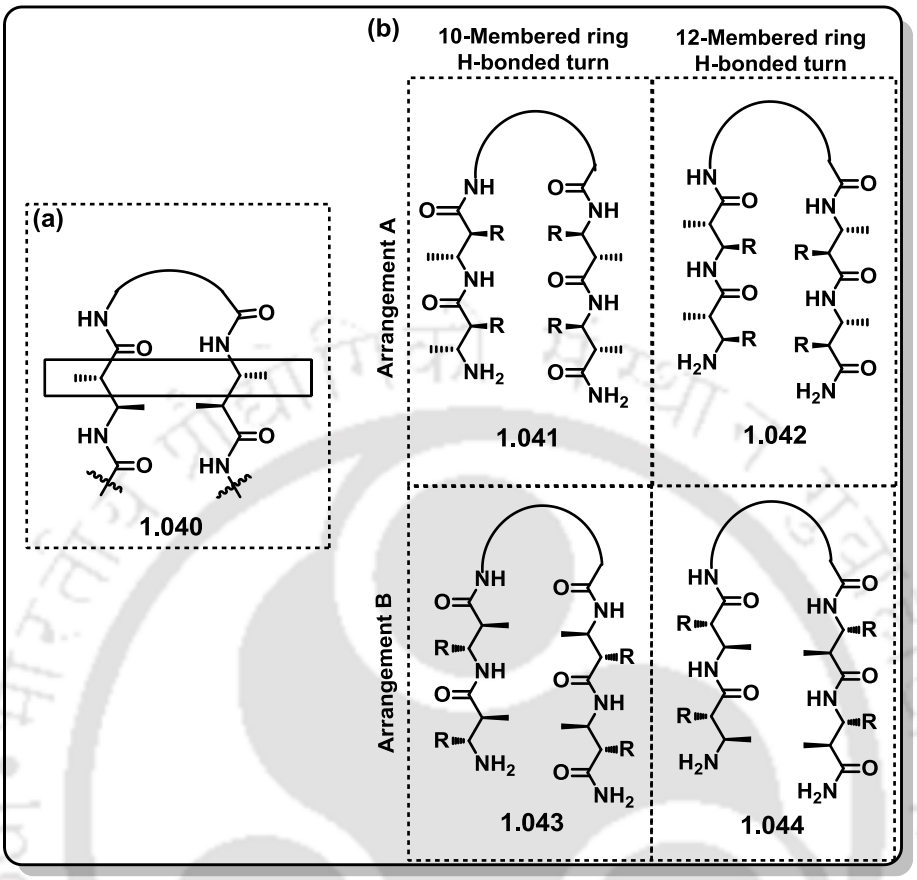

Figure 1.14. (a) General structure of an antiparallel β- hairpin peptide **1.040**, with "side chain pairs" boxed. (b) Definition of the two possible side chain arrangements for antiparallel β-peptide hairpins (**1.041-1.044**).[23]

Donald Hilvert and coworkers have incorporated photoinducible β-Hairpin secondary structure in synthesized peptides (**1.045**, **Figure 1.15**). Their synthesized photochromic azobenzene linker was incorporated into an amino acid sequence as a turn inducer in such a way that the peptide folds into a β-hairpin structure in aqueous solution (**1.045-1.046**, **Figure 1.15**). The photo-inducible molecular scaffold present in the thermodynamically favourable trans form, prohibited structure determination. Conformational change of the linker to the cis form from trans after induction of light, exhibited a well-defined β-hairpin structure supported by ^{1}H NMR analysis. The cis-to-trans isomerization of the peptide containing azobenzene unit was 30% slower compared to that of the unsubstituted chromophore. Thus suitably substituted azobenzenes unit can be used as photo-inducible turn elements and can control the stabilization of β-hairpin secondary structure.[24]

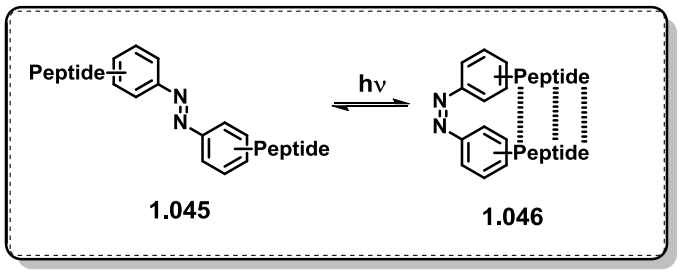

Figure 1.15. A Photoinducible β-hairpin formation with azobenzene molecular scaffold (**1.045-1.046**).[24]

Chakraborty and coworkers and Jagadeesh and coworkers synthesized pyrrole (**1.047**, **Figure 1.16**) and furan (**1.048**, **Figure 1.16**) based molecular scaffold. These scaffolds when incorporated in peptides, showed β-sheet formation in the peptide backbone (**1.049-1.050**, **Figure 1.16**). The peptide was stabilized through intramolecular H-bonding interaction between Pyrrole-NH and furan ›CO. Various conformational analysis supported the β-hairpin formation within the peptide through hydrogen bonding interaction.[25]

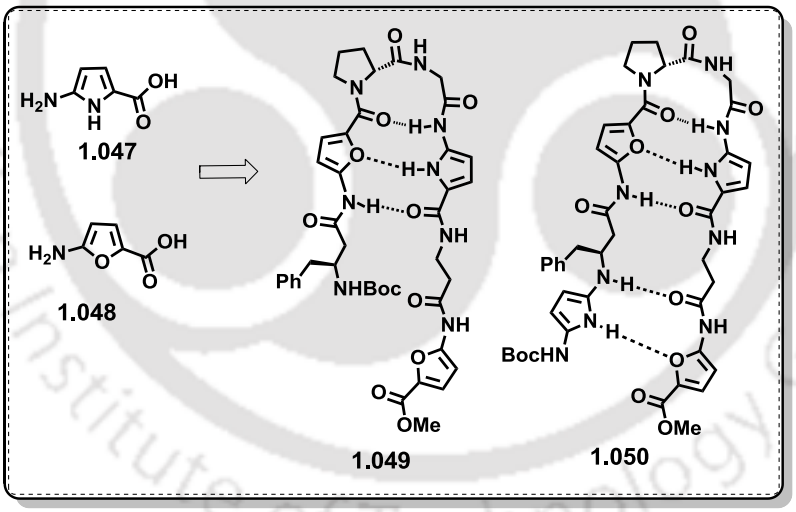

Figure 1.16. Pyrrole and furan based γ-amino acids (**1.047-1.048**) and hybrid peptides (**1.049-1.050**).[25]

Balaram *et al.* have synthesized hybrid peptide segments with α and γ amino acids. They have used 1-aminomethylcyclohexaneacetic acid as stereochemically constrained γ amino acid residue where the torsion angles C^{γ}-C^{β} and C^{β}-C^{α} were mainly restricted to gauche conformations. The hybrid peptide sequence was Boc–Leu–Phe–Val–Aib–Gpn–Leu–Phe–Val–OMe (**1.051**, **Figure 1.17**) and Boc–Gpn–Aib–Gpn–Aib–Gpn–Aib–Gpn–Aib–OMe (**1.052**, **Figure 1.17**). Peptide **1.052** forms α-helix over the Aib(2)–Aib(6) segment, wheather peptide **1.051** forms a β-hairpin

structure. This structure is stabilized by hydrogen bonds with the Aib–Gpn part leading to the generation of a nonhelical C12 turn. Theoretical calculations permitted the energetically feasible hydrogen bonded structures in αγ and γα sequences.[26]

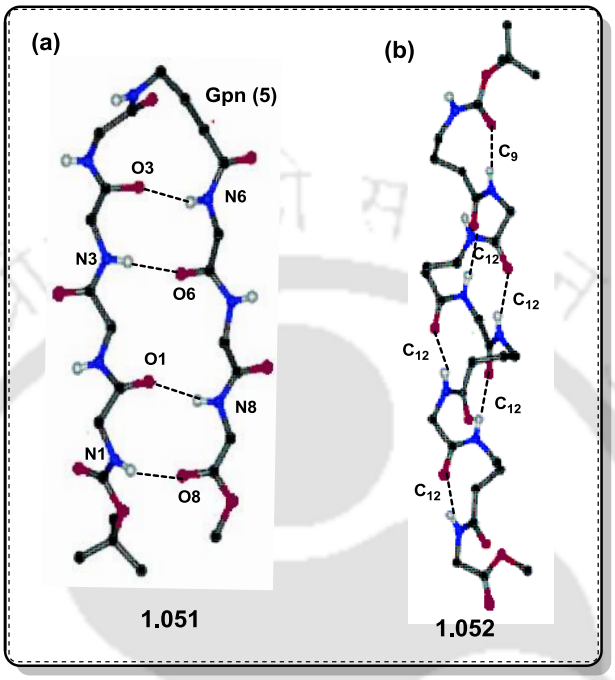

Figure 1.17. (a) β-hairpin conformations of peptide **1.051** and (b) α-helix conformations of peptide **1.052** determined in crystals. [26] Copyright (2009) from American Chemical Society.

Padmanabhan Balaram and coworkers have synthesized octapeptide Boc–LFV^{D}P^{L}PLFV–OMe, which favors the type II′ β-turn nucleated β-hairpin conformation (**1.053**, **Figure 1.18**). The molecular scaffold that nucleates the hairpin conformation is D–Pro–L–Pro dipeptide. However, in 14 residue peptide Boc–LFV^{D}P^{L}PLFVA^{D}P^{L}PLFV–OMe (**1.054**, **Figure 1.18**) two centrally positioned ^{D}Pro–^{L}Pro segments enabled the β-sheet formation with three strands. In both the peptides Phe2 and Phe7 side chains have been placed in proximity (**1.055**-**1.056**, **Figure 1.18**). The intramolecularly hydrogen bonded NH groups and observation of specific cross strand NOEs established the folded conformations of peptides **1.053** and **1.054**. The study proposes clustering of aromatic residues into antiparallel strands, which may resulted the appropriate positioning of an additional aromatic side chains and enhanced the size of the aromatic cluster (**1.057**, **Figure 1.18**).[27]

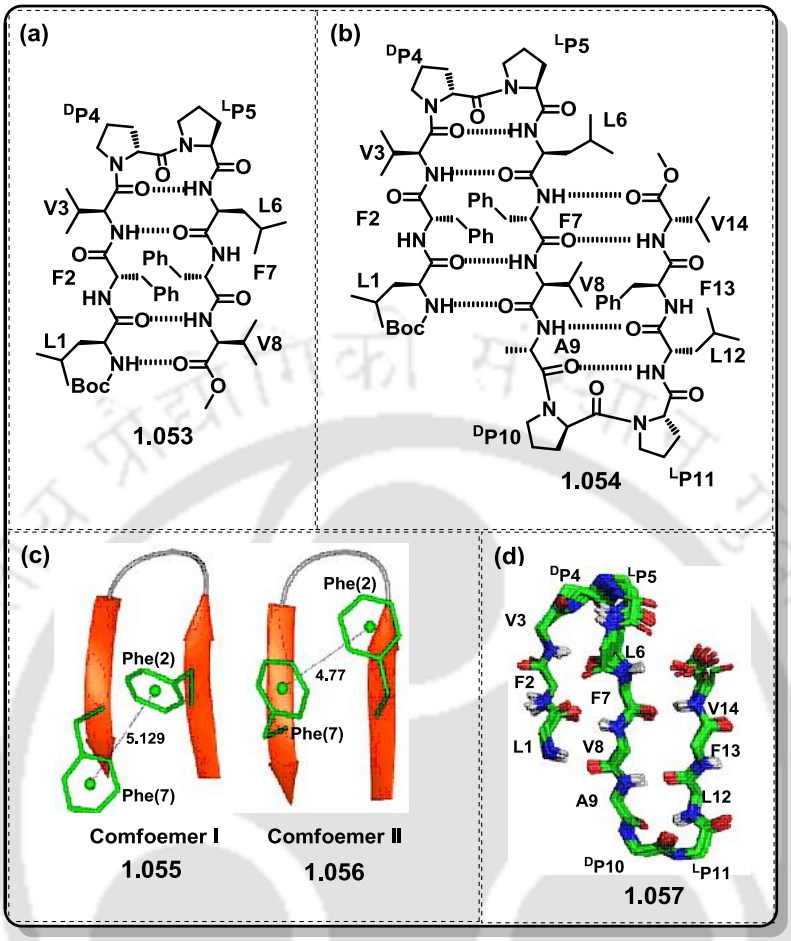

Figure 1.18. (a-b) Schematic representation of peptides **1.053** and **1.054**. (c) Schematic representation of different conformers in crystals of Boc–LFV–$^{D}P^{L}P$–LFV–OMe (**1.055-1.056**). (d) Macromoldel study **1.057** of peptide **1.054** using NOE constrained from the ROESY spectra in $CDCl_3$.[27] Copyright (2012) from American Chemical Society.

Okumura *et al.* have synthesized an 18-residue peptide with sequence INYWLAHAKAGYIVHWTA, which showed the transformation between α-helix and β-hairpin secondary structures (**1.061-1.062**, **Figure 1.19**). Helix-strand replica exchange MD simulation method established that this peptide had both α-helix and β-hairpin structures in aqueous solution (**1.058-1.060**, **Figure 1.19**). This method reproduced the conformations closer to experimental value. They calculated the free-energy and showed the transformation between the α-helix and β-hairpin structures. From MD simulation the calculated free-energy difference between the two structures was almost zero, which was a good agreement of experimental results.[28]

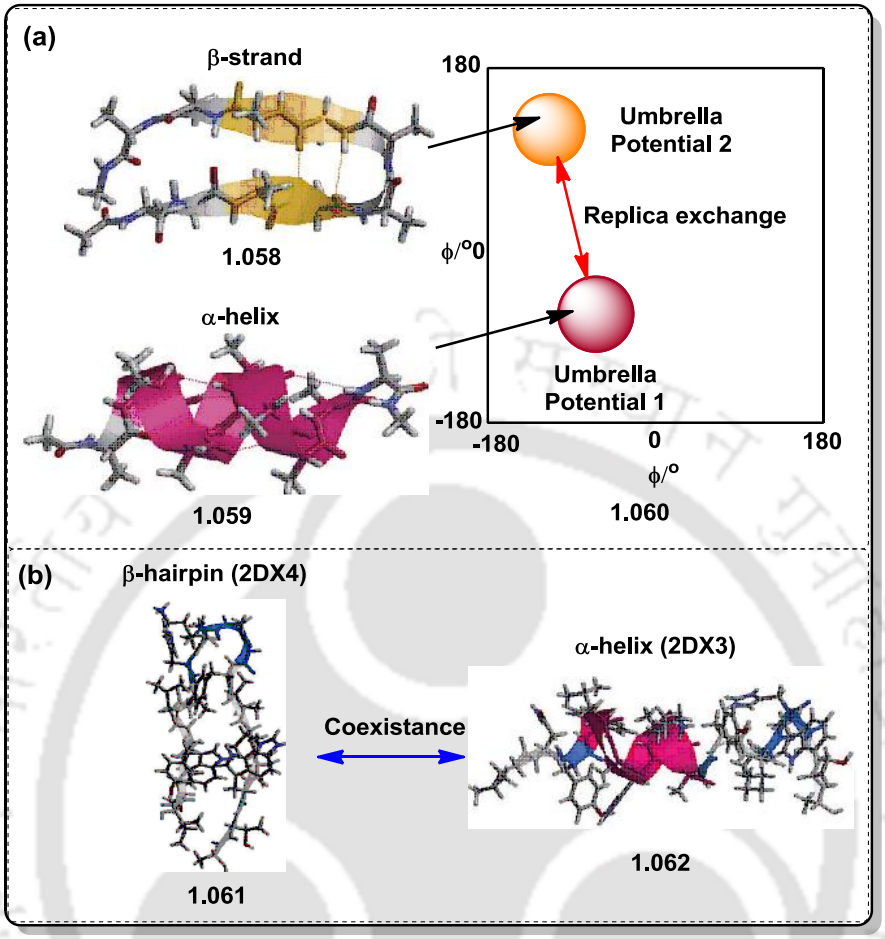

Figure 1.19. (a) Schematic illustration of the helix-strand replica-exchange method (**1.058-1.060**). (b) Experimental conformations of the designed peptide showing the coexistance of the α-helix and β-hairpin structures (**1.061-1.062**) in peptide.[28] Copyright (2013) from Royal Society of Chemistry.

John A. Robinson and coworkers have synthesized macrocyclic β-hairpin-shaped peptidomimetics (**1.063**, **Figure 1.20**) with D-Pro–L-Pro dipeptide as a conformationally constrained molecular scaffold, which acts specifically against Pseudomonas. This peptide targeted the outer membrane protein LptD, which facilitates lipopolysaccharide conveyance to the cell surface during outer membrane biogenesis. From NMR spectroscopy analysis, it was concluded that the folded β-hairpin structure of the peptide was responsible for the binding to target LptD (**1.064**, **Figure 1.20**).[29]

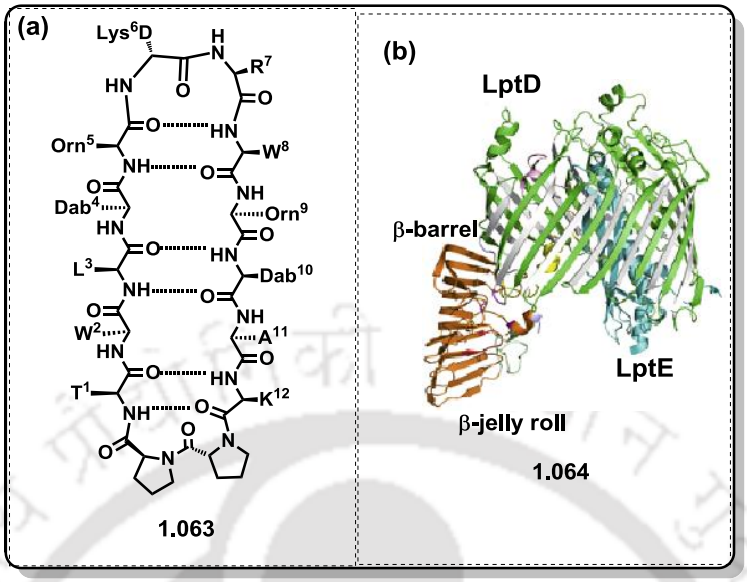

Figure 1.20. (a) designed β-hairpin peptide **1.063** (Dab = L-2,4-diaminobutyric acid; Orn = L-ornithine). (b) Ribbon representation of the Shigella flexneri LptD/E **1.064**.[29] Copyright (2013) from Elsevier.

1.3. The Approaches to β-Sheet Peptidomimetics

β-sheets consist of β-strands connected laterally by at least two or three backbone hydrogen bonds, form a generally twisted, pleated sheet.[30]

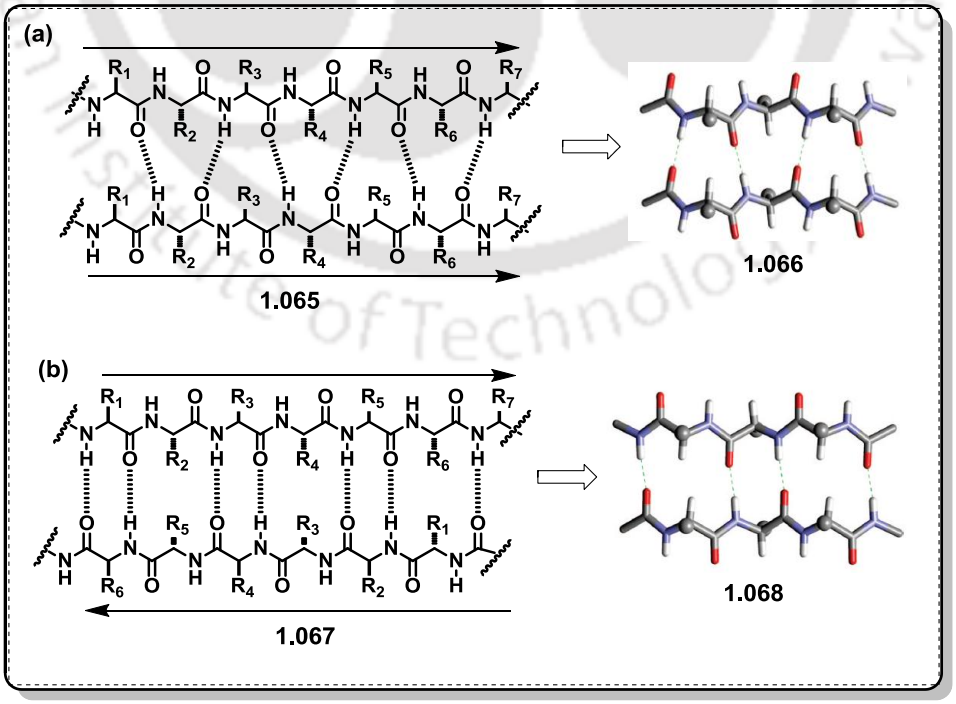

Figure 1.21. Schematic representation of (a) parallel (**1.065**, **1.066)** and (b) antiparallel (**1.067**, **1.068)** β-sheet. Amino acid side chains are represented by R.[30]

A β-strand is a stretch of polypeptide chain typically 3 to 10 amino acids with backbone in an extended conformation. Over 30% of all protein structures are found to contain β-sheet secondary structure. In β-sheet secondary structure two or more paired β-strands organized in either parallel, antiparallel, or mixed orientations held together by interstrand hydrogen bonding interaction (**1.065-1.068**, **Figure 1.21**).[30]

The β-strands that propagate in the same direction and are characterized by a series of 12-membered hydrogen-bonded rings are known as parallel β-sheets. On the other hand, when the strands propagate in opposite directions and are found to contain alternating 10- and 14- membered hydrogen-bonded rings are known as antiparallel β-sheets. The parallel β-sheets generally have dihedral angles Φ = -119°, Ψ = 113° and antiparallel has Φ = -139°and Ψ = 135° (**1.069**, **Figure 1.22**).[31]

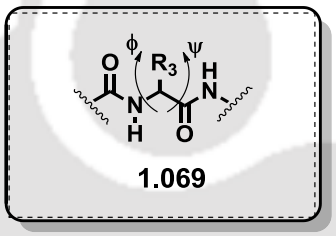

Figure 1.22. Phi (Φ) and psi (Ψ) angles for β-strand and β-sheets **1.069**.[31]

1.4. Toward β-Sheet Mimetics

Small molecules based on the secondary structural elements like α-helices, β- or γ-turns, or β-strands/sheets can show the bioactivity of proteins stems. For example a 19-membered macrocyclic peptide cyclotheonamide (**1.070**, **Figure 1.23**) shows β-sheet secondary structure which moderately inhibits the serine protease thrombin.

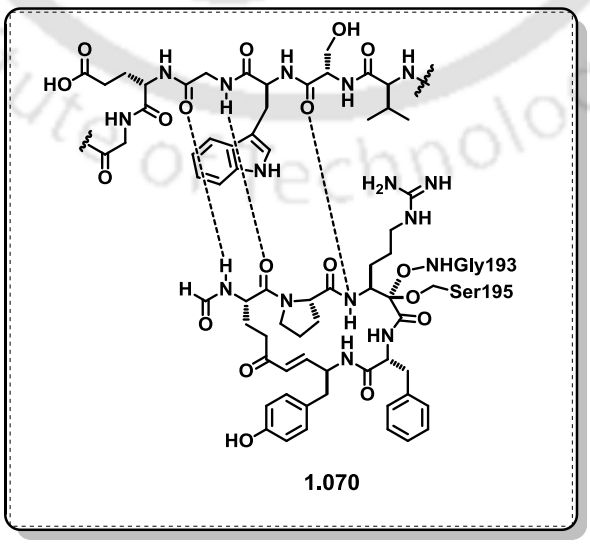

Figure 1.23. Schematic representation of the interaction between the β-strands **1.070** of cyclotheonamide A and thrombin.[32]

Moreover it is a good inhibitor of serine proteases trypsin and streptokinase. In this peptide the NH-CHR–C(O)–Pro–Arg residue forms a hydrogen bonded antiparallel β-sheet with Ser214/Trp215/ Gly216. This protease-binding phenomenon was observed in solid as well as solution phase.[32]

B. R. Bowen and coworkers synthesized epindolidione moiety as conformationally constrained molecular scaffold (**1.071**, **Figure 1.24**), which served as a central strand of the β-sheet. However, strand-strand side chain interactions were not observed because of the planar geometry of the scaffold. Turn was induced in the peptide by introduction of L-Pro–D-Ala dipeptide unit. NMR analysis proves the formation of antiparallel β-sheet formation (**1.072**, **Figure 1.24**).[33]

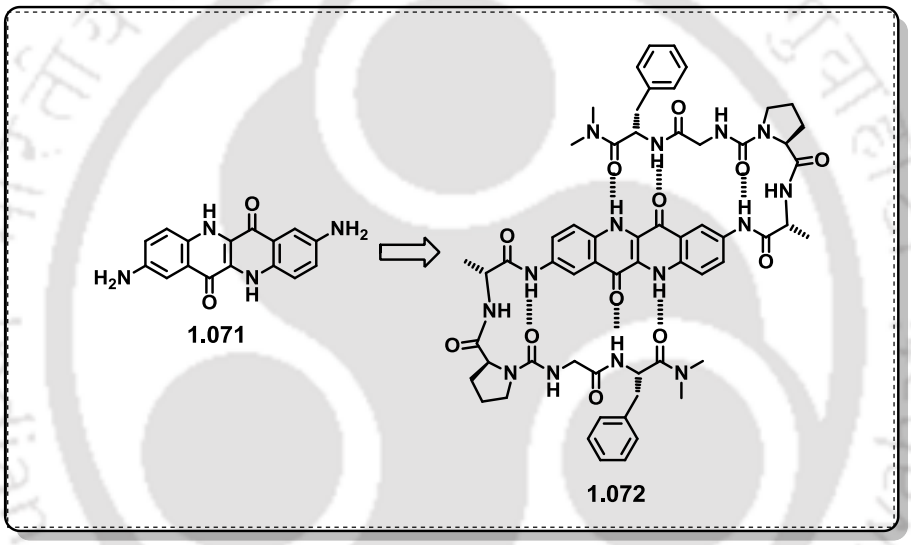

Figure 1.24. Epindolidione scaffold **(1.071)** and its peptide showing antiparallel β-sheet secondary structure **(1.072).** [33]

Rebek and coworkers have synthesized xanthene-based molecular scaffold 2,7-di-tert-alkyl-9,9-dimethylxanthene-4,5-dicarboxylic acid (**1.073**, **Figure 1.25**). It was a U-shaped molecule that had the ability to form β-sheet like structure through intramolecular hydrogen bonding (**1.074**, **Figure 1.25**).[34] To the best of our knowledge, this motif is the first reported β-sheet inducing molecular scaffold though not in a peptide but in an organic framework.

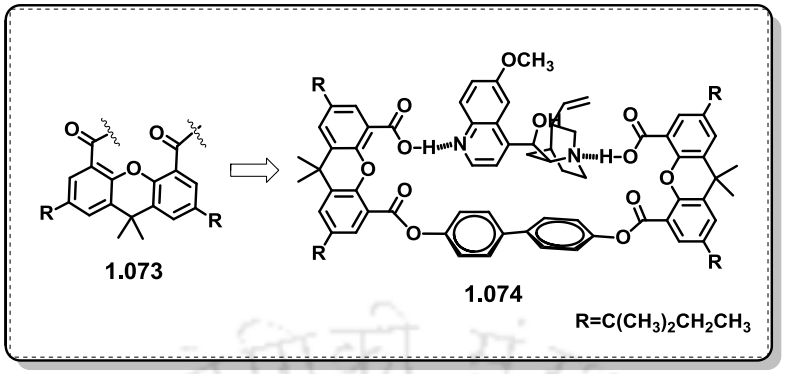

Figure 1.25. xanthene-based molecular scaffold **(1.073)** and its ~~utility~~ β-sheet like structure **(1.074)**.[34]

Feigel *et al.* synthesized pseudo-amino acid scaffold containing biphenyl system (**1.075**, **Figure 1.26**) incorporated into peptide backbone resulted in the formation of antiparallel β-sheet secondary structure (**1.076**, **Figure 1.26**). In solution phase, the peptides were showing interconverting (R,R)-, (S,S)-, and (R,S)-diastereomers due to the atropisomerism of the biphenyl units. NMR analysis and MD simulation study concluded that the major diastereomer of biphenyl scaffold containing peptide adopted the antiparallel β-sheet conformation in the (R,R)-isomer.[35]

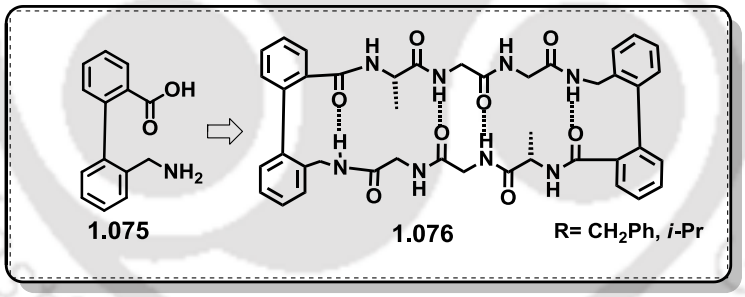

Figure 1.26. Design of biphenyl containing scaffold (**1.075**) and its peptide showing antiparallel β-sheet secondary structure (**1.076**).[35]

Jeffery W. Kelly and coworkers have synthesized 4-(2-aminoethyl)-6-dibenzofuranpropanoic acid as β-sheet nucleating molecular scaffold **1.078**. This molecular scaffold have been utilized to create an acyclic peptidomimetic (**1.079**, **Figure 1.27**) with antimicrobial /antibacterial activity equivalent to the cyclic peptide gramicidin S, **1.077**.[36]

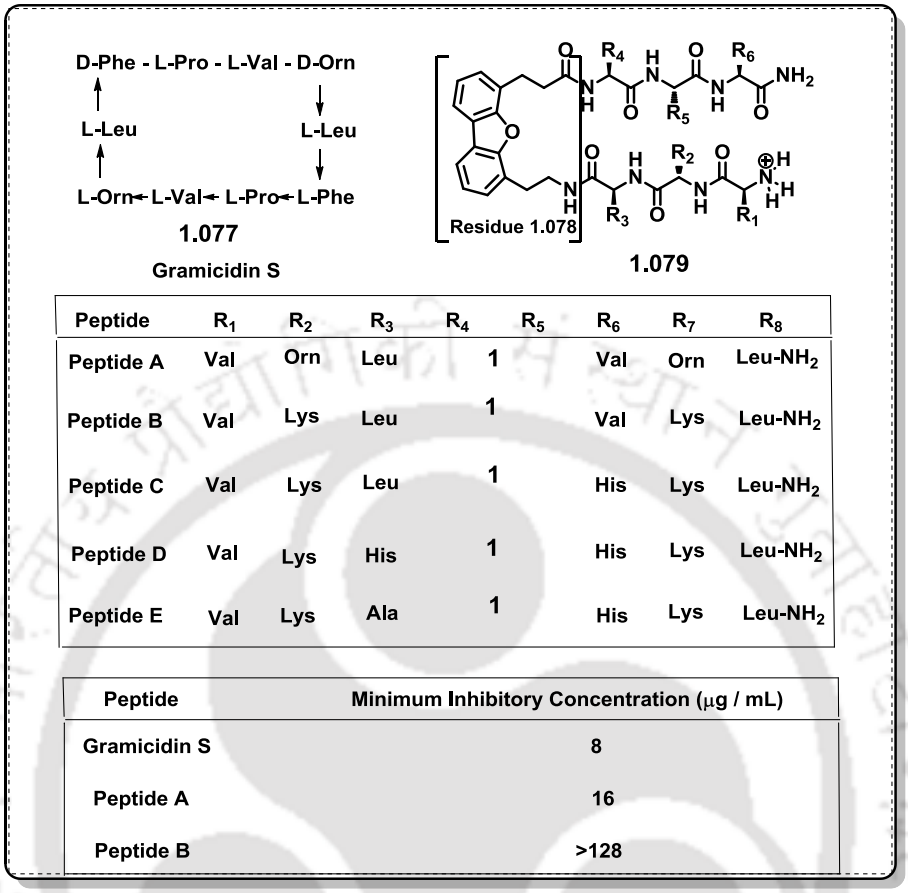

Peptide	R_1	R_2	R_3	R_4	R_5	R_6	R_7	R_8
Peptide A	Val	Orn	Leu	1		Val	Orn	Leu-NH_2
Peptide B	Val	Lys	Leu	1		Val	Lys	Leu-NH_2
Peptide C	Val	Lys	Leu	1		His	Lys	Leu-NH_2
Peptide D	Val	Lys	His	1		His	Lys	Leu-NH_2
Peptide E	Val	Lys	Ala	1		His	Lys	Leu-NH_2

Peptide	Minimum Inhibitory Concentration (μg / mL)
Gramicidin S	8
Peptide A	16
Peptide B	>128

Figure 1.27. (**a**) Structural template for peptides A-E and gramicidin S (**1.077**-**1.079**) and antibacterial activity of gramicidin S and synthesized peptides.[36]

Feigel. *et al.* have synthesized two rigid spacers phenoxathim-4,6dicarboxylic acid and 2,8-dlmethyl-4,6-bis(aminomethyl)phenoxathiin-10,10-dioxide using these molecular scaffold they have synthesized the cyclic structures **1.080** (5-Val/Val-6) and **1.081** (5-Phe/Phe-6). These two rigid molecular scaffolds with diacid and diamino groups offer a distance of the short peptides that allows hydrogen bond formation similar to that of a parallel β-sheet. NMR analysis supports the β-sheet formation in peptides (**1.082**-**1.083**, **Figure 1.34**).[37]

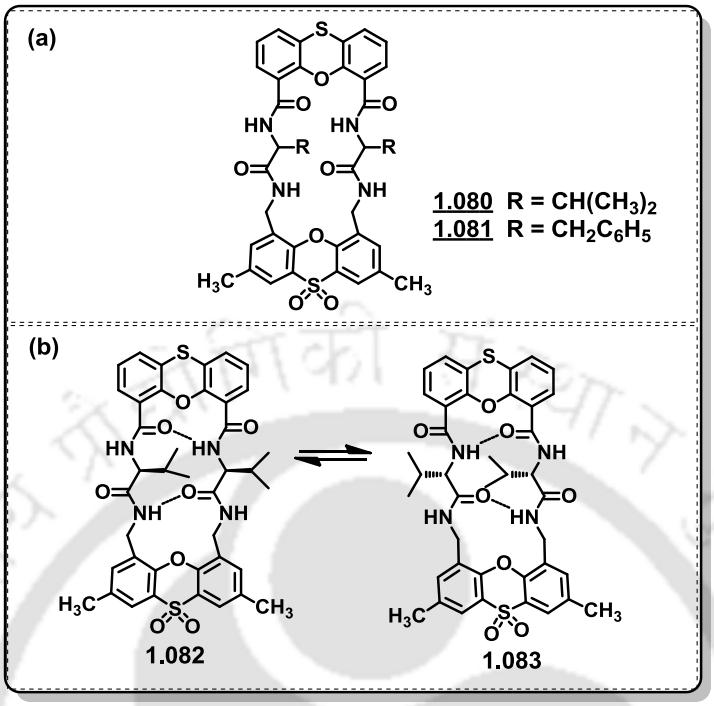

Figure 1.28. (a) Macrocyclic β-sheet peptides with phenoxathim-4,6dicarboxylic acid (**1.080-1.081**) (b) Degenerate exchange proposed for parallel β-sheet conformation (**1.082-1.083**).[37]

Karle *et al.* have synthesized endo-(2S,3R)-2-amino-3-carboxynorbornene as conformationally constrained molecular scaffold, which induces β-sheet like structure when present in a peptide backbone (**1.084**, **Figure 1.29**). The unnatural peptide containing norbornene unit adopted parallel β-sheet conformation in $CDCl_3$, which is supported by NMR analysis. The peptide strands are stabilized by intramolecular hydrogen bonding in between the NHs of Ala and Val units (**1.085**, **Figure 1.29**). Thus the norbornene containing amino acid scaffold acts as a good nucleator for β-sheet peptides (**1.086**, **Figure 1.29**).[38]

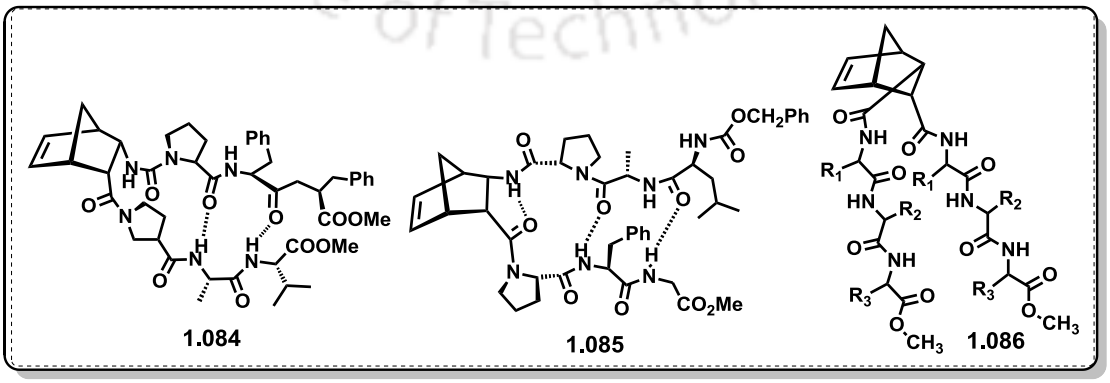

Figure 1.29. Norbornene containing peptidomimetics (**1.084-1.086**).[38]

Nowick and coworkers have synthesized a new class of artificial β-sheet peptides with 5-amino-2-methoxybenzamide template that is connected with phenylalanylleucine dipeptide by a hydrogen-bonded turn unit 1,2-diaminoethane diurea (**1.087**, **Figure 1.30**). This peptide can be elongated via peptide coupling with terminal NH or CO group (**1.087**-**1.089**, **Figure 1.30**).[39]

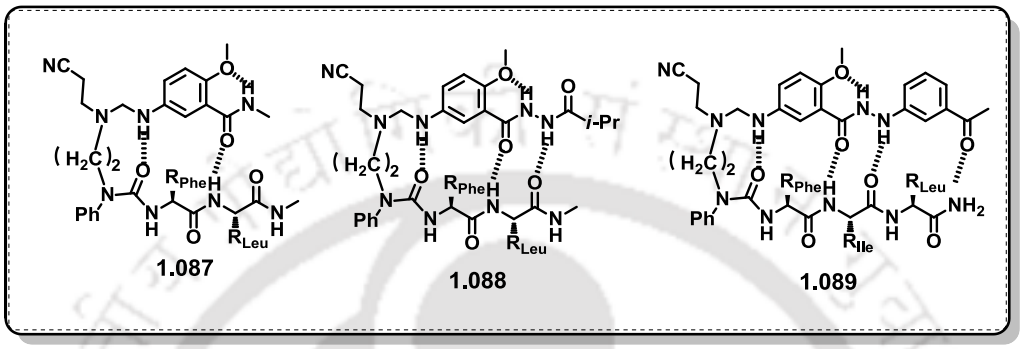

Figure 1.30. Structures of artificial β-sheet peptides (**1.087**-**1.089**).[39]

Balaram *et al.* have synthesized peptides having β-hairpin conformation and extended β-pleated sheet assembly (**1.090**, **Figure 1.31**). The sequence of the peptide was t-butoxycarbonyl β-Phe–β-Phe–D-Pro–Gly–β-Phe–β-Phe–methyl ester. D-Pro–Gly dipeptide acts as a molecular scaffold and nucleates a chain reversal wherein forming a type II β-turn conformation (**1.091**-**1.092, Figure 1.31**). The peptide is stabilized by intramolecular cross-strand hydrogen bonding interaction. The poor solubility of synthesized peptide indicates strong intermolecular interactions present in the solid state.[40]

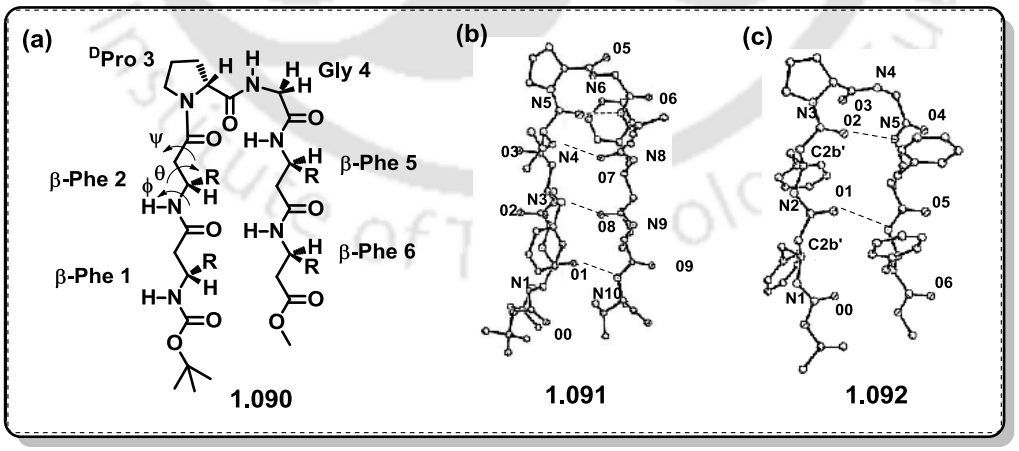

Figure 1.31. (a) Schematic representation of the β-hairpin peptide **(1.090)**. (b) Stereodiagram of synthesized peptide with only one pair of facing β-Phe residues **(1.091)**. (c) Stereodiagram drawn from coordinates obtained in the crystal structure of peptide (**1.092)**.[40]

Nowick and coworkers established the sequence-selective dimerization between two pairs of β-sheets by playing with the placement of two threonine (Thr) or valine (Val) residues in their synthesized peptide (**1.093**, **Figure 1.32a**). As a result peptides formed selectively homodimers or heterodimers depending on their sequential preferences (**1.094-1.096**, **Figure 1.32a**). The four peptides were assorted in all six possible binary combinations established that homo Thr–Thr pair and Val–Val pair are 0.6 kcal/mol more stable than two hetero Thr–Val pairs (**1.097**, **Figure 1.32 b**).[41]

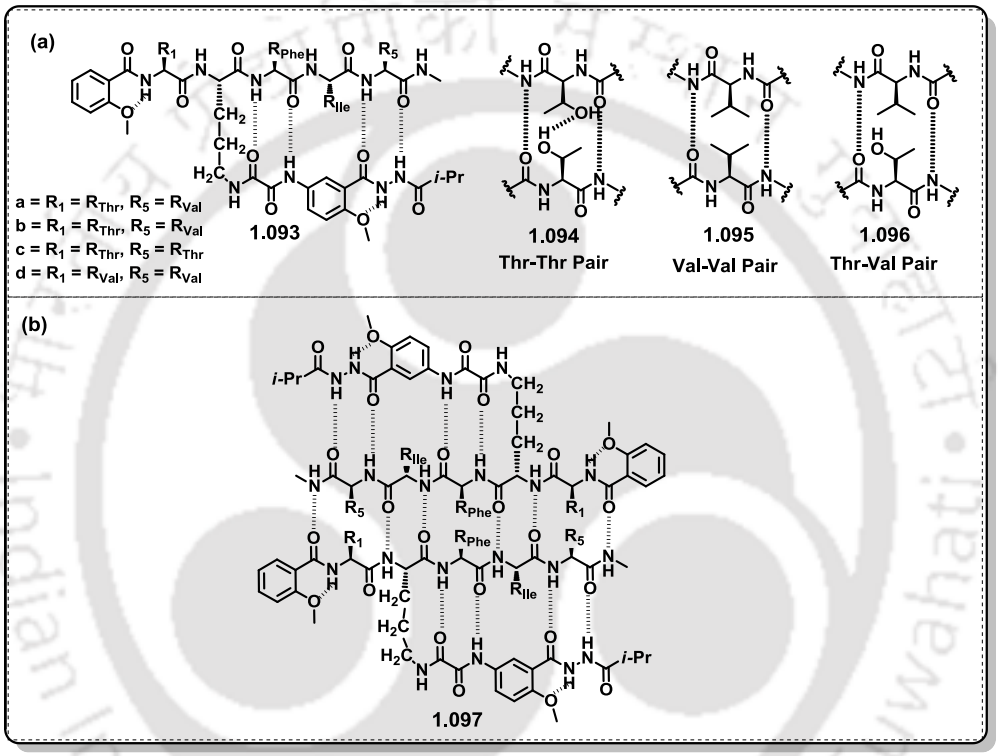

Figure 1.32. (a) Structures of artificial β-sheet peptides and its relative stability with different aliphatic variants **(1.093-1.096)**. (b) Possible homodimerization of the peptide **(1.097).**[41]

Thomas Schrader and coworkers have synthesized a combination of two aminopyrazole ligands with di- or tripeptides which were taken from the main fragment of water-soluble Aβ-specific ligands that allow the investigations of β-sheet peptides in water. It has been investigated that the nucleation site of the aggregation of the Alzheimer's peptide is KLVFF sequence, which is situated in the central region of Aβ. The synthesized β-sheet peptide **1.098** contains aminopyrazole as rigid molecular scaffold which helps inducing β-sheet conformation in peptide which was supported by conformational analysis. The newly synthesized peptide backbone shows the hydrogen bonds and hydrophobic interactions between aminopyrazole unit and Phe residues. The attraction of KKLVFF fragment and synthesized ligands depends on the sequence and composition of artificial amino acids. So, for the first

time they have shown the complexation of aminopyrazole containing β-sheet ligands with peptides which was taken directly from Aβ (**1.099**, **Figure 1.33**). The MD simulation studies also supported similar phenomena (**1.100-1.102**, **Figure 1.33**).[42]

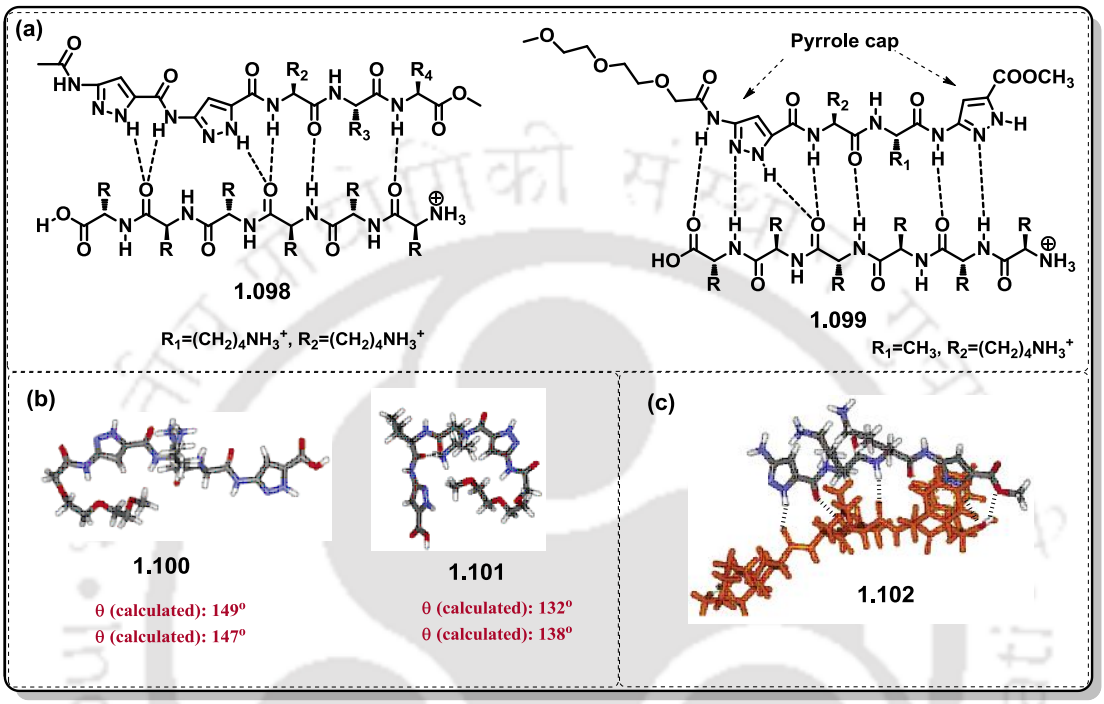

Figure 1.33. (a) The β-sheets conformation shown when ligand and their complexes interact with a hexapeptide **(1.098**, **1.099)**. (b) Monte Carlo simulation and corresponding torsion angles for the free ligands **(1.100**, **1.101)**. (c) Molecular dynamics calculation of the complex formed between KKLVFF and hybrid ligand **(1.102)**.[42] Copyright (2005) from American Chemical Society

Basak *et al.* have synthesized ω- enediynyl amino acid scaffold (**1.103**, **Figure 1.34**) and incorporated into peptide backbone. Enediyne molecules were widely used for their cytotoxic activity and possible use as anticancer drug. The conformational analysis of synthesized peptides supported β-sheet like structure stabilize through intramolecular H-bond formation (**1.104-1.105**, **Figure 1.34**).[43]

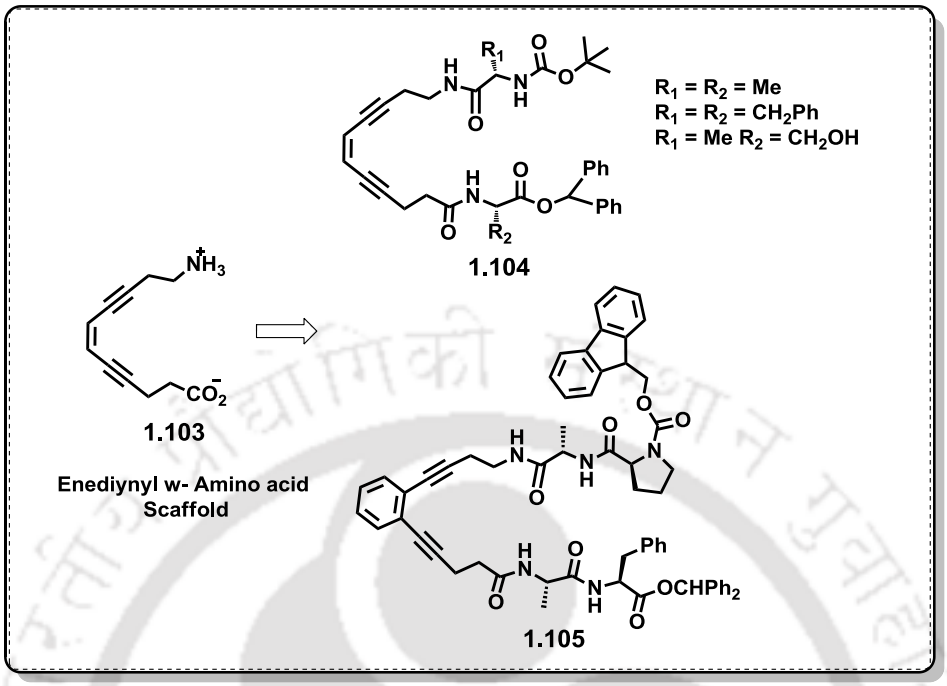

Figure 1.34. Example of enediyne **(1.103)** based peptidomimetics **(1.104- 1.105)**.[43]

Carsten Schmuck and coworkers have synthesized flexible zwitterionic peptide which shows a β-sheet like structure on bending of the two strands in protic solvent methanol (**1.106**, **Figure 1.35**).[44]

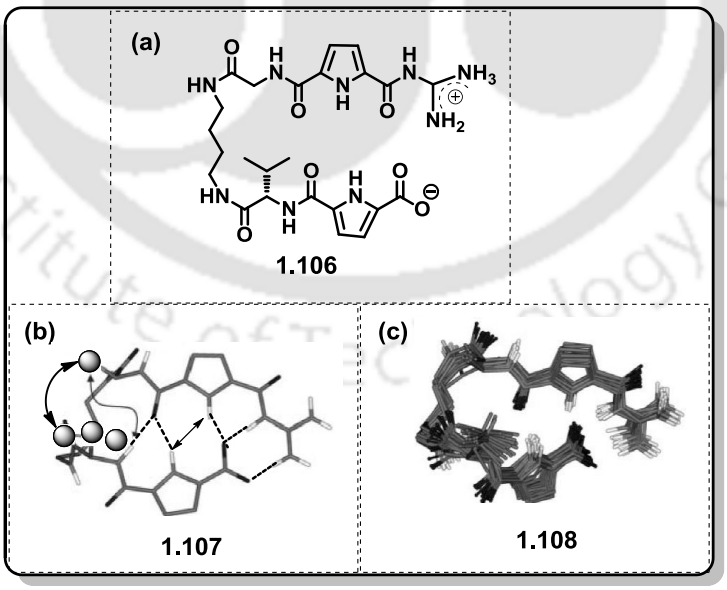

Figure 1.35. (a) Structure of flexible zwitterionic peptide **1.106**. (b) Calculated structure of Peptide showing intramolecular H-bonds and non-sequential NOEs **1.107**. (c) MD simulation of structure **1.108** of zwitterionic peptide.[44] Copyright (2007) from American Chemical Society

The guanidiniocarbonyl pyrrole moiety serves the purpose of a highly efficient oxoanion binding site, and a pyrrole-2-carboxylate unit as complementary binding sites. Butylene spacer acts as molecular scaffold. The intramolecular zwitterion formation among the carboxylate and the (guanidiniocarbonyl) pyrrole cation helps to form a well-defined β-sheet structure which has been characterized by NMR analysis (**1.107-1.108**, **Figure 1.35**).[44]

Brian R. Linton and coworkers have synthesized cysteine derived β-sheet peptides wherein the cysteine acts as a scaffold. The -S-S- bond removes the internal barrier for the β-sheet formation and adopts conformations in organic solvents that mimic small β-sheets (**1.109**, **Figure 1.36**). In the synthesized small peptide relative hydrogen bond strengths, β-strand aggregation, and the hydrogen bond donors and acceptors were recognized through hydrogen/deuterium exchange (**1.110**, **Figure 1.36**).[45]

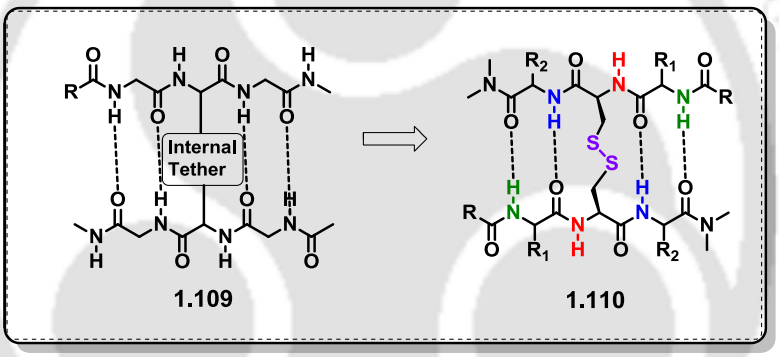

Figure 1.36. A strategy for β-sheet peptidomimetics using an internal tether **(1.109-1.110)** between two peptide α-carbons.[45]

Samuel H. Gellman and coworkers have synthesized diacid units of cyclohexane derivative (**1.111**, **Figure 1.37**) which endorse the generation of two-stranded parallel β-sheet secondary structure in between the peptides that were attached via their *N*-termini (**1.113**, **Figure 1.37**). In this case, the rigid molecular scaffold was cis-1,2-cyclohexanedicarboxylic acid (**1.112,** CHDA) and the linker unit was glycine which again linked to one carboxyl group of the molecular scaffold CHDA. Parallel β-sheet secondary structure was formed when the CHDA-Gly unit was joined with L-residue of peptide strands.[46]

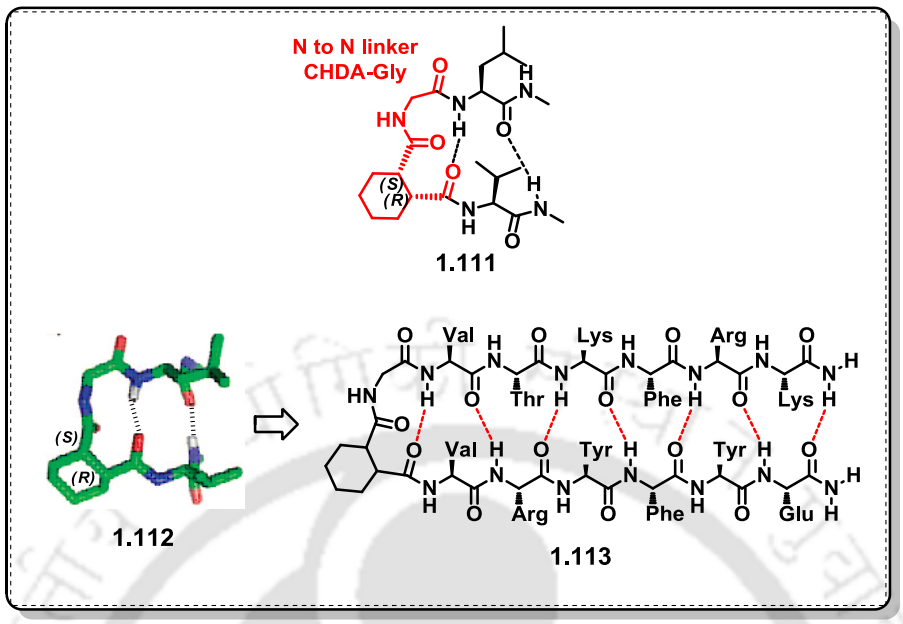

Figure 1.37. Tetrapeptide mimics containing parallel N-to-N linkers **(1.111)**. Hydrogen bonding pattern in synthesized peptide containing cis-1,2-cyclohexanedicarboxylic acid molecular scaffold (**1.112**) for the desired parallel β-sheet conformation **(1.113)**.[46] Copyright (2008) from American Chemical Societ

James S. Nowick and coworkers have synthesized 5-aminoanisic oxalamide template based model peptide that dimerizes through parallel β-sheet interactions in solution phase (**1.114**, **Figure 1.38**). The C-terminally linked dipeptides were connected through 5-aminoanisic oxalamide scaffold. NMR analysis concluded the formation of β-sheet secondary structure and dimerization. Noncovalent interactions among parallel β-sheets may have provoked peptide and protein aggregation.[47]

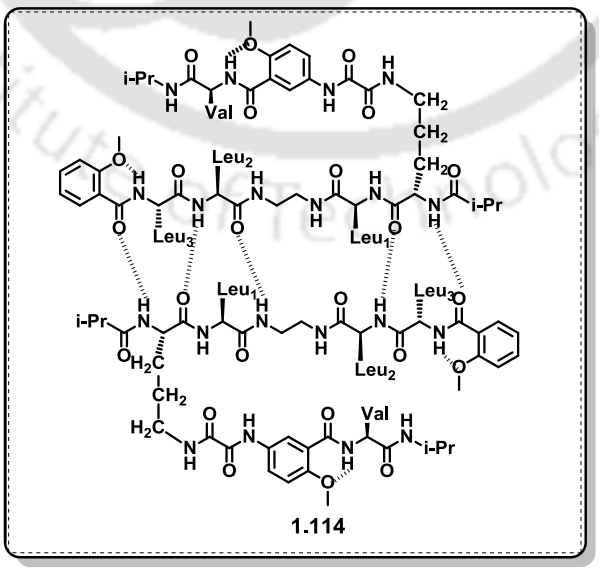

Figure 1.38. Design of peptide that dimerizes through parallel β-sheet interactions **1.114**. [47]

Juan R. Del Valle and coworkers have synthesized conformationally constrained dipeptide scaffold based on imidazo[1,2-a]pyridine. This scaffold, on incorporation into the host peptide, induced β-sheet conformation, as revealed from structural analysis based on NMR spectroscopy (**1.115-1.117**, **Figure 1.39**).[48]

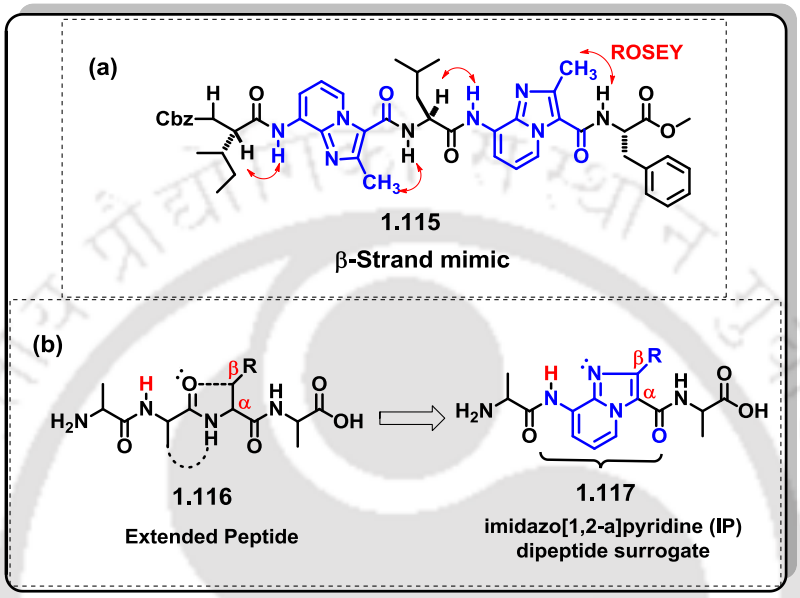

Figure 1.39. Design of imidazo[1,2-a]pyridine molecular scaffold based β-strand mimics (**1.115-1.117**).[48]

Mayo *et al.* have synthesized calix[4]arene-based β-sheet like peptidomimetics (**1.118-1.123**, **Figure 1.40**). These newly designed peptides are powerful anti-tumor agents. Among the synthesized peptides **1.120** encourages cell cycle capture and stops tumor growth by about 50-times better than parent **1.118**. These all calixarene scaffold based peptides can be used as useful therapeutics against cancer.[49]

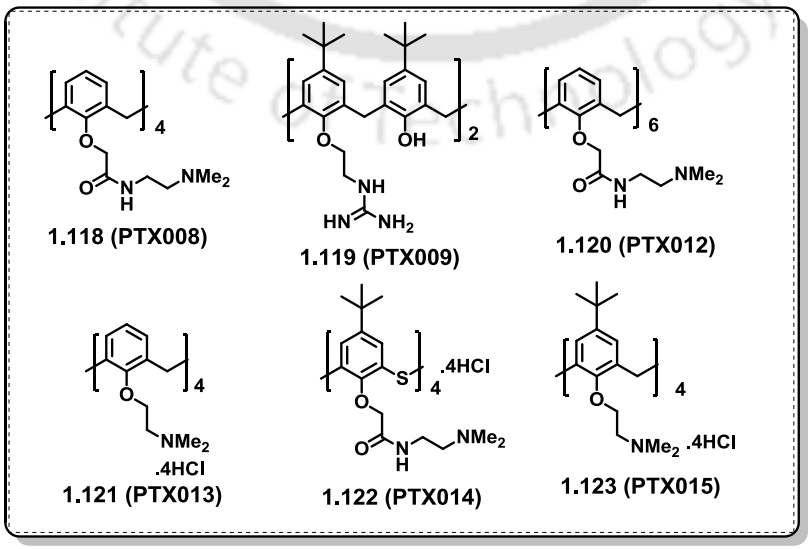

Figure 1.40. Structural representations of calix[4]arene diguanidine compound PTX009 and tetra-amine compounds PTX008, PTX012, PTX013, PTX014, and PTX015 (**1.118-1.123**).[49]

1.5. Summary and Future Prospect

This review chapter comprises of a literature survey of synthesis of conformationally constrained molecular scaffolds and their applications to peptidomimetic chemistry. The basic concepts and approaches to peptidomimetic chemistry covers a diverse array of compounds and synthetic strategies such as 'click chemistry' for the purpose of generating an array of molecular scaffold mimicking the structural and biological features of an active part of protein. In this respect, β-sheet/ β-hairpin peptidomimetics with conformationally constrained molecular scaffold have attracted great interest. The generation of foldamers bearing amino acid side-chain isosteres has the potential to show secondary structural frameworks like β-hairpin/ β-sheet or α-helix conformation and expected to be the next-generation therapeutics in medicine. Peptidomimetic inhibitors, found to be potent against the HIV-1 protease, can show the improved therapeutic profile against drug-resistant viral strains.

On the other hand, β-strand mimicking and β-sheet like structures in a designed fluorescent peptide aiming at the fundamental aspects that a particular conformation can have an impact on the photophysics has received little attention. Investigating such an impact might find widespread applications for the study of interbiomolecular interactions in cell and the design of new peptide based drug candicates. Considerable efforts, though separately have been invested in the design of scaffolded β-sheet peptidomimetics in one hand and fluorescent peptide probes for studying peptide–protein interaction, very few efforts have been undertaken simultaneously to consider the both. Therefore, the generation of scaffolded peptidomimetics with interesting fluorescence property of fundamental importance appears to be highly demanding. Such probes could be of immense importance for the dual applicability (a) mimicking a protein's particular secondary structure, such as β-sheet, of pharmacological importance and b) studying fundamental level biological process involving protein–peptide interaction with the help of fluorescent photophysical property.

1.6. References

1. Fosgerau, K.; Hoffmann, T. *Drug Discov Today*, **2015**, 20, 122.
2. Pantoja-Uceda, D.; Santiveri, C. M.; Jiménez, M. A. *Methods Mol Biol.* **2006**, *340*, 27.
3. (a) Hruby, V. J.; Al-Obeidi, F.; Kazmierski, W. *Biochem J.* **1990**, *268*, 249. (b) Hruby, V. J. Life Sci. **1982**, *31*, 189. (c) Bursavich M. G.; Rich, D. H. *J. Med. Chem.* **2002**, *45*, 541. (d) Bursavich M. G.; West, C. W.; Rich, D. H. *Org. Lett.* **2001**, *3*, 2317. (e) Goodman, M.; Kossoy, A. *J. Am. Chem. Soc.* **1966**, *88*, 5010. (f) Goodman, M.; Feng, Y.; Melacini, G.; Taulane, J. P. *J. Am. Chem. Soc*. **1996**, *118*, 5156. (g) Olson, G. L.; Bolin, D. R.; Bonner, M. P.; BOs, M.; Cook, C. M.; Fry, D. C.; Graves, B. J.; Hatada, M.; Hill, D. E.; Kahn, M.; Madison, V. S.; Rusiecki, V. K.; Sarabu, R.; Sepinwall, J.; Vincent, G. P.; Matthew, E. *J. Med. Chem.* **1993**, *36*, 3039.
4. Kieber-Emmons, T.; Murali, R.; Greene, M. I. *Curr Opin Biotechnol.* **1997**, *8*, 435.
5. (a) Feigel, M. *J. Am. Chem. Soc.* **1986**, *108*, 181. (b) Brandmeier,V.; Sauer, W. H. B.; Feigel, M. *Helv. Chim. Acta.* **1994**, *77*, 70.
6. (a) Saweczko, P.; Enright, G. D.; Kraatz, H. B. *Inorg. Chem.* **2001**, *40*, 4409. (b) Galka, M. M.; Kraatz, H. B. *ChemPhysChem*. **2002**, *4*, 356. (c) Moriuchi, T.; Yoshida, K.; Hirao, T. *Org. Lett.* **2003**, *5*, 4285.
7. Moriuchi, T.; Yoshida, K.; Hirao, T. *Organometallics* **2001**, *20*, 3101.
8. (a) Kyte, J. Structure in Protein Chemistry, Garland, New York, 1995; (b) C. Branden and J. Tooze, Introduction to Protein Structure, 2nd edn., Garland, New York, 1998.
9. Robinson, J. A. *Acc Chem Res.* **2008**, *41*, 1278.
10. Gunasekaran, K.; Ramakrishnan, C.; Balaram, P. *Protein Eng.* **1997**, *10*, 1131.
11. (a) Johannesson, P.; Lindeberg. G.; Tong, W.; Gogoll, A.; Karlén, A.; Hallberg, A. *J Med Chem.* **1999**, *42*, 601. (b) Legrand, B.; Mathieu, L.; Lebrun, A.; Andriamanarivo, S.; Lisowski, V.; Masurier, N.; Zirah, S.; Kang, Y. K.; Martinez, J.; Maillard, L. T. *Chemistry* **2014**, *20*, 6713.
12. Liang, G.-B. B.; Rito, C. J.; Gellman, S. H. *J. Am. Chem. Soc.* **1992**, *114*, 4440.
13. (a) Marchini, M.; Mingozzi, M.; Colombo, R.; Guzzetti, I.; Belvisi, L.; Vasile, F.; Potenza, D.; Piarulli, U.; Arosio, D.; Gennari, C. *Chemistry* **2012**, *18*, 6195. (b) Diaz, H.; Espina, J. R.; Kelly, J. W. *J. Am. Chem. Soc.* **1992**, *114*, 8316. (c) Soth, M. J.; Nowick, J. S. *J. Org. Chem*. **1999**, *64*, 276.
14. Gardner, R. R.; Liang, G. B.; Gellman, S. H. *J. Am. Chem. Soc.* **1999**, *121*, 1806.
15. Nowick, J. S.; Brower, J. O. *J. Am. Chem. Soc.* **2003**, *125*, 876.
16. Daura, X.; Gademann, K.; Schaefer, H.; Jaun, B.; Seebach, D.; van Gunsteren, W. F. *J. Am. Chem. Soc.* **2001**, *123*, 2393.

17. Nakamura, G. R.; Starovasnik, M. A.; Reynolds, M. E.; Lowman, H. B. *Biochemistry* **2001**, *40*, 9828.
18. Chung, Y. J.; Huck, B. R.; Christianson, L. A.; Stanger, H. E.; Krauth, S.; Powell, D. R.; Gellman, S. H. *J. Am. Chem. Soc.* **2000**, *122*, 3995.
19. Belvisi, L.; Gennari, C.; Madder, A.; Mielgo, A.; Potenza, D.; Scolastico, C. *Eur. J. Org. Chem.* **2000**, 695.
20. Cochran, A. G.; Tong, R. T.; Starovasnik, M. A.; Park, E. J.; McDowell, R. S.; Theaker, J. E.; Skelton, N. J. *J. Am. Chem. Soc.* **2001**, *123*, 625.
21. Lai, J. R.; Huck, B. R.; Weisblum, B.; Gellman, S. H. *Biochemistry* **2002**, *41*, 12835.
22. Lahr, S. J.; Engel, D. E.; Stayrook, S. E.; Maglio, O.; North, B.; Geremia, S.; Lombardi, A.; DeGrado, W. F. *J. Mol. Biol.* **2005**, *346*, 1441.
23. Langenhan, J. M.; Gellman, S. H. *Org. Lett.* **2004**, *6*, 937.
24. Aemissegger, A.; Kräutler, V. Van-Gunsteren, W. F.; Hilvert, D. *J. Am. Chem. Soc.* **2005**, *127*, 2929.
25. (a) Chakraborty, T. K.; Srinivasa, R. K.; Kiran, M. U.; Jagadeesh, B. *Tetrahedron Lett.* **2009**, *50*, 4350.
26. Chatterjee, S.; Vasudev, P. G.; Raghothama, S.; Ramakrishnan, C.; Shamala, N.; Balaram, P. *J. Am. Chem. Soc.* **2009**, *131*, 5956.
27. Sonti, R.; Rai, R.; Ragothama, S.; Balaram, P. *J. Phys. Chem. B* **2012**, *116*, 14207.
28. Okumura, H.; Itoh, S. G. *Phys. Chem. Chem. Phys.* **2013**, *15*, 13852.
29. Schmidt, J.; Patora-Komisarska, K.; Moehle, K.; Obrecht, D.; Robinson, J. A. *Bioorg Med Chem.* **2013**, *21*, 5806. (b) Krishna, Y.; Sharma, S.; Ampapathi, R. S.; Koley, D. *Org. Lett.* **2014**, *16*, 2084. (c) Sun, Q.; Xu, B.; Niu, Y.; Xu, F.; Liang, L.; Wang, C.; Yan, J. G. Y.; Wang, W.; Jin, H.; Xu, P. *Chem. Med. Chem.* **2015**, *10*, 498.
30. Loughlin, W. A.; Tyndall, J. D.; Glenn, M. P.; Hill, T. A.; Fairlie, D. P. *Chem Rev.* **2010**, *104*, 6085.
31. Voet, D.; Voet, J. G.; Pratt, C. W. *Fundamentals of Biochemistry*; Wiley: New York: **1999**.
32. Lee, A. Y.; Hagihara, M.; Karmacharya, R.; Albers, M. W.; Schreiber, S. L.; Clardy, J. *J. Am. Chem. Soc.* **1993**, *115*, 12619. (b) Janetka, J. W.; Raman, P.; Satyshur, K.; Flentke, G.; Rich, D. H. *J. Am. Chem. Soc.* **1997**, **119**, 441.
33. Kem, D. S.; Bowen, B. R. *Tetrahedron Lett.* **1988**, *29*, 5081
34. Nowick, J. S.; Ballester, P.; Ebmeyer, F.; Rebek, J., Jr. *J. Am. Chem. Soc.* **1990**, *112*, 8902.
35. Brandmeier, V.; Sauer, W. H. B.; Feigel, M. *Helv. Chim. Acta*. **1994**, *77*, 70.
36. Graciani, N. R.; Tsang, K. Y.; McCutchen, S. L.; and Kelly, J. W. *Bioorg. Med. Chem. Lett.* **1994**, *2*, 999.

37. Wagner, G.; Feigel, M. *Tetrahedron* **1993**, *49*, 10831.
38. Ranganathan, D.; Haridas, V.; Kurur, S.; Thomas, A.; Madhusudanan, K. P.; Nagaraj, R.; Kunwar, A. C.; Sarma, A. V. S.; Karle, I. L. *J. Am. Chem. Soc*. **1998**, *120*, 8448.
39. Smith, E. M.; Holmes, D. L.; Shaka, A. J.; Nowick, J. S. *J. Org. Chem.* **1997**, *62*, 7906.
40. Karle, I.; Gopi, H. N.; Balaram, P. *Proc. Natl. Acad. Sci.* **2002**, *99*, 5160.
41. Nowick, J. S.; Chung, D. M. *Angew. Chem. Int. Ed.* **2003**, *42*, 1765.
42. Rzepecki, P.; Schrader, T. *J. Am. Chem. Soc.* **2005**, *127*, 3016.
43. (a) Basak, A.; Bag, S. S.; Basak, A. *Bioorg. Med. Chem. Lett.* **2005**, *13*, 4096. (b) Basak A.; Bag, S. S.; Bdour, H. M. M. *Chem. Comm.* **2003**, *20*, 2614. (c) Basak, A.; Rudra.; Rani, K.; Bag, S. S.; Basak, A. *J. Chem. Soc., Perkin Trans. 1*. **2002**, *15*, 1805.
44. Schmuck, C.; Dudaczek, J. *Eur. J. Org. Chem*. **2007**, 3326.
45. Cashman, T. J.; Linton, B. R. *Org. Lett.* **2007**, *9*, 5457.
46. Freire, F.; Fisk, J. D.; Peoples, A. J.; Ivancic, M.; Guzei, I. A.; and Gellman, S. H. *J. Am. Chem. Soc.* **2008**, *130*, 7839.
47. Levin, S.; Nowick, J. S. *Org. Lett.* **2009**, *11*, 1003.
48. Kang, C. W.; Sun, Y.; Del Valle, J. R. *Org. Lett.* **2012**, *14*, 6162.
49. Dings, R. P. M.; Levine, J. I.; Brown, S. G.; Astorgues-Xerri, L.; MacDonald, J. R.; Hoye, T. R.; Raymond, E.; Mayo, K. H. *Invest. New Drugs* **2013**, *31*, 1142.

2.1. Introduction

The three dimensional form of local segments of proteins are known as protein secondary structure. The α-helix, β-sheet and β-turn are the most common secondary structural elements of protein. The secondary structure of proteins paves the way for tertiary structure formation. The pattern of hydrogen bonds between the amine hydrogen and carbonyl oxygen atoms in the peptide backbone defines the secondary structure of protein. Secondary structure may alternatively be defined based on the regular pattern of backbone dihedral angles in a particular region of the Ramachandran plot regardless of whether it has the correct hydrogen bonds.

Kaj Ulrik Linderstrøm first introduced the concept of protein secondary structure. Peptide chains often form orderly hydrogen bonded arrangements with carbonyl oxygen atoms and amide N–H-hydrogens. These hydrogen-bonded arrangements are the motif of the secondary structure of the protein.

The α-helical secondary structure is a right hand-spiral conformation in which every backbone N−H group forms hydrogen bond with the backbone C=O group of the amino acid located three or four residues earlier along the protein sequence. β-sheets consist of β-strand connected laterally by at least two to three backbone hydrogen bonds, form a generally twisted, pleated sheet.

2.1.1. Protein Secondary Structure: β-Sheet Peptidomimetics

Out of several protein secondary structures, β-sheet is the major secondary structural element found in globular proteins. Historically, it was first detected in the form of keratin fibers. In 1933 Astbury described the β-sheet secondary structure as straight, extended chains with alternating side chain direction and hydrogen bonds between adjacent antiparallel chains.[1] The correct hydrogen-bonding patterns for both antiparallel and parallel β sheet, and also “pleated,” sheet structures with α-Carbons successively a little above and below the plane of the sheet have been described by Pauling and Corey.[2]

The β-sheets in combination of two or more β-strands, not only act as a key scaffolding agent to stabilize proteins but also serve the purpose of a key recognition motifs that binds other specific proteins and/or DNA.[3] Over 30% of all proteins consist of β-sheet secondary structure.

The β-strands are organized together forming an extensive hydrogen bonding network with their neighbors with N-H groups in the backbone of one strand and the >C=O groups in the backbone of the adjacent strands. In a β-sheet secondary structure the adjacent β-strands are aligned so that their C^{α} atoms are adjacent and their side chains point in the same way. The "pleated" appearance of β-strands rises from

tetrahedral chemical bonding at the C^{α} atom. As a result of pleating in β-sheet structure, the distance between the two strands decreases to approximately 6 Å as compare to that of 7.6 Å (2 × 3.8 Å) expected from two fully extended trans peptides.

2.1.2. Hydrogen Bonding Patterns in β-Sheet Structure

β-strands too can be said to be directional, as the peptide chains have a directionality conferred by their *N*-terminus and *C*-terminus. Adjacent β-strands can form hydrogen bonds in antiparallel, parallel, or mixed arrangements (**2.01-2.02**, **Figure 2.1**). All the *N*-termini of consecutive β-strands are oriented in the same direction in a parallel arrangement. The introduction of non-planarity in the inter-strand hydrogen bonding pattern makes the arrangement slightly less stable. The dihedral angles (φ, ψ) are about (–120°, 115°) in parallel sheets (**Table 2.1**). On the other hand, less than five interacting parallel strands in a motif are rare to find out. However, parallel β-sheet may be more stable since small amyloidogenic sequences seems to usually aggregate into β-sheet fibrils composed of primarily parallel β-sheet strands.

The consecutive β-strands alternate orientation wherein the *N*-terminus of one strand is adjacent to the *C*-terminus of the next forming an antiparallel arrangement. In this arrangement the strongest inter-strand stability is observed because it allows the inter-strand hydrogen bonds between carbonyls and amines to be planar, as their preferred orientation. In antiparallel β-sheets, peptide backbone dihedral angles (φ, ψ) are found to be –140° and 135°, respectively (**2.03**, **Figure 2.1** and **Table 2.1**).

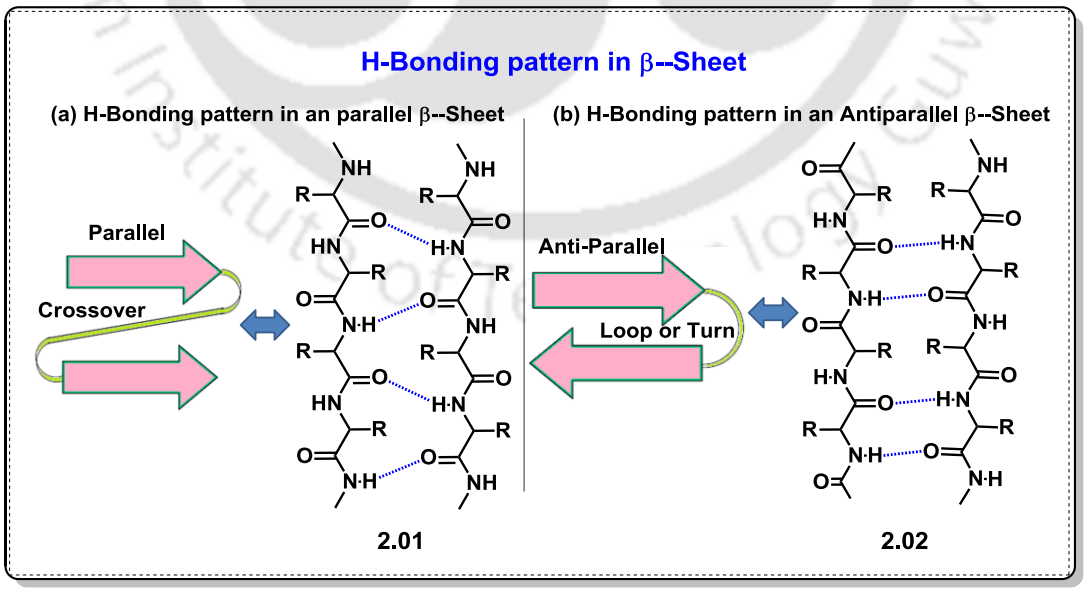

Figure 2.1. The structure of β-sheets- (a) Parallel (**2.01**) and (b) Anti-parallel (**2.02**).[2]

Table 2.1. Ideal Phi (Φ) and Psi (Ψ) Angles for a β-sheet in comparison to a-helix and one β-turn

2.03	**secondary structure**	**Φ**	**Ψ**
	parallel β-sheet	−119	113
	antiparallel β-sheet	−139	135
	α-helix	−58	−47
	β-turn Type I	−60	−30

2.1.3. Importance of Folded β-Sheet

The β-sheet shows mostly a scaffolding role in protein architecture. However, it sometimes acts as a key recognition motif in some protein−protein and protein−DNA interactions that are important in many biological processes and in some diseases.[3] The β-sheet structure with intermolecular interactions between the hydrogen-bonding edges establishes essential form of biomolecular recognition (like DNA base pairing) (**2.04**-**2.07**, **Figure 2.2**) that elaborates protein quaternary structure, peptide and protein aggregation and protein-protein interactions.[4-6]

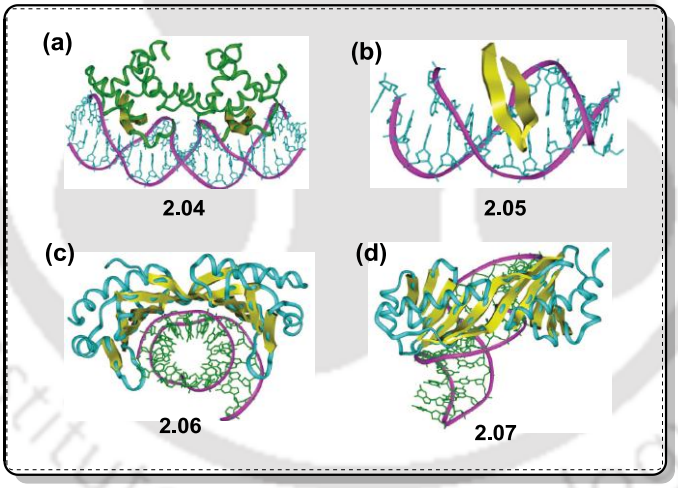

Figure 2.2. DNA recognition of β-sheets. Complex of two arc repressor protein dimers with DNA illustrating (a) the overall interactions (**2.04**) and (b) β-sheet interaction (**2.05**) (c) protein straddling the DNA strand (**2.06**) and (d) displays the positioning of the β-sheet over the DNA strand (**2.07**).[3-6] Copyright (2010) from American Chemical Society

β-sheets are not only important for normal biological activities, but also involved in many diseases including HIV, cancer, and neurodegenerative diseases. Therefore creating model systems that fold to form β-sheet like structures or participate in intermolecular interactions among β-strands would provide valuable tools to study β-

sheet folding and interactions.[7] To modulate the natural systems which may eventually lead to the synthesis of new drugs synthetic chemical models are used. The molecular scaffolds that act as turn unit have been introduced into peptides to mimic the structures of parallel and antiparallel β-sheets. The hydrogen-bonded β-sheet structure with molecular scaffold helps to prevent the formation of complex and ill-defined aggregates. The hydrogen bond formation in β-sheet prevents aggregation and promotes the generation of simple monomeric and dimeric units.[8] The importance of hydrogen-bonding complementarity, size complementarity and chiral complementarity has been elucidated by NMR studies of artificial folded β-sheets.[9-10] The sequence selectivity in the molecular recognition between β-sheets has also been demonstrated by these pairing preferences. The necessity of intermolecular edge-to-edge interactions of β-sheets in peptides and proteins has been illustrated by these studies. Ultimately, these chemical model systems with molecular scaffold containing folded β-sheets may lead to new direction of controlling β-sheet interactions and treating diseases.

2.1.4. Incorporation of Molecular Scaffold to Nucleate the β-Sheet

The molecular scaffold in the peptide backbone can organize a peptide structure by controlling the intramolecular interaction of peptide or peptidomimetic strands. Kelly's group have developed dibenzofuran unit (**2.08**, **Figure 2.3**) as an important heterocyclic as well as aromatic scaffold that has been found to induce β-sheet secondary structure when present in a peptide backbone (**2.09**, **Figure 2.3**). The distance between C4 and C6 (4.9 Å) of the dibenzofuran molecular scaffold is close to the antiparallel β-sheet strands. So, it can be placed in a peptide backbone to nucleate β-sheet conformation. The 4-(2-aminoethyl)-6-dibenzofuranpropionic acid scaffold (**2.08**) also can act as a hydrophobic cluster composed of the dibenzofuran skeleton. Due to the formation of intramolecular hydrogen bonding between the attached amino acid residues the hydrophobic side chains were flanked. This dibenzofuran unit can selectively nucleate the β-sheet secondary structure.[11]

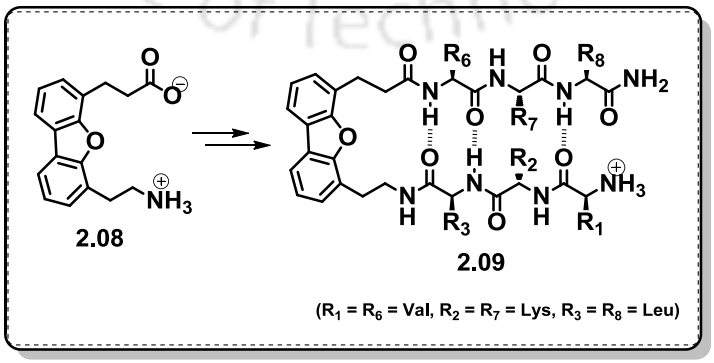

Figure 2.3. Kelly's dibenzofuran molecular scaffold (**2.08**) and incorporation of the scaffold into peptide backbone in order to nucleate the peptide into β-sheet secondary structure (**2.09**).[11]

The Bipyridine-based molecular scaffolds (**2.10**, **2.12**, **Figure 2.4**) have been incorporated into peptide backbones to stimulate β-sheet folding upon the addition of Cu(II) ions in the peptide solution. The attached peptide strands were elongated to the appropriate direction upon the coordination of the Cu(II) in a cisoid square planar conformation (**2.11**, **Figure 2.4**) which leads to the β-sheet formation into the peptide backbone (**2.13**, **Figure 2.4).**[12]

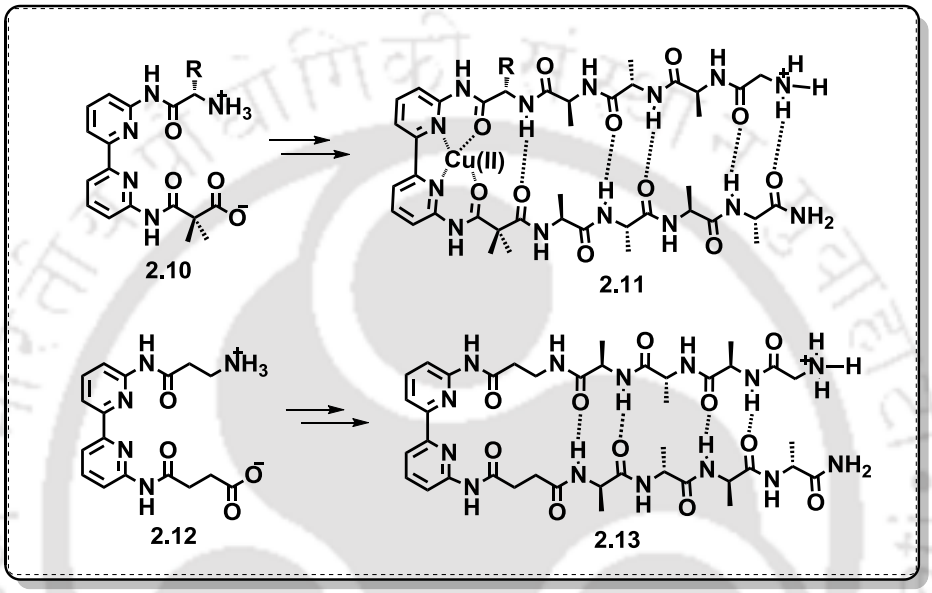

Figure 2.4. Bipyridine-based molecular scaffolds (**2.10**, **2.12**) induce to stimulate β-sheet structure upon the addition of Cu(II) ions (**2.11**).[12]

Endo-(2S,3R)-2-amino-3–Carboxynorbornene acts as a conformationally constrained molecular scaffold. Norbornene β-amino acid scaffold (**2.14**) is quite similar to that of turn-inducer proline and thus, can induce β-sheet structure in peptide (**2.14-2.16**, **Figure 2.5**).[13] The built-in U-architecture, small in size and low molecular weight make these norbornene derivatives advantageous for using as constrained molecular scaffold.[14] I. L. Karle and coworkers have synthesized endo-(2S,3R)-norbornene dicarbonyl (**2.17**) as a molecular scaffold, which is a reverse-turn mimetic scaffold that nucleates parallel β-sheet structure (**2.18**, **Figure 2.5**).

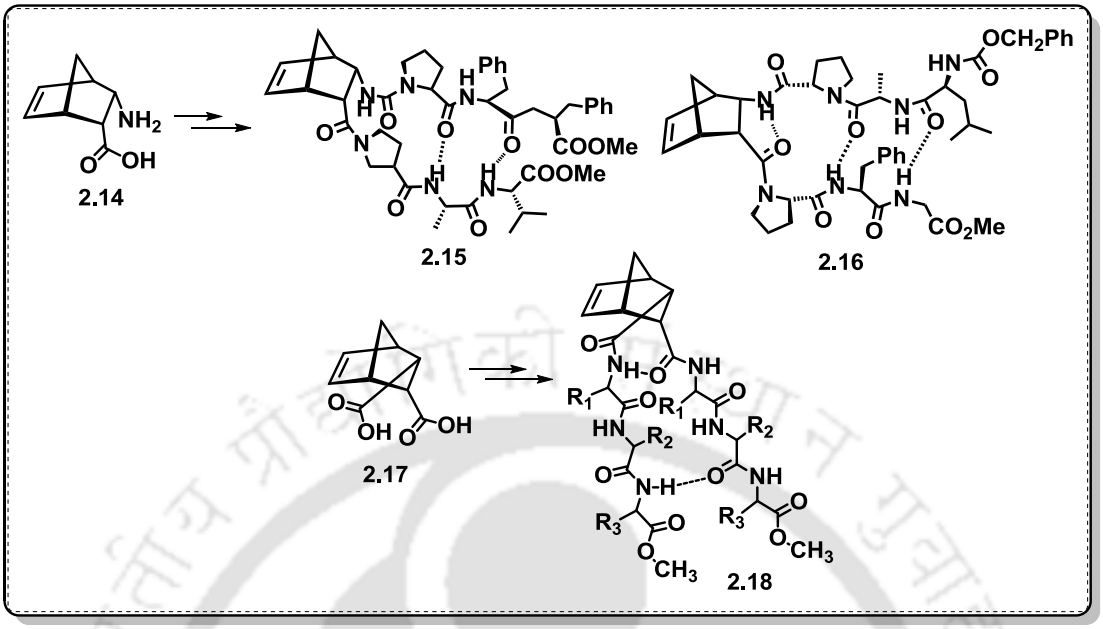

Figure 2.5. endo-(2S,3R)-norbornene-based molecular scaffolds as β-sheet inducer (**2.14**-**2.18**).[14]

Oligourea molecular scaffold can hold more than one peptide strands in proximity. Thus, Nowick and coworkers have synthesized diurea based molecular scaffold, oligoureas (**2.19**), via the treatment of diamine with peptide isocyanates. This scaffold is able to stabilize the β-sheet secondary structure in peptide backbone through intramolecular hydrogen bonding interaction **(2.20**-**2.21**, **Figure 2.6**).[15a]

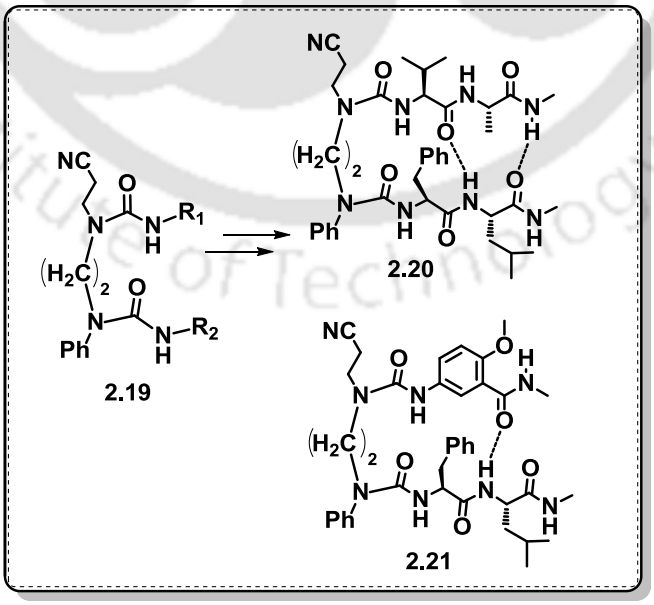

Figure 2.6. Oligourea molecular scaffold **(2.19)** as a β-sheet inducer (**2.20**-**2.21**).[15a]

Urea based molecular scaffold has been introduced into peptide backbone in order to achieve hydrogen-bonded duplex in peptides. The dipeptidyl urea bears *C*-terminal pyridyl moiety (**L-Ala–L-Pro–NHPy**) in the two dipeptide chains (**2.22**-**2.23**, **Figure 2.7)**. The two pseudopeptide molecule forms a β-sheet like hydrogen-bonded duplex when the molecules held together through intermolecular hydrogen bonding formation (**2.24**, **Figure 2.7**).[15b]

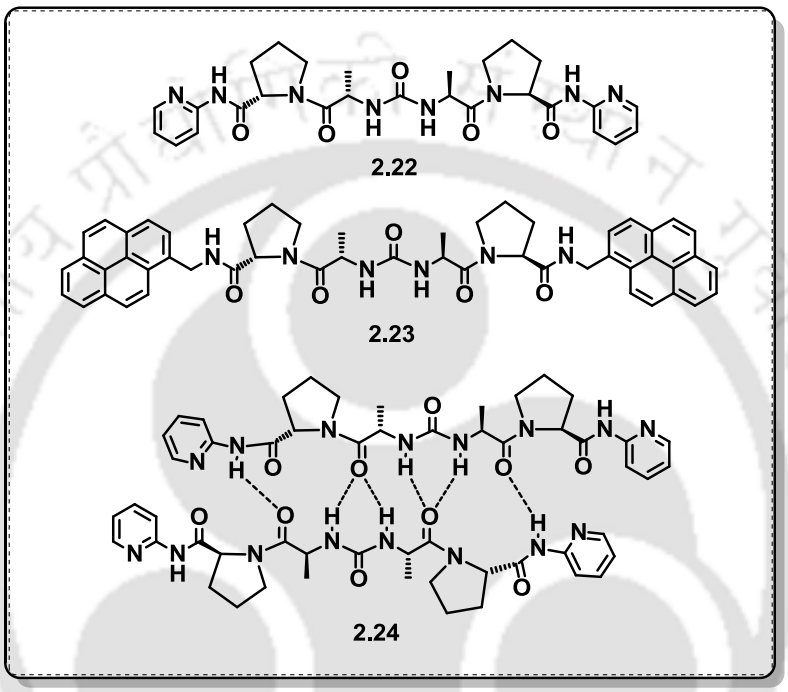

Figure 2.7. Urea based molecular scaffold forms β-sheet like hydrogen-bonded duplex in peptide backbone (**2.22**-**2.24**).[15b]

2.1.5. Fluorescently Labeled Peptides and Application of FRET/ Exciplex /Excimer Emission Process

Fluorescence resonance energy transfer (FRET) is a process where the excited state energy is transferred to an acceptor (A) from the initially excited donor (D) unit.[16,17] The emission spectra of the donor unit overlaps with the absorption of the acceptors unit. Thus energy transfer occurs from donor to acceptor and the emission intensity of the donor unit decreases with the increase of the intensity of the acceptor. FRET process is a distance-dependent process of interaction between donor and acceptor molecules in their electronic excited states, without emission of a photon.[16,18] A long-range dipole-dipole interaction between the donor and acceptor is resulted in a FRET process.[16,19] The donor molecule in its excited state has several routes to release its energy and return to the ground state (**Figure 2.8**). The excited state energy of the

donor molecule can degenerate to the environment (as light or heat) or directly transferred to an acceptor molecule to its excited state. The latter process is called FRET.

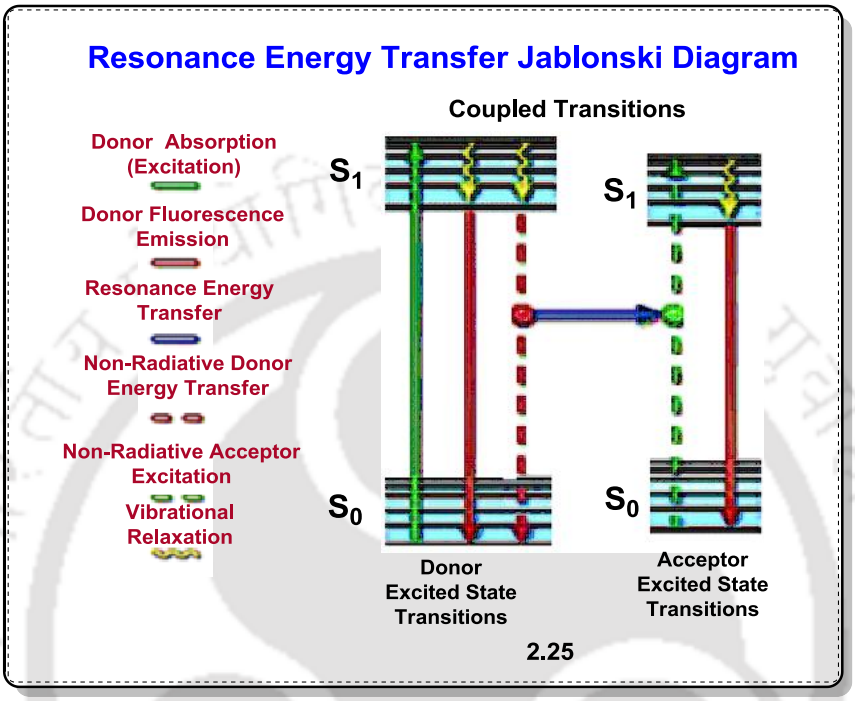

Figure 2.8. Jablonski diagram illustrating the coupled transitions involved between the donor emission and acceptor absorbance in fluorescence resonance energy transfer (**2.25**).

FRET emission is a fluorescence photophysical phenomena, which find widespread applications such as elucidating biophysical events of proteins/peptides in a cell. FRET event has been utilized to monitor the conformational changes in biomolecules such as nucleic acids and proteins.[20] The efficiency of energy transfer between a donor and acceptor is utilized to measure the intermolecular association/distance in between macromolecules.[21, 22]

Stephen J. Benkovic and coworkers have synthesized fluorescent amino acids 4-biphenyl–L-phenylalanine (**2.28**, **Figure 2.9**) and 4-methylenecoumaryl–L-alanine (**2.29**, **Figure 2.9**). These amino acids have been incorporated in dihydrofolate reductase (DHFR) at 17 and 115 positions (**2.26**, **Figure 2.9**). This model system allowed the study of conformational changes related to inhibitor binding. When irradiated the modified DHFRs at 280 nm, the excited fluorophore **2.28** transfers its energy to the other fluorophore **2.29** leading to an emission at 450 nm (**2.27**, **Figure**

2.9). This phenomena reveals that sensitive monitoring of changes in DHFR conformation can be measured when amino acids containing small fluorophoric units were introduced into DHFR with minimal disruption of function.[23]

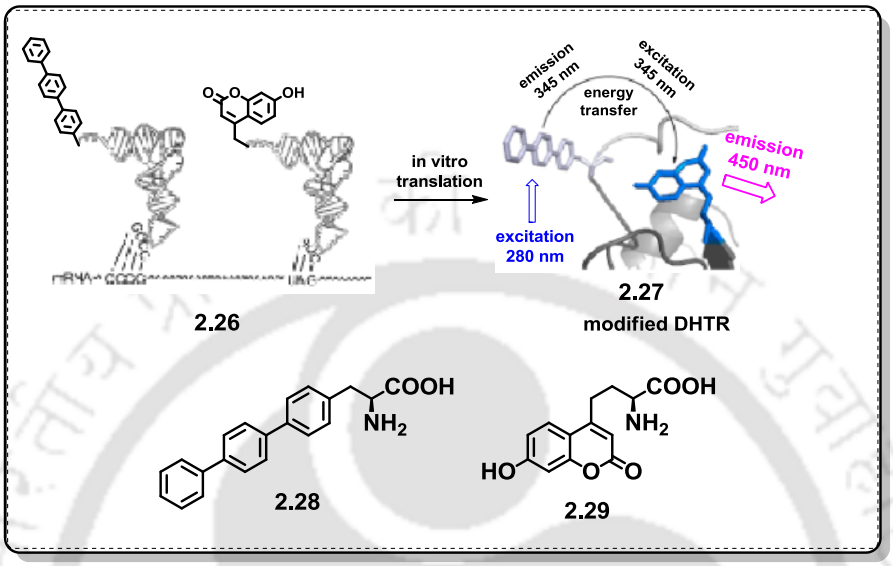

Figure 2.9. Incorporation of two fluorophoric units **2.28** and **2.29** into DHFR at Positions 17 and 115, respectively (**2.26**) and elucidation of FRET process (**2.27**).[23] Copyright (2013) from American Chemical Society.

In 2009 Dehua Pei and coworkers designed a solid supported peptide probe system wherein the *C*- and *N*-termini contained fluorescent donor (Edans) and quencher (Dabcyl) pair **(2.30**, **Figure 2.10)**. This peptide can monitor the cleavage of proteases. Before cleavage the peptide showed very little fluorescence. But the cleavage caused the separation between donor and quencher and an enhancement of fluorescence of donor fluorophore was observed. For the systematic profiling and the substrate specificity of endopeptidases this strategy was utilized (**2.31**, **Figure 2.10**).[24]

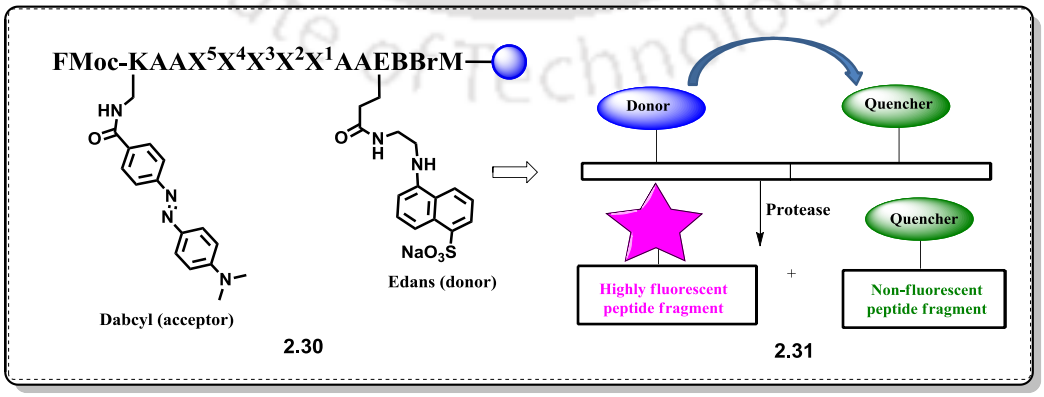

Figure 2.10. Schematic presentation of FRET based peptide (**2.30**) designed for systematic profiling the substrate specificity of endopeptidases (**2.31**).[24]

In 1998 Johansson and coworkers showed p–Cyanophenylalanine (PheCN) and tryptophan (Trp) unit as an efficient FRET pair, which serves better than commonly used dye pairs.[25] Feng Gai and coworkers have observed the overall applicability of their reported FRET pair in protein folding-unfolding studies. Two small proteins, villin headpiece subdomain (HP35) and the lysin motif (LysM) domain were applied to the urea-induced unfolding transitions for this study. They showed that the unfolding transition of HP35 reported by FRET happens at a denaturant concentration (**2.32**, **2.33**, **Figure 2.11**). This study reveals FRET process as a widely applicable tool for conformational studies especially for relatively small proteins. [26]

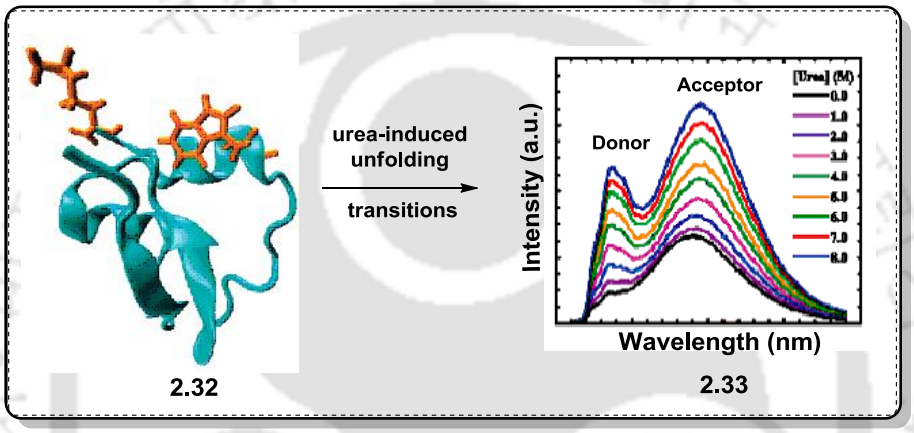

Figure 2.11. Application of FRET process for protein conformational studies especially for the relatively small proteins (**2.32-2.33**).[26] Copyright (2008) from American Chemical Society

Kevin W. Plaxco and coworkers have synthesized a peptide beacon (**2.34**, **Figure 2.12**) directed against an antibody diagnostic of HIV infection which was based on excimer emission. They employed a highly antigenic, six-residue epitope into it. The epitope can adopt a prolonged conformation in both the native protein and complexed state with its target antibody. Peptide beacon (PB) produces a large excimer peak at 475 nm in absence of the target. However, with increasing concentration of human anti-p17 antibody, the excimer emission decreases 2-fold and at last it vanishes and only the broad shoulder of monomer emission was observed (**2.35**, **Figure 2.12**). Thus, this approach was found to be helpful to monitor presence of polypeptide-binding targets and characterizing excimer-based PBs that is directed against an anti-HIV antibody.[27]

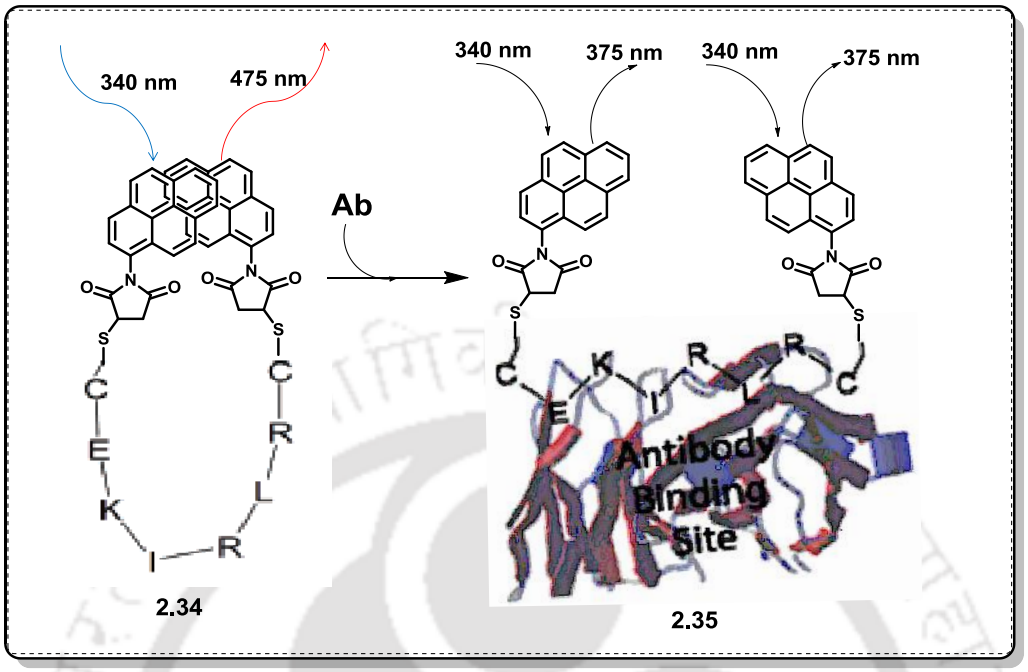

Figure 2.12. The excimer-based PB architecture is composed of two N–(1-pyrenyl)maleimides conjugated to a recognition peptide. In the absence of target (**2.34**), permits excimer formation. But upon target antibody binding (**2.35**), the pyrene moieties are separated and pyrene monomer emission was observed.[27]

In 2015 Wen-Sheng Chung evaluated the results of probe structures of biomolecules in pyrene-pyrene overlapping modes on their emission properties on the protein surface (**2.36-2.38**, **Figure 2.13**). They have synthesized and conjugated to two cysteine residues in the A55C/C77S/V169C mutant of adenylate kinase (**Adk**). Adenylate kinase showed a structural change in between its Open and Closed forms **(2.38-2.39, Figure 2.13).** They labeled a pyrene probe in the closed form of Adenylate kinase. When pyrene unit is stacked on the protein surface, excimer emission was found due to the ground-state association of pyrenes. The fluctuation in pyrene association modes on the spectral assets appeared at both ground and excited states with the increase in linker length. Steady-state fluorescence and time-resolved spectroscopic analysis were used to understand the interaction fashion between pyrene–Labeled biomolecules.[28]

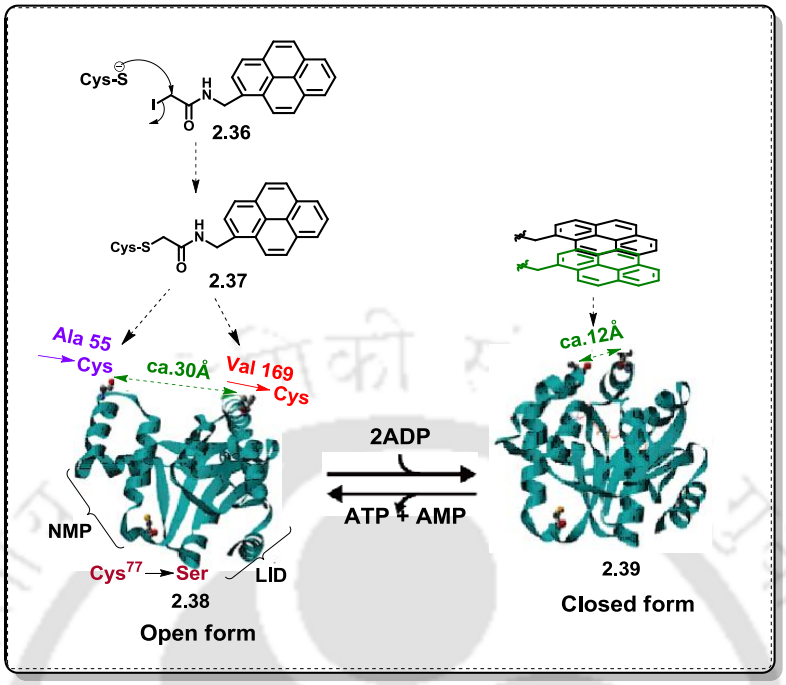

Figure 2.13. Reversible switching system for excimer emission property of pyrene.[28] Copyright (2015) from American Chemical Society

Masahiko Sisido and coworkers have synthesized a polypeptide with α-helix chain wherein *p*-(dimethy1amino) phenyl group (D) and a naphthyl group (N) were placed at the middle of the α-helix. The distance between the two fluorescent groups was altered by inserting different numbers (m) of alanyl units (**2.40**, **Figure 2.14**). They observed the quenching of fluorescence from either D or N groups or exciplex formation in the polypeptides when m = 0 and 2. But none of them was observed for the m = 1 polypeptide. This phenomenon indicates that the electron-transfer interactions in the polypeptides are happening through space. The quenching efficiency of the D-N pair in the polypeptide was insensitive to their relative orientation, but the exciplex formation was sensitive to their orientation.[29]

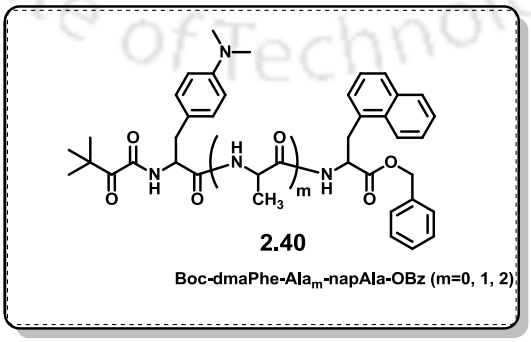

Figure 2.14. Polypeptide with α-helix chain containing p-(dimethy1amino)phenyl group (D) and a naphthyl group (N).[29]

2.2. Background

It is clear that considerable efforts separately have been invested in the design of scaffolded β-sheet peptidomimetics in one hand and fluorescent peptide probes on the other hand for studying peptide-protein interactions. However, β-strand mimicking and β-sheet like structures in a designed fluorescent peptide aiming at the fundamental aspects that a particular conformation can have an impact on the photophysics has received no or little attention. Investigating such an impact might find widespread applications in studying interbiomolecular interactions in cell and the design of new peptide based drug candidates. Therefore, the generation of scaffolded peptidomimetics with interesting fluorescence property of fundamental importance is highly demanding. Such probes could be of immense importance which can be applied dually-for mimicking a protein's particular secondary structure, such as β-sheet, of pharmacological importance and studying biological process involving protein-peptide interaction at least at the fundamental level in a model system**.**

2.3. Objective

With this above back ground and concept, we framed our objective as below

(a) Synthesis of uracil-di-aza-amino acid (**U^rAA**, **2.43**) as a new family of novel molecular scaffold for β-hairpin mimic (**Figure 2.15**).

(b) Synthesis of fluorescent peptide **2.61** **[BocNH–^{TMnap}Ala^{Do}–Leu–U^rAA–Leu–^{TPy}Ala^{Do}–CONMe(OMe)]**, and peptide **2.64** **[BocNH–^{TPy}Ala^{Do}–Leu–U^rAA–Leu–^{TPy}Ala^{Do}–CONMe(OMe)].**

(c) Conformational analysis of the synthesized peptides.

(d) Study of their photophysical properties towards establishing the concept of exciplex emission and excimer emission in their respective conformations.

(e) Study of interaction of the synthesized peptides with BSA protein.

2.3.1. The Logics Behind our Choice of Uracil Nucleobase to be the Scaffold

(a) It's easy associability with biological targets.

(b) Expectedly high propensity to nucleate β-sheet conformation owing to its conformational restriction at ω_i angle.

(c) Better understandable pharmacological implications of uracil than those of other heterocycles.

(d) The nucleobase-amino acid hybrid peptide would be the probe of choice for studying peptide-protein/peptide-DNA interaction as the hybrid

construct of nucleobase-amino acid could find application in future drug design process which is a newly emergent strategy to molecular diversity.

The concept is very promising and advantageous over a combinatorial approach of drug discovery as the biological activity of several new hybrids often exceeds that of the parent compounds. Therefore, the simple uracil scaffold would be advantageous over the reported other scaffolds for the nucleation of β-sheet structure in a short peptide sequence because the it is very simple, easy to synthesise, low cost and less time consuming which is an issue for the success of the design of a β-sheet nucleator (**Figure 2.15**). There are also no precedented examples of utilizing nucleobase-peptide hybrid construct with the nucleobase acting as a β-sheet inducer. This type of hybrid construct might interact with the biomolecules efficiently through the uracil base via H-bonding interaction.

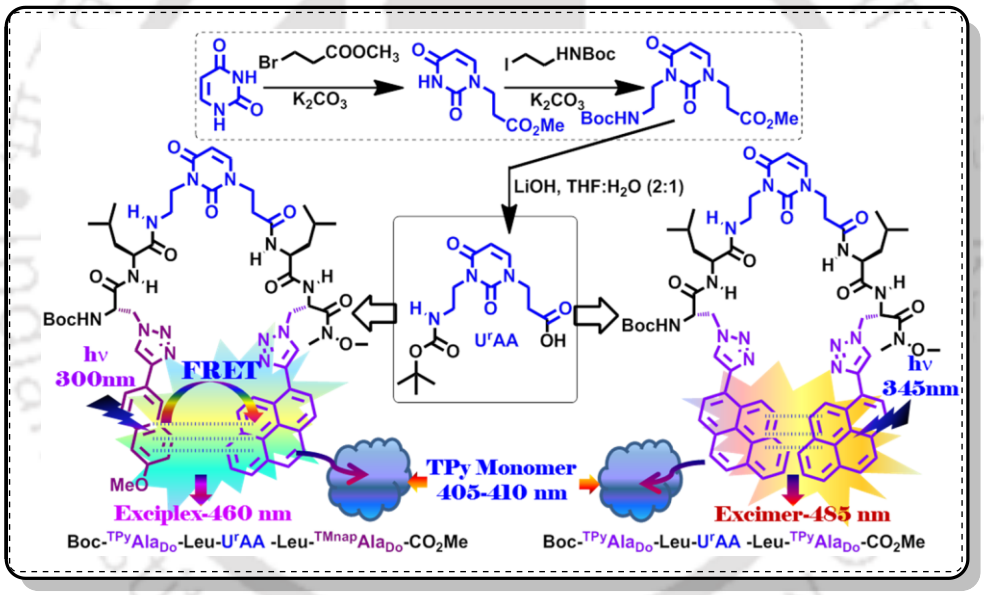

Figure 2.15. Synthesis of uracil-di-aza-amino acid, **U^{r}AA** as constrained molecular scaffold and structures of designed peptidomimetics **2.61-2.64** with predefined conformation and predicted photophysics.

2.4. Result and Discussion

2.4.1. Synthesis of Uracil Amino Acid Scaffold (U^{r}AA, 2.43) and Corresponding Peptides.

Synthesis of uracil amino acid was started from uracil nucleobase **2.41** which was treated with 3-bromo methyl propanoate and K_2CO_3 in dry DMSO for 12 hours at room temperature to get one side protected uracil **2.42**. Next it was treated with Boc

protected 2-iodoethanamine and K_2CO_3 at room temperature for 12 hours to get uracil amino acid (**U^{r}AA**) **2.43** in deprotected form. The ester group was then hydrolyzed with LiOH in THF : H_2O = 2 : 1 solvent to get –COOH protected **U^{r}AA 2.44** (**Scheme 2.1**).

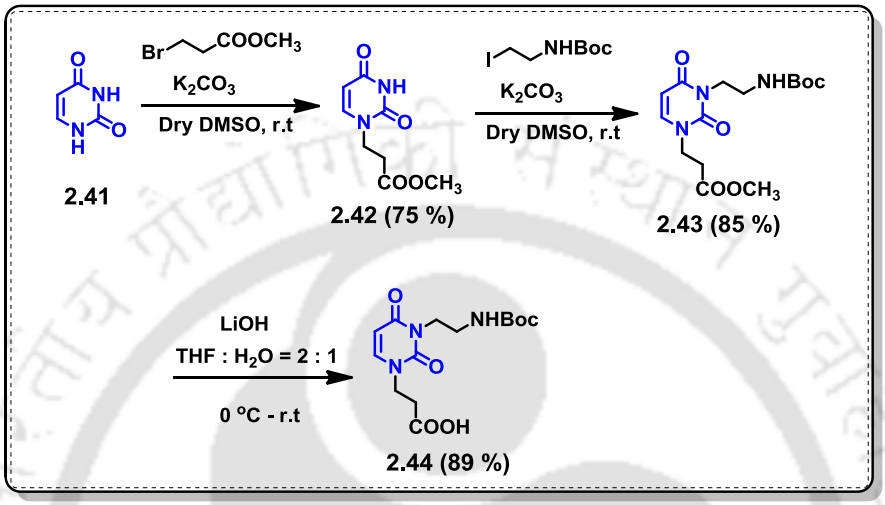

Scheme 2.1. Scheme for the synthesis of uracil amino acid scaffold (**U^{r}AA**).

To explore the constrained property and to determine the effect exerts by the scaffold **2.43** on the conformation of a peptide, we, next, incorporated it into two pseudo-symmetric fluorescent pentapeptides **2.61** (**Scheme 2.3**) and **2.64** (**Scheme 2.4**) differing only in the *C*-terminal fluorescent amino acids.

All the peptides were synthesized following simple peptide coupling protocol by solution phase reaction conditions. For the synthesis of the dipeptide, we have started from serine azide **2.45**. *N*-terminus of serine azide **2.45** was deprotected using TFA and DCM. The TFA salt serine azide **2.46** was then reacted with Boc protected leucine **2.47** via EDC.HCl/HOBT mediated peptide coupling reaction, afforded [**BocNH–Leu–Ser(N$_3$)–CONMe(OMe)**] dipeptide. Next the *N*-side deprotection of the synthesized dipeptide **2.48** was carried out again by TFA and DCM. The *C*-protected dipeptide was then allowed to react with our previously synthesized **U^{r}AA** scaffold **2.44** via EDC.HCl/DMAP mediated peptide coupling protocol getting **U^{r}AA** containing tripeptide azide **2.50**. Azide **2.50** was treated with pyrene alkyne (**2.51**) via (3+2)π cycloaddition reaction yielding fluorescent tripeptide **2.52** and then Boc deprotection of fluorescent tripeptide was carried out using TFA and DCM (**Scheme 2.2**).

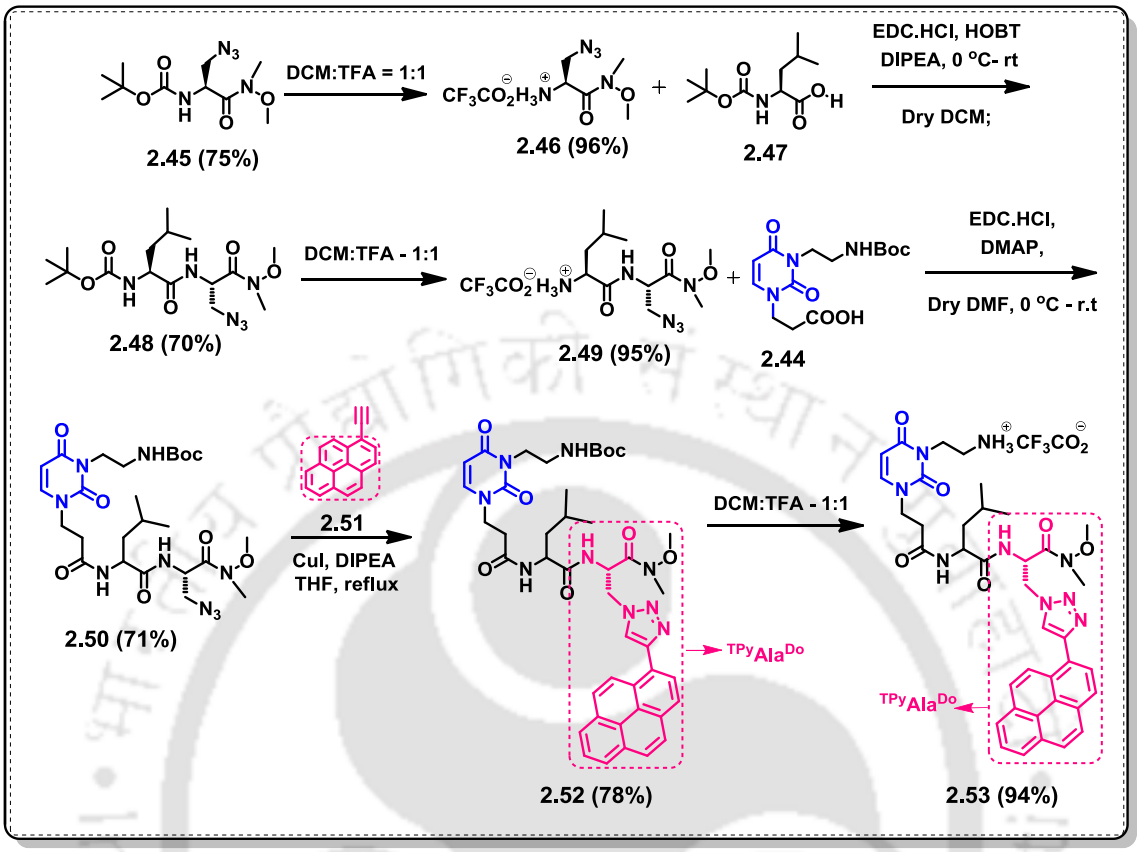

Scheme 2.2. Scheme for the synthesis of uracil amino acid scaffolded tripeptide **2.53** [**TFA$^{(-)}$NH$_3^{(+)}$–U^{r}AA–Leu–^{TPy}Ala^{Do}–CONMe(OMe)**]

The synthesis of another dipeptide strand also started from serine azide **2.45**. Then lithium hydroxide mediated ester hydrolysis and then EDC.HCl/HOBT mediated peptide coupling with COOH protected leucine **2.56** yielded dipeptide **2.57** [**BocNH–Ser(N$_3$)–Leu–COOCH$_3$**]. The synthesized dipeptide was then allowed to react with 6-Methoxy-2-naphyl alkyne **2.58** to get our desired fluorescent dipeptide **2.59**. Next the ester hydrolysis was carried out using LiOH. The *N*-protected fluorescent dipeptide acid **2.60** was then reacted with previously synthesized amine TFA salt **2.53** again via EDC.HCl/HOBT mediated peptide coupling reaction yielded our desired final **ExcipFRET-peptide 2.61** (**Scheme 2.3**).

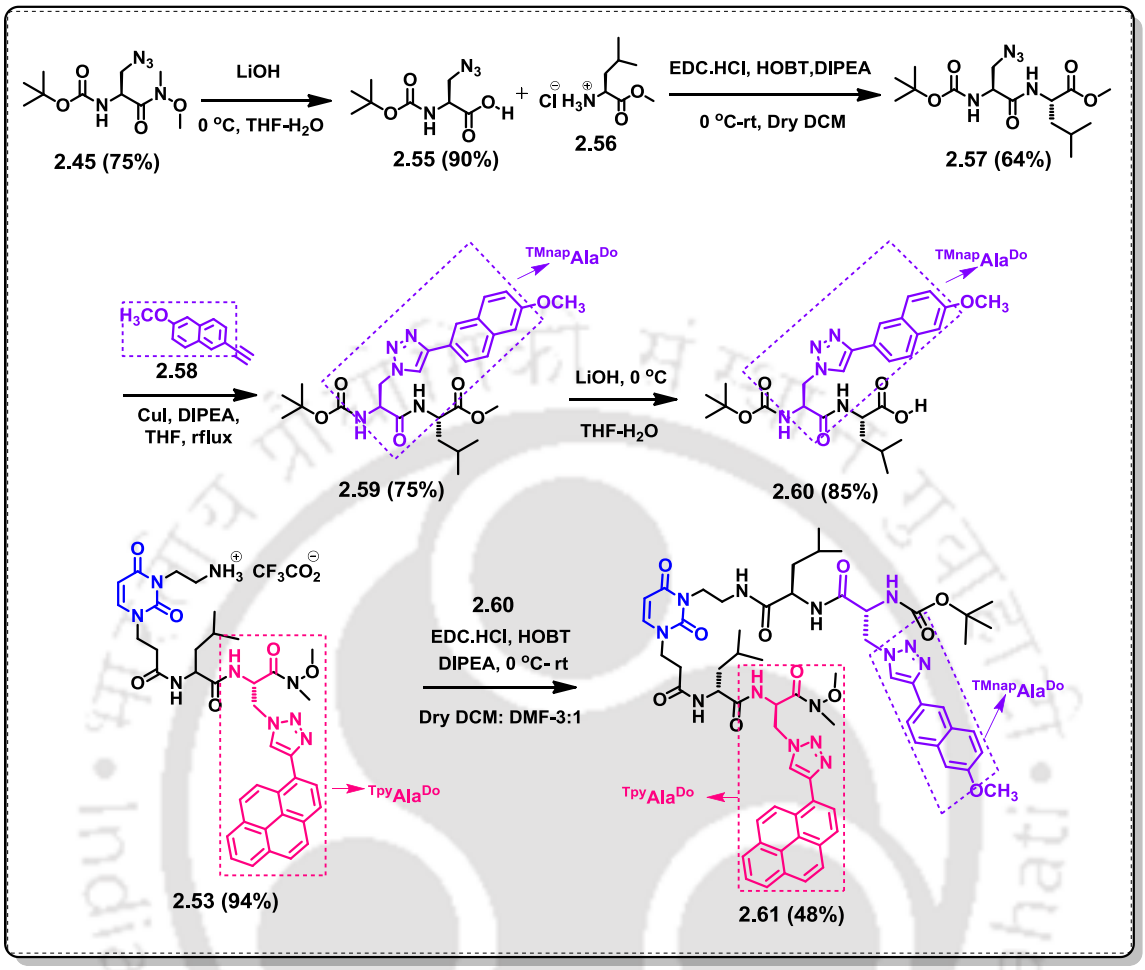

Scheme 2.3. Scheme for the synthesis of the **ExcipFRET-peptide 2.61** [**BocNH–^{TMnap}Ala^{Do}–Leu–U^{r}AA–Leu–^{TPy}Ala^{Do}–CONMe(OMe)**]

The synthesis of another pentapeptide [**BocNH–^{TPy}Ala^{Do}–Leu–U^{r}AA–Leu–^{TPy}Ala^{Do}–CONMe(OMe)**] was carried out using the similar protocol as described earlier. The 6-methoxy-2-naphthyl alkyne was replaced by 1-Pyrene alkyne *via* the EDC.HCl/HOBT mediated peptide coupling reaction of fluorescent dipeptide acid **2.63** and *C*-protected fluorescent tripeptide **2.53**, we obtained our desired **Excim-peptide 2.64** with **U^{r}AA** at the backbone of the peptide (**Scheme 2.4**).

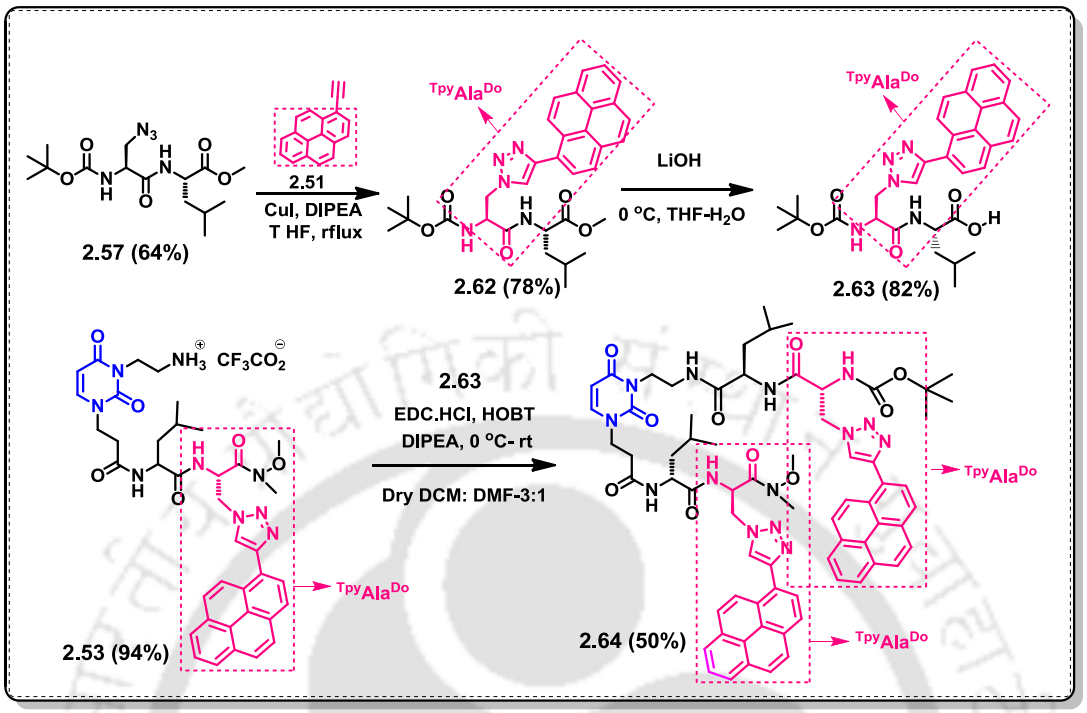

Scheme 2.4. Scheme for the synthesis of **Excim-peptide 2.64** [**BocNH–^{TPy}Ala^{Do}–Leu–U^{r}AA–Leu–^{TPy}Ala^{Do}–CONMe(OMe)**]

Next we have synthesized the monomer units, for FRET and excimer comparison of our synthesized pentapeptides. Serine azide **2.45** was allowed to react with 6-methoxy-2-naphthyl alkyne and 1-Pyrene alkyne separately under click reaction conditions to get monomeric units (**^{TPy}Ala^{Do}**) **2.65** and (**^{TMnap}Ala^{Do}**) **2.66** (**Scheme 2.5**).

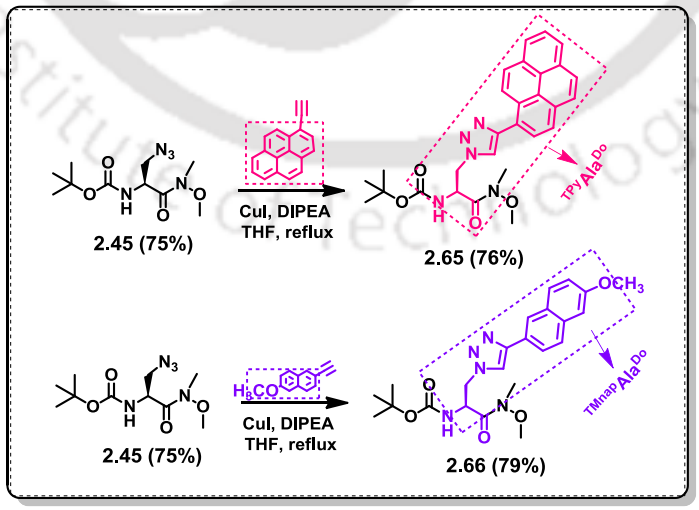

Scheme 2.5. Scheme for the synthesis of monomeric amino acids **^{TPy}Ala^{Do}** (**2.65**) and **^{TMnap}Ala^{Do}** (**2.66**) in *N*,*C*-protected form.

All the synthesized compounds (final and intermediate) were obtained in the pure form by column chromatography using silica-gel (60-120 mesh) and characterized via ^{1}H, ^{13}C, IR, MS/ HRMS. Next we have studied the secondary structure of the peptides by various spectroscopic techniques.

2.4.2. Conformational Study of Peptides 2.61 and 2.64 using CD, IR, NMR, Spectroscopic Techniques.

Study of Circular Dichroism Spectroscopy: Using a CD spectropolarimeter CD spectra were recorded with a cell path length of 1 mm at in different solvent at room temperature and variable temperature. All the samples were with 60 μM concentration and prepared in spectroscopic grade solvents. The secondary structure determination in methanol/acetonitrile/buffer using CD spectropolarimeter revealed a negative band at around 208-215 nm and a positive band at 195 nm indicating a predominantly β-sheet conformation in both the peptides **2.61-2.64** (**Figure 2.16**).[30]

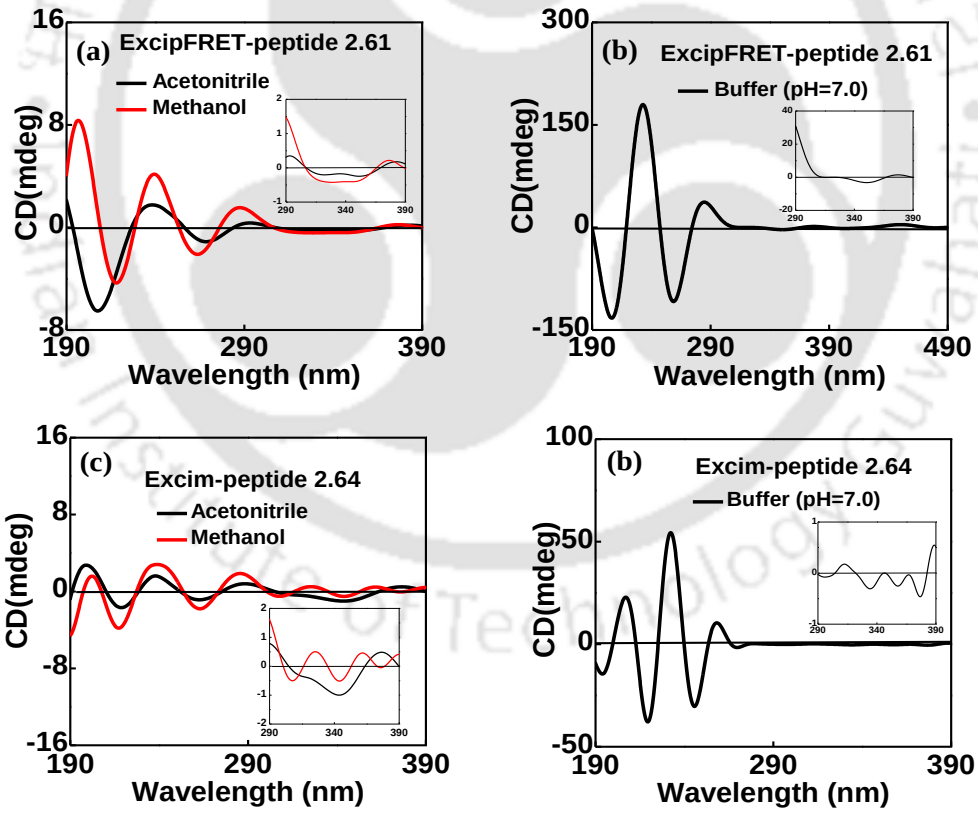

Figure 2.16. Deconvoluted CD spectra of (a)-(b) **ExcipFRET-peptide 2.61 [BocNH–^{TMnap}Ala^{Do}–Leu–U^{r}AA–Leu–^{TPy}Ala^{Do}–CONMe(OMe)]** and (c)-(d) **Excim-peptide 2.64 [BocNH–^{TPy}Ala^{Do}–Leu–U^{r}AA–Leu–^{TPy}Ala^{Do}–CONMe(OMe)]** in Acetonitrile, MeOH and Buffer solvents (60 μM concentration; 25 ^{o}C).

The signature of aromatic π-π stacking interaction between two terminal chromophores in both the peptides was evident in the CD spectra. The CD spectra exhibited ICD bands in the chromophoric absorbance region (300-350 nm) along with the signature peaks of β-sheet. These observations indicated that the uracil amino acid scaffold (**U^{r}AA**) induced folding between two peptide arms bringing two terminal fluorophoric units closer.

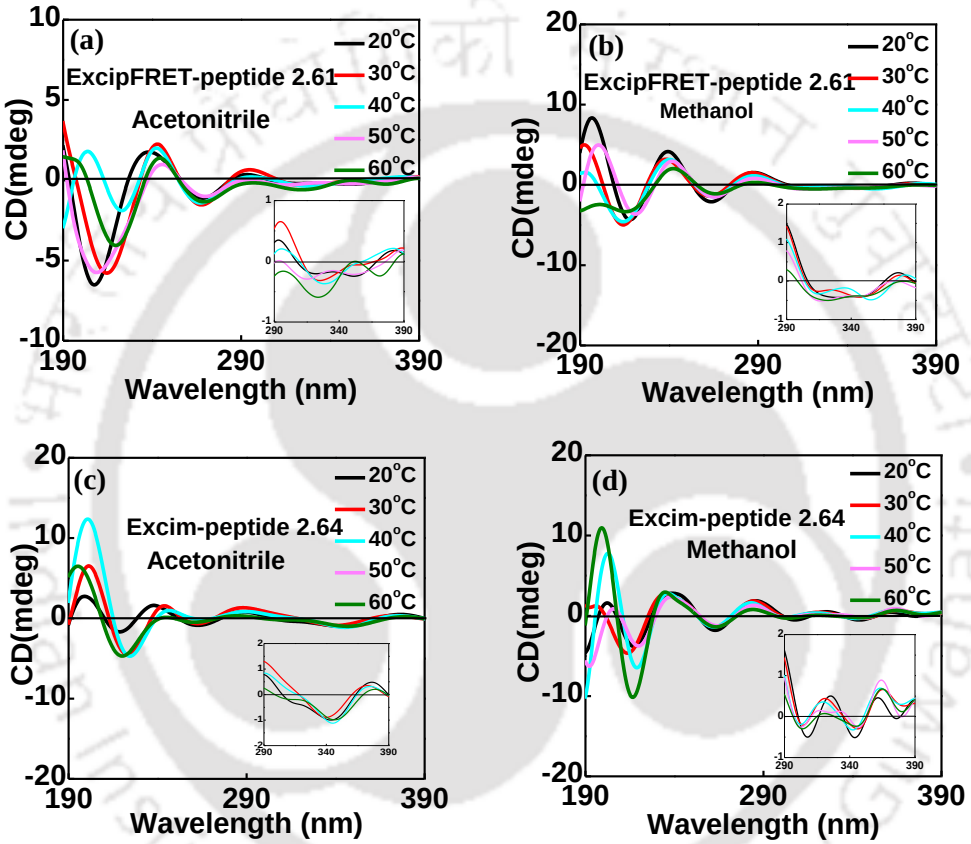

Figure 2.17. Variable temperature CD spectra of (a)-(b) **ExcipFRET-peptide 2.61** [**BocNH–^{TMnap}Ala^{Do}–Leu–U^{r}AA–Leu–^{TPy}Ala^{Do}–CONMe(OMe)**] and (c)-(d) **Excim-peptide 2.64** [**BocNH–^{TPy}Ala^{Do}–Leu–U^{r}AA–Leu–^{TPy}Ala^{Do}–CONMe(OMe)**] in acetonitrile and MeOH solvents (60 μM concentration; 25 ^{o}C).

Evidence of Intramolecular H-Bonding from FT-IR Spectroscopy: IR spectroscopic technique was utilized to prove the intramolecular H-bonding formation in synthesized peptide strand. So, using dry KBr, IR spectra were recorded, which showed the presence of intramolecular H-bonded and free amide -NH stretching absorptions at 3463-3320 and 3480-3297 cm^{-1} for **ExcipFRET-peptide 2.61** and **Excim-peptide 2.64** respectively, supported β-sheet like structures in peptide

backbone. The IR spectra of peptide **2.61** showed a sharp N-H stretching absorption at $\bar{\upsilon}$ =3320 cm^{-1}, C=O stretching at $\bar{\upsilon}$ =1708 cm^{-1} and 1853 cm^{-1}. The IR spectra of peptide **2.64** showed N-H stretching absorption at $\bar{\upsilon}$ =3297 cm^{-1}, C=O stretching at $\bar{\upsilon}$ =1707 cm^{-1} and 1855 cm^{-1}. The absorption peaks were independent of the sample concentration.[31]

Evidence of Intramolecular H-Bonding from Variable Temperature ^{1}H NMR (VT-NMR): Variable temperature ^{1}H NMR analysis was carried out to support the intramolecular Hydrogen bonding interaction in peptide **2.61** and **2.64** in d_6-DMSO in which all NHs exhibited different chemical shifts. From VT-NMR analysis intramolecular H-bonding formation was indicated in both peptide **2.61** and **2.64**. All the amide NH's, and triazole C-H exhibited ($\Delta\delta/\Delta T$) values that are moderate to close to Kessler limit of -3 to -6 ppb/K indicating presence of strong to moderate intramolecular H-bonding and supported the predominant turn or turn like structure of the peptides (**Table 2.2**, **Figure 2.18**).[32]

Table 2.2. Values of temperature coefficients of chemical shifts of amide NHs or triazole–CH in **ExcipFRET-peptide 2.61** and **Excim-peptide 2.64**

NHs from ExcipFRET-peptide 2.61	**$\Delta\delta/\Delta T$ (ppb/k)**	**NHs from Excim-peptide 2.64**	**$\Delta\delta/\Delta T$ (ppb/k)**
*N-t*erminal-Ser-NH1	- 6.9 ppb/k	*N*-terminal-Ser-NH1	- 6.26 ppb/k
N-terminal–Leu-NH2	- 7.04 ppb/k	*N*-terminal–Leu-NH2	- 5.21 ppb/k
N-terminal-^{Mnap}**TAA**–CH1	-1.8 ppb/k	*N*-terminal-^{Py}**TAA**–CH1	-1.78 ppb/k
C-terminal-^{Py}**TAA**–CH2	-1.2 ppb/k	*C*-terminal-^{Py}**TAA**–CH2	-1.57 ppb/k
C-terminal –Leu-NH4	-4.38 ppb/k	*C*-terminal –Leu-NH4	-4.00 ppb/k
N-terminal -Ser-NH5	-5.7 ppb/k	*C*-terminal -Ser-NH5	-5.7 ppb/k
U^{r}AA-NH3	-4.9 ppb/k	**U^{r}AA**-NH3	-4.00 ppb/k

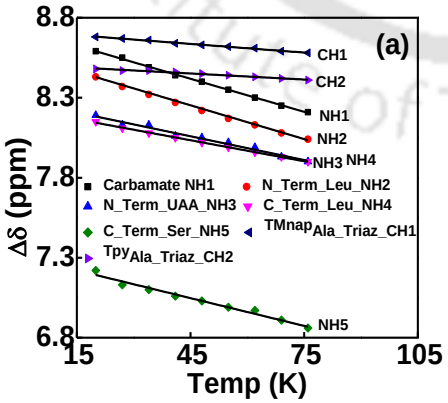

Figure 2.18. Temperature dependence of amide -NH/triazole –CH chemical shift of Pentapeptide **2.61**(**a**) and of Pentapeptide **2.64** (**b**)**.**

Conformational Analysis using 2D NMR Experiment: Next, the 2D NMR analysis in DMSO-d_6 was carried out to support the β-sheet conformation in peptide backbone. The proton signals were divided into groups or coupling with the help of ^{1}H-^{1}H TOCSY (Total Correlated Spectroscopy). Thus, for both **ExcipFRET-peptide 2.61** and **Excim-peptide 2.64** TOCSY experiment was carried out in d_6-DMSO to identify various NH's protons and triazole CH's. The analysis of solution conformations from NOESY and ROESY spectra in d_6-DMSO of both the peptide **2.61- 2.64** revealed that the scaffold adopted a rigid hairpin shape. The backbone H-bonding and hydrophobic/stacking interactions between terminal chromophores helped the scaffold nucleating the peptide strands to adopt overall β-sheet conformation. The 2D NMR supported the close proximity and possibility of a photophysical interaction between the two terminal fluorescent unnatural amino acids (**^{TMNap}Ala^{Do}/^{TPy}Ala^{Do}** for **2.61** and **^{TPy}Ala^{Do}/^{TPy}Ala^{Do}** for **2.64** (**Figure 2.19 a-b**).

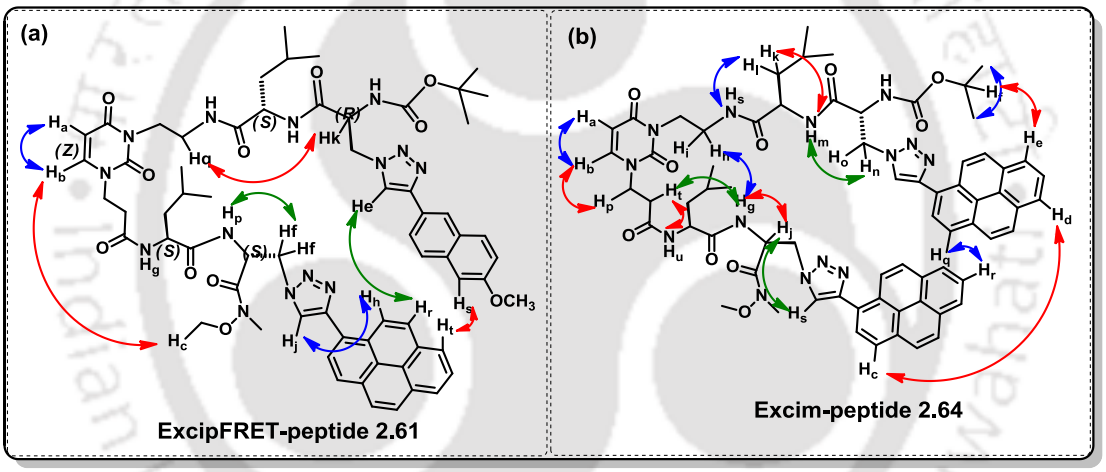

Figure 2.19. Pictorial presentation of long range proton-proton interaction of **ExcipFRET-peptide 2.61** (a) and **Excim-peptide 2.64** (b) as evident from 2D NMR.

Conformational Analysis Using Macromodel Study*:* Next, we have carried out MD simulations for the peptides using an OPLS 2005 force field. The starting structures for the peptides were the global minimum conformers. The MD simulations were performed using Schrodinger Macromodel (Maestro vs. 9.1) software package with OPLS 2005 force field in which the systems were subjected to 100 ps simulations time (with time step of 1.5 fs and equilibrium time 1.0 ps) at constant temperature (300 K) and pressure (1 atm) with shaking bonds to hydrogens. An optimal minimization method was chosen for minimizing the generated structures (with maximum iteration of 1000) with gradiant convergence threshold of 0.05.[33]

The Pyrene unit of the *C*-terminal amino acid (**^{TPy}Ala^{Do}**) and the Methoxynapthalene moiety of *N*-terminal amino acid (**^{TMnap}Ala^{Do}**) in Pentapeptide

2.61, were chosen as freely moving moieties during the simulation. The two Pyrene units in Pentapeptide **2.64**, were chosen as freely moving moieties during the simulation.

Figure 2.20 showed the final structures of the **ExcipFRET-peptide 2.61** and **Excim-peptide 2.64** obtained after the MD simulations. As shown in the figure it was observed that none of the peptide was distorted and retained their global minimum conformation.

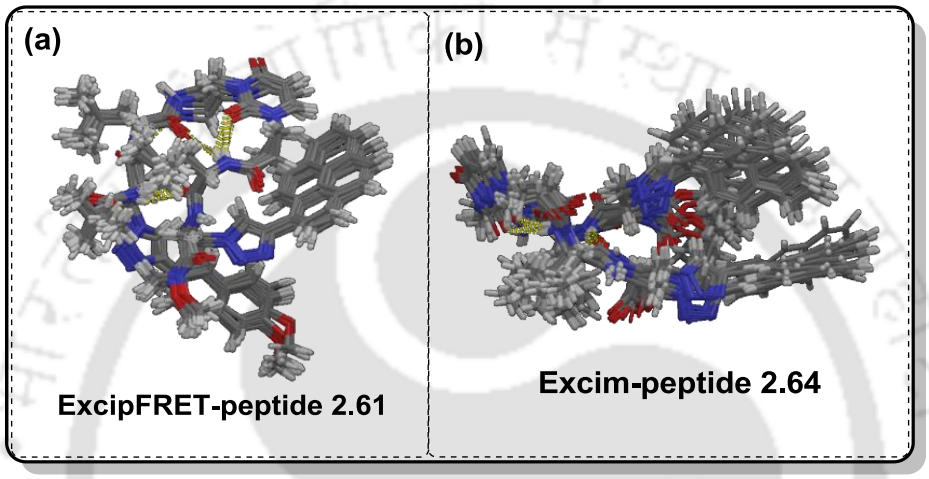

Figure 2.20. Clustering of structures (within 21 kJ/mole global minima) obtained from molecular dynamics simulation for the peptides. (a) **ExcipFRET-peptide 2.61 [BocNH–^{TMnap}Ala^{Do}–Leu–U^{r}AA–Leu–^{TPy}Ala^{Do}–CONMe(OMe)]** and (b) **Excim-peptide 2.64 [BocNH–^{TPy}Ala^{Do}–Leu– U^{r}AA–Leu–^{TPy}Ala^{Do}–CONMe(OMe)]**.

2.4.3. Study of Photophysical Properties

We have studied the photophysical properties of **ExcipFRET-peptide 2.61** and **Excim-peptide 2.64** in various solvents after establishing the β-sheet conformation in peptide backbone. The UV-visible spectra of the ^{TMnap}**Ala**^{Do} monomer exhibited a structured absorption band of methoxynaphthalene unit at around 290-300 nm in various solvents (**Figure 2.21**). When excited at the absorption maxima of ^{TMnap}**Ala**^{Do} in each solvent showed a broad emission band at 365 nm (**Figure 2.21**). ^{TPy}**Ala**^{Do} monomer showed broad absorption at around 347 nm in dioxane and exhibit blue shift of 4 nm as the solvent polarity increases from dioxane to methanol (**Figure 2.22**). Upon excitation on the absorption maxima of ^{TPy}**Ala**^{Do} it showed a structured emission at around 384, 405 and 427 nm (**Figure 2.22**). The quantum yield also follows the same trend as the intensity in various organic solvents (**Table 2.3** and **2.4**).

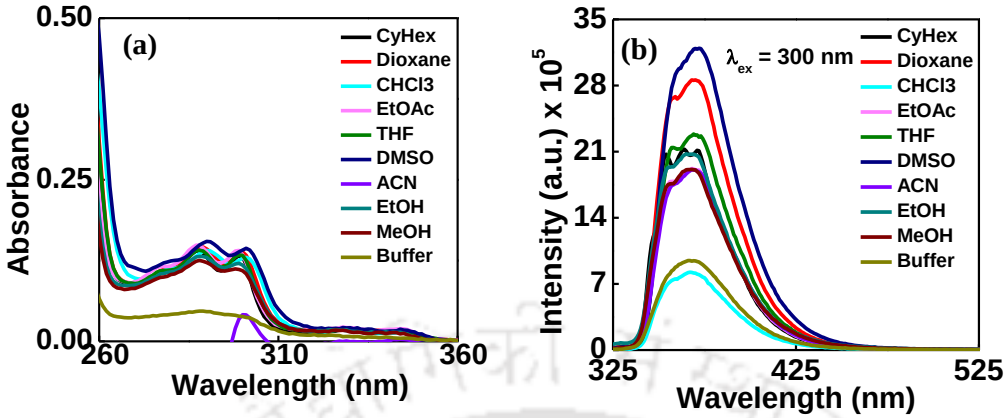

Figure 2.21. UV-Visible (a), fluorescence emission at 300 nm (b) of **UNNA 2.66 [**^{TMnap}**Ala**^{Do}), Considered as the monomeric donor unit in FRET study**]** in different solvents [10 µM, r.t.; $\lambda_{ex} = \lambda_{max} \approx 300$ nm in each solvent].

Table 2.3. Summary table of photophysical properties of the **UNNA 2.66 (**^{TMnap}**Ala**^{Do}**)**

Entry	**Solvents**	**UV-Vis & Fluorescence**			
		λ_{max}^{abs} **(nm)**	λ_{max}^{fl} **(nm)**	$\varepsilon_{max \times 10^3}$ **(Lmol^{-1}cm^{-1})**	Φ_f
[^{TMnap}**Ala**^{Do}**]; [The Donor Chromophore Only]**	CyHex	255, 288, 299	354, 363, 371	12.9	0.31
	Dioxane	256, 288, 299	357, 370	13.8	0.43
	$CHCl_3$	256, 290, 301	367	12.8	0.12
	EtOAc	255, 288, 299	356, 370	13.4	0.29
	THF	256, 288, 299	357, 370	13.3	0.34
	DMSO	257, 290, 301	360, 371	14.1	0.49
	EtOH	255, 288, 299	367	14.1	0.28
	ACN	300	368	11.8	0.32
	MeOH	253, 288, 298	356, 368	10.9	0.29
	Buffer (pH=7.0)	253, 288, 300	367	03.8	0.15

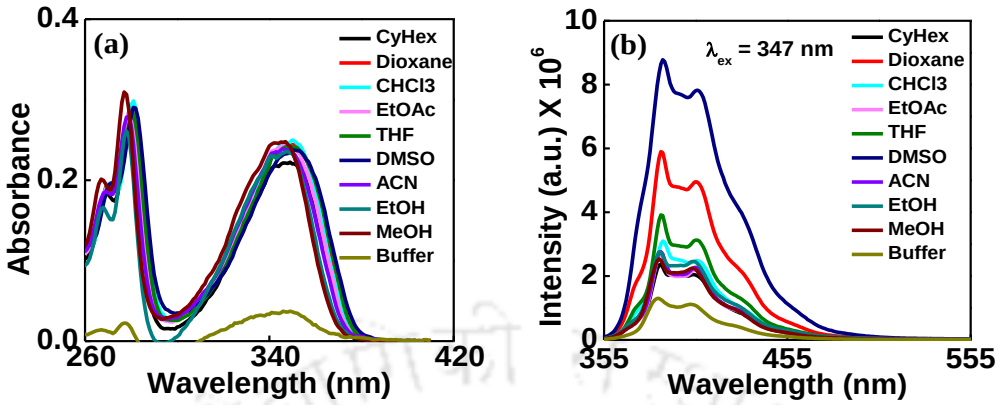

Figure 2.22. UV-Visible (a), fluorescence emission at 350 nm (b) of **UNNA 2.65** [^{TPy}**Ala**^{Do}**;** Considered as the monomeric unit in Excimer study] in different solvents [10 µM, r.t.; $\lambda_{ex} = \lambda_{max} \approx 347$ nm in each solvent].

Table 2.4. Summary table of photophysical properties of **UNNA 2.65 (^{TPy}Ala^{Do})**

Entry	**Solvents**	**UV-Vis & Fluorescence**			
		λ_{max}^{abs} **(nm)**	λ_{max}^{fl} **(nm)**	$\varepsilon_{max \times 10^3}$ **(Lmol^{-1}cm^{-1})**	Φ_f
(^{TPy}Ala^{Do}) [The Acceptor Chromophore Only]	CyHex	269, 280, 347	384, 405, 427	22.1	0.15
	Dioxane	270, 280, 347	384, 405, 427	24.2	0.36
	$CHCl_3$	270, 281, 347	385, 405, 428	24.4	0.18
	EtOAc	269, 279, 347	384, 405, 427	24.3	0.15
	THF	270, 280, 347	384, 405, 427	24.1	0.22
	DMSO	271, 281, 350	386, 405, 428	23.3	0.59
	EtOH	267, 278, 347	384, 405, 427	23.8	0.16
	ACN	268, 278, 347	384, 405, 427	23.5	0.17
	MeOH	267, 277, 343	384, 405, 427	24.8	0.15
	Buffer (pH=7.0)	266, 277, 347	384, 405, 427	3.6	0.15

The **ExcipFRET-peptide 2.61** showed absorbance around 300 and 345 nm respectively with very little solvatochromic shift and exhibit structured emission band at around 355, 372, 384, 404 and 427 nm upon excitation at 300 nm (**Figure 2.23**, **Table 2.5**). **Excim-peptide 2.64** shows absorbance maxima at 349 nm with 4 nm blue shift from nonpolar $CHCl_3$ to polar MeOH solvent **Excim-peptide 2.64** exhibit structured emission band of pyrene at around 386, 405, 429 nm with a broad excimer band at around 385 nm (**Figure 2.24**, **Table 2.6**) upon excitation at its absorption maxima.

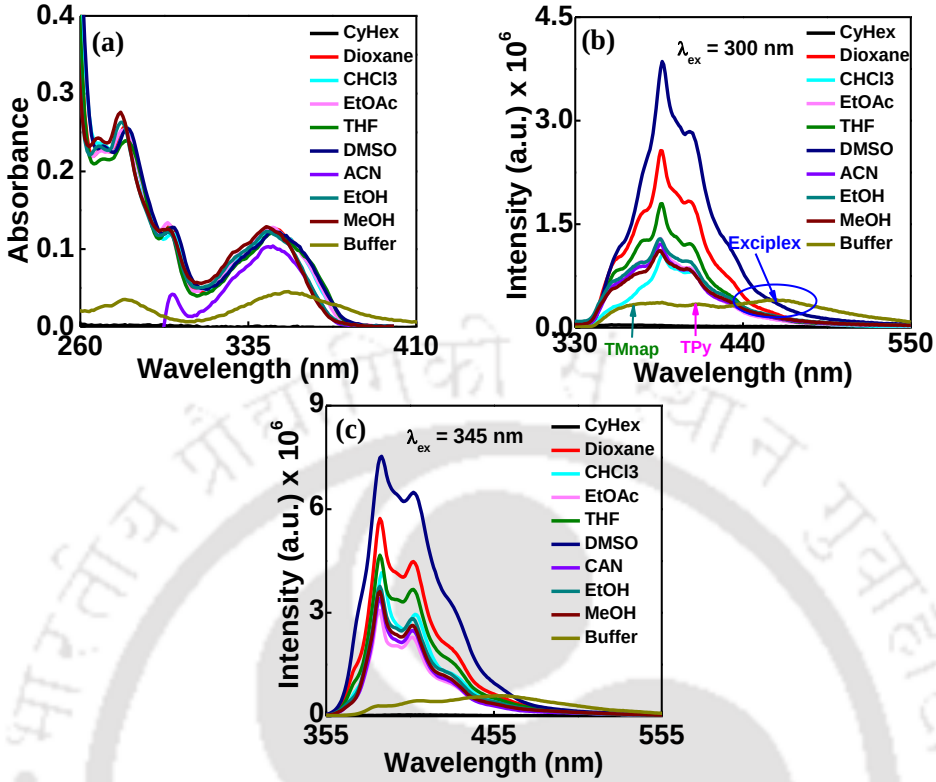

Figure 2.23. (a) UV visible, (b) Fluorescence emission (λ_{ex} ≈ 300 nm) and (c) Fluorescence emission (λ_{ex} ≈ 345 nm) of **ExcipFRET-peptide 2.61** [**BocNH–^{TMnap}Ala^{Do}–Leu–U^{r}AA–Leu–^{TPy}Ala^{Do}–CONMe(OMe)**] in different solvents [10 µM, r.t.

Table 2.5. Summary table of photophysical properties of **ExcipFRET-peptide 2.61 [BocNH–^{TMnap}Ala^{Do}–Leu–U^{r}AA–Leu–^{TPy}Ala^{Do}–CONMe(OMe)]**

Entry	Solvents	UV-Vis & Fluorescence			
		λ_{max}^{abs} (nm)	λ_{max}^{fl} (nm)	$\varepsilon_{max} \times 10^3$ ($Lmol^{-1}cm^{-1}$)	Φ_f
Exip FRET-peptide 2.61	CyHex	280, 300	355, 372, 384	0.2	0.02
	Dioxane	269, 280, 300, 345	355, 372, 384, 404, 427	12.4	0.44
	$CHCl_3$	270, 280, 301, 345	355, 372, 386, 405, 427	12.2	0.19
	EtOAc	269, 270, 299, 345	355, 372, 384, 404, 427	12.7	0.24
	THF	270, 280, 299, 346	357, 372, 386, 405, 429	11.9	0.32
	DMSO	270, 281, 301, 345	355, 372, 386, 405, 427	12.0	0.66
	EtOH	268, 278, 299, 343	355, 372, 384, 404, 427	10.3	0.24
	ACN	300, 344	355, 372, 384, 404, 427	12.2	0.27
	MeOH	267, 278, 299, 343	355, 372, 384, 404, 427	12.8	0.24
	Buffer (pH=7.0)	282, 300, 345	355, 372, 384, 404, 427, 465	5.0	0.25

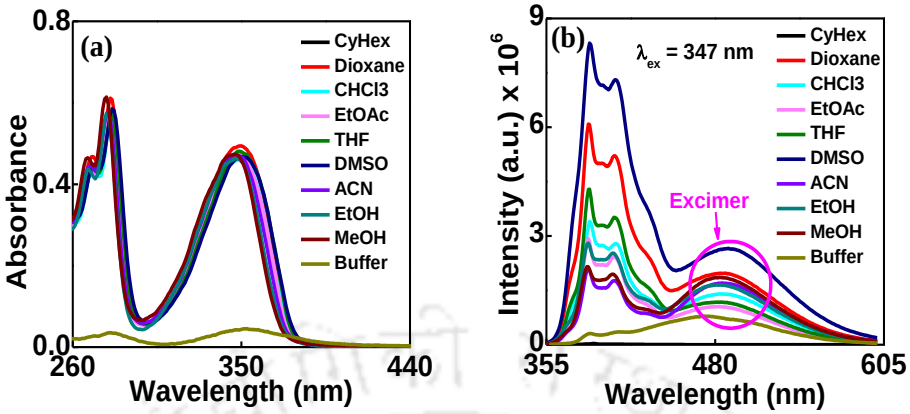

Figure 2.24. (a) UV-Visible and (b) fluorescence emission spectra of **Excim-peptide 2.64**, **[BocNH–^{TMnap}Ala^{Do}–Leu–U^{r}AA–Leu–^{TPy}Ala^{Do}–CONMe(OMe)]**, in different solvents [10 μM, r.t.; $\lambda_{ex} = \lambda_{max} \approx 350$ nm in each solvent].

Table 2.6. Summary table of photophysical properties of **Excim-peptide 2.64 [BocNH–^{TMnap}Ala^{Do}–Leu–U^{r}AA–Leu–^{TPy}Ala^{Do}–CONMe(OMe)]**

Entry	Solvents	UV-Vis & Fluorescence			
		λ_{max}^{abs} (nm)	λ_{max}^{fl} (nm)	$\varepsilon_{max} \times 10^3$ ($Lmol^{-1}cm^{-1}$)	Φ_f
Exim-peptide 2.64	CyHex	278, 350	389, 405, 482	0.5	0.14
	Dioxane	270, 280, 349	386, 405, 429, 484	49.4	0.48
	$CHCl_3$	270, 281, 350	386, 406, 429, 483	46.0	0.30
	EtOAc	269, 279, 347	386, 404, 429, 482	47.2	0.24
	THF	271, 281, 349	386, 405, 429, 482	48.0	0.32
	DMSO	271, 281, 347	387, 406, 429, 490	46.7	0.72
	EtOH	269, 278, 346	385, 405, 429, 484	46.5	0.26
	ACN	268, 278, 347	385, 404, 429, 482	45.6	0.30
	MeOH	268, 277, 346	385, 405, 429, 483	45.8	0.29
	Buffer (pH=7.0)	280, 352	385, 405, 473	8.0	0.21

2.4.3.1. Establishment of Dual Door Entry to Exciplex Formation and Excimer Formation in ExcipFRET-Peptide 2.61 and Excim-Peptide 2.64

To establish our concept of dual door entry to exciplex emission either via FRET or via excitation of a FRET acceptor in **ExcipFRET-peptide 2.61** and an excimer emission in **Excim-peptide 2.64** in their β-sheet conformation we, next, examined the photophysical interaction between the terminal triazolyl unnatural amino acids in both the fluorescent pentapeptides in aqueous buffer. The UV-visible and fluorescence

photophysical properties of the fluorescent triazolyl amino acid monomers indicated a possibility of FRET process from donor, ^{TMNap}**Ala**^{Do} to acceptor, ^{TPy}**Ala**^{Do} in peptide **2.61** (**Figure 2.25 a**, **b**). Moreover, at the absorption wavelength (λ_{abs}^{max} = 300 nm) of ^{TMNap}**Ala**^{Do}, the amino acid ^{TPy}**Ala**^{Do} absorb negligibly indicating that the peptide **2.61** could selectively be excited at 300 nm. Thus, based on our designed concept and the above observations we turned our attention to study the FRET process/exciplex emission in details in peptide **2.61** in buffer solvent. Thus, upon excitation at the absorption maximum of the donor, ^{TMNap}**Ala**^{Do} (λ_{ex} = 300 nm), the **ExcipFRET**-peptide **2.61** showed an weak and overlapped emission at 365 nm corresponding to the emission from ^{TMNap}**Ala**^{Do}, along with another broad emission which could be resolved into two bands, 405 and 465 nm. The band at 405 nm is most expectedly the emission from **TPy** *via* FRET and the broad long wavelength emission at 465 nm is most likely from an exciplex of **TMNap**–**TPy** (**Figure 2.25 d**). Further analysis revealed that the emission intensity of the donor, ^{TMNap}**Ala**^{Do}, decreased seven times of that of the free donor fluorescence in buffer (**Figure 2.25 d**).

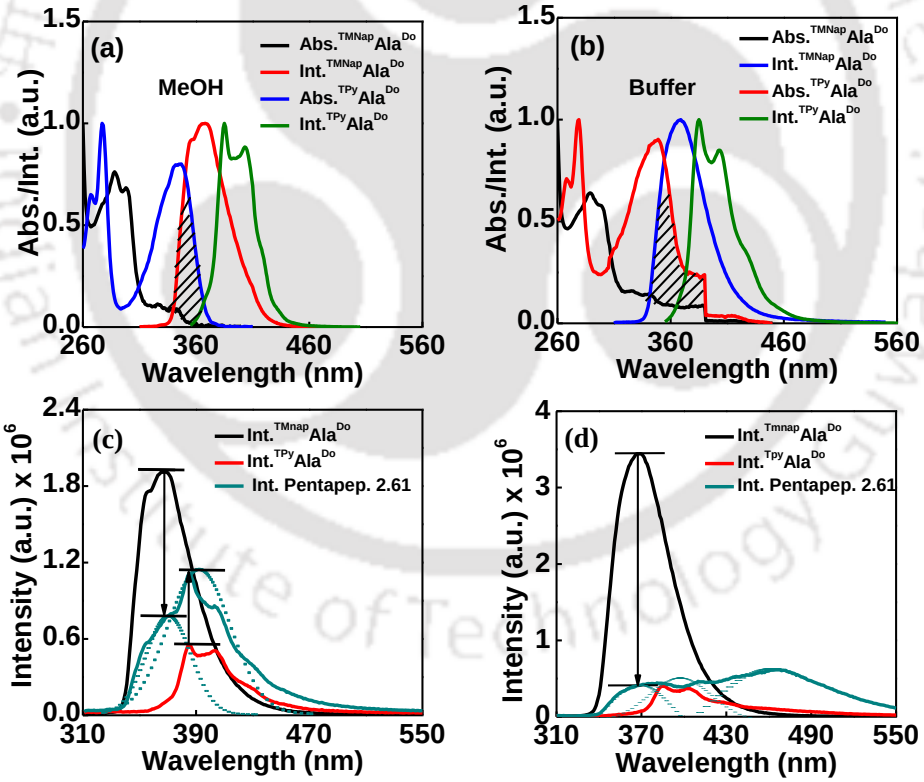

Figure 2.25. Overlap spectra of two monomers ^{TPy}**Ala**^{Do} and ^{TMNap}**Ala**^{Do} in MeOH (a) and Buffer (b). Steady state intensity comparison spectra of two monomers ^{TPy}**Ala**^{Do}, ^{TMNap}**Ala**^{Do} and Pentapep. **2.61** (λ_{ex} = 300 nm) in MeOH (c) and Buffer (d).

While in methanol, a two times increase in emission intensity of the acceptor, ^{TPy}**Ala**^{Do} was observed with no band at 465 nm (**Figure 2.25 c**), in buffer the ^{TPy}**Ala**^{Do} monomer emission from peptide **2.61** decreased compared to the free acceptor emission along with a new emission (exciplex) band at 465 nm (**Figure 2.25 d**). Therefore, the change in donor/acceptor emissions supported a FRET process from ^{TMNap}**Ala**^{Do} to ^{TPy}**Ala**^{Do} in peptide **2.61** in both solvents.

A gradual decrease in the emission intensity as well as life time of emission at 465 nm with increasing temperature indicated a breakdown of π-stacked excited state complex (exciplex) between **TMNap** and **TPy** confirming the exciplex emission in peptide **2.61** (**Figure 2.26 a-b**). The close proximity guided high possibility of formation of π-π stacked complex between excited state triazolylpyrene (**TPy**) at the *C*-terminus and ground state triazolyl methoxynaphthalene (**TMNap**) at the *N*-terminus was supported from a 2D NMR (**Figure 2.19**) as well as by a molecular dynamics (MD) simulation (**Figure 2.20**). Moreover, the excitonic interactions among the terminal fluorescent amino acids as was seen in the absorption/emission spectra further supported π-π stacked complexation between **TPy** and **TMNap**. All the observations evident our fundamental concept of FRET mediated exiplex emission in a β-sheet fluorescent pentapeptide **2.61**.

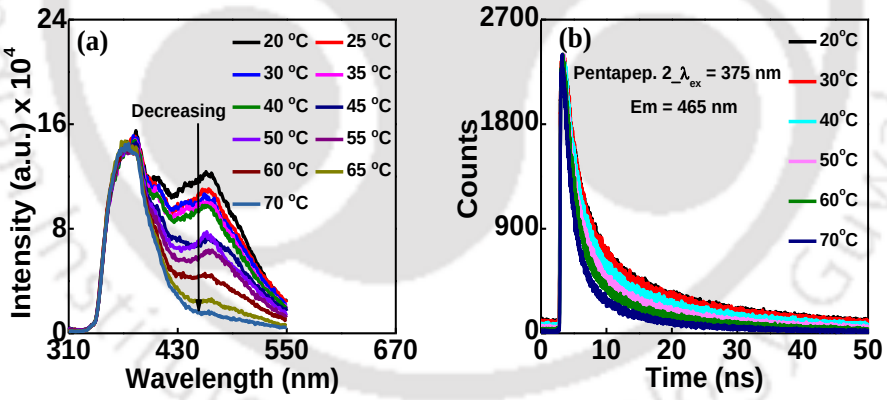

Figure 2.26. Temperature variable fluorescence spectra (a) and time resolved spectra (b) of peptide **2.61** in buffer showing FRET-mediated exciplex emission.

After investigation and establishing the fundamental aspects of exciplex emission via FRET in the peptide **2.61**, we turned our attention to prove the second path of exciplex formation via direct excitation at the FRET acceptor, **TPy**. Thus, upon excitation at the absorption wavelength of FRET acceptor, **TPy**, of *N*-terminal ^{TPy}**Ala**^{Do} (λ_{ex} = 347 nm), the peptide **2.61** showed two emission bands at 405 and 465 nm which are superimposable to the spectrum obtained when excited at the donor absorbance maximum (λ_{ex} = 300 nm of **TMNap**, of *C*-terminal ^{TMNap}**Ala**^{Do}) and are

unambiguously assigned as monomer emission from **TPy** and the exciplex emission from π-stacked **TPy-TMNap** complex, respectively. The second path of exciplex emission was further supported both from a variable temperature steady state as well as time resolve fluorescence experiment (**Figure 2.26**, **a-b**).

The occurrence of a FRET process was also evident from a time resolved fluorescence study wherein we observed a decrease in donor life time ($^{\mathbf{TMNap}}\mathbf{Ala}^{\mathbf{Do}}$; λ_{ex} = 290 nm, λ_{em} = 365 nm) from 8.8 to 7.1 ns. However, we observed a decrease in acceptor (**TPy**) emission intensity as well as life time ($^{\mathbf{TPy}}\mathbf{Ala}^{\mathbf{Do}}$; λ_{ex} = 290 nm, λ_{em} = 405 nm) from 67.2 ns to 16.6 ns with an appearance of exciplex band at 465 nm of life time 19 ns. The decreased acceptor's intensity/life time could be explained considering n-π* quenching of **TPy** monomer (acceptor) emission by closely spaced donor **TMNap** through –OMe group leading to decrease in monomer emission and formation of **TPy–TMNap** exciplex complex (**Figure 2.27**, **Table 2.8**).

The nucleation by the $\mathbf{U^rAA}$ scaffold into a β-sheet conformation played an important role in bringing the two terminal fluorescent amino acids closer and to interact photophysically leading to an exciplex emission in peptide **2.61** (**ExciFRET-peptide**) via two path-either via FRET or via direct excitation of the FRET acceptor. To the best of our knowledge this fundamental phenomenon is new and will open an avenue for designing such probes for application in chemical biology. This is neither an accidental discovery nor a system to show merely the **TPy–TMNap** exciplex emission but a judiciously designed and properly positioned donor/acceptor pair involved in π-π stacking interaction in the fluorescent peptide-probe reporting for the first time. Here $\mathbf{U^rAA}$ scaffolded predefined secondary structure impacted greatly to offer predicted photophysical property.

After establishing the fundamental concept of dual door entry to exciplex emission in **ExcipFRET-peptide 2.61**, we next studied the photophysical interaction between the two terminal **TPy** moieties in **Excim-peptide 2.64**. The UV-visible absorption spectra of peptide **2.64** showed bands at 268, 277 and 347 nm corresponding to the uracil absorption, and absorption of **TPy**, respectively, in methanol (**Figure 2.24 a**). Upon excitation at long wavelength absorption band (λ_{ex} = 347 nm), the peptide showed dual emission centred at 405 nm corresponds to the structured triazolyl pyrene monomer emission and unstructured broad emission at 475 nm which was unambiguously assigned as an excimer emission (**Figure 2.24 b**). Support for an excimer emission also came from a fluorescence life time experiment (**Table 2.9**), where excimer emission band shows the life time 17.6 ns and 22.1 ns in methanol and buffer solvent respectively (**Figure 2.28 b**, **Table 2.9**). The H-bonding and side chain hydrophobic interaction between the two dipeptide arms of the scaffold in the β-sheet conformation allowed the terminal $^{\mathbf{TPy}}\mathbf{Ala}^{\mathbf{Do}}$ to come closer to involve in π-π-stacking

interaction leading to **TPy–TPy** excimer emission. This was also supported by CD, 2D NMR spectroscopy as well as a molecular dynamics (MD) simulation study.

Table 2.8. Summary table of time resolved fluorescence spectroscopy of **ExcipFRET-peptide 2.61**, and monomers ^{TMnap}**Ala**^{Do} and ^{TPy}**Ala**^{Do} at λ_{ex} **= 290 nm.**

Entry	Solvents	Φ_f	λ [nm]	τ_1 [ns]	τ_2 [ns]	<τ> [ns]	k_f [$10^8 s^{-1}$]	k_{nr} [$10^8 s^{-1}$]	χ^2
^{TMnap}**Ala**^{Do}	**MeOH**	0.29	365	1.5 (6 %)	7.1 (94 %)	6.8	0.04	0.10	1.02
	Buffer	0.14	365	8.8 (100 %)	--	8.8	0.02	0.1	1.07
^{TPy}**Ala**^{Do}	**MeOH**	0.15	405	17.7 (100%)	---	17.7	0.01	0.05	1.04
	Buffer	0.15	405	7.9 (4 %)	69.6 (96%)	67.2	0.002	0.012	0.99
ExcipFRET-peptide 2.61	**MeOH**	0.09	365	0.9 (13 %)	5.4 (87 %)	4.9	0.02	0.19	0.98
	Buffer	0.07	365	6.4 (85 %)	10.9 (15%)	7.2	0.01	0.13	1.03
ExcipFRET-peptide 2.61	**MeOH**	0.2	405	6.0 (23%)	19.2 (77%)	16.1	0.01	0.05	1.02
	Buffer	0.043	405	1.8 (31 %)	7.0 (45 %) / 51.9 (24 %)	16.6	0.003	0.06	1.05
	Buffer	0.13	465	6.4 (49 %)	30.6 (51%)	19.0	0.007	0.05	1.1

For lifetimes of the fluorescent amino acids and peptides at λ_{ex} = 290 nm; Concentration of each compound = 10 μM; <τ>, k_f, and k_{nr} are weighted means from the biexponential/triexponential fits: $<\tau> = 1/(\alpha_1/\tau_1 + \alpha_2/\tau_2)$, $k_f = \Phi_f/<\tau>$, and $k_{nr} = (1 - \Phi_f)/<\tau>$.

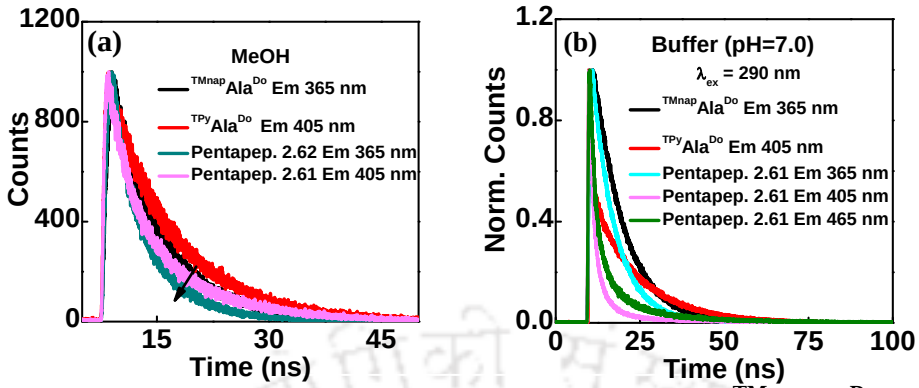

Figure 2.27. Time resolved fluorescence of two monomers ^{TMnap}**Ala**^{Do} (**2.66**), ^{TPy}**Ala**^{Do} (**2.65**) and **ExcipFRET-peptide 2.61** using λ_{ex} **= 290** (a) λ_{em} = 365, 405 in MeOH and (b) λ_{em} = 365, 405, 465 in buffer solvent.

Table 2.9: Summary table of fluorescence lifetimes of monomers ^{TMnap}**Ala**^{Do} (**2.66**), ^{TPy}**Ala**^{Do} (**2.65**), **ExcipFRET-peptide 2.61** and **Excim-peptide 2.64** at λ_{ex} **= 375 nm**

Entry	Solvents	Φ_f	λ [nm]	τ_1 [ns]	τ_2 [ns]	$\langle\tau\rangle$ [ns]	k_f [$10^8 s^{-1}$]	k_{nr} [$10^8 s^{-1}$]	χ^2
^{TPy}**Ala**^{Do}	**MeOH**	0.15	405	17.4 (100%)	---	17.4	0.01	0.05	0.9
	Buffer	0.15	405	9.2 (35 %)	60.7 (85 %)	42.8	0.002	0.02	1.0
ExcipFRET-peptide 2.61	**MeOH**	0.22	405	4.6 (32 %)	17.5 (68 %)	29.5	0.007	0.03	1.0
	Buffer	0.043	405	1.6 (61 %)	7.3 (39 %)	3.9	0.01	0.3	1.0
	Buffer	0.13	465	2.5 (30 %)	14.3 (70 %)	12.5	0.01	0.07	1.0
Excim-peptide 2.64	**MeOH**	0.1	405	5.6 (44 %)	15.0 (56 %)	10.8	0.01	0.08	0.9
	Buffer	0.013	405	7.8 (81 %)	43.5 (19 %)	14.9	0.001	0.07	1.1
Excim-peptide 2.64	**MeOH**	0.18	485	17.8 (100 %)	---	17.8	0.01	0.05	0.9
	Buffer	0.2	475	8.9 (49 %)	34.6 (51 %)	22.1	0.01	0.04	1.1

For lifetimes of the fluorescent amino acids and peptides at λ_{ex} = 336 nm; Concentration of each compound = 10 μM; $\langle\tau\rangle$, k_f, and k_{nr} are weighted means from the biexponential/triexponential fits: $\langle\tau\rangle = 1/(\alpha_1/\tau_1 + \alpha_2/\tau_2)$, $k_f = \Phi_f/\langle\tau\rangle$, and $k_{nr} = (1-\Phi_f)/\langle\tau\rangle$.

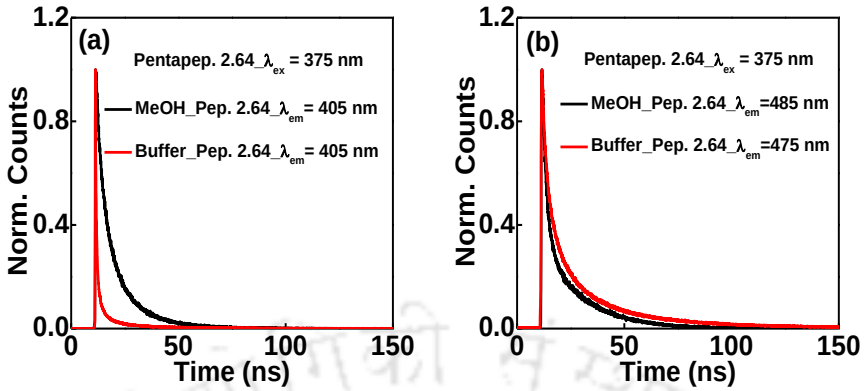

Figure 2.28. Time resolved fluorescence of monomer ^{TPy}**Ala**^{Do} (**2.65**) and **Excim-peptide 2.64** using λ_{ex} **= 375** (a) λ_{em} = 405 nm and (b) λ_{em} = 485, 475 nm.

2.4.3.2. Calculation of the Forster distance and FRET efficiency in Methanol Solvent:

For the FRET the fluorescence resonance energy transfer (FRET) and the Förster distance were calculated using the following three equations. The efficiency of energy transfer, *E*, was calculated using the equation (1)

$$E = \frac{R_0^6}{R_0^6 + r^6} = 1 - \frac{F}{F_0} \quad \text{.....(1)}$$

where *F* and F_0 are the fluorescence intensity of donor in the presence and absence of acceptor, *r* is the distance between donor and the acceptor and R_0 is the critical distance when the energy*v* transfer efficiency is 50% . The Förster distance R_0 (Å) was calculated by the following equation (2)

$$R_0 = [8.79\times10^{-5}\kappa^2 n^{-4}\Phi_D J(\lambda)]^{1/6} \text{ .....(2)}$$

where κ^2 is the orientation, *n* is the refractive index of the medium, Φ_D is the quantum yield of the donor in the absence of acceptor $J(\lambda)$ is the overlap integral of the fluorescence emission spectrum of the donor and the absorption spectrum of the acceptor given by the following equation (3)

$$J = \frac{\int_0^\infty F_D(\lambda)\varepsilon_A(\lambda)\lambda^4 d\lambda}{\int_0^\infty F_D(\lambda) d\lambda} \text{.....(3)}$$

where $F_D(\lambda)$ is the fluorescence intensity of the donor in the wavelength range λ to $\lambda + \Delta\lambda$ with the total intensity normalized to unity. $\varepsilon_A(\lambda)$ is the molar extinction coefficient of the acceptor as a function of wavelength (λ).

For calculating the Förster radius we chose two possible values for the orientation factor (κ^2) following a literature report.[35] Though the chromophoric units were placed in two side chains of two terminal amino acids via a triazole rigid linker, the β-sheet induction by the scaffold made the two connected dipeptidic arms flexible and allowed the terminal amino acid containing chromophores to freely move and to come closer for a photophysical interaction. Therefore the κ^2 was considered to most possibly be 0.666 (considering rapid dynamic averaging within the donor excited-state lifetime). However, as we are at this stage unable to provide angles between the transition dipoles, i.e., the characteristic angular parameter κ^2, so we also calculated R_0 values considering rigid donor acceptor conformation i.e. by considering $\kappa^2 = 0.476$ to test the deviations in calculations we primarily chose both the κ^2 values for evaluating R_0 values.[35-37]

Thus, using the values of $\kappa^2 = 2/3$, $n = 1.33$, $\Phi_D = 0.24$, and the obtained overlap integral, $J(\lambda) = 4.14 \times 10^{16}$, the R_0 and r values were calculated which were found to be $R_0 = 75$ Å and $r = 71$ Å. On the other hand, R_0 and r values were found to be = 71 Å and $r = 67$ Å, respectively, using $\kappa^2 = 0.476$. Therefore, a deviation of $\pm$ 4 Å in R_0 measurement was the result. Following this minimal deviation we consider $\kappa^2 = 0.666$ and calculated all other parameters throughout the thesis. R_0 is the critical distance when the energy transfer efficiency is 50 % and r is the distance between the donor and acceptor.

Energy Transfer efficiency (E) = $1 - F/F_0 = 59$ %. F and F_0 are the fluorescence intensity of donor in the presence and absence of acceptor.

2.4.4. Study of Interaction of our Synthesized peptides with BSA Protein

The exciplex and excimer emissive peptides could serve as sensitive probes for studying protein–peptide/peptide–DNA interaction and in wider application such as for visualizing intracellular events and understanding molecular interactions inside a cell.[30] We thought that the monomer/exciplex and monomer/excimer emission from peptide **2.61** and **2.64**, respectively, might offer some interesting insight into model BSA-peptide interaction.

Among various major soluble and transport proteins found in blood plasma, serum albumins have many biological functions.[38] They serve as a transporter for many compounds like fatty acids bilirubin, bile salts, lecithin nutrients, steroids, hormones and a variety of therapeutic drugs.[39] Out of available serum albumins, BSA is the most studied model as it is easily available and structurally similar to human serum albumin (HSA).[40] The sequence of BSA displays 75% identity and 87% similarity with HSA. The shape of the protein is roughly heart shaped and has three domains I, II, III and two binding sites Site-I and site-II. Studies on the drug binding

events with BSA revealed that site-I dominated by strong hydrophobic interaction and site-II dominated by interaction of hydrophobic, H-bonding and electrostatic interaction. The ligands in site-I are generally remained in the vicinity of tryptophan, that serve as an efficient energy donor. Therefore BSA was chosen as a model protein for studying peptide–protein interaction with the help of UV-Vis and fluorescence spectroscopy.

Thus, we, finally, studied the interaction using UV-visible absorption spectroscopy. In phosphate buffer the probe **ExcipFRET-peptide 2.61** and **Excim-peptide 2.64** exhibited weak and structureless absorptions at around 300 and 347 nm, corresponding to **TMNap** and **TPy**, respectively (**Figure 2.29 a-c**). Upon gradual addition of BSA to a solution of the **ExcipFRET-peptide 2.61** and/or **Excim-peptide 2.64**, the absorption bands experienced strong hyperchromicity along with a hypsochromic shift of 18 and 10 nm, respectively, indicating a strong binding interaction between both the probes and BSA in the hydrophobic region (**Figure 2.29**).

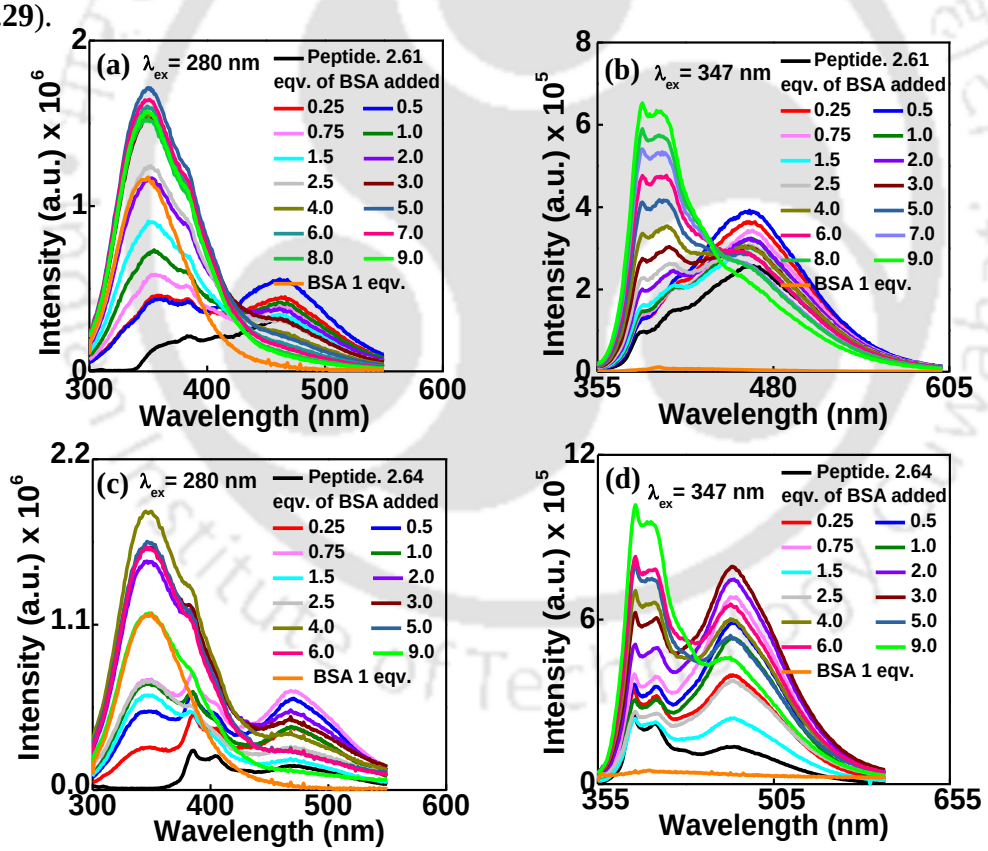

Figure 2.29. Fluorescence titration of **ExcipFRET-peptide** probe **2.61** (a-b) and **Excim-peptide 2.64** (c-d) in presence and absence of increasing concentration of BSA showing dual path entry to exciplex in **2.61** and excimer in **2.64** [λ_{ex} = 280 nm; for (a), (c) and λ_{ex} = 347 nm for (b), (d), concentration of peptide = 5 μM]. All the experiments were carried out in 5 mM phosphate buffer, pH 7.0, r.t.

The Job's plots suggested a 1:1 probe: BSA binding events in all the cases with association constants ranging from 0.5-1.3 x 10^5 M^{-1} and binding free energy of around -6 to -7 kcal/$mole^{-1}$.

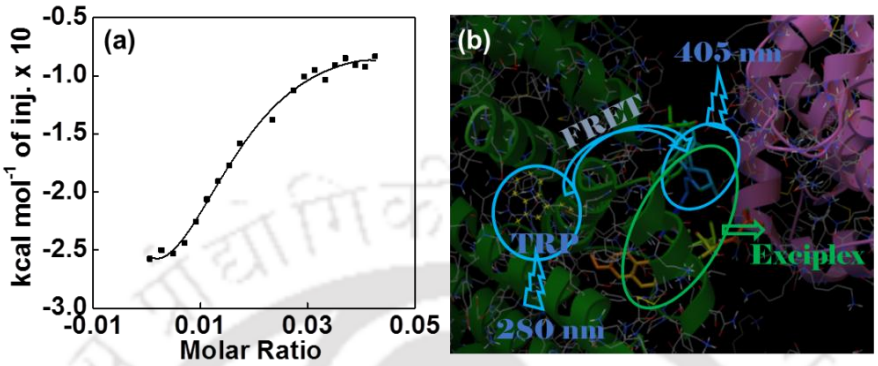

Figure 2.30. (a) Integrated heat profile of the ITC with non–Linear-squares fit to a one-site binding model and (b) docking pose of **ExcipFRET-peptide 2.61** in presence of BSA.

In addition to this, a fluorescence titration experiment was carried out to investigate the protein sensing ability and to gain insight into the interaction of the probes with BSA. Thus, the **ExcipFRET**-peptide **2.61** showed a regularly increased **TPy** monomer emission (405 nm) and exciplex emission (465 nm) when excited either at BSA (280 nm) or **TMNap** (300 nm) upon gradual addition of an increasing amount of BSA (**Figure 2.29-a**). Analysis of emission of BSA, probe **2.61** and a 1:1 mixture indicated a decrease in emission of BSA or **TMNap** along with an enhancement of **TPy** monomer emission and of **TPy–TMNap** exciplex emission clearly indicating a FRET mediated exciplex emission. Similar increase in both the emission at 405 nm (**TPy** emission) and at 470 nm (exciplex) was observed when excited at **TPy** (350 nm) upon gradual increase in the concentration of BSA (**Figure 2.29-b**). All the observations were further supported from ~~a~~ time resolve fluorescence study. The exciplex emission intensity decreased slightly at high BSA concentration possibly due to encumbering **TPy** moiety in the hydrophobic pocket that restricts formation of π-π- stacked **TPy–TMNap** complex leading to an ultimate increase in **TPy** monomer emission. This explanation was also supported from anisotropy experiment, a small excimer/monomer intensity ratio and life time experiment. Therefore, the **ExcipFRET-peptide 2.61** maintained its photophysics in BSA microenvironment and behaved as a system of dual path to exciplex emission-either via FRET (from **BSA** or **TMNap** to **TPy**) or direct excitation of a FRET acceptor (**TPy**). The backbone H-bond mediated intrastrand β-sheet conformation in both the peptides nucleated by the scaffold **U^rAA** played an important role in bringing two

terminal chromophoric amino acids closer leading to predefined photophysical interactions and exciplex/excimer formation.

On the other hand, on addition of an increasing concentration of BSA, both the monomer at 405 nm and the excimer emission at 475 nm of the probe **2.64** increased gradually (λ_{ex} = 280 nm) (**Figure 2.29 c**). Closer look at emission of only BSA, only probe **2.64** and 1:1 mixture indicated a decrease in emission of BSA and an increase in both monomer emission from **TPy** (405 nm) as well as **TPy**–T**Py** excimer emission at 475 nm when excited at BSA absorption (280 nm) (**Figure 2.29 c**). Moreover, on excitation at **TPy** (λ_{ex} = 347 nm), both the monomer emission at 405 nm and the excimer emission at 485 nm of the probe **2.64** increased gradually as BSA concentration increases (**Figure 2.29 d**). All spectroscopic outcomes unambiguously indicated the excimer emission via FRET from BSA to **TPy** in peptide **2.26** when excited at BSA (280 nm) which was also supported from time resolved fluorescence study. Therefore, in BSA microenvironment, the probe **2.64** behaved as a system of dual path to excimer emission-eitheir via FRET (from **BSA** to **TPy**) or direct excitation of a FRET acceptor (**TPy**). The slight decrease in excimer emission at high BSA concentration, a small change in anisotropy and excimer/monomer intensity ratio indicated that the **TPy**–T**Py** excimer formation was restricted as the concentration of BSA increased which was also supported from ~~a~~ life time experiment. All the observations could be explained if we consider single site binding of the probe **2.64** leading to encumbering **TPy** moiety in the hydrophobic pocket of BSA which might be the possible cause of low FRET efficiency as the concentration of BSA increased ultimately leading to a restricted **TPy–TPy** excimer formation. The binding event was also supported from an ITC experiment as well as from a molecular docking calculation. The binding events from an ITC experiment indicated a single event binding with affinity of 0.5 $\times 10^5$ M^{-1} and a free energy change of -6 to -6.9 kcal/mol (**Figure 2.30 a**). The docking study showed the binding of the probes in hydrophobic pocket of site I in the vicinity of Trp 134 supporting the close proximity and FRET incidences in both the cases (**Figure 2.30 b**).

2.5. Conclusion

In summary, the newly designed uracil-amino acid (**U^{r}AA**) in the peptide backbone marked a novel class of unnatural peptide building block with ability to induce β-sheet conformation. We established the dual mechanism of exciplex emission in a designed **ExcipFRET-peptide 2.61** and excimer emission in an **Excim-peptide 2.64**. Both the peptides maintainning their predefined photophysics were found to interact with a model biomolecule with fluorescence swith-on response. This is the first report of design of a fluorescent peptide with a predefined secondary

structure together with predicted photophysical properties. Under study is the exploration of sequence specific DNA binding event of uracil-amino acid (**U^{r}AA**) scaffold and study of interaction with other protein biomolecules.

2.6. Experimental Section

2.6.1. Materials and Methods

All reactions were carried out under inert atmosphere using flame-dried glassware. Combined organic layers were dried over anhydrous sodium sulfate. After work up solvents were removed in a rotary evaporator under reduced pressure. For column chromatography Silica gel (60-120 mesh) was used. Reactions were monitored by TLC on silica gel 60 F254 (0.25). BSA, Na_2HPO4 and $NaH_2PO_4.H_2O$ (for preparation of phosophate buffer) were purchased from Merck, India and used without further purification. Milli-Q Water was taken for solution preparation. All solutions were prepared freshly before doing the experiments. The probe molecules (**ExcipFRET-peptide 2.61** and **Excim-peptide 2.64**) were synthesized and purified according to the procedure described.

^{1}H NMR spectra were recorded either at 400 MHz or at 600 MHz and ^{13}C NMR spectra were recorded either at 100 MHz or at 150 MHz (mentioned accordingly). Coupling constants (*J* value) were reported in hertz (Hz). The chemical shifts were shown in ppm downfield form tetramethylsilane (TMS), using residual chloroform (δ = 7.26 in ^{1}H NMR, δ = 77.23 in ^{13}C NMR), DMSO (δ = 2.5 in ^{1}H NMR, δ = 39.5 in ^{13}C NMR), as an internal standard. Mass spectra were recorded with a HR mass spectrometer and data analysed by using built-in software. IR spectra were recorded in KBr on a FT-IR spectrometer. All 2D NMR Experiments were carried out on 600 MHz spectrometer at room temperature using 7 - 10 mM concentration in d_6-DMSO solvent. Spectra were acquired with 2048 x 256 in both dimension (F2 and F1) and other parameters are given below.

TOCSY : Free induction decay (FID) with NS = 16 and DS =32, relaxation delay (D1) 2s, mixing time (D9) 0.08s, acquisition time (AQ) 0.085s, spectral width 12019 Hz.

ROESY : Free induction decay (FID) with NS = 16 and DS =16, relaxation delay (D1) 2s, mixing time (P15) 0.02s, acquisition time (AQ) 0.085s, spectral width (SWH) 12019 Hz.

NOESY : Free induction decay (FID) with NS = 8 and DS =16, relaxation delay (D1) 2s, mixing time (D8) 0.6s, acquisition time (AQ) 0.085s, spectral width (SWH) 12019 Hz.

2.6.2. General Procedures for the Synthesis of Uracil Amino Acid Scaffold and Target Peptides

General procedure for the peptide coupling: *N*-protected amino acid or peptide (1.0 equivalent) is taken in dry DCM or 3:1 mixture of dry DCM and DMF, then 1-[3-dimethyl amino propyl]-3-ehtylcarbo-diimide hydrochloride (EDC.HCl) (1.2 equivalent) and HOBT (1.2 equivalent) were added simultaneously to the reaction mixture at 0 ^{o}C under inert N_2 atmosphere. The reaction mixture was kept under stirring for 1h maintaining 0 ^{o}C. –COOH protected amino acids or peptides (1.0 equivalent) was added followed by diisopropylethylamine (DIPEA) (2.4 equivalent) and stirring was continued for 0.5 h maintaining 0 ^{o}C. The ice bath was then removed and the reaction mixture was stirred for another 12-15 h at room temperature. The solvent was dried by rotary evaporator, and the work up was done with EtOAc and aqueous $NaHCO_3$ solution. The combined organic layer was washed with brine solution dried over anhydrous Na_2SO_4 and concentrated under reduced pressure. The residue was purified by column chromatography on silica gel (eluent: petroleum ether/ethyl acetate) to afford the peptides and characterized.

General procedure for [3+2] cyclo-addition reaction: The azide compound was taken in dry THF under nitrogen atmosphere. Alkyne (1.1 equivalent) was added followed by 1 mol % CuI. Then 1.2 equivalent DIPEA was added to the reaction mixture and it was allowed to stir for 10-12 h at about 65 to 70 ^{o}C. Upon completion of reaction (monitored by TLC), the reaction mixture was concentrated by rotary evaporator and then diluted with EtOAc. Work up was done with EtOAc and NH_4Cl solution. The combined organic layer was washed with brine solution dried over anhydrous Na_2SO_4 and concentrated under reduced pressure. The residue was purified by column chromatography on silica gel (eluent: petroleum ether/ethyl acetate) to afford the title trizolyl unnatural peptides and characterized.

General procedure for the deprotection of the methyl ester: COOH protected amino acid or peptide was taken in THF : H_2O = 2 : 1, then lithium hydroxide (1.5 equivalent) was added at 0 ^{o}C. The reaction mixture was stirred for about 1-2 hour. Upon completion of reaction (monitored by TLC), solvent was dried by rotary evaporator. Then water (4-5 ml) was added to the reaction mixture and cooled to 0 ^{o}C. 1(N) HCl was added to the reaction mixture to adjust pH- 3 to 4. Work up was done with EtOAc and water. The combined organic layer was washed with brine solution

dried over anhydrous Na_2SO_4 and concentrated under reduced pressure. The hydrolysed compound was isolated by column chromatography (Si-gel, $CHCl_3$: MeOH = 10:1). Yield was 90-96%.

General procedure for the deprotection of the** BocNH–**protecting group: Respective NH–Boc protected amino acids or peptides were taken in dry RB, then dissolved in CH_2Cl_2 and allowed to cool to 0 °C. TFA (equal amount as the solvent) was added to the solution and it was allowed to warm to room temperature. After stirring at room temperature until starting material was consumed (TLC monitoring), the reaction mixture was concentrated *in vacuo*. The residual TFA was evaporated by evaporating the mixture with dry toluene thrice, evaporated thrice and dried in high vaccum to afford the product in quantitative yield.

2.6.3. Synthesis of Uracil Amino Acid Scaffold (2.43, U^{r}AA)

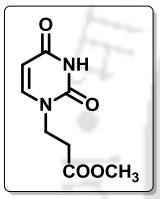

Synthesis of methyl 3-(2,4-dioxo-3,4-dihydropyrimidin-1(2H)-yl)propanoate (2.42): Natural uracil **2.41** (1000 mg, 8.93 mmol) was taken in a dry RB then dry DMSO was added to it, then methyl 3-bromopropanoate (1.22 ml, 11.16 mmol) is added into it followed by K_2CO_3 (1540.4 mg, 11.16 mmol) and the mixture was allowed to stirr at room temperature for 12 hours. After completion of the reaction (Monitered by TLC), the reaction mixture was diluted with EtOAc and washed with water. Combined organic layer was dried over anhydrous Na_2SO_4, concentrated in *vacuo* and purified by coloumn chromatography (Si-gel, PE:EA = 1:3). Compound **2.42** obtained in pure form 1400mg as white solid. Yield 79%. mp 117-120 ^oC. IR (KBr) 3012, 1733, 1703, 1667, 1422, 1375, 1177, 898 cm^{-1}. ^1H NMR (CD_3OD; 600 MHz) δ 2.74 (2H, t, J = 5.4 Hz), 3.64 (3H, s), 3.94 (2H, t, J = 5.4 Hz), 5.61 (1H, d, J = 7.8 Hz), 7.40 (1H, d, J = 7.2 Hz). ^{13}C NMR (CD_3OD; 150 MHz) δ 32.5, 45.2, 51.9, 101.5, 146.1, 151.1, 164.8, 171.9. HRMS calcd. for $C_8H_{11}N_2O_4$ $[M + H]^+$ 199.0713, found 199.0713.

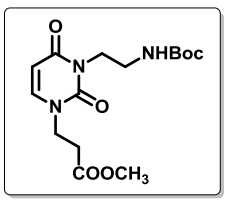

Synthesis of U^{r}AA (2.43): Methyl 3-(2,4-dioxo-3,4-dihydropyrimidin-1(2H)-yl)propanoate **2.42** (1400 mg, 7.07 mmol) was taken in a dry RB andthen dry DMSO was added to it, tert-butyl (2-iodoethyl) carbamate (2300 mg, 8.48 mmol) is added into it followed by K_2CO_3 (1171 mg, 8.48 mmol) and the mixture was allowed to stirr at room temperature for 12 hours. After completion of the reaction (Monitered by TLC), work up is done with EtOAc and water. Combined organic layer was dried over anhydrous Na_2SO_4, concentrated in vacuo and purified by coloumn chromatography (Si-gel, PE:EA = 1:1) in pure form 2050 as white solid. Yield 85%. mp 94-98 ^oC; IR (KBr) 3295, 2980, 1741, 1700,

1652, 1536, 1461, 1367, 1211, 1165, 981, 768 cm-1. ^{1}H NMR ($CDCl_3$; 600 MHz) δ 1.37 (9H, s), 2.80 (2H, s), 3.41 (2H, d, J = 4.2 Hz), 3.68 (3H, s), 3.99 (2H, t, J = 5.4 Hz), 4.08 (2H, s), 4.95 (1H, bs), 5.67 (1H, d, J = 7.8 Hz), 7.34 (1H, d, J = 7.8 Hz). ^{13}C NMR ($CDCl_3$; 150 MHz) δ 28.4, 77.3, 80.9, 83.5, 119.2, 122.1, 122.8, 126.8, 129.1, 138.5, 152.7. ^{13}C NMR ($CDCl_3$; 150 MHz) δ 28.4, 32.7, 39.2, 40.7, 46.2, 52.2, 79.2, 101.2, 143.9, 151.6, 156.2, 163.7, 172.2. HRMS calcd. for $C_{15}H_{24}N_3O_6$ $[M + H]^+$ 342.1660, found 342.1660.

Synthesis of BocNH–U^{r}AA–COOH (2.44): Using the general procedure of ester hydrolysis, starting from 2050 mg (6.01 mmol) of **2.43**, 1750 mg (5.35 mmol) of the title compound **2.44** was isolated as a white solid material. Yield 89%. mp 110-115 ^{o}C; IR (KBr) 3363, 2981, 1734, 1680, 1645, 1610, 1529, 1466, 1283, 1159, 800, 646 cm^{-}1. ^{1}H NMR ($CDCl_3$; 600 MHz) δ 1.34 (9H, s), 2.72 (2H, s), 3.33 (2H, d, J = 4.8 Hz), 3.97 (2H, d, J = 6.0 Hz), 4.01 (2H, d, J = 3.6 Hz), 5.65 (1H, d, J = 7.8 Hz), 7.39 (1H, bs). ^{13}C NMR ($CDCl_3$; 150 MHz) δ 28.3, 32.7, 38.6, 40.8, 46.3, 49.0, 79.5, 100.9, 144.7, 151.7, 156.8, 164.4, 173.5. –APCI-MS calcd. for $C_{14}H_{20}N_3O_6$ $[M - H]^-$ 326.13, found 326.12.

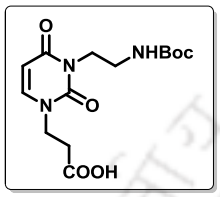

2.6.4. Synthesis of Fluorescent Pentapeptides 2.61, 2.64 and Triazolyl Unnatural Fluorescent Amino Acids 2.65 and 2.66.

Synthesis of BocNH–Ser(N$_3$)–CONMe(OMe) (2.45): From our previously published method from 2500 mg (12.5 mmol) of NBocNH–protected L-serine, 1350 mg (4.93 mmol) of the title compound **2.45** was preapred. Overall Yield 75 %.

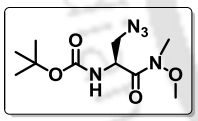

Synthesis of TFA salt of BocNH–Ser(N$_3$)–CONMe(OMe) (2.46): Using the general procedure of BocNH–deprotection, BocNH–Ser(N$_3$)–CONMe(OMe) (500 mg, 1.832 mmol) was reacted with TFA to get the compound **2.46** in quantitative (96 %) yield and was used for the next step without further purification and characterization.

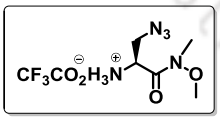

Synthesis of BocNH–Leu–Ser(N$_3$)–CONMe(OMe) (2.48) : Using general procedure of peptide coupling, BocNH–protected leucine **2.47** (1000 mg, 4.32 mmol) was taken as as starting material then 752 mg (4.32 mmol) of Boc-deprodected serine azide was reacted with it. After completion of reaction 1165 mg (3.02 mmol) of the title compound **2.48** was isolated in pure form by column chromatography (Si-gel, PE : EtOAc = 2:1) as colourless gummy material. Yield 70%. IR (KBr) 3331, 2964, **2105**, 1684, 1649, 1524, 1277, 1174, 1046, 993, 614 cm-1. ^{1}H NMR ($CDCl_3$; 600 MHz) δ 0.93 (6H, t, J = 4.8 Hz), 1.44 (9H, s), 1.48-1.54 (1H,

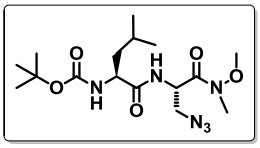

m), 1.67 (2H, bs), 3.23 (3H, s), 3.55-3.66 (2H, m), 3.76 (3H, s), 4.17 (1H, bs), 4.88 (1H, bs), 5.06 (1H, bs), 7.11 (1H, bs), ^{13}C NMR ($CDCl_3$; 150 MHz) δ 21.9, 23.2, 24.9, 28.5, 32.5, 41.5, 49.8, 52.0, 53.5, 61.9, 80.4, 155.8, 169.1, 172.8. +APCI-MS calcd. for $C_{16}H_{31}N_6O_5$ $[M + H]^+$ 387.23, found 387.22.

Synthesis of TFA salt of BocNH–Leu-Ser(N_3)–CONMe(OMe) (2.49): Using the general procedure of BocNH–deprotection, compound **2.48** was reacted with TFA to get the compound **2.49** in quantitative (95%) yield and was used for the next step without further purification and characterization.

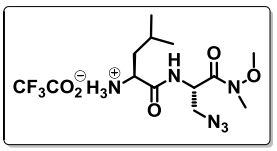

Synthesis of BocNH–U^{r}AA–Leu–Ser(N_3)–CONMe(OMe) (2.50) : U^{r}AA scaffold **2.44** (872 mg, 2.65 mmol) was taken in dry DMF, 1-[3- dimethyl amino propyl]-3-ehtylcarbo-diimide hydrochloride (EDC.HCl) (612 mg, 3.204 mmol), followed by DMAP (717 mg, 5.874 mmol) were added at 0 ^{o}C. Then compound **2.49** was added and the reaction mixture was stirred for 1h at 0 ^{o}C, after that ice bath is removed and the reaction mixture was allowed to stir at room temperature for 18h. After completion of the reaction (monitored by TLC), the solvent was dried by rotary evaporator. Work up was done with EtOAc and $NaHCO_3$ solution. Combined organic layer was washed with brine solution and concentrated in reduced pressure. The product tripeptide **2.50** (1130 mg, 1.89 mmol) was isolated in pure form by column chromatography (Si-gel, PE : EtOAc = 1:3) as colorless gummy material . Yield 71%. IR (KBr) 3452, 2960, 2108, 1702, 1548, 1658, 1461, 1367, 1171, 768 cm^{-1}. ^{1}H NMR ($CDCl_3$; 600 MHz) δ 0.91 – 0.86 (6H, m), 1.41 (9H, s), 1.63 (2H, s), 1.89 (1H, s), 3.22 (3H, s), 3.49 – 3.35 (2H, m), 3.62 (2H, s), 3.77 (3H, s), 3.81 (2H, d, *J* = 12.4 Hz,), 3.94 (1H, d, *J* = 12.4 Hz), 4.16 (1H, d, *J* = 13.5 Hz), 4.54 – 4.44 (1H, m), 4.90 (1H, m), 5.51 (1H, d, *J* = 7.8 Hz), 6.85 (1H, s), 7.14 (1H, d, *J* = 7.2 Hz), 7.20 (1H, d, *J* = 27.0 Hz). ^{13}C NMR ($CDCl_3$; 150 MHz) δ 21.8, 23.1, 24.9, 28.5, 32.4, 33.8, 38.8, 38.9, 39.4, 39.6, 40.4, 41.4, 48.5, 50.1, 51.5, 52.7, 62.1, 80.1, 100.5, 144.6, 151.9, 157.4, 163.3, 170.9, 174.2. +APCI-MS calcd. for $C_{25}H_{42}N_9O_8$ [M + H]+ 596.32, found 596.32.

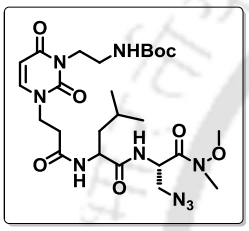

Synthesis of BocNH–U^{r}AA–Leu–T^{Py}Ala^{Do}–CONMe(OMe) (2.52): Using general procedure of [3+2] cyclo-addition reaction, 600 mg (1.008 mmol) of azide derivative of tripeptide **2.50** and 245 mg (1.109 mmol) of 9-ethynyl pyrene **2.51** was reacted. After completion of reaction 646 mg (0.786 mmol) of the title compound **2.52** was isolated in pure form as a light yellowish brown gummy material (Si-gel, PE : EtOAc = 1:2). Yield 78%. IR (KBr) 3305, 2959, 2106, 1704, 1654, 1532, 1456, 1171, 850, 792 cm^{-1}. ^{1}H NMR ($CDCl_3$; 600 MHz) δ 0.89 – 0.85 (6H, m). 1.53 (9H, s), 1.78 – 1.55 (2H, m), 3.07 – 2.91 (1H, m), 3.22 (3H, s), 3.30 (3H, s), 3.48 – 3.38 (1H, m), 3.76 (3H, s), 3.85 (3H, s), 4.11 (1H, dd, *J* = 48.1, 12.9 Hz), 4.47 (1H, d, *J* = 10.7

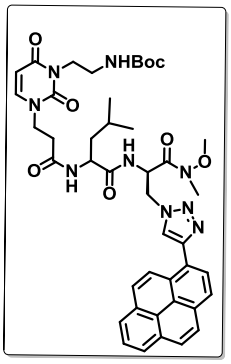

Hz), 4.86 (1H, d, *J* = 12.9 Hz), 5.12 (1H, s), 5.47 (1H, dd, *J* = 53.6, 7.5 Hz), 6.84 (1H, s), 6.98 (1H, d, *J* = 7.4 Hz), 7.06 (1H, s), 7.15 (1H, d, *J* = 7.5 Hz), 7.21 (1H, d, *J* = 7.7 Hz), 8.01 (1H, t, *J* = 7.0 Hz), 8.09 (3H, dd, *J* = 33.1, 8.8 Hz), 8.20 (2H, dd, *J* = 31.7, 6.6 Hz), 8.42 (1H, s), 8.52 (1H, d, *J* = 6.7 Hz), 8.75 (1H, s), 8.94 (1H, d, *J* = 7.1 Hz. ^{13}C NMR ($CDCl_3$; 150 MHz) δ 15.4, 21.7, 21.8, 23.1, 23.1, 24.9, 28.5, 28.8, 29.9, 32.5, 33.0, 33.4, 33.8, 48.5, 48.6, 49.8, 50.1, 51.6, 52.7, 52.7, 53.5, 62.0, 62.2, 80.1, 100.4, 100.5, 125.1, 125.2, 125.3, 125.4, 126.2, 127.4, 127.5, 127.9, 128.2, 144.6, 151.8, 157.4, 163.2, 170.9, 171.4, 174.6. HRMS calcd. for $C_{43}H_{52}N_9O_8$ $[M + H]^+$ 822.3933, found 822.4006.

Synthesis of TFA salt of BocNH–U^{r}AA–Leu–T^{Py}Ala^{Do}–CONMe(OMe) (2.53) : Using the general procedure of BocNH–deprotection, compound **2.52** (640 mg, 0.78 mmol) was reacted with TFA to get the product **2.53** in quantitative (94%) yield and was used for the next step without further purification and characterization.

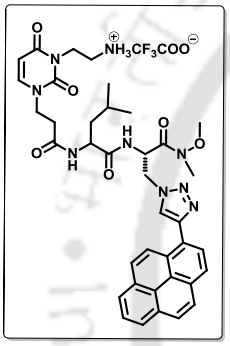

Synthesis of BocNH–Ser(N_3)–COOH (2.55): Using the general procedure of ester hydrolysis, starting from 1350 mg (4.93 mmol) of **2.45**, 1020 mg (5.35 mmol) of the title compound **2.55** was isolated as a colourless gummy material. Yield 89%.

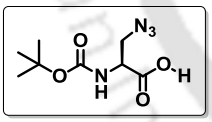

Synthesis of BocNH–Ser(N_3)–Leu–$COOCH_3$ (2.57): Using general procedure of peptide coupling, BocNH–protected serine azide **2.55** (1000 mg, 4.35 mmol) was taken as as starting material then 790 mg (4.35 mmol) of methyl ester of leucine **2.56** was reacted with it. After completion of reaction 990 mg (2.77 mmol) of the title compound **2.57** was isolated in pure form by column chromatography (Si-gel, PE : EtOAc = 2:1) as colourless gummy material. Yield 64%. IR (KBr) 3326, 2960, 2873, 2105, 1745, 1666, 1524, 1368, 1250, 1023, 858, 780 cm^{-1}. ^{1}H NMR ($CDCl_3$; 400 MHz) δ 0.88 (6H, d, *J* = 5.6 Hz), 1.41 (9H, s), 1.63-1.51 (3H, m), 3.51 (1H, dd, *J* = 4.8 Hz, 6.8 Hz), 3.68 (3H, s), 3.74-3.70 (1H, m), 4.30 (1H, bs), 4.56 (1H, bs), 5.51 (1H, d, *J* = 6.4 Hz), 6.97 (1H, d, *J* = 6.4 Hz), ^{13}C NMR ($CDCl_3$; 100 MHz) δ 21.9, 22.8, 24.8, 28.3, 41.3, 51.0, 52.2, 52.4, 53.7, 80.8,

155.5, 169.5, 173.1. HRMS calcd. for $C_{15}H_{27}N_5O_5Na$ ($[M + Na]^+$) 380.1908, found 380.1909.

Synthesis of BocNH–^{TMnap}Ala^{Do}–Leu–COOCH$_3$ (2.59): Using general procedure of [3+2] cyclo-addition reaction, 225 mg (0.583 mmol) of azide derivative of dipeptide **2.57** and (117 mg, 0.641 mmol) of 2-ethynyl-6-methoxynaphthalene **2.58** was reacted. After completion of reaction (monitored by TLC) 236 mg (0.437 mmol) of the title compound **2.59** was isolated in pure form as a white solid (Si-gel, PE : EtOAc = 1:1). Yield 75%. mp 149-152 ^oC. IR (KBr) 3364, 2960, 1758, 1691, 1660, 1514, 1162, 1028, 855 cm^{-1}. ^1H NMR ($CDCl_3$; 600 MHz) δ 0.70 (6H, d, J = 5.4 Hz), 1.41-1.43 (1H, m), 1.47 (9H, s), 1.72 (2H, d, J = 19.2 Hz), 3.68 (3H, s), 3.93 (3H, s), 4.51-4.55 (1H, q, J = 5.4, 9.0 Hz), 4.73 (1H, d, J = 14.4 Hz), 4.78 (1H, bs), 5.01 (1H, d, J = 13.2 Hz), 5.88 (1H, bs), 6.93 (1H, bs), 7.13 (1H, s), 7.16 (1H, d, J = 8.4 Hz), 7.77 (2H, t, J = 9.0 Hz), 7.85 (1H, d, J = 9.0 Hz), 7.95 (1H, s), 8.22 (1H, s), ^{13}C NMR ($CDCl_3$; 150 MHz) δ 21.6, 22.8, 24.6, 28.4, 41.3, 51.0, 52.5, 54.6, 55.5, 81.2, 105.9, 119.5, 121.9, 124.4, 124.5, 125.6, 127.5, 129.1, 129.8, 134.5, 148.0, 158.1, 169.0, 172.9 . HRMS calcd. for $C_{28}H_{38}N_5O_6$ $[M + H]^+$ 540.2817, found 540.2818.

Synthesis of BocNH–^{TMnap}Ala^{Do}–Leu–COOH (2.60): Using the general procedure of ester hydrolysis, starting from 235 mg (0.437 mmol) of title compound **2.59**, 195 mg (0.371 mmol) of the title compound **2.60** was isolated as a light white solid. Yield 85%. mp 178-182 ^oC. IR (KBr) 3419, 2959, 1703, 1660, 1501, 1220, 1163, 1028, 854 cm^{-1}. ^1H NMR ($CDCl_3$; 600 MHz) δ 0.80 (6H, m). 1.33 (9H, s), 1.49 (3H, m), 3.65 – 3.54 (1H, m), 3.88 (3H, s), 4.38 (1H, bs), 4.77 (2H, m), 7.13 – 7.02 (2H, m), 7.70 (2H, m), 7.80 – 7.77 (1H, m), 7.98 (1H, s), 8.15 (1H, d, J = 10.6 Hz),^{13}C NMR ($CDCl_3$; 150 MHz) δ 21.3, 28. 22.8, 24.7, 24.8, 28.0, 40.8, 48.55, 48.7, 48.8, 48.9, 49.12, 54.2, 55.2, 80.8, 105.7, 119.2, 121.7, 124.2, 124.3, 124.3, 125.3, 127.4, 128.9, 129.6, 134.4, 147.9, 157.9, 169.2. –APCI-MS calcd. $C_{27}H_{34}N_5O_6$ $[M - H]^-$ 524.25, found 524.23.

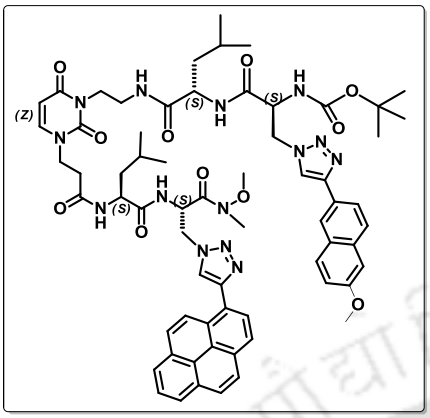

Synthesis of BocNH–^{TMnap}Ala^{Do}–Leu–U^{r}AA–Leu–^{TPy}Ala^{Do}–CONMe(OMe) (2.61): Using general procedure of peptide coupling, the acid compound **2.60** (200 mg, 0.37 mmol) was taken as as starting material then (302 mg, 0.37 mmol) of amine compound **2.53** was reacted with it. After completion of reaction 241 mg (0.196 mmol) of the title compound **2.61** was isolated in pure form by column chromatography (Si–gel, PE : EtOAc =1:4) as light brown solid material. Yield 53%. mp 108–112 ^{o}C. IR (KBr) 3403, 3320, 2925, 2107, 1707, 1653, 1456, 1222, 1162, 1026, 805 cm^{-1}. ^{1}H NMR ($CDCl_3$; 600 MHz) δ 0.78–0.83 (12H, m), 1.29 (9H, s), 1.38-1.45 (6H, m), 2.30- 2.40 (1H, m), 2.55- 2.63 (1H, m), 3.11 (2H, s), 3.16 (3H, s), 3.88 (3H, s), 4.23 (1H, bs), 4.32-4.36 (2H, m), 4.56-4.59 (2H, m), 4.71 – 4.75 (2H, m), 4.76 – 4.82 (1H, m), 4.85 (1H, d, *J* = 9.9 Hz), 5.32 (1H, bs), 5.44 (1H, t, *J* = 6.9 Hz), 5.59 (1H, d, *J* = 6.8 Hz), 7.17 (2H, s), 7.23 (1H, t, *J* = 8.0 Hz), 7.32 (2H, s), 7.53 (1H, d, *J* = 6.8 Hz), 7.88 (5H, d, *J* = 7.3 Hz), 8.09 (1H, t, *J* = 6.0 Hz), 8.15 (2H, d, *J* = 6.6 Hz), 8.21 (2H, s), 8.24 (1H, s), 8.27 (2H, d, *J* = 6.7 Hz), 8.31 (3H, m), 8.37 (1H, m), 8.43 (1H, bs), 8.47-8.49 (1H, m), 8.60 (1H, bs), 8.69 (1H, s), 8.83 (1H, d, *J* = 9.2 Hz). ^{13}C NMR ($CDCl_3$; 150 MHz) δ 21.3, 21.4, 22.1, 22.9, 23.1, 23.1, 23.9, 24.1, 24.1, 28.0, 29.0, 33.8, 36.2, 40.4, 40.7, 45.6, 45.7, 45.9, 46.9, 48.7, 49.5, 49.8, 50.6, 50.6, 51.0, 51.2, 51.3, 54.3, 55.2, 78.7, 78.8, 79.12, 99.7, 99.7, 106.0, 113.4, 119.1, 120.5, 121.9, 122.0, 123.3, 123.9, 124.1, 124.3, 124.6, 124.9, 125.2, 125.4, 125.5, 125.8, 125.9, 126.0, 126.5, 126.8, 127.1, 127.3, 127.6, 127.7, 127.8, 127.9, 128.2, 128.5, 129.1, 129.5, 130.0, 130.4, 130.6, 130.8, 130.9, 131.9, 133.8, 145.1, 145.9, 146.4, 148.3, 150.7, 151.0, 155.0, 157.4, 162.6, 166.0, 168.7, 169.4, 171.7, 172.3, 190.3. HRMS calcd. for $C_{65}H_{77}N_{14}O_{11}$ $[M + H]^+$ 1229.5891, found 1229.5881.

Synthesis of BocNH–^{TPy}Ala^{Do}–Leu–COOCH$_3$ (2.62): Using general procedure of [3+2] cyclo-addition reaction, 225 mg (0.583 mmol) of azide derivative of dipeptide **2.57** and 216 mg (0.641 mmol) of 1-ethynyl pyrene was reacted. After completion of reaction 265 mg (0.455 mmol) of the title compound **2.62** was isolated in pure form as a light yellow solid (Si-gel, PE : EtOAc = 1:1). Yield 78%. mp 118-122 ^{o}C. IR (KBr) 3334, 2956, 1743, 1661, 1518, 1367, 1248, 1162, 847 cm-1. ^{1}H NMR ($CDCl_3$; 600 MHz) δ 0.70 (6H, d, *J* = 5.4 Hz), 1.49 (9H, s), 1.52-1.53 (1H, m), 1.67 (2H, s), 3.69 (3H, s), 4.54-4.58 (1H, q, *J* = 9, 13.8 Hz), 4.86-4.84 (2H, m), 5.12 (1H, d, *J* = 12.0 Hz), 5.98 (1H, d, *J* = 6.0 Hz), 7.01 (1H, bs), 8.03 (1H, d, *J* = 7.8 Hz), 8.07-8.13

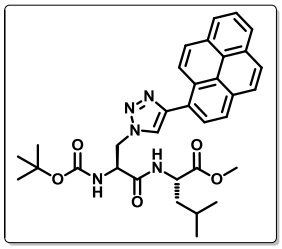

(4H, m), 8.19-8.24 (4H, m), 8.70 (1H, d, , J = 9.0 Hz), ^{13}C NMR ($CDCl_3$; 150 MHz) δ 21.7, 22.8, 24.7, 28.4, 41.3, 51.1, 52.6, 54.6, 81.3, 124.8, 124.9, 125.2, 125.3, 125.6, 126.3, 127.2, 127.5, 128.1, 128.4, 128.6, 130.9, 131.5, 147.6, 155.8, 169.0, 172.9. HRMS calcd. for $C_{33}H_{38}N_5O_5$ $[M + H]^+$ 584.2867, found 584.2877.

Synthesis of BocNH–^{TPy}Ala^{Do}–Leu–COOH (2.63): Using the general procedure of ester hydrolysis, starting from 260 mg (0.455 mmol) of title compound **2.62**, 212 mg (0.373 mmol) of the title compound **2.63** was isolated as a light yellow solid. Yield 82%. mp 143-147 ^{o}C; IR (KBr) 3420, 2958, 1718, 1662, 1519, 1367, 1162, 847 cm-1. ^{1}H NMR ($CDCl_3$; 600 MHz) δ 0.90 (6H, s), 1.39 (9H, s), 1.60 (1H, d, J = 7.8), 1.68 (2H, bs), 4.83 (2H, d, J = 12 Hz), 5.05 (1H, d, J = 11.4 Hz), 8.03 (4H, m), 8.17-8.20 (4H, m), 8.34 (1H, s), 8.60 (1H, d, J = 8.4 Hz), ^{13}C NMR ($CDCl_3$; 150 MHz) δ 14.5, 21.1, 22.5, 24.3, 27.6, 41.0, 50.9, 52.3, 54.0, 65.3, 79.8, 124.1, 124.2, 124.4, 124.6, 124.7, 125.0, 125.7, 126.7, 126.8, 127.4, 127.6, 128.0, 130.3, 130.8, 146.4, 155.3, 168.5.–APCI-MS calcd. for $C_{32}H_{34}N_5O_5$ ($[M - H]^-$) 568.26, found 568.50.

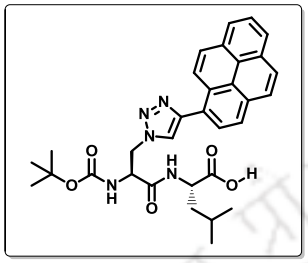

Synthesis of BocNH–^{TPy}Ala^{Do}–Leu–U^{r}AA–Leu–^{TPy}Ala^{Do}–CONMe(OMe) (2.64) : Using general procedure of peptide coupling acid compound **2.63** (200 mg, 0.35 mmol) was taken as starting material then (290 mg, 0.35 mmol) of amine compound **2.53** was reacted with it. After completion of reaction (223 mg, 0.175 mmol) of the title compound **2.64** was isolated in pure form by column chromatography (Si-gel, PE : EtOAc =1:4) as light brown solid material. Yield 50%. mp 154-157 ^{o}C. IR (KBr) 3480, 3297, 2924, 2105, 1707, 1655, 1537, 1454, 1 165, 848 cm-1. ^{1}H NMR ($CDCl_3$; 600 MHz) δ 0.66-0.72 (12H, m), 1.27 (9H, s), 1.36-1.39 (3H, m), 1.42-1.44 (2H, m), 3.14 (3H, s), 3.41-3.52 (1H, m), 3.64 (1H, s), 3.68 (2H, s), 3.74 (3H, s), 3.82-3.87 (1H, m), 4.17-4.19 (1H, m), 4.21-4.25 (1H, m), 4.31-4.35 (1H, m), 4.61-4.67 (2H, m), 4.70-4.73 (1H, m), 4.84 (2H, d, J = 12.0 Hz), 4.90 (1H, d, J = 12.0 Hz), 5.30 (1H, bs), 5.40 (1H, d, J = 12.0 Hz), 5.55 (1H, t, J = 6.0 Hz), 7.24-7.30 (2H, m), 7.50 (1H, t, J = 6.0 Hz), 8.06-8.09 (3H, m), 8.10-8.13 (2H, m), 8.18-8.24 (5H, m), 8.28-8.35 (7H, m), 8.56 (1H, bs), 8.61-8.66 (2H, m), 8.06-8.09 (2H, m), 8.81 (2H, d, J = 12.0 Hz). ^{13}C NMR ($CDCl_3$; 150 MHz) δ 21.2, 21.3, 21.4, 22.9, 23.0, 23.1, 23.1, 23.9, 23.9, 24.0, 24.1, 32.0, 33.7, 33.8, 36.1, 45.6, 45.7, 45.8, 48.6, 49.5, 49.8, 50.6, 50.6, 50.8, 51.0, 51.2, 51.3, 54.3, 78.6, 99.6, 123.9, 123.9, 124.2, 124.3, 124.8, 124.9, 125.0, 125.1, 125.1, 125.1, 125.4, 125.5, 126.4, 126.9, 127.1, 127.3, 127.3, 127.4, 127.6, 127.6,

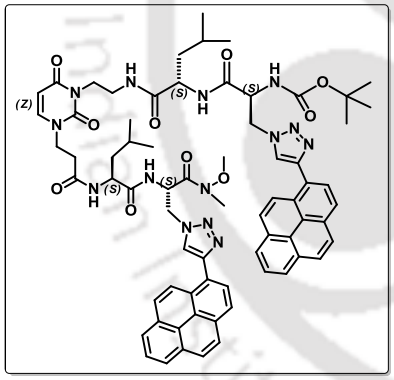

127.9, 127.9, 130.3, 130.5, 130.5, 130.9, 145.7, 145.9, 150.7, 150.9, 155.1, 162.3, 162.5, 168.6, 169.5, 171.8, 172.2, 172.3. HRMS calcd. for $C_{70}H_{77}N_{14}O_{10}$ $[M + H]^+$ 1273.5942, found 1273.5938.

Synthesis of $^{TPy}Ala^{Do}$ (2.65): Using general procedure of [3+2] cyclo-addition reaction 48 mg (0.18 mmol) of chiral serine azide **2.45** and 44mg (0.19 mmol) of 2-ethynyl pyrene reacted each other gives 68 mg (0.137 mmol) of the title compound **2.65** was isolated as a light brown solid. Yield 72.4%; IR (KBr) 3421, 2976, 2930, 2103, 1712, 1663, 1164, 849, 757 cm-1. ^{1}H NMR ($CDCl_3$; 400 MHz) δ 1.39 (9H, s), 3.24 (3H, s), 3.77 (3H, s), 4.84-4.85 (2H, d, J = 4.8 Hz), 5.18-5.20 (1H, m), 5.73-5.75 (1H, d, J = 7.6 Hz), 7.95-8.00 (2H, m), 8.03-8.06 (2H, m), 8.07 (1H, s), 8.12-8.12 (3H, m), 8.61-8.63 (1H, d, J = 9.2 Hz), ^{13}C NMR ($CDCl_3$; 100 MHz) δ 22.9, 28.5, 29.9, 32.6, 51.4, 62.0, 77.1, 77.4, 77.7, 124.3, 124.8, 125.0, 125.2, 125.3, 125.5, 126.2, 127.4, 127.5, 127.9, 128.2, 128.7, 131.0, 131.4, 131.5, 147.5, 155.4, 169.2. HRMS calcd. for $C_{28}H_{30}N_5O_4$ ($[M + H]^+$) 500.2376, found 500.2323.

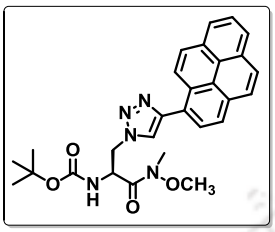

Synthesis of $^{TMnap}Ala^{Do}$ (2.66): Using general procedure of [3+2] cyclo-addition reaction, 50 mg (0.18 mmol) of azide derivative of serine **2.45** and 37 mg (0.2 mmol) of 2-ethynyl-6-methoxynaphthalene was reacted. After completion of reaction (monitored by TLC) 236 mg (0.437 mmol) of the title compound **2.66** was isolated in pure form as a white solid (Si-gel, PE : EtOAc = 1:1). Yield 79%. IR (KBr) 3341, 2970, 1660, 1524, 1164, 1029, 855, 653 cm^{-1}. 1H NMR ($CDCl_3$; 400 MHz) δ 1.38 (9H, s), 3.21 (3H, s), 3.74 (3H, s), 3.89 (3H, s), 4.7 - 4.77 (2H, m), 5.07-5.13 (1H, m), 5.56 (1H, d, J = 6.8 Hz), 7.12 (2H, t, J = 4.8 Hz), 7.74 (2H, dd, J = 3.6 Hz, 8.4 Hz), 7.82 (1H, s), 7.85 (1H, s), 8.21 (1H, s), ^{13}C NMR ($CDCl_3$; 100 MHz) δ 28.7, 33.0, 51.6, 55.8, 62.3, 81.0, 106.3, 119.7, 120.9, 124.8, 124.9, 126.2, 127.8, 129.0, 129.4, 130.2, 134.8, 148.4, 155.5, 158.4, 169.3; HRMS calcd for $C_{23}H_{29}N_5O_5$ ($[M + H]^+$) 456.2241, found 456.2242.

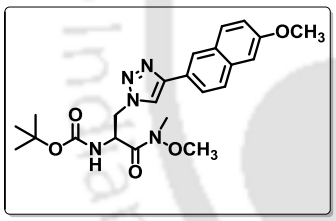

2.7. Photophysical Studies of the Synthesized Peptides.

UV-visible measurements: The *UV* –visible spectra of all final peptides and UNNAs (10 µM) were measured in different solvents using a UV-Visible spectrophotometer (**SHIMADZU**, **UV-2550**) with a cell of 1 cm path length. The measurements were done in absorbance mode. The sample solutions absorbance values were measured in the wavelength range of 200–700 nm. All the sample solutions were prepared freshly just before doing the experiment.

Fluorescence experiments: All the sample solutions for fluorescence measurements (**HORIBA Scientific**, **Fluoromax-4**) were also prepared freshly just before doing the experiment. Fluorescence spectra were obtained using a fluorescence spectrophotometer at 25 °C using 1 cm path length cell. The wavelengths for excitation in all the cases were set at the absorption maxima of each sample in each solvent. The emission spectra were measured in the wavelength regime of 300–700 nm with an integration time of 0.2 sec. From 2.0 ml 500 μM stock solution, 2 ml of 10 μM concentration of solution was used for fluorescence experiment in 1 ml cell. Fluorescence emissions were recorded by exciting the sample solutions at their absorption maxima. Steady-state fluorescence emission spectra were recorded at room temperature as an average of five scans using an excitation slit of 3.0 nm, emission slit 3.0 nm, and scan speed of 120 nm/min. Using quinine sulphate as a reference, the fluorescence quantum yields (Φ_f) were determined with the known Φ_f (0.55) in 0.1 molar solution in sulphuric acid. Following equation was used to calculate the quantum yield,

$$\Phi_S = \Phi_R \frac{Fl_S^{Area}}{Fl_R^{Area}} \frac{Abs_R}{Abs_S} \frac{n_S^2}{n_R^2}$$

where, Φ_R is the quantum yield of standard reference, Fl_S^{Area} (sample) and Fl_R^{Area} (reference) are the integrated emission peak areas, Abs_S (sample) and Abs_R (reference) are the absorbances at the excitation wavelength, and n_S (sample) and n_R (reference) are the refractive indices of the solutions.

A time resolved fluorescence spectrophotometer (*Eddinburg Instruments FSP920*) was utilized to perform fluorescence lifetime experiments. Working condition was maintained at 25^{o}C and results were recorded at an excitation wavelength of 290 nm LED and 375 nm laser using a cuvette having path length 1 cm. To analyze the lifetime data time correlated single photon counting (TCSPC) method was used and analysis was done using a software package with range 205 – 4000 channels.

Error analysis in spectroscopic studies: All the photophysical experiments were done four times. The experimental standard errors (SE, Equation 2) were calculated based on their individual standard deviations (SD, Equation 1) for four consecutive run for the same experiment under same experimental condition.

$$SD = \sqrt{\sum_{i=1}^{n} \frac{1}{n-1} (x - \overline{x})^2}$$

……Equation 1

where SD is standard deviation, *x* is individual data points, $\bar{x}$ is the mean value of the experiments and n is the total number of observations.

The standard error (*SE*) was measured by sample standard deviation obtained divided by the square root of number of observations

$$SE = \frac{SD}{\sqrt{n}} \quad \text{.....Equation 2}$$

The experimental errors in wavelength for both the UV-Visible and fluorescence measurement were found to be in the range of 1-2 nm. Error in Quantum yield calculation lies in the range of 8-10%. The experimental error for lifetime measurement lies between ± 0.5 ns range.

2.8. Studies On the Interaction of Peptides (2.61, 2.64) with BSA

***Preparation of BSA solution*:** BSA (Merck) solution was prepared using Phosphate buffer of pH 7.02, by dissolving 0.08 gm of BSA in 1 mL phosphate buffer (20 mM). The stock solution (1000 μM) of the compound was prepared in DMSO, due to poor solubility of compound in buffer.

General experimental on interaction study of BSA by photophysical study: Spectral measurements were done at room temperature. The interaction of compound with BSA was studied by titrating aqueous solution of Peptides (**2.61** and **2.64**) with increasing concentrations of BSA solution (ranging from 0, 1.25, 2.5, 3.75, 5, 7.5, 10, 12.5, 15, 20, 25, 30, 45 μM). Total volume of each sample was 3 ml, which contains 2-3% DMSO. 2-3% DMSO may not cause any structural changes of our synthesized peptides. Before doing spectral measurement each sample solution were mixed well.

***UV-Visible study with BSA*:** UV-visible spectrophotometer (**SHIMADZU**, **UV-2550**) was used to carry out UV–Visible absorbance measurements. The experiments were done in 20 mM phosphate buffer of pH 7.02 at 25^{o}C, where 2-3% DMSO was used to solubilize the probe peptides. The spectral measurements were carried out in absorbance mode and absorbance values were measured in wavelength regime of 200–700 nm. Freshly prepared sample solutions were used to carry out all the experiments.

Fluorescence study with BSA: Steady state fluorescence and anisotropy measurements were carried out using steady state fluorescence spectrophotometer (**HORIBA Scientific**, **Fluoromax-4**) with a cell of 1 cm path length at 25^{o}C. The

excitation wavelengths were set at the absorption maxima in each sample. Steady state fluorescence spectrophotometer was used to measure steady state anisotropy. Fluorescence lifetime experiment was done using similar procedure as described above.

UV and fluorescence experiments were also repeated four times. Standard experimental error was calculated by above mentioned procedure, for UV and fluorescence measurement which lies between 2-3% and for lifetime measurement lies between ± 0.5 range.

2.9. Some Selected Spectra

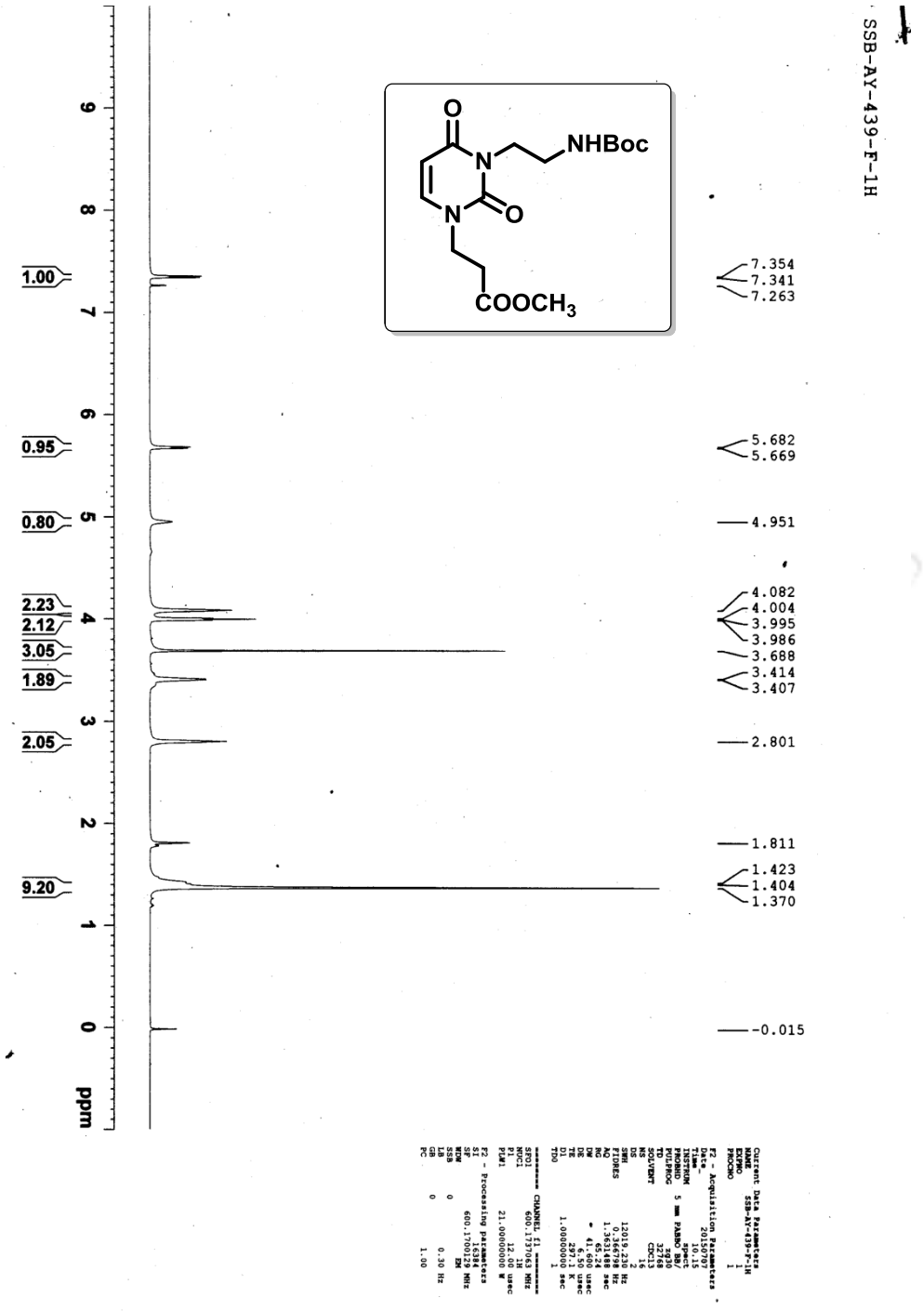

Figure 2.31. ^{1}H Spectra of synthesized compound **2.43.**

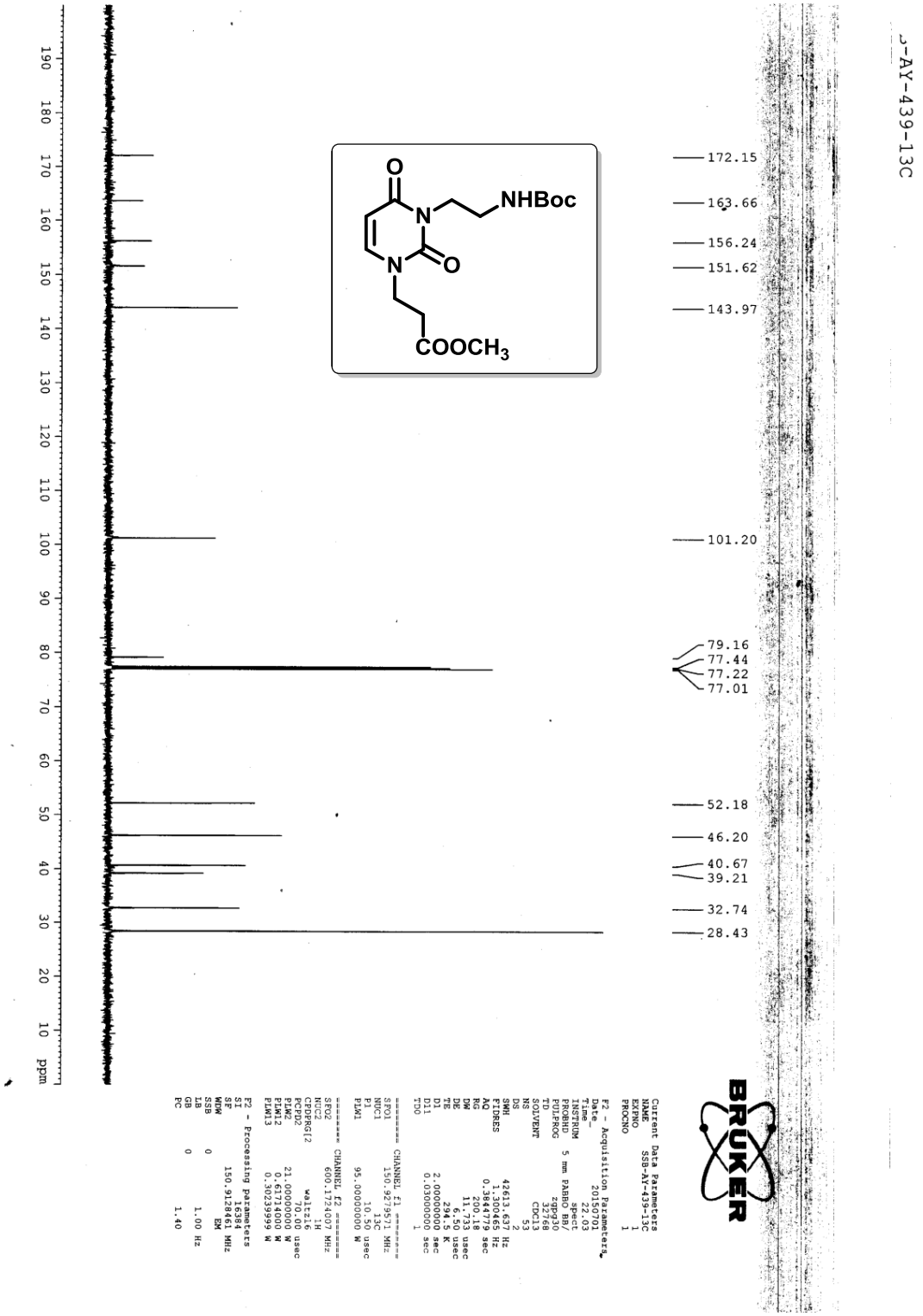

Figure 2.32. ^{13}C Spectra of synthesized compound **2.43.**

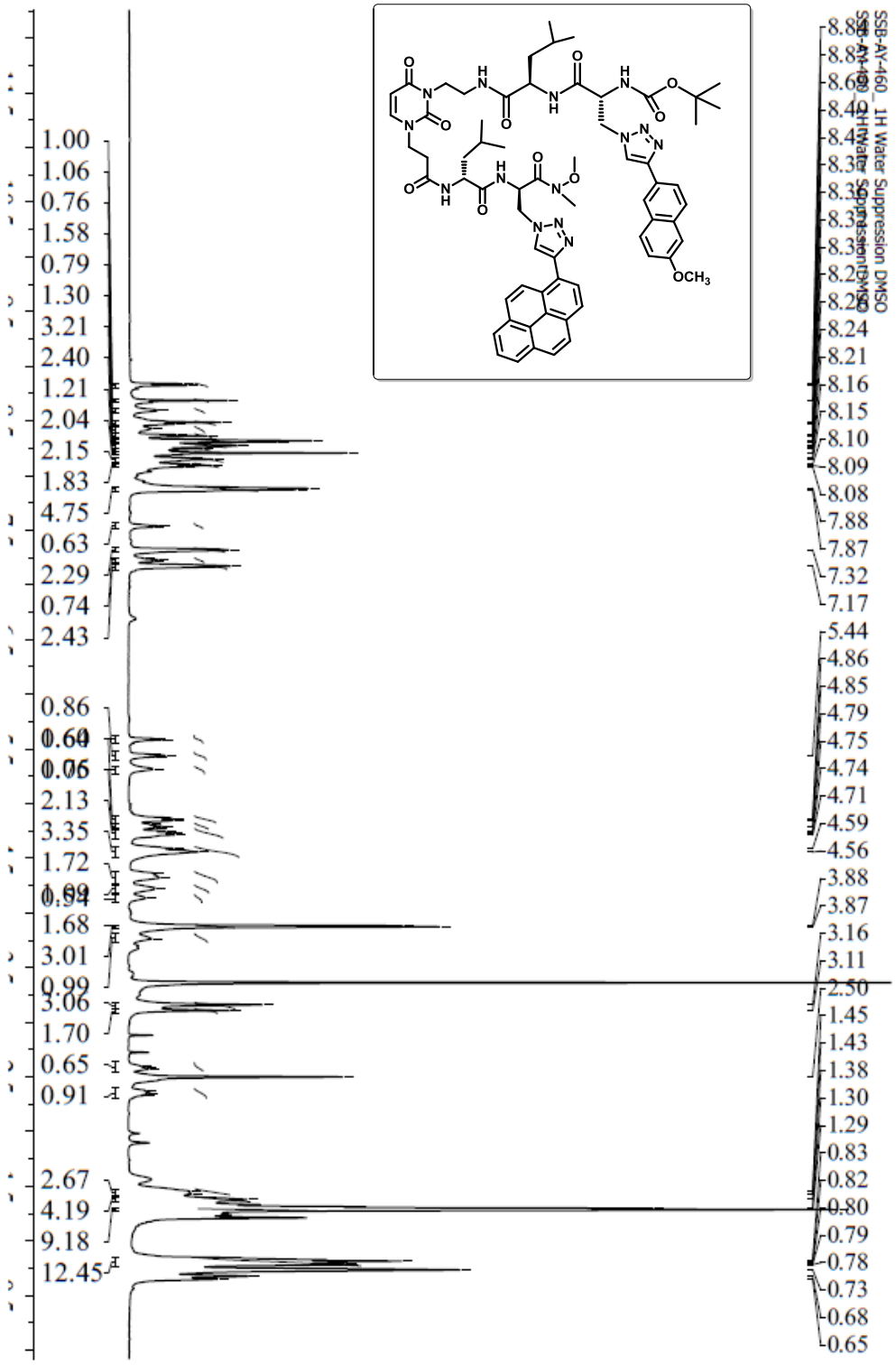

Figure 2.33. ^{1}H Spectra of synthesized compound **2.61.**

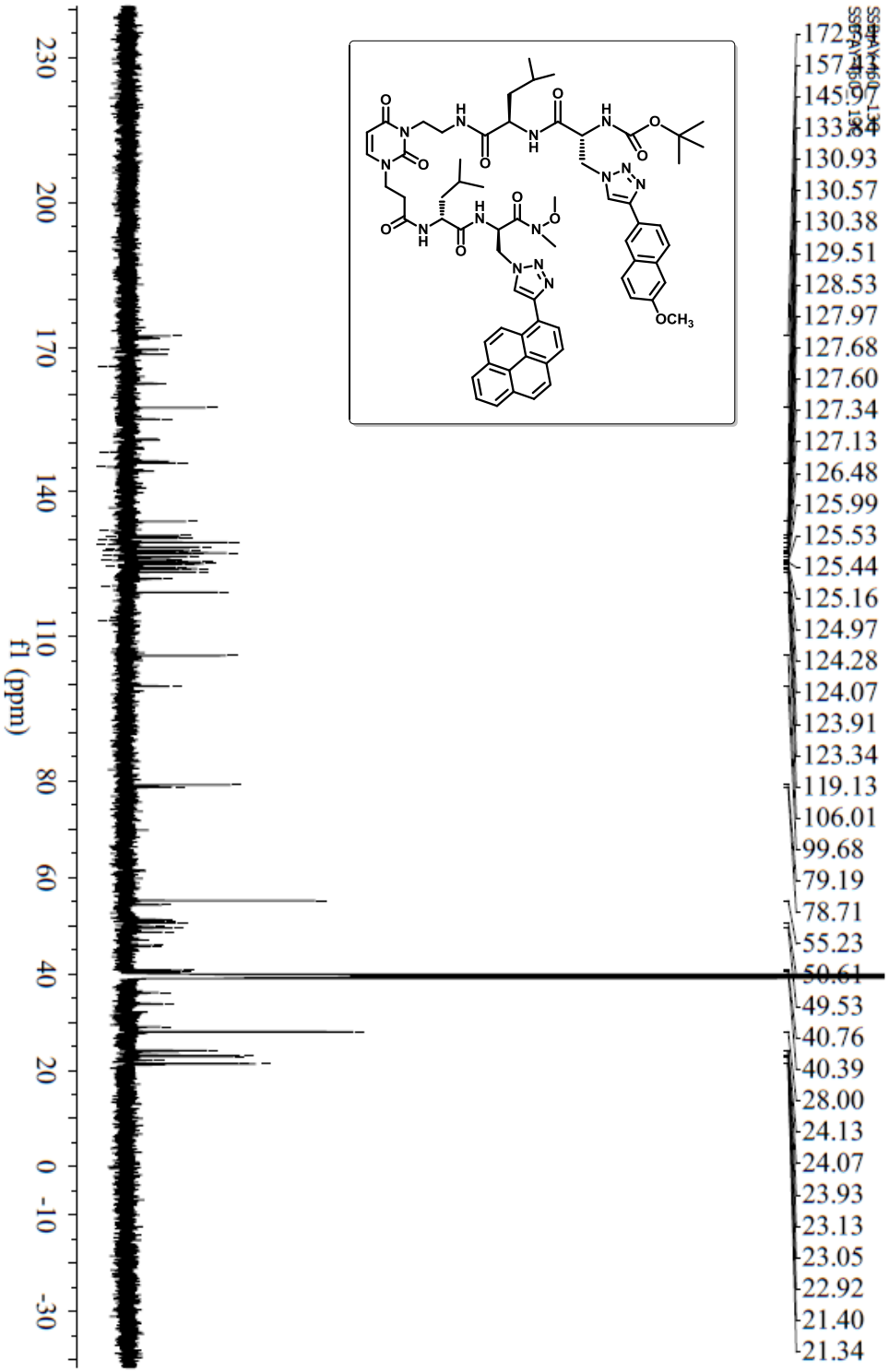

Figure 2.34. ^{13}C Spectra of synthesized compound **2.61.**

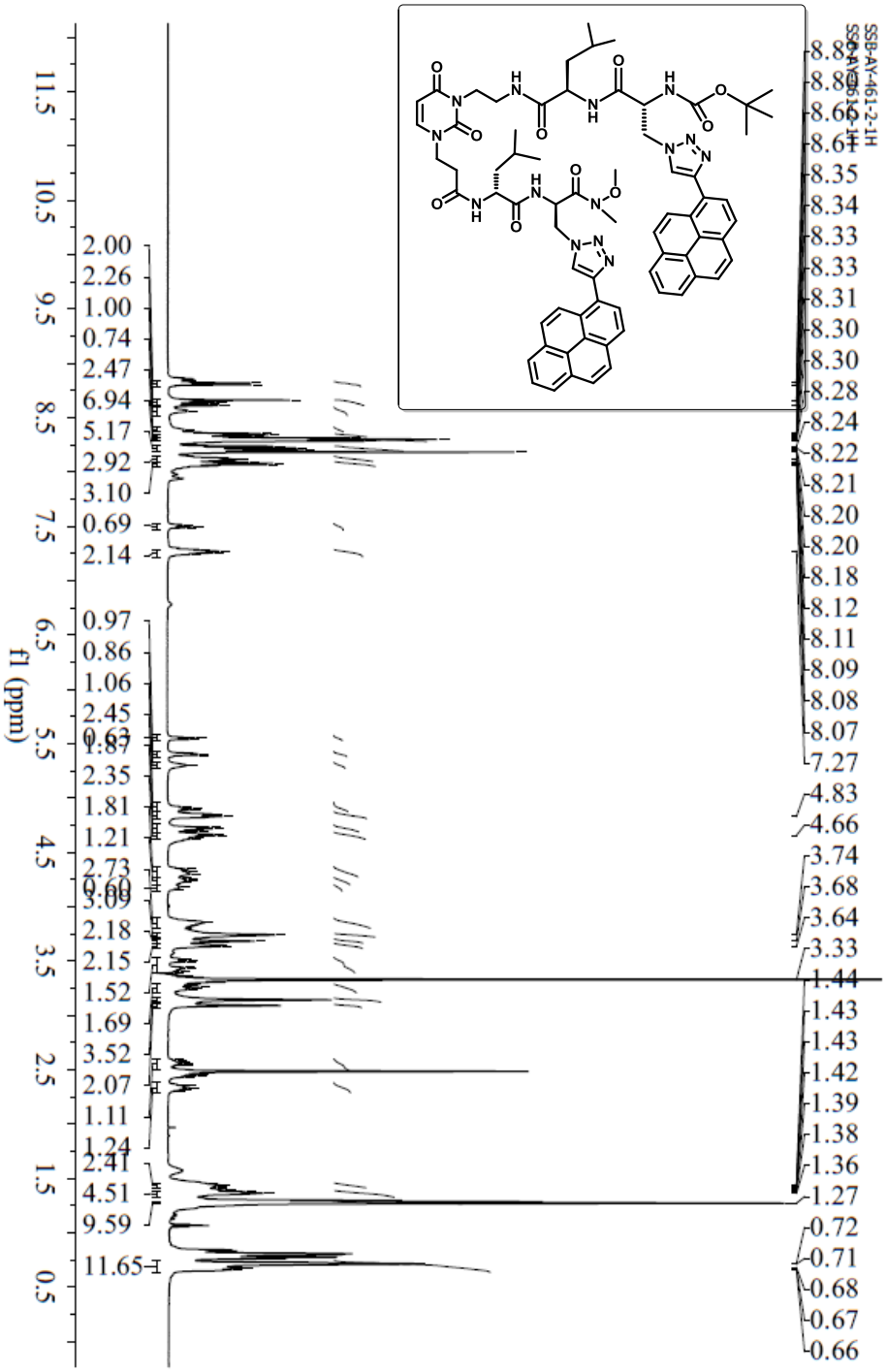

Figure 2.35. ^{1}H Spectra of synthesized compound **2.64.**

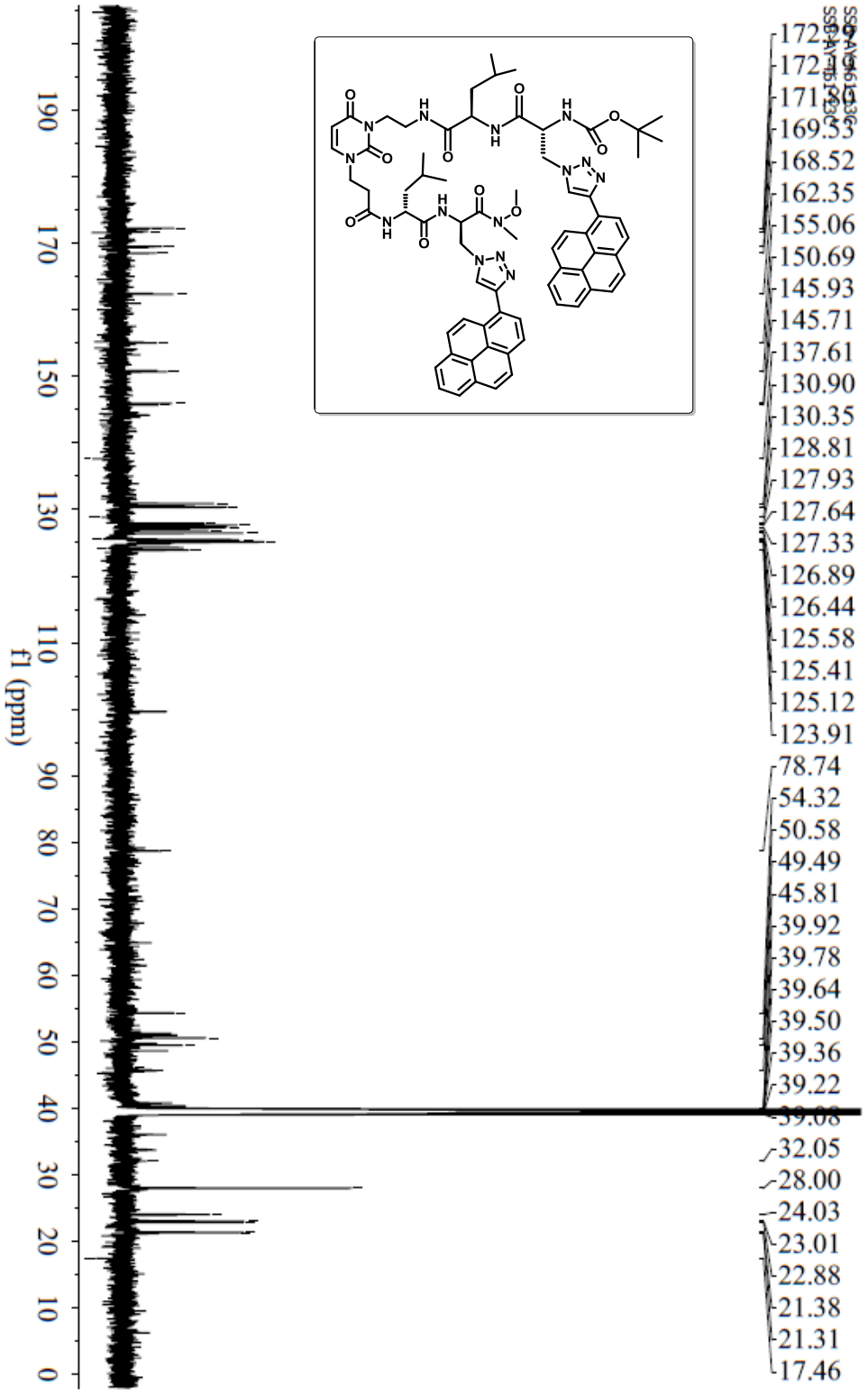

Figure 2.36. ^{13}C Spectra of synthesized compound **2.64.**

2.10. References

1. (a) Astbury, W. T., and A. Street. *X-ray studies of the structure of hair, wool and related fibers. I. General. Trans. Roy. Soc. 230A*: pp. 75–101, **1931**.
(b) Astbury, W. T.; H. J. Woods. *X ray studies of the structure of hair, wool, and related fibres. II. The molecular structure and elastic properties of hair keratin. Phil. Trans. R. Soc. Lond. A. 232*: pp. 333–394, **1933**.

2. (a) Pauling, L.; Corey, R. B.; Branson, H. R. *Proc. Natl. Acad. Sci.* **1951**, *37*, 205
(b) Pauling, L.; Corey, R. B. *J. Am. Chem. Soc.* **1950**, *72*, 5349.
(c) Corey, R. B.; Donohue, J. *Ibid*. **1950**, *72*, 2899.
(d) Lévy, H. A.; Corey, R. B. *Ibid.* **1941**, *63*, 2095.

3. Loughlin W. A.; Tyndall J. D.; Glenn. M. P. Hill, T. A.; Fairlie, D. P. *Chem. Rev*. **2004**, *104*, 6085.

4. Nikolov, D. B.; Chen, H.; Halay, E. D.; Usheva, A. A.; Hisatake, K.; Lee, D. K.; Roeder, R. G.; Burley, S. K. *Nature* **1995**, *377*, 119.

5. Kim, J. L.; Nikolov, D. B.; Burley, S. K. *Nature* **1993**, *365*, 520.

6. Kim, Y.; Geiger, J. H.; Hahn, S.; Sigler, P. B. *Nature* **1993**, *365*, 512.

7. (a) Man, S. H *Curr Opin Chem Biol* **1998**, 2, 717. (b) Searle, M. S. *J. Chem. Soc. Perkin Trans.* **2001**, *2*, 1011. (c) Venkatraman, J.; Shankaramma, S. C.; Balaram, P.; *Chem Rev.* **2001**, *101*, 3131. (d) Searle, M. S.; Ciani, B.; *Curr. Opin. Struct. Biol.* **2004**, *14*, 458. (e) Hughes, R. M.; Waters, M. L.; *Curr Opin Struct Biol* **2006**, *16*, 514.

8. Nowick, J. S. *Acc. Chem. Res*. **2008**, *41*, 1319.

9. Nowick, J. S.; Smith, E. M.; Pairish, M. *Chem. Soc. Rev.* **1996**, *25*, 401.

10. (a) Nowick, J. S. *Acc. Chem. Res.* **1999**, *32*, 287.
(b) Nowick, J. S. *Org. Biomol. Chem*. **2006**, *4*, 3869.

11. (a) Díaz, H.; Tsang, K. Y.; Choo, D.; Espina, J. R. Kelly, J. W. *J. Am. Chem. Soc.* **1993**, *115*, 3790.
(b) Graciani, N. R.; Tsang, K. Y.; McCutchen, S. L.; Kelly, J. W. *Biorg. Med. Chem*. **1994**, *2*, 999.

12. Schneider, J. P. Kelly, J. W. *J. Am. Chem. Soc.* **1995**, *117*, 2533.

13. Jones, I. G.; Jones, W.; North, M. *J. Org. Chem.* **1998**, *63*, 1505.

14. (a) Ranganathan, D.; Haridas, V.; Kurur, S.; Thomas, A.; Madhusudanan, K. P.; Nagaraj, R.; Kunwar, A. C.; Sarma, A. V. S.; Karle, I. L. *J. Am. Chem. Soc.* **1998**, *120*, 8448;
(b) Hackenberger, C. P. R.; Schiffers, I.; Runsink, Bolm, J. C. *J. Org. Chem*. **2004**, *69*, 739.

15. (a) Nowick, J. S.; Smith, E. M.; Noronha, G. *J. Org. Chem*. **1995**, *60*, 7386.

(b) Moriuchi, T.; Tamura, T.; Hirao, T. *J. Am. Chem. Soc.* **2002**, *124*, 9356.

16. Lakowicz, J. R. *Principles of Fluorescence Spectroscopy*; 3rd ed.; Springer: New York, **2006**.

17. Moriuchi, T.; Tamura, T.; Hirao, T. *J. Am. Chem. Soc.* **2002**, *124*, 9356.

18. Cheng, P. –C. *Handbook of Biological Confocal Microscopy*. New York, NY: Springer. pp. 162, **2006**.

19. Helms, V. *Principles of Computational Cell Biology*. pp. 202, **2008**.

20. Harris, D. C. *Quantitative Chemical Analysis.* pp. 419, **2010**.

21. (a) Dietrich, A.; Buschmann, V.; Müller, C.; Sauer, M. *Rev. Mol. Biotechnol.* **2002**, *82*, 211.
(b) Jares-Erijman, E. A.; Jovin, T. M. *Nat. Biotechnol.* **2003**, *21*, 1387.
(c) Dickenson, N. E.; Picking, W. D. *Int. J. Mol. Sci.* **2012**, *13*, 15137.
(d) Okumoto, S.; Jones, A.; Frommer, W. B. *Annu. Rev. Plant Biol.* **2012**, *63*, 663.

22. (a) Periasamy, A. *J. Biomed. Opt.* **2001**, *6*, 287.
(b) Grohmann, D.; Klose, D.; Klare, J. P.; Kay, C. W. M.; Steinhoff, H.-J.; Werner, F. *J. Am. Chem. Soc.* **2010**, *132*, 5954.

23. Chen, S.; Fahmi, N. E.; Wang, L.; Bhattacharya, C.; Benkovic, S. J.; Hecht, S. M. *J. Am. Chem. Soc.* **2013**, *135*, 12924.

24. Ekici, O. D.; Zhu, J.; Chung, I. Y. W.; Paetzel, M.; Dalbey, R. E.; Pei, D. *Biochemistry* **2009**, *48*, 5753.

25. Karolin, J.; Fa, M.; Wilczynska, M.; Ny, T.; Johansson, L. B.- A. *Biophys. J.* **1998**, *74*, 11.

26. Glasscock, J. M.; Zhu, Y.; Chowdhury, P.; Tang, J. and Gai, F. *Biochemistry* **2008**, *47*, 11070.

27. Oh, K. J.; Cash, K. J.; Plaxco, K. W. *J. Am. Chem. Soc.* **2006**, *128*, 14018.

28. Fujii, A.; Sekiguchi, Y.; Matsumura, H.; Inoue, T.; Chung, W. –S.; Hirota, S. and Matsuo, T. *Bioconjugate Chem.* **2015**, *26*, 537.

29. Sisido,M.; Tanaka, R.; Inai, Y.; Imanishif, Y. *J. Am. Chem. Soc*. **1989**, *111*, 6190.

30. (a) Woody, R. W. In *Circular Dichroism. Principles and Applications;* Nakanishi, K. Berova, N.; Woody, R. W. Eds., **1994**, 473–496, VCH, New York. (b) Proulx, C.; Lubell, W. D. *J. Org. Chem.* **2010**, *75*, 5385. (c) Chen, Y. H.; Yang, J. T. *Biochem. Biophys. Res. Commun.*, **1971**, *44*, 1285. (d) Krysmann, M. J.; Castelletto, V.; Kelarakis, A.; Hamley, I. W.; Hule, R. A.; Pochan, D. J. *Biochemistry* **2008**, *47*, 4597.

31. Kim, K.; Germanas, J. P. *J. Org. Chem.* **1997**, *62*, 2847.

32. Kessler, H. *Angew. Chem., Int. Ed. Engl.*, **1982**, *21*, 512.

33. (a) MacroModel, Version 9.9 Schrodinger, LLC, New York, NY, **2012**. (b) Kolossvry, I. W.; Guida, C. *J. Am. Chem. Soc.***1996**, *118*, 5011.

34. Sahoo, H.; Roccatano, D.; Hennig, A.; Nau, W. M. *J. Am. Chem. Soc*. **2007**, *129*, 9762

35. Sahoo, H.; Roccatano, D.; Hennig, A.; Nau, W. M. *J. Am. Chem. Soc.* **2007**, 129, 9762.

36. Steinberg, I. Z. *J. Chem. Phys.* **1968**, *48*, 2411-2413.

37. Steinberg, I. Z. *Annu. Rev. Biochem.* **1971**, *40*, 83-114.

38. (a) Gelamo, E.L.; Silva, C. H.; Imasato, H.; Tabak, M. *Biochim. Biophys. Acta* **2002**, *1594*, 84. (b) Naveenraj, S.; Anandan, S.; Kathiravan, A.; Renganathan, R.; Ashokkumar, M. *J. Pharm. Biomed. Anal.* **2010**, *53*, 804.

39. (a) Yamasaki, K.; Maruyama, T.; Kragh-Hansen, U.; Otagiri, M. *Biochim. Biophys. Acta* **1996**, *1295*, 147. (b) He, X. M.; Carter, D. C. *Nature* **1992**, *358*, 209.

40. Mandeville, J. S.; Tajmir-Riahi, H. A. *Biomacromolecules* **2010**, *11*, 465.

3.1. Introduction

β-Turn is one of the most important structure of protein among the different type of secondary structures.[1] It is one of the three major secondary structural elements of peptides and proteins. The β-turn[2] also been referred to as the β-bend, β-loop or reverse turn. The β-turn peptides play critical roles in the myriad of recognition events in biological systems.

Classifications of β-Turns based on their ϕ and ψ angles are the i+1 and i+2 residues. The existence of a number of turn types (I, I', II, II', III, III', IV, V, Va, VIa, VIb, VII, and VIII) the C_α^{i} to C_α^{i+3} distance varies from 4-7 Å.[3]

Vankatachalam has predicted the ideal value of torsion angles of β-turn structure and it is given in the **Table 3.1**. Based on the value of torsion angle phi (ϕ) and psi (ψ) (*) that must be a cis-proline, β-turn structures has been classified.[4]

Table 3.1. Torsional angels of β-turn conformation

Torsion angles of β-turn secondary structure				
Type	φ_{i+1}	ψ_{i+1}	φ_{i+2}	ψ_{i+2}
I	-60	-30	-90	0
II	-60	120	80	0
VIII	-60	-30	-120	120
I'	60	30	90	0
II'	60	-120	-80	0
VIa1	-60	120	-90	0*
VIa2	-120	120	-60	0*
VIb	-135	135	-75	160*
IV	turns excluded from all the above categories			

Though, an exponential growth on the development of constrained non-peptidic molecular scaffolds as peptidomimetics is observed, very few peptide-based drugs have been developed. Therefore, there is a need to renovate the existing design principles with newer concepts, chemistry and protocols to introduce conformationally constrained nonpeptide isosteres or small molecule scaffold into peptide backbones in order to achieve desirable secondary structures along with pharmacologically viable peptide-based drug candidates of enhanced metabolic stability.

According to the ϕ and ψ angles of the i+1 and i+2 residues β-turns are classified (**3.01-3.04**, **Figure 3.1-3.2**).[5] In addition the C_α^{i} to C_α^{i+3} distance varies from 4-7 Å, to the existence of a number of turn types (I, I', II, II', III, III', IV, V, Va, VIa, VIb, VII and VIII).[6]

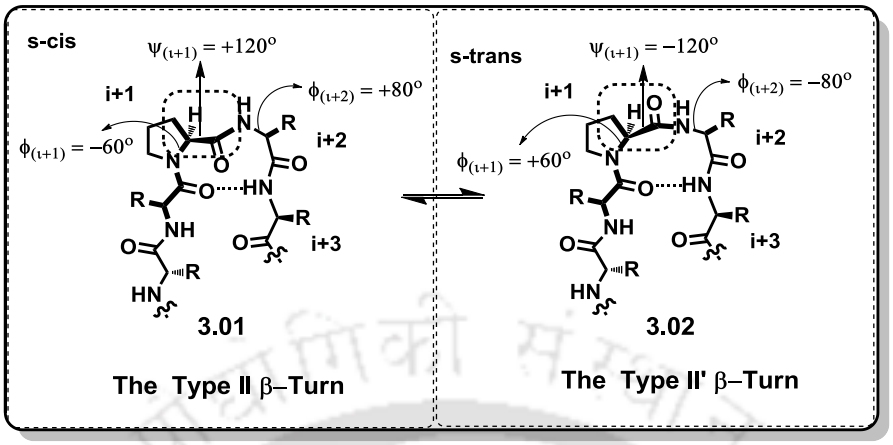

Figure 3.1. The type II- and II'-β-turn motif (**3.01-3.02**).[6]

The success of many efforts has been measured by the ability of a scaffold to adopt a turn motif, while the retention or improvement of biological activity is the ultimate indicator of that successful design. The turn structure has been measured using spectroscopic methods such as circular dichroism (CD)[7] or solution phase NMR.[8]

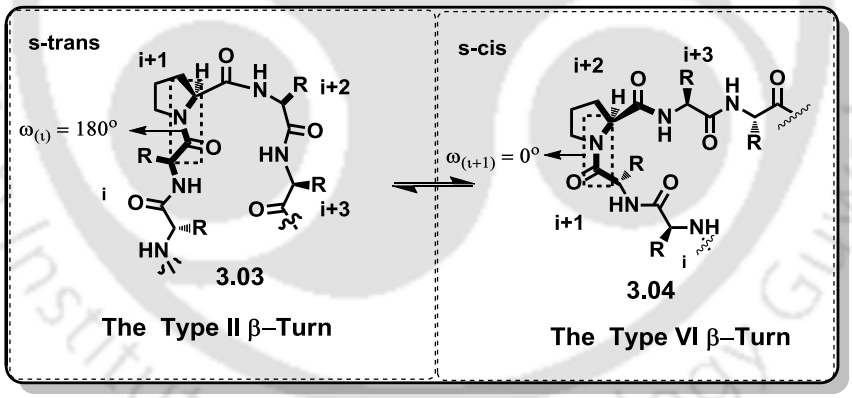

Figure 3.2. The type II- and VI- β-turn motif (**3.03-3.04**).[8]

The simplest defined loop structure of β-turns were determined by residues at two positions (i+1, i+2). Smith *et al.* have reviewed the conformational characteristics of simplest defined loop structure of β-turn.[9]

Katzenellenbogen *et al*. has designed a tetrapeptide mimic (**3.05**) based on biological active neuropeptides.[10] Type-1 β-turn conformation was adopted by the synthesized peptide **3.05** and the structure was also confirmed by NMR experiment analysis, molecular modeling study and X-ray crystallography (**Figure 3.3**). The

Type-1 β-turn conformations was stabilized through intramolecular hydrogen bonding interaction (**3.06-3.08, Figure 3.3**) and were stable in both the hydrogen bonding and non-hydrogen bonding solvents at various temperatures, which was supported by NMR experiment analysis.

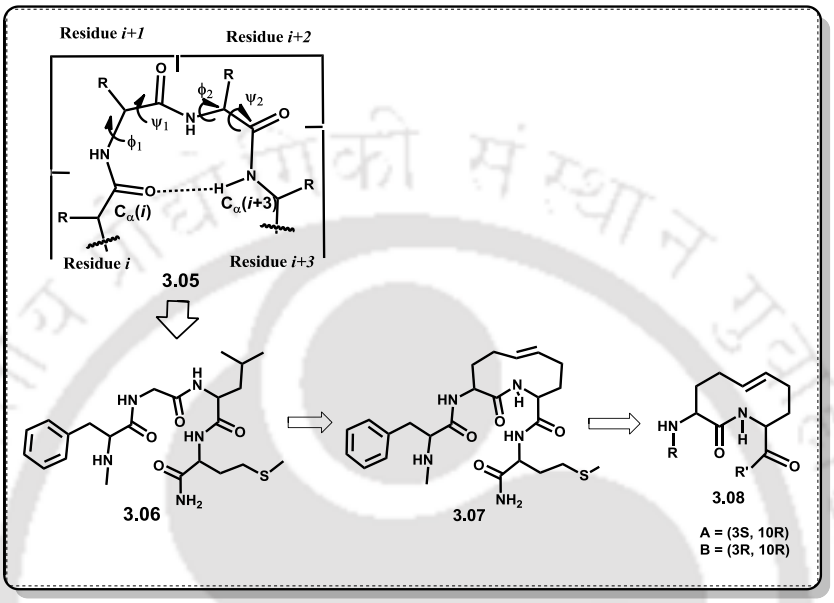

Figure 3.3. Type-I β -turn peptidomimetic (**3.05-3.08**).[10]

A series of β-turn peptides with biological importance have been synthesized by Pramanik and coworkers.[11] The influence of solvent polarity and steric interaction on the adopted conformation of the peptide backbone and interconversion of secondary structure between β-turn and β-sheet have been studied. The model tripeptides I-III, [BocNH–Ile–Aib–R–COOMe (R = Val for peptide I; Leu for II and Phe for peptide III), Aib (Aib = α-amino isobutyric acid)] have been synthesized by them. The steric residue part of the tripeptide was changed to investigate the conformational interconversion. Aib (α-amino isobutyric acid) was placed in center of the peptide through which it can adopt β-turn secondary structure. The peptide BocNH–Ile-Aib-Val-OMe [Peptide I, R= $CH(CH_3)_2$, **Figure 3.4**] exhibited the type-II β-turn structure (**3.09-3.11, Figure 3.4**) and the structure was stabilized through intramolecular hydrogen bonding interaction between CO of i^{th} residue and NH of i+3 residue creating pseudo ten membered ring (**3.12, Figure 3.4**). The adopted β-turn secondary structure of the peptide I was also confirmed by X-ray diffraction analysis. Similarly peptide II forms a hydrated β-turn representing the solvent mediated intermediate for the interconversion between β-turn and β-strand and peptide III adopts a completely unfolded β-strand like structure.

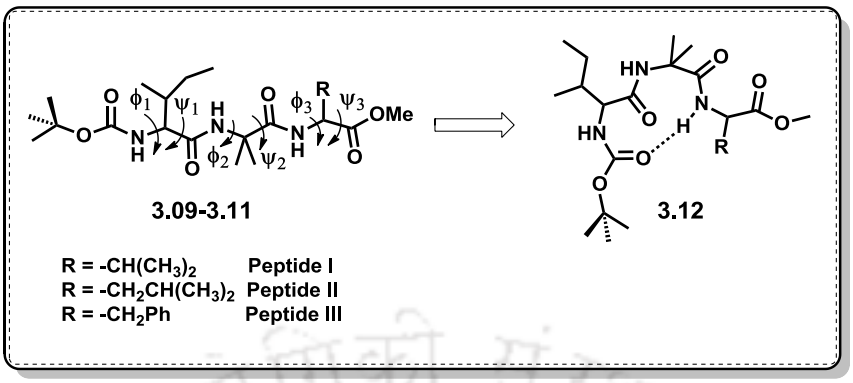

Figure 3.4. Type-II β-turn peptides containing **Aib** (α-amino isobutyric acid) in the center of the peptide strand (**3.09-3.12**).[11]

The residues Gly113–Asn113–Pro114–Tye115 can form a hairpin like type-VI revers turn in native RNase (**3.15, Figure 3.5**) was established by Ronald T. Raines and coworkers. The turn creating unit Asn113-Pro114 (**3.13**) was replaced by two β-amino acid residues, R-nipecotic acid-S-nipecotic acid (**3.14**). These two units when incorporated into the peptide backbone, stabilized the type-VI revers turn through N-H…O=C hydrogen bonded 12- membered ring formation. It was found to be resistant to degradation by protease enzyme.[12]

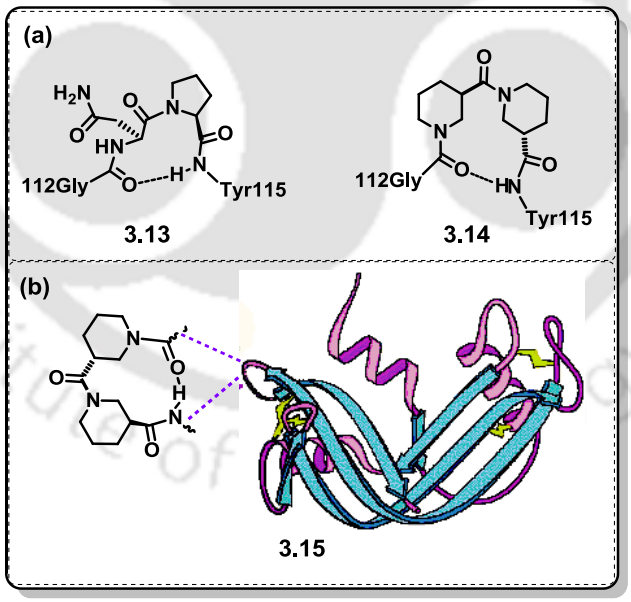

Figure 3.5. (a) Hydrogen bonding in Ribonuclease A variants containing Asn-Prolin (**3.13**) and R-nipecotic acid-S-nipecotic acid (**3.14**, R-Nip-S-Nip), (b) Semisynthesis of ribonuclease A by expressed protein ligation (**3.15**).[12] Copyright (2002) from American Chemical Society.

A novel revers turn peptidomimetics containing **Asx**-Pro-mimietics **3.18** was developed by Gmeiner and coworkers (**3.16-3.18**, **Figure 3.6**).[13] The **Asx**-Pro-turn (high frequency in protein structures nucleating type I β-turns) in peptide backbone was stabilized through intramolecular hydrogen bonding between i and i+3 residues. The revers turn in that peptide was also supported by NMR experiment. A stable intramolecular hydrogen bonding in peptide **3.18** was indicated by low $\Delta\delta/\Delta T$ value of -4.7 ppb/k in the solvent containing 30% DMSO in $CDCl_3$.

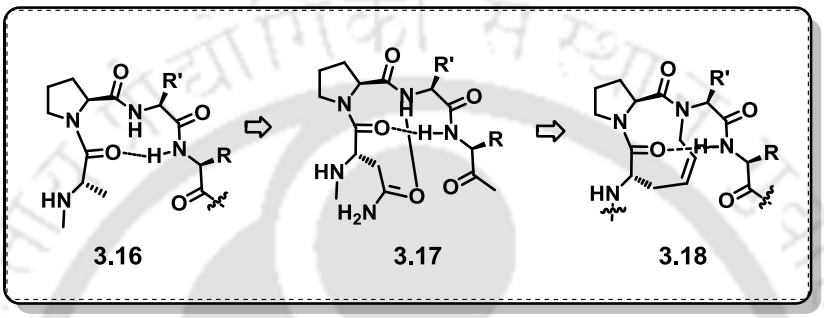

Figure 3.6. Ring-closing olefin metathesis based classical β-turn structure (**3.16-3.18**).[13]

A series of piperazine acid based β-turn peptidomimetics (**3.20-3.22**, **Figure 3.7**) have been synthesized by Russell and coworkers.[14] A library of tetrapeptides with 10 membered hydrogen bonding ring, where the distance of i and i + 3 residue varies from 4 to 7 Å was defined by them (**3.19**, **Figure 3.7**). They have studied the effect of piperazine acid as the key element of turn unit.

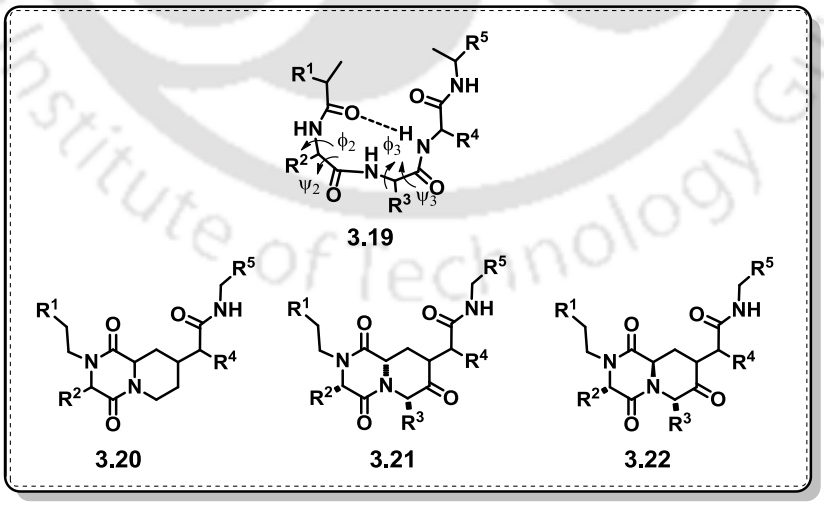

Figure 3.7. Peptidic β-turn and piperazine acid based β-turn mimetic peptides.[14]

A library of 1,4-diphenyl-1,2,3-triazole-based β-turn peptidomimics using click chemistry (**3.23-3.25**, **Figure 3.8**) was introduced by Zhan-Ting Li and his co-workers. The conformational analysis of synthesized compounds (**3.26-3.31**, **Figure 3.8**) in both solution and solid phase indicates the formation of β-hairpin or β-sheet like structures in peptide backbone. The compounds were stabilized via intramolecular hydrogen bonding. The scaffold helped the formation of β-sheets secondary structure in peptide strands attached in the two arms of the scaffold.[15]

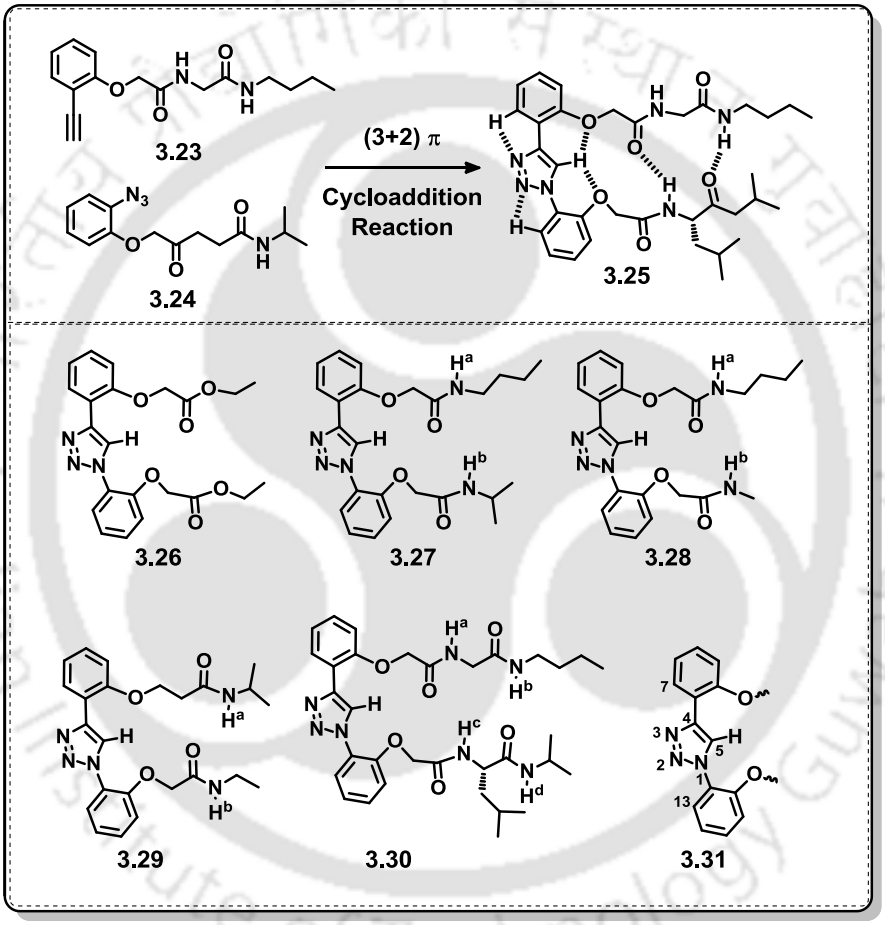

Figure 3.8. 1,4-diphenyl -1,2,3-triazole-based β-turn mimic as β-sheet nucleator (**3.23-3.25**).[15]

3.2. Relay FRET Process in Biomolecules

In 1999 there was a report of a sequential energy transfer system in oligonucleotides containing three chromophores those were located on the three separate strands.[16] In 2001 Nicholas J. Turro, Jingyue Ju and coworkers have synthesized trichromophoric DNA, labeled with three dyes with different absorption

and emission property. They have built up a multiple numbers of fluorescent chromophores that can serve the purpose of multiplex biological assays. The energy transfer system contained covalently attached three different fluorophores to a single stranded DNA molecule (**3.32**, **Figure 3.9**). This triple fluorescence energy transfer system showed the increase in acceptor emission with a large "Stokes shift".[17] This trichromophore-labeled DNA with constant fluorescence signature, were independent of the length of DNA fragments. This trichromophoric labeling approach in DNA can further be prolonged to more than three chromophores and can be applicable to wide-ranging applications in biological labeling and imaging.

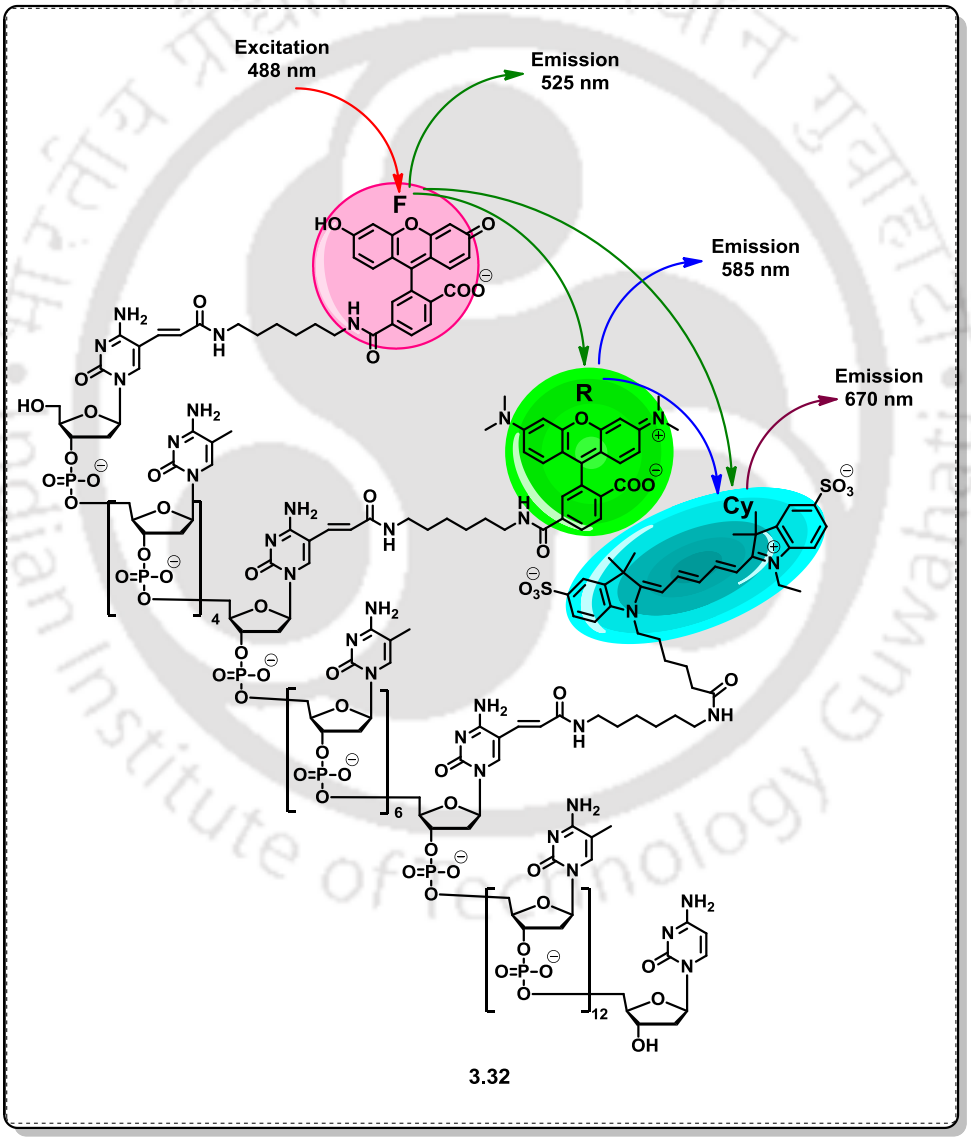

Figure 3.9. The interaction of the three chromophores that are separated by defined number of nucleotides allows efficient ET to take place in three fluorophoric units of DNA (**3.32**).[17]

In 2011 Gregory A. Sotzing and coworkers have utilized a DNA thin film and tagged it with three fluorescent dyes (**3.33-3.35**, **Figure 3.10**). They incorporated three chromophores in solid state DNACTMA thin films. They established an efficient long-range energy transfer through relay FRET process in a solid-state matrix of DNA-CTMA where no covalent attachments were necessary (**3.36**, **Figure 3.10**). The better ability of DNA to interact with the encapsulated dyes and to provide the required proximity and orientation was improved the FRET efficiency.[18]

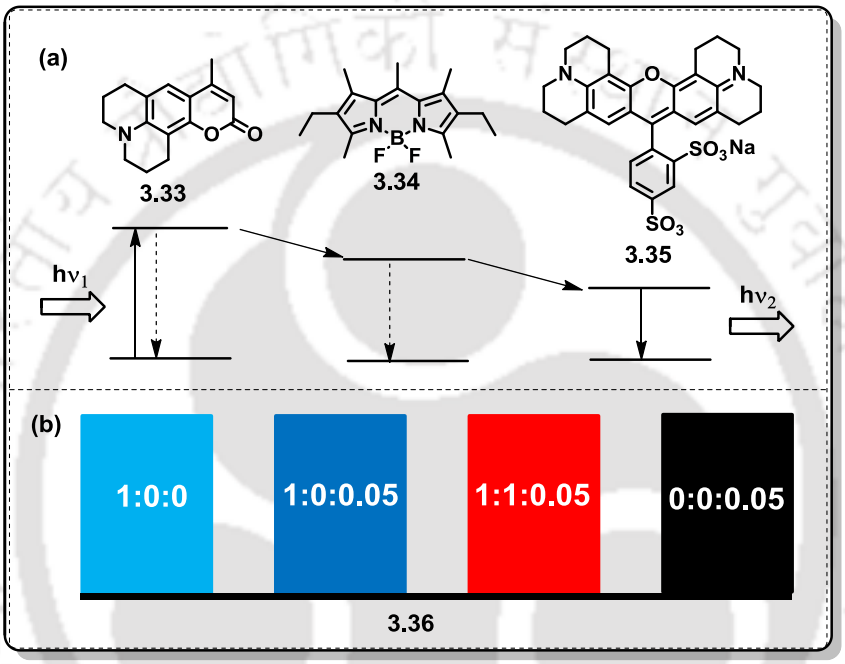

Figure 3.10. (a) Schematics of the cascade FRET process in DNA thin film (**3.33-3.35**), (b) Digital photographs of DNA films illuminated less than 365 nm UV light (**3.36**).[18]

In 2011 Michael Gratzel and coworkers employed multiple energy relay dyes in liquid dye sensitized solar cells. They employed 4-(dicyanomethylene)-2-methyl-6-(4-dimethylaminostyryl)-4H-pyran (**3.38**, DCM) with zinc phthalocyanine (**3.37**, TT1) Rhodamine B (**3.39**, RB) and Rhodamine BE (**3.40**, RBE) dyes having complementary absorption spectra. When these dyes were placed inside the porous network of the nanocrystalline TiO_2 film, high yields of energy transfer was resulted (**Figure 3.11**). This FRET phenomena enhanced the solar-to-electric power conversion efficiency by 35 %.[19]

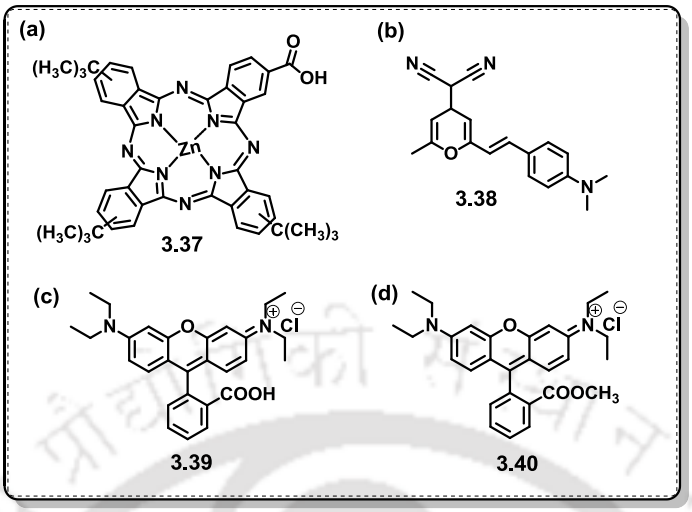

Figure 3.11. Molecular structures of (a) TT1 (**3.37**), (b) DCM (**3.38**), (c) RB (**3.39**) and (d) RB E (**3.40**) that were used in liquid dye sensitized solar cells.[19]

János Szöllősi and coworkers have developed a method that allows the determination of FRET efficiency on a flow cytometer in three-dye systems.[20] This Triple FRET process that was measured in two-dye systems, regenerated the energy transfer efficiency of the system (**3.42-3.44**, **Figure 3.12**) indicating the existence of trimeric complexes which was not possible with conventional FRET methods (**3.41**, **Figure 3.12**).[21]

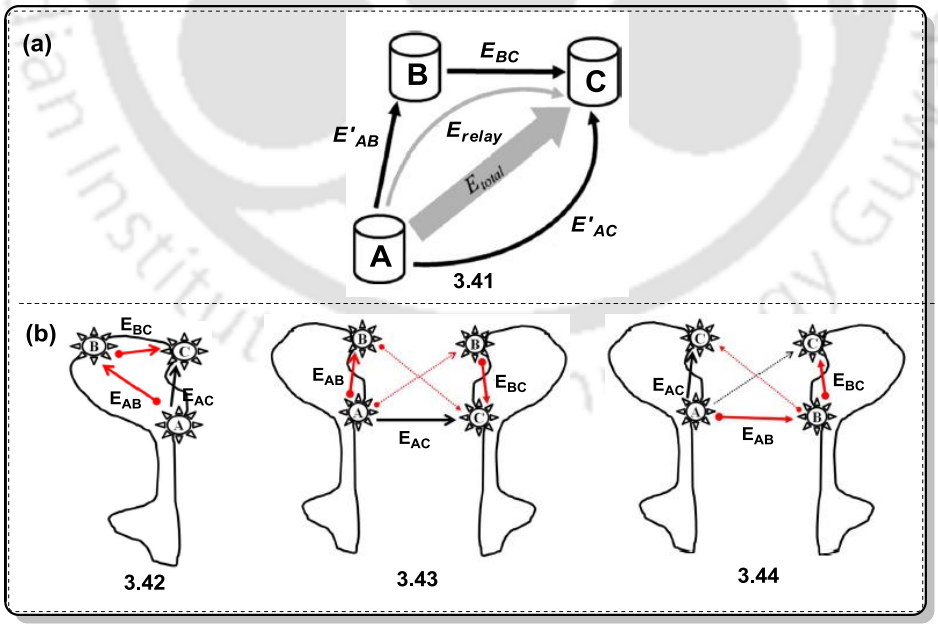

Figure 3.12. (a) Schematic drawing of a three-dye system with possible energy transfer routes (**3.41**). (b) Schemes for providing the alternative spatial distribution and possible transfer routes between fluorescently tagged antibodies (**3.42-3.44**).[21] Copyright (2013) from Wiley Online Library.

Daniel Moses, Alan J. Heeger and coworkers have designed a process that accumulated a complex containing conjugated polymer (CCP) and a dsDNA containing three fluorophores (**3.47-3.49**, **Figure 3.13**). In this system the two step FRET process was observed. The energy transfer occurs from cationic conjugated polymer to a fluorescein molecule linked to one terminus of the DNA to an ethidium bromide (EB) molecule introduced into the dsDNA unit (**3.46**, **Figure 3.13**). The direct energy transfer from the CCP to EB results from the near orthogonality of their transition moments which was supported by time-dependent anisotropy measurements (**3.45**, **Figure 3.13**). Here the fluorescein molecule acts as intermediate molecule that relays the FRET energy from complex containing conjugated polymer (CCP) to ethidium bromide (EB). This type of sequential energy-transfer mechanism containing polymer units have been used to elucidate the efficient energy transfer in the photosynthetic light-harvesting arrangements.[22]

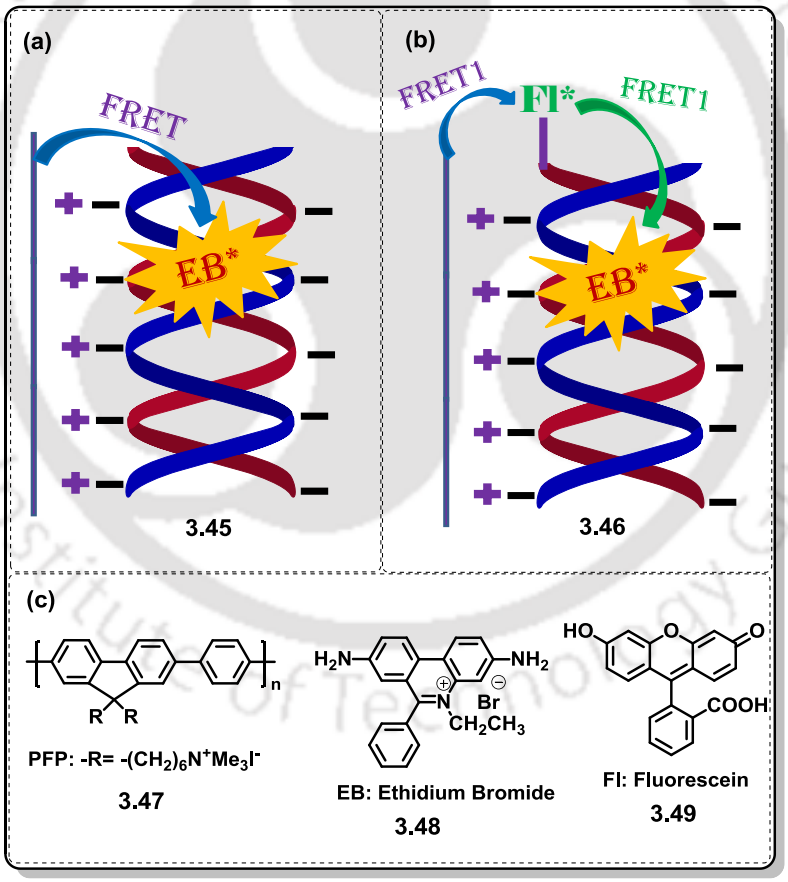

Figure 3.13. Schematic representation of DNA sequence detection by FRET from CCP to intercalated dyes in the absence (a, **3.45**) and presence (b, **3.45**) of fluorescein. (c) The molecular structures of the CCP (PFP), FL, and EB (**3.47-3.49**).[22]

In many biological processes peptide-membrane interactions play a crucial role, for example membrane lysis, fertilization, and viral infection.[23] Gai *et al*. have studied the kinetics of the helix formation through the peptide-membrane association using FRET phenomenon among *p*-cyano-l-phenylalanine and tryptophan FRET pair (**3.50-3.52**).

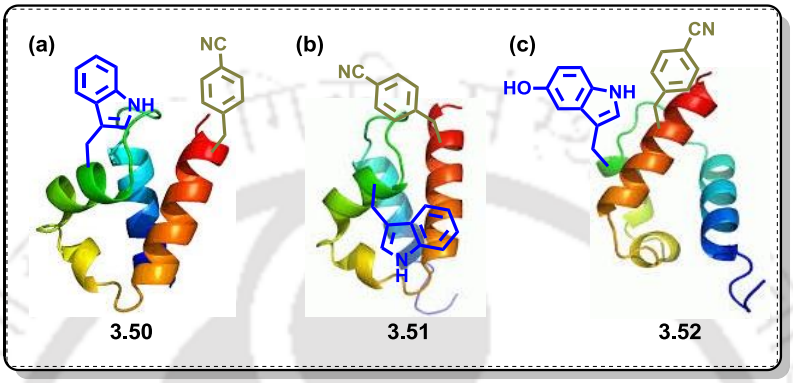

Figure 3.14. (a) FRET based protein for study the kinetics of the helix formation accompanied by the peptide–membrane association utilising FRET phenomenon among a FRET pair, *p*-cyano-l-phenylalanine and tryptophan (**3.50**). (b) FRET phenomena for studying the urea-induced unfolding transitions of two small proteins (**3.51**). (c) The 7-azatryptophane (7AW) and 5-hydroxytryptophane (5HW) as FRET acceptor to Phe-CN in proteins utilized to demonstrate the urea-induced unfolding transitions of protein (**3.52**).[23]

Igor L. Medintz and coworkers have established the utilization of hybrid fluorescent protein semiconductor quantum dot (QD) sensor to monitor caspase **3** proteolytic activity using FRET phenomena (**3.53**, **Figure 3.15**). The fluorescent protein can serve the purpose of an efficient fluorescence resonance energy transfer acceptor due to the closeness to the QD. The addition of caspase **3** enzyme to the QD-fluorescent protein conjugates specifically cleaved the fluorescent protein linker sequence which can alter the energy transfer with the QD and monitor its proteolytic activity quantitatively (**3.54, Figure 3.15**). This type of sensing approach contains bacterial appearance of the protease substrate including FRET event, facilitate self-assembly to QDs, and can modify the substrate to target other proteases.[24]

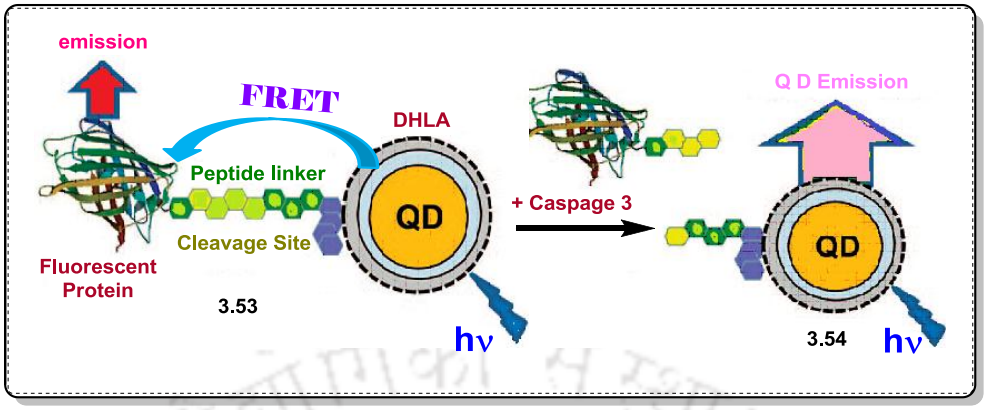

Figure 3.15. Schematic diagram of the QD-fluorescent protein sensor. Fluorescent protein with an *N*-terminal linker expressing the caspase **3** cleavage site, resulting in FRET quenching of the QD and sensitized emission from the fluorescent protein acceptor (**3.53-3.54**). Copyright (2009) from American Chemical Society.

Subhendu Sekhar Bag and coworkers have synthesyzed aromatic triazolo amino acid scaffold as a turn mimetic β-sheet nucleator. They have also described the photophysical result from an ^{Ar}**TAA** scaffolded trichromophoric fluorescent pentapeptide and its application in sensing BSA. After analysis of the photophysical properties of trichromophoric fluorescent pentapeptide, it established the concept of dual door entry to excimer emission. Both the processes of excitation of **TPy** of ^{TPy}**Ala**^{Do}-either energy transfer from excited scaffold amino acid, ^{Ar}**TAA** (FRET) to **TPy** or direct excitation of **TPy**-led to the excimer emission in pentapeptide (**3.55**, **Figure 3.16 a**).[25]

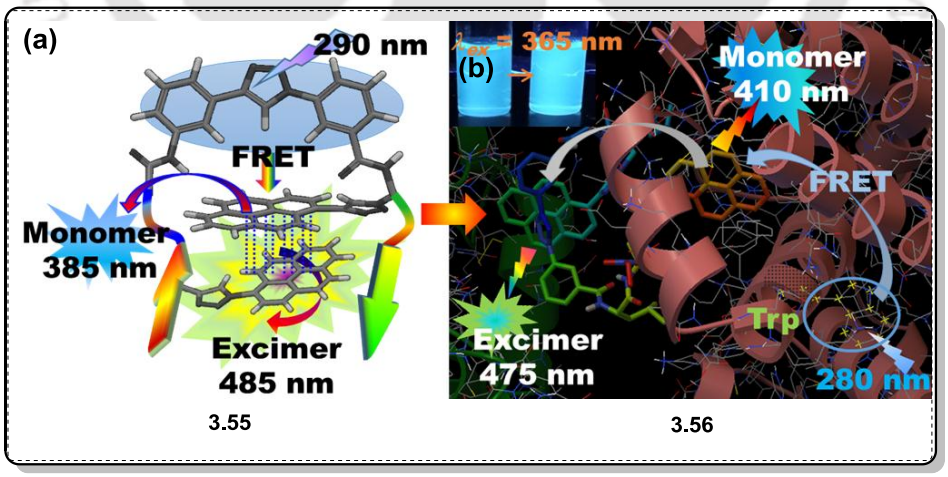

Figure 3.16: (a) Schematic presentation of the aromatic triazolyl amino acid scaffold ^{Ar}**TAA** based dual door entry system trichromophoric fluorescent pentaptide (**3.55**) and (b) protien–Peptide interaction (**3.56**).[25] Copyright (2016) from Royal Society of Chemistry.

This study would provide fundamental guidelines to design such conceptual fluorescent probe of dual door entry system to excimer emission which would start of a new generation of probes that find wide applications in the field of chemical biology. Moreover, the probe of dual door entry to excimer emission system was creating an effective fluorescence light-up probe for studying protein (BSA)–peptide interactions in solution (**3.56**, **Figure 3.16 b**).[25]

3.3. Background

For peptides and proteins one of the major secondary structural elements is β-turn. The β-turn peptides the residue which contains potentially critita1 pharmacophoric information is predominates, thus, this secondary structure plays a critical role of recognition events in biological system. Now a day the β-turn mimetics is a po werful tool examine the relationship between structure-function of complex proteins and peptides. Therefore a great deal of efforts have been paid to synthesize conformationally constrained small molecule scaffolds that can create 'nucleating turn mimics' and induce the secondary structure in peptide strands. As for an example Kelly *et al.* have synthesized dibenzofuran unit to nucleate anti-parallel β-sheets. Soth *et al.* have synthesized peptide/oligourea/azapeptide hybrid oligomer as β-turn nucleating agent, which contains two intramolecular hydrogen bonds and adopt a hairpin turn. Smith, Hirschmann *et al.* have used of 3, 5-linked pyrrolin-4-one to create a hydrogen-bonded turn-like structure as β-strand mimic. However, limited attempt have been undertaken to design a fluorescent peptide aiming at the fundamental aspects that a particular conformation can have an impact on the photophysics. Investigating such an impact might find widespread applications in studying interbiomolecular interactions in cell and the design of new peptide based drug candidates. Therefore, the generation of scaffolded peptidomimetics with interesting fluorescence property of fundamental importance is highly demanding.

3.4. Objective

As a part of our ongoing research activity, we previously designed aromatic triazolyl amino acid as constrained molecular scaffold to establish a β-sheet structure in a Leu-enkephaline analogue peptide and in a designed trichromophoric pentapeptide with interest dual door entry to excimer emission property. Inspired by our previous work and work presented in **Chapter 2** we thought that *o,o*- or *o,m*-aromatic triazolyl amino acid could serve as interesting scaffold for peptide secondary structure induction and thereby helping in generation of interesting photophysical property. Thus, we framed our objective as below

(a) Synthesize of *ortho,meta*-aromatic amino acid scaffold *via* click chemistry.
(b) Synthesis of trichromophoric pentapeptide and study of conformation.
(c) Study photophysical property toward establishing our concept of a relay FRET process.

We thought that the scaffold ($^{o,m\text{-}Ar}$**TAA**) would adopt a hairpin turn and induce the two chromophores at the two termini to come closer thereby allowing them possibly in dipolar photophysical interaction. From a priori knowledge that the *m,m*-aromatic triazolyl amino acid scaffold (^{Ar}**TAA**) and pyrene form a FRET pair while a Pyrene-Perylene also form the same pair. Therefore, we envisioned that a pentapeptide with the scaffold in the backbone if decorated with triazolyl perylene amino acid (^{TPer}**Ala**^{Do}) at the *N*-terminus and triazolylpyrene amino acid (^{TPy}**Ala**^{Do}) at the *C*-terminus, we could achieve a FRET relay process from the scaffold $^{o,m\text{-}Ar}$**TAA** to ^{TPy}**Ala**^{Do} to ^{TPer}**Ala**^{Do} upon exciting the peptide at the absorption (λ_{max} = 290 nm) of scaffold wherein no or negligible absorption is exhibited by other two chromophore.

(d) Study of interaction of trichromophoric fluorescent pentapeptide with protein BSA.

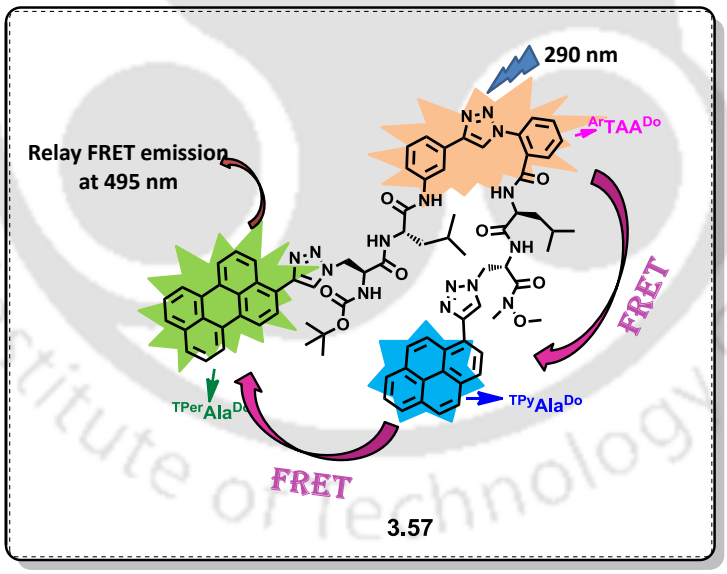

Figure 3.17. Graphical presentation of *ortho,meta*-triazolo aromatic amino acids, the Leu-Enkephalin peptide and the possible photophysics in a designed fluorescent pentapeptide.

3.5. Result and Discussion

3.5.1. Synthesis of *ortho,meta*-Triazolo Aromatic Amino Acids Scaffold ($^{o,m\text{-}Ar}$TAA) and Corresponding Peptides

Our first target was to synthesize triazolo ***o,o***-aromatic amino acid scaffold **3.65** ($^{o,o\text{-}Ar}$**TAA**) and its corresponding Leu-enkephalin analogue and fluorescent pentapeptide. However, we only could synthesize a tripeptide analogue to Leu-enkephalin **3.67** (**BocNH–$^{o,o\text{-}Ar}$TAA–Phe–Leu–COOMe**) containing this triazolo *o,o*-aromatic amino acid scaffold (**Scheme 3.1**).

For the synthesis of *o,o*-aromatic triazolyl amino acid scaffold, we first synthesized, *N*-Boc protected 2-ethynyl-aniline **3.64** from 2-bromo aniline **3.61** via $PdCl_2(PPh_3)_2$ catalyzed sonogashira coupling and the deprotection of the TMS group with KOH in MeOH solvent at room temperature. 3-azido methyl benzoate **3.60** was prepared starting from anthranilic acid. Anthranilic acid **3.58** was reacted with $SOCl_2$/ MeOH and the product was reacted with $NaNO_2$ / NaN_3 in acidic medium at 0 ^oC to get ortho azido methyl benzoate.

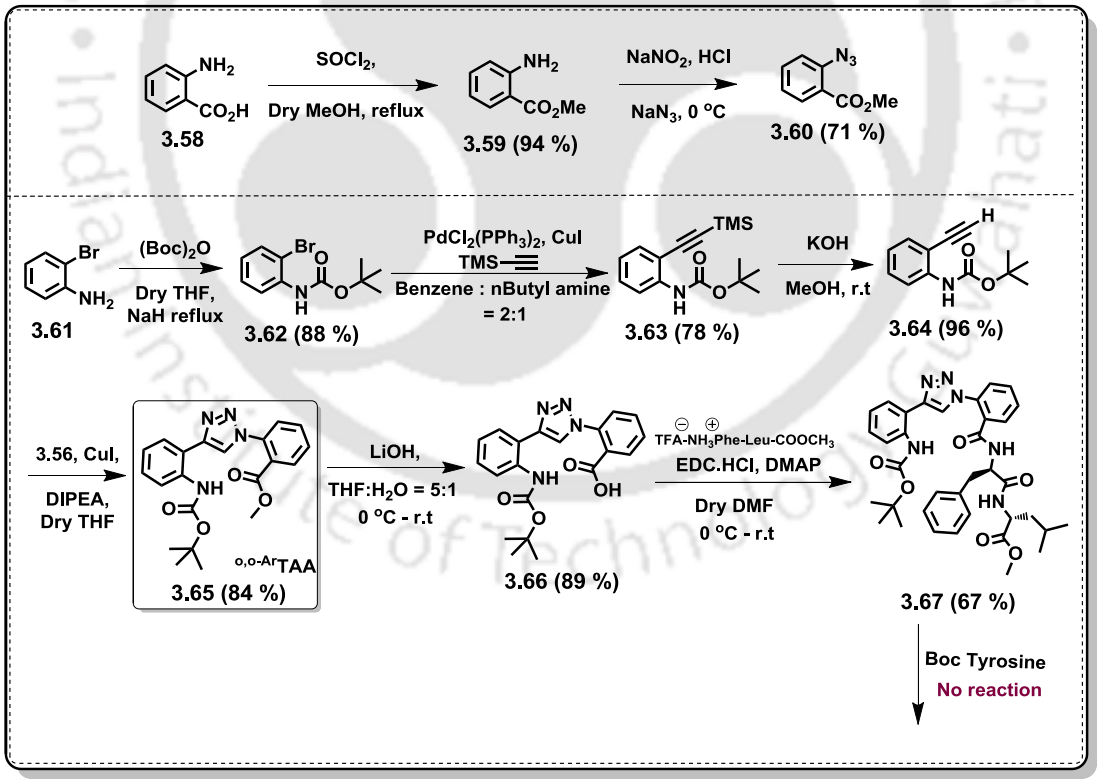

Scheme 3.1. Synthesis of ($^{o,o\text{-}Ar}$**TAA**) containing tripeptide [**BocNH–$^{o,o\text{-}Ar}$TAA–Phe–Leu–COOCH$_3$**].

Next, ortho azido methyl benzoate **3.60** and *N*-Boc protected 2-ethynyl-aniline **3.64** were reacted under click reaction condition to get *o,o*-aromatic triazolyl amino acid scaffold **3.65** in both C and N protected form. The scaffold was then reacted with LiOH to hydrolyze methyl ester getting *N–P*rotected *o,o*-aromatic triazolyl amino acid scaffold **3.66** (**Scheme 3.1**).

The synthesized scaffold was then subjected to react with Boc deprotected TFA salt of Phe–Leu–$COOCH_3$ to afford the tripeptide **3.67** containing *o,o*-aromatic triazolyl amino acid scaffold (**Scheme 3.1**). The incorporation of tyrosine at the *N*-terminus of the scaffold was unsuccessful to complete the synthesis of Leu-enkephalin analogue. This is possibly because of steric reason. However, this tripeptide enabled us to test the conformational induction by the scaffold and set the path to think for the alternative scaffold, i.e. *o,m*-analogue.

Therefore, we planned to synthesize the triazolo *ortho,meta*-aromatic amino acid scaffold (**$^{o,m\text{-Ar}}$TAA**) and incorporate into a trichromophoric fluorescent pentapeptide containing triazolyl perylene amino acid (**^{TPer}Ala^{Do}**) at the *N*-terminus and triazolyl pyrene amino acid (**^{TPy}Ala^{Do}**) at the *C*-terminus via a solution phase pepetide coupling protocol [**3.79, BocNH–^{TPer}Ala^{Do}–Leu–$^{o,m\text{-Ar}}$TAA–Leu–^{TPy}Ala^{Do}–CONMe(OMe)].** We also incorporated it into a tetrapeptide sequence analogous to Leu-enkephalin (**3.82, BocNH–Tyr–$^{o,m\text{-Ar}}$TAA–Phe–Leu–CO_2Me**) to test the conformational induction by the scaffold.

For the synthesis of **3.72** (**$^{o,m\text{-Ar}}$TAA**) we followed the similar protocol as we have mentioned for the synthesis of **3.65** (**$^{o,o\text{-Ar}}$TAA**) starting from 3-bromo aniline **3.68** and anthranilic acid **3.58** (**Scheme 3.2**).

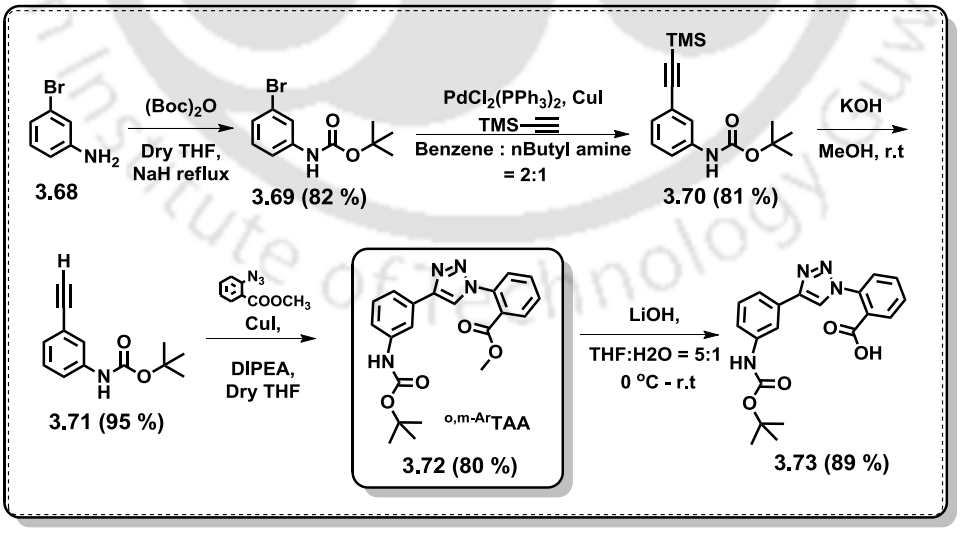

Scheme 3.2. Synthesis of *o,m*-aromatic triazolyl amino acid scaffold **3.72** (**$^{o,m\text{-Ar}}$TAA**).

Next we have incorporated our synthesized scaffold, $^{o,m\text{-}Ar}$**TAA,** in a designed fluorescent pentapeptide **3.79** and a linear Leu-enkephalin analogue peptide **3.82** to investigate the constrained properties of our synthesized molecular scaffold. All intermediate and final peptides were synthesized following a solution phase peptide coupling protocol. Thus the $^{o,m\text{-}Ar}$**TAA** (**3.72**) was coupled via EDC.HCl/DMAP mediated peptide coupling protocol with azido [**TFA-NH$_3$–Leu–Ser–CONMe(OMe)**] dipeptide **2.49** to get $^{o,m\text{-}Ar}$**TAA** containing *N*, *C*-protected azido tripeptide **3.76**. After that via (3+2)π cycloaddition reaction we have obtained the fluorescent tripeptide **3.77**.

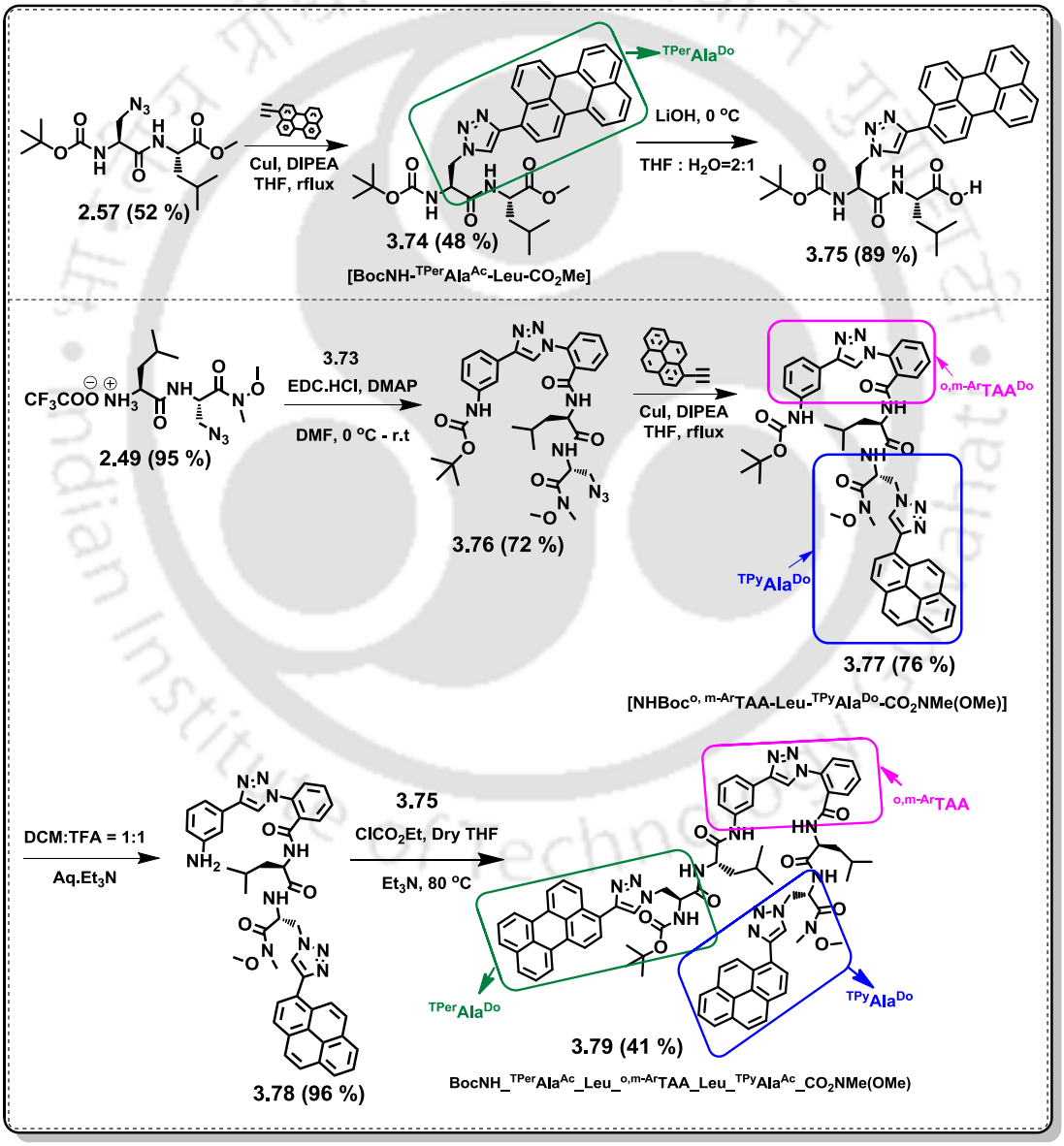

Scheme 3.3. Synthetic scheme of aromatic triazolyl amino acid scaffold based unnatural **pentapeptide 3.79 [BocNH–^{TPer}Ala^{Do}–Leu–$^{o,m\text{-}Ar}$TAA–Leu–^{TPy}Ala^{Do}–CONMe(OMe)].**

The Boc deprotection of the fluorescent tripeptide (**3.78**) was carried out using TFA in DCM solvent. Free amine derivative we have obtained by washing the tripeptide solution with aqueous Et_3N. The Boc deprotected tripeptide was then allowed to couple with BocNH–protected dipeptide **3.75** (**BocNH–^{TPer}Ala^{Do}–Leu–CO_2H**) via EDC.HCl/HOBT mediated peptide coupling protocol afforded our desired fluorescent pentapeptide **3.79** with triazolyl pyrene and triazolyl perylene at the two termini (**Scheme 3.3**).

The Leu-enkephalin analogue, using $^{o,m\text{-}Ar_r}$**TAA** was synthesised following similar procedure to study the conformation, which was induced by $^{o,m\text{-}Ar_r}$**TAA**. Thus, TFA salt of COOH protected Phe–Leu–$COOCH_3$ dipeptide was reracted with $^{o,m\text{-}Ar_r}$**TAA** via EDC.HCl/DMAP mediated peptide coupling protocol yielded tripeptide **3.80**. The *N*-terminus of the tripeptide was then deprotected using TFA and DCM solvent. The BocNH–tyrosine was then attached to the *N*-terminus of *N*-BocNH–deprotected tripeptide **3.81** to get the desired tetrapeptide **3.82** containing $^{o,m\text{-}Ar_r}$**TAA** molecular scaffold (**Scheme 3.4**).

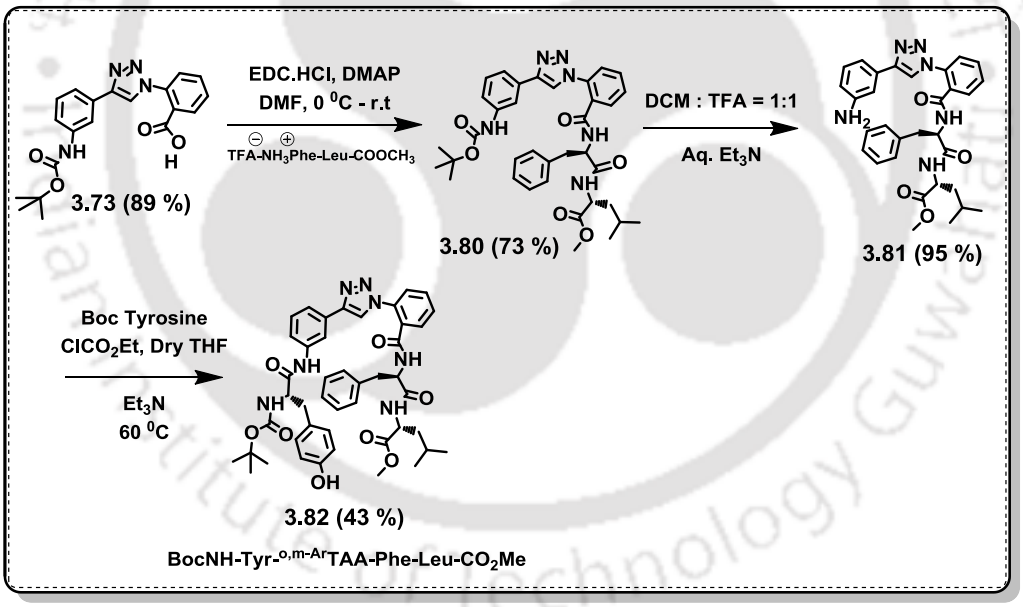

Scheme 3.4. Synthetic scheme of *ortho,meta*-triazolyl aromatic amino acid scaffold based Leu-enkephalin analogue natural **Tetrapeptide 3.82** [**BocNH–Tyr–$^{o,m\text{-}Ar_r}$TAA–Phe–Leu–COOMe**]**.**

Next we have synthesized the monomer units, for FRET comparison of our synthesized pentapeptide. Serine azide was allowed to react with 1-Pyrene alkyne and 3-Perylene alkyne separately under click reaction condition to get monomeric units

[BocNH–^{TPy}Ala^{Do}–CONMe(OMe)] 2.65 and **[BocNH–^{TPer}Ala^{Do}–CONMe(OMe)] 3.83** (**Scheme 3.5**).

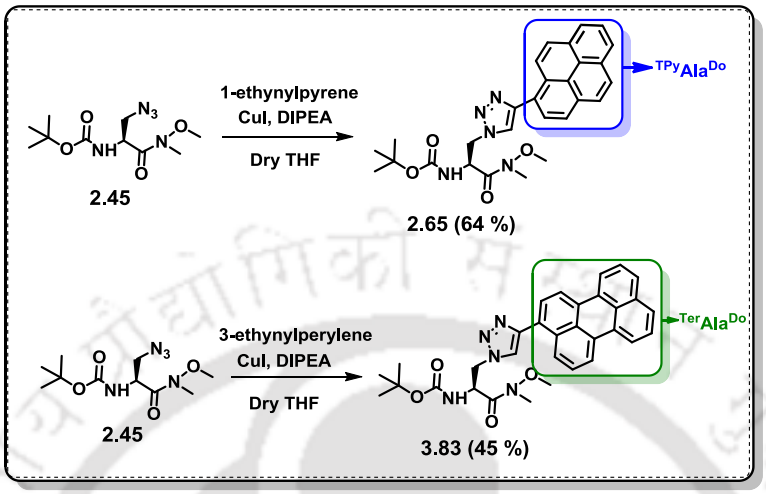

Scheme 3.5. Synthetic scheme for monomeric amino acids ^{TPy}**Ala**^{Do} (**2.65**) and ^{TPer}**Ala**^{Do} (**3.83**) in *N*, *C*-protected form.

All the synthesized pentapeptides (final and intermediate) were obtained in the pure form by column chromatography using silica-gel (60-120 mesh) and characterized via ^{1}H, ^{13}C, 2D NMR, IR, HR-mass spectrometry. Next we have studied the secondary structure of the pentapeptides were studied by various spectroscopic techniques.

3.5.2. Conformational Study of Pentapeptide 3.79 and Tetrapeptide 3.82 using CD, IR, NMR, Spectroscopic Techniques.

Study of Circular Dichroism Spectroscopy: CD spectra were recorded using a CD spectropolarimeter with a cell path length of 1 mm at in different solvent at room temperature. All the samples were with 50 μM concentration and prepared in spectroscopic grade solvents.

First we analyzed the CD spectra of the scaffolds (**3.65, 3.72**). From circular dichroism spectra it was revealed that the scaffolds adopted hairpin turn structure (-196, +200 and +207 nm) with negative induced CD signals corresponding to the absorption wavelengths of the scaffolds at 250 and 283 nm in polar protic solvent MeOH. The chirality was found to be inversed in polar aprotic solvent acetonitrile (+195, -200, +232 nm) with an appearance of a red shifted ICD bands at 257 and 296 nm having positive CD intensity.

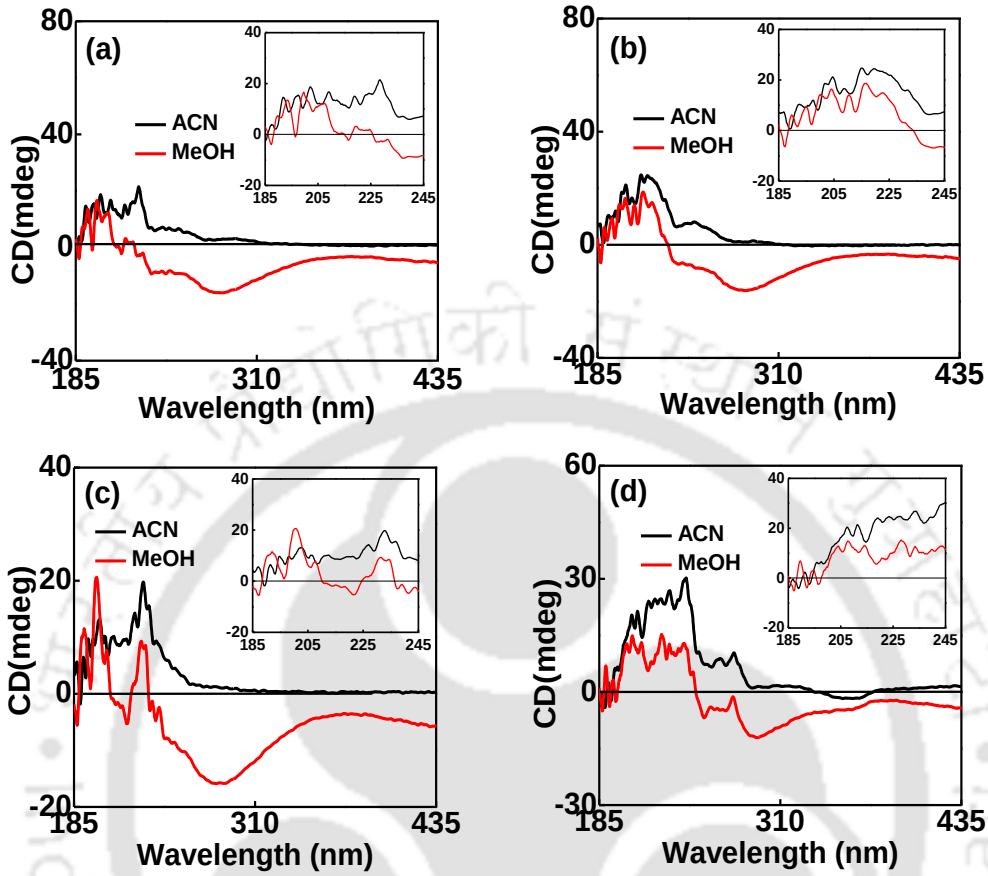

Figure 3.18. CD spectra of (a) $^{o,o\text{-Ar}}$**TAA** (**3.65**), (b) Tripeptide **3.67** [**BocNH–**$^{o,o\text{-Ar}}$**TAA–Phe–Leu–COOMe**], (c) $^{o,m\text{-Ar}}$**TAA** (**3.72**) (d) Tripeptide **3.77** [**BocNH–**$^{o,m\text{-Ar}}$**TAA–Leu–**^{TPy}**Ala**^{Do}**–CONMe**(**OMe**)] in acetonitrile and methanol solvents (50 μM concentration; 25 ^{o}C).

This results indicated the H-bond mediated inversion of chirality/conformation which might again due to the out of-planarity of o-aminophenyl unit with respect to rest part of the scaffold, a result similar to what was observed in our earlier designed triazolyl-*m,m*-aromatic amino acid scaffold.[25] Similar observation were observed in case of tripeptide **3.67** containing scaffold $^{o,o\text{-Ar}}$**TAA** (**3.65**) and fluorescent tripeptide **3.77** containing scaffold $^{o,m\text{-Ar}}$**TAA** (**3.72**).

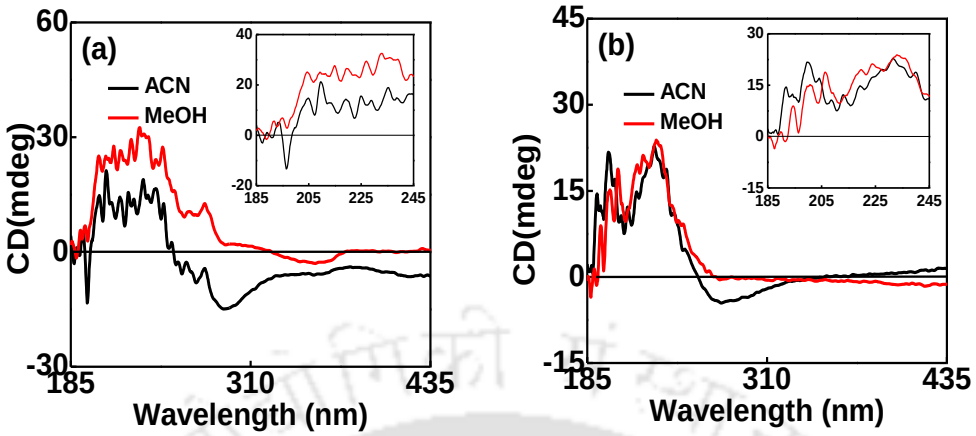

Figure 3.19. (a) CD spectra of **Pentapeptide 3.79** [**BocNH–^{TPer}Ala^{Do}–Leu–$^{o,m\text{-}Ar}$TAA–Leu–^{TPy}Ala^{Do}–CONMe(OMe)**] and (b) **Tetrapeptide 3.82** [**BocNH–Tyr–$^{o,m\text{-}Ar}$TAA–Phe–Leu–COOMe**] in acetonitrile and methanol solvents (50 μM concentration; 25 ^{o}C).

The secondary structure determination via CD study of both the Leu-enkephalin analogue **3.82** and fluorescent pentapeptide **3.79** containing $^{o,m\text{-}Ar}$**TAA** in the backbone, showed predominantly turn induced β-sheet like structures.

Intramolecular H-Bonding Interaction Using the Study of FT-IR Spectroscopy: To prove the intramolecular H-bond formation in the two strands of the synthesized peptides, IR spectroscopic technique was used. So, IR spectra were recorded using dry KBr pellets, which showed the presence of intramolecular H-bonded and free amide -NH stretching absorptions at 3463-3294 and 3480-3320 cm^{-1} for fluorescent pentapeptide **3.79** and Leu-enkephalin analogue tetrapeptide **3.82** supporting β-sheet like structures in both the peptides. The IR spectrum of peptide **3.79** showed a sharp N-H stretching absorption at $\bar{\upsilon}$ =3294 cm^{-1}, C=O stretching at $\bar{\upsilon}$ =1722 cm^{-1} and 1654 cm^{-1} and for Leu-enkephalin analogue **3.82** IR spectra showed N-H stretching absorption at $\bar{\upsilon}$ =3320 cm^{-1}, C=O stretching at $\bar{\upsilon}$ =1743 cm^{-1} and 1658 cm^{-1}. The absorption peaks does not dependent on the sample concentration.[26]

Intramolecular H-Bonding Interaction Using the Study of Variable Temperature ^{1}H NMR (VT-NMR): Variable temperature ^{1}H NMR analysis was carried out in d_6-DMSO to support the intramolecular Hydrogen bonding interaction in fluorescent pentapeptide **3.79** and Leu-enkephalin analogue tetrapeptide **3.82** in which all NHs showed different chemical shifts. Intramolecular H-bonding formation was indicated in both peptide **3.79** and **3.82** from VT-NMR analysis. Almost all the amide NH's, and triazole C-H exhibited ($\Delta\delta/\Delta T$) values that are moderate to close to

Kessler limit of -3 to -6 ppb/K (**Figure 3.20, Table 3.2**) indicating presence of strong to moderate intramolecular H-bonding and supported the predominant turn induced β-sheet like structure of the peptides.

Table 3.2. Values of temperature coefficients of chemical shifts of amide NHs or triazole-CH in (a) **Pentapeptide 3.79** [**BocNH–^{TPer}Ala^{Do}–Leu–$^{o,m\text{-}Ar}$TAA–Leu–^{TPy}Ala^{Do}–CONMe(OMe)**] and (b) **Tetrapeptide 3.82** [**BocNH–Tyr-$^{o,m\text{-}Ar}$TAA–Leu–Phe–COOMe**].

NHs from Fluorescent Pentapeptide 3.79	**$\Delta\delta/\Delta T$ (ppb/k)**	**NHs from Tetrapeptide 3.82**	**$\Delta\delta/\Delta T$ (ppb/k)**
N-terminal–Ser–NH1	- 5.00 ppb/k	*N*-terminal-Tyr–NH1	- 12.5 ppb/k
N-terminal–Leu–NH2	- 5.43 ppb/k	$^{o,m\text{-}Ar}$TAA–NH2	- 6.49 ppb/k
$^{o,m\text{-}Ar}$TAA –NH3	- 4.63 ppb/k	*C*-terminal–Phe–NH3	-9.0 ppb/k
C-terminal–Leu–NH4	- 5.26 ppb/k	*C*-terminal–Leu–NH4	-7.54 ppb/k
C-terminal–Ser–NH5	- 6.31 ppb/k	$^{o,m\text{-}Ar}$TAA-triazole-CH1	-1.63 ppb/k
$^{o,m\text{-}Ar}$TAA-CH1	- 1.00 ppb/k	Tyr-OH	-5.63 ppb/k
C-terminal–P^{y}Tz_CH2	- 1.07 ppb/k		
N-terminal–P^{er}Tz-CH3	- 1.00 ppb/k		

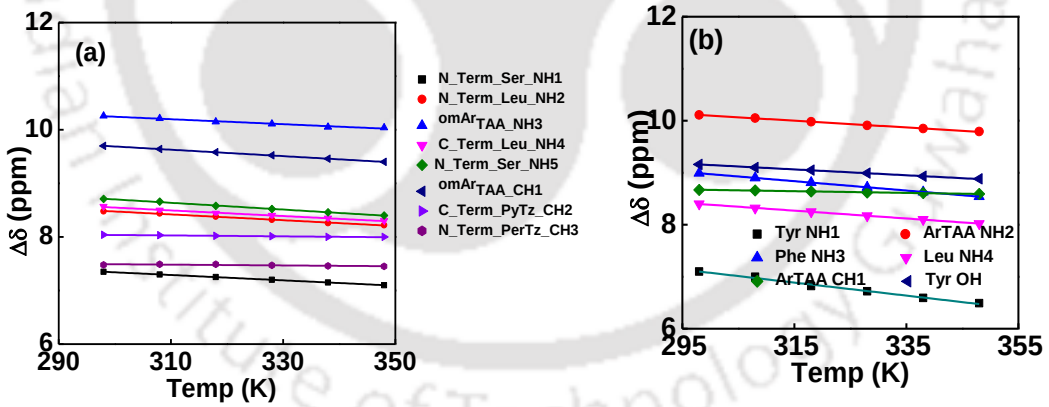

Figure 3.20. Temperature dependence of amide–NH/triazole-CH chemical shift of (a) **Pentapeptide 3.79** [**BocNH–^{TPer}Ala^{Do}–Leu–$^{o,m\text{-}Ar}$TAA–Leu–^{TPy}Ala^{Do}–CONMe(OMe)**] and (b) **Tetrapeptide 3.82** [**BocNH–Tyr–$^{o,m\text{-}Ar}$TAA–Leu–Phe–COOMe**].

Conformational Analysis using 2D NMR Experiment: Next, the 2D NMR analysis in DMSO-d_6 was carried out to support the secondary structural conformation. The proton signals were divided into groups or coupling with the help of ^{1}H-^{1}H TOCSY. Thus, for both pentapeptide **3.79** and tetrapeptide **3.82** TOCSY

experiment was carried out in d_6-DMSO to identify various NH's protons. The interaction of various protons in the solution conformations was revealed from NOESY and ROESY spectra in d_6-DMSO of both the peptides **3.79** and **3.82** (**Figure 3.21**). The H-bonding formation between the two peptide strands and the hydrophobic/stacking interactions between terminal chromophores helped the scaffold to nucleate the peptide into turn induced β–Sheet conformation. The 2D NMR supported the close proximity of the two terminal fluorescent unnatural amino acids and thus the possibility of a photophysical interaction between ^{TPer}**Ala**^{Do} and ^{TPy}**Ala**^{Do} in pentapeptide **3.79** was observed.

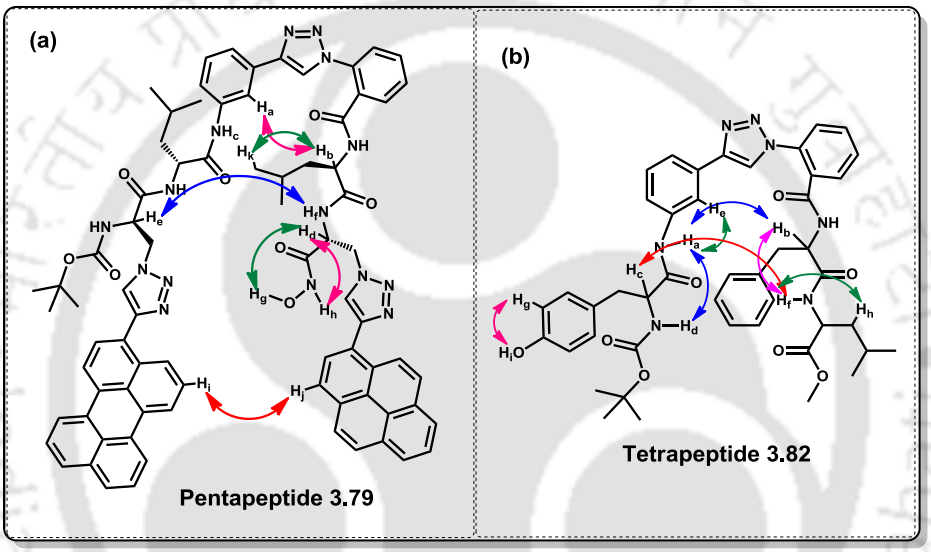

Figure 3.21. Pictorial presentation of long range proton-proton interaction of (a) **Pentapeptide 3.79** and (b) **Tetrapeptide 3.82** as evident from 2D NMR.

Conformational Analysis Using Macromodel Study: Next MD simulations for the peptides were carried out using an OPLS 2005 force field in Schrodinger Macromodel (Maestro vs. 9.1) software package. The starting structures of the peptides were the global minimum conformers. The minimization method was chosen for minimizing the generated structures (with maximum iteration of 1000) with gradient convergence threshold of 0.05.

The triazolyl pyrene and perylene moities in **pentapeptide 3.79** were chosen as freely moving moieties during the simulation.

The clustering of the MD simulated structures of the **pentapeptide 3.79** and **tetrapeptide 3.82** were shown in **Figure 3.22 a-b.** The peptide containing *ortho,meta*-triazolo aromatic amino acid scaffold ($^{o,m\text{-}Ar}$**TAA**) supported the turn induced β-sheet conformation as was revealed from the MD simulation. The observed H-bonding possibility revealed from the MacroModel study was also supported from

the VT-NMR study in all the cases. The close proximity of triazolyl pyrene and perylene units was revealed from NMR studies as which was also supported from the MD simulation.

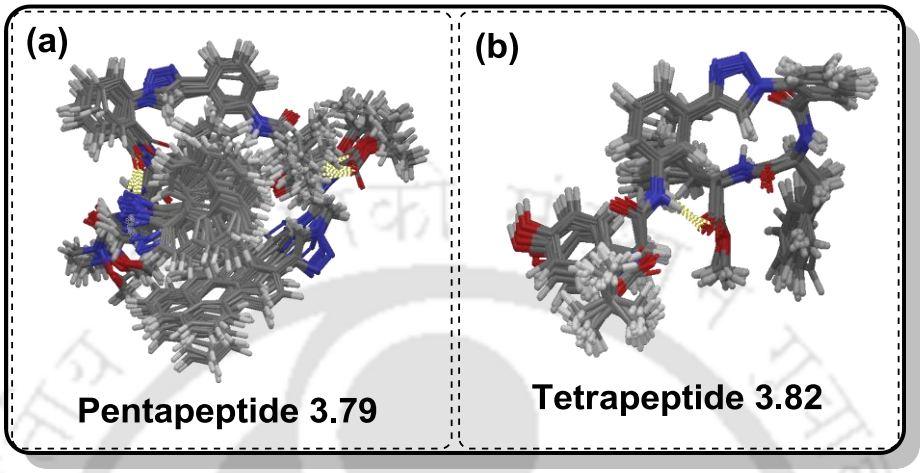

Figure 3.22. Clustering of structures (within 21 kJ/mole global minima) obtained from molecular dynamics simulation for (a) **Pentapeptide 3.79** [**BocNH–^{TPer}Ala^{Do}–Leu–$^{o,m\text{-}Ar}$TAA–Leu–^{TPy}Ala^{Do}–CONMe(OMe)**] and (b) **Tetrapeptide 3.82** (**BocNH–Tyr–$^{o,m\text{-}Ar}$TAA–Phe–Leu–COOMe**).

3.5.3. Study of Photophysical Properties

Next, we have studied the photophysical properties of **pentapeptide 3.79** and the three monomer units **$^{o,m\text{-}Ar}$TAA, ^{TPy}Ala^{Do}** and **^{TPer}Ala^{Do}** in various solvents. The UV-visible spectra of the **$^{o,m\text{-}Ar}$TAA** monomer exhibited a unstructured band at around 290 nm in various solvents (**Figure 3.23, Table 3.3**). When excited at the absorption maxima of in each solvent it showed different broad and structureless emission bands in each solvent.

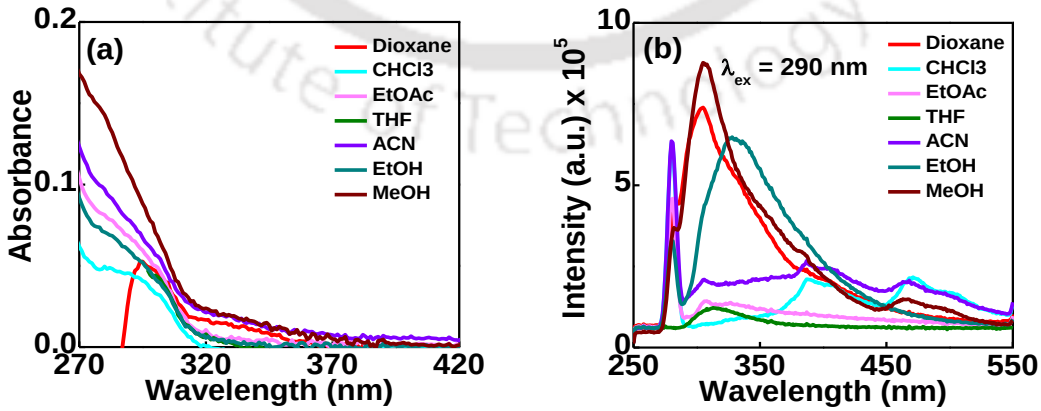

Figure 3.23. (a) UV-Visible, (b) fluorescence emission spectra of **$^{o,m\text{-}Ar}$TAA,** in different solvents [10 μM, r.t.; $\lambda_{ex} = \lambda_{max} \approx 290$ nm in each solvent]

Table 3.3. Summary table of photophysical properties of the $^{o,m\text{-}Ar}$**TAA, 3.72.**

Entry	Solvents	UV-Vis & Fluorescence		
		λ_{max}^{abs} (nm)	λ_{max}^{fl} (nm)	Φ_f
BocNH_$^{o,m\text{-}Ar}$TAA_COOMe (3.72)	Dioxane	294	304	0.23
	$CHCl_3$	290	392, 470	0.14
	EtOAc	290	308, 327	0.09
	THF	290	312	0.07
	ACN	290	306, 390, 465	0.18
	EtOH	290	305	0.23
	MeOH	290	329	0.25

^{TPy}**Ala**^{Do} (**2.65**) monomer showed broad absorption at around 347 nm which showed 4 nm blue shift as the solvent polarity increases from nonpolar dioxane to polar and protic methanol (**Figure 3.24-a, Table 3.4**). Upon excitation on the absorption maxima of ^{TPy}**Ala**^{Do} it showed a less structured emission of pyrene at around 384, 405 and 427 nm (**Figure 3.24-b, Table 3.4**). The quantum yield also follows the same trend as the steady state fluorescence.

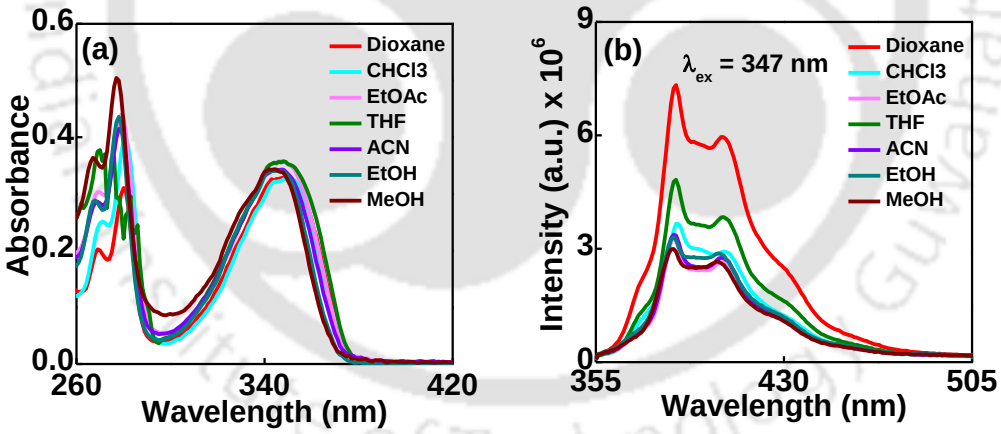

Figure 3.24. (a) UV-Visible, (b) fluorescence emission spectra of **UNNA 2.65** [(^{TPy}**Ala**^{Do})**;** Considered as the monomeric acceptor unit in FRET study] in different solvents [10 µM, r.t.; $\lambda_{ex} = \lambda_{max} \approx 347$ nm in each solvent].

Table 3.4. Summary table of photophysical properties of ^{TPy}**Ala**^{Do}**, 2.65**.

Entry	Solvents	UV-Vis & Fluorescence		
		λ_{max}^{abs} (nm)	λ_{max}^{fl} (nm)	Φ_f
^{TPy}**Ala**^{Do} (**2.65**)	Dioxane	270, 280, 347	384, 405, 427	0.29
	$CHCl_3$	270, 281, 347	385, 405, 428	0.15
	EtOAc	269, 279, 347	384, 405, 427	0.14
	THF	270, 280, 347	384, 405, 427	0.19
	ACN	267, 278, 347	384, 405, 427	0.14
	EtOH	268, 278, 345	384, 405, 427	0.15
	MeOH	267, 277, 343	384, 405, 427	0.14

^{TPer}**Ala**^{Do} (**3.83**) monomer showed broad absorption at around 450 nm which showed 4 nm blue shift as the solvent polarity increases from nonpolar $CHCl_3$ to polar and protic methanol (**Figure 3.25-a, Table 3.5**). Upon excitation on the absorption maxima of ^{TPer}**Ala**^{Do} it showed a less structured emission of pyrene at around 470 and 497 nm (**Figure 3.25-b, Table 3.5**). The quantum yield also follows the same trend as the intensity.

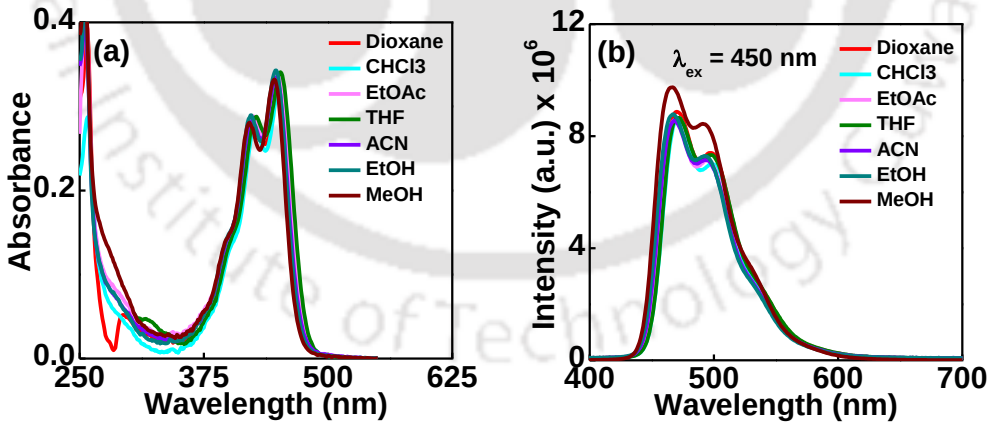

Figure 3.25. (a) UV-Visible, (b) fluorescence emission spectra of **UNNA 3.83** [(^{TPer}**Ala**^{Do})**,** Considered as the monomeric acceptor unit in FRET study] in different solvents [10 µM, r.t.; $\lambda_{ex} = \lambda_{max} \approx 450$ nm in each solvent].

Table 3.5. Summary table of photophysical properties of the **UNNA 3.83** (**^{TPer}Ala^{Do}**)

Entry	Solvents	UV-Vis & Fluorescence		
		λ_{max}^{abs} (nm)	λ_{max}^{fl} (nm)	Φ_f
(**^{TPer}Ala^{Do}**) (**3.83**)	Dioxane	397, 422, 450	470, 497	0.68
	$CHCl_3$	397, 422, 452	470, 497	0.65
	EtOAc	397, 422, 450	470, 497	0.65
	THF	397, 422, 450	470, 497	0.67
	ACN	397, 422, 450	470, 497	0.65
	EtOH	397, 422, 450	470, 497	0.67
	MeOH	397, 422, 448	466, 497	0.74

The tripeptide **3.77** [**BocNH–$^{o,m\text{-}Ar}$TAA–Leu–^{TPy}Ala^{Do}–CONMe(OMe)**] showed a structures absorbance at around 290 nm (corresponding to **$^{o,m\text{-}Ar}$TAA** unit) and 347 nm with very (corresponding to pyrene unit) with very little solvatochromic shift (**Figure 3.26-a, Table 3.6**).

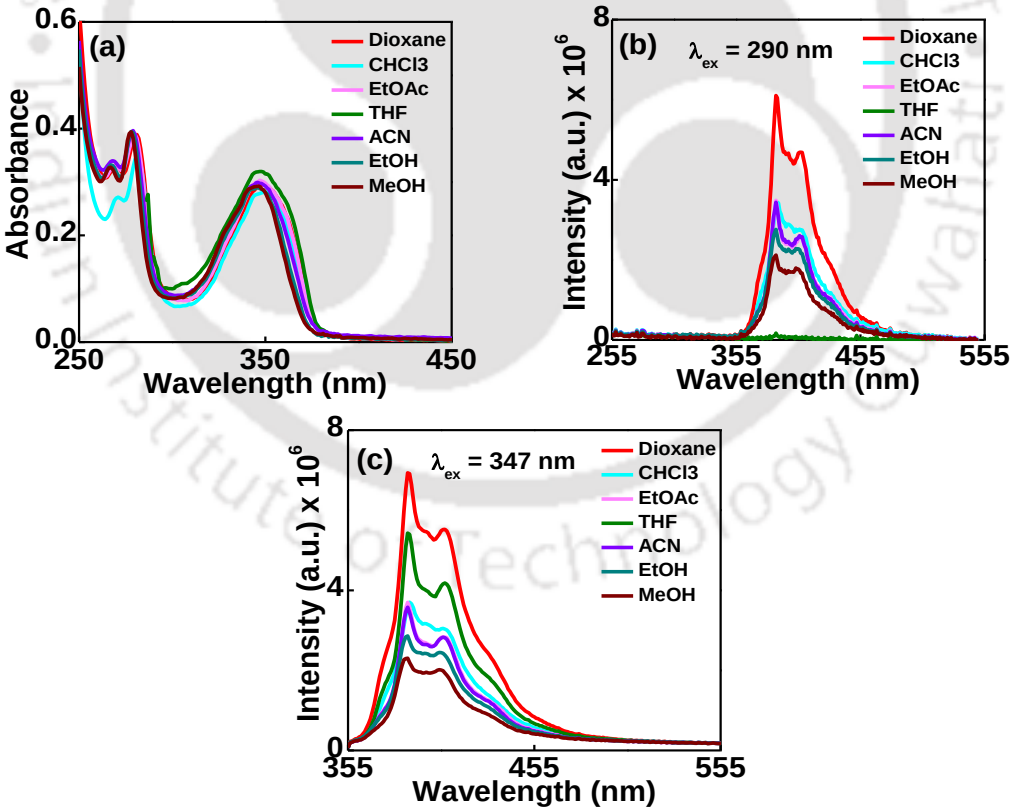

Figure 3.26. (a) UV-Visible, (b) fluorescence emission at $\lambda_{ex} \approx 290$ nm, fluorescence emission at $\lambda_{ex} \approx 347$ nm (c) of **Tripeptide 3.77** [**BocNH-$^{o,m\text{-}Ar}$TAA–Leu–^{TPy}Ala^{Do}-CONMe(OMe)**] in different solvents [10 µM, r.t.; $\lambda_{ex} = \lambda_{max} \approx 290$ and 347 nm in each solvent].

When excited at 290 nm, the tripeptide **3.77** showed low intensity corresponding to molecular scaffold and high intensity of pyrene emission (**Figure 3.26-b, Table 3.6**). This may be due to FRET emission process from scaffold to pyrene unit.

Table 3.6. Summary table of photophysical properties of **Tripeptide 3.77** [**BocNH–$^{o,m\text{-Ar}}$TAA –Leu–^{TPy}Ala^{Do}–CONMe(OMe)**]

Entry	**Solvents**	**UV-Vis & Fluorescence**		
		λ_{max}^{abs} **(nm)**	λ_{max}^{fl} **(nm)**	Φ_f
[BocNH–$^{o,m\text{-}Ar}$TAA–Leu-^{TPy}Ala^{Do}–CONMe(OMe)](3.77)	Dioxane	268, 278, 348	386, 407, 429	0.33
	$CHCl_3$	268, 279, 348	386, 407, 429	0.2
	EtOAc	268, 278, 347	386, 406, 429	0.18
	ACN	268, 278, 347	386, 406, 429	0.18
	EtOH	268, 278, 347	386, 407, 429	0.16
	MeOH	268, 278, 347	386, 406, 429	0.14

The pentapeptide **3.79** showed an absorbance band at around 347 nm (corresponding to **TPy**) and 450 nm (corresponding to **TPer**) both of which showed a blue shift about 6-8 nm from nonpolar $CHCl_3$ to polar and protic MeOH solvent with an appearance of a clear isobestic point at around 378 nm (**Figure 3.27-a, Table 3.7**). Upon excitation at 290 nm corresponding to the absorbance of $^{o,m\text{-Ar}}$**TAA**, pentapeptide **3.79** showed negligible emission corresponding to scaffold, and highly intense emission at 405 nm, corresponding to **TPy** and at 495 nm corresponding to **TPer** (**Figure 3.27-b, Table 3.7**). Upon excitation at around 350 nm at the absorbance of ^{TPy}**Ala**^{Do}, the pentapeptide **3.79** showed low intensity of pyrene emission and high intensity of perylene emission (**Figure 3.27-c, Table 3.7**). At last upon excitation at around 450 nm corresponding to **TPer** absorbance, pentapeptide **3.79** showed less structured emission band of perylene at around 495 nm (**Figure 3.27-d, Table 3.7**).

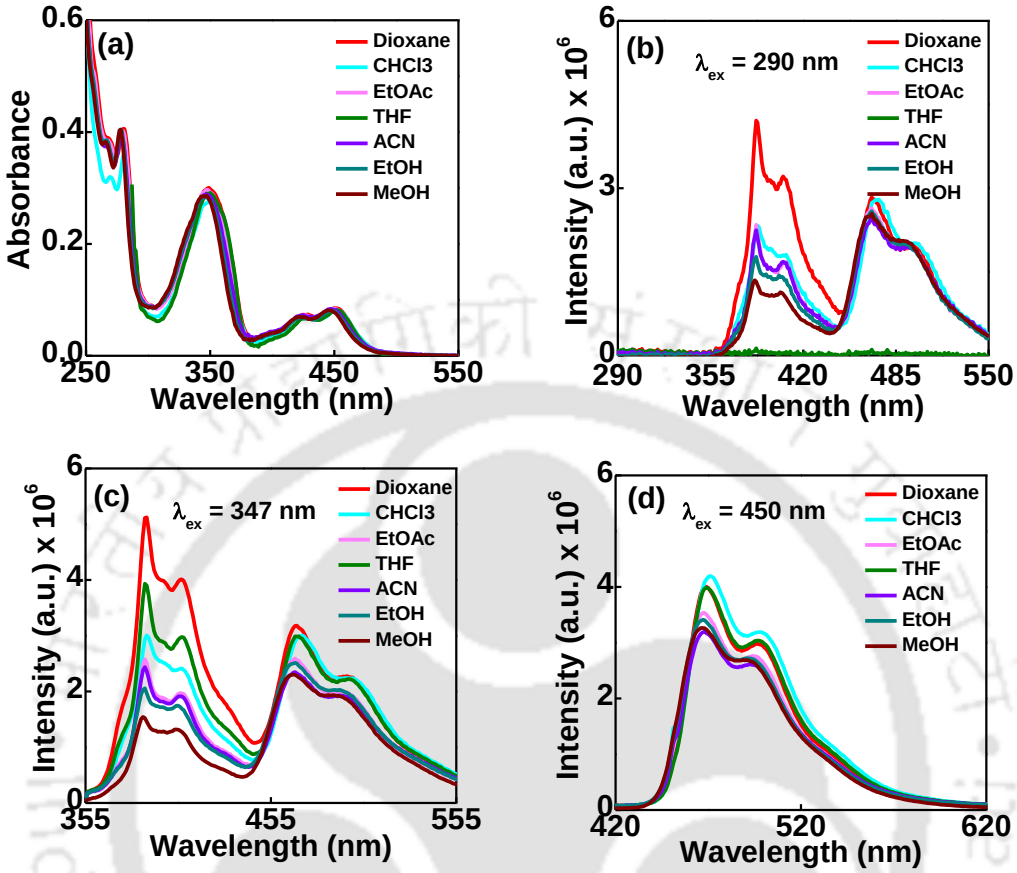

Figure 3.27. (a) UV-Visible, (b) fluorescence emission at $\lambda_{ex} \approx 290$ nm (c) fluorescence emission at $\lambda_{ex} \approx 347$ nm, (d) fluorescence emission at $\lambda_{ex} \approx 450$ nm of Fluorescent **Pentapeptide 3.79** [**BocNH–^{TPer}Ala^{Do}–Leu–$^{o,m\text{-}Ar}$TAA–Leu–^{TPy}Ala^{Do}–CONMe(OMe)**] in different solvents [10 μM, r.t.].

Table 3.7. Summary table of photophysical properties of **Pentapeptide 3.79** [**BocNH–^{TPer}Ala^{Do}–Leu–$^{o,m\text{-}Ar}$TAA–Leu–^{TPy}Ala^{Do}–CONMe(OMe)].**

Entry	Solvents	UV-Vis & Fluorescence		
		λ_{max}^{abs} (nm)	λ_{max}^{fl} (nm)	Φ_f
[BocNH–^{TPer}Ala^{Do}–Leu–$^{o,m\text{-}Ar}$TAA–Leu–^{TPy}Ala^{Do}–CONMe(OMe)] (**3.79**)	Dioxane	267, 279, 349, 425, 447	387, 407, 467, 497	0.51
	$CHCl_3$	267, 279, 350, 426, 452	388, 407, 468, 496	0.55
	EtOAc	267, 279, 347, 425, 448	386, 406, 468, 495	0.47
	THF	267, 279, 347, 426, 450	386, 406, 468, 495	0.52
	ACN	267, 279, 348, 426, 448	386, 406, 468, 495	0.45
	EtOH	267, 279, 346, 422, 447	386, 406, 468, 495	0.47
	MeOH	267, 279, 344, 422, 446	386, 406, 468, 495	0.43

3.5.3.1. Establishment of Relay FRET Process in Fluorescent Pentapeptide 3.79.

Next, we have studied the photophysical properties of the fluorescent pentapeptide **3.79** to test our hypothesis of FRET relay process. The UV-visible and fluorescence photophysical properties of scaffold $^{o,m\text{-}Ar}$**TAA,** fluorescent triazolyl amino acid monomers ^{TPy}**Ala**^{Do} and ^{TPer}**Ala**^{Do} indicated a possibility of FRET process from donor $^{o,m\text{-}Ar}$**TAA** to acceptor ^{TPy}**Ala**^{Do} and from donor ^{TPy}**Ala**^{Do} to acceptor ^{TPer}**Ala**^{Do} in pentapeptide **3.79** (**Figure 3.28 a, b**). Thus, upon excitation at the scaffold (λ_{ex} = 290 nm) we observed three emission bands at 320 nm (negligible) corresponding to the emission of the scaffold, at 405 nm corresponding to **TPy** of ^{TPy}**Ala**^{Do} and at 495 nm corresponding to the emission from **TPer** of ^{TPer}**Ala**^{Do} (**Figure 3.28 c**). Analysis revealed that upon excitation of the pentapeptide **3.79** at λ_{ex} = 290 nm, the emission intensity of the donor $^{o,m\text{-}Ar}$**TAA** appeared negligible whereas that of the acceptors **TPy** and **TPer** increased by about 1.5 and 1.25 times, respectively, in methanol solvent.

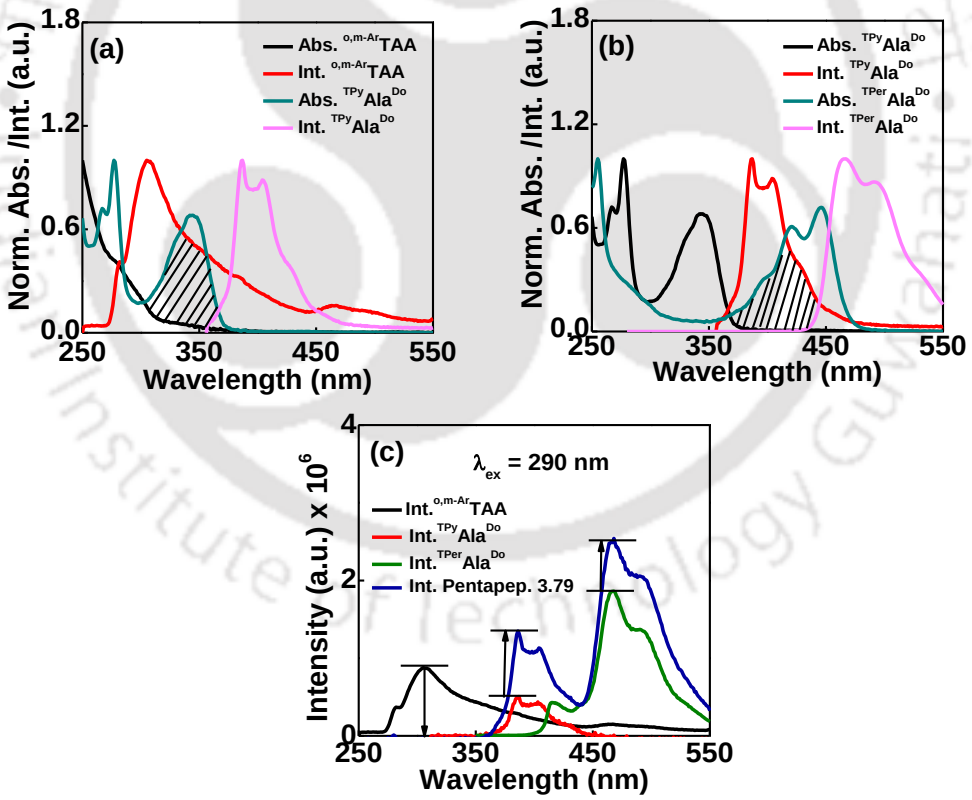

Figure 3.28. Overlap spectra of two monomers (a) $^{o,m\text{-}Ar}$**TAA,** ^{TPy}**Ala**^{Do} and (b) ^{TPy}**Ala**^{Do} , ^{TPer}**Ala**^{Do}. (c) Fluorescence emission spectra of donor $^{o,m\text{-}Ar}$**TAA** and acceptor ^{TPy}**Ala**^{Do}**,** ^{TPer}**Ala**^{Do} and the **Pentapeptide 3.79** which contain these three units (10 μM each, r.t.; λ_{ex} = 290 nm) in solvent MeOH.

The time resolved fluorescence study showed that there is a decrease in donor life time ($^{o,m\text{-Ar}}$**TAA**; λ_{ex} = 290 nm, λ_{em} = 320 nm) from 4.79 to 3.86 ns with an increase in acceptor (**TPy** and **TPer**) life time (^{TPy}**Ala**^{Do}; λ_{ex} = 290 nm, λ_{em} = 405 nm) from 15.2 ns to 16.15 ns and (^{TPer}**Ala**^{Do}; λ_{ex} = 290 nm, λ_{em} = 495 nm) from 3.8 ns to 4.66 ns (**Table 3.8**). Thus, at λ_{ex} = 290 nm the decrease in donor with the increase in acceptor (**TPy** and **TPer**) life time was an evidence of relay FRET process from $^{o,m\text{-Ar}}$**TAA** to ^{TPy}**Ala**^{Do} to ^{TPer}**Ala**^{Do}.

We have also analysed the separate FRET process. That the FRET occurred from scaffold to **TPy** (1st FRET) is evident from the decrease in intensity as well as life time of the scaffold and increase in intensity and life time of the **TPy** upon excitation at 290 nm (**Figure 3.29**).

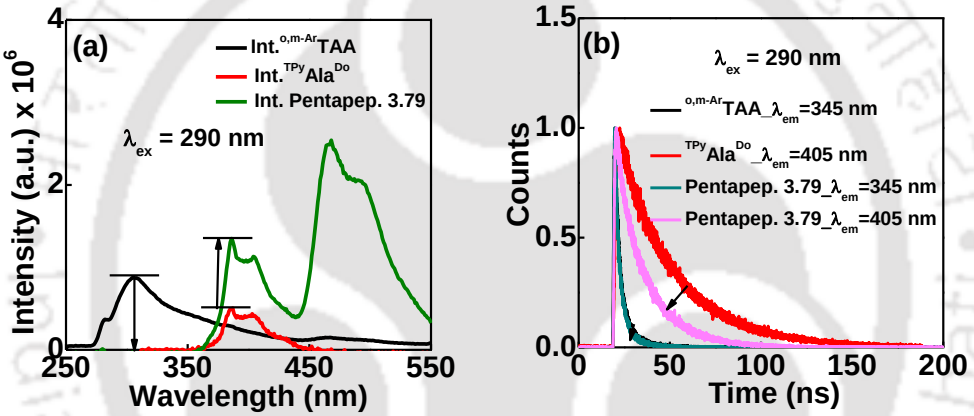

Figure 3.29. (a) Fluorescence emission spectra of donor $^{o,m\text{-Ar}}$**TAA** and acceptor ^{TPy}**Ala**^{Do} and the **Pentapeptide 3.79** which contain these two units (10 μM each, r.t.; λ_{ex} = 290 nm) in solvent MeOH. (b) Time resolved fluorescence of donor and acceptor chromophore $^{o,m\text{-Ar}}$**TAA** and ^{TPy}**Ala**^{Do} and **Pentapeptide 3.79** using λ_{ex} = 290 nm λ_{em} = 405 nm in acetonitrile solvent. Decrease in lifetime of $^{o,m\text{-Ar}}$**TAA** as well as increase in life time of ^{TPy}**Ala**^{Do} is an evidence of FRET from $^{o,m\text{-Ar}}$**TAA** to ^{TPy}**Ala**^{Do}.

Further the 2nd FRET process also analysed separately. Thus, upon excitation at **TPy,** the intensity as well as lifetime of **TPy** decreased while for **TPer** were found to increase (**Figure 3.30**). The time resolved fluorescence spectra showed that the donor life time (^{TPy}**Ala**^{Do}; λ_{ex} = 375 nm, λ_{em} = 405 nm) remained approximately same but an increase in acceptor (**TPer**) life time (^{TPer}**Ala**^{Do}; λ_{ex} = 375 nm, λ_{em} = 495 nm) from 3.8 ns to 4.71 ns (**Table 3.9**) was observed.

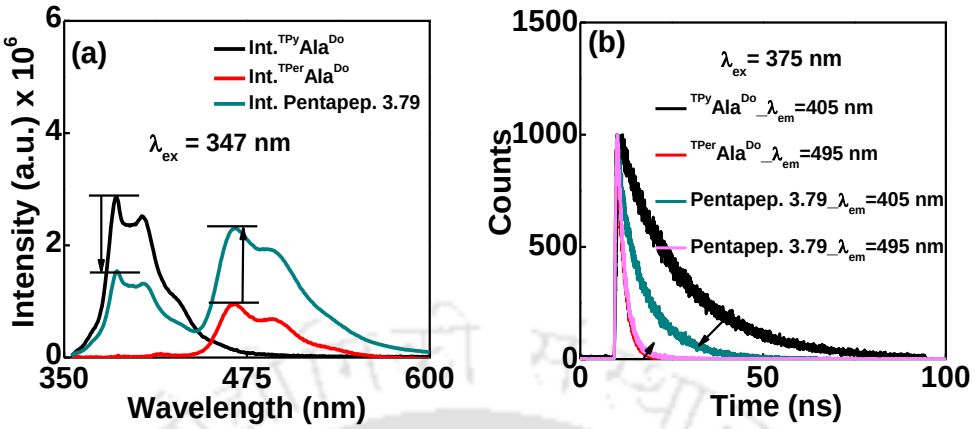

Figure 3.30. (a) Fluorescence emission spectra of donor ^{TPy}**Ala**^{Do} and acceptor ^{TPer}**Ala**^{Do} and the **Pentapeptide 3.79** which contain these two units (10 μM each, r.t.; λ_{ex} = 347 nm) in solvent MeOH. (b) Time resolved fluorescence of donor and acceptor chromophore ^{TPy}**Ala**^{Do} and ^{TPer}**Ala**^{Do} and **Pentapeptide 3.79** using λ_{ex} = 375 nm λ_{em} = 405, 495 nm in acetonitrile solvent. Decrease in lifetime of ^{TPy}**Ala**^{Do} as well as increase in life time of ^{TPer}**Ala**^{Do} is an evidence of FRET from ^{TPy}**Ala**^{Do} to ^{TPer}**Ala**^{Do}

Table 3.8: Summary table of fluorescence lifetimes of $^{o,m\text{-}Ar}$**TAA,** ^{TPy}**Ala**^{Do}, ^{TPer}**Ala**^{Do} and **Pentapeptide 3.79** at λ_{ex} = 290 nm in acetonitrile solvent.

Entry	Φ_f	λ [nm]	τ_1 [ns]	τ_2 [ns]	$\langle\tau\rangle$ [ns]	k_f [$10^8 s^{-1}$]	k_{nr} [$10^8 s^{-1}$]	χ^2
$^{o.m\text{-}Ar}$**TAA**	0.18	350	2.3 (59 %)	8.3 (41 %)	4.79	0.04	0.17	0.95
^{TPy}**Ala**^{Do}	0.14	405	15.2 (100 %)	---	15.2	0.011	0.05	1.05
^{TPer}**Ala**^{Do}	0.65	495	3.8 (100 %)	---	3.8	0.17	0.09	0.95
Tripep. 3.77	0.01	350	3.62 (100 %)	---	3.62	0.003	0.27	1.2
3.77	0.17	405	3.8 (3 %)	17.3 (97%)	16.98	0.01	0.05	1.03
PentaPep. 3.79	0.001	350	1.9 (58 %)	6.5 (42 %)	3.86	0.0002	0.26	0.94
PentaPep. 3.79	0.12	405	2.9 (6 %)	16.9 (94 %)	16.15	0.007	0.05	0.96
PentaPep. 3.79	0.33	495	3.67 (83 %)	9.5 (17 %)	4.66	0.07	0.14	0.94

For lifetimes of the fluorescent amino acids and peptides at λ_{ex} = 290 nm; Concentration of each compound = 10 μM; $\langle\tau\rangle$, k_f, and k_{nr} are weighted means from the biexponential fits: $\langle\tau\rangle = 1/(\alpha_1/\tau_1 + \alpha_2/\tau_2)$, $k_f = \Phi_f/\langle\tau\rangle$, and $k_{nr} = (1 - \Phi_f)/\langle\tau\rangle$.

Table 3.9: Summary table of fluorescence lifetimes of **UNAA 2.65**, **3.83** Tripeptide **3.77** and **Pentapeptide 3.79** at λ_{ex} = 375 nm in acetonitrile solvent.

Entry	Φ_f	λ [nm]	τ_1 [ns]	τ_2 [ns]	<τ> [ns]	k_f [$10^8 s^{-1}$]	k_{nr} [$10^8 s^{-1}$]	χ^2
^{TPy}Ala^{Do}	0.14	405	15.16 (100 %)	---	15.16	0.011	0.055	1.01
^{TPer}Ala^{Do}	0.65	495	3.8 (100 %)	---	3.8	0.17	0.09	1.04
Tripep. 3.77	0.17	405	4.7 (11 %)	17.1 (89 %)	15.78	0.011	0.052	1.01
PentaPep. 3.79	0.12	405	3.99 (13 %)	17.1 (87 %)	15.29	0.008	0.057	1.06
PentaPep. 3.79	0.33	495	3.54 (80 %)	9.38 (20 %)	4.71	0.07	0.14	0.98
For lifetimes of the fluorescent amino acids and peptides at λ_{ex} = 375 nm; Concentration of each compound = 10 μM; <τ>, k_f, and k_{nr} are weighted means from the biexponential fits: $<\tau> = 1/(\alpha_1/\tau_1 + \alpha_2/\tau_2)$, $k_f = \Phi_f/<\tau>$, and $k_{nr} = (1-\Phi_f)/<\tau>$.								

Table 3.10: Summary table of fluorescence lifetimes of **UNAA 3.83** (^{TPer}Ala^{Do}) and Pentapep. **3.79** at λ_{ex} = 405 nm in acetonitrile solvent.

Entry	Φ_f	λ [nm]	τ_1 [ns]	τ_2 [ns]	<τ> [ns]	k_f [$10^8 s^{-1}$]	k_{nr} [$10^8 s^{-1}$]	χ^2
^{TPer}Ala^{Do}	0.65	495	3.71 (100 %)	---	3.71	0.17	0.09	1.06
PentaPep. 3.79	0.33	495	2.85 (57 %)	5.2 (43 %)	3.85	0.09	0.17	1.05
For lifetimes of the fluorescent amino acids and peptides at λ_{ex} = 405 nm; Concentration of each compound = 10 μM; <τ>, k_f, and k_{nr} are weighted means from the biexponential fits: $<\tau> = 1/(\alpha_1/\tau_1 + \alpha_2/\tau_2)$, $k_f = \Phi_f/<\tau>$, and $k_{nr} = (1-\Phi_f)/<\tau>$.								

Calculation of the Forster distance and FRET efficiency in Methanol Solvent:

Using the values of κ^2= 2/3, n = 1.33, Φ_D = 0.25, and the obtained overlap integral, $J(\lambda)$ = 5.88 x 10^{16}, the R_0 and r values were calculated using the equations mentioned in **Chapter 2**, section **2.4.3.2** which were found to be R_0 = 80.6 Å and r = 54.12 Å. R_0 is the critical distance when the energy transfer efficiency is 50 % and r is the distance between the donor $^{o,m\text{-}Ar}$**TAA** and acceptor **TPy.**

Energy Transfer efficiency (E_1) = 1- F/F_0 = 91.6 %. F and F_0 are the fluorescence intensity of donor in the presence and absence of acceptor.

Using the similar values of κ^2= 2/3, n = 1.33 and Φ_D = 0.14, and the obtained overlap integral, $J(\lambda)$ = 1.42 x 10^{17}, the R_0 and r values were calculated and found R_0 = 84.8 Å and r = 86.7 Å. R_0 is the critical distance when the energy transfer efficiency is 50 % and r is the distance between the donor **TPy** and acceptor **TPer**.

Energy Transfer efficiency (E_2) = 1- F/F_0 = 46.7 %. F and F_0 are the fluorescence intensity of donor in the presence and absence of acceptor.

3.5.4. Studies on the Interaction of Pentapeptide 3.79 With BSA Protein

As an application study of interaction with protein BSA we used the pentapeptide **3.79** as a possible probe for sensing BSA protein. The overlapping spectra of emission BSA protein and absorbance of pentapeptide **3.79** indicated that there might be a possibility of energy transfer from Trp unit of BSA to pyrene unit of pentapeptide **3.79.**

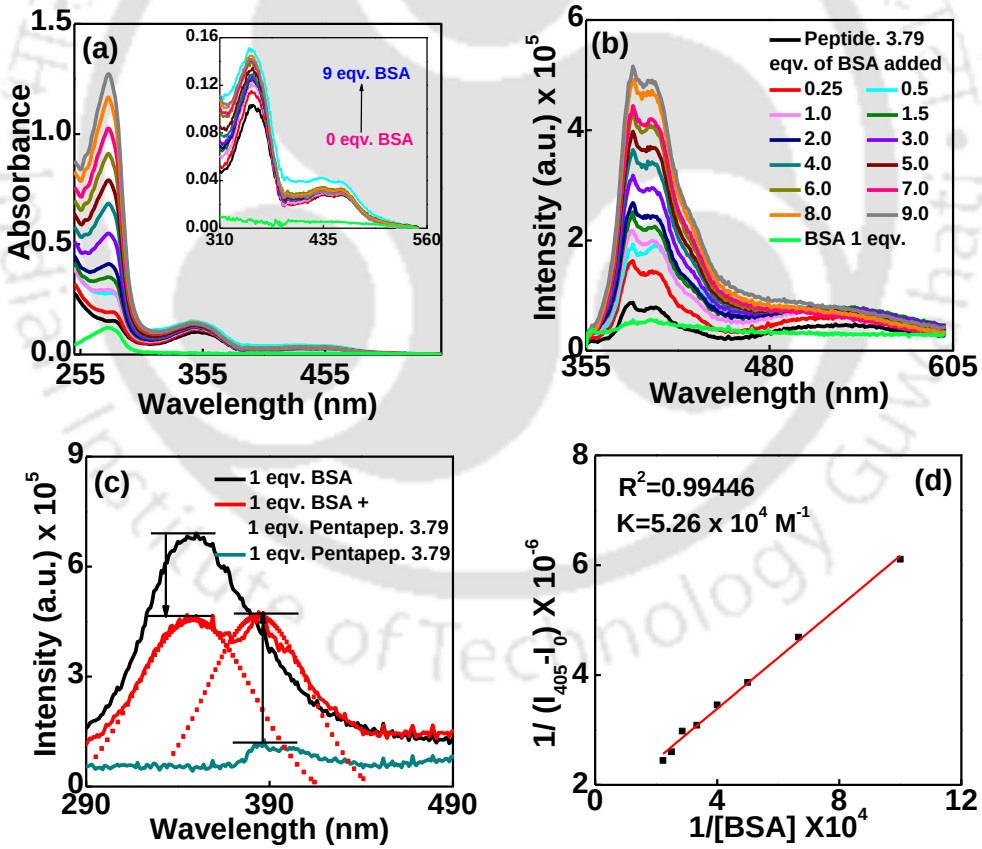

Figure 3.31. Titration of probe **Pentapeptide 3.79** with increasing concentration of BSA solution (a-b) UV visible and fluorescence emission spectra at λ_{ex} = 280 nm, (c) steady state fluorescence intensity comparison spectra of BSA, **Pentaeptide 3.79** and 1:1 mixture of both of them, showing visual evidence of FRET from BSA to peptide

3.79. (d) Benesi-Hildebrand plot at λ_{em} = 405 nm. [Concentration of peptide = 5µM]. All the experiments were carried out in 20 mM phosphate buffer, pH 7.0, r.t.

Thus as we excited at absorption of BSA (280 nm) we observed decrease in BSA emission intensity as well as increase in pyrene emission (**Figure 3.31**) intensity, which is a visual evidence of FRET from BSA protein to pentapeptide **3.79.** Time resolved fluorescence study also supported this FRET phenomena.

The association constant of probe with BSA was found to be 5.26 x 10^4 M^{-1}, determined by Benesi-Hildebrand plot and the free energy of binding was found ΔG = -6.502 kcal/mol (**Figure 3.31 d**).

Molecular Docking Calculation: Docking calculations with BSA protein and pentapeptide **3.79** were carried out using Autodock4 (Bikadi, Hazai, 2009). Following is the BSA sequence which was used to generate the 3D model. >gi|3336842|emb|CAA76847.1| bovine serum albumin [Bos taurus]
MKWVTFISLLLLFSSAYSRGVFRRDTHKSEIAHRFKDLGEEHFKGLVLIAFSQ
YLQQCPFDEHVKLVNELTEFAKTCVADESHAGCEKSLHTLFGDELCKVASLR
ETYGDMADCCEKQEPERNECFLSHKDDSPDLPKLKPDPNTLCDEFKADEKKF
WGKYLYEIARRHPYFYAPELLYYANKYNGVFQECCQAEDKGACLLPKIETM
REKVLTSSARQRLRCASIQKFGERALKAWSVARLSQKFPKAEFVEVTKLVTD
LTKVHKECCHGDLLECADDRADLAKYICDNQDTISSKLKECCDKPLLEKSHCI
AEVEKDAIPENLPPLTADFAEDKDVCKNYQEAKDAFLGSFLYEYSRRHPEYA
VSVLLRLAKEYEATLEECCAKDDPHACYSTVFDKLKHLVDEPQNLIKQNCDQ
FEKLGEYGFQNALIVRYTRKVPQVSTPTLVEVSRSLGKVGTRCCTKPESERMP
CTEDYLSLILNRLCVLHEKTPVSEKVTKCCTESLVNRRPCFSALTPDETYVPK
AFDEKLFTFHADICTLPDTEKQIKKQTALVELLKHKPKATEEQLKTVMENFVA
FVDKCCAADDKEACFAVEGPKLVVSTQTALA

The association constant of probe with BSA determined by Benesi-Hildebrand plot (**Figure. 2.32**) was found to be 5.26 x 10^4 M^{-1} with an experimental free energy of binding, ΔG = -6.502 kcal/mol is very closer to docking result. Visualization of docking result clearly showed the close proximity of **TPy** of probe **3.79** and Trp of BSA and hence the possibility of occurrence of FRET process was also supported by a molecular docking calculation with Autodoc programme. The Probe–Peptide **3.79** was located in the vicinity of tryptophan (Trp-134) and remained surrounded by other hydrophobic amino acids of the hydrophobic pocket of site I of BSA protein (**Figure 5.32b**).

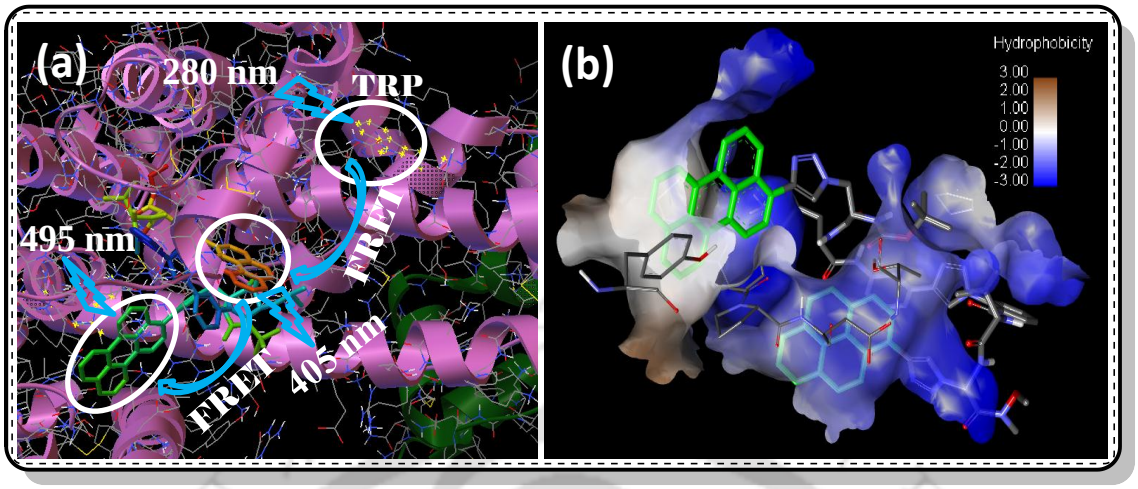

Figure 3.32. (a) docking pose of **Pentapeptide 3.79** in presence of BSA. (b) **Pentapeptide 3.79** hydrophobic interaction with the hydrophobic pocket of BSA.

Isothermal titration calorimetric measurement: Isothermal titration calorimetric measurement is a used to determine thermodynamic characterization of non–COvalent, equilibrium interactions involving small molecules with macromolecule (Protein). Here the ITC study of **pentaeptide 3.79** with BSA was performed in phosphate buffer pH 7.00 at 298 K. The protein solution (2 µm) was taken in a sample cell and **peptide 3.79** was used as titrant solution (15 µm) was fitted in the syringe. In **Figure 3.33 panel a** each peak in binding isotherm shows a single injection of pentapeptide **3.79** into BSA solution and **panel b** of the same figure shows the amount of heat liberated per injection as a function of molar ratio of the peptide to BSA. The resulting data was fitted to a sigmoidal curve involving one binding site. Here **panel a** of **Figure 3.33** shows that BSA shows a negative deflection, which means that the binding process is exothermic in nature at 298 K. The negative value of enthalpy (ΔH = -5.063 x 10^7) indicates the binding is enthalpycally favored but entropically opposed (ΔS = -1.70 x 10^5). The binding constant (K), binding stoichiometry (N) and change in free energy were obtained from the fitted data (**Table 3.11**).

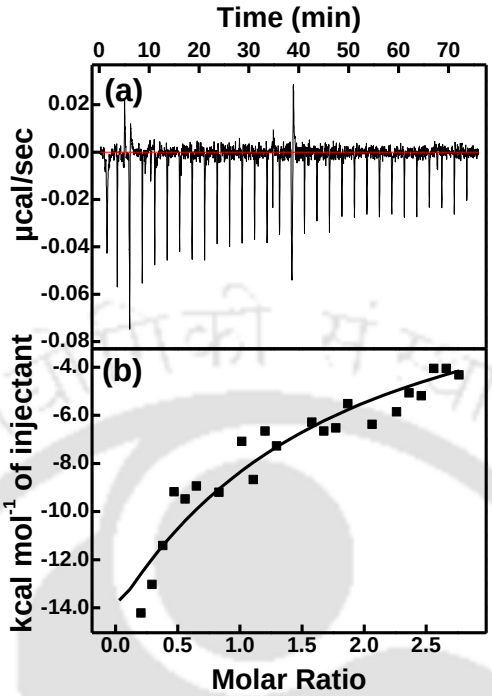

Figure 3.33. Plot of isothermal titration calorimetry.

Table 3.11: Thermodynamical parameter of **BSA-Pentapeptide 3.79** system from ITC measurement.

Model : One Sites				
K_1 (M^{-1})	N	ΔH_1 (cal/mol)	ΔS_1 (cal/mol/deg)	ΔG_1 (Kcal)
1.15×10^5	0.00118	-5.063×10^7	-1.70×10^5	- 6.9

3.6. Conclusion

In conclusion we successfully introduced a new *o,m*-triazolyl aromatic scaffold. The designed *ortho,meta*-triazolo aromatic amino acid scaffold was found to adopt a hairpin shape and induces turn induced β-sheet structure in peptide backbone. The fluorescent peptide in the turn conformation was found to show FRET relay process from **scaffold** to **TPy** to **TPer**. This is newly designed fluorescent peptide which might found wider application in chemical biology. The pentapeptide **3.79** was also used for studying interaction with BSA protein. Sensing of other specific proteins and DNA with this probe is future focus of this work.

3.7. Experimental Procedures

3.7.1. Materials and Methods

All reactions were carried out under inert atmosphere using flame-dried glassware. Combined organic layers were dried over anhydrous sodium sulfate. After work up solvents were removed in a rotary evaporator under reduced pressure. For column chromatography Silica gel (60-120 mesh) was used. Reactions were monitored by TLC on silica gel 60 F254 (0.25). BSA, Na_2HPO_4 and $NaH_2PO_4.H_2O$ (for preparation of phosophate buffer) were purchased from Merck, India and used without further purification. Milli-Q Water was taken for solution preparation. All solutions were prepared freshly before doing the experiments. The probe molecules (pentapeptide **3.79**) were synthesized and purified according to the procedure described.

^{1}H NMR spectra were recorded either at 400 MHz or at 600 MHz and ^{13}C NMR spectra were recorded either at 100 MHz or at 150 MHz (mentioned accordingly). Coupling constants (*J* value) were reported in hertz (Hz). The chemical shifts were shown in ppm downfield form tetramethylsilane, using residual chloroform (δ = 7.26 in ^{1}H NMR, δ = 77.23 in ^{13}C NMR), DMSO (δ = 2.5 in ^{1}H NMR, δ = 39.5 in ^{13}C NMR), as an internal standard. Mass spectra were recorded with a HR mass spectrometer and data analyzed by using built-in software. IR spectra were recorded in KBr on a FT-IR spectrometer. All 2D NMR Experiments were carried out on 600 MHz spectrometer at room temperature using 7 - 10 mM concentration in d_6-DMSO solvent. Spectra were acquired with 2048 x 256 in both dimension (F2 and F1) and other parameters are given below.

TOCSY: Free induction decay (FID) with NS = 16 and DS =32, relaxation delay (D1) 2s, mixing time (D9) 0.08s, acquisition time (AQ) 0.085s, spectral width 12019 Hz.

ROESY: Free induction decay (FID) with NS = 16 and DS =16, relaxation delay (D1) 2s, mixing time (P15) 0.02s, acquisition time (AQ) 0.085s, spectral width (SWH) 12019 Hz.

NOESY: Free induction decay (FID) with NS = 8 and DS =16, relaxation delay (D1) 2s, mixing time (D8) 0.6s, acquisition time (AQ) 0.085s, spectral width (SWH) 12019 Hz.

3.7.2. Some General Procedure for Our Synthetic Scheme of Peptides

***General procedure for the peptide coupling*:** To a solution *N*-protected amino acids/peptides in 3:1 mixture of dry DCM and DMF, 1-[3-dimethyl amino propyl]-3-ehtylcarbo-diimide hydrochloride (EDC.HCl) (1.2 equiv.) and HOBT (1.2 equiv.) were added and the reaction mixture was stirred for 1h at 0 ^{o}C. Then the amine salt of wienreb amide or methyl ester protected corresponding amino acids or dipeptides (1.0 equiv.) were added followed by diisopropylethylamine (DIPEA) (2.4 equiv.). The reaction mixture was stirred for another 18-20 h at 0 ^{o}C to room temperature. Then solvent was dried by rotary evaporator, after which it was partitioned between EtOAc and aqueous $NaHCO_3$ solution (50 ml each). The organic layer was washed with brine solution. Pure product was isolated in pure form by column chromatography.

***General procedure of [3+2] cyclo-addition reaction*:** The azido derivative of compounds were taken in dry THF and degassed for 5 min with nitrogen gas. After adding alkyne (1.1 equiv.) degassing were continued for the next 5 min. Then, 1 mol% powderd CuI was added. Then 1.2 equiv. DIPEA was added and reaction mixture was degassed and allowed to precede for 12 h about 65 to 70 ^{o}C. After total consumption of the starting azide (Monitored by TLC), the reaction mixture was evaporated completely and work up was done by EtOAc and NH_4Cl solution. The organic layer was washed with brine and dried over Na_2SO_4. The targeted trizolyl compounds were separated by column chromatography and characterized.

***General procedure for the deprotection of the methyl ester*:** To a solution of the respective methyl ester protected peptide in THF : H_2O = 5 : 1, lithium hydroxide (1.5 equivalent) was added at 0 ^{o}C. The reaction mixture was stirred about 3-4 hour until starting material was consumed. Reaction was monitored by TLC. After completion of the reaction, solvent dried by rotary evaporator. Then water (4-5 ml) was added to the reaction mixture and cooled to 0 ^{o}C. The dilute acetic acid was added to the reaction mixture to adjust pH- 3 to 4. The reaction mixture was extracted with EtOAc. The combined organic layers were dried over Na_2SO_4. The hydrolyzed compound was isolated by column chromatography (Si-gel, $CHCl_3$: MeOH = 10:1). Yield was 90-96%.

General procedure for the deprotection of the BocNH–group: The respective BocNH– protected amino acids and peptides was dissolved in CH_2Cl_2 and cooled to 0 ^{o}C. TFA (equal amount as the solvent) was added and the solution was allowed to warm to room temperature. The stirring was continue at room temperature until the starting material was consumed (monitored by TLC). The reaction mixture was evaporated in vacuum. The residual TFA was evaporated by triturating the mixture

with dry toluene thrice, evaporated thrice and dried to afford the product in quantitative yield.

But in some cases to get free amine, water (4-5 ml) was added to the reaction mixture after evaporation of reaction solvent and cooled at 0 ^{o}C temperature. Then diluted aq.Et_3N was added to the reaction mixture to adjust pH-8. The reaction mixture was extracted with EtOAc. The combined organic layers were dried over Na_2SO_4 and evaporated in vacuum to yield the crude product in quantitative yield to use for next step.

3.7.3. Synthetic route of unnatural aromatic triazolyl amino acid scaffolds (3.65, $^{o,o\text{-Ar}}$TAA), (3.72, $^{o,m\text{-Ar}}$TAA) and corresponding peptides.

Synthesis of methyl 2-aminobenzoate (3.59): Anthranilic acid **3.58** (1500 mg, 10.95 mmol) was taken in a dried RB in dry methanol solvent. Reaction mixture was taken under ice bath, and then 1.5 equivalent $SOCl_2$ was added. After 15 minutes the ice bath was removed and reaction mixture was refluxed for 5-6 hours. When the spot of the starting material was vanished (monitored by TLC) the solvent was dried in rotary evaporator and work up was done with EtOAc and water. The title compound **3.59** was isolated in quantitative yield.

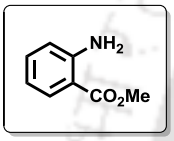

Synthesis of methyl 2-azidobenzoate (3.60): Starting material **3.59** (1000 mg) was taken in a conical then it dissolved by adding water and it was acidified with dil. HCl under ice cool condition. Then drop by drop 1.5 equivalent $NaNO_2$ solution consequently 1.5 equiv. NaN_3 solution was added slowly to the reaction mixture maintaining ice cold condition. After 10 minutes to complete the reaction (monitored by TLC), work up was done by ethyl acetate. The combined organic layer was washed by brine solution dried over Na_2SO_4. The title compound **3.60** was isolated by column chromatography (si-gel, PE) in pure form as colourless oil (832 mg, Yield 71 %). IR (KBr) 2953, 2844, **2115**, 1727, 1585, 1484, 1443, 1300, 1140, 752 cm^{-1}.

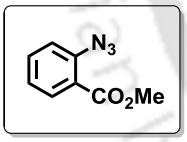

Synthesis of tert-butyl (2-bromophenyl)carbamate (3.62): A portion of NaH (1.1 eqv.) (washed by hexane) and 2-bromo aniline **3.61** (1 ml, 8.7 mmol) was taken in dry THF. The reaction mixture was heated to reflux for one hour then cooled to room temperature. Boc anhydride (1.5 ml, 10.4 mmol) was added and reaction mixture was stirred for further 30 minutes. After that the second portion of sodium hydride (same eqv. amount again) was added to the reaction mixture and refluxed it overnight. The reaction mixture was cooled to room temperature, excess NaH was quenched carefully by water. Work up was done by EtOAc and water. The combined organic

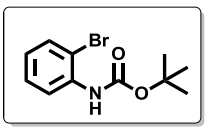

layer was dried over Na_2SO_4 and purified by column chromatography (Si-gel, PE : EtOAc = 10:1) to get pure compound **3.62**. (2070 mg, 7.6 mmol, Yield 88 %).

Synthesis of tert-butyl (2-((trimethylsilyl)ethynyl)phenyl)carbamate (3.63): 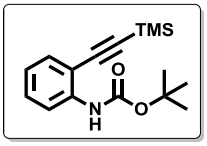

Boc protected 2-bromo aniline **3.62** (800 mg, 2.95 mmol) was taken in a dry R.B, solvent benzene : n-butyl amine = 2:1 was added to it then $PdCl_2(PPh_3)_2$ (103.6 mg, 0.147 mmol) and CuI (11.2 mg, 0.06 mmol) was added and degassed by N_2 gas. After fifteen minute TMS acetylene (600 µl, 4.42 mmol) was added and heated to 80 ^oC for about 12 hour. Completion of reaction was monitored by TLC. Then solvent was evaporated, work up was done with EtOAc and aqueous NH_4Cl solution. Combined organic layer was washed with brine solution. Pure product **3.63** (665 mg, 2.3 mmol) was isolated by column chromatography (Si-gel, PE : EtOAc = 10:1). Yield 78 %. ^1H NMR ($CDCl_3$; 400 MHz) δ 0.29 (9H, s). 1.53 (9H, s), 6.93 (1H, t, J = 7.6 Hz), 7.29 (1H, t, J = 7.9 Hz), 7.41 – 7.33 (2H, m), 8.11 (1H, d, J = 8.3 Hz); ^{13}C NMR ($CDCl_3$; 100 MHz) δ -0.13. 28.6, 76.7, 77.0, 77.3, 80.6, 100.5, 102.0, 110.9, 117.14, 121.8, 129.9, 131.2, 140.2, 152.3.

Synthesis of tert-butyl (3-ethynylphenyl)carbamate (3.64): 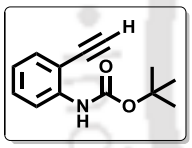

Tert-butyl (2-((trimethylsilyl)ethynyl)phenyl)carbamate **3.63,** 650 mg (2.24 mmol) was dissolved in 8 ml methanol, 314 mg (5.6 mmol) KOH was added to the solution at room temperature and stirrer. Completion of the reaction was monitored by TLC. Then solvent was dried by rotary evaporator, work up was done with EtOAc and water. Combined organic layer was washed with brine solution. Pure product **3.64** (468 mg, 2.15 mmol) was isolated by column chromatography (Si-gel, PE : EtOAc = 10:1). Yield 96 %. ^1H NMR ($CDCl_3$; 400 MHz) δ 11.51 (9H, s). 3.46 (1H, s), 6.92 (1H, t, J = 7.5 Hz), 7.27 (1H, d, J = 6.7 Hz), 7.31 (1H, d, J = 8.3 Hz), 7.39 (1H, d, J = 7.7 Hz), 8.14 (1H, d, J = 8.4 Hz); ^{13}C NMR ($CDCl_3$; 100 MHz) δ 28.4. 76.9, 77.2, 77.5, 79.4, 80.9, 84.3, 109.9, 117.7, 122.1, 130.2, 132.3, 140.4, 152.5.

Synthesis of $^{o,o\text{-}Ar}$TAA (3.65): 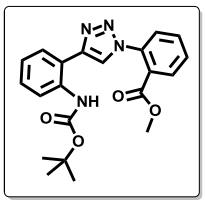

Tert-butyl (2-ethynylphenyl)carbamate **3.64** (450 mg, 2.06 mmol) was taken in dry THF. Methyl 2-azidobenzoate **3.60**, 403 mg (2.3 mmol), 1 mol % CuI, and 1.2 eqv. DIPEA was added and reaction mixture was refluxed for 12 hour. After completion of reaction (monitored by TLC) the reaction mixture was evaporated completely. Work up was done with EtOAc and NH_4Cl solution. Combined organic layer was washed with brine solution, dried over Na_2SO_4 and concentrates under high vacuum. Pure product **3.65** (600 mg, 1.52 mmol) was isolated by column chromatography (Si-gel, PE : EtOAc = 2:1). Yield 84 %. IR (KBr) 3296, 3127, 2980, 1733, 1612, 1538, 1303, 1155, 756 cm^{-1}. ^1H NMR ($CDCl_3$, 400 MHz) δ 1.53 (9H, s), 3.72 (3H, s), 7.04 (1H, t, J = 7.5 Hz),

7.34 (1H, t, *J* = 7.9 Hz), 7.49 (1H, d, *J* = 7.7 Hz), 7.55 (1H, d, *J* = 7.7 Hz), 7.65 (1H, t, *J* = 7.6 Hz), 7.72 (1H, t, *J* = 7.6 Hz), 8.05 (1H, d, *J* = 7.7 Hz), 8.09 (1H, s), 8.39 (1H, d, *J* = 8.4 Hz), 10.30 (1H, s); ^{13}C NMR ($CDCl_3$,100 MHz) δ 28.6. 52.9, 80.3, 117.0, 120.3, 122.4, 122.8, 126.9, 127.6, 127.7, 129.4, 130.44 131.6, 133.0, 136.1, 137.4, 147.6, 153.7, 165.6; HRMS calcd for $C_{21}H_{23}N_4O_4$ ($[M + H]^+$) 395.1714, found 395.1722.

Synthesis of BocNH–$^{o,o\text{-Ar}}$TAA–COOH (3.66): Using the general procedure of methyl ester hydrolysis, starting from 600 mg (1.52 mmol) of **3.65**, 515 mg (1.36 mmol) of the title compound **3.66** was isolated as a white solid material in pure form by column chromatography ($CHCl_3$: MeOH = 50 : 1). Yield 89 %. IR (KBr) 3307, 2979, 1717, 1603, 1239, 1159, 1055, 761; ^{1}H NMR (CD_3OD, 600 MHz) δ 1.50 (9H, s), 7.30 – 7.25 (2H, m), 7.42 – 7.36 (1H, bs), 7.48 (1H, d, *J* = 7.5 Hz), 7.52 (1H, d, *J* = 7.6 Hz), 7.58 (1H, t, *J* = 7.6 Hz), 7.67 (1H, t, *J* = 7.7 Hz), 8.06 (1H, s), 8.07 (1H, s); ^{13}C NMR (CD_3OD, 150 MHz) δ 28.5, 39.7, 81.2, 115.6, 116.2, 118.5, 118.6, 120.8, 121.3, 122.6, 125.8, 127.1, 128.3, 129.7, 129.9, 130.2, 130.6, 130.9, 131.9, 132.1, 133.1, 134.9, 136.5, 139.1, 140.9, 147.4, 167.9, 173.3, 176.4; HRMS calcd for $C_{20}H_{19}N_4O_4$ $[M - H]^-$ 379.1412, found 379.1439.

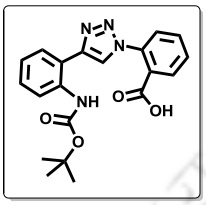

Synthesis of TFA salt of BocNH–Phe–Leu–COOCH$_3$: Using our previous method of peptide coupling we obtained **BocNH–Phe–Leu-COOCH$_3$**. And by treating TFA : DCM = 1:1 of 1500 mg of Phenylalanine Leucine dipeptide we obtained BocNH–deprotected material in quantitative yield.

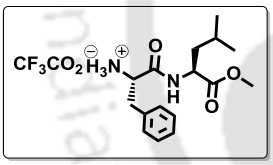

Synthesis of BocNH–$^{o,o\text{-Ar}}$TAA–Phe–Leu–COOCH$_3$ (3.67): COOH deprotected $^{o,o\text{-Ar}}$TAA scaffold **3.66** (155 mg, 0.4 mmol) was taken in dry DMF, then EDC.HCl (115 mg, 0.6 mmol), followed by DMAP (182 mg, 1.5 mmol) were added at 0 ^{o}C. Then Boc deprotected leucine phenylalanine dipeptide (150 mg, 0.4 mmol), was added and the reaction mixture and it was stirred for 1h at 0 ^{o}C, after that ice bath is removed and the reaction mixture was allowed to stir at room temperature for 18h. After completion of the reaction (monitored by TLC), the solvent was dried. Work up was done with EtOAc and $NaHCO_3$ solution. Combined organic layer was washed with brine solution and concentrated under reduced pressure. The product tripeptide **3.67** (174 mg, 0.27 mmol) was isolated in pure form by column chromatography (Si-gel, PE : EtOAc = 1:1) as colorless gummy material. Yield 67 %; IR (KBr) 3348, 3256, 2958, 1747, 1734, 1653, 1533, 1444, 1241, 1156, 1021, 754 cm^{-1}. ^{1}H NMR ($CDCl_3$; 600 MHz); δ 0.83 – 0.81 (6H, m). 1.49 – 1.40 (2H, m), 1.50 (9H, s), 1.56 – 1.52 (1H, m),

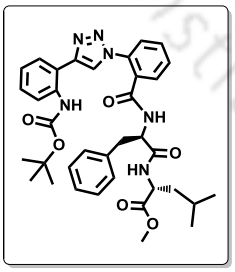

3.07 (2H, dd, *J* = 11.8, 7.1 Hz), 3.65 (3H, s), 4.47 (1H, dd, *J* = 11.0, 5.6 Hz), 4.74 – 4.67 (1H, m), 6.18 (1H, dd, *J* = 26.7, 7.8 Hz), 6.63 (1H, dd, *J* = 21.5, 7.5 Hz), 7.03 (1H, t, *J* = 7.5 Hz), 7.19 (2H, dd, *J* = 15.7, 7.3 Hz), 7.28 – 7.23 (3H, m), 7.33 (1H, t, *J* = 7.9 Hz), 7.49 (1H, dd, *J* = 7.7, 1.0 Hz), 7.57 – 7.50 (3H, m), 7.64 – 7.60 (1H, m), 8.20 (1H, d, *J* = 3.3 Hz), 8.37 (1H, d, *J* = 8.4 Hz), 10.24 (1H, s); ^{13}C NMR ($CDCl_3$; 150 MHz); *δ* 22.0, 22.8, 24.9, 28.6, 37.9, 41.3, 51.3, 52.5, 55.0, 80.3, 116.9, 120.3, 122.4, 123.0, 126.3, 127.4, 127.8, 128.9, 129.1, 129.5, 130.3, 131.7, 132.1, 134.4, 136.2, 137.3, 148.0, 153.6, 166.3, 170.2, 172.8. HRMS calcd for $C_{36}H_{43}N_6O_6$ ([M + H]$^+$) 655.3239, found 655.3242.

Synthesis of tert-butyl (3-bromophenyl)carbamate (3.69): In a dry THF, NaH (1.1 eqv.) (washed by hexane) and 3-bromo aniline **3.68** (2000 mg, 5.8 mmol) were taken. The reaction mixture was heated to reflux for one hour then cooled to room temperature. Boc anhydride (2.42 ml, 6.4 mmol) was added and reaction mixture was stirred for 30 minute. A second portion of sodium hydride (same eqv. amount again) was added to the reaction mixture and refluxed overnight. The reaction mixture was cooled to room temperature, carefully quenched by water. The reaction mixture was extracted with EtOAc. The combined organic layers were dried over Na_2SO_4. The Pure product **3.69** was isolated by column chromatography (Si-gel, PE : EtOAc = 10:1). (1300 mg, 4.8 mmol, Yield 82 %).

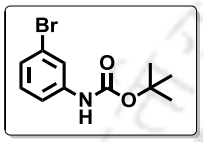

Synthesis of tert-butyl (3-((trimethylsilyl)ethynyl)phenyl)carbamate (3.70): In a dry R.B, compound **3.69** (1300 mg, 4.8 mmol) was taken with dry solvent benzene : n-butyl amine = 2:1 then catalyst $PdCl_2(PPh_3)_2$ (168 mg, 0.24 mmol) was added and degassed by N_2 gas. After fifteen minute of stirring the reaction mixture, TMS acetylene (1.02 ml, 7.2 mmol) and CuI (46 mg, 0.24 mmol) was added and heated to 80 ^{o}C temperature for 12 hour. Then solvent was dried by rotary evaporator, and it was partitioned between EtOAc and aqueous NH_4Cl solution (20 ml each). The organic layer was washed with brine solution. Pure product **3.70** (1124 mg, 3.9 mmol) was isolated in pure form by column chromatography (Si-gel, PE : EtOAc = 10:1). Yield 81 %. ^{1}H NMR ($CDCl_3$; 400 MHz) *δ* 0.15 (9H, s); 1.42 (9H, s); 6.52 (1H, bs); 7.04 (1H, d, *J* = 6.8 Hz); 7.1 (1H, t, *J* = 8.2 Hz); 7.17 (1H, d, *J* = 8.4 Hz); 7.48 (1H, s); ^{13}C NMR ($CDCl_3$; 100 MHz) *δ* 0.1, 28.4, 80.8, 94.3, 104.9, 118.8, 121.8, 126.7, 128.9, 130.3, 138.4, 152.7.

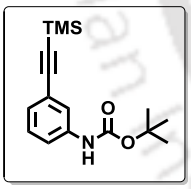

Synthesis of tert-butyl (3-ethynylphenyl)carbamate (3.71): Compound **3.70,** (500 mg, 1.73 mmol) was treated with methanol and KOH (145 mg, 2.6 mmol) at room temperature and stirrer for 1 hour. Then solvent was dried by rotary evaporator, work up was done with EtOAc and water. Pure product **3.71** (360 mg, 1.64 mmol) was isolated in pure

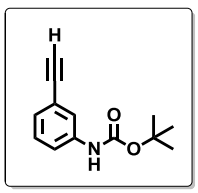

form by column chromatography (Si-gel, PE : EtOAc = 10:1). Yield 95 %. ^{1}H NMR ($CDCl_3$; 400 MHz) δ 1.5 (9H, s); 3.04 (1H, s); 6.63 (1H, s); 7.14 (1H, d, J = 7.6 Hz); 7.19 (1H, t, J = 8 Hz); 7.43 (1H, d, J = 8 Hz); 7.53 (1H, s); ^{13}C NMR ($CDCl_3$; 100 MHz) δ 28.4, 77.3, 80.9, 83.5, 119.2, 122.1, 122.8, 126.8, 129.1, 138.5, 152.7.

Synthesis of $^{o,m\text{-Ar}}$TAA (3.72): Tert-butyl (3-ethynylphenyl) carbamate **3.71**, (360 mg, 1.64 mmol) was taken in dry THF and degassed for 5 min with nitrogen gas. Methyl 2-azidobenzoate **3.60**, 320 mg (1.8 mmol), 1 mol % CuI, and 1.2 eqv. DIPEA was added and reaction mixture was refluxed for 12 hour. After completion of reaction (monitored by TLC) the reaction mixture was evaporated completely and the work up was done by EtOAc and NH_4Cl solution. The organic layer was washed with brine, dried over Na_2SO_4 and concentrates under high vaccum. Pure product **3.72** (520 mg, 1.3 mmol) was isolated by column chromatography (Si-gel, PE : EtOAc = 2:1). Yield 80 %. IR (KBr) 3346, 2978, 1726, 1598, 1529, 1437, 1299, 1159, 1051, 761 cm^{-1}. ^{1}H NMR ($CDCl_3$, 600 MHz) δ 1.52 (9H, s). 3.70 (3H, s), 6.66 (1H, s), 7.36 (2H, d, J = 4.4 Hz), 7.51 (1H, d, J = 8.2 Hz), 7.60 (2H, t, J = 7.5 Hz), 7.68 (1H, t, J = 7.5 Hz), 7.95 (1H, s), 8.01 (1H, d, J = 7.7 Hz), 8.08 (1H, s); ^{13}C NMR ($CDCl_3$,150 MHz) δ 15.5, 28.5, 52.8, 80.9, 115.9, 118.5, 120.7, 121.8, 126.8, 127.8, 129.8, 130.1, 131.3, 131.5, 132.9, 136.3, 139.2, 147.6, 152.9, 165.9; HRMS calcd for $C_{21}H_{23}N_4O_4$ ([M + H]$^+$) 395.1712, found 395.1757.

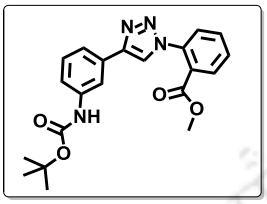

Synthesis of BocNH–$^{o,m\text{-Ar}}$TAA–COOCH$_3$ (3.73): Using the general procedure of methyl ester hydrolysis, starting from 600 mg (1.52 mmol) of **3.72**, 515 mg (1.36 mmol) of the title compound **3.73** was isolated as a white solid material in pure form by column chromatography ($CHCl_3$: MeOH = 50 : 1). Yield 89 %. IR (KBr) 3307, 2979, 1717, 1603, 1239, 1159, 1055, 761; ^{1}H NMR (CD_3OD, 600 MHz) δ 1.50 (9H, s), 7.30 – 7.25 (2H, m), 7.42 – 7.36 (1H, bs), 7.48 (1H, d, J = 7.5 Hz), 7.52 (1H, d, J = 7.6 Hz), 7.58 (1H, t, J = 7.6 Hz), 7.67 (1H, t, J = 7.7 Hz), 8.06 (1H, s), 8.07 (1H, s); ^{13}C NMR (CD_3OD, 150 MHz) δ 28.5, 39.7, 81.2, 115.6, 116.2, 118.5, 118.6, 120.8, 121.3, 122.6, 125.8, 127.1, 128.3, 129.7, 129.9, 130.2, 130.6, 130.9, 131.9, 132.1, 133.1, 134.9, 136.5, 139.1, 140.9, 147.4, 167.9, 173.3, 176.4.

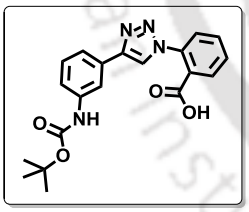

Synthesis of di, tri, tetrapeptides and triazolyl donor/acceptor unnatural pentapeptide (3.79): The targeted peptides were synthesized following the general procedure of peptide coupling protocol as was earlier discussed. The pure product was isolated by column chromatography.

Synthesis of BocNH–^{TPer}Ala^{Do}–Leu–COOCH$_3$ (3.74): Using general procedure of [3+2] cyclo-addition reaction, starting from 200 mg (0.52 mmol) of azide derivative of dipeptide **2.57** (Synthetic procedure described in **Chapter 2**) and 157 mg (0.57 mmol) of 1-ethynyl perylene, (160 mg, 0.252 mmol) of the title compound **3.74** was isolated as a dark brown solid material (Si-gel, PE : EtOAc = 1:1). Yield 48 %; IR (KBr) 3298, 2957, 1477, 1721, 1661, 1520, 1249, 1163, 810, 765 cm^{-1}. ^{1}H NMR (CDCl$_3$; 600 MHz); δ 0.76 (6H, s). 1.41 (2H, s), 1.48 (9H, s), 1.60 – 1.52 (1H, m), 3.70 (3H, s), 4.56 (1H, d, J = 6.9 Hz), 4.82 (2H, d, J = 14.6 Hz), 5.03 (1H, d, J = 11.7 Hz), 5.96 (1H, d, J = 6.3 Hz), 7.07 (1H, s), 7.47 (3H, dd, J = 15.7, 7.7 Hz), 7.66 (3H, d, J = 7.1 Hz), 7.97 (1H, s), 8.17 (4H, dd, J = 18.2, 7.2 Hz), 8.24 (1H, d, J = 8.6 Hz); ^{13}C NMR (CDCl$_3$; 150 MHz); δ 21.8, 22.9, 24.8, 28.5, 29.9, 41.3, 51.2, 52.6, 54.6, 81.3, 117.3, 119.9, 120.7, 122.9, 125.4, 126.7, 126.8, 127.3, 128.0, 128.0, 128.2, 128.6, 129.3, 131.0, 131.4, 131.6, 131.9, 132.4, 134.7, 147.0, 155.6, 169.1, 172.9. HRMS calcd. for $C_{37}H_{40}N_5O_5$ ([M + H]$^+$) 634.3024, found 634.3020.

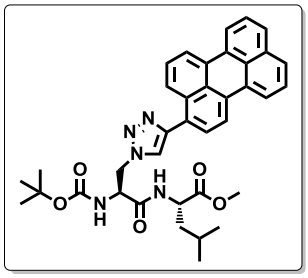

Synthesis of (BocNH–^{TPer}Ala^{Do}–Leu–COOH (3.75): Using the general procedure of ester hydrolysis, starting from 160 mg (0.252 mmol) of **3.74**, 140 mg (0.224 mmol) of the title compound **3.75** was isolated as a dark brown solid material. Yield 89%. This compound is used for the next step without further characterisation.

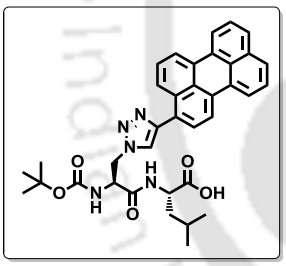

Synthesis of BocNH–$^{o,m\text{-}Ar}$TAA–Leu–Ser(N$_3$)–CONMe(OMe) (3.76): $^{o,m\text{-}Ar}$**TAA** scaffold **3.73** (116 mg, 0.266 mmol) was taken in dry DMF, then EDC.HCl (77 mg, 0.4 mmol), followed by DMAP (81 mg, 0.665 mmol) were added at 0 ^{o}C. Then Boc deprotected Leucine-serine dipeptide **2.49** (Synthetic procedure described in **Chapter 2**) (100 mg, 0.266 mmol), was added and the reaction mixture and it was stirred for 1h at 0 ^{o}C, after that ice bath is removed and the reaction mixture was allowed to stir at room temperature for 18h. After completion of the reaction (monitored by TLC), the solvent was dried. Work up was done with EtOAc and NaHCO$_3$ solution. Combined organic layer was washed with brine solution and concentrated under reduced pressure. The product tripeptide azide **3.76** (124 mg, 0.19 mmol) was isolated in pure form by column chromatography (Si-gel, PE : EtOAc = 1:1) as colorless gummy material. Yield 72 %; IR (KBr) 3450, 2958, 2928, 2102, 1653, 1509, 1390, 1167, 1049, 848

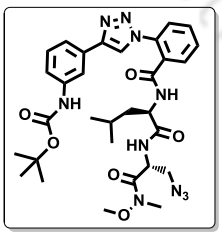

cm^{-1}. ^1H NMR ($CDCl_3$; 600 MHz); δ 0.75 (6H, t, J = 6.8 Hz), 1.50 (9H, m), 1.41 (2H, m), 1.51 (1H, s), 3.19 (3H, s), 3.49 (2H, d, J = 5.0 Hz), 3.70 (3H, s), 4.51 (1H, dd, J = 14.2, 8.3 Hz), 4.99 (1H, bs), 6.68 (1H, d, J = 7.9 Hz), 6.98 (1H, bs), 7.20 (1H, d, J = 7.9 Hz), 7.32 (1H, t, J = 7.9 Hz), 7.59 – 7.45 (5H, m), 7.68 (1H, d, J = 7.2 Hz), 7.84 (1H, s), 8.17 (1H, s); ^{13}C NMR ($CDCl_3$; 150 MHz); δ 15.4, 21.8, 23.0, 24.8, 28.5, 32.5, 41.1, 49.7, 51.8, 52.7, 61.9, 66.0, 80.8, 116.0, 119.1, 120.6, 122.3, 126.3, 129.4, 129.7, 130.2, 130.8, 131.5, 131.6, 132.3, 134.2, 138.9, 148.0, 152.8, 166.7, 169.0, 171.6. HRMS calcd. for $C_{31}H_{41}N_{10}O_6$ ($[M + H]^+$) 649.3205, found 649.3211.

Synthesis of BocNH–$^{o,m\text{-Ar}}$TAA–Leu–^{TPy}Ala^{Do}–CONMe(OMe) (3.77): Using the general procedure of [3+2] cyclo-addition reaction, starting from (120 mg, 0.185 mmol) of azide derivative of tripeptide **3.76** and 44 mg (0.2 mmol) of 1-ethynyl pyrene, (122 mg, 0.14 mmol) of the title compound **3.77** was isolated as a light brown solid material (Si-gel, PE : EtOAc = 1:2). Yield 76 %; IR (KBr) 3296, 2958, 1725, 1653, 1531, 1437, 1158, 849, 762 cm^{-1}. ^1H NMR ($CDCl_3$, 600 MHz) δ 0.77 (6H, dd, J = 10.1, 6.6 Hz), 1.47 (9H, s), 1.54 (3H, m), 3.77 (3H, s), 3.25 (3H, s), 4.49 (1H, d, J = 6.0 Hz), 4.83 (2H, d, J = 14.9 Hz), 5.39 (1H, bs), 6.83 (1H, s), 6.96 (1H, s), 7.09 (1H, s), 7.14 (1H, s), 7.16 (1H, s), 7.23 – 7.18 (1H, m), 7.40 – 7.32 (2H, m), 7.43 (1H, d, J = 5.2 Hz), 7.52 (1H, s), 7.70 (1H, s), 7.91 (1H, s), 7.99 – 7.92 (3H, m), 8.02 (2H, t, J = 8.2 Hz), 8.09 (2H, d, J = 7.0 Hz), 8.14 (1H, d, J = 7.1 Hz), 8.20 (1H, s), 8.60 (1H, d, J = 8.8 Hz); ^{13}C NMR ($CDCl_3$, 150 MHz) δ 15.4, 21.8, 23.0, 249, 28.5, 32.8, 40.6, 50.5, 50.7, 52.8, 62.1, 66.0, 77.0, 77.2, 77.4, 80.5, 115.9, 118.5, 120.2, 121.8, 124.8, 124.9, 125.0, 125.2, 125.2, 125.3, 126.1, 127.3, 127.5, 127.8, 128.1, 128.5, 128.9, 129.6, 129.6, 130.6, 131.0, 131.1, 131.2, 131.5, 131.6, 134.1, 139.3, 147.3, 147.8, 152.9, 157.2, 167.0, 168.4, 172.0; HRMS calcd for $C_{49}H_{51}N_{10}O_6$ ($[M + H]^+$) 875.3988, found 875.3990.

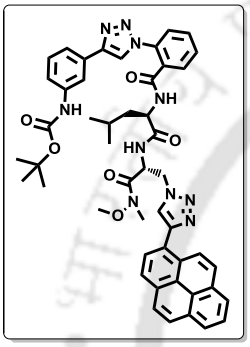

Synthesis of NH_2-$^{o,m\text{-Ar}}$TAA–Leu–^{TPy}Ala^{Do}–CONMe(OMe) (3.78): Using the general procedure of BocNH–deprotection, we have deprotected compound **3.77**. Then the reaction mixture was concentrates under vacuum, diluted with EtOAc and neutralized with Et_3N. The organic layer was then partitioned by EtOAc and water. Combined organic layer was washed with brine solution and dried over Na_2SO_4. Mixture concentrates under high vacuum. The product **3.78** was obtained in quantitative yield and was used without further purification and characterization.

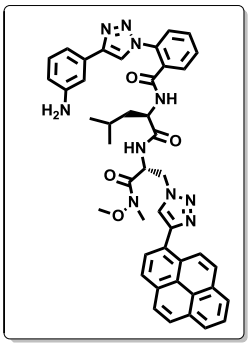

Synthesis of BocNH–^{TPer}Ala^{Do}–Leu-$^{o,m\text{-}Ar}$TAA–Leu–^{TPy}Ala^{Do}–CONMe(OMe) (3.79): The acid compound **3.75,** 120 mg (0.2 mmol) was taken in a dry 50 ml RB. Then dry THF was added to the RB under nitrogen atmosphere maintaining the solution to stir at 0 ^{o}C temperature. Then ethyl chloroformate (0.028 ml, 0.3 mmol) and tri-ethylamine (0.04 ml, 0.3 mmol) were added maintaining 0 ^{o}C. Then free amine of tripeptide **3.78**, 150 mg (0.2 mmol) was added to the reaction mixture and allowed to stirrer about half an hour. Then the ice bath was removed and the reaction mixture was refluxed about 6 hours at 80 ^{o}C. Completion of reaction was monitored by TLC. Pure product **3.79**, 113 mg (0.12 mmol) was isolated as a dark brown solid material (Si-gel, PE : EtOAc = 1:3). Yield 41 %. IR (KBr) 3294, 2923, 1722, 1655, 1532, 1223, 1159, 1050, 849, 763 cm^{-1}. ^{1}H NMR (d_6-DMSO; 600 MHz) δ 0.65 (6H, s), 0.75 – 0.90 (6H, m), 1.21 (9H, s), 1.28 (4H, d, J = 18.2 Hz,), 1.42 (2H, s), 3.15 (3H, s), 3.76 (3H, s), 4.34 (1H, s), 4.72 (3H, s), 4.79 (1H, s), 5.33 (1H, s), 7.09 (2H, d, J = 32.3 Hz), 7.37 – 7.11 (3H, m), 7.41 (1H, s), 7.60 (7H, dd, J = 73.1, 43.1 Hz), 7.78 (1H, s), 8.08 (2H, s), 8.14 (5H, d, J = 34.0 Hz), 8.27 (6H, dd, J = 23.1, 16.5 Hz), 8.37 (2H, s), 8.48 (1H, s), 8.72 – 8.51 (4H, m), 8.78 (2H, s), 9.70 (1H, s), 10.29 (1H, s); ^{13}C NMR (d_6-DMSO; 150 MHz) δ 14.0, 14.6, 21.2, 22.1, 23.0, 24.0, 28.1, 29.1, 31.4, 32.1, 37.6, 49.7, 51.9, 59.2, 61.6, 78.6, 119.2, 121.1, 122.6, 123.9, 124.3, 125.1, 125.5, 126.5, 127.2, 127.4, 127.7, 127.9, 127.9, 128.3, 129.1, 129.3, 130.4, 130.6, 130.9, 132.4, 134.0, 134.3, 136.4, 138.2, 139.8, 146.0, 146.4, 153.5, 154.2, 155.1, 159.6, 162.2, 165.6, 166.3, 168.5, 168.8, 172.3, 173.5; HRMS calcd for $C_{80}H_{78}N_{15}O_8$ ([M + H]$^{+}$) 1376.6152, found 1376.6139.

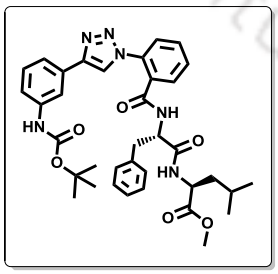

Synthesis of BocNH–$^{o,m\text{-}Ar}$TAA–Phe–Leu–COOCH$_3$ (3.80): A solution of N-protected aromatic triazolyl amino acid **$^{o,m\text{-}Ar}$TAA 3.73,** (116 mg, 0.266 mmol) in dry DMF**,** was taken in a dry R.B. Under ice cold condition (EDC.HCl) (76 mg, 0.4 mmol), DMAP (81 mg, 0.66 mmol) were added and stirred for 5 minutes then the amine salt of methyl ester protected phenyl alanine leucine dipeptide was added and stirring was continued for another 30 minutes maintaining 0 ^{o}C. Then the reaction mixture was bringing to room temperature and stirred for another 18 h. After completion of the reaction, the solvent was dried. Work up was done with EtOAc and water. Combined organic layer was washed with brine solution and purified by column chromatography (Si-gel, PE: EtOAc = 1:1). Pure product **3.80** (125 mg, 0.19 mmol) was isolated as solid compound. Yield 73 %; IR

(KBr) 3302, 2957, 1730, 1652, 1531, 1236, 1158, 1051, 761 cm^{-1}. ^1H NMR ($CDCl_3$, 600 MHz) δ 0.75 (6H, t, J = 6.8 Hz), 1.44 (2H, d, J = 9.2 Hz), 1.51 (10H, s), 3.49 (2H, d, J = 5.0 Hz), 3.70 (3H, s), 4.51 (1H, dd, J = 14.2, 8.3 Hz), 4.99 (1H, bs), 6.68 (1H, d, J = 7.9 Hz), 6.98 (1H, s), 7.20 (1H, d, J = 7.9 Hz), 7.32 (1H, t, J = 7.9 Hz), 7.58 – 7.44 (5H, m), 7.68 (1H, d, J = 7.2 Hz), 7.84 (1H, s), 8.17 (1H, s); ^{13}C NMR (d_6-DMSO; 150 MHz); δ 21.9. 22.8, 24.9, 28.5, 29.9, 37.8, 40.9, 51.4, 52.4, 54.9, 80.7, 116.0, 118.6, 120.6, 121.8, 125.7, 127.2, 128.8, 128.9, 129.5, 129.7, 129.9, 130.9, 131.5, 131.9, 134.5, 136.5, 139.3, 147.9, 153.1, 166.7, 170.5, 173.0; HRMS calcd for $C_{36}H_{43}N_6O_6$ ($[M + H]^+$) 655.3239, found 655.3241.

Synthesis of NH_2-$^{o,m\text{-Ar}}$TAA–Phe–Leu–$COOCH_3$ (3.81): Using the general procedure of BocNH–deprotection, we are getting the free amine derivative of compound **3.80** (100 mg, 0.18 mmol). The product **3.81** was obtained in quantitative yield and was used without further purification and characterization.

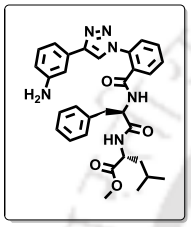

Synthesis of BocNH–Tyr-$^{o,m\text{-Ar}}$TAA-Phe–Leu–$COOCH_3$ (3.82): In a solution of *N*-Boc tyrosine (60.93 mg, 0.213 mmol) in dry THF at 0 ^0C temperature, ethyl chloroformate (24µl , 0.256 mmol) and triethyl amine (0.035 ml, 0.256 mmol) were added. After five minutes free amine and *C*-terminal protected tripeptide **3.81** (100 mg, 0.19 mmol) was added and stirred at half an hour at cold condition. Then reaction mixture was refluxed about 6 hours. Completion of the reaction (monitored by TLC), the solvent was dried by rotary evaporator, Work up was done with EtOAc and water. Combined organic layer was washed with brine solution and concentrates under high vacuum. Pure product **3.82** (70 mg, 0.08 mmol) was isolated by column chromatography (Si-gel, PE : EtOAc = 1:1) as white solid. Yield 43 %; IR (KBr) 3320, 2958, 1743, 1658, 1618, 1537, 1516, 1368, 1254, 1164, 1030, 790 cm^{-1}. ^1H NMR (d_6-DMSO; 600 MHz) δ 0.70 (3H, d, J = 4.2 Hz). 0.81 (3H, d, J = 4.3 Hz), 1.32 (9H, s), 1.48 (1H, bs), 1.58 (2H, d, J = 8.2 Hz), 2.78 – 2.68 (1H, m), 2.86 (2H, dd, J = 29.4, 16.4 Hz), 3.13 (2H, dd, J = 22.0, 9.1 Hz), 3.62 (3H, s), 4.28 (2H, s), 4.58 (1H, s), 6.64 (1H, d, J = 7.4 Hz), 7.01 (1H, d, J = 7.8 Hz), 7.10 (1H, d, J = 7.5 Hz), 7.17 – 7.12 (1H, m), 7.22 – 7.18 (1H, m), 7.30 (3H, d, J = 7.9 Hz), 7.34 (2H, d, J = 6.7 Hz), 7.39 (1H, t, J = 7.4 Hz), 7.60 – 7.54 (2H, m), 7.63 (1H, d, J = 7.7 Hz), 7.67 (1H, t, J = 7.6 Hz), 7.74 (1H, d, J = 7.7 Hz), 8.22 (1H, s), 8.40 (1H, d, J = 6.3 Hz), 8.67 (1H, s), 9.00 (1H, d, J = 7.9 Hz), 9.16 (1H, s), 10.11 (1H, s); ^{13}C NMR (d_6-DMSO; $CDCl_3$; 150 MHz), δ 21.9, 23.2, 24.8, 28.8, 37.4, 39.7, 39.9, 40.0, 40.2, 40.3, 40.4, 40.6, 51.4, 52.5, 54.8, 57.6, 78.7, 115.5, 116.5, 119.6, 121.3,

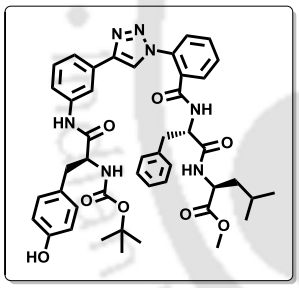

122.9, 125.8, 125.9, 127.0, 128.6, 128.8, 128.9, 129.3, 129.6, 129.7, 129.9, 130.8, 131.4, 131.6, 131.9, 134.6, 138.6, 140.2, 147.1, 156.1, 156.4, 166.8, 171.8, 172.1, 173.5; HRMS calcd for $C_{45}H_{52}N_7O_8$ ($[M + H]^+$) 818.3872, found 818.3876.

Synthesis of $^{TPer}Ala^{Do}$ (3.83): Using general procedure of [3+2] cyclo-addition reaction, 0.060 g (0.219 mmol) of azide derivative of serine **2.45** and 0.072 g (0.263 mmol) of 1-ethynyl perylene was reacted. After completion of reaction (monitored by TLC) 0.058 g (0.105 mmol) of the title compound **3.83** was isolated in pure form as a brown solid (Si-gel, PE : EtOAc = 1:1). Yield 79%. IR (KBr) 3296, 2925, 2103, 1718, 1662, 1498, 1367, 1164, 1023, 809, 765 cm^{-1}. ^1H NMR ($CDCl_3$; 400 MHz) δ 1.40 (9H, s); 3.25 (3H, s); 3.78 (3H, s); 4.86–4.77 (2H, m); 5.14 (1H, bs); 5.62 (1H, d, *J* = 5.6 Hz); 7.43 (2H, d, *J* = 7.6 Hz); 7.51–7.47 (1H, m); 7.65 (2H, m); 7.82 (1H, s); 7.88 (1H, d, *J* = 8 Hz); 8.01 (1H, d, *J* = 8.4 Hz); 8.17–8.05 (4H, m); ^{13}C NMR (CDCl3; 100 MHz); d 28.4, 32.7, 51.4, 51.5, 62.1, 80.7, 120.1, 120.6, 120.7, 125.6, 126.7, 126.8, 127.2, 128.0, 128.1, 128.2, 128.7, 129.3, 131.1, 131.4, 131.6, 131.8, 134.8, 147.0, 155.3, 169.1; HRMS calcd for $C_{32}H_{32}N_5O_4$ ($[M+H]^+$) 550.2449, found 550.2450.

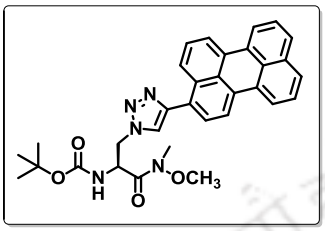

3.8. Photophysical Studies of the Synthesized Peptides, Amino Acids and Scaffolds:

UV-visible measurements: The *UV* –visible spectra of all final peptides and UNNAs (10 µM) were measured in different solvents using a UV-Visible spectrophotometer (**SHIMADZU**, **UV-2550**) with a cell of 1 cm path length. The measurements were done in absorbance mode. The sample solutions absorbance values were measured in the wavelength range of 200–700 nm. All the sample solutions were prepared freshly just before doing the experiment.

Fluorescence experiments: All the sample solutions for fluorescence measurements (**HORIBA Scientific**, **Fluoromax-4**) were also prepared freshly just before doing the experiment. Fluorescence spectra were obtained using a fluorescence spectrophotometer at 25 °C using 1 cm path length cell. The wavelengths for excitation in all the cases were set at the absorption maxima of each sample in each solvent. The emission spectra were measured in the wavelength regime of 300–700 nm with an integration time of 0.2 sec. From 2.0 ml 500 µM stock solution, 2 ml of 10 µM concentration of solution was used for fluorescence experiment in 1 ml cell. Fluorescence emissions were recorded by exciting the sample solutions at their absorption maxima. Steady-state fluorescence emission spectra were recorded at room temperature as an average of five scans using an excitation slit of 3.0 nm, emission

slit 3.0 nm, and scan speed of 120 nm/min. Using quinine sulphate as a reference, the fluorescence quantum yields (Φ_f) were determined with the known Φ_f (0.55) in 0.1 molar solution in sulphuric acid. Following equation was used to calculate the quantum yield,

$$\Phi_S = \Phi_R \frac{Fl_S^{Area}}{Fl_R^{Area}} \frac{Abs_R}{Abs_S} \frac{n_S^2}{n_R^2}$$

where, Φ_R is the quantum yield of standard reference, Fl_S^{Area} (sample) and Fl_R^{Area} (reference) are the integrated emission peak areas, Abs_S (sample) and Abs_R (reference) are the absorbances at the excitation wavelength, and n_S (sample) and n_R (reference) are the refractive indices of the solutions.

A time resolved fluorescence spectrophotometer (*Eddinburg Instruments FSP920*) was utilized to perform fluorescence lifetime experiments. Working condition was maintained at 25^{o}C and results were recorded at an excitation wavelength of 290 nm LED and 375 nm laser using a cuvette having path length 1 cm. To analyze the lifetime data time correlated single photon counting (TCSPC) method was used and analysis was done using a software package with range 205 – 4000 channels.

All the experiments were done four times. The experimental errors were found within 1-2 nm. The experimental standard errors were calculated based the following equations for four consecutive run for the same experiment at same condition.

$$SD = \sqrt{\sum_{i=1}^{n} \frac{1}{n-1} (x - \overline{x})^2}$$

……Equation 1

where SD is standard deviation, *x* is individual data points, $\overline{x}$ is the mean value of the experiments and n is the total number of observations.

The standard error (*SE*) was measured by sample standard deviation obtained divided by the square root of number of observations

$$SE = \frac{SD}{\sqrt{n}}$$

……..……....Equation 2

The experimental errors in wavelength for both the UV-Visible and fluorescence measurement were found to be in the range of 1-2 nm. Error in Quantum yield calculation lies in the range of 8-10%. The experimental error for lifetime measurement lies between ± 0.4 ns range.

3.9. Studies On the Interaction of Peptides (3.79) with BSA

***Preparation of BSA solution*:** BSA (Merck) solution was prepared using Phosphate buffer of pH 7.02, by dissolving 0.08 gm of BSA in 1 mL phosphate buffer (20 mM). The stock solution (1000 μM) of the compound was prepared in DMSO, due to poor solubility of compound in buffer.

General experimental on interaction study of BSA by photophysical study: Spectral measurements were done at room temperature. The interaction of compound with BSA was studied by titrating aqueous solution of Peptides (**3.79**) with increasing concentrations of BSA solution (ranging from 0, 1.25, 2.5, 3.75, 5, 7.5, 10, 12.5, 15, 20, 25, 30, 45 μM). Total volume of each sample was 3 ml, which contains 2-3% DMSO. 2-3% DMSO may not cause any structural changes of our synthesized peptides. Before doing spectral measurement each sample solution were mixed well.

***UV-Visible study with BSA*:** UV-visible spectrophotometer (**SHIMADZU**, **UV-2550**) was used to carry out UV–Visible absorbance measurements. The experiments were done in 20 mM phosphate buffer of pH 7.02 at 25^{o}C, where 2-3% DMSO was used to solubilize the probe peptides. The spectral measurements were carried out in absorbance mode and absorbance values were measured in wavelength regime of 200–700 nm. Freshly prepared sample solutions were used to carry out all the experiments.

Fluorescence study with BSA: Steady state fluorescence and anisotropy measurements were carried out using steady state fluorescence spectrophotometer (**HORIBA Scientific**, **Fluoromax-4**) with a cell of 1 cm path length at 25^{o}C. The excitation wavelengths were set at the absorption maxima in each sample. Steady state fluorescence spectrophotometer was used to measure steady state anisotropy. Fluorescence lifetime experiment was done using similar procedure as described above.

UV and fluorescence experiments were also repeated four times. Standard experimental error was calculated by above mentioned procedure, for UV and fluorescence measurement which lies between 2-3% and for lifetime measurement lies between ± 0.4 ns range.

3.10. Some Selected Spectra

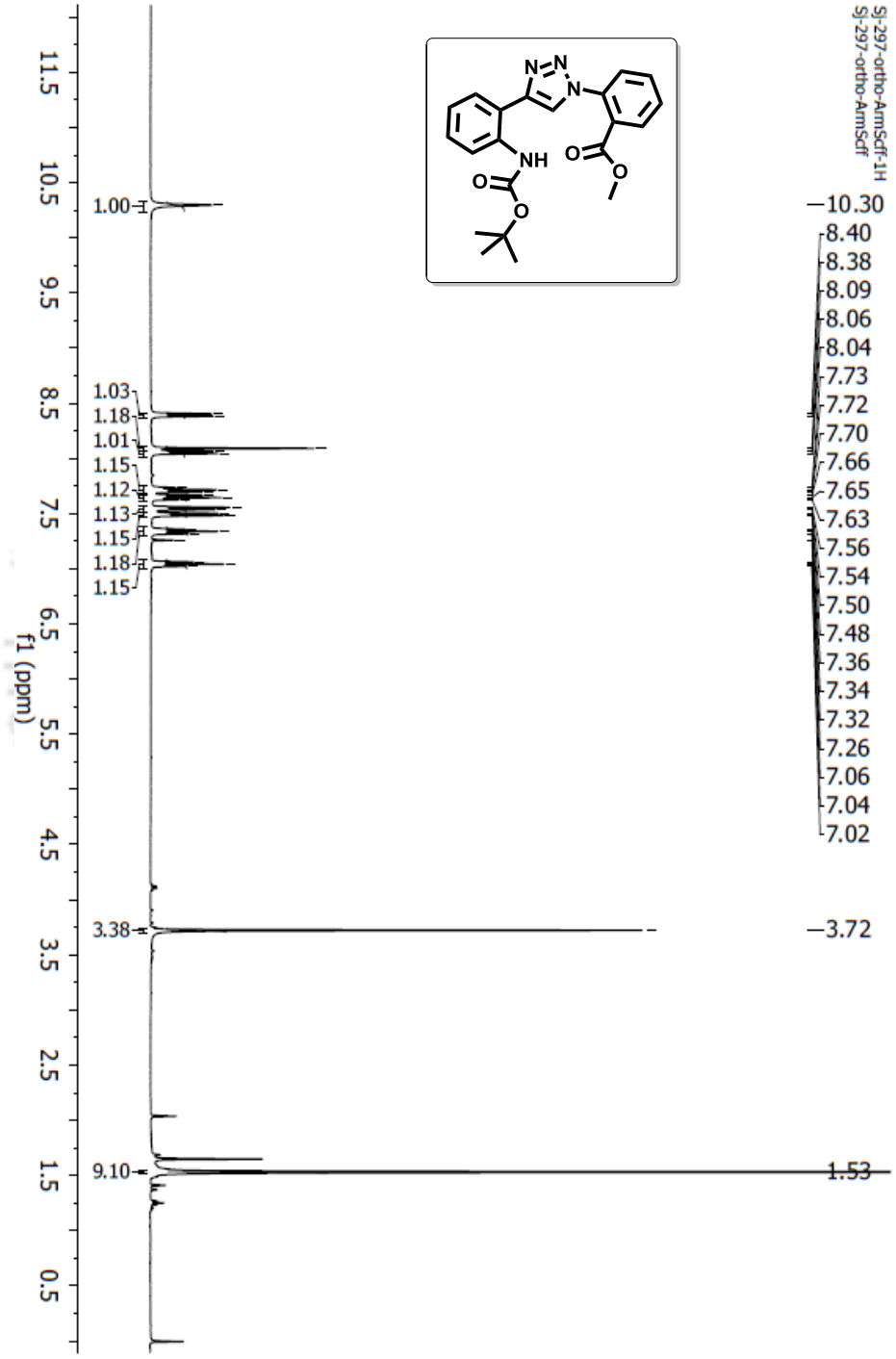

Figure 3.33: ^{1}H Spectra of synthesized compound **3.65**

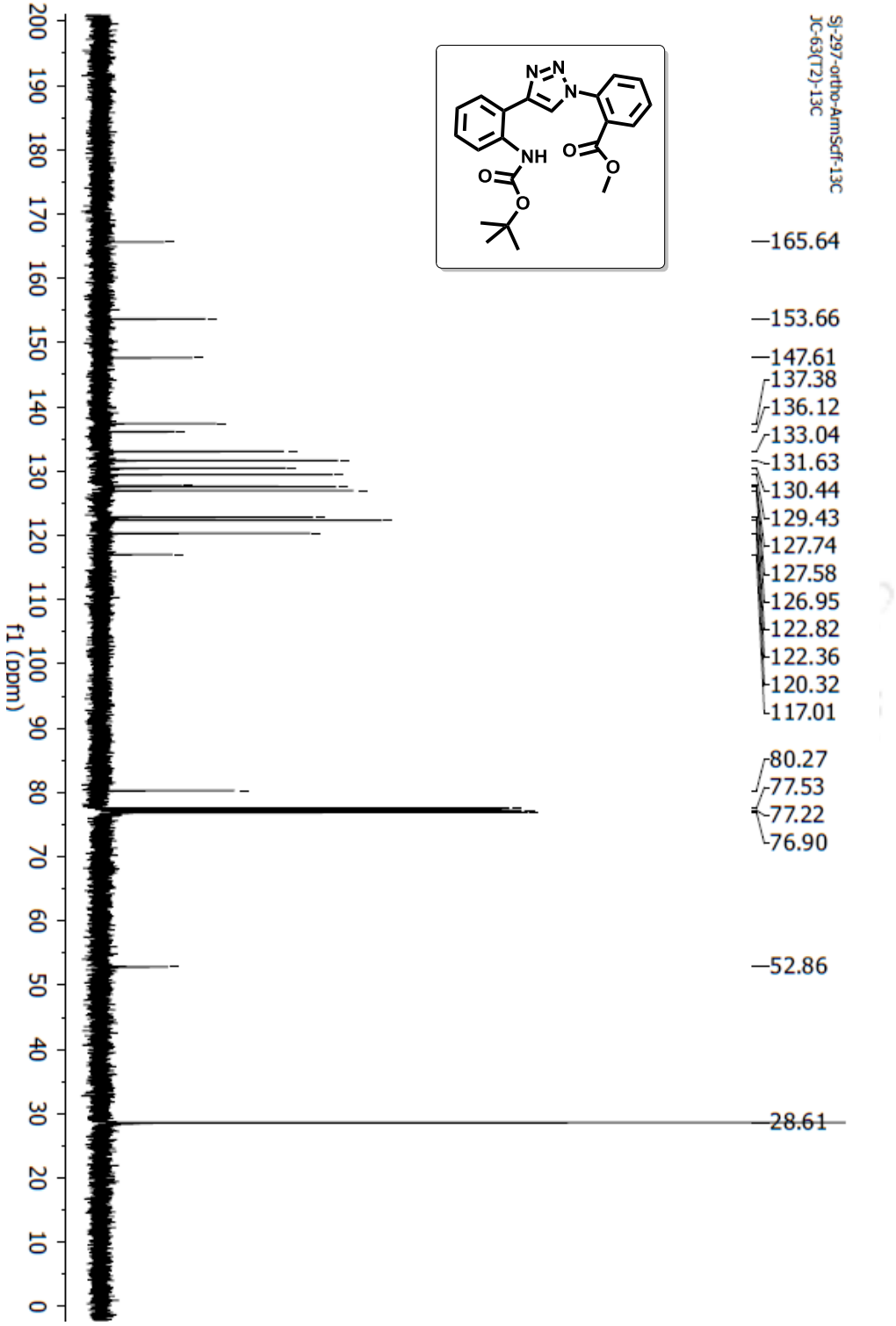

Figure 3.34: ^{13}C Spectra of synthesized compound **3.65.**

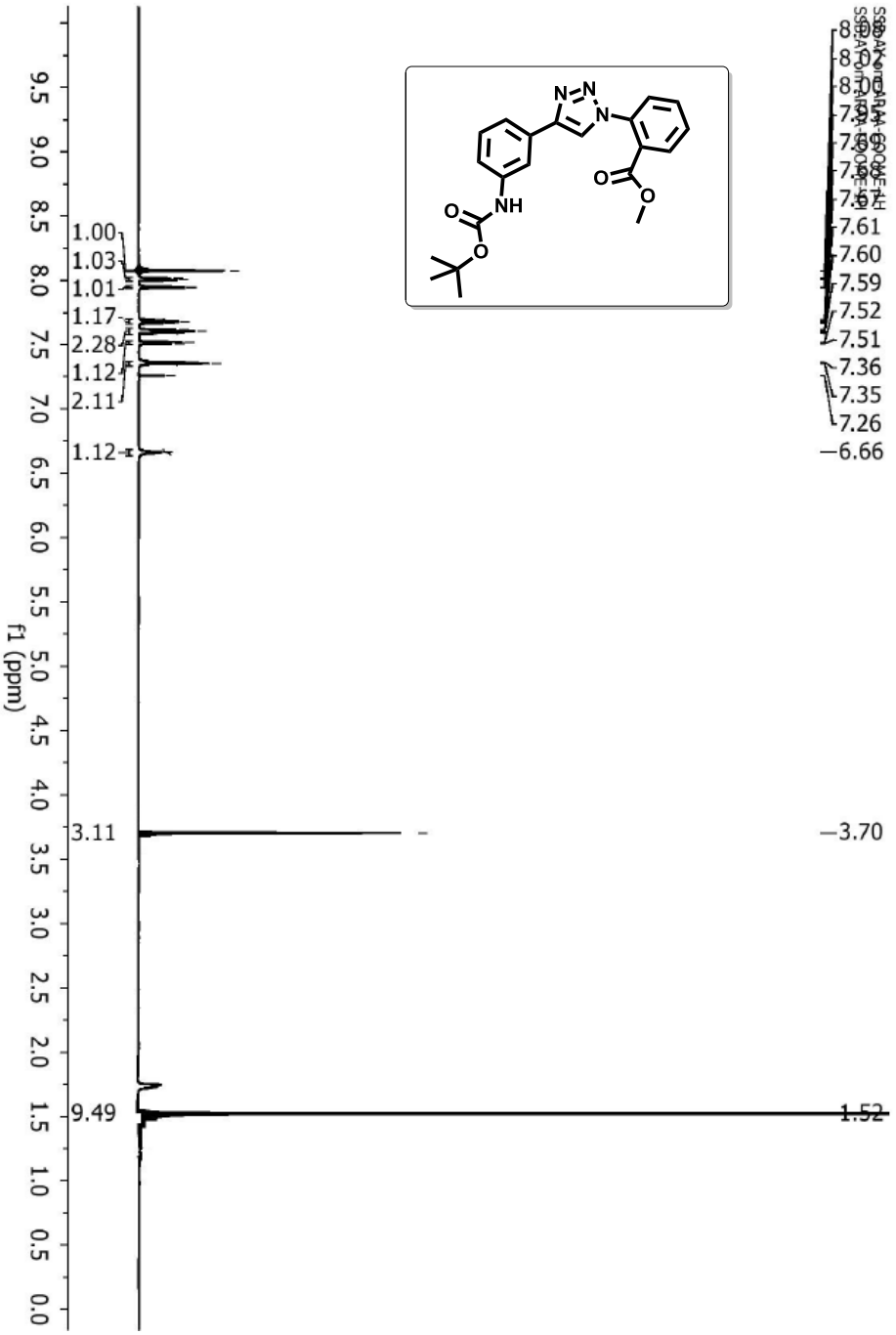

Figure 3.35: ^{1}H Spectra of synthesized compound **3.72.**

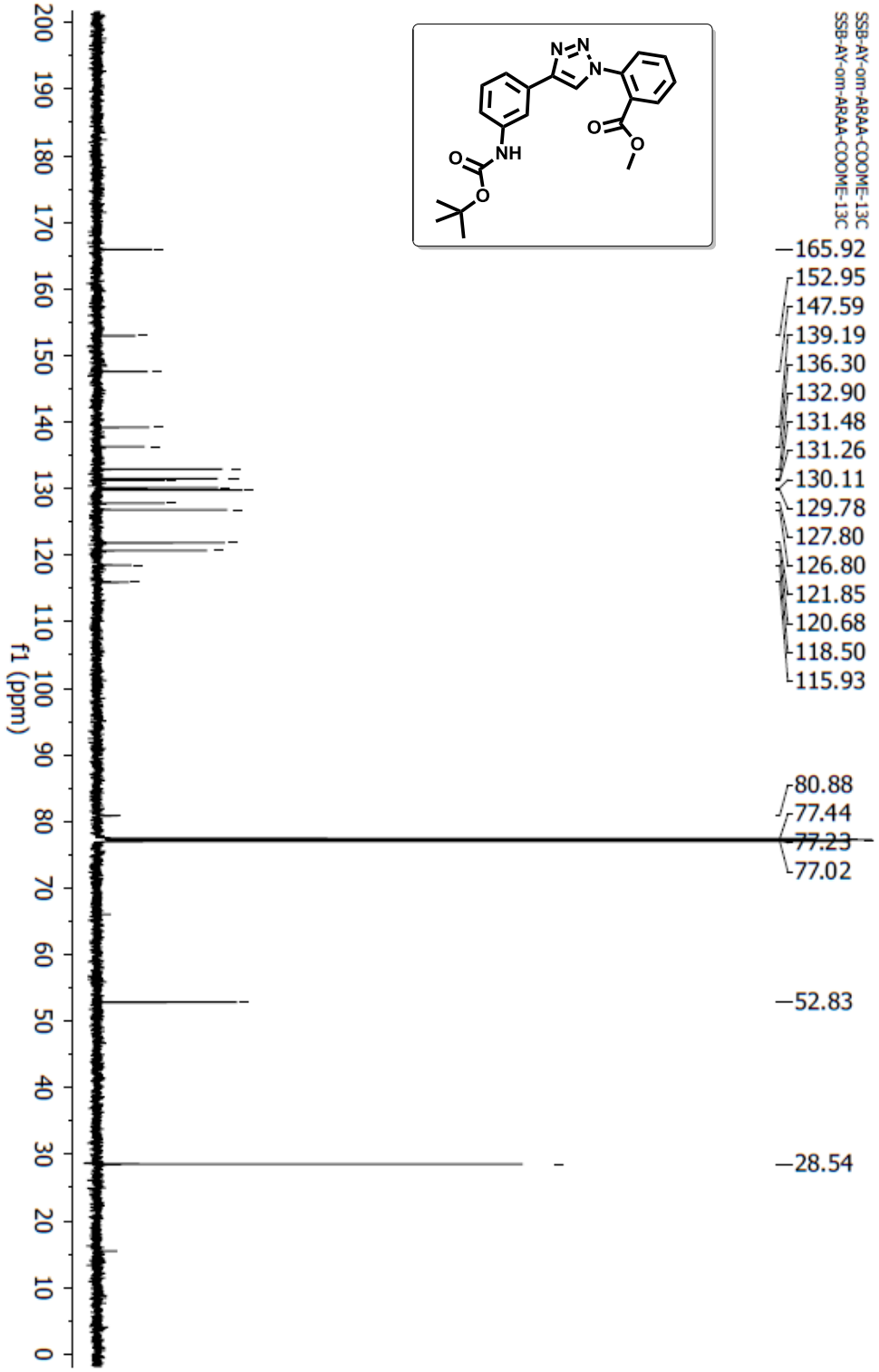

Figure 3.36: ^{13}C Spectra of synthesized compound **3.72.**

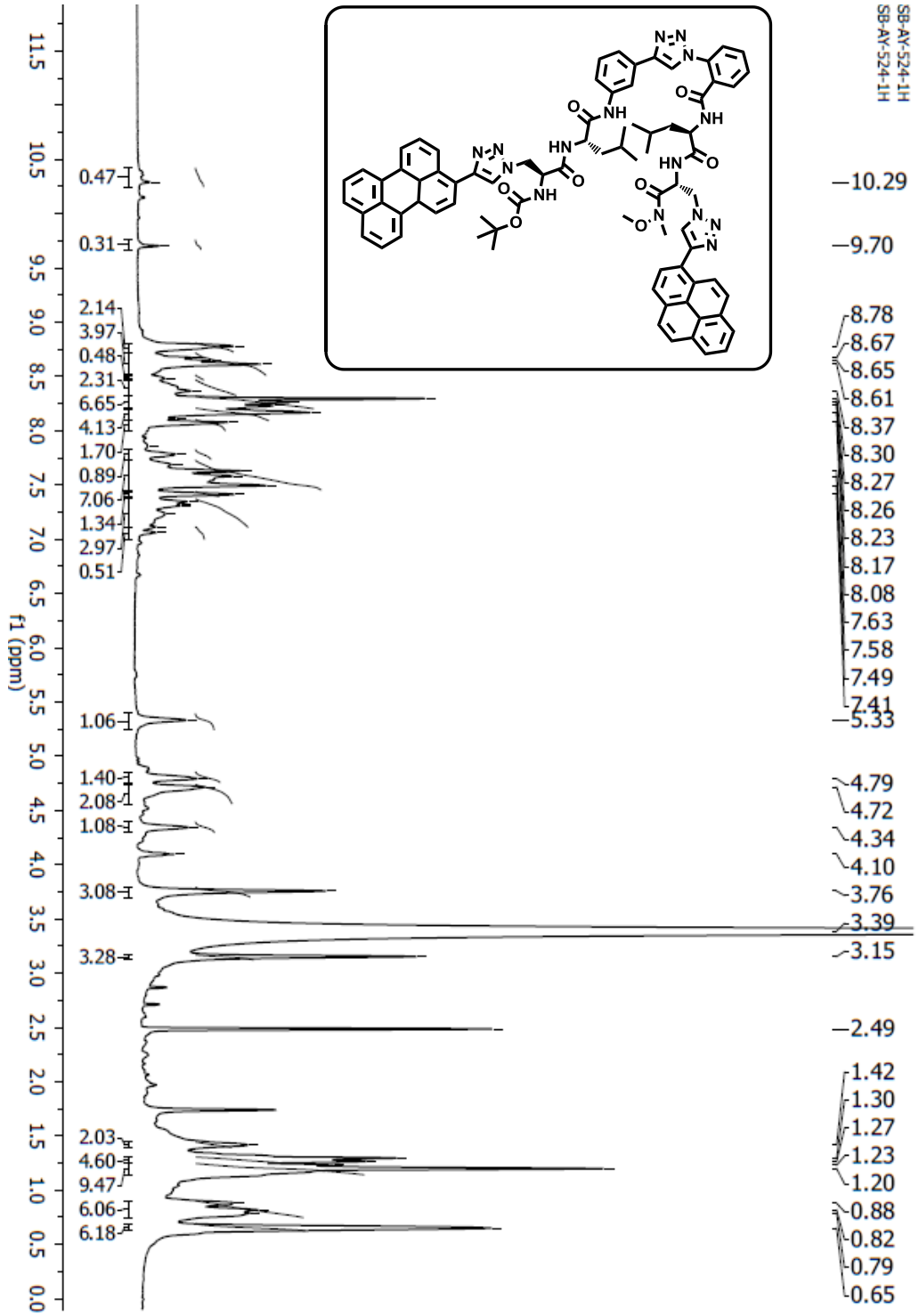

Figure 3.37: ^{1}H Spectra of synthesized compound **3.79.**

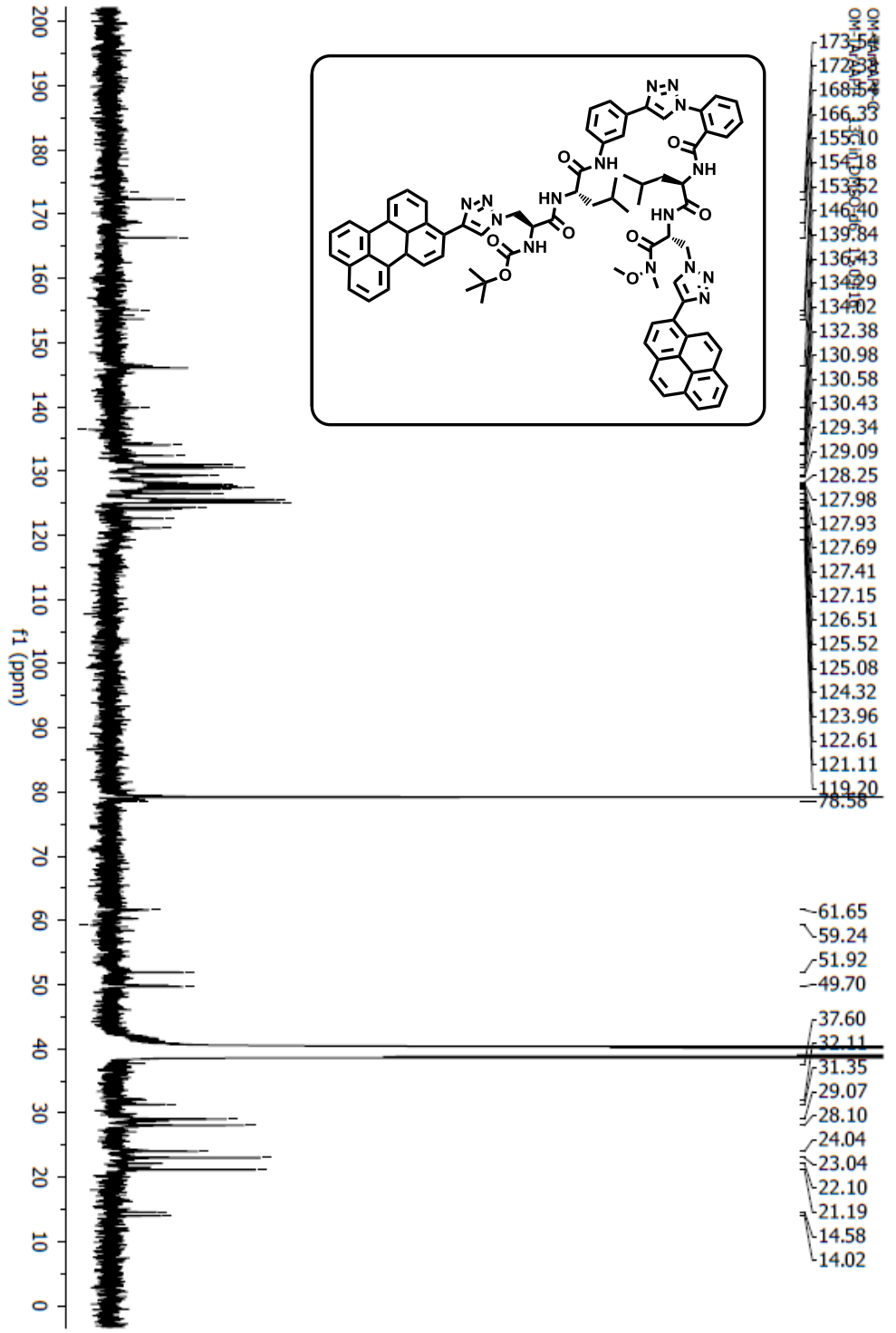

Figure 3.38: ^{13}C Spectra of synthesized compound **3.79.**

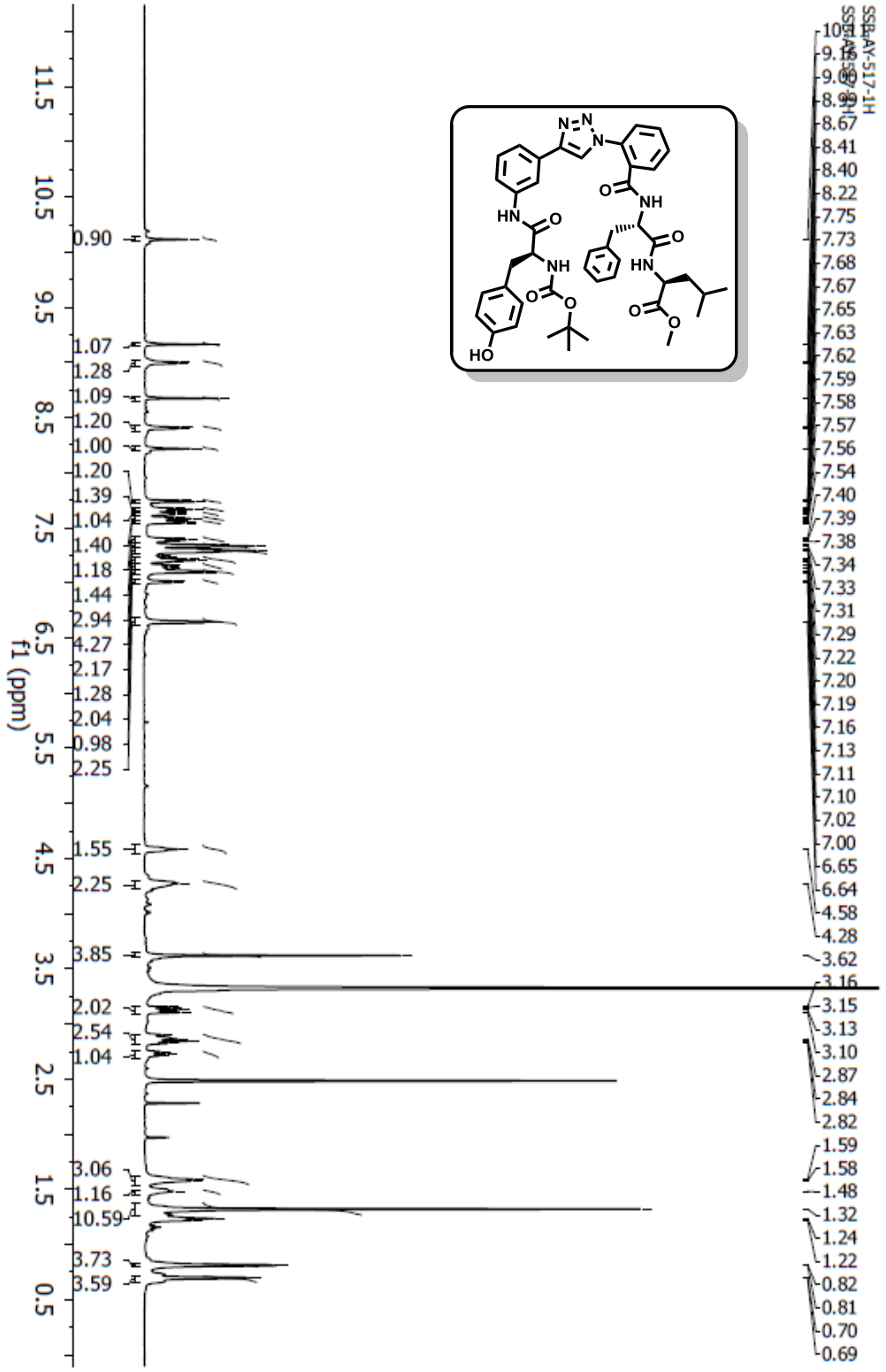

Figure 3.39: ^{1}H Spectra of synthesized compound **3.82.**

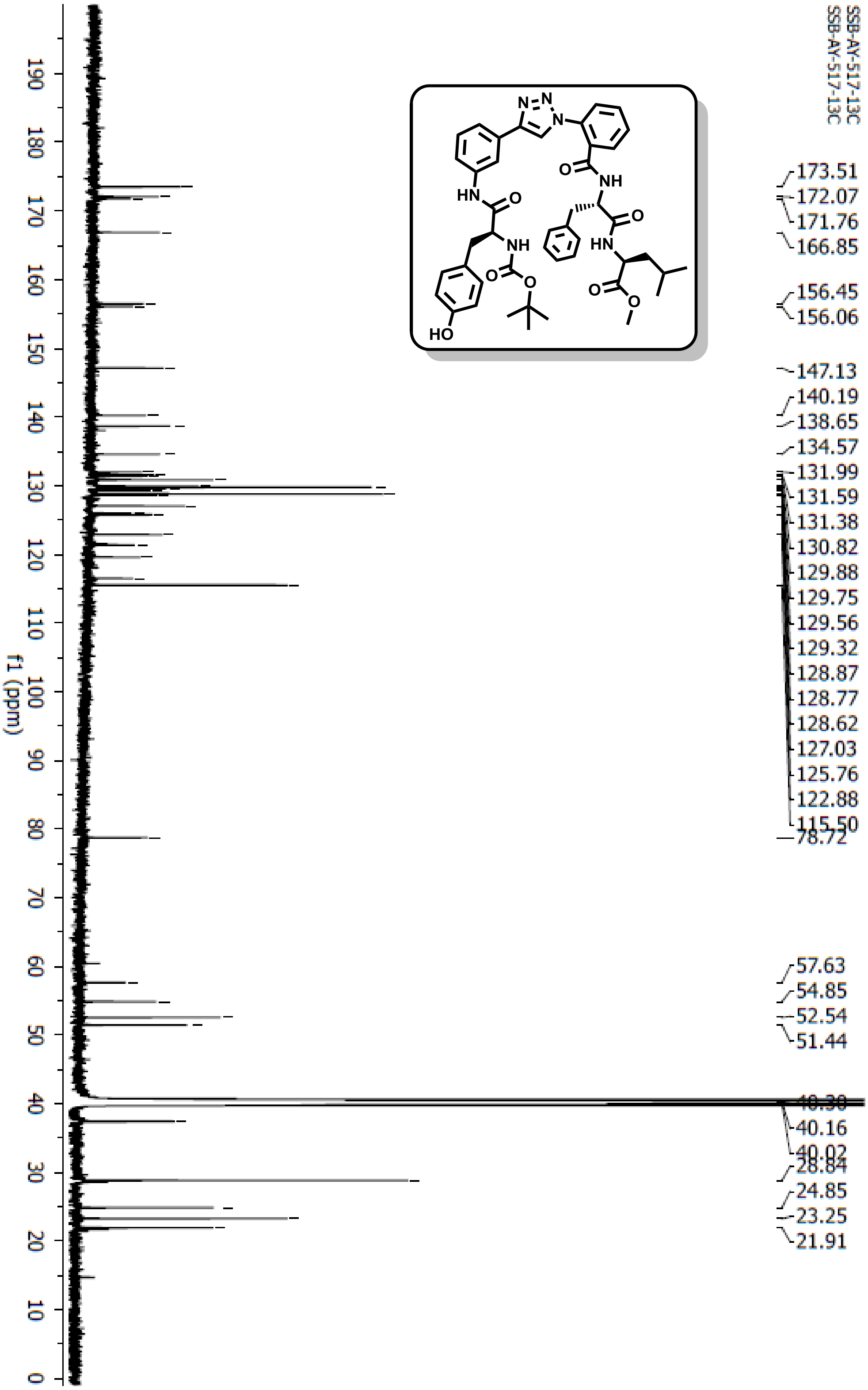

Figure 3.40: ^{13}C Spectra of synthesized compound **3.82.**

3.11. Reference

1. (a) Schulz, G. E.; R. Schirmer, H. In *Principles of Protein Structure*; Springer, New York, **1979**.
(b) Branden, C.; Tooze, J. In *Introduction to Protein Structure*; Garland, New York, **1991**.

2. (a) Souers, A. J.; Rosenquist, A.; jarvie, E. M.; Ladlow, M.; Fenuik, W.; Ellman, J. A. *Biorg. Med. Chem. Lett*. **2000**, *10*, 2731.
(b) Souers, A. J.; Virgilio, A. A.; Rosenquist, A.; Fenuik, W.; Ellman, J. A. *J. Am. Chem. Soc.* **1999**, *121*, 1817.
(c) Gardner, B.; Nakanishi, H.; Kahn, M. *Tetrahedron* **1993**, *49*, 3433.
(d) Giannis, A.; Kolter, T. *Angew. Chem. Int. Ed. Engl.* **1993**, *32*, 1244.

3. Wilmot, C. M.; Thornton, J. M. *J. Mol. Biol.* **1988**, *203*, 221.

4. Venkatachalam, C. M. *Biopolymers* **1968**, *6*, 1425.

5. (a) R. F. Wissner, S. Batjargal, C. M. Fadzen, J. E. Petersson, *J. Am. Chem. Soc.* **2013**, *135*, 6529.
(b) H. S. Lee, J. Guo, E. A. Lemke, R. D. Dimla, P. G. Schultz, *J. Am. Chem. Soc.* **2009**, *131*, 12921.

6. Wilmot, C. M.; Thornton, J. M. *J. Mol. Biol.* **1988**, *203*, 221.

7. (a) Toniolo, C.; Polese, A.; Formaggio, F.; Crisma, M.; Kamphuis, J. *J. Am. Chem. Soc.* **1996**, *118*, 2744.
(b) Engel, M.; Williams, R. W.; Erickson, B. W. *Biochemistry* **1991**, *30*, 3161.
(c) Kemp, D. S.; Allen, T. J.; Oslick, S. L. *J. Am. Chem. Soc.* **1995**, *117*, 6641.

8. (a) Plateau, P.; Gueron, M. *J. Am. Chem. Soc.* **1982**, *104*, 7310.
(b) Wishart, D. S.; Sykes, B. D.; Richards, F. M. *J. Mol. Biol.* **1991**, *222*, 311.
(c) Plateau, P.; Gueron, M. *J. Am. Chem. Soc.* **1982**, *104*, 7310.
(d) Wishart, D. S.; Sykes, B. D.; Richards, F. M. *J. Mol. Biol.* **1991**, *222*, 311.
(e) Dyson, H. J.; Wright, P. E. *Ann. Rev. Biophys. Biophys. Chem.* **1991**, *20*, 519.

9. (a) Smith, J. A.; Pease, L. G. CRC *Crit. Rev. Biochem.* **1980**, *8*, 315.
(b) Rose, G. D.; Gierasch, L. M.; Smith, J. A. *Adv. Protein Chem.***1985**, *37*, 1.
(c) Shamala, N.; Nagaraj, R.; Balaram, P. *Biochem. Biophys. Res. Commun.* **1977**, *79*, 292.

10. (a) Benedetti, E. *Biopolymers* **1996**, *40*, 3.
(b) Ravi, A.; Prasad, B. V. V.; Balaram, P. *J. Am. Chem. Soc.* **1983**, *105*, 105.
(c) Fink, B. E.; Kym, P. R. Katzenellenbogen, J. A. *J. Am. Chem. Soc*. **1998**, *120*, 4334.

11. (a) Dutt, A.; Frohlich, R.; Pramanik, A. *Org. Biomol. Chem*. **2005**, *3*, 661.

(b) Dutt, A.; Drew, M. G. B.; Pramanik, A. *Tetrahedron* **2005**, *61*, 11163.
(c) Dutt, A.; Dutta, A.; Mondal, R.; Spencer, E. C.; Howardb, J. A. K.; Pramanik, A. *Tetrahedron* **2007**, *63*, 10282.

12. Arnold, U.; Hinderaker, M. P.; Nilsson, B. L. Huck, B. R.; Gellman, S. H.; Raines, R. T. *J. Am. Chem. Soc*. **2002**, *124*, 8522.

13. (a) Pinsker, A.; Einsiedel, J.; Härterich, S.; Waibel, R.; Gmeiner, P. *Org. Lett*. **2011**, *13*, 3502.
(b) Bittermann, H.; Gmeiner, P. *J. Org. Chem*. **2006**, *71*, 97.

14. Golebiowski, A.; Klopfenstein, S. R.; Shao, X.; Chen, J. J.; Colson, A.-O.; Grieb, A. L. Russell, A. F *Org. Lett*. **2000**, *2*, 2615.

15. Wu, C. -F.; Zhao, X.; Lan, W. –X.; Cao, C.; Liu, J. –T.; Jiang, X. –K.; Li, Z. -T. *J. Org. Chem*. **2012**, *77*, 4261.

16. Kawahara, S.; Uchimaru, T.; Murata, S. *Chem. Commun.* **1999**, 563.

17. Tong, A. K.; Jockusch, S.; Li, Z.; Zhu, H,-R.; Akins, D. L.; Turro, N. J.; Ju, J. *J. Am. Chem. Soc.* **2001**, *123*, 12923.

18. Navarathne, D.; Ner, Y.; Grote, J. G.; Sotzing, G. A. *Chem. Commun.* **2011**, *47*, 12125.

19. Yum, J.-Ho.; Hardin, B. E.; Hoke, E. T.; Baranoff, E.; Zakeeruddin, S. M.; Nazeeruddin, M. K.; Torres, T.; McGehee, M. D.; Gratzel, M.; *ChemPhysChem* **2011**, *12*, 657.

20. Santoro, S. W.; Joyce, G. F. *Proc. Natl. Acad. Sci.* **1997**, *94*, 4262.

21. Fábián Á, Horváth G, Vámosi G, Vereb G, Szöllősi J. *Cytometry A.* **2013** *83A*, 375.

22. Xu, Q.-H.; Wang, S.; Korystov, D.; Mikhailovsky, A.; Bazan, G. C.; Moses, D.; Heeger. A. J. *Proc. Natl. Acad. Sci.* **2005**, *102*, 530.

23. (a) Zasloff, M. *Nature* **2002**, *415*, 389.
(b) Rinaldi, A. C. *Curr. Opin. Chem. Biol.* **2002**, *6*, 799.

24. Boeneman, K.; Mei, B. C.; Dennis, A. M.; Bao, G.; Deschamps, J. R.; Mattoussi, H.; Medintz, I. L. *J. Am. Chem. Soc*. **2009**, *131*, 3828.

25. Bag, S. S.; Jana, S.; Pradhan, M. K.; Pal, S. *RSC Adv.* **2016**, *6*, 72654.

26. (a) Oh, K.; Guan, Z. *Chem. Commun*. **2006**, 3069. (b) Feher-Voelger, A.; Borges-Gonzlez, J.; Carrillo, R.; Morales. E. Q.; Gonzlez-Platas, J.; Martn, T. *Chem. Eur. J.* **2014**, *20*, 1.

4.1. Introduction

4.1.1. Triazole Ring as a Conformationally Constrained Molecular Scaffold

The Huisgenazide-alkyne cycloaddition reaction has broadly been utilized as conjugation strategy in composite biomimetic architectures as the triazole ring replaces peptide/amide and phosphodiester bonds. Several reports established the fact that the 1,2,3-triazole units can be utilized as surrogates for biologically relevant amide bonds. There are some factors that describes why 1,2,3-triazole units can be used widely in peptidomimetic chemistry.

(a) 1,2,3-triazole units can be used as highly stable passive linker that can replace more labile linkers in biologically active compounds.

(b) The triazole ring displays similar electronic content and dipole moment and planarity as the amide bond.

(c) A good non-classical bioisostere of the peptidic bond with an improved stability in biological systems can be reflected by 1,2,3-triazole units (**4.01-4.02**, **Figure 4.1**).[1]

(d) The analogous H-bonding profile as an amide bond can be done by 1,2,3-triazole units.

(e) The ring can serve the purpose of a peptidomimetic scaffold.

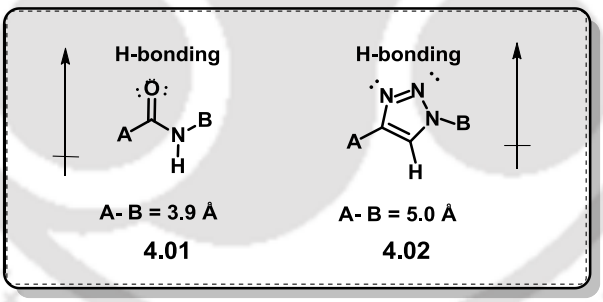

Figure 4.1. Bioisosteric relationship between the amide bond and triazole ring (**4.01-4.02**).[1]

4.1.2. The 1,2,3-Triazole Units Containing Peptidomimetics

Wong *et al.* have described the utilization of triazole unit as HIV protease inhibitors. The HIV protease has been synthesized by the replacement of amide bond of central peptide with the triazole ring as the isostere. The newly synthesized triazole-based peptide showed inhibition towards HIV protease in the nanomolar range. Thus the triazole unit containing peptidomimetic inhibition profile can be compared as a reference inhibitor (**4.03-4.04**, **Figure 4.2**).[2]

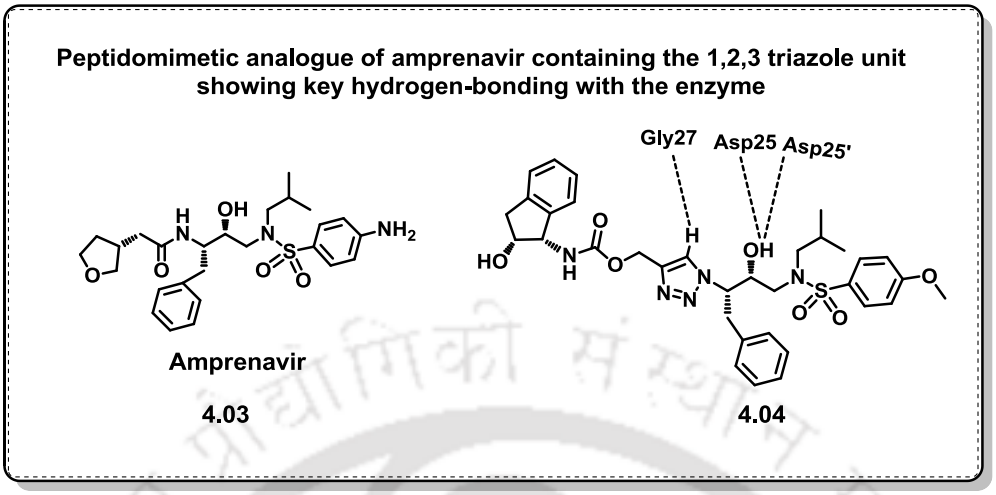

Figure 4.2. (a) Peptidomimetic analogue of Amprenavir containing the 1,2,3-triazole as amide bond isostere in the central unit (**4.03**-**4.04**).[2]

Guan and coworkers have utilized this strategy and synthesized triazole linked peptides with turn unit.[4] The synthesized peptides with triazole unit revealed a β-turn secondary structure and hence the triazole unit serves the purpose of a reverse turn inducer (**4.05**-**4.06**, **Figure 4.3**).

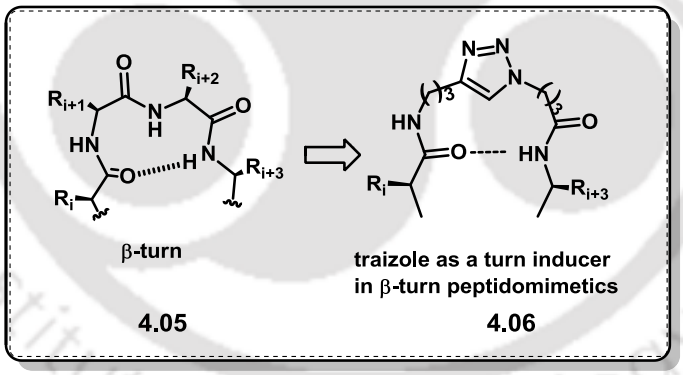

Figure 4.3. Comparison between a β-turn (**4.05**) and β-turn peptidomimetics containing the triazole ring (**4.06**) connecting the two peptide β-strands.[4]

Burgess *et al.* synthesized cyclic peptide derivatives from linear peptide with the help of click chemistry.[5] The synthesized peptides containing triazole unit showed β-turn structures. The peptides were highly stable as verified by NMR and CD analysis. From their study it is revealed that the triazole molecular scaffold can nucleate the cyclic peptides to adopt type I and type II β-turn conformations (**4.07**-**4.09**, **Figure 4.4**).

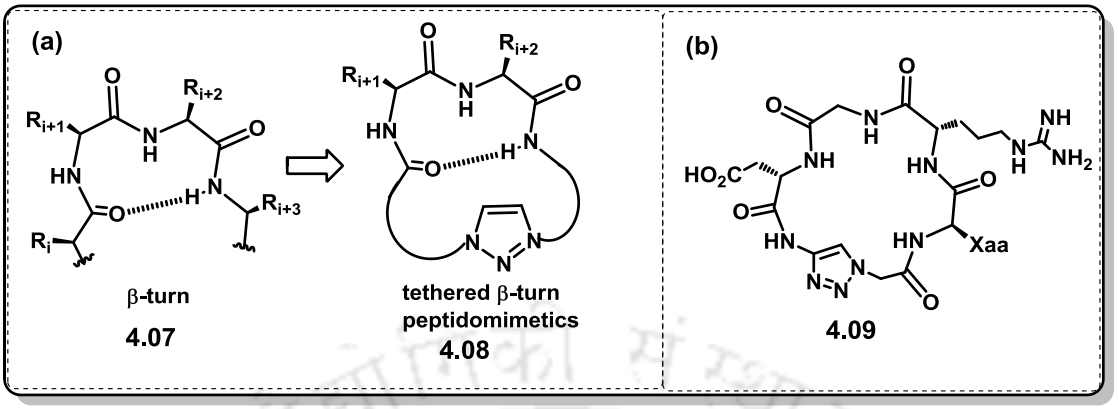

Figure 4.4. (a) The triazole ring as the inducer/scaffold for macrocyclic β-turn peptidomimetics (**4.07-4.08**), (b) Cyclic RGD peptidomimetic with the triazole ring (**4.09**) as a turn-inducing element.[5]

James *et al.* have synthesized a library of cyclic tetrapeptides using click reaction (**4.10-4.11**, **Figure 4.5**) with β-turn structures with high yield (**4.12-4.14**, **Figure 4.5**). The intramolecular hydrogen bonding between carbonyl of phenyl alanine at i^{th} and NH of glycine at i+3 is clearly evident from a crystallographic study indicating a β-turn secondary structure. The secondary structural conformation was supported by 1D, 2D and variable temperature (VT)-^{1}H NMR spectroscopy.[6]

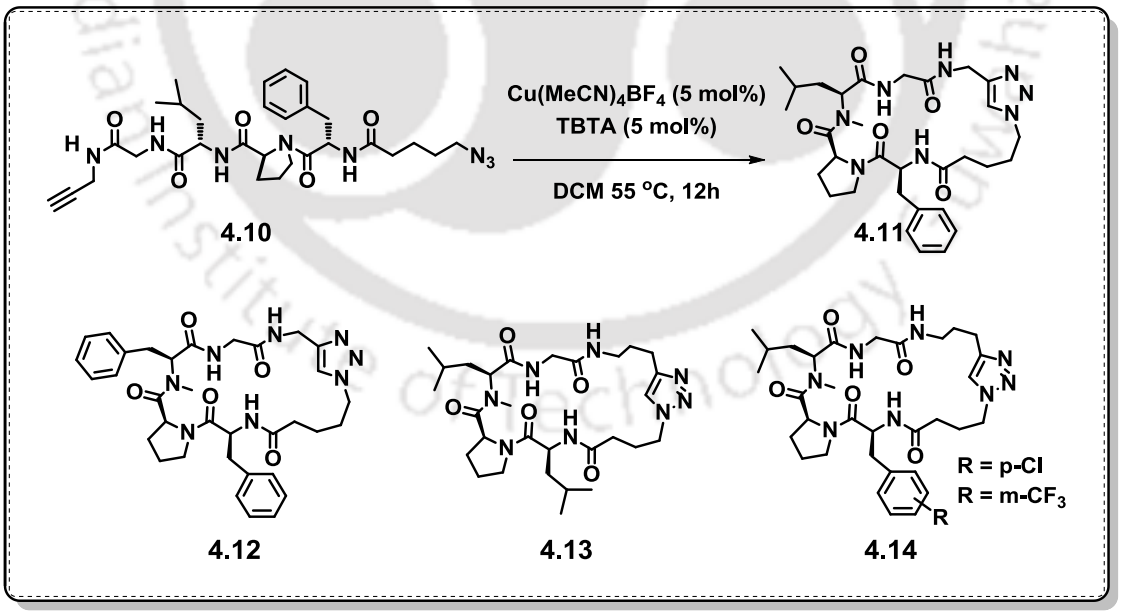

Figure 4.5. Copper catalyzed synthesis of cyclic tetrapeptides (**4.10-4.14**). [6]

.

4.1.3. Distance Dependent FRET study

Förster resonance energy transfer (FRET) becomes a valuable strategy for the assessment of distances in many biomolecular systems.[7] FRET among various donor/acceptor pairs allows determining the distance between them. Short polypeptides which is flexible and with 10-20 amino acids in their backbone, the end-to-end distance can be calculated by FRET measurement.[8]

Werner M. Nau and coworkers have used 2,3-diazabicyclo[2.2.2]oct-2-ene (**4.15**, DBO) as an acceptor unit and tryptophan (Trp) as a donor unit form a convenient donor/acceptor pair having the R_0 value of 10 Å. They have synthesized flexible and structureless Trp–(Gly–Ser)$_n$–Dbo–NH_2 peptides with n = 0-10. This FRET pair allows to measure the end-to-end distances in these short peptides (**Figure 4.6**). The distances and distribution functions were measured by them from steady state and time-resolved fluorescence and compare with those from MD simulations. They have introduced Trp/Dbo FRET pair as a unique tool to evaluate distribution functions for short flexible peptides.[8]

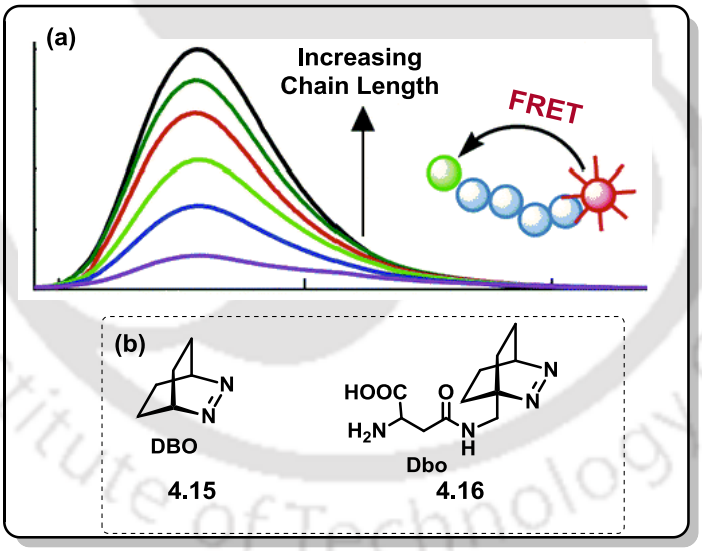

Figure 4.6. (a) Schematic diagram of distance distributions of short polypeptides recovered by FRET study in the 10 Å domain. (b) Structures of DBO and Dbo that were used in this study (**4.15-4.16**).[8] Copyright (2007) from American Chemical Society

FRET is a photophysical phenomenon between two flurophores that only occurs when the fluorophores are in sufficient proximity (10-100 Å) with each other. The primary condition for FRET to occur is the overlap between the emission spectrum of

the donor and the excitation spectrum of the acceptor.[9] Study with two auto fluorescent protein in combination with the receptor protein may afford a sensor protein. That sensor protein responds to a dynamic fluctuation of intracellular ligand concentration by a ratiometric fluorescence change. The receptor when binds the substrate, it causes a large structural change of the substrate, that was measured by FRET study (**4.17**-**4.18**, **Figure 4.7**). This strategy would be the most straight forward way to integrate the signal transduction function into the receptor of interest.

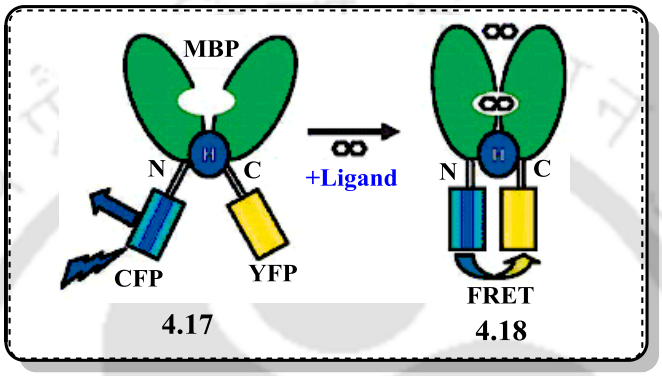

Figure 4.7. Intramolecular FRET-based biosensors exploit the protein domains with a large structural change upon the ligand-binding event (**4.17**-**4.18**).[9] Copyright (2006) from Willey Online Library.

Nau *et al.* have synthesized short and structureless random-coil polypeptides (**4.19, Figure 4.8**) where 2,3-diazabicyclo[2.2.2]oct-2-ene (DBO) is attached as a fluorescent probe at one end of the peptide and the another end contains tryptophan amino acid.[10] Tryptophan and DBO were good donor/acceptor pair in FRET study in peptides of the general structure Trp-$(Pro)_n$-Dbo–NH_2 (n = 1-6).[10] FRET was measured by steady-state and time-resolved fluorescence spectroscopy as well as by molecular dynamics (MD) simulations. The FRET efficiency depends on the spacer length (number of proline residues) of the peptides and it was ranged between 2-72% (**4.19**, **Figure 4.8**). The donor-acceptor distances were calculated from FRET study 8 Å (n = 1) and 16 Å (n = 6) in water and was found to be comparable or slightly higher in propylene glycol. From the study it was revealed that in polyprolines the donor-acceptor distances extracted by FRET can be correlated with the Förster radii of the employed FRET pairs.

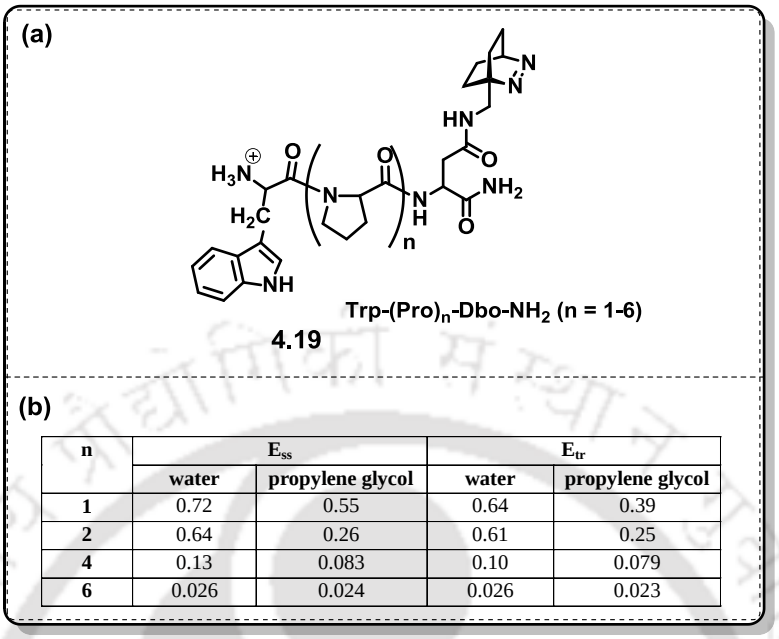

n	E_{ss}		E_{tr}	
	water	propylene glycol	water	propylene glycol
1	0.72	0.55	0.64	0.39
2	0.64	0.26	0.61	0.25
4	0.13	0.083	0.10	0.079
6	0.026	0.024	0.026	0.023

Figure 4.8. (a) Molecular structures of the investigated polyproline, labeled amino acid and peptides (**4.19**). (b) Steady-state energy transfer efficiencies (E_{ss}) and Energy transfer efficiency obtained from time resolved fluorescence (E_{tr}) of the investigated polyprolines. [10]

Janda *et al.* have demonstrated a monitoring of HIV gp41 core disruption based on FRET assay.[11] They have chosen 7-methoxycoumerin-4-acetic acid (MCA) and 2,4 dinitrophenyl (Dnp) groups as fluorophore and quencher, for this purpose. This FRET pair (MCA **4.23** and Dnp **4.24**) is having small size, can avoid large polycyclic entities and could interact with peptide or nonpeptide inhibitor through π-stacking interaction.

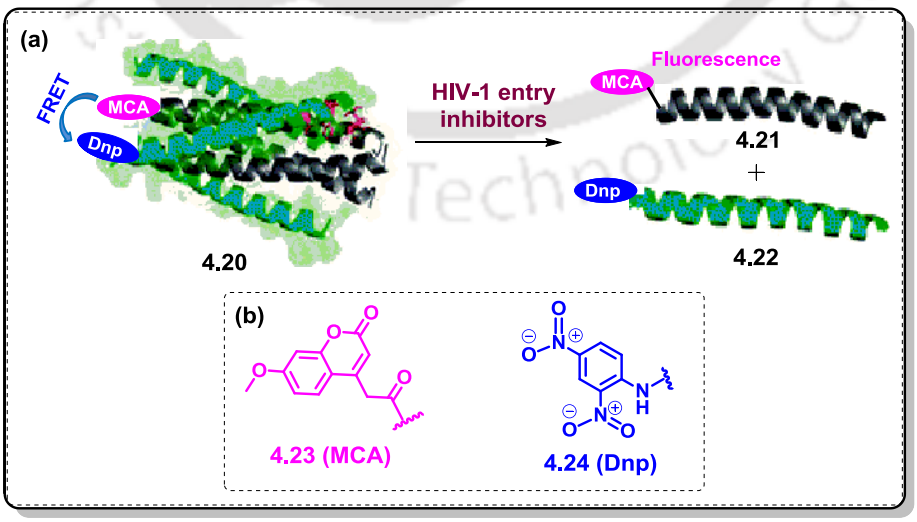

Figure 4.9. (a) Schematic diagram for the disruption of FRET between Dnp and MCA on introduction of HIV-1 inhibitor (**4.20-4.22**). (b) Structures of MCA (**4.23**) and Dnp (**4.24**) used for FRET assay.[11]

Thus, they have reported the design, synthesis, and development of *N*-and *C*-terminal peptide FRET pair for screening of gp41 six-helix bundle disruption (**4.20-4.22**, **Figure 4.9**). By strategically placing two FRET probes on two peptides, they were able to monitor the intermolecular co-association by fluorescence quenching between the fluorescence donor and acceptor.[11]

Werner M. Nau and coworkers have investigated the conformational changes of short polypeptides upon phosphorylation (**4.25-4.27**, **Figure 4.10**).[12] The peptides were probed by short-distance FRET pair ($R_0 \approx 10$ Å) based on tryptophan as natural FRET donor and (**Dbo**) as synthetic FRET acceptor. They investigated it for two peptides LeuArgArgTrpSerLeuGly-Dbo and TrpLysArgThrLeuArgArg-Dbo (**4.25**). An increase in FRET efficiency for peptide **4.25** was shown upon phosphorylation as was evident from steady-state and time-resolved fluorescence experiments in H_2O. This was due to the conformational change of the peptide **4.25** upon phosphorylation which helped bringing the FRET pairs close together and FRET efficiency was thus, increased. Thus, Trp/Dbo FRET pair can deal with the conformational changes that accompanied the methylation or phosphorylation of peptides, or their response to external variations like salt effects, pH changes, and temperature.

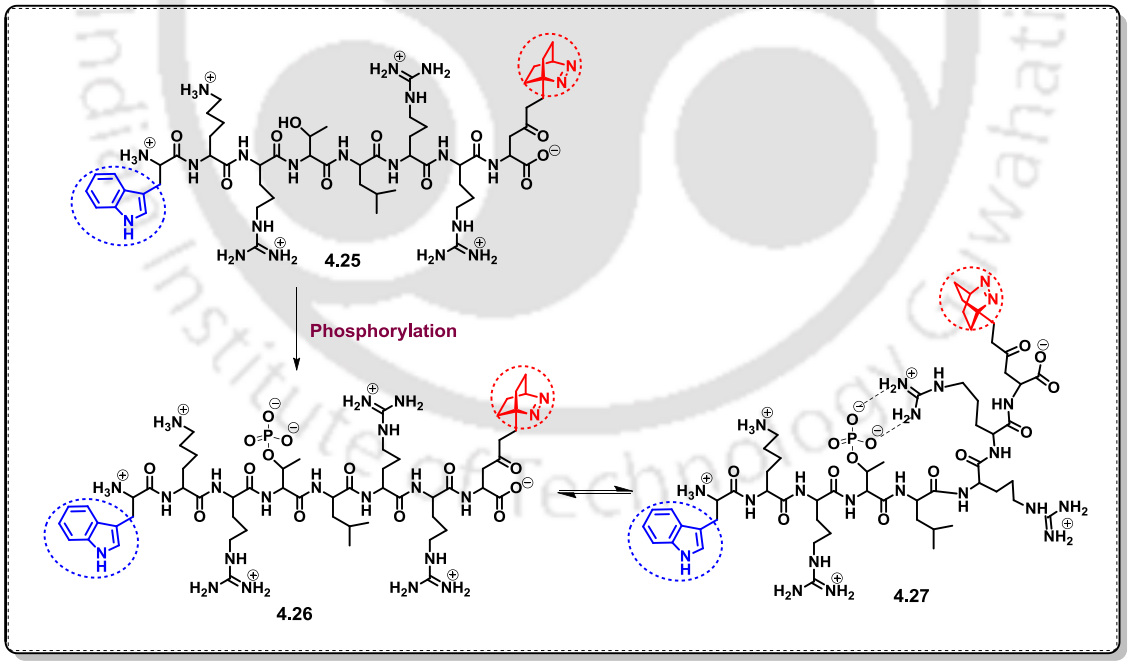

Figure 4.10. Salt-bridge formation and distance dependent FRET measurement upon phosphorylation in synthesized peptide (**4.25-4.27**).[12]

4.2. Background

Förster resonance energy transfer (FRET) is a process of energy transfer between two chromophores. A donor chromophore from its excited electronic state transfers the energy to an acceptor chromophore through nonradiative dipole–dipole coupling. The efficiency of this energy transfer is inversely proportional to the sixth power of the distance between donor and acceptor, making FRET extremely sensitive to small changes in distance. Measurements of FRET efficiency can be used to determine if two fluorophores are within a certain distance of each other. Such measurements are used as a research tool in fields including biology and chemistry. FRET was first described over 50 years ago, that is being used more and more in biomedical research and drug discovery today. FRET is one of few tools available for measuring nanometer scale distances and the changes in distances, both in vitro and in vivo.[13] Due to its sensitivity to distance, FRET has been used to investigate molecular level interactions. One common donor-acceptor pair in biology used is a cyan fluorescent protein (CFP) – yellow fluorescent protein (YFP) pair.[14] Both are color variants of green fluorescent protein (GFP) which can be attached to a host protein by genetic engineering and a fusion of CFP and YFP linked by a protease cleavage sequence can be used as a cleavage assay.[15] Many more advanced research results and designed chromophoric pairs have been reported aiming at the uncovering the structure, function, dynamics and interactions involving biomolecules inside a cell. However, a number of issues that needs to be considered while designing FRET experiments such as

(a) Close proximity which needs either to be established or removed during an assay, resulting in a change in signal that can be measured

(b) Appropriate donor/acceptor pairs need to have enough spectral overlap for efficient energy transfer to take place and difference in spectrums as to be distinguishable from one another.

Factors such as concentration, cellular localization *etc.* also played important roles in controlling the success or failure of FRET process. Therefore, a critical design of efficient FRET pair as well as their proper placement within a molecular entity is critical which is more important in biomolecular investigations as the FRET efficiency would depend on the spatial disposition of the chromophores in an adopted biomolecular conformation.

4.3. Objective

The above background and vast applications of FRET inspired us to take a challenge of designing scaffold amino acids of arm length differed by 1-2 carbon

atoms. For investigating the factors that affect the folding, stability and interactions of peptides and proteins a number of β-turn mimics employing various templates have been developed.

With this concept and background information we framed our objective as below

(a) Synthesis of triazolyl amino acids with various spacer lengths via cycloaddition reaction between the corresponding alkynyl ester and azides.

(b) Incorporation into fluorescent pentapeptides wherein two fluorescent amino acids (^{TMnap}**Ala**^{Do} and ^{TPy}**Ala**^{Do}) have been placed at the two termini which constitute a FRET pair.

(c) Study of conformation with the help of CD, IR, 2D NMR, variable temperature NMR and MD simulation.

(d) Study of photophysical property towards establishing our concept of distance dependent FRET.

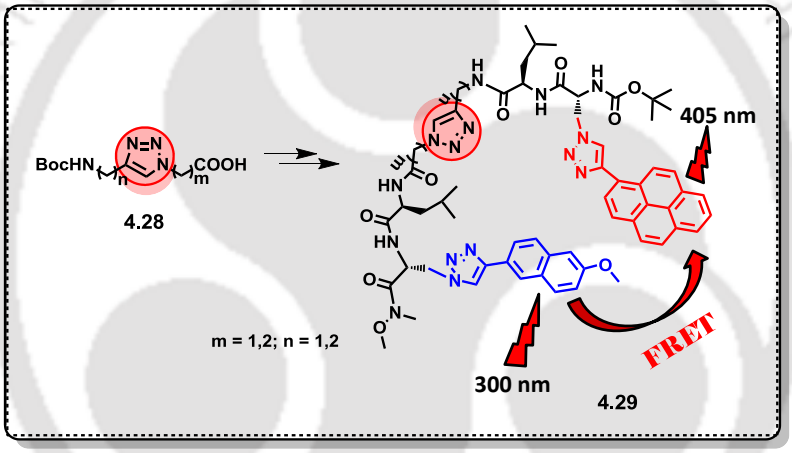

Figure 4.11. Graphical presentation of aliphatic triazolo amino acids with different spacer lengths (**4.28**) and distance dependant FRET phenomena in the designed fluorescent pentapeptides (**4.29**).

Based on our earlier concept of triazolyl aliphatic amino acid as peptidomimetic scaffolds, we thought that altering the length of amine or acid terminus or both and embedding the same in a peptide backbone could end up with β-sheet peptides.[16] However, the propensity to form turn/sheet secondary structure would depend on the length of the spacers that connect the amine and acid in the two arms to the triazole ring of the scaffold triazolyl amino acid. Furthermore, we envisioned that the extent of through space interaction/photophysical dipolar interaction between two fluorescent amino acids if placed at the two termini of a pentapeptide containing the scaffold at the center would be different due to different spacer length. Thus, these two fluorescent amino acids if constitute a FRET pair, efficiency of Forster resonance energy transfer from donor to acceptor fluorescent amino acid upon excitation at the

absorption wavelength of donor amino acid would vary depending on the spacer length. We, then, further envisioned that the FRET efficiency would be higher at a smallest spacer length while largest one would give lowest FRET efficiency maintaining the secondary structure/conformation of the pentapeptides in all cases.

4.4. Result and Discussion

4.4.1. Synthesis of Aliphatic Triazolyl Amino Acid Scaffolds with Different Spacer Lengths and Corresponding Peptides

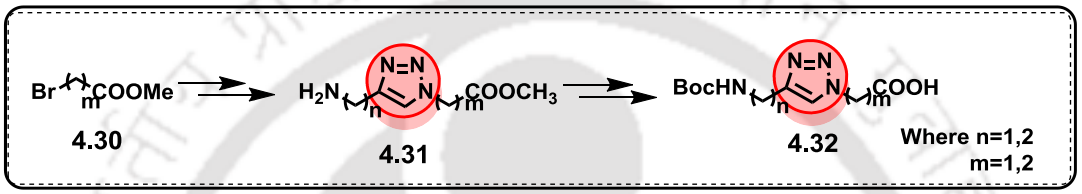

Scheme 4.1. General scheme for the synthesis of triazolyl amino acid scaffolds with different spacer lengths (**4.30-4.32**).

4.4.2. Synthetic scheme for Boc protected aliphatic amino acid scaffolds

Based on Cu(I) catalyzed click chemistry the synthesis of aliphatic triazolyl amino acid scaffolds was carried out. For the synthesis of 1/1 aliphatic triazolyl amino acid scaffold, we have started the reaction from ethyl bromoacetate (**4.33**) which was treated with NaN_3 in water/acetone (1:3) solvent at 60 ^oC to get ethyl azidoacetate (**4.34**). The synthesized ethyl azidoacetate, **4.34** underwent (3+2)π cycloaddition reaction with propargyl alcohol under click reaction condition and generated corresponding triazolyl alcohol (**4.35**) which was then allowed to react with mesyl chloride in presence of triethyl amine as base at 0 ^oC in dry DCM solvent to get mesylate derivative (**4.36**) of the corresponding alcohol. The mesylate derivative (**4.36**) was then reacted with NaN_3 in dry DMF solvent at 50 ^oC to afford azido derivative of triazolyl scaffold (**4.37**). The hydrolysis of ethyl ester was carried out by lithium hydroxide mediated hydrolysis reaction condition. Then the reduction of azide under Pd/C and hydrogen atmosphere in dry methanol solvent afforded the NH_2 and COOH deprotected unnatural triazolyl amino acid **4.39**, $^{1/1\text{-Al}}$**TAA**. Boc-protection of synthesized scaffold using Boc-anhydried in dioxane–water system finally yielded the BocNH-triazolyl amino acid scaffold (**4.40**, $^{1/1\text{Al}}$**TAA**) (**Scheme 4.2**).

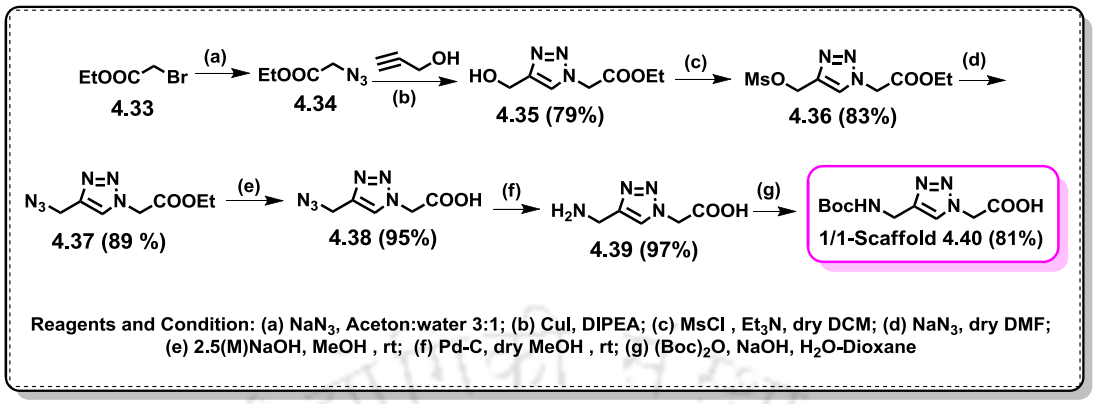

Scheme 4.2. Synthesis of aliphatic triazolyl amino acid scaffold (**4.40**, $^{1/1Al}$**TAA**).

The synthesis of other aliphatic triazolyl amino acid scaffolds ($^{1/2Al}$**TAA**, $^{2/1Al}$**TAA**, $^{2/2Al}$**TAA**) were carried out by similar reaction conditions as described earlier following **Scheme 4.2.**

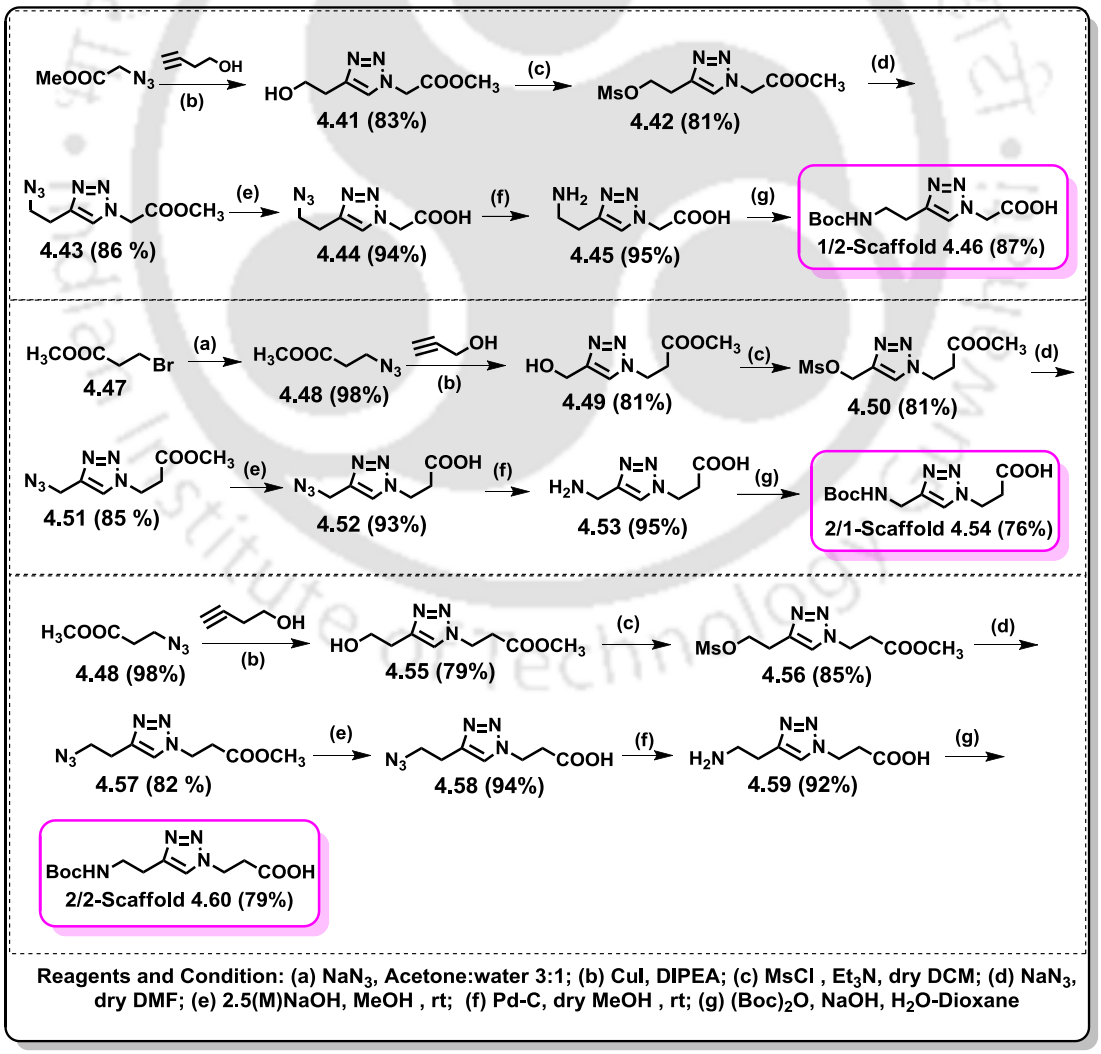

Scheme 4.3. Synthetic scheme for the synthesis of three triazolyl aliphatic amino acid scaffolds $^{1/2Al}$**TAA** (**4.46**), $^{2/1Al}$**TAA** (**4.54**), $^{2/2Al}$**TAA** (**4.60**).

4.4.3. Synthesis of Unnatural Fluorescent Pentapeptides Based on Aliphatic Amino acid scaffolds

Next, the fluorescent pentapeptide with $^{1/1\text{-Al}}$**TAA** (**4.40**) scaffold in backbone was synthesized in a similar way (as described in **Chapter 2**, **Section 2.4.1**) via the peptide coupling reaction of Boc-deprotected tripeptide [**TFA.NH$_3$–$^{1/1\text{-Al}}$TAA–Leu-^{TPy}Ala^{Do}–CONMe(OMe)**] (**4.64**) and Boc-protected dipeptide (**BocNH–^{TMnap}Ala^{Do}–Leu–CO$_2$H**, **2.60**), containing unnatural fluorescent triazolyl amino acids [^{TMnap}**Ala**^{Do} and ^{TPy}**Ala**^{Do}, respectively] wherein the scaffold $^{1/1\text{-Al}}$**TAA** (**4.40**) was placed in the middle of the peptide backbone (**Scheme 4.4**). Synthetic procedure of fluorescent triazolyl dipeptide and tripeptide derivatives was discussed in **Chapter 2**.

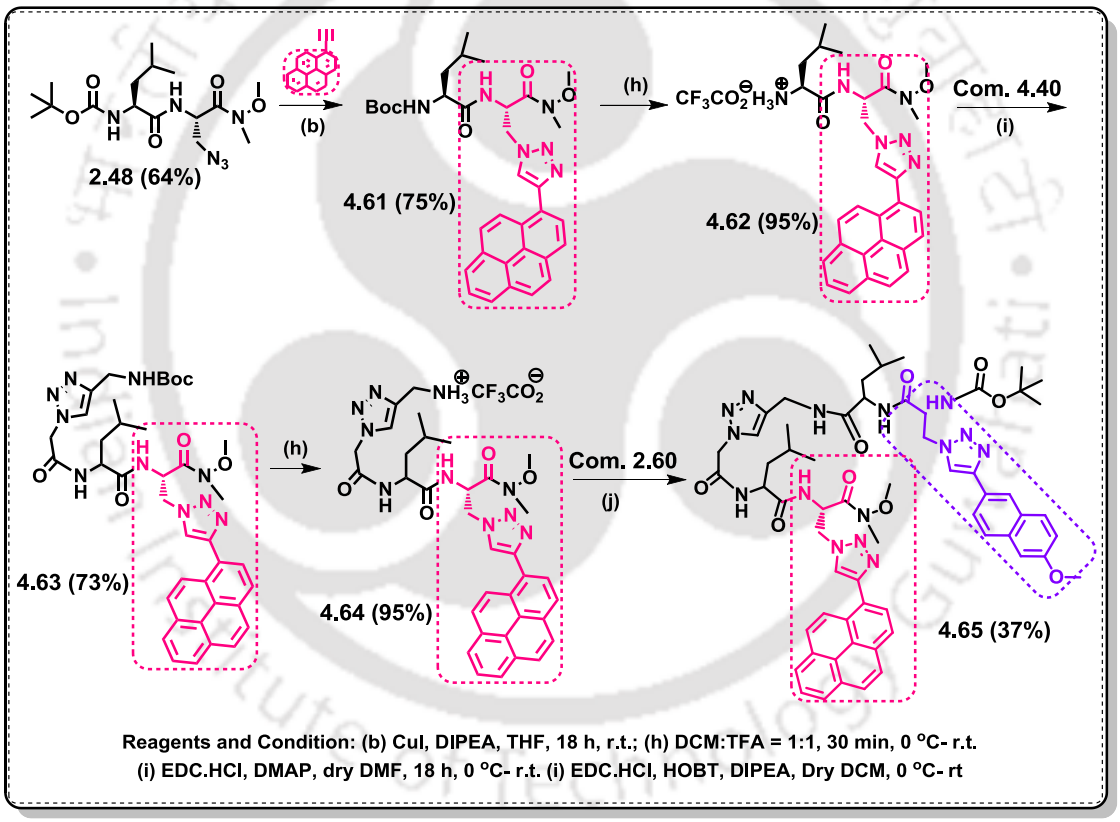

Scheme 4.4. Synthetic scheme of $^{1/1\text{Al}}$**TAA** (**4.40**) scaffold based unnatural pentapeptide **4.65** [**BocNH–^{TMnap}Ala^{Do}–Leu–$^{1/1\text{Al}}$TAA–Leu–^{TPy}Ala^{Do}–CONMe(OMe)**].

The synthesis of another aliphatic triazolyl amino acid scaffold with different spacer length [$^{1/2\text{-Al}}$**TAA** (**4.46**, **Scheme 4.3**), $^{2/1\text{-Al}}$**TAA** (**4.54**, **Scheme 4.3**), $^{2/2\text{Al}}$**TAA** (**4.60**, **Scheme 4.3**)] containing unnatural pentapeptides were carried out using similar peptide coupling reaction conditions as described earlier following the **Scheme 4.4.**

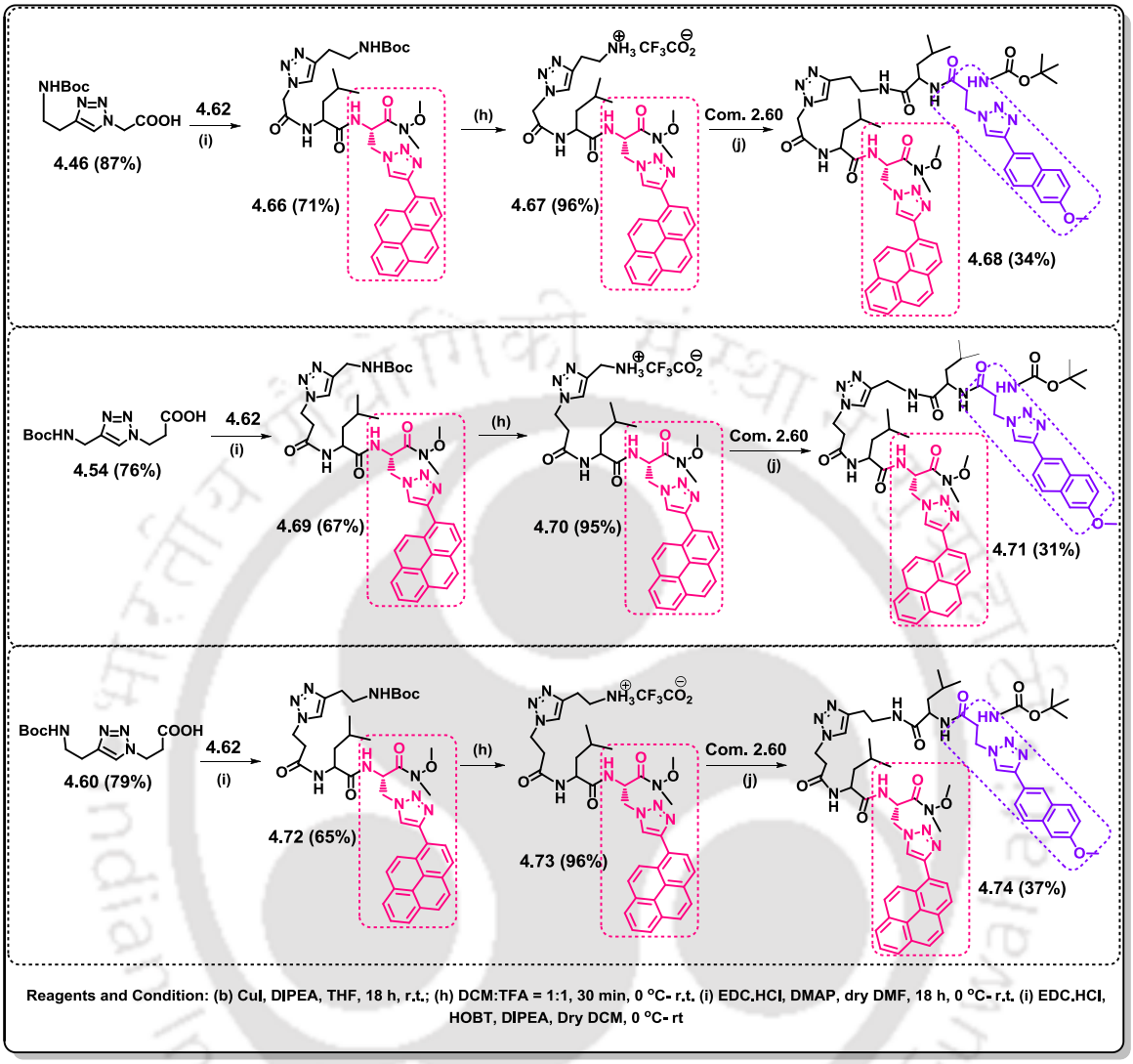

Scheme 4.5. Synthetic scheme of $^{1/2Al}$**TAA** (**4.46**), $^{2/1Al}$**TAA** (**4.54**), $^{2/2Al}$**TAA** (**4.60**) scaffold based unnatural pentapeptides **4.68**, **4.71** and **4.74.**

All the intermediate peptides and final peptides were purified by silica-gel (60-120 mesh) column chromatography and characterized by both 1D and 2D NMR, IR, and HR-mass spectrometry. After getting our target peptides in pure form in hand, we, next, studied their secondary structure using various spectroscopic techniques.

4.4.4. Conformational Study of Pentapeptides 4.65, 4.68, 4.71 and 4.74 using CD, IR, NMR Spectroscopic Techniques.

Study of Circular Dichroism Spectra: The secondary structure determination via CD spectrometer of the four fluorescent pentapeptides **4.65**, **4.68**, **4.71**, **4.74** containing aliphatic triazolyl amino acid scaffolds with different spacer lengths (**4.44**, **4.46**, **4.54**, **4.60**) in the backbone, showed predominantly β-sheet like structures in each peptide. CD spectra were recorded using a CD spectrometer with a cell path length of 1 mm at in different solvent at room temperature and variable temperature. All the samples were with 50 μM concentration and prepared in spectroscopic grade solvents. From circular dichroism spectra it was revealed that the unnatural pentapeptides adopted β-sheet like structures. In all peptides positive bands at around 196 and negative band at around 212 nm supported the β-sheet like structure (**Figure 4.12**). The appearance of ICD bands in the chromophoric absorbance region (300-350 nm) in all the peptides indicated the π-π stacking interactions between the two terminal chromophores.[17]

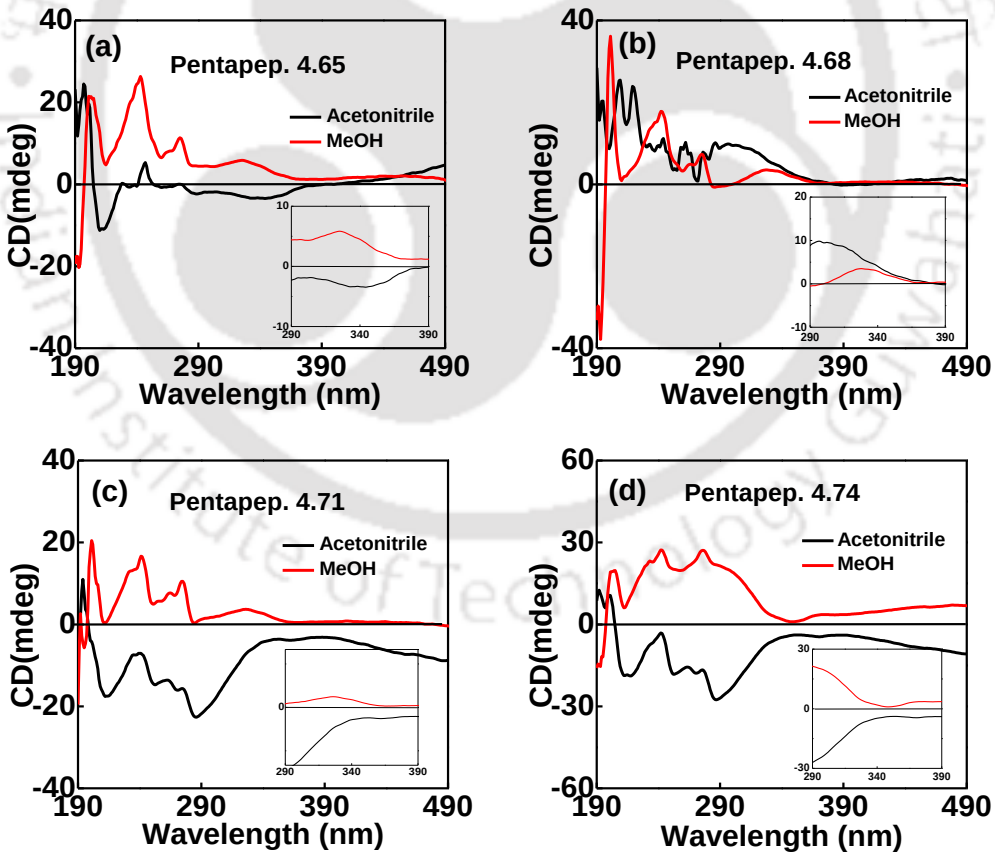

Figure 4.12. CD spectra of (a) **Pentapeptide 4.65**, (b) **Pentapeptide 4.68**, (c) **Pentapeptide 4.71**, (d) **Pentapeptide 4.74** in acetonitrile and methanol solvents (50 μM concentration, 25 ^{o}C).

Intramolecular H-Bonding interaction using the study of FT-IR Spectroscopy: To prove the intramolecular H-bond formation in synthesized peptide strands, IR spectroscopic technique was used. So, IR spectra were recorded using dry KBr and solid dry compound, which showed the presence of intramolecular H-bonded and free amide –NH stretching absorptions at around 3310-3296 cm^{-1} for all fluorescent pentapeptides which supported β-sheet like structure. The IR spectrum of all peptides showed a sharp N-H stretching absorption at around $\bar{\upsilon}$ = 3310-3296 cm^{-1}, C=O stretching at $\bar{\upsilon}$ = 1885-1660 cm^{-1}. The absorption peaks does not dependent on the sample concentration.[18]

Intramolecular H-Bonding formation using the Study of Variable Temperature ^{1}H NMR (VT-NMR): Variable temperature ^{1}H NMR spectra were recorded and analysed (d_6-DMSO) to support the intramolecular hydrogen bonding formation in fluorescent pentapeptides **4.65**, **4.68**, **4.71** and **4.74** in which all NHs showed different chemical shifts. Intramolecular H-bonding interaction was indicated in all the from VT-NMR analysis. Almost all the amide NH's exhibited ($\Delta\delta/\Delta T$) values in the range of -5 to -8 ppb/K indicating the presence of weak intramolecular H-bonding between the peptide strands (**Table 4.1**, **4.2**, **Figure 4.13**).[19]

Table 4.1. Values of temperature coefficients of chemical shifts of amide NHs or in **Pentapeptides 4.65** and **4.68.**

NHs from Fluorescent Pentapeptide 4.65	**$\Delta\delta/\Delta T$ (ppb/k)**	**NHs from Fluorescent Pentapeptide 4.68**	**$\Delta\delta/\Delta T$ (ppb/k)**
N-terminal–Ser–NH1	- 7.84 ppb/k	*N*-terminal–Ser–NH1	- 6.67 ppb/k
N-terminal–Leu–NH2	- 6.39 ppb/k	*N*-terminal–Leu–NH2	- 7.21 ppb/k
$^{1/1Al}$**TAA** –NH3	- 6.65 ppb/k	$^{1/2Al}$**TAA**–NH3	-5.94 ppb/k
C-terminal–Leu–NH4	- 6.67 ppb/k	*C*-terminal–Leu–NH4	-7.52 ppb/k
C-terminal–Ser–NH5	- 6.77 ppb/k	*C*-terminal–Ser–NH5	-6.89 ppb/k

Table 4.2. Values of temperature coefficients of chemical shifts of amide NHs or in **Pentapeptides 4.71** and **4.74.**

NHs from Fluorescent Pentapeptide 4.71	**$\Delta\delta/\Delta T$ (ppb/k)**	**NHs from Fluorescent Pentapeptide 4.74**	**$\Delta\delta/\Delta T$ (ppb/k)**
N-terminal–Ser–NH1	- 7.45 ppb/k	*N*-terminal–Ser–NH1	- 8.88 ppb/k
N-terminal–Leu–NH2	- 7.24 ppb/k	*N*-terminal–Leu–NH2	- 7.14 ppb/k
$^{2/1Al}$**TAA** –NH3	- 6.84 ppb/k	$^{2/2Al}$**TAA** –NH3	-7.3 ppb/k
C-terminal–Leu–NH4	- 5.51 ppb/k	*C*-terminal–Leu–NH4	-7.24 ppb/k
C-terminal–Ser–NH5	- 7.3 ppb/k	*C*-terminal–Ser–NH5	-6.98 ppb/k

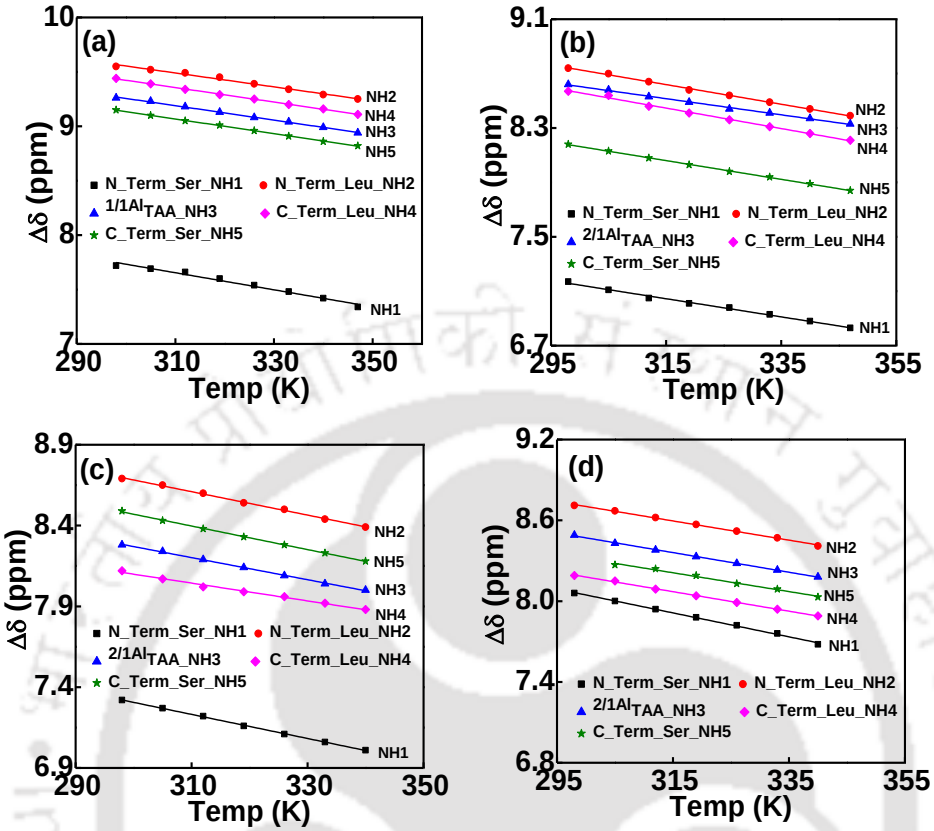

Figure 4.13. Temperature dependence of amide–NH/triazole-CH chemical shift of fluorescent pentapeptides **4.65** (a), **4.68** (b), **4.71** (c) and **4.74** (d).

Conformational Analysis using 2D NMR Experiment: Next, the 2D NMR analysis in DMSO-d_6 was carried out to support the secondary structural conformation in peptide backbone. The proton signals were divided into groups or coupling with the help of ^{1}H-^{1}H TOCSY (Total Correlated Spectroscopy). Thus, for pentapeptide **4.65**, **4.68**, **4.71** and **4.74** TOCSY experiment was carried out in d_6-DMSO to identify various NH's protons. The interaction of various protons in the solution conformations was revealed from NOESY and ROESY spectra in d_6-DMSO of all the pentapeptides (**Figure 4.14**). The H-bonding formation between the two peptide strands and the hydrophobic/stacking interactions between terminal chromophores helped the scaffold to nucleate the peptide into turn induced β-sheet conformation. The 2D NMR supported the close proximity of the two terminal fluorescent unnatural amino acids and possibility of a photophysical interaction between (^{TMnap}**Ala**$_{Do}$/^{TPy}**Ala**$_{Do}$) for all pentapeptides.

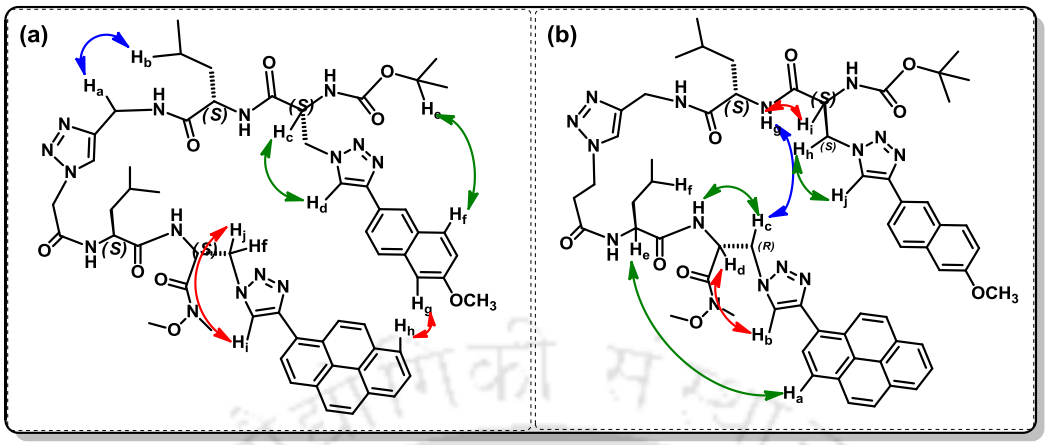

Figure 4.14. Pictorial presentation of long range proton-proton interaction of **Pentapeptide 4.65** (a) and **Pentapeptide 4.71** (b) as evident from 2D NMR.

Conformational Analysis Using Macromodel Study: Next, MD simulations for the pentapeptides were carried out with Schrodinger Macromodel (Maestro vs. 9.1) software package using an OPLS 2005 force field. The starting structures for the were the global minimum conformers.

The triazolylpyrene and methoxynaphthalene moiety in all pentapeptides were chosen as freely moving moieties during the simulation. After the MD simulations the final structures of the pentapeptides **4.65** and **4.71** was showed in **Figure 4.15.** The peptide backbone containing aliphatic amino acid scaffold with different spacer length supports the β-sheet conformation in. The observed H-bonding possibility revealed from the Modeling study was also supported from the VT-NMR study in all cases. The close proximity of triazolylpyrene and triazolylmethoxynaphthalene units was revealed from NMR studies was also supported by the MD simulation.

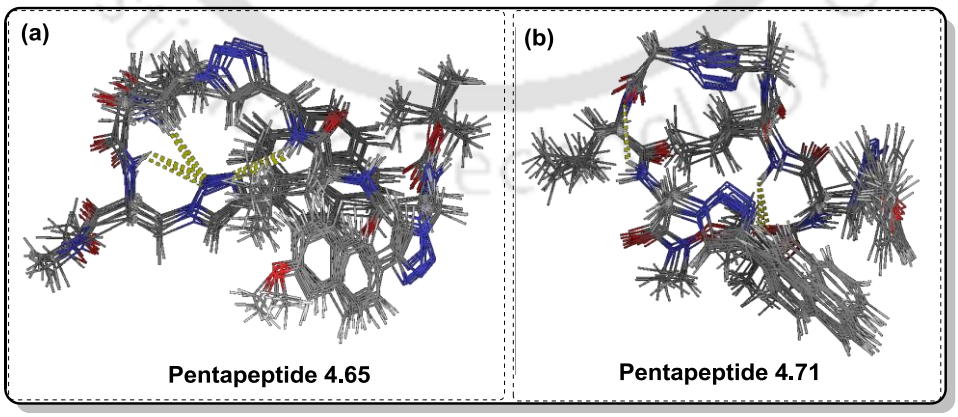

Figure 4.15. Clustering of structures (within 21 kJ/mole global minima) obtained from molecular dynamics simulation for the peptides. (a) **Pentapeptide 4.65 [BocNH–^{TMNap}Ala^{Do}–Leu-$^{1/1Al}$TAA–Leu–^{TPy}Ala^{Do}–CONMe(OMe)]** (b) **Pentapeptide 4.71 [BocNH–^{TMNap}Ala^{Do}–Leu-$^{2/1Al}$TAA–Leu–^{TPy}Ala^{Do}–CONMe(OMe)]**

4.4.5. Study of Photophysical Properties

Next we have studied the photophysical properties of all the peptides and monomer units in various solvents. The UV-visible and fluorescence spectra of the monomer units ^{TMnap}**Ala**^{Do} and ^{TPy}**Ala**^{Do} (**Figure 4.16/4.17**, **Table 4.3/4.4**) were similar to that we have discussed in **Chapter 2**. The UV-visible and fluorescence photophysical properties of the fluorescent triazolyl amino acid monomers indicated that there is a possibility of FRET process from donor ^{TMNap}**Ala**^{Do} to acceptor ^{TPy}**Ala**^{Do} in all peptides (**Figure 4.22 a**).

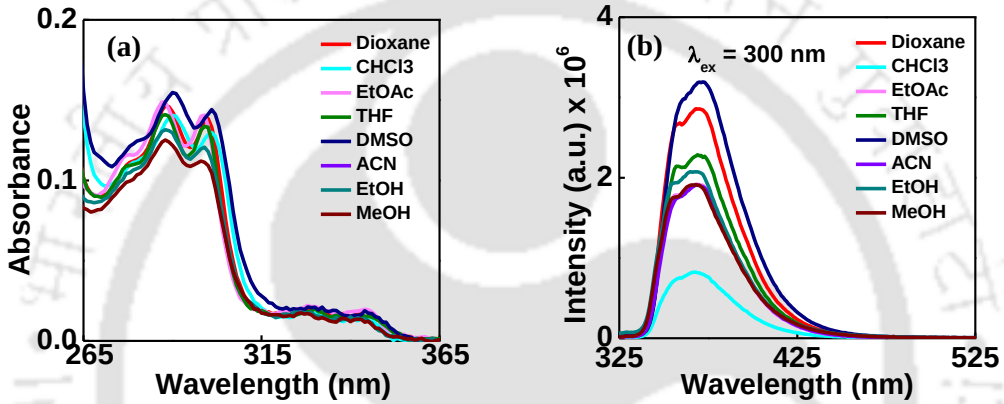

Figure 4.16. UV-Visible (a), fluorescence emission at λ_{ex} = 300 nm (b) of ^{TMnap}**Ala**^{Do}, in different solvents [10 µM, r.t., $\lambda_{ex} = \lambda_{max} \approx 300$ nm in each solvent].

Table 4.3. Summary table of photophysical properties of ^{TMnap}**Ala**^{Do} [**The Donor Chromophore**]

Entry	**Solvents**	**UV-Vis & Fluorescence**			
		λ_{max}^{abs} **(nm)**	λ_{max}^{fl} **(nm)**	ε_{max}	Φ_f
^{TMnap}**Ala**^{Do},[**The Donor Chromophore Only**]	Dioxane	256, 288, 299	357, 370	0.01385	0.43
	$CHCl_3$	256, 290, 301	367	0.01284	0.12
	EtOAc	255, 288, 299	356, 370	0.01339	0.29
	THF	256, 288, 299	357, 370	0.01331	0.34
	DMSO	257, 290, 301	360, 371	0.01412	0.49
	EtOH	255, 288, 299	367	0.00413	0.285
	ACN	300	368	0.0118	0.322
	MeOH	253, 288, 298	356, 368	0.01092	0.294

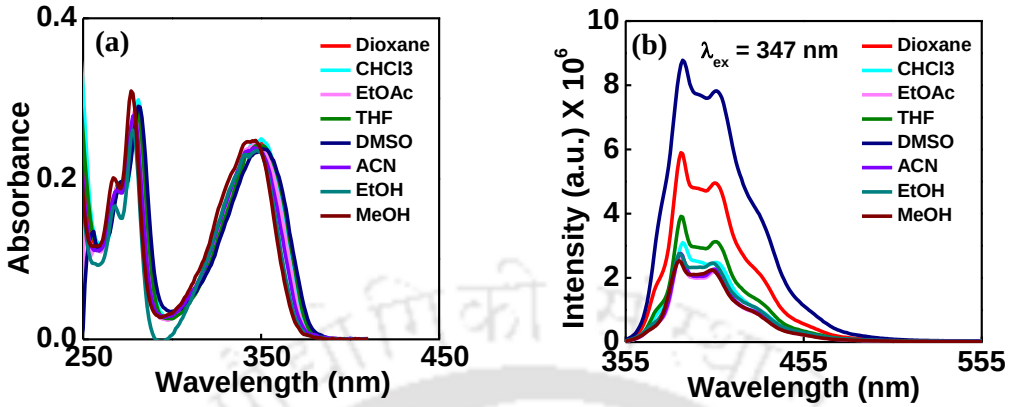

Figure 4.17. UV-Visible (a), fluorescence emission at $\lambda_{ex} \approx 347$ nm (b) of ^{TPy}**Ala**^{Do}, in different solvents [10 µM, r.t., $\lambda_{ex} = \lambda_{max} \approx 347$ nm in each solvent]

Table 4.4. Summary table of photophysical properties of ^{TPy}**Ala**^{Do} [**The Acceptor Chromophore**]

Entry	**Solvents**	**UV-Vis & Fluorescence**			
		λ_{max}^{abs} **(nm)**	λ_{max}^{fl} **(nm)**	ε_{max}	Φ_f
^{TPy}**Ala**^{Do} [**The Acceptor Chromophore Only**]	Dioxane	270, 280, 347	384, 405, 427	0.02423	0.36
	$CHCl_3$	270, 281, 347	385, 405, 428	0.0244	0.18
	EtOAc	269, 279, 347	384, 405, 427	0.0243	0.15
	THF	270, 280, 347	384, 405, 427	0.02413	0.22
	DMSO	271, 281, 347	386, 405, 428	0.02327	0.59
	EtOH	267, 278, 347	384, 405, 427	0.02379	0.16
	ACN	268, 278, 347	384, 405, 427	0.0235	0.17
	MeOH	267, 277, 343	384, 405, 427	0.02478	0.15

Looking at the pattern of UV visible spectra of ^{TMNap}**Ala**^{Do} and ^{TPy}**Ala**^{Do} , we can say that, at the absorption wavelength of ^{TMNap}**Ala**^{Do} (λ_{abs}^{max} = 300 nm), the amino acid ^{TPy}**Ala**^{Do} absorb negligibly indicating that the pentapeptide **4.65** could selectively be excited at 300 nm. Thus, upon excitation at the absorption maximum of the donor, ^{TMNap}**Ala**^{Do} (λ_{ex} = 300 nm), the pentapeptide **4.65** showed a weak and overlapped emission at 365 nm corresponding to the emission from ^{TMNap}**Ala**^{Do}, accompanied by another broad emission at 405 nm (**Figure 4.18**, **Table 4.5**).

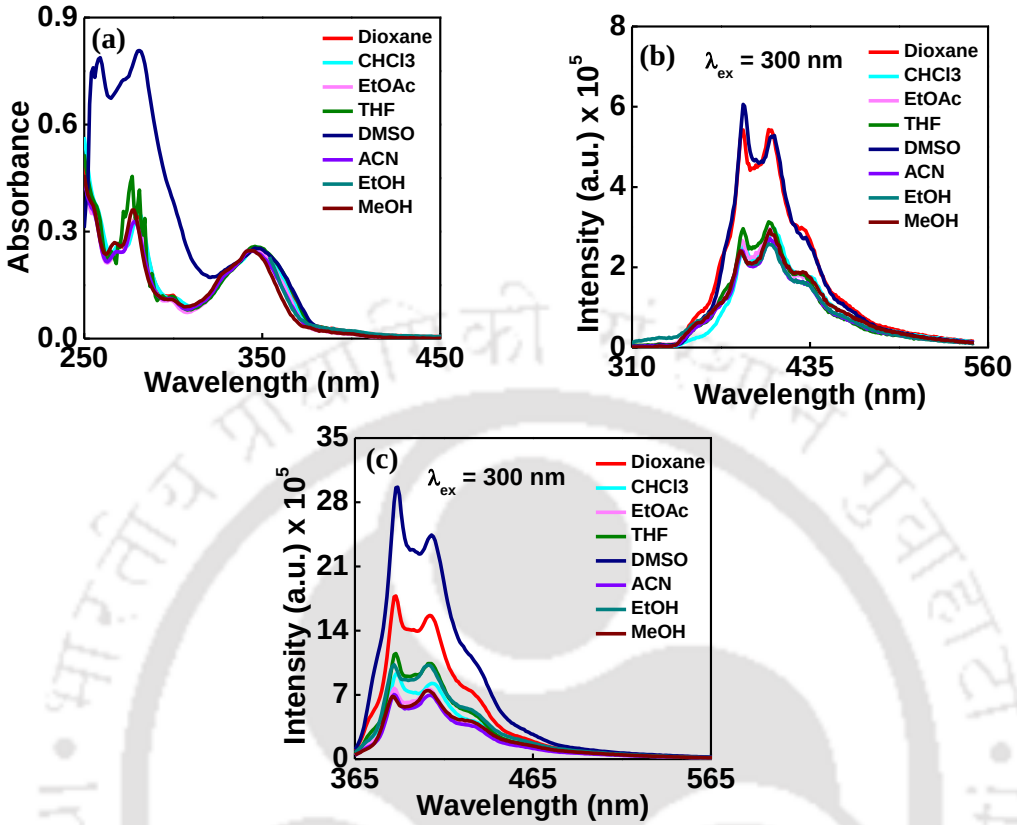

Figure 4.18. UV-Visible (a), fluorescence emission at $\lambda_{ex} \approx 300$ nm (b), fluorescence emission at $\lambda_{ex} \approx 347$ nm (c) of **Pentapeptide 4.65**, in different solvents [10 µM, r.t.]

Table 4.5. Summary table of photophysical properties of **Pentapeptide 4.65**

Entry	Solvents	UV-Vis & Fluorescence			
		λ_{max}^{abs} (nm)	λ_{max}^{fl} (nm)	ε_{max}	Φ_f
Pentapeptide 4.65	Dioxane	269, 278, 346	362, 387, 407, 429	0.02509	0.22
	$CHCl_3$	270, 280, 347	362, 388, 409, 430	0.02547	0.13
	EtOAc	269, 279, 346	362, 387, 406, 427	0.02518	0.11
	THF	346	362, 387, 406, 427	0.02586	0.15
	DMSO	271, 281, 348	362, 388, 409, 430	0.0254	0.35
	ACN	268, 278, 346	362, 387, 407, 428	0.02439	0.1
	EtOH	341	362, 387, 407, 427	0.02863	0.15
	MeOH	266, 276, 343	362, 386, 406, 427	0.02439	0.11

The band at 405 nm is most expectedly the emission from **TPy** via FRET (**Figure 4.21 b**). The occurrence of a FRET process was also evident from a time resolved

fluorescence study wherein we observed a decrease in donor life time (^{TMNap}**Ala**^{Do}, λ_{ex} = 290 nm, λ_{em} = 365 nm) from 6.8 to 3.38 ns (in pentapeptide **4.65**) (**Figure 4.23**, **Table 4.9**).

Other pentapeptide **4.68** also showed a weak emission at 365 nm corresponding to the emission from ^{TMNap}**Ala**^{Do}, accompanied by a broad emission at 405 nm (**Figure 4.19**, **Table 4.6**) when excited at the absorption wavelength of ^{TMNap}**Ala**^{Do} (λ_{abs}^{max} ≈ 300 nm). Only the extent of intensities was different. Here also the occurrence of FRET process was evident from a time resolved fluorescence study wherein we observed a decrease in donor life time (^{TMNap}**Ala**^{Do}, λ_{ex} = 290 nm, λ_{em} = 365 nm) from 6.8 to 3.15 ns (in pentapeptide **4.68**) (**Figure 4.23**, **Table 4.9**).

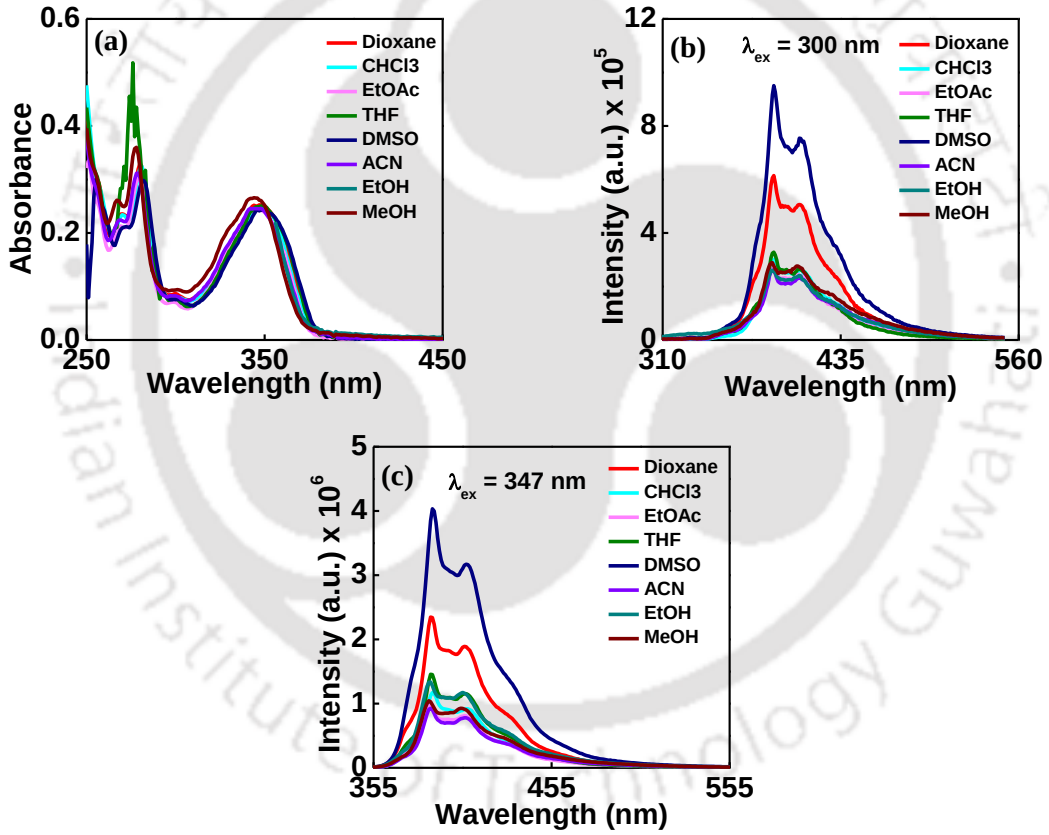

Figure 4.19. UV-Visible (a), fluorescence emission at λ_{ex} ≈ 300 nm (b), fluorescence emission at λ_{ex} ≈ 347 nm (c) of **Pentapeptide 4.68**, in different solvents [10 µM, r.t.]

Table 4.6. Summary table of photophysical properties of **Pentapeptide 4.68**

Entry	Solvents	UV-Vis & Fluorescence			
		λ_{max}^{abs} (nm)	λ_{max}^{fl} (nm)	ε_{max}	Φ_f
Pentapeptide 4.68	Dioxane	270, 280, 346	366, 387, 407, 427	0.02504	0.29
	$CHCl_3$	269, 279, 346	366, 388, 407, 428	0.02448	0.16
	EtOAc	269, 279, 346	366, 387, 406, 427	0.02423	0.12
	THF	346	366, 387, 407, 427	0.02489	0.19
	DMSO	270, 281, 348	366, 388, 408, 429	0.02436	0.49
	ACN	268, 278, 346	366, 387, 406, 427	0.02455	0.124
	EtOH	343	366, 386, 406, 427	0.02944	0.22
	MeOH	267, 277, 343	366, 385, 405, 427	0.02651	0.17

Other pentapeptides **4.71** and **4.74** showed the results similar to that of the pentapeptides **4.65** and **4.68**. Their photophysical properties and summary table were discussed bellow (**Figure 4.20/4.21**, **Table 4.7/4.8**).

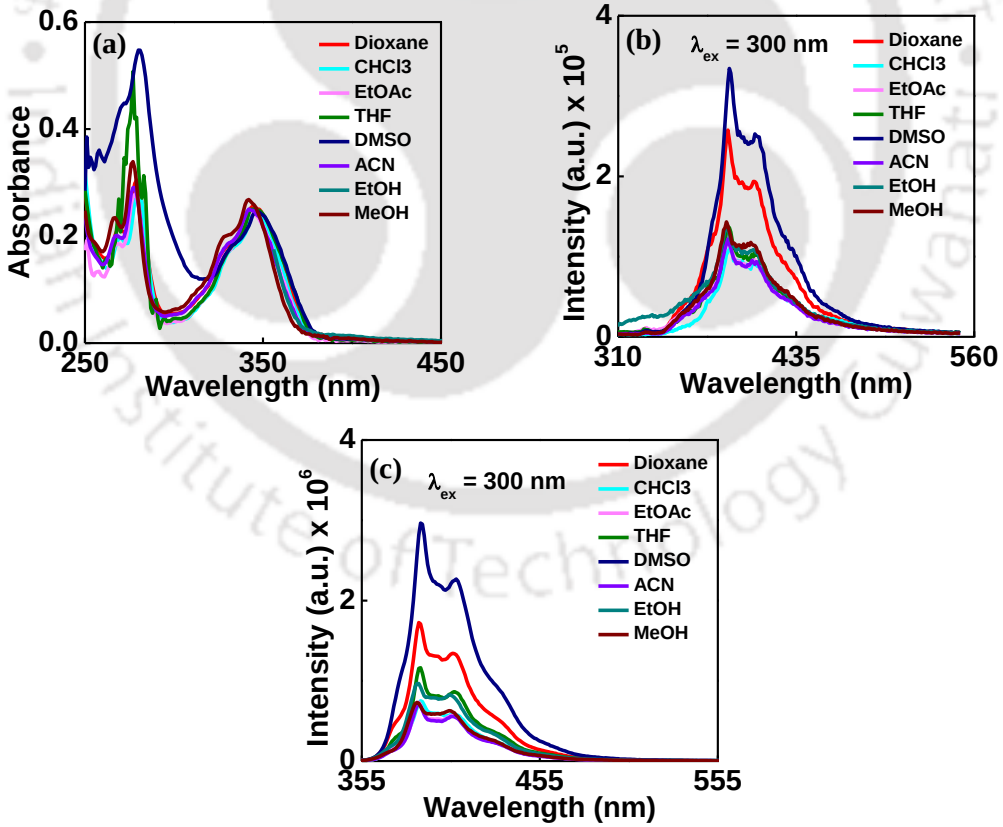

Figure 4.20. UV-Visible (a), fluorescence emission at $\lambda_{ex} \approx 300$ nm (b), fluorescence emission at $\lambda_{ex} \approx 347$ nm (c) of **Pentapeptide 4.71**, in different solvents [10 µM, r.t.]

Table 4.7. Summary table of photophysical properties of Pentapepeptide 4.71

Entry	Solvents	UV-Vis & Fluorescence			
		λ_{max}^{abs} (nm)	λ_{max}^{fl} (nm)	ε_{max}	Φ_f
Pentapeptide 4.71	Dioxane	269, 279, 330, 345	368, 387, 405, 428	25.21×10^3	0.18
	$CHCl_3$	269, 279, 332, 345	368, 388, 406, 428	23.02×10^3	0.08
	EtOAc	268, 278, 330, 343	368, 386, 406, 427	24.4×10^3	0.08
	THF	330, 344	368, 386, 406, 428	24.97×10^3	0.12
	DMSO	271, 280, 333, 347	368, 388, 408, 430	22.72×10^3	0.32
	ACN	268, 277, 330, 343	368, 387, 406, 428	24.84×10^3	0.07
	EtOH	327, 342	368, 386, 406, 427	30.73×10^3	0.11
	MeOH	266, 276, 328, 341	368, 385, 405, 426	26.5×10^3	0.08

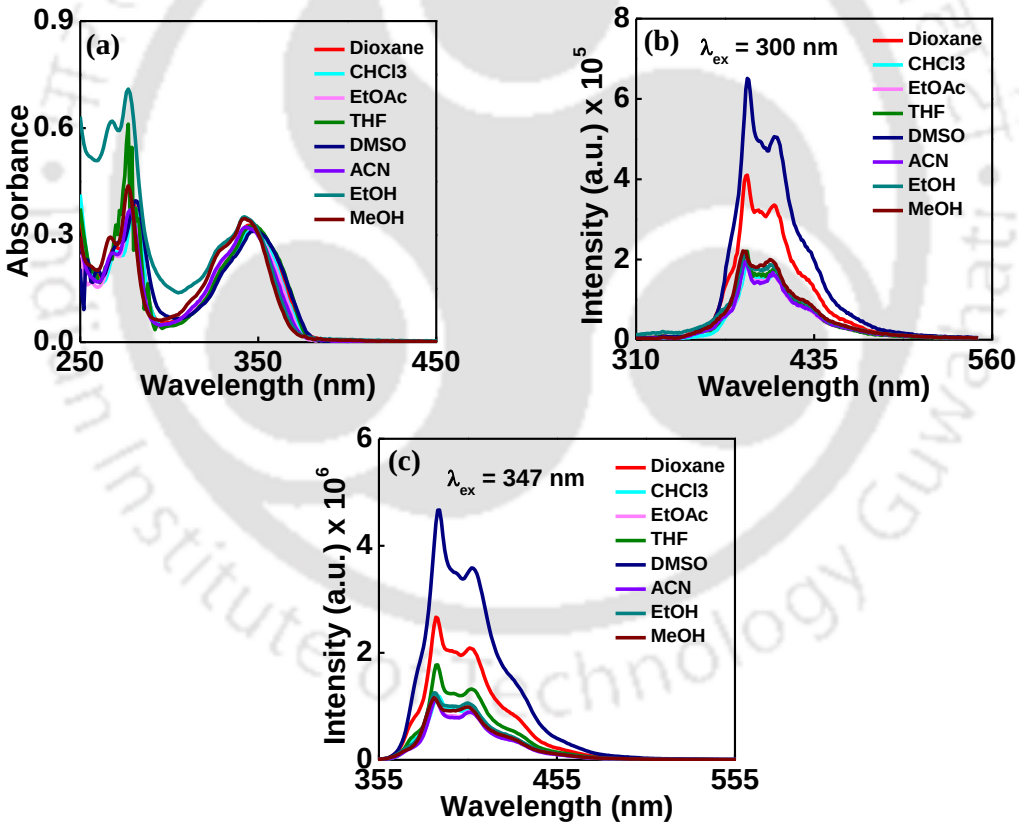

Figure 4.21. UV-Visible (a), fluorescence emission at $\lambda_{ex} \approx 300$ nm (b), fluorescence emission at $\lambda_{ex} \approx 347$ nm (c) of **pentapeptide 4.74**, in different solvents [10 µM, r.t.]

Table 4.8. Summary table of photophysical properties of **Pentapepeptide 4.74**

Entry	Solvents	UV-Vis & Fluorescence			
		λ_{max}^{abs} (nm)	λ_{max}^{fl} (nm)	ε_{max}	Φ_f
Pentapeptide 4.74	Dioxane	269, 279, 345	368, 387, 397, 407, 430	32.71×10^3	0.24
	$CHCl_3$	270, 280, 347	368, 387, 397, 407, 430	31.73×10^3	0.11
	EtOAc	269, 279, 347	368, 386, 397, 406, 430	31.79×10^3	0.1
	THF	346	368, 386, 396, 407, 430	32.45×10^3	0.15
	DMSO	271, 281, 348	368, 388, 399, 407, 430	30.57×10^3	0.42
	ACN	268, 278, 342	368, 386, 396, 406, 430	31.93×10^3	0.1
	EtOH	342	368, 385, 397, 403, 430	34.4×10^3	0.12
	MeOH	266, 276, 342	368, 384, 395, 404, 430	34.06×10^3	0.11

4.4.6. Establishment of Distance Dependent FRET Process in Fluorescent Pentapeptides.

Next, we have studied the photophysical property of the fluorescent pentapeptides **4.65**, **4.68**, **4.71** and **4.74** to test our hypothesis of distance dependent FRET process. The possibility of FRET process was supported from the overlap spectra (**Figure 4.22 a**).

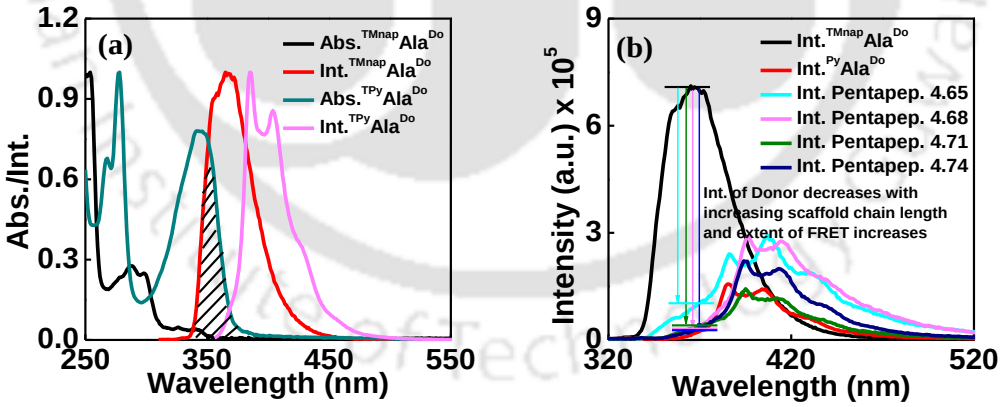

Figure 4.22. (a) Overlaping of emission spectra of **Monomeric amino acid ^{TMnap}Ala^{Do}** (act as a FRET donor) and the absorption spectra of **Monomeric amino acid ^{TPy}Ala^{Do}** (act as a FRET acceptor), (b) Fluorescence spectra of individual donor **^{TMnap}Ala^{Do}** and acceptor amino acid **^{TPy}Ala^{Do}** and the All fluorescent pentapeptides which contain these two **UNNA**s (10 μM each, r.t., λ_{ex} = 300 nm) in MeOH solvent.

Thus, upon excitation at the ^{TMnap}**Ala**^{Do} (λ_{ex} = 290 nm) we observed the emission bands at 365 nm (negligible) corresponding to the emission of the ^{TMnap}**Ala**^{Do} and a broad emission band at 405 nm corresponding to **TPy** of ^{TPy}**Ala**^{Do} (**Figure 4.22 b**). The relative intensities and the time resolved spectroscopy suggested that the extent of FRET process from ^{TMnap}**Ala**^{Do} to ^{TPy}**Ala**^{Do} was different in all the pentapeptides. As the scaffold induces β-sheet secondary structure into the peptide backbone the two termini of the peptide come close together and would show the FRET interaction. As the length of the spacers of triazolyl amino acid scaffold are different the extent of FRET are expected to be different. In scaffold **4.60** the chain length (containing a C-2/C-2 spacer) is highest, its flexibility and the extent of fluorescence termini of coming closer is also highest. So, it is expected that the pentapeptide **4.74** will show highest extent of FRET (**Figure 4.22 b**).

The efficiency of FRET was calculated in all pentapeptides, which was highest for **pentapeptide 4.74** (96.4%), lowest for **pentapeptide 4.65** (85.3%) and moderate for **pentapeptide 4.68** (95.1%) and **pentapeptide 4.71** (94.2%) from steady state fluorescence spectra (**Figure 4.22**). This may be due to the increase of flexibility of the molecular scaffold to help getting turn in such a way that two termini come close together and the extent of FRET increases.

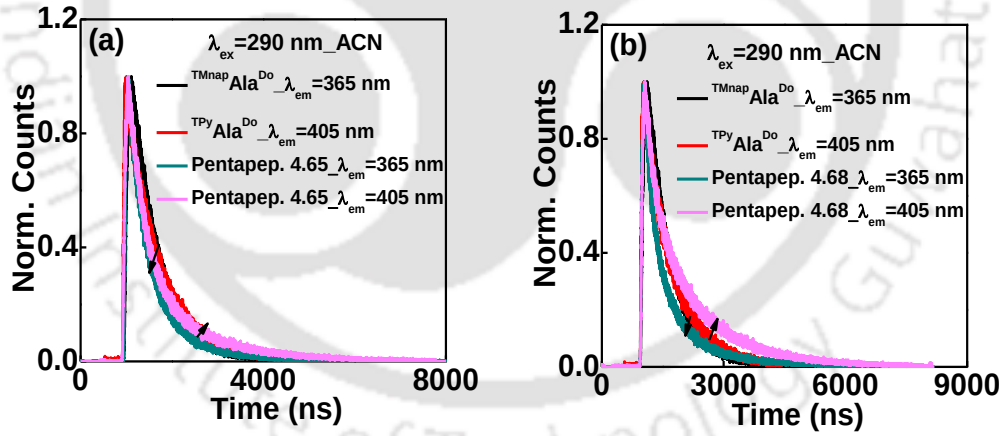

Figure 4.23. Time resolved fluorescence of donor and acceptor chromophore ^{TMnap}**Ala**^{Do} and ^{TPy}**Ala**^{Do}and **Pentapeptide 4.65** (**a**), **Pentapeptide 4.68** (**b**) using λ_{ex} = **290** nm λ_{em} = 365, 405 nm in Acetonitrile solvent. Decrease in lifetime of ^{TMnap}**Ala**^{Do} as well as increase in life time of ^{TPy}**Ala**^{Do} is an evidence of FRET from ^{TMnap}**Ala**^{Do} to ^{TPy}**Ala**^{Do}.

Table 4.9: Summary table of fluorescence lifetimes of **Pentapeptides 4.65**, **4.68**, **4.71**, **4.74** and monomers ^{TMnap}**Ala**^{Do}, ^{TPy}**Ala**^{Do} at λ_{ex} **= 290** nm in acetonitrile solvent.

Entry	Φ_f	λ [nm]	τ_1 [ns]	τ_2[ns]	τ_3[ns]	<τ> [ns]	k_f [$10^8 s^{-1}$]	k_{nr} [$10^8 s^{-1}$]	χ^2
^{TMnap}**Ala**^{Do}	0.32	365	1.54 (6 %)	7.1 (94 %)	---	6.8	0.047	0.1	1.02
^{TPy}**Ala**^{Do}	0.17	405	3.64 (28 %)	18.24 (72 %)	---	14.1	0.012	0.06	1.01
Pentapep. 4.65	0.01	365	0.466 (54 %)	5.07 (36 %)	12.66 (10 %)	3.38	0.003	0.29	1.08
Pentapep. 4.65	0.09	405	0.772 (16 %)	4.34 (59 %)	15.82 (25 %)	6.71	0.0134	0.14	1.07
Pentapep. 4.68	0.006	365	0.494 (60 %)	4.573 (29 %)	14.13 (11 %)	3.15	0.0019	0.32	1.04
Pentapep. 4.68	0.118	405	0.72 (39 %)	3.77 (24 %)	15.38 (37 %)	6.91	0.017	0.13	1.06
Pentapep. 4.71	0.006	365	0.802 (16 %)	5.36 (58 %)	12.58 (26 %)	6.57	0.001	0.15	1.07
Pentapep. 4.71	0.064	405	0.725 (16 %)	3.86 (34 %)	15.41 (50 %)	9.125	0.007	0.1	1.07
Pentapep. 4.74	0.001	365	5.27 (42 %)	0.533 (27 %)	14.5 (31 %)	6.83	0.0001	0.15	1.05
Pentapep. 4.74	0.09	405	0.684 (17 %)	3.75 (28 %)	15.48 (55 %)	9.75	0.009	0.09	1.03

For lifetimes of the fluorescent amino acids and peptides at λ_{ex} = 290 nm, Concentration of each compound = 10 μM, <τ>, k_f, and k_{nr} are weighted means from the biexponential/ triexponential fits: $<\tau> = 1/(\alpha_1/\tau_1 + \alpha_2/\tau_2)$, $k_f = \Phi_f/<\tau>$, and $k_{nr} = (1- \Phi_f)/<\tau>$.

Table 4.10: Summary table of fluorescence lifetimes of **Pentapeptides 4.65**, **4.68**, **4.71**, **4.74** and monomers ^{TMnap}**Ala**^{Do}, ^{TPy}**Ala**^{Do} at λ_{ex} **= 375** nm in acetonitrile solvent.

Entry	Φ_f	λ [nm]	τ_1 [ns]	τ_2[ns]	τ_3[ns]	<τ> [ns]	k_f [$10^8 s^{-1}$]	k_{nr} [$10^8 s^{-1}$]	χ^2
^{TPy}**Ala**^{Do}	0.17	405	3.32 (65 %)	13.98 (35 %)	---	8.58	0.02	0.097	1.14
Pentapep. 4.65	0.09	405	0.624 (11 %)	4.17 (76 %)	11.35 (13 %)	4.71	0.019	0.19	0.96
Pentapep. 4.68	0.118	405	0.493 (31 %)	3.77 (36 %)	14.7 (33 %)	6.37	0.018	0.14	1.09
Pentapep. 4.71	0.064	405	0.298 (29 %)	3.59 (37 %)	14.76 (35 %)	6.54	0.01	0.143	1.1
Pentapep. 4.74	0.09	405	0.246 (17 %)	3.89 (46 %)	15.14 (37 %)	7.41	0.012	0.123	1.09

For lifetimes of the fluorescent amino acids and peptides at λ_{ex} = 375 nm, Concentration of each compound = 10 μM, <τ>, k_f, and k_{nr} are weighted means from the biexponential/ triexponential fits: $<\tau> = 1/(\alpha_1/\tau_1 + \alpha_2/\tau_2)$, $k_f = \Phi_f/<\tau>$, and $k_{nr} = (1- \Phi_f)/<\tau>$.

4.5. Conclusion

In conclusion we have successfully synthesized aliphatic triazolo amino acid molecular scaffolds with different chain length and incorporate them into designed fluorescent pentapeptide backbone in order to achieve turn into peptide backbone. With the increase in chain length of the molecular scaffold the extent of flexibility also increases and the extent of FRET increases.

4.6. Experimental Section

4.6.1. Materials and Methods

All reactions were carried out under inert atmosphere using flame-dried glassware. Combined organic layers were dried over anhydrous sodium sulfate. After work up solvents were removed in a rotary evaporator under reduced pressure. For column chromatography Silica gel (60-120 mesh) was used. Reactions were monitored by TLC on silica gel 60 F254 (0.25).

^{1}H NMR spectra were recorded either at 400MHz or at 600 MHz and ^{13}C NMR spectra were recorded either at 100 MHz or at 150 MHz (mentioned accordingly).

Coupling constants (*J* value) were reported in hertz (Hz). The chemical shifts were shown in ppm downfield form tetramethylsilane, using residual chloroform (δ = 7.26 in ^{1}H NMR, δ = 77.23 in ^{13}C NMR), DMSO (δ = 2.5 in ^{1}H NMR, δ = 39.5 in ^{13}C NMR), as an internal standard. Mass spectra were recorded with a HR mass spectrometer and data analyzed by using built-in software. IR spectra were recorded in KBr on a FT-IR spectrometer. All 2D NMR Experiments were carried out on 600 MHz spectrometer at room temperature using 7 - 10 mM concentration in d_6-DMSO solvent. Spectra were acquired with 2048 x 256 in both dimension (F2 and F1) and other parameter are given below.

TOCSY : Free induction decay (FID) with NS = 16 and DS =32, relaxation delay (D1) 2s, mixing time (D9) 0.08s, acquisition time (AQ) 0.085s, spectral width 12019 Hz.

ROESY : Free induction decay (FID) with NS = 16 and DS =16, relaxation delay (D1) 2s, mixing time (P15) 0.02s, acquisition time (AQ) 0.085s, spectral width (SWH) 12019 Hz.

NOESY : Free induction decay (FID) with NS = 8 and DS =16, relaxation delay (D1) 2s, mixing time (D8) 0.6s, acquisition time (AQ) 0.085s, spectral width (SWH) 12019 Hz.

4.6.2. Some General Procedure for Our Synthetic Scheme of Pentapeptides

General procedure for the preparation of azide from bromo: To a solution of bromo compound (1 equiv.) in water/acetone (1:3) was added NaN_3 (1.5 equiv.) and the mixture was heated at 60 ^{o}C for 4 hours. Then the reaction mixture was diluted with DCM and washed with water. The organic layer was dried over anhydrous Na_2SO_4 and concentrated in vacuum. The crude material was obtained in quantitative yield. This can be used for next step without further purification.

General procedure for [3+2] cyclo-addition (Click reaction) reaction: The prepared azido compound taken in dry THF and degassed for 5 min with nitrogen gas. After adding alkyne (1.1 equivalent) degassing was continued for the next 5 min. Then 1 mol % powdered CuI was added. Then 1.2 equivalent DIPEA was added and reaction mixture was degassed and allowed to proceed for 18-20 h at room temperature. After total consumption of the starting azide, the reaction mixture was evaporated completely and work up was done by EtOAc and NH_4Cl solution. The organic layer was washed with brine, dried over Na_2SO_4.The title trizolyl compound was separated by column chromatography and characterized.

General procedure for the preparation of mesyl derivative from hydroxyl group: In a dry R.B -OH compound (1 equivalent) was loaded in a dry CH_2Cl_2. Mesyl chloride (1.4 equivalent) and triethylamine (1.3 equivalent) were added to the reaction mixture at 0^oC. The reaction mixture was stirred at 0 ^oC till the starting material was consumed. After that the reaction mixture was diluted with DCM and washed with water and dried over Na_2SO_4 and then evaporated in vacuum. The pure compound was then isolated by column chromatography and utilized immediately for the next step without further characterization.

General procedure for the deprotection of the methyl ester: To a solution of the respective methyl ester protected peptide in THF: H_2O = 5 : 1, lithium hydroxide (1.5 equivalent) was added at 0 ^oC. The reaction mixture was stirred for about 3-4 hour until starting material was fully consumed. Reaction was monitored by TLC. After completion of the reaction, solvent was dried by rotary evaporator. Then water (4-5 ml) was added to the reaction mixture and cooled to 0 ^oC. The dilute acetic acid was added to the reaction mixture to adjust pH- 3 to 4. The reaction mixture was extracted with EtOAc. The combined organic layers were dried over Na_2SO_4. The hydrolyzed compound was isolated by column chromatography (Si-gel, $CHCl_3$:MeOH = 10:1). Yield was 90-96%.

General procedure for the preparation of azide from mesyl derivative: To a solution of mesyl compound (1 equivalent) in dry DMF was added NaN_3 (1.5 equiv.) and the mixture was stirred at room temperature. Then the reaction mixture was diluted with DCM and washed with water. The organic layer was dried over anhydrous Na_2SO_4 and concentrated in vacuum. The product was isolated by column chromatography and characterized. Yield was 70-75%.

General procedure for the preparation of amine from azide derivative: To a solution of the azide compound in methanol Pd/C is added and to it hydrogen gas balloon was set and stirred the reaction mixture for 3-4 hours. The solvent methanol was then evaporated and the crude mass was dissolved in water and then filtered, filtrate is evaporated to afford the compound with quantitative yield.

General procedure for the Boc protection of amine group: In a solution of amine compound (1 equivalent) in 1:1 mixture of 1,4 dioxane and water (3 ml each) was added NaOH (2 equivalent) followed by di-tert-butyl dicarbonate (1.5 equiv.) maintaining the pH between 7.5-8.5. The reaction mixture was stirred at room temperature for 20 hours. The reaction mixture was washed with ethyl acetate (2 x 10 ml) and the aqueous phase was treated with dilute HCl to bring pH 4 in cold

condition. Immediately the solution was extracted with ethyl acetate and the organic layer was washed with water, brine, dried and evaporated under vacuum to furnish the Boc-protected amine derivative as white solid in pure form.

General procedure for the Peptide coupling: To a solution *N*-protected amino acids in 3:1 mixture of dry DCM and DMF, 1-[3-dimethyl amino propyl]-3-ehtylcarbo-diimide hydrochloride (EDC.HCl) (1.2 equivalent) and HOBT (1.2 equivalent) were added and the reaction mixture was stirred for 1h at 0^{o}C. Then the amine salt of wienreb amide or methyl ester protected corresponding amino acids or dipeptide (1.1 equivalent) were added followed by diisopropylethylamine (DIPEA) (2.4 equivalent). The reaction mixture was stirred for another 18-20 h at 0^{o}C to room temperature. Then solvent was dried by rotary evaporator, after which it was partitioned between EtOAc and aqueous $NaHCO_3$ solution (50 ml each). The organic layer was washed with brine solution. Pure product was isolated by column chromatography.

General procedure for the deprotection of the Boc-group: The respective both side protected amino acids and peptides was dissolved in CH_2Cl_2 and cooled to 0^{o}C. TFA (equal amount as the solvent) was added and the solution was allowed to warm to room temperature. The stirring was continuing at room temperature until the starting material was consumed (monitored by TLC). The reaction mixture was evaporated in vacuum. The residual TFA was evaporated by triturating the mixture with dry toluene thrice, evaporated thrice and dried to afford the product in quantitative yield.

4.6.3. Synthesis of the Targeted Molecular Scaffolds and Peptides

Synthesis of ethyl azido acetate (4.34): To a solution of ethyl bromoacetate (1510 mg, 9.04 mmol) in water/acetone (1:3) was added NaN_3 (881.6 mg, 13.56 mmol) and the mixture was heated at 60^{o}C for 4 hours. Then the reaction mixture was diluted with DCM and washed with water. The organic layer was dried over anhydrous Na_2SO_4 and evaporated in vacuum. The crude material was obtained in quantitative yield. The product **4.34** is oily liquid. Yield 97%. IR (KBr) 2955, 2103, 1741, 1441, 1372, 1175, 1064 cm^{-1}. The azide was used for the next step without further purification and characterization.

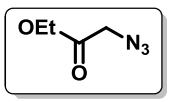

Synthesis of ethyl 2-(4-(hydroxymethyl)-1H-1,2,3-triazol-1-yl) acetate (4.35): The prepared ethyl azido acetate **4.34** (500 mg, 3.876 mmol) and propargyl alcohol (0.246 ml, 5.8 mmol) was undergone click reaction to get the corresponding triazolyl alcohol

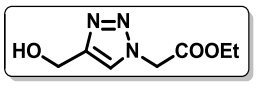

compound. The title alcohol compound **4.35** was isolated by column chromatography (Si-gel, PE:EA = 1:1) in pure form as white solid (560 mg, Yield 79%). ^{1}H NMR ($CDCl_3$, 600 MHz) δ 1.26 (3H, t, J = 3.0 Hz), 4.21 (2H, q, J = 5.4 Hz), 4.74 (2H, d, J = 7.8 Hz), 5.10 (2H, s), 7.63 (1H, s). ^{13}C NMR ($CDCl_3$, 150 MHz) δ 13.9, 50.7, 55.7, 62.3, 123.8, 148.2, 166.6. +APCI-MS calcd. for $C_7H_{12}N_3O_3$ $[M + H]^+$ 186.1, found 186.1.

Synthesis of ethyl 2-(4-(((methylsulfonyl)oxy)methyl)-1H-1,2,3-triazol-1-yl)acetate (4.36): Compound **4.35** (100 mg, 0.54 mmol) was taken in a dry CH_2Cl_2. Mesyl chloride (0.06 ml, 0.81 mmol) and triethyl amine (0.113 ml, 0.81 mmol) were added to the reaction mixture at 0 ^{o}C. The reaction mixture was stirred at 0^{o}C till the starting material was consumed. After that the reaction mixture was diluted with DCM and washed with water and dried over Na_2SO_4 and then evaporated in vacuum. The pure compound **4.36** was then isolated by column chromatography (si-gel, PE:EA = 2:1) as a colourless oil (129 mg, Yield 83%) and utilized immediately for the next step without further characterization.

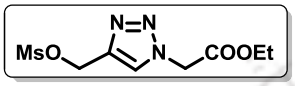

Synthesis of ethyl 2-(4-(azidomethyl)-1H-1,2,3-triazol-1-yl)acetate (4.37): To a solution of the mesyl derivative **4.36** (129 mg, 0.523mmol) in dry DMF (5 ml), NaN_3 (40.7 mg, 0.627 mmol) was added and stirrer for 18 h at 50 ^{o}C. The reaction mixture was partitioned between EtOAc and water (20 ml each). The organic layer was washed with brine solution, dried with Na_2SO_4, filtered and then evaporated. The title compound **4.37** was isolated by column chromatography (si-gel, PE:EA = 5:1) in pure form as white solid (98 mg, Yield 89%). mp 43-44 ^{o}C, IR (KBr) 3447, 3138, 3006, 2108, 1739, 1634, 1464, 1407, 1259, 1021, 771 cm^{-1}.^{1}H NMR ($CDCl_3$, 600 MHz) δ 1.29 (3H, t, J = 6.6 Hz), 4.27 (2H, q, J = 7.2 Hz), 4.51 (2H, s), 5.17 (2H, s), 7.17 (1H, s). ^{13}C NMR ($CDCl_3$, 150 MHz) δ 14.0, 45.5, 50.9, 62.5, 124.0, 142.9, 166.2. +APCI-MS calcd. for $C_7H_{10}N_6O_2$ $[M + H]^+$ 211.1, found 211.1.

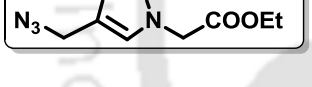

Synthesis of 2-(4-(azidomethyl)-1H-1,2,3-triazol-1-yl)acetic acid (4.38): To a solution of compound **4.37** in methanol, 2.5 (M) NaOH solution was added and stirred for about 2-3 hours at room temperature until starting material was vanished. After that in the reaction mixture, dilute HCl was added until the pH became 4. Then it was partitioned between EtOAc and water (20 ml each). The organic layer was washed with brine solution, dried with Na_2SO_4, filtered and then evaporated. The prepared title compound **4.38** was used for next step without further purification (Yield 95%). IR (KBr) 3153, 2101, 1725, 1557, 1447, 1414, 1362, 1333, 1231, 1068, 822 cm^{-1}. ^{1}H NMR (CD_3OD, 400 MHz) δ 4.49 (2H, s), 5.30 (2H, s), 8.06 (1H, s). ^{13}C

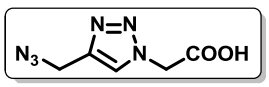

NMR (CD_3OD, 100 MHz) δ 46.1, 51.8, 126.6, 144.0, 169.9. –APCI-MS calcd. for $C_5H_5N_6O_2$ $[M - H]^-$ 181.1, found 181.2.

Synthesis of 2-(4-(aminomethyl)-1H-1,2,3-triazol-1-yl)acetic acid (4.39): To a solution of the compound **4.38** in methanol (200 mg, 1.1 mmol) Pd/C is added and to it hydrogen gas balloon was set and stir the reaction mixture for 3-4 hours. The solvent methanol was then evaporated and the crude mass was dissolved in water and then filtered, filtrate is evaporated to afford the title compound **4.39** with quantitative yield. mp 285-286 ^oC, IR (KBr) 3418, 3153, 1614, 1393, 1308, 1233 cm^{-1}. ^1H NMR (D_2O, 600 MHz) δ 4.34 (2H, s), 5.06 (2H, s), 8.07 (1H, s). ^{13}C NMR (D_2O, 150 MHz) δ 34.0, 53.2, 126.3, 139.6, 173.1.HRMS calcd. for $C_5H_9N_4O_2$ $[M + H]^+$ 157.0727, found 157.0713.

Synthesis of $^{1/1Al}$TAA (4.40): In a solution of 2-(4-(azidomethyl)-1H-1,2,3-triazol-1-yl)acetic acid **4.39** (200 mg, 1.28 mmol) in 1:1 mixture of 1,4 dioxane and water (3 ml each) was added NaOH (102.6 mg, 2.56 mmol) followed by di-t-butyl dicarbonate (0.44 ml, 1.92 mmol) maintaining the pH between 7.5-8.5. The reaction mixture was stirred at room temperature for 20 h. The reaction mixture was washed with ethyl acetate (2 x 10 ml) and the aqueous phase was treated with dil. HCl to bring pH 4 in cold condition. Immediately the solution was extracted with ethyl acetate and the organic layer was washed with water, brine, dried and evaporated under *vacuo* to furnish the Boc-protected 2-(4-(azidomethyl)-1H-1,2,3-triazol-1-yl) acetic acid **4.40** as white solid in pure form (265.4 mg, Yield 81%). mp 105-106 ^oC, ^1H NMR (CD_3OD, 400 MHz) δ 1.43 (9H, s), 4.31 (2H, s), 5.25 (2H, s), 7.87 (1H, s). ^{13}C NMR (CD_3OD, 100 MHz) δ 28.9, 36.8, 51.8, 80.6, 125.6, 147.4, 158.4, 170.0. HRMS calcd. for $C_{10}H_{15}N_4O_4$ $[M - H]^-$ 255.254, found 255.2255.

Synthesis of methyl 2-(4-(2-hydroxyethyl)-1H-1,2,3-triazol-1-yl)acetate (4.41): Using general procedure of click reaction, we have got title compound **4.41** (1.577g) from methyl azido acetate (1.90g) and homopropergyl alcohol. product yield = 83%. ^1H NMR ($CDCl_3$, 400 MHz) δ 2.95 (2H, t, J = 6.0 Hz), 3.79 (3H, s), 3.92 (2H, bs), 5.14 (2H, s), 7.53 (1H, s). ^{13}C NMR ($CDCl_3$, 100 MHz) δ 28.9, 50.8, 53.2, 61.6, 123.3, 146.1, 167.2. HRMS calcd. for $C_7H_{12}N_3O_3$ $[M + H]^+$ 186.0873, found 186.0877.

Synthesis of methyl 2-(4-(2-((methylsulfonyl)oxy)ethyl)-1H-1,2,3-triazol-1-yl)acetate(4.42): Using general procedure for the synthesis of mesylate derivative from alcohol, we have got the title compound **4.42** (1.215g) from methyl 2-(4-(2-hydroxyethyl)-1H-1,2,3-triazol-1-yl)acetate(1.5g). Product yield = 81%.

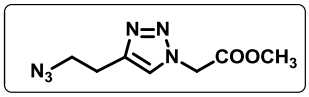

Synthesis of methyl 2-(4-(2-azidoethyl)-1H-1,2,3-triazol-1-yl)acetate (4.43): Using general procedure for the synthesis of azide from mesylate, we have got the title compound **4.43** (1.032g) from methyl 2-(4-(2-((methylsulfonyl)oxy)ethyl)-1H-1,2,3-triazol-1-yl)acetate (1.2g). Product yield =86%. ^{1}H NMR ($CDCl_3$, 400 MHz) δ 3.03 (2H, t, J = 6.8 Hz), 3.64 (2H, t, J = 6.4 Hz), 3.81 (3H, s), 5.17 (2H, s), 7.56 (1H, s). ^{13}C NMR ($CDCl_3$, 100 MHz) δ 25.7, 50.6, 50.8, 53.1, 123.4, 144.8, 166.9. HRMS calcd. for $C_7H_{11}N_6O_2[M + H]^+$ 211.0938, found 211.0943

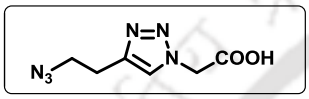

Synthesis of 2-(4-(2-azidoethyl)-1H-1,2,3-triazol-1-yl)acetic acid (4.44): Using general procedure of methyl ester hydrolysis reaction, we have got the title compound **4.44** (0.94g) from methyl 2-(4-(2-azidoethyl)-1H-1,2,3-triazol-1-yl)acetate (1.0g). Product yield = 94%. ^{1}H NMR (CD_3OD, 600 MHz) δ 3.02 (2H, t, J = 7.2 Hz), 3.63 (2H, t, J = 6.4 Hz), 5.16 (2H, s), 7.68 (1H, s). ^{13}C NMR ($CDCl_3$, 150 MHz) δ 25.3, 50.3, 50.8, 123.7, 144.4, 168.2. HRMS calcd. for $C_6H_7N_6O_2$ $[M + H]^-$ 195.0636, found 195.0633.

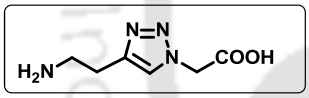

Synthesis of 2-(4-(2-aminoethyl)-1H-1,2,3-triazol-1-yl)acetic acid (4.45): Using general procedure for the conversion of azide to amine, we have got the title compound **4.45** (0.855g) from2-(4-(2-azidoethyl)-1H-1,2,3-triazol-1-yl)acetic acid (0.9g). Product yield = 95%. ^{1}H NMR (D_2O, 600 MHz) δ 3.13 (2H, t, J = 6.6 Hz), 3.35 (2H, t, J = 6.6 Hz), 5.04 (2H, s), 7.88 (1H, s). ^{13}C NMR ($CDCl_3$, 100 MHz) δ 25.5, 41.7, 55.8, 127.9, 145.6, 175.9.

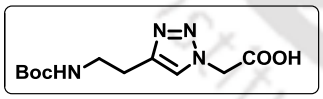

Synthesis of $^{1/2Al}$TAA (4.46): Using general procedure for Boc protection, we have got title compound **4.46** (0.696g)from2-(4-(2-aminoethyl)-1H-1,2,3-triazol-1-yl)acetic acid (0.8g).Product yield =87%. ^{1}H NMR ($CDCl_3$, 400 MHz) δ 1.43 (9H, s), 2.91 (2H, t, J = 6.4 Hz), 3.40 (2H, q, J = 8 Hz, J = 14 Hz), 5.14 (2H, s), 7.60 (1H, s). ^{13}C NMR ($CDCl_3$, 100 MHz) δ 29.8, 32.1, 43.6, 54.6, 83.4, 127.4, 149.4, 160.5, 172.2. HRMS calcd. for $C_{11}H_{17}N_4O_4$ $[M + H]^-$ 269.1255, found 269.1251.

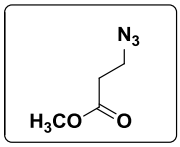

Synthesis of methyl 3-azidopropanoate (4.48): Using general procedure for the conversion of bromo to azide, we have got the title compound **4.48** (1.96 g) from methyl 3-bromopropanoate (2.0 g). product yield = 98%.

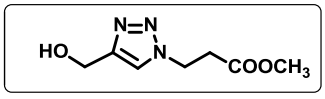

Synthesis of methyl 3-(4-(hydroxymethyl)-1H-1,2,3-triazol-1-yl)propanoate (4.49): Using general procedure for click reaction, we

have got the title compound **4.49** (1.539g) from methyl 3-azidopropanoate (1.90 g). product yield = 81% . ^{1}H NMR ($CDCl_3$, 400 MHz) δ 2.91 (2H, t, J = 6.4 Hz), 3.63 (3H, s), 4.36-4.37 (1H, d), 4.58 (2H, t, J = 6.4 Hz), 4.67-4.68 (2H, d, J = 5.6 Hz), 7.63 (1H, s). ^{13}C NMR ($CDCl_3$, 100 MHz) δ 34.1, 45.4, 51.9, 55.5, 122.8, 147.7, 170.9. HRMS calcd. for $C_7H_{12}N_3O_3$ $[M + H]^+$ 186.0873, found 186.0872.

Synthesis of methyl 3-(4-(((methylsulfonyl)oxy)methyl)-1H-1,2,3-triazol-1-yl)propanoate (4.50): Using general procedure for the conversion of alcohol to mesylate derivative, we have got the title compound **4.50** (1.215 g) from methyl 3-(4-(hydroxymethyl)-1H-1,2,3-triazol-1-yl)propanoate (1.5 g). product yield = 81%.

Synthesis of methyl 3-(4-(azidomethyl)-1H-1,2,3-triazol-1-yl)propanoate (4.51): Using general procedure for the conversion of mesylate to azide derivative, we have got the title compound **4.51** (1.02 g) from methyl 3-(4-(((methylsulfonyl)oxy)methyl)-1H-1,2,3-triazol-1-yl)propanoate (1.2 g). product yield = 85%. ^{1}H NMR ($CDCl_3$, 400 MHz) δ 2.899 (2H, t, J = 6.0 Hz), 3.59 (3H, s), 4.37 (2H, s), 4.58 (2H, t, J = 6.4 Hz), 7.66 (1H, s). ^{13}C NMR ($CDCl_3$, 100 MHz) δ 34.2, 45.4, 45.6, 52.1, 123.4, 142.2, 170.9. HRMS calcd. for $C_7H_{11}N_6O_2$[M + H]$^+$ 211.0938, found 211.0938.

Synthesis of 3-(4-(azidomethyl)-1H-1,2,3-triazol-1-yl)propanoic acid (4.52): Using general procedure for methyl ester hydrolysis, we have got the title compound **4.52** (0.93 g) from methyl 3-(4-(azidomethyl)-1H-1,2,3-triazol-1-yl)propanoate (1.0g). product yield = 93%. ^{1}H NMR ($CDCl_3$, 400 MHz) δ 2.99 (2H, t, J = 6.4 Hz), 4.47 (2H, s), 4.69 (2H, t, J = 6.4 Hz), 7.95 (1H, s). ^{13}C NMR ($CDCl_3$, 100 MHz) δ 35.2, 47.3, 48.6, 125.6, 143.9, 173.9. HRMS calcd. for $C_6H_7N_6O_2$[M + H]$^-$ 195.0636, found 195.0618.

Synthesis of 3-(4-(aminomethyl)-1H-1,2,3-triazol-1-yl)propanoic acid (4.53): Using general procedure for the conversion of azide to amine, we have got the title compound **4.53** (0.855g) from 3-(4-(azidomethyl)-1H-1,2,3-triazol-1-yl)propanoic acid (0.9g). Product yield = 95%. ^{1}H NMR ($CDCl_3$, 600 MHz) δ 2.81 (2H, t, J = 6.6 Hz), 4.33 (2H, s), 4.67 (2H, t, J = 6.6 Hz), 8.08 (1H, s). ^{13}C NMR ($CDCl_3$, 150 MHz) δ 33.9, 37.4, 47.7, 125.1, 139.4, 178.4.

Synthesis of $^{2/1Al}$TAA (4.54): Using general procedure for Boc protection, we have got the title compound **4.54** (0.608g) from 3-(4-(aminomethyl)-1H-1,2,3-triazol-1-yl)propanoic acid (0.80g). Product yield = 76%. ^{1}H NMR ($CDCl_3$, 600

MHz) δ 1.40 (9H, s), 2.96 (2H, t, J = 6.6 Hz), 4.34 (2H, d, J = 5.4 Hz), 4.67 (2H, t, J = 5.4 Hz), 7.69 (1H, s). ^{13}C NMR ($CDCl_3$, 150 MHz) δ 28.4, 34.6, 35.8, 46.0, 80.2, 123.4, 145.3, 156.4, 173.4. HRMS calcd. for $C_{11}H_{17}N_4O_4$ $[M + H]^-$ 269.1255, found 269.1247.

Synthesis of methyl 3-(4-(2-hydroxyethyl)-1H-1,2,3-triazol-1-yl) propanoate (4.55): Using general procedure for click reaction, we have got the title compound **4.55** (1.501g) from methyl 3-azidopropanoate(1.90g). product yield = 79%. ^{1}H NMR ($CDCl_3$, 400 MHz) δ 2.86-2.93 (4H, m), 3.19-3.28 (1H, bs), 3.66 (3H, s), 3.86-3.87 (2H, bd, J = 4 Hz), 4.55-4.60 (2H, q, J = 6.0 Hz, 11.2 Hz), 7.47 (1H, s). ^{13}C NMR ($CDCl_3$, 100 MHz) δ 28.8, 34.5, 45.5, 52.3, 61.5, 122.6, 145.5, 171.2.

Synthesis of methyl 3-(4-(2-((methylsulfonyl)oxy)ethyl)-1H-1,2,3-triazol-1-yl)propanoate (4.56): Using general procedure for the conversion of alcohol to mesylate, we have got the title compound **4.56** (1.19g) from methyl 3-(4-(2-hydroxyethyl)-1H-1,2,3-triazol-1-yl) propanoate(1.4g).product yield = 85%.The product is used without further characterization.

Synthesis of methyl 3-(4-(2-azidoethyl)-1H-1,2,3-triazol-1-yl)propanoate (4.57): Using general procedure for the conversion of mesylate to azide derivative, we have got the title compound **4.57** (0.902g) from methyl 3-(4-(2-((methylsulfonyl) oxy)ethyl)-1H-1,2,3-triazol-1-yl)propanoate (1.1g). product yield = 82 %. ^{1}H NMR ($CDCl_3$, 400 MHz) δ 2.87-2.91 (4H, m), 3.52 (2H, t, J = 7.2 Hz), 3.66 (3H, s), 4.55 (2H, t, J = 6.8 Hz), 7.47 (1H, s). ^{13}C NMR ($CDCl_3$, 100 MHz) δ 25.6, 34.4, 45.4, 50.5, 52.1, 122.6, 144.0, 170.9.

Synthesis of 3-(4-(2-azidoethyl)-1H-1,2,3-triazol-1-yl)propanoic acid (4.58): Using general procedure for the methyl ester hydrolysis, we have got the title compound **4.58** (0.752g) from methyl 3-(4-(2-azidoethyl)-1H-1,2,3-triazol-1-yl) propanoate (0.8 g). Product yield = 94 %. ^{1}H NMR ($CDCl_3$, 400 MHz) δ 2.95-3.02 (4H, m), 3.57 (2H, t, J = 6.4 Hz), 4.62 (2H, t, J = 6.8 Hz), 7.55 (1H, s). ^{13}C NMR ($CDCl_3$, 100 MHz) δ 25.6, 34.6, 45.8, 52.1, 123.3, 144.2, 174.2.

Synthesis of 3-(4-(2-aminoethyl)-1H-1,2,3-triazol-1-yl)propanoic acid (4.59): Using general procedure for the conversion of azide to amine, we have got the title compound **4.59** (0.644g) from3-(4-(2-azidoethyl)-1H-1,2,3-triazol-1-yl)propanoic acid (0.7g). Product yield = 92%. ^{1}H NMR (D_2O, 400 MHz) δ 2.79 (4H, m), 3.11

(2H, t, *J* = 6.8 Hz), 3.34 (2H, t, *J* = 7.2 Hz), 7.88 (1H, s). ^{13}C NMR ($CDCl_3$, 100 MHz) δ 22.9, 37.6, 47.7, 57.9, 124.1, 142.9, 178.6.

Synthesis of $^{2/2Al}$TAA (4.60): Using general procedure for Boc protection, we have got the title compound **4.60** (0.474g) from 3-(4-(2-aminoethyl)-1H-1,2,3-triazol-1-yl) propanoic acid (0.6g). Product yield = 79%. ^{1}H NMR ($CDCl_3$, 600 MHz) δ 1.41 (9H, s), 2.88 (2H, t, *J* = 6.5 Hz), 2.98 (2H, t, *J* = 5.8 Hz), 3.42 (2H, s), 4.63 (2H, t, *J* = 6.3 Hz), 5.14 (1H, s), 7.53 (1H, s). ^{13}C NMR ($CDCl_3$, 150 MHz) δ 26.2. 28.6, 34.7, 40.1, 45.9, 79.8, 122.9, 145.4, 156.5, 173.4.

Synthesis of BocNH–Leu-^{TPy}Ala^{Do}–CONMe(OMe) (4.61): Using the general procedure of [3+2]cyclo-addition reaction, starting from 200 mg (0.52 mmol) of azide derivative of dipeptide **2.48** (synthetic procedure was described in **Chapter 2**) and 140 mg (0.62 mmol) of 1-ethynyl pyrene, 247 mg (0.40 mmol) of the title compound **4.61** was isolated as a light brown solid material (Si-gel, PE : EtOAc = 1:1). Yield 78%, IR (KBr) 3450, 2958, 2928, 2102, 1653, 1509, 1390, 1167, 1049, 848 cm^{-1}. ^{1}H NMR ($CDCl_3$, 600 MHz), δ 0.89 (6H, d, *J* = 5.4 Hz), 1.38 (9H, s), 1.52-1.48 (1H, m), 1.67-1.59 (2H, m), 3.29 (3H, s), 3.7 (3H, s), 4.11 (1H, bs), 4.89 (1H, dd, *J* = 4.2 Hz, 9.6 Hz), 4.95 (1H, d, *J* = 6.6 Hz), 5.05 (1H, bs), 5.36 (1H, bs), 7.22 (1H, d, *J* = 5.4 Hz), 7.99 (1H, t, *J* = 7.2 Hz), 8.06 (2H, d, *J* = 4.8 Hz), 8.09 (1H, t, *J* = 9.0 Hz), 8.18-8.15 (3H, m), 8.30 (1H, s), 8.31 (1H, s), 8.79 (1H, d, *J* = 9.0 Hz), ^{13}C NMR ($CDCl_3$, 150 MHz), δ 21.9, 23.1, 24.9, 28.4, 32.9, 41.1, 50.4, 50.7, 53.9, 62.1, 80.4, 124.8, 124.9, 125.0, *150*.2, 125.3, 125.4, 126.1, 127.4, 127.5,127.8, 128.2, 128.7, 131.1, 131.4, 131.5, 147.8, 155.9, 168.2, 173.2. HRMS calcd for $C_{34}H_{41}N_6O_5$ [M + H]$^+$ 613.3133, found 613.3132.

Synthesis of TFA salt of BocNH–Leu-^{TPy}Ala^{Do}–CONMe(OMe) (4.62): Using the general procedure of Boc-deprotection, the compound **4.61** (240 mg, 0.40 mmol) was deprotected and the product **4.62** was obtained in quantitative yield and were used without further purification and characterization.

Synthesis of BocNH–$^{1/1Al}$TAA–Leu-^{TPy}Ala^{Do}–CONMe(OMe) (4.63): To a solution of *N*-protected aliphatic amino acid scaffold (**4.40**, 160 mg, 0.625 mmol) in dry DMF, (EDC.HCl) (178 mg, 0.937 mmol), followed by DMAP (288 mg, 1.87 mmol) were added at 0 ^{o}C. Next, the amine salt of Weinreb amide, the

dipeptide **4.62** (390 mg, 0.625 mmol) was added and the reaction mixture was stirred for 30 min at 0°C and then 18h at room temperature. After completion of the reaction (monitored by TLC) the work up was done with EtOAc and water. The organic layer was washed with brine solution. The product tripeptide **4.63** (342 mg, 0.456 mmol) was isolated in pure form by column chromatography (Si-gel, EtOAc) as light brown solid compound. Yield 73%. ^{1}HNMR ($CDCl_3$, 600 MHz) δ 0.81 – 0.91 (6H, m), 1.37 (9H, s), 1.49 - 1.63 (3H, m), 3.27 (3H, s), 3.80 (3H, s), 4.22 (2H, s), 4.44 - 4.53 (1H, m), 4.87 (2H, s), 4.97 (1H, d, J = 8.1 Hz), 5.01 - 5.07 (1H, m), 5.08 - 5.14 (1H, m), 5.20 (1H, s), 5.41 (1H, d, J = 6.3 Hz), 7.51 (1H, bs), 7.56 (1H, s), 8.00 – 8.10 (m, 5H), 8.14 - 8.23 (4H, m), 8.64 (1H, d, J = 8.9 Hz). ^{13}C NMR ($CDCl_3$, 100 MHz) δ 21.9, 22.9, 24.9, 29.9, 32.8, 36.3, 40.2, 40.3, 43.4, 50.5, 51.9, 52.5, 52.6, 52.7, 54.8, 61.9, 62.1, 62.3, 79.7, 113.9, 113.9, 116.3, 116.8, 123.1, 123.9, 123.9, 124.0, 124.2, 124.6, 124.7, 124.8, 124.9, 125.0, 125.1, 125.3, 125.4, 125.6, 125.7, 125.8, 125.8, 126.3, 126.4, 127.3, 127.5, 128.1, 128.4, 128.5, 128.5, 128.6, 128.7, 128.9, 131.0, 131.4, 131.5, 131.9, 135.0, 135.1, 142.0, 142.3, 147.6, 151.9, 155.9, 161.4, 166.1, 171.9. HRMS calcd. for $C_{39}H_{47}N_{10}O_6$ $[M + H]^+$ 751.3675, found 751.3675.

Synthesis of TFA salt of BocNH–$^{1/1Al}$TAA–Leu-^{TPy}Ala^{Do}–CONMe(OMe) (4.64): Using the general procedure of Boc-deprotection, compound **4.63** (300 mg, 0.4mmol) was reacted with TFA to get the product **4.64** in quantitative (95 %) yield and was used for the next step without further purification and characterization.

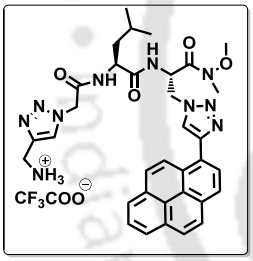

Synthesis of BocNH–^{TMnap}Ala^{Do}–Leu–$^{1/1Al}$TAA–Leu–^{TPy}Ala^{Do}–CONMe(OMe) (4.65): Using general procedure of peptide coupling, the acid compound **2.60** (synthetic procedure was described in **Chapter 2**) (200 mg, 0.38mmol) was taken as starting material then (290 mg, 0.38mmol) of amine compound **4.64** was reacted with it. After completion of reaction 162 mg (0.141mmol) of the title compound **4.65** was isolated in pure form by column chromatography (Si-gel, PE : EtOAc =1:4) as light brown solid material. Yield 37%. IR (KBr) 3423, 3310, 2925, 2106, 1673, 1557, 1456, 1432, 1163, 1027, 849 cm^{-1}. ^{1}H NMR ($CDCl_3$, 600 MHz) δ 0.48 – 0.72 (12H, m), 1.20 (9H, s), 1.53 – 1.61 (6H, m), 3.14 (3H, s), 3.31 (3H, s), 3.86 (3H, s), 4.30 (4H, dd, J = 26.2, 11.2 Hz), 4.48 – 4.58 (2H, m), 4.75 (2H, dd, J = 13.9, 3.8 Hz), 4.83 (2H, d, J = 9.2

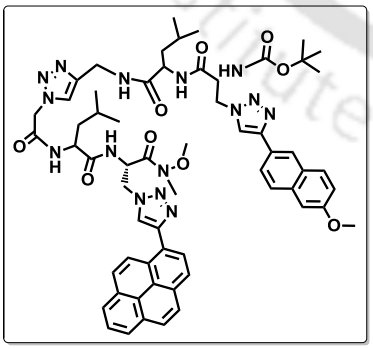

Hz), 4.97-5.04 (1H, m), 5.07 – 5.16 (2H, m), 7.85 (2H, d, *J* = 8.6 Hz), 8.05 – 8.13 (2H, m), 8.23 (5H, ddd, *J* = 15.8, 8.8, 4.8 Hz), 8.27 – 8.38 (7H, m), 8.47 (2H, s), 8.52 (1H, s), 8.70 (1H, s), 8.79 (2H, t, *J* = 9.2 Hz). ^{13}C NMR ($CDCl_3$, 150 MHz) δ 21.4, 21.7, 22.1, 22.7, 22.9, 23.1, 23.2, 24.1, 24.2, 24.3, 28.0, 29.0, 43.4, 45.9, 49.5, 49.7, 51.4, 51.5, 51.7, 55.0, 55.3, 79.2, 123.3, 123.3, 123.9, 124.3, 125.0, 125.1, 125.4, 125.9, 126.3, 126.5, 126.8, 127.4, 127.5, 127.5, 127.6, 127.8, 127.9, 128.0, 128.7, 129.6, 130.4, 130.6, 130.6, 130.9, 132.1, 133.2, 133.9, 141.3, 141.4, 145.8, 146.0, 155.1, 165.4, 167.7, 168.8, 175.3, 177.2. HRMS calcd. for $C_{61}H_{72}N_{15}O_9$ $[M + H]^+$ 1158.5632, found 1158.5646.

Synthesis of BocNH–$^{1/2Al}$TAA–Leu–^{TPy}Ala^{Do}–CONMe(OMe) (4.66): Following the similar procedure of DMAP mediated peptide coupling reaction, we have got tripeptide **4.66** from *N*-protected aliphatic amino acid scaffold **4.46** (160 mg, 0.625 mmol) as light brown solid compound. Yield 71 %. ^{1}H NMR ($CDCl_3$, 600 MHz) δ 0.82 – 0.91 (6H, m), 1.37 (9H, s), 1.49-1.63 (3H, m), 2.59 (1H, s), 2.87 (1H, s), 3.28 (3H, s), 3.33 - 3.43 (3H, m), 3.50 - 3.61 (1H, m), 3.81 (3H, s), 4.42 - 4.50 (1H, m), 4.52 - 4.62 (1H, m), 4.88 (1H, s), 4.98 (2H, s), 5.04 (1H, m), 5.09 - 5.18 (1H, m), 5.42 (1H, s), 7.04 (3H, bs), 7.55 (2H, s), 7.97-8.12 (5H, m), 8.15-8.24 (4H, m), 8.64 (1H, d, *J* = 9.2 Hz). ^{13}C NMR ($CDCl_3$, 150 MHz) δ 21.9, 22.9, 23.0, 24.9, 24.9, 26.2, 26.4, 28.6, 32.5, 32.8, 39.7, 40.1, 41.0, 49.8, 50.5, 51.9, 52.5, 52.8, 61.9, 62.2, 66.0, 79.3, 123.5, 123.6, 124.7, 124.7, 124.8, 124.9, 125.0, 125.1, 125.3, 125.4, 125.7, 125.8, 126.4, 126.5, 127.4, 127.5, 128.1, 128.5, 128.7, 129.9, 131.0, 131.5, 147.5, 151.6, 155.9, 165.8, 166.2, 171.8. HRMS calcd. for $C_{40}H_{49}N_{10}O_6$ $[M + H]^+$ 765.3831, found 765.3839.

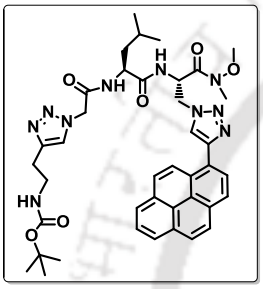

Synthesis of TFA salt of BocNH–$^{1/2Al}$TAA–Leu–^{TPy}Ala^{Do}–CONMe(OMe) (4.67): Using the general procedure of Boc-deprotection, compound **4.66** (300 mg, 0.39mmol) was reacted with TFA to get the product **4.67** in quantitative (96 %) yield and was used for the next step without further purification and characterization.

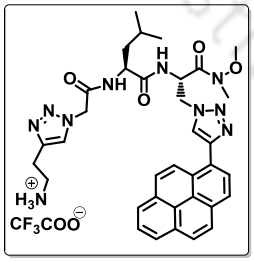

Synthesis of BocNH–^{TMnap}Ala^{Do}–Leu-$^{1/2Al}$TAA–Leu–^{TPy}Ala^{Do}–CONMe(OMe) (4.68): Using general procedure of peptide coupling reaction, the acid compound **2.60** (200 mg, 0.38 mmol) was taken as a starting material then (296 mg, 0.38mmol) of amine compound **4.67** was reacted with it. After completion of reaction 151 mg (0.129

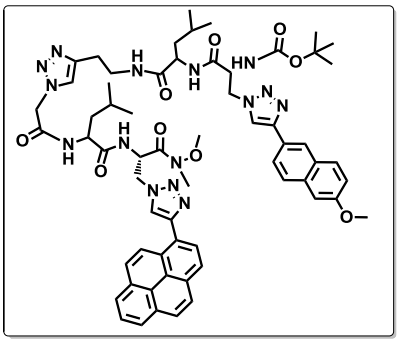

mmol) of the title compound **4.68** was isolated in pure form by column chromatography (Si-gel, PE : EtOAc =1:4) as light brown solid material. Yield 34 %. IR (KBr) 3308, 2924, 2105, 1680, 1657, 1549, 1465, 1246, 1163, 1024, 849 cm^{-1}. ^1H NMR ($CDCl_3$, 600 MHz) δ 0.80 – 0.91 (12H, m), 1.29 (9H, s), 1.39 – 1.51 (6H, m), 3.16 (3H, s), 3.41 (3H, s), 3.74 (2H, d, *J* = 22.0 Hz), 3.87 (3H, s), 4.37 (2H, s), 4.53 (1H, s), 4.55 – 4.63 (1H, m), 4.72 – 4.79 (2H, m), 4.85 (2H, d, *J* = 13.3 Hz), 4.98 (1H, s), 5.03 (1H, d, *J* = 3.4 Hz), 5.09 (2H, d, *J* = 8.8 Hz), 5.37 (1H, s), 7.18 (1H, d, *J* = 7.9 Hz), 7.83 – 7.92 (2H, m), 8.07 – 8.14 (2H, m), 8.24 (5H, dd, *J* = 7.9, 5.4 Hz), 8.30 – 8.36 (6H, m), 8.39 (1H, d, *J* = 7.9 Hz), 8.44 (1H, s), 8.48 (1H, s), 8.53 (1H, s), 8.68 (1H, s), 8.82 (1H, d, *J* = 9.3 Hz). ^{13}C NMR ($CDCl_3$, 150 MHz) δ 21.5, 21.6, 21.7, 22.7, 22.9, 23.1, 23.1, 23.2, 24.1, 28.0, 28.1, 49.4, 49.8, 51.4, 51.7, 52.4, 55.1, 55.5, 78.4, 123.9, 124.3, 124.4, 124.9, 125.2, 126.3, 126.5, 126.6, 126.7, 127.0, 127.1, 127.4, 127.6, 127.7, 127.8, 127.9, 128.0, 128.1, 128.3, 128.5, 130.4, 130.6, 130.7, 130.7, 130.9, 131.1, 133.3, 145.8, 146.0, 148.8, 149.4, 154.8, 165.2, 167.8, 170.9, 172.0. HRMS calcd.for $C_{62}H_{74}N_{15}O_9$ $[M + H]^+$ 1172.5788, found 1172.5771.

Synthesis of BocNH–$^{2/1Al}$TAA–Leu–^{TPy}Ala^{Do}–CONMe(OMe) (4.69): Following the similar procedure of DMAP mediated peptide coupling we have got tripeptide **4.69** from *N*-protected aliphatic amino acid scaffold **4.54** (160 mg, 0.625 mmol) as yellowish brown gummy compound. Yield 67 %.^1H NMR ($CDCl_3$, 600 MHz) δ 0.84 – 0.94 (6H, m), 1.25 (9H, s), 1.50 (2H, m), 1.59 – 1.65 (1H, m), 2.69 (2H, s), 3.31 (3H, s), 3.86 (3H, s), 4.31 – 4.44 (1H, m), 4.48 – 4.66 (2H, m), 4.74 – 4.85 (5H, m), 4.94 (2H, dd, *J* = 19.7, 9.6 Hz), 5.07 (1H, s), 5.40 (1H, d, *J* = 2.0 Hz), 5.56 (6H, s), 5.99 (1H, dd, *J* = 26.0, 7.3 Hz), 6.35 (6H, d, *J* = 23.5 Hz), 7.32 (1H, d, *J* = 8.8 Hz), 7.98 - 8.13 (5H, m), 8.17 – 8.28 (4H, m), 8.72 (3H, d, *J* = 9.3 Hz). ^{13}C NMR ($CDCl_3$, 150 MHz) δ 21.8, 22.8, 24.7, 28.4, 32.5, 36.1, 40.4, 50.2, 50.4, 52.3, 52.4, 62.0, 79.5, 122.5, 123.1, 123.8, 124.6, 126.3, 126.5, 126.8, 127.1, 127.3, 128.4, 128.9, 130.1, 130.3, 130.6, 131.2, 145.6, 146.6, 155.9, 165.9, 168.2, 172.1. HRMS calcd.for $C_{40}H_{49}N_{10}O_6$ $[M + H]^+$ 765.3831, found 765.3826.

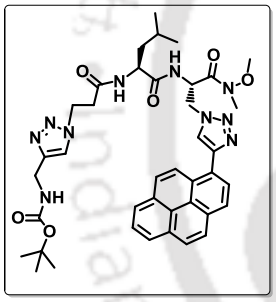

Synthesis of TFA salt of BocNH–$^{2/1Al}$TAA–Leu–^{TPy}Ala^{Do}–CONMe(OMe) (4.70): Using the general procedure of Boc-deprotection, compound **4.69** (300 mg, 0.39mmol) was reacted with TFA to get the product **4.70** in quantitative (95 %) yield and was used for the next step without further purification and characterization.

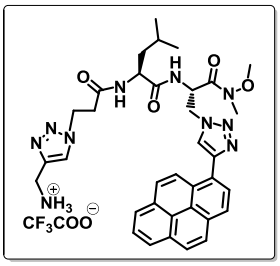

Synthesis of BocNH–^{TMnap}Ala^{Do}–Leu-$^{2/1Al}$TAA–Leu–^{TPy}Ala^{Do}–CONMe(OMe) (4.**71**): Using general procedure of peptide coupling, the acid compound **2.60** (200 mg, 0.38mmol) was taken as a starting material then (296 mg, 0.38 mmol) of amine compound **4.70** was reacted with it. After completion of reaction 138 mg (0.118mmol) of the title compound **4.71** was isolated in pure form by column chromatography (Si-gel, PE : EtOAc =1:4) as light brown solid material. Yield 31 %. IR (KBr) 3299, 2957, 2106, 1683, 1660, 1541, 1389, 1163, 1056, 848 cm^{-1}. ^{1}H NMR ($CDCl_3$, 600 MHz) δ 0.82-0.87 (12H, m), 1.68 (9H, s), 1.80-1.87 (6H, m), 3.17 (3H, s), 3.41 (3H, s), 3.76 (4H, s), 3.90 (2H, d, *J* = 9.3 Hz), 4.32 (3H, m), 4.68 (1H, dd, *J* = 13.7, 7.5 Hz), 4.76 (2H, m), 4.78 – 4.93 (3H, m), 5.34 (2H, bs), 5.51 (1H, bs), 7.50 (1H, d, *J* = 7.9 Hz), 8.02 – 8.06 (1H, m), 8.13 (3H, dt, *J* = 14.9, 7.8 Hz), 8.24-8.29 (6H, m), 8.33-8.39 (7H, m), 8.41 (1H, d, *J* = 7.9 Hz), 8.52 (1H, bs), 8.74 (1H, s), 8.85 (1H, d, *J* = 9.3 Hz). ^{13}C NMR ($CDCl_3$, 150 MHz) δ 22.0, 22.1, 23.0, 23.5, 23.7, 24.7, 24.8, 25.2, 25.3, 28.0, 29.6, 29.7, 32.8, 50.1, 50.4, 51.5, 51.7, 51.9, 53.5, 53.7, 59.5, 62.2, 79.8, 124.4, 124.6, 124.9, 125.3, 125.7, 125.8, 125.9, 126.2, 126.3, 126.6, 127.1, 127.3, 127.7, 127.9, 128.0, 128.2, 128.3, 128.4, 128.6, 128.9, 128.9, 130.3, 131.0, 131.2, 131.4, 131.6, 141.5, 146.5, 150.7, 157.5, 169.5, 169.9, 172.3, 173.1, 173.3. HRMS calcd. for $C_{62}H_{74}N_{15}O_9$ $[M + H]^+$1172.5788, found 1172.5719.

Synthesis of BocNH–$^{2/2Al}$TAA–Leu-^{TPy}Ala^{Do}–CONMe(OMe) (4.72): Following the similar procedure of DMAP mediated peptide coupling we have got tripeptide **4.72** from *N*-protected aliphatic amino acid scaffold **4.60** (160 mg, 0.625 mmol) as yellowish brown gummy compound. Yield 65 %. ^{1}H NMR ($CDCl_3$, 600 MHz) δ 0.79 - 0.92 (6H, m), 1.38 (9H, s), 1.48 - 1.66 (3H, m), 2.31 (2H, d, *J* = 15.7 Hz), 2.68 (1H, dt, *J* = 31.1, 12.2 Hz), 2.92 - 2.74 (1H, m), 3.20 (1H, s), 3.26 (3H, s), 3.50-3.64 (1H, m), 3.72 (1H, d, *J* = 1.5 Hz), 3.80 (3H, s), 4.20 (2H, d, *J* = 5.5 Hz), 4.33 (1H, dd, *J* = 15.2, 7.6 Hz), 4.42 (1H, s), 4.57 (1H, dd, *J* = 8.3, 4.2 Hz), 4.88 (2H, s), 5.42 (1H, d, *J* = 5.2 Hz), 7.04 (1H, d, *J* = 20.9 Hz), 7.22 (1H, s), 7.49 (1H, s), 7.93 - 8.09 (5H, m), 8.11 - 8.20 (4H, m), 8.67 (1H, dd, *J* = 24.4, 9.0 Hz). ^{13}C NMR ($CDCl_3$, 150 MHz) δ 21.8, 22.0, 23.0, 23.1, 24.8, 24.9, 28.6, 29.9, 32.8, 40.4, 41.5, 46.0, 50.6, 51.9, 52.3, 62.2, 66.0, 79.7, 124.7, 124.8, 124.9, 125.0, 125.1, 125.3, 125.5, 125.6, 126.2, 126.3, 127.4, 127.5, 127.9, 128.0, 128.3, 128.4, 128.7, 130.9, 131.0, 131.4, 131.4, 131.5, 131.5, 131.5, 132.1, 145.2, 147.5,

155.9, 168.4, 169.9, 172.6. HRMS calcd. for $C_{41}H_{51}N_{10}O_6$ $[M + H]^+$ 779.3988, found 779.3991.

Synthesis of TFA salt of BocNH–$^{2/2Al}$TAA–Leu–^{TPy}Ala^{Do}–CONMe(OMe) (4.73): Using the general procedure of Boc-deprotection, compound **4.72** (300 mg, 0.39mmol) was reacted with TFA to get the product **4.73** in quantitative (96 %) yield and was used for the next step without further purification and characterization.

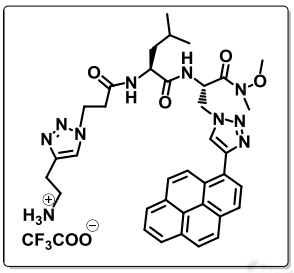

Synthesis of BocNH–^{TMnap}Ala^{Do}–Leu-$^{2/2Al}$TAA–Leu–^{TPy}Ala^{Do}–CONMe(OMe) (4.74): Using general procedure of peptide coupling, the acid compound **2.60** (200 mg, 0.38 mmol) was taken as starting material then (301 mg, 0.37 mmol) of amine compound **4.73** was reacted with it. After completion of reaction 166 mg (0.14mmol) of the title compound **4.74** was isolated in pure form by column chromatography (Si-gel, PE : EtOAc = 1:4) as light brown solid material. Yield 37 %. IR (KBr) 3296, 2924, 2105, 1648, 1546, 1435, 1171, 1053, 849 cm^{-1}. ^1H NMR ($CDCl_3$, 600 MHz) δ 0.67 – 0.71 (6H, m), 0.83 (6H, m), 1.25 – 1.36 (3H, m), 1.39 - 1.51 (3H, m), 1.73 (9H, s), 3.12 (3H, d, *J* = 18 Hz), 3.15 (3H, s), 3.47 – 3.53 (1H, m), 3.70 (2H, s), 3.75 (5H, s), 4.19 – 4.35 (4H, m), 4.66 (1H, dd, *J* = 13.8, 7.4 Hz), 4.74 (2H, dd, *J* = 13.9, 8.3 Hz,), 4.83 (3H, dt, *J* = 21.1, 7.7 Hz,), 5.32 (2H, s), 5.49 (1H, s), 7.99 – 8.04 (1H, m), 8.10 (3H, dt, *J* = 11.4, 7.6 Hz), 8.16 – 8.27 (6H, m), 8.27 – 8.36 (8H, m), 8.39 (1H, d, *J* = 7.9 Hz), 8.48 (1H, bs), 8.71 (2H, s), 8.82 (1H, d, *J* = 9.3 Hz). ^{13}C NMR ($CDCl_3$, 150 MHz) δ 20.3, 22.0, 22.1, 22.2, 23.0, 23.1, 23.5, 23.7, 24.7, 24.8, 25.5, 32.7, 39.3, 39.7, 39.9, 40.0, 40.1, 40.3, 40.4, 40.6, 40.7, 41.2, 41.5, 49.3, 50.1, 50.4, 51.3, 51.5, 51.9, 58.7, 62.1, 63.7, 65.6, 87.5, 124.4, 124.4, 124.6, 124.7, 124.9, 125.0, 125.3, 125.5, 125.7, 125.8, 125.9, 126.1, 126.1, 126.2, 126.5, 127.1, 127.4, 127.7, 127.8, 128.0, 128.1, 128.2, 128.3, 128.5, 128.6, 129.2, 131.0, 131.1, 131.2, 131.3, 131.6, 146.6, 154.5, 169.9, 171.3, 173.1, 173.2, 173.3.

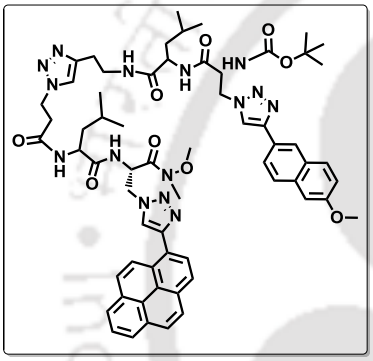

4.7. Photophysical Studies of the Synthesized Peptides.

UV-visible measurements: The *UV* –visible spectra of all final peptides and UNNAs (10 µM) were measured in different solvents using a UV-Visible

spectrophotometer (**SHIMADZU**, **UV-2550**) with a cell of 1 cm path length. The measurements were done in absorbance mode. The sample solutions absorbance values were measured in the wavelength range of 200–700 nm. All the sample solutions were prepared freshly just before doing the experiment.

Fluorescence experiments: All the sample solutions for fluorescence measurements (**HORIBA Scientific**, **Fluoromax-4**) were also prepared freshly just before doing the experiment. Fluorescence spectra were obtained using a fluorescence spectrophotometer at 25 °C using 1 cm path length cell. The wavelengths for excitation in all the cases were set at the absorption maxima of each sample in each solvent. The emission spectra were measured in the wavelength regime of 300–700 nm with an integration time of 0.2 sec. From 2.0 ml 500 μM stock solution, 2 ml of 10 μM concentration of solution was used for fluorescence experiment in 1 ml cell. Fluorescence emissions were recorded by exciting the sample solutions at their absorption maxima. Steady-state fluorescence emission spectra were recorded at room temperature as an average of five scans using an excitation slit of 3.0 nm, emission slit 3.0 nm, and scan speed of 120 nm/min. Using quinine sulphate as a reference, the fluorescence quantum yields (Φ_f) were determined with the known Φ_f (0.55) in 0.1 molar solution in sulphuric acid. Following equation was used to calculate the quantum yield,

$$\Phi_S = \Phi_R \frac{Fl_S^{Area}}{Fl_R^{Area}} \frac{Abs_R}{Abs_S} \frac{n_S^2}{n_R^2}$$

where, Φ_R is the quantum yield of standard reference, Fl_S^{Area} (sample) and Fl_R^{Area} (reference) are the integrated emission peak areas, Abs_S (sample) and Abs_R (reference) are the absorbances at the excitation wavelength, and n_S (sample) and n_R (reference) are the refractive indices of the solutions.

A time resolved fluorescence spectrophotometer (*Eddinburg Instruments FSP920*) was utilized to perform fluorescence lifetime experiments. Working condition was maintained at 25^{o}C and results were recorded at an excitation wavelength of 290 nm LED and 375 nm laser using a cuvette having path length 1 cm. To analyze the lifetime data time correlated single photon counting (TCSPC) method was used and analysis was done using a software package with range 205 – 4000 channels.

All the experiments were done four times. The experimental errors were found within 1-2 nm. The experimental standard errors were calculated based the following equations for four consecutive run for the same experiment at same condition.

$$SD = \sqrt{\sum_{i=1}^{n} \frac{1}{n-1}(x - \overline{x})^2}$$

……Equation 1

where SD is standard deviation, *x* is individual data points, $\overline{x}$ is the mean value of the experiments and n is the total number of observations.

The standard error (*SE*) was measured by sample standard deviation obtained divided by the square root of number of observations

$$SE = \frac{SD}{\sqrt{n}}$$

……Equation 2

The experimental errors in wavelength for both the UV-Visible and fluorescence measurement were found to be in the range of 1-2 nm. Error in Quantum yield calculation lies in the range of 8-10%. The experimental error for lifetime measurement lies between ± 0.5 ns range.

4.8. Some Selected Spectra

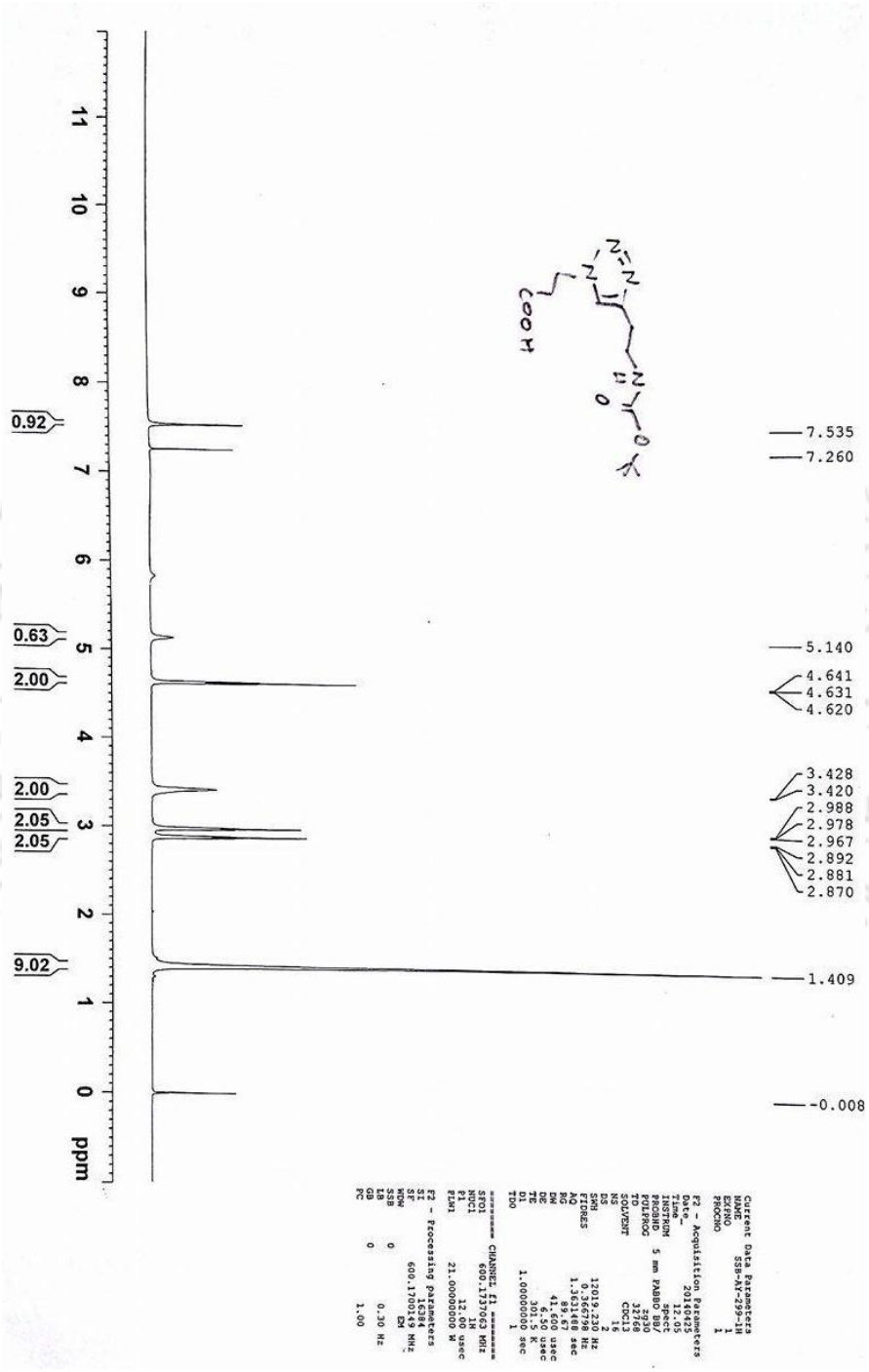

Figure 4.24. ^{1}H Spectra of synthesized compound **4.60.**

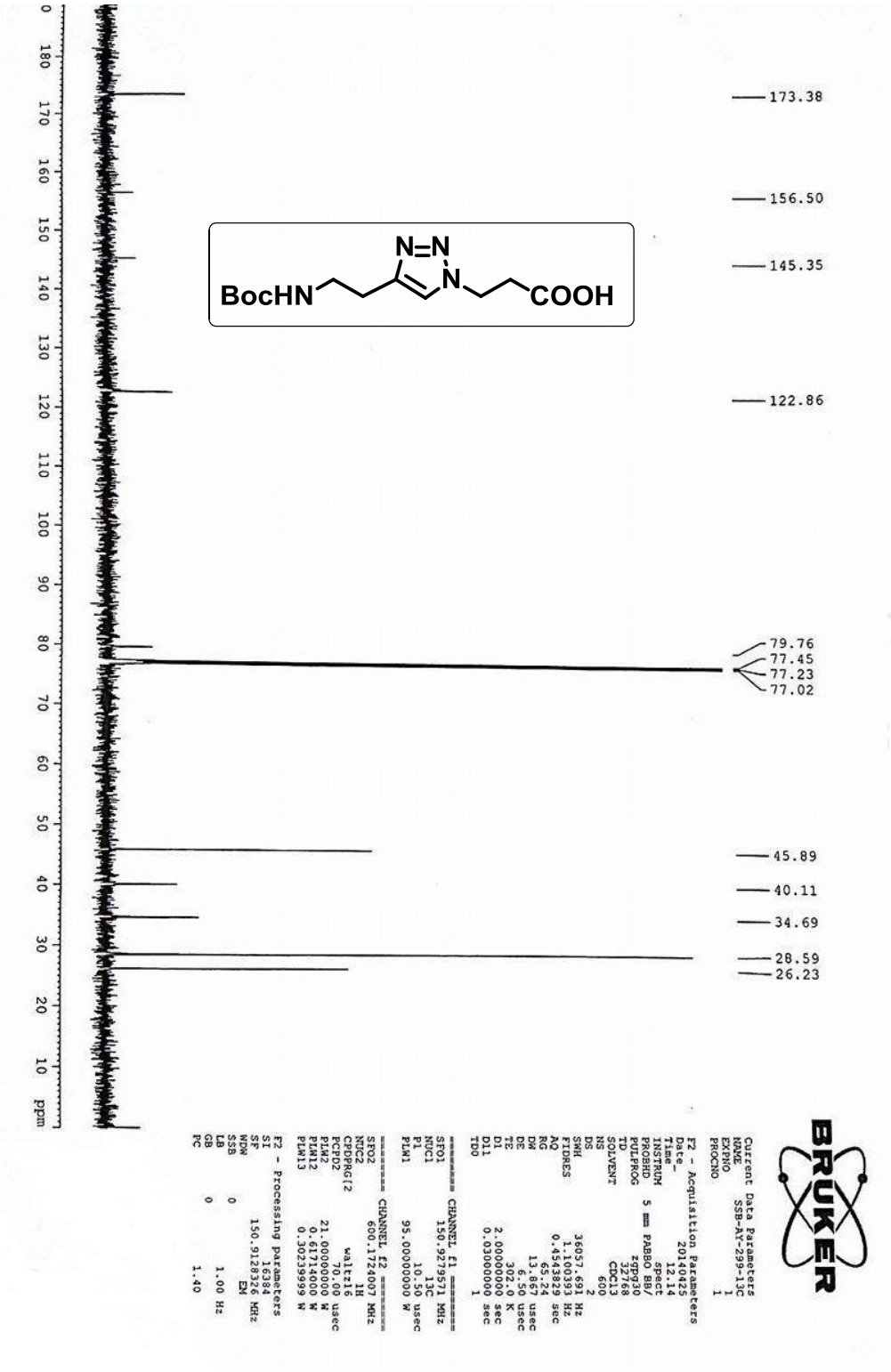

Figure 4.25. ^{13}C Spectra of synthesized compound **4.60.**

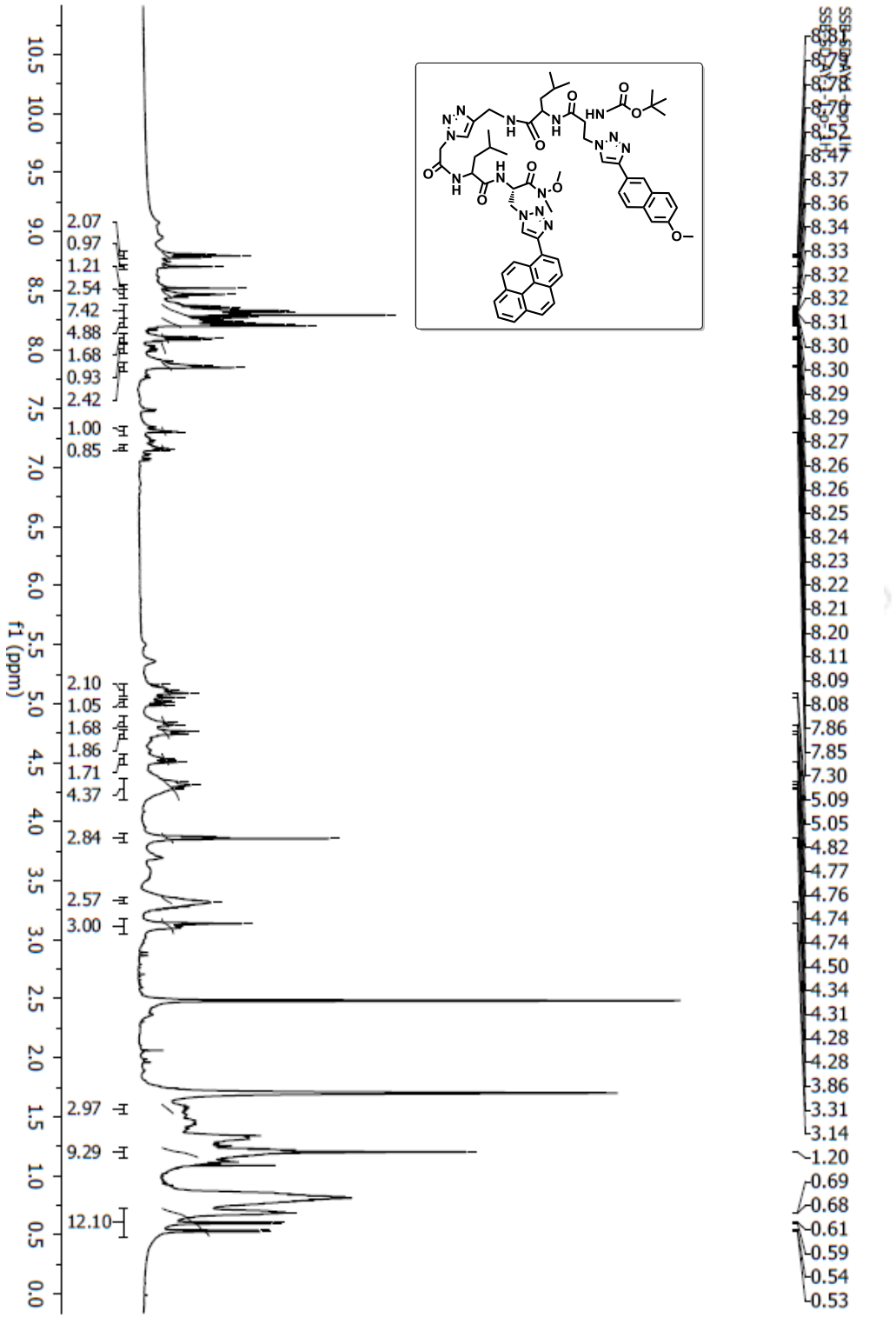

Figure 4.26. ^{1}H Spectra of synthesized compound **4.65**.

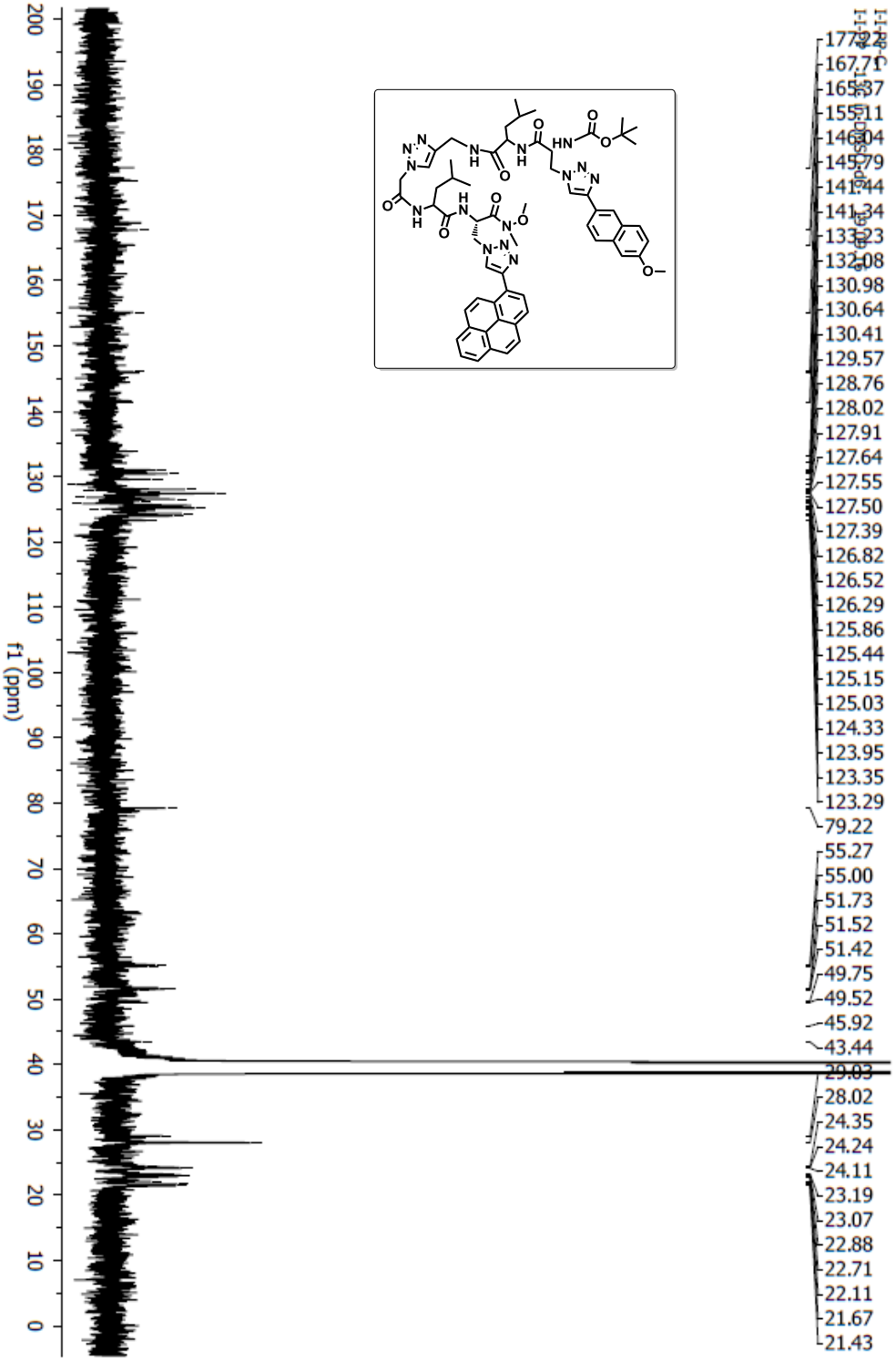

Figure 4.27. ^{13}C Spectra of synthesized compound **4.65.**

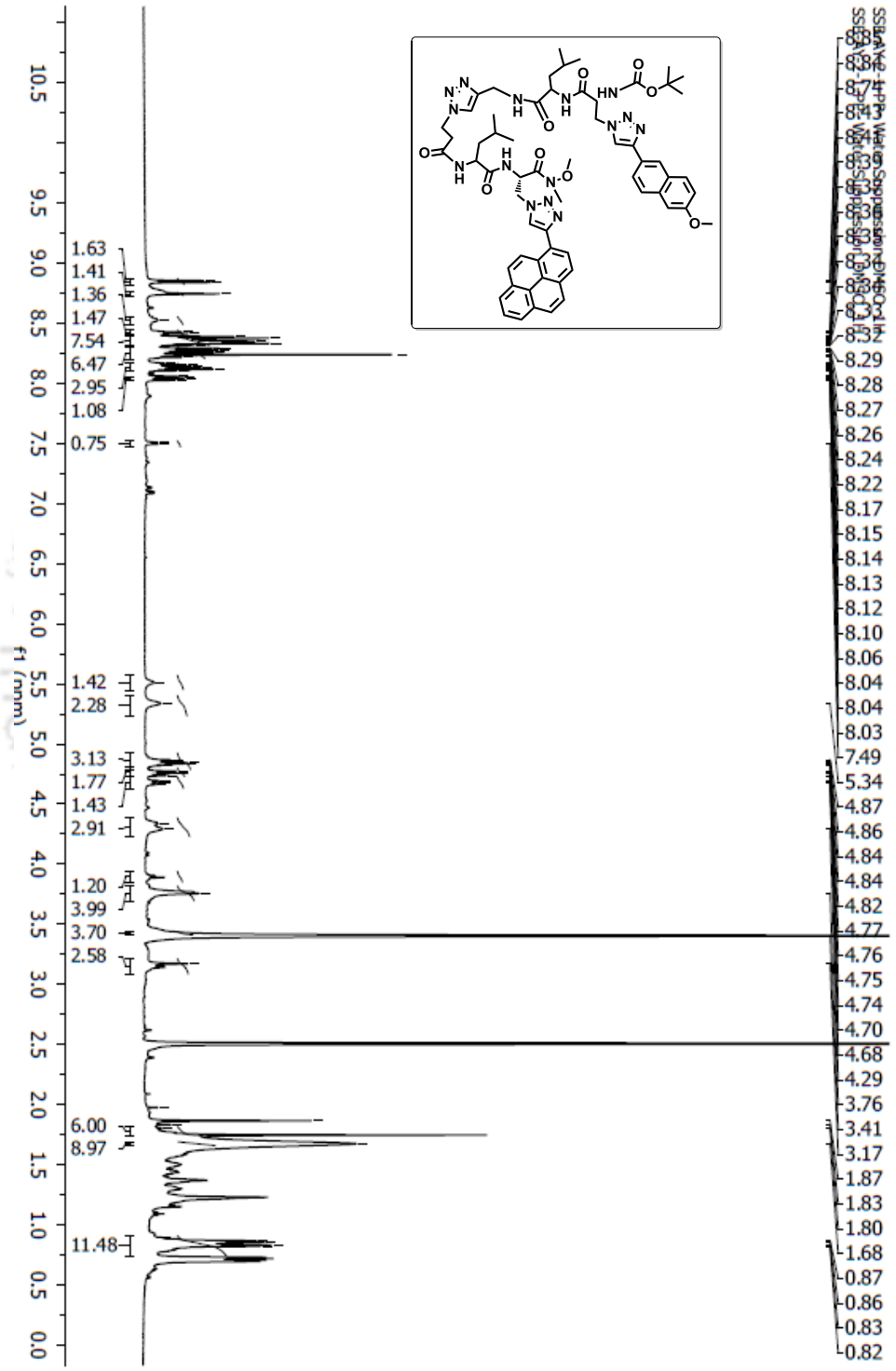

Figure 4.28. ^{1}H Spectra of synthesized compound **4.71.**

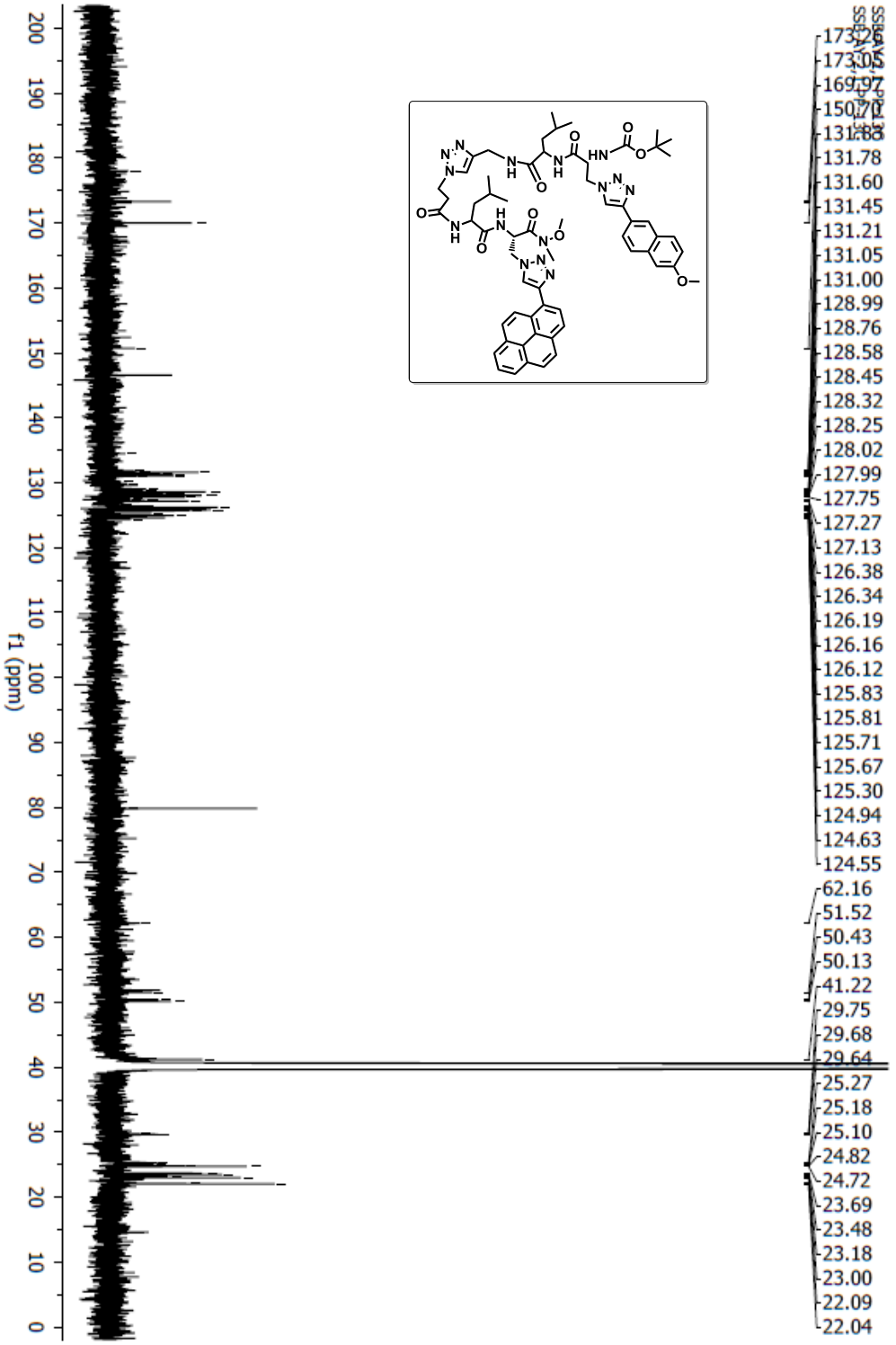

Figure 4.29. ^{13}C Spectra of synthesized compound **4.71.**

4.9. Reference

1. (a) Himo, F.; Lovell, T.; Hilgraf, R. *J. Am. Chem. Soc*.**2005**, *127*, 210. (b) Bock, V. D.; Hiemstra, H.; van Maarseveen, J. H. *Eur. J. Org. Chem.*, **2006**, 68.
2. (a) Brik, A.; Muldoon, J.; Lin, Y. C. Elder, J. H.; Goodsell, D. S.; Olson, A. J.; Fokin, V. V.; Sharpless, K. B.; and Wong, C. H. *ChemBioChem***2003**,*4*, 1246. (b) Brik, A.; Alexandratos, J.; Lin, Y. -C. Elder, J. H.; Olson, A. J.; Alexander, W.; Goodsell, D. S.; Wong, -C. H. *ChemBioChem*, **2005**,*6*, 1167.
3. Horne, W. S.; Yadav, M. K.; Stout, C. D.; Ghadiri, M. R. *J. Am. Chem. Soc*. **2004**, *126*, 15366.
4. Oh, K.; Guan, Z. *Chem. Commun*. **2006**, 3069.
5. Ko, E.; Liu, J.; Perez, L. M.; Lu, G.; Schaefer, A.; Burgess, K. *J. Am. Chem. Soc*.**2011**, *133*, 462.
6. Chouhan, G.; James, K. *Org. Lett*. **2013**, *15*, 1206.
7. (a) Selvin, P. R. *Methods Enzymol*.**1995**, *246*, 300. (b) Lakowicz, J. R. Principles of Fluorescence Spectroscopy; Kluwer Academic/Plenum: New York, **1999**.
8. (a)Yeh, I.-C.; Hummer, G. *J. Am. Chem. Soc*.**2002**, *124*, 6563. (b) Roccatano, D.; Nau, W. M.; Zacharias, M. *J. Phys. Chem. B***2004**, *108*, 18734.
9. Sapsford, K.E.; Berti, L. and Medintz, I.L. *Angew. Chem. Int. Ed.***2006**, *45*, 4562.
10. (a) Sahoo, H.; Roccatano, D.; Hennig, A.; Nau, W. M. *J. Am. Chem. Soc.* **2007**, 129, 9762. (b) Sahoo, H.; Hennig, A.; Florea, M.; Roth, D.; Enderle, T. and Nau, W. M. *J. Am. Chem. Soc*.**2007**, *129*, 15927.
11. Xu, Y.; Hixon, M. S.; Dawson, P. E.; Janda, K. D. *J. Org. Chem*. **2007**, *72*, 6700.
12. Sahoo, H. and Nau, W. M. *ChemBioChem***2007**, *8*, 567 .
13. Haas, E.; M. Wilchek, E.; Katchalski-Katzir, I. Z. Steinberg. *Proc. Natl. Acad. Sci.* **1975**, *72*, 1807
14. (a) Erickson M. G.; Moon D. L.; Yue D. T. *Biophys. J*. **2003**, *85*, 599. (b) Patterson G. H.; Piston D. W.; Barisas B. G. *Anal. Biochem.* **2000**, *284*, 438. (c) Pollok, B. A.; Heim, R. *Trends Cell Biol.* **1999**, *9*, 57.
15. Badorff, C.; Berkely, N.; Mehrotra, S.; Talhouk, J. W.; Rhoads, R. E.; Knowlton, K. U. *J. Biol. Chem*. **2000**, *275*, 11191.
16. Bag, S. S.; Jana; S.; Yashmeen; A.; De; S. *Chem. Commun.* **2015**, *51*, 5242.
17. (a) Rubinov, B.; Wagner, N.; Rapaport, H.; Ashkenasy, G. *Angew. Chem., Int. Ed*. **2009**, *121*, 6811. (b) Tsang, K. Y.; Diaz, H.; Graciani, N.; Kelly, J. W. *J. Am. Chem. Soc.*, **1994**, *116*, 3988. (c) Fuller, A. A.; Du, D.; Liu, F.; Davoren, J. E.; Kroon, G.; Powers, E. T.; Wipf, P.; Gruebele, M.; Kelly, J. W. *Proc. Natl. Acad. Sci.* **2009**, *106*, 11067. (d) Fujii, A.; Hirota, S.; Matsuo, T. *Bioconjugate Chem*. **2013**, *24*, 1218. (e) Fujii, A.; Sekiguchi, Y.; Matsumura, H.; Inoue, T.; Chung, W. –S.; Hirota, S.; Matsuo, T.; *Bioconjugate Chem*. **2015**, *26*, 537.

18. Oh, K.; Guan, Z. *Chem. Commun*. **2006**, 3069.
19. Kessler, H. *Angew. Chem., Int. Ed. Engl.* **1982**, *21*, 512.

5.1. Introduction

Molecular design that mimic the structure, conformation of proteins or active site of an enzyme are very much effective to show interaction with biomolecules and thus biological activity or can be utilized as probe of biophysical study. As for an example, the bacterial transpeptidase enzyme recognizes D-Ala–D-Ala peptide sequence for the bacterial cell wall biosynthesis known as the transpeptidation that crosslinks the peptide side chains of peptidoglycan strands providing the protection to bacteria.[1] The β-lactam core is structurally similar to D-Ala–D-Ala terminus of peptidoglycan terminus. Therefore the β-lactam antibiotics such as penicillins are being misrecognized by bacterial transpeptidases for the TPase catalytic reaction, thereby irreversibly inhibit the enzyme and stopping the bacterial cell wall synthesis required for bacterial survival. Thus, penicillin irreversibly binds to and inhibits the activity of the transpeptidase enzyme by forming a highly stable penicilloyl-enzyme intermediate. Because of the interaction between penicillin and transpeptidase, this enzyme is also known as penicillin-binding protein (PBP). The potent antibacterial activity by β-lactams helped control not only the spread of life-threatening illness, but have also prevented the onset of opportunistic infections in immune-deficient patients.[2,3] About 60% of the worldwide sales of antibacterial substances can be allocated to the β-lactam antibiotics and it can be estimated that β-lactam antibiotics account for about 10% of the total sale of drugs. However, the emergence of various resistant strains of pathogens, such as β-lactamases. Therefore combating with β-lactamases really need the newer design and synthesis of β-lactam which will either be inhibitor or can stop activity of lactamases covalently.

Now a day fluorescent β-lactams also serves as an important role in biological and medicinal chemistry. It is demonstrated that fluorescent β-lactams can serve as a sensitive fluorogenic reporter for imaging Tetrahymena ribozyme activity in living cells.[4] Fluorescent labeled β-lactam represents a successful model in the construction of "switch-on" fluorescent biosensor.[5] And also it is also explored that fluorescent β-lactams are used to block bacterial growth by generating reactive oxygen species (ROS).[6]

The development of efficient β-lactam antibiotics with novel, sensitive and rapid detection method for monitoring β-lactamase activity is currently an active research area to combat with bacterial resistance. Modification of the N-acyl side chain and attaching a membrane-penetrating functionality may leads to a design of modified penicillin which can be good antibiotics for bacterial resistance. Though there are few reports of modified penicillins, but they are still prone to hydrolysis by β-lactamases demanding newer design concept. Furthermore, though a number of fluorescent probes have been reported for the detection of the activity of β-lactamases however,

most probes lack specificity or need help of other inhibitors. Given the challenges, the development of new β-lactam antibiotics as well as methodologies that can provide rapid information on bacterial resistance and/or antibiotic susceptibility would be valuable.

There are some factors in the β-lactam ring structure which are responsible for their antibacterial activities.[6] Thus many kind of β-lactams were synthesized with different N3 moiety to show large antibacterial spectrum. As 4-Alkyliden-azetidin-2-ones were synthesized that shows in vitro antibacterial activity and was evaluated against 43 recent clinical isolates of antibiotic-susceptible and resistant Gram-positive and Gram-negative pathogens (**5.01**-**5.05**, **Figure 5.1**).[7]

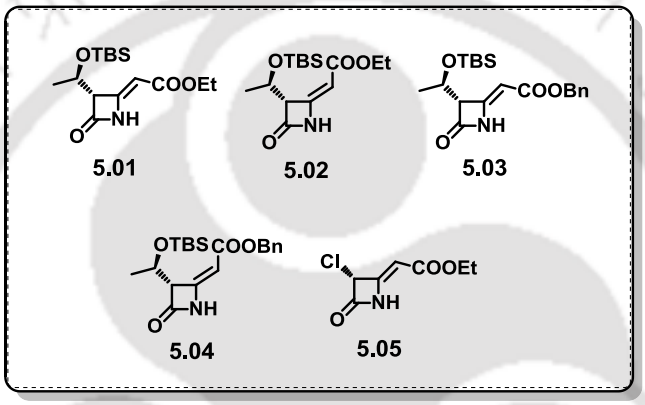

Figure 5.1. Structures of 4-Alkyliden β-lactams (**5.01**-**5.05**).[7]

Owing to the above concept and based on structure activity relationship study several β-lactam analogs have been designed by modification of the N-acyl side chain which showed superior antibacterial activity (**5.06**-**5.11**, **Figure 5.2**).[8–10]

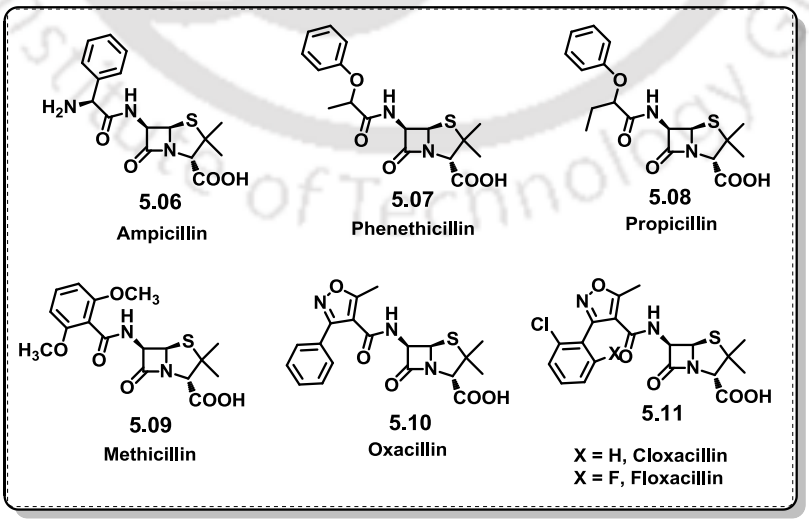

Figure 5.2. The structure of some acid- resistant and β-lactamase-resistant penicillins (**5.06**-**5.11**).[8-10]

Thus, recent studies have shown that the attachment of functional groups, such as incorporation of structural feature like peptidoglycan, in place of N-acyl side chain could result the Penicillin binding protein (PBP) specific β-lactams and cephalosporins.[11] Penicillin binding proteins can also tolerate a variety of non-amide groups at the C-6 and C-7 positions of penicillins and cephalosporins.[12] Some of these non-amide β-lactam analogs (**5.12-5.14**, **Figure 5.3**) possessing potent antibacterial activity, have shown differential affinity for PBP isoforms.

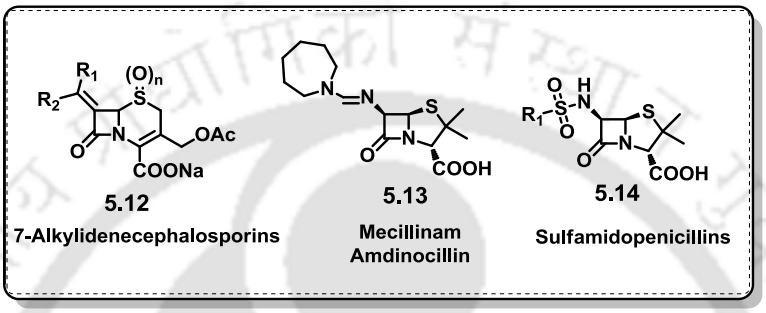

Figure 5.3. Structure of amide isosteric β-lactams (**5.12-5.14**).[12]

5.1.1. β-lactam reactivity and biological activity

The remarkable antibacterial and chemical activity of penicillin molecule is due to the fusion of the β-lactam ring with the thiazolidine ring. The strain, which is developed due to the fusion of the five-membered thiazolidine ring and four-membered β-lactam ring leads to non-planarity of the molecule which results in a large angle and torsional rotation.[13,14] These factors make the penicillin molecule labile to any kind of nucleophilic attack and susceptible to degrade in the presence of acid, alkali or even neutral molecules like water and alcohol. But the strain is somewhat released via delocalization of the lone pair of electrons on the adjoining N-atom with the C=O group. This greater instability of penicillin molecule was mainly responsible for hindering early progress and development of the chemistry and biology of penicillins.

In 1958, Sheehan *et al*. have reported the procedure for the synthesis of natural penicillin V starting from t-butyl phthalimido malonaldehydate (**5.14**) and D and DL–penicillamine (**5.15-5.20**, **Scheme 5.1**).[15] As a result they got crystalline DL-penicillin V, which was resolved to give L-penicillin V having less than 1% of the bioactivity of the natural enantiomer. This methodology has a broad application to produce efficiently the natural penicillin V and also it shows the path to prepare other modified penicillins.

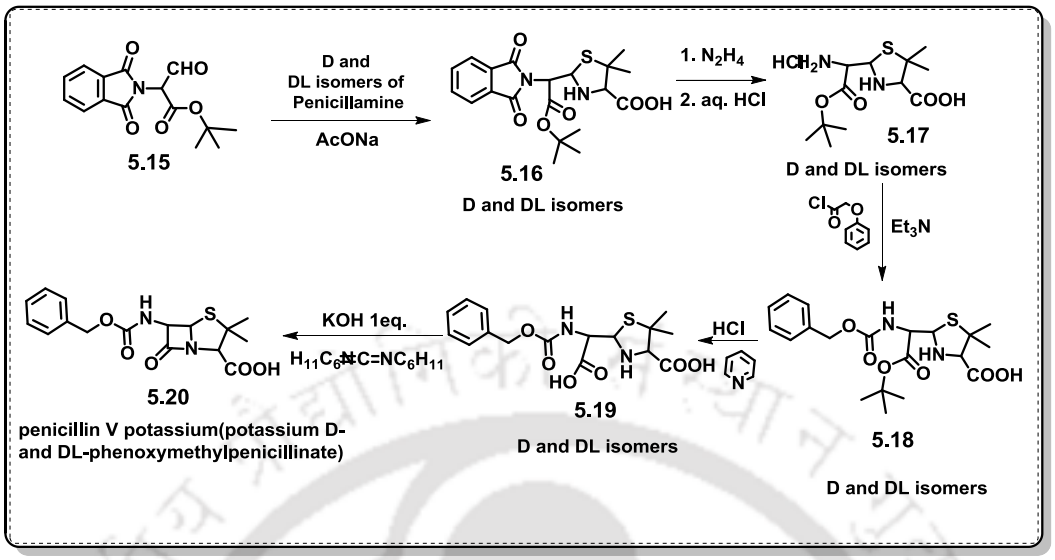

Scheme 5.1. Synthesis of natural penicillin V from phthalimido malonaldehydate (**5.15-5.20**).[15]

The modification at position C6 and C7 of penicillin and C7 and C3 in cephalosporin nucleus have resulted in providing hundreds of novel cephalosporin analogues with better antibacterial activity. A few lakhs of semisynthetic penicillins and cephalosporins were thus prepared for obtaining more potent and useful drugs, but only a few of them have gained prominence in the present antibacterial market in their own right. The search for newer β-lactams has reached to a point where there is availability of a wide range of antibacterial drugs. The medicinal chemists and microbiologist are still seeking new and improved antibacterial agents.[16]

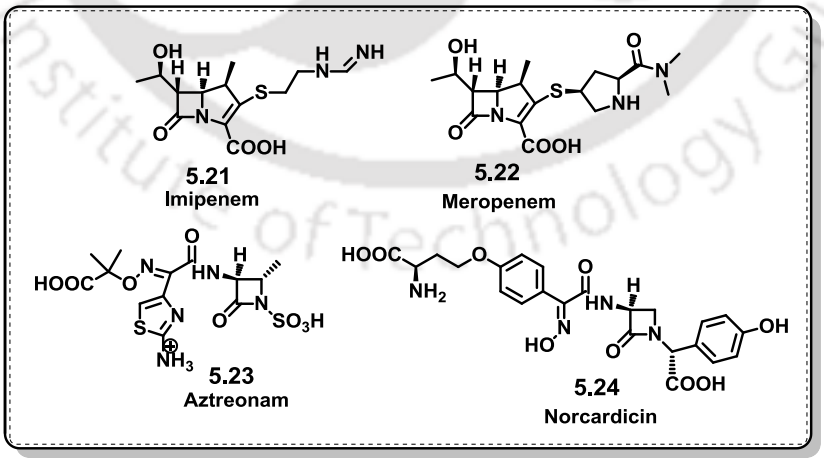

Figure 5.4. Some non-classical β-lactam antibiotics (**5.21-5.24**).[16]

The progress in search for new β-lactams remained same till the end of 1980 with success. Thus some non-classical β-lactams like Imipenem, Meropenem, Aztreonam,

Norcardicin (**5.21-5.24**, **Figure 5.4**) with broad-spectrum activity against certain key pathogens, e.g. P. aeruginosa and/or MRSA with improved pharmacokinetic properties has been discovered.

5.1.2. Why fluorescent β-lactams?

The β-lactam antibiotics, which are a major class of antimicrobial agents to treat bacterial infection in clinics but, the overuse of these antibiotics has resulted in a large number of bacteria with β-lactamases. Fluorescent β-lactams also serves as an important role in biological and medicinal chemistry. It is demonstrated that fluorescent β-lactams can serve as a sensitive fluorogenic reporter for imaging Tetrahymena ribozyme activity in live cells. Fluorescent labeled β-lactam represents a successful model in the construction of "switch-on" fluorescent biosensor. Moreover, it has been explored that fluorescent β-lactams could block bacterial growth by generating reactive oxygen species (ROS). Photodynamic therapy (PDT) is a promising option for generating reactive oxygen species (ROS). PDT is a photochemistry-based technology that relies on the wavelength specific light activation of certain nontoxic photosensitizers (PSs) to produce active molecular species that are toxic to targeted biomolecules/compounds.[17] PSs have been conjugated to antibodies or peptides for the treatment of bacterial infections, but the inter or intracellular targets are large, and labeling of antibodies or peptides with photosensitizers is experimentally challenging.[18] Therefore, developing the specific compounds with photosensitizing activity is very necessary. Xing and co-workers reported a simple and specific conjugation of vancomycine porphyrins to use for fluorescent imaging and antibacterial studies on VRE.

In 2011 Shi *et al.* have reported a novel fluorescent compound which is a unique conjugation of norvancomycin− fluorescein (VanF) for photo inactivation of Bacillus subtilis. The compound was characterized by UV-vis and fluorescence spectroscopy and confirmed by MALDI-TOF mass spectrometry. The photodynamic assay of norvancomycin-fluorescein (**5.25**) indicated that **5.25** effectively inactivated the Gram-positive Bacillus subtilis from clinic with inactivation rate of 30-70% within 1−7.5 μM (**5.25-5.27**, **Figure 5.5**).[19]

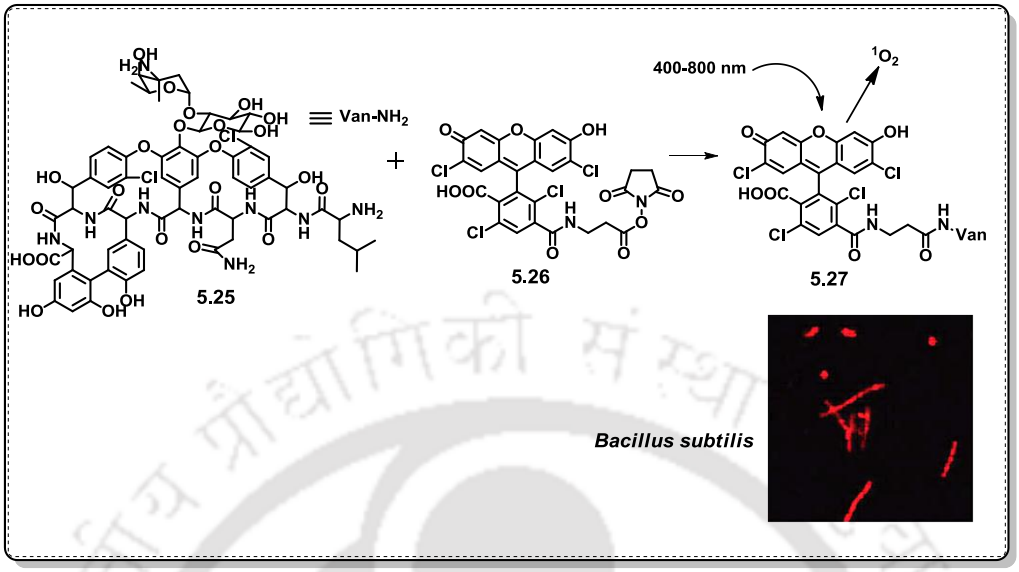

Figure 5.5. Fluorescent imaging of *Bacillus subtilis* labeled with VanH (**5.25-5.27**).[19]

Two fluorescent cephalosporins have been reported by Yang *et.al*. which has been utilized to block bacterial growth by generating reactive oxygen species (ROS).[20]

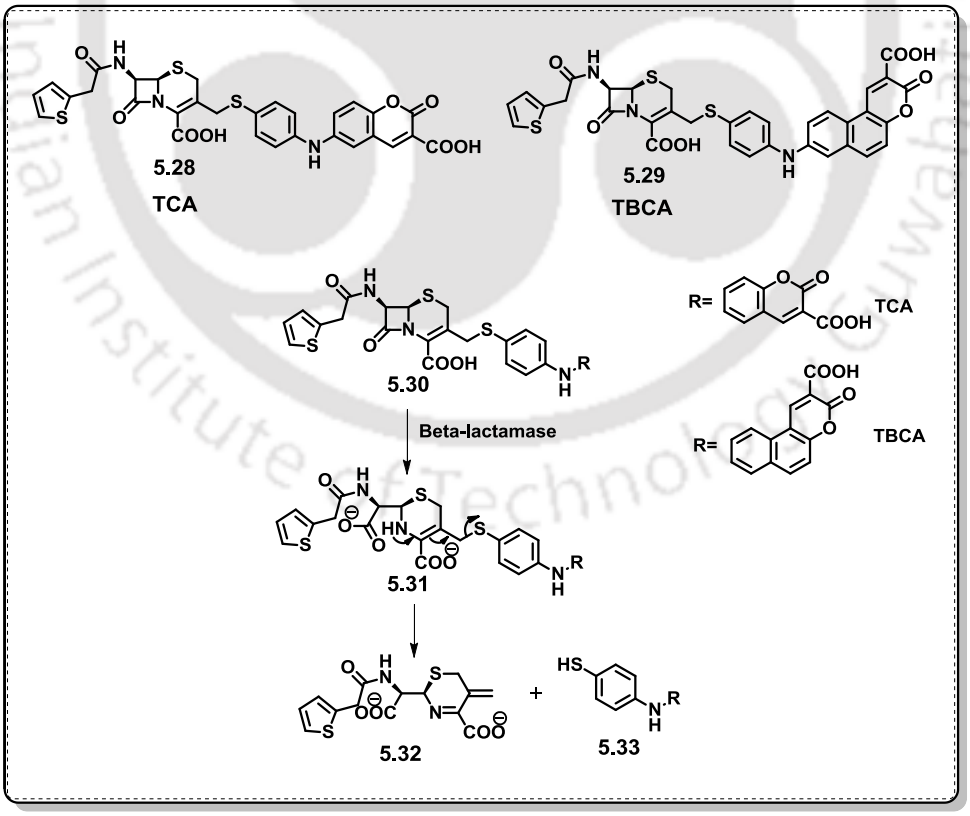

Figure 5.6. Hydrolysis of the fluorescent cephalosporins (TCA. **5.28** and TBCA **5.29**) with β-lactamases (**5.30-5.33**).[20]

They have synthesized two fluorescent cephalosporins, TCA and TBCA (**5.28** and **5.29**) which were characterized by ^{1}H, ^{13}C NMR, UV, and fluorescence spectroscopy. From a biological activity assay it has been demonstrated that TCA inactivate a Klebsiella pneumonia strain that expressed extended-spectrum β-lactamases (**5.30-5.33**, **Figure 5.6**). Incubation of 6 mM TCA with K. pneumonia cultures resulted in cell death for 84% of the cells. In vitro, TCA exhibited a MIC ¼ 0.5 mg/mL with Staphylococcus aureus. TBCA exhibited stronger binding affinities to a Gram-positive bacterial strain.

In 2008 Wong *et al*. have reported fluorescein-labeled E166C mutant of the PenPC -lactamase (**5.36**) which represents a successful model in the construction of "switch-on" fluorescent biosensors from nonallosteric proteins (**5.38-5.39**, **Figure 5.7**). The E166Cf biosensor changes its fluorescence upon-lactam binding and hydrolysis. When an enzyme-substrate complex is formed, it enhances the fluorescence of E166Cf (**5.37**). Upon regeneration of the free enzyme the restoration of the weak fluorescence of E166Cf is the result. These phenomena have been studied utilising mass spectrometry and stopped-flow fluorescence spectroscopy of E166Cf with cefuroxime, penicillin G, and 6-aminopenicillanic acid (**5.34-5.36**, **Figure 5.7**).[21]

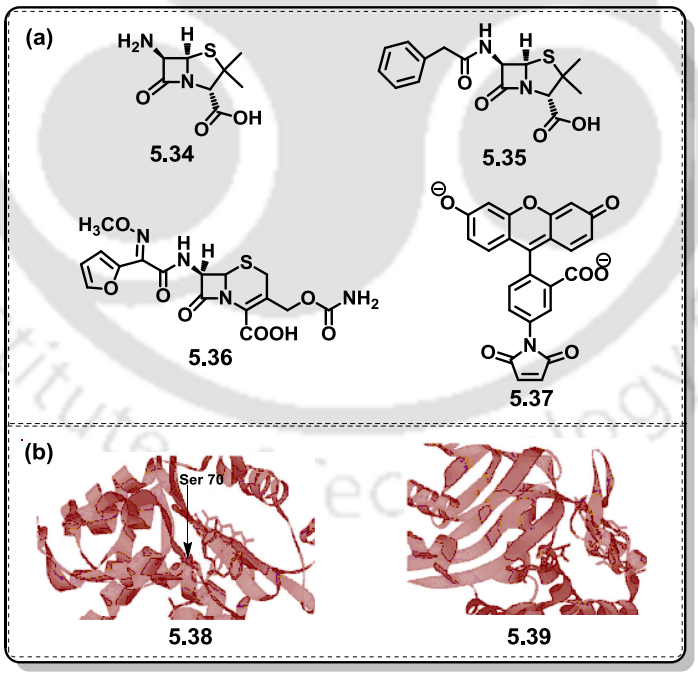

Figure 5.7. (a) Structures of the β-lactam antibiotics (**5.34, 5.35** and **5.36**) and fluorescein-5-maleimide (E166C, **5.37**). (b) Molecular models of E166Cf with penicillin G (**5.38** and **5.39**). [21]

Rao *et al*. have synthesized a new class of small nonfluorescent fluorogenic substrates (**5.40**, **Figure 5.8**) which becomes brightly fluorescent after β-lactamase hydrolysis with up to 153-fold enhancement in the fluorescence intensity (**5.41-5.42**, **Figure 5.8)**. By this phenomena less than 500 fM of β-lactamase in cell lysates can be readily detected, and β-lactamase expression in living cells can imaged with red fluorescence (**Figure 5.8**). These newly synthesized fluorogenic substrates should be useful in clinical diagnostics and facilitate the applications of β-lactam as a biosensor.[22]

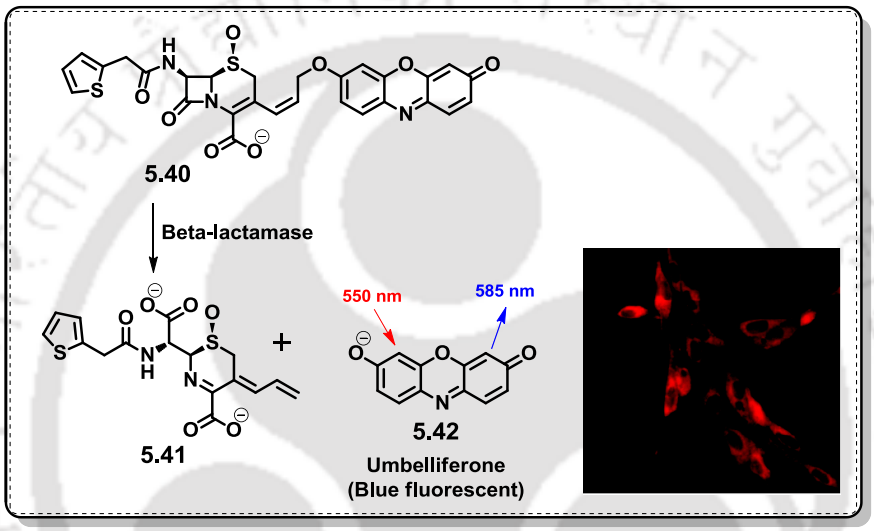

Figure 5.8. Synthesized β-lactams before (**5.40**) and after (**5.41, 5.42**) β-lactamase treatment and fluorescence images of Bla-stably transfected C6 glioma cells loaded with compound **5.40** at room temperature.[22]

5.1.3. Degradation of β-lactams

Penicillin contains unstable, highly strained and reactive 4-membered lactam ring. The degradation of penicillin may takes place in alkaline or acidic condition, in the presence of enzyme β-lactamase or treatment of weak nucleophiles like water, alcohol and metal ions. The strained bicyclic system in penicillin is supposed to remain in equilibrium with pseudopenicillin (**5.46**) under neutral condition which undergoes further isomerization to penicillenicic acid (**5.49**) which can be characterized by its strong UV absorption at 322 nm. The highly strained β-lactam ring and its lactam bond breaks in the presence of acid (**5.43-5.47**, **Scheme 5.2**)[23,24] giving an array of complex products, including penilloic acid, penicillamine and penilloaldehyde through the highly unstable intermediate. Penicilloic acid (**5.48**) exists in its isomeric form, i.e. penamaldic acid (**5.50**) which has been characterized by its UV peak around 320 nm under strong acid condition. It may also undergo ready decarboxylation to

give penilloic acid (**5.44**). In strong acidic medium (pH 2 or less), it undergoes rearrangement through oxazoline formation giving rise to penillic acid (**5.47**).[25] It was thought to protect the degradation of penicillins under acidic conditions by putting some electron-withdrawing groups in the α-position of the N-acyl side chain.

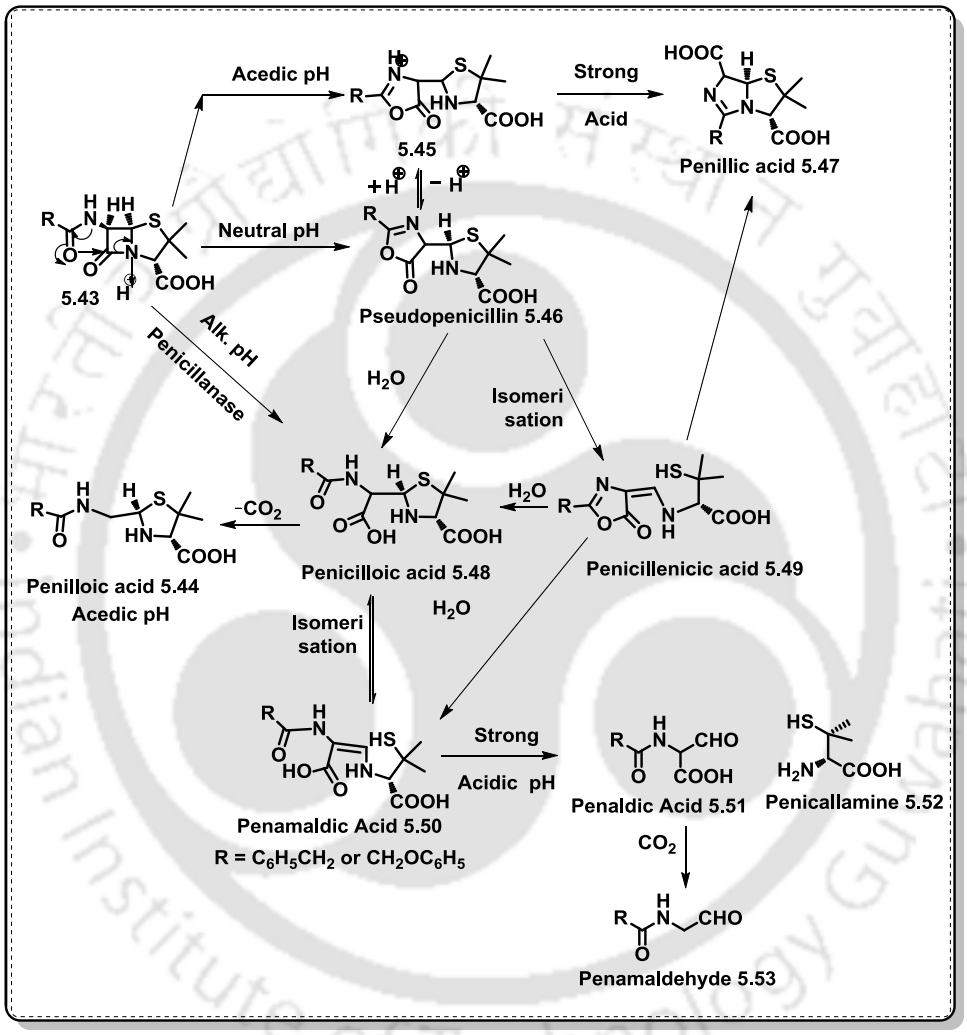

Scheme 5.2. Pathways of degradation of penicillin in acidic and alkaline conditions (**5.43-5.53**).[16]

The instability of penicillin is due to β-lactam carbonyl group and acyl side chain that undergo neighbouring group participation leading to opening of β-lactam ring. Thus penicillin always suffers from in-built self-destructing mechanism (**5.43-5.55**, **Scheme 5.3**).

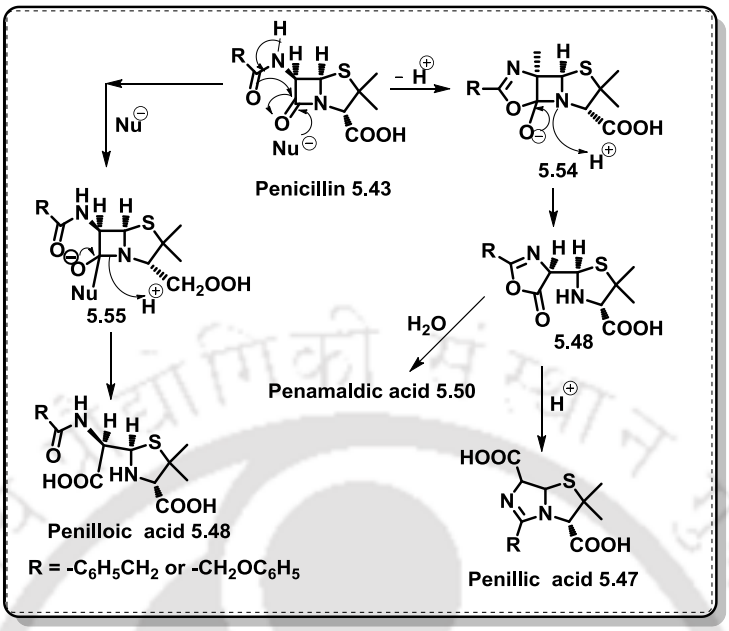

Scheme 5.3. Nucleophilic ring opening and acid sensitivity of penicillin due to the influence of N-acyl side chain (**5.43-5.55**).[25]

Liu *et al*. have synthesized a new class of thiazolidine amides that are produced through N4-C7 β-lactam ring opening of penicillin V methyl ester (**5.57**) with various aliphatic, aromatic, and heterocyclic primary amines (**5.58-5.63**, **Scheme 5.4**).[27]

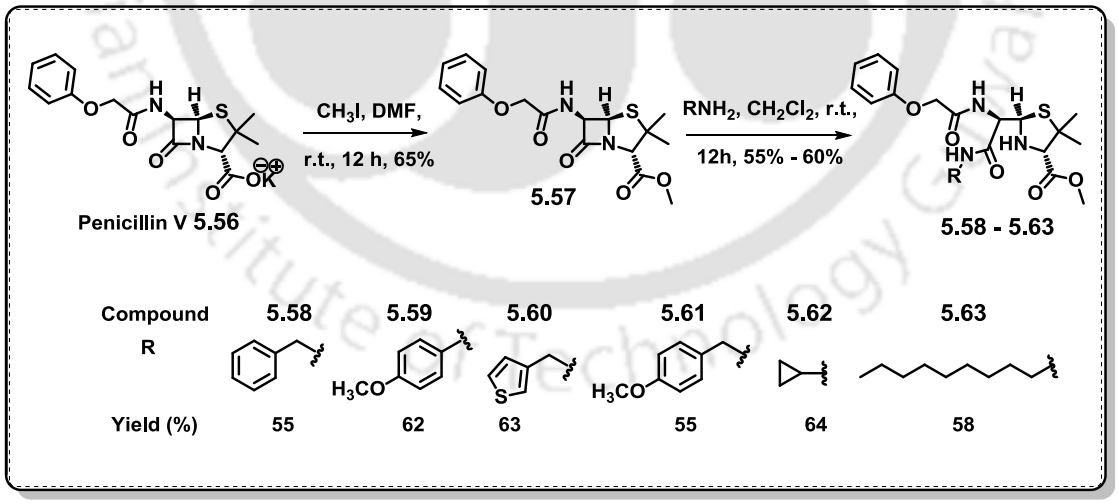

Scheme 5.4. Ring opening of β-lactams of penicillin V methyl ester (**5.56-5.63**).[27]

Styring *et al*. have synthesized amides derived from penicillin V by opening of β-lactam ring using benzyl amine as nucleophile (**5.64-5.67**, **Scheme 5.5a**). Coupling with racemic (R/S)-2-aminobutanol **5.68** shows significantly higher toxicity than the pure diastereomers prepared from homochiral 2-aminobutanol which has been

attributed to conformational changes in the resolved product that has been brought through hydrogen-bonded self-assembly in the intermediate (**5.68**, **Scheme 5.5b**).[26]

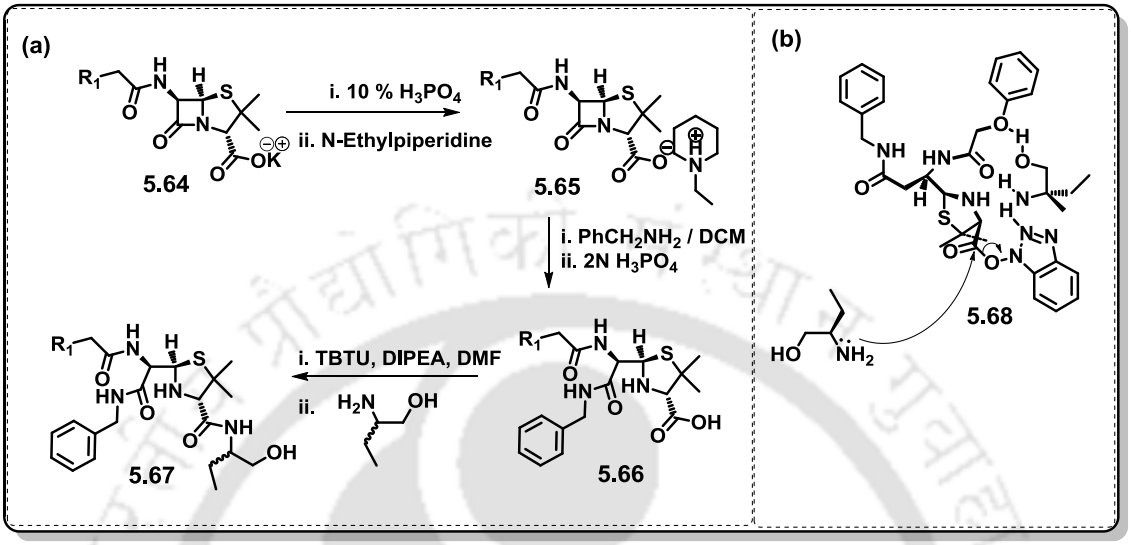

Scheme 5.5. (a) General scheme for the synthesis of amides through nucleophilic ring opening of penicillin V (**5.64-5.67**). (b) Nucleophilic attack of (R)-2-aminobutanol at the activated ester of the self-assembled intermediate showing 'bound' (S)-2-aminobutanol (**5.68**).[26]

5.2. Background

The development of efficient β-lactam antibiotics with novel, sensitive and rapid detection method for monitoring β-lactamase activity is currently an active research area to combat with bacterial resistance. Modification of the N-acyl side chain and attaching a membrane-penetrating functionality may leads to a design of modified peniciline which can be good antibiotics for bacterial resistance. Nevertheless, though there are few reports of modified penicilines, they are still prone to hydrolysis by β-lactamases demanding newer design concept. Furthermore, though a number of fluorescent probes have been reported for the detection of the activity of β-lactamases, most probes lack specificity or need help of other inhibitors. Given the challenges, the development of new β-lactam antibiotics as well as methodologies that can provide rapid information on bacterial resistance and/or antibiotic susceptibility would be valuable.

5.3. Objective

The growing demand of newer β-lactam and β-lactamase assay inspired us to take a project on the generation of fluorescent β-lactams, particularly triazolyl donor/acceptor chromophore decorated fluorescent penicillanic acids.

The logics behind choosing triazole hybrid into β-lactam are-

(a) Triazoles are metabolically inert, the mimic of trans amide bond,

(b) They can easily get associated with biomolecular/biological targets via H-bonding and

(c) Triazoles show a wide range of biological activities such as antibacterial, herbicidal, fungicidal, antiallergic, and anti-HIV.

Therefore, we planned to replace the acid sensitive N-6 acyl bond of penicilin with a triazole ring containing donor/acceptor aromatics. The electron charge density at C-3 of β-lactam core may influence the electrophilicity of lactam carbonyl against the nucleophilic attack. Moreover, the triazole ring can facilitate cell permeability for β-lactams into bacterial cell if conjugated with cell penetrating groups. We envisaged that replacing the N-6 acyl unit by triazole would modulate the fluorescence property of the attached donor-acceptor aromatics as well as would render stabile electronic property onto the lactam ring.[21] The susceptibility of modified β-lactam ring towards cleavage with a fluorogenic hydroxyl or amines as nucleophile is facile. The ring cleavage was then be signaled by a new fluorescence property at higher wave length region by virtue of a photophysical interaction among the two fluorophores in the ring-opened form. Thus, a rapid and highly sensitive fluorescence based method could be achieved for assessing activity of β-lactam antibiotics in presence of a fluorogenic nucleophile. The initial fluorescent β-lactam would act as a model fluorescent molecular probe which might be utilised for monitoring the antibiotic susceptibility.

After nucleophilic ring opening with pyrenyl amine, the two fluorophores come close together resulting in a dipolar photophysical/π-π-stacking interaction in the excited state. Thus, in hetero-chromophoric pair wherein the chromophore in probe is β-lactam and that in the incoming nucleophile are different, leads to FRET emission or π-π-stacking interaction leading to exciplex emission or both. On the other hand, if the second chromophore in the nucleophile is same as in the probe β-lactam, results a homo-chromophoric system after ring cleavage and would lead to the formation π-π-stacked complexation and corresponds to excimer emission. This model can be utilized to monitor fluorimetrically the β-lactamase resistance and β-lactam antibiotic activity. Such assay system in real enzymatic world would be more beneficial as the read-out for the assay is optical rather than bacterial viability or based on growth of bacteria.

With this concept, we aimed to

(a) generate triazolyl fluorescent β-lactams and

(b) investigate the change in photophysical proterty upon chemical clevage which could be treated as a complentary model to study the susceptibility of β-lactam antibiotics.

In our design the N-5 acyl unit was replaced by triazolyl donor-acceptor aromatics as a source of stability as well as fluorescence property. The β-lactam ring was attempted to cleave with fluorogenic amines as nucleophiles. We targeted two fluorescent β-lactams-one with triazolylmethoxynaphthyl (**TMNap**) and other with triazolylpyrene (**TPy**) chromophore for the model ring opening by a fluorogenic nucleophile, namely, aminomethylpyrene (**AMePy**). Thus, upon ring cleavage we observed FRET as well as exciplex and established dual mechanism for exciplex emission in the β-lactams with triazolylmethoxynaphthalene (^{TMNap}**β-Lac**^{Do}) and an excimer emission in triazolylpyrene (^{TPy}**β-Lac**^{Do}) containg β-lactam (**Figure 5.9**). These two systems are models and might help in designing such system to use in real enezyme world.

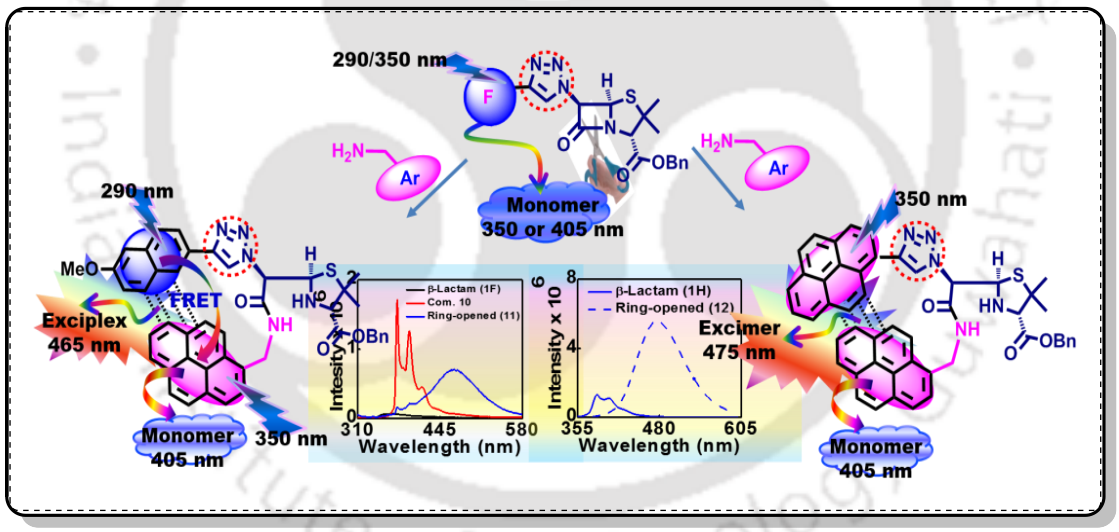

Figure 5.9. Schematics of fluorescence discrimination of fluorescent triazolyl β-lactam from the ring opened form.

5.4. Result and Discussion

5.4.1. Synthesis of Triazolyl Donor/Acceptor β-Lactams

The synthesis of the triazolyl β-lactams started with 6-aminopenicillanic acid (**5.69**), the amino functionality of which was converted to azide (**5.74**) following a modified literature protocol (**Scheme 5.6**). First of all the 6-aminopenicillanic acid (**5.69**) was converted to *N*,*C*- diprotected penicillanic acid **5.71** in good yield. Next, the 6-amino penicillanic-3-benzyl carboxylate ester **5.72** was obtained via deprotection of 6-*N*-protecting group with *p*-toluene sulphonic acid and subsequent neutralization of PTSA salt **5.72** with $NaHCO_3$ in water. Ultimately, the free 6-amino group of **5.73** was converted to azide via diazo-transfer reaction with triflyl azide in toluene to afford only azide **5.74** in very good yield (**Scheme 5.6**). All the intermediates and the azide were purified by silica gel column chromatography and were well characterized by NMR and mass spectrometry.

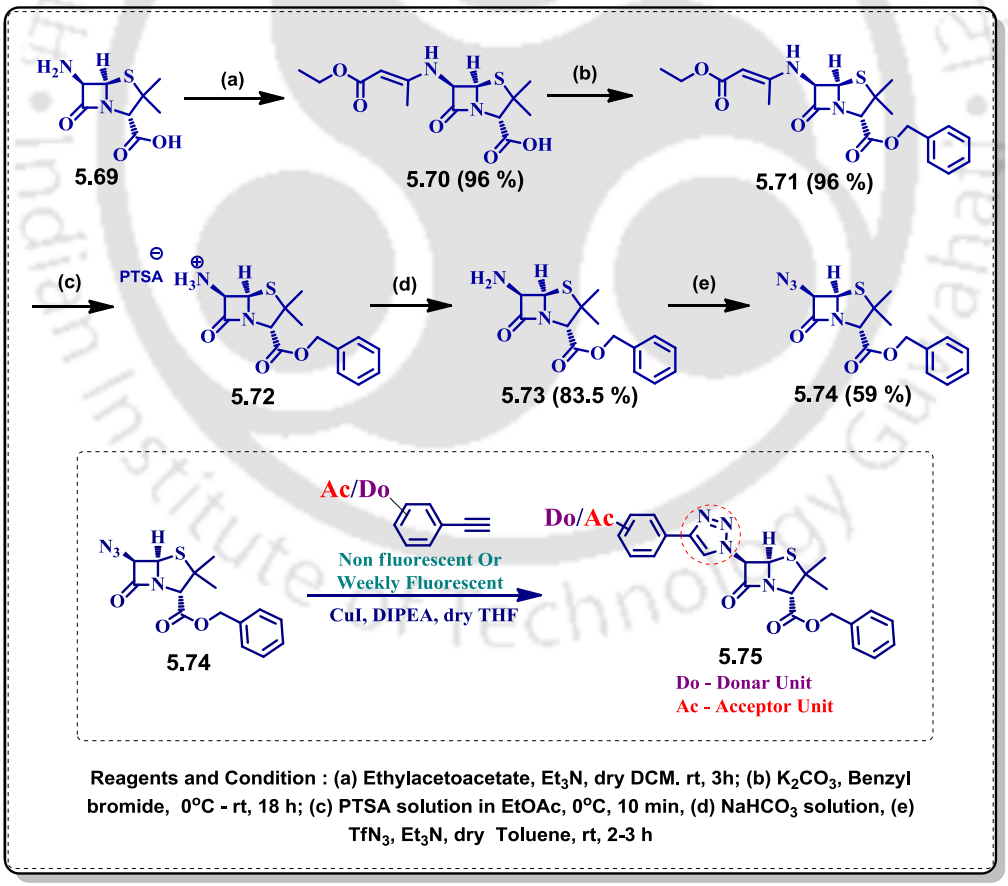

Scheme 5.6. Synthetic scheme for the synthesis of Benzyl Protected Azido Penicillin and (3+2) π cycloaddition reaction between benzyl protected 6-azidopenicillin and various donor and acceptor alkynes.

The azido transfer reaction occurred with retention of configuration which was supported by the β-orientation of the azide group in **5.74** as was revealed from coupling constant value from ^{1}H NMR ($J_{5,6}$ = 4.0 Hz).[11] After getting the 6-azido penicillanic-3-benzyl carboxylate ester **5.74** in pure form various alkynes of donor/acceptor substituted aromatics and polyaromatic hydrocarbons were subjected to react with **5.74** under click reaction condition to obtain the desired designed 6-(donor/acceptor aromatic substituted) triazolyl-penicillanic-3-benzyl carboxylates **5.76-5.87** in very good to excellent yields (**Scheme 5.6** and **Figure 5.10**) and were characterized by NMR and mass spectrometry.

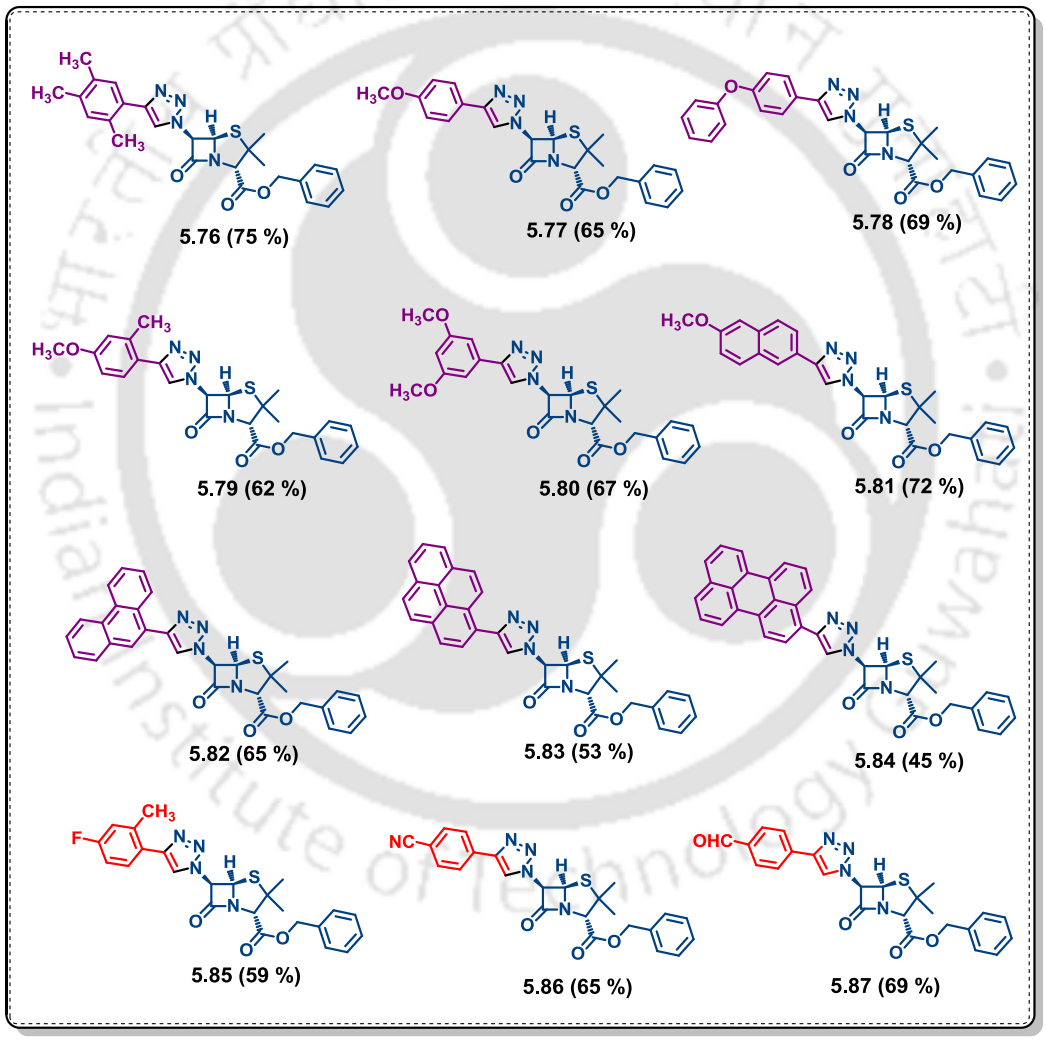

Figure 5.10. Structures of synthesized β-lactam compounds.

After synthesizing all the β-lactam compounds, we have chosen two of them for ring opening with alkyl (Benzyl/ Pyrinyl) amine (**Scheme 5.7**). The photophysical property of the ring opened compound was explored.

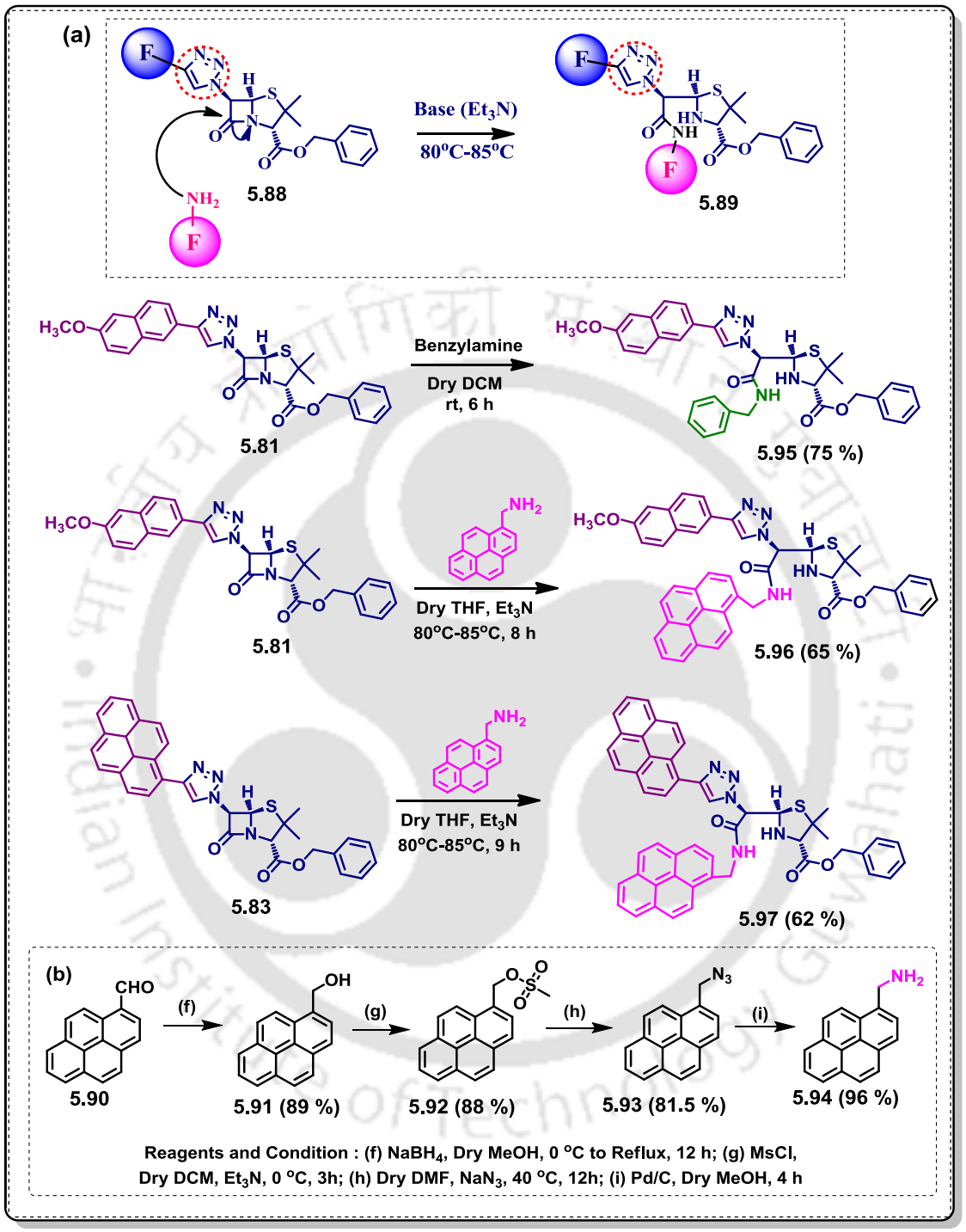

Scheme 5.7: (a) Scheme for ring opening of β-lactam by Benzyl/Pyrinyl amine (b) Scheme for synthesis of Pyren-1-yl methanamine (**AMePy, 5.94**).

All the synthesized modified β-lactams and ring opened compounds were purified by column chromatography and characterized by NMR and HRMS analysis. Assignments are given in the experimental section.

5.4.2. Study of photophysical properties

After characterization of all the β-lactam compounds, we have studied their photophysical properties in organic solvents of different polarities to check their solvatochromic nature. The UV–visible spectra were recorded in a UV-visible spectrophotometer with a cell of 1 cm path length at 25 ^{o}C and 1 nm slit width with freshly prepared sample having concentration 10 µM. Fluorescence emission spectra were recorded in a fluorescence spectrophotometer using a cell of 1 cm path length and 2/5 nm excitation/emission slit width at 25 ^{o}C. To record the emission spectra, excitation wavelengths were set at maximum wavelength of absorbance (λ_{max}^{abs}) in each case. The fluorescence quantum yield (Φ_f) was determined using quinine sulphate / perylene as a reference with the known Φ_f = 0.54 respectively, in 0.1 molar solution in sulphuric acid / hexane.

The β-lactam **5.76** (**Benzyl 2, 4, 5-trimethylphenyl-6-triazolylpenicillanate**) containing 2, 4, 5-trimethylphenyl donor aromatic unit showed two absorption bands at around 245 and 281 nm with no solvatochromicity in organic solvents tested. Upon excitation at the absorption maxima, it showed broad emission at around 360 nm which red shifted about 61 nm from nonpolar dioxane to polar protic MeOH solvent. Quantum yield also follows the same sequence as steady state fluorescence for β-lactam **5.76** (**Figure 5.12, Table 5.1**).

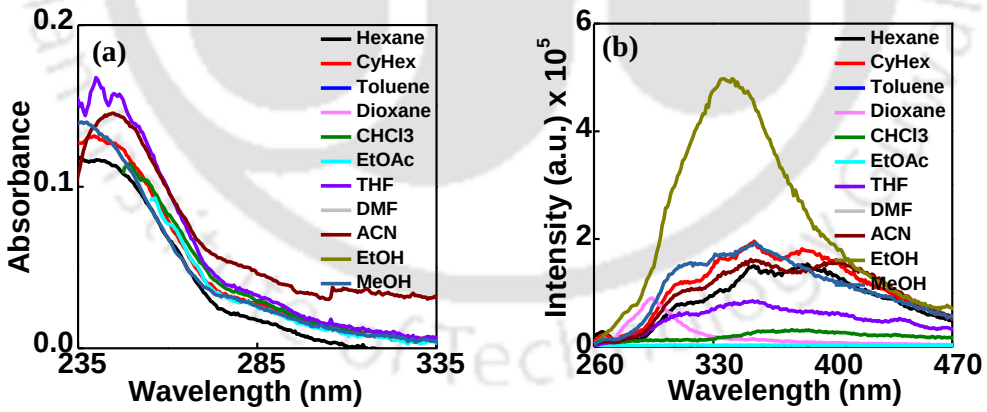

Figure 5.12. (a) UV-visible absorption, (b) fluorescence emission spectra of **Benzyl 2, 4, 5-trimethylphenyl-6-triazolylpenicillanate** in various organic solvents. Excitation wavelength was the λ_{max}^{abs} in each solvent and the concentration of each β-lactam was 10 µM.

Table 5.1. Summary of photophysical properties of β-lactam **5.76** (**Benzyl 2, 4, 5-trimethylphenyl-6-triazolylpenicillanate**)

Entry →	**5.76 (Benzyl 2, 4, 5-trimethylphenyl-6-triazolylpenicillanate)**							
Solvents →	**CyHex**	**Diox.**	**$CHCl_3$**	**EtOAc**	**THF**	**DMF**	**ACN**	**MeOH**
λ_{max}^{abs} **(nm)**	292	---	281	281	281	281	281	281
$\varepsilon_{max\ X}\ 10^3$	1.1	--	3.4	2.8	3.6	2.55	5	2.9
λ_{max}^{fl} **(nm)**	302	294	361	365	354	357	353	355
Φ_f	0.001	0.003	0.0055	0.0038	0.008	0.0035	0.023	0.021

The β-lactam **5.77** (**Benzyl 4-methoxyphenyl-6-triazolylpenicillanate**) containing 4-methoxyphenyl aromatic donor unit exhibited a structure-less broad absorption at around 256 nm with almost no shift in wavelength as the polarity of the solvent increases. Upon excitation at its absorption maxima the β-lactam **5.77** showed an emission band at around 290 nm in nonpolar solvents like hexane and toluene, which was red shifted in polar solvents. The emission band showed a red shift about 67 nm from nonpolar cyclohexane to polar THF solvent with a high intensity in polar solvents like Acetonitrile, Ethanol and DMF. Quantum yield also follows the same sequence as steady state fluorescence in β-lactam **5.77** (**Figure 5.13, Table 5.2**).

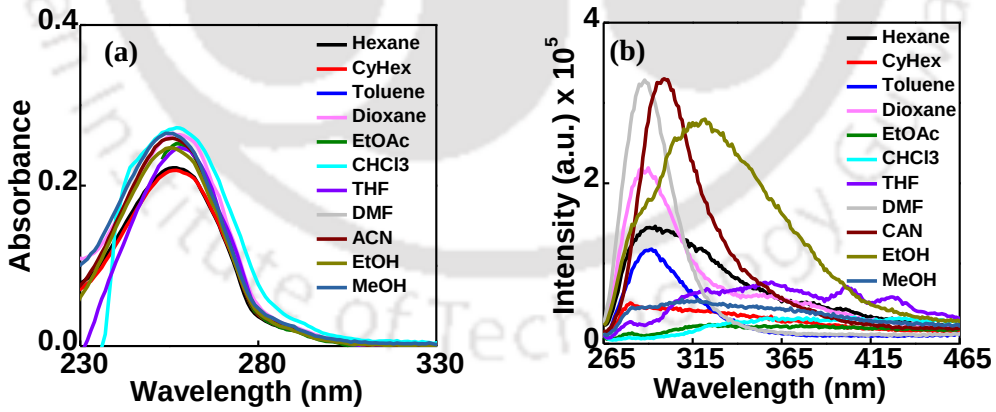

Figure 5.13. (a) UV-visible absorption, (b) fluorescence emission spectra of **Benzyl 4-methoxyphenyl-6-triazolylpenicillanate** in various organic solvents. Excitation wavelength was the λ_{max}^{abs} in each solvent and the concentration of each β-lactams was 10 μM.

Table 5.2. Summary of photophysical properties of β-lactams **5.77** (**Benzyl 4-methoxyphenyl-6-triazolyl penicillanate**)

Entry →	**5.77 (Benzyl 4-methoxyphenyl-6-triazolylpenicillanate)**							
Solvents →	**CyHex**	**Diox.**	**$CHCl_3$**	**EtOAc**	**THF**	**DMF**	**ACN**	**MeOH**
λ_{max}^{abs} **(nm)**	256	256	257	256	257	256	256	255
ε_{max} $x\ 10^3$	21.8	26.5	24.9	27.0	24.3	21.7	25.9	26.5
λ_{max}^{fl} **(nm)**	280	319	357	318	357	287	299	307
Φ_f	0.004	0.01	0.004	0.003	0.007	0.009	0.013	0.005

The **Benzyl-4-phenoxyphenyl-6-triazolylpenicillanate** β-lactam (**5.78**) containing 4-phenoxyphenyl donor aromatic unit showed broad and strong absorption band at around 257 nm with no solvatochromicity in all organic solvents tested. When excited at its absorption maxima, it exhibited a strong emission band at around 288 nm in nonpolar solvents and was red shifted about 32 nm as the polarity of the solvent increases (from nonpolar hexane to polar protic MeOH). Quantum yield also follows the same trend as steady state fluorescence in β-lactam **5.78** (**Figure 5.14, Table 5.3**).

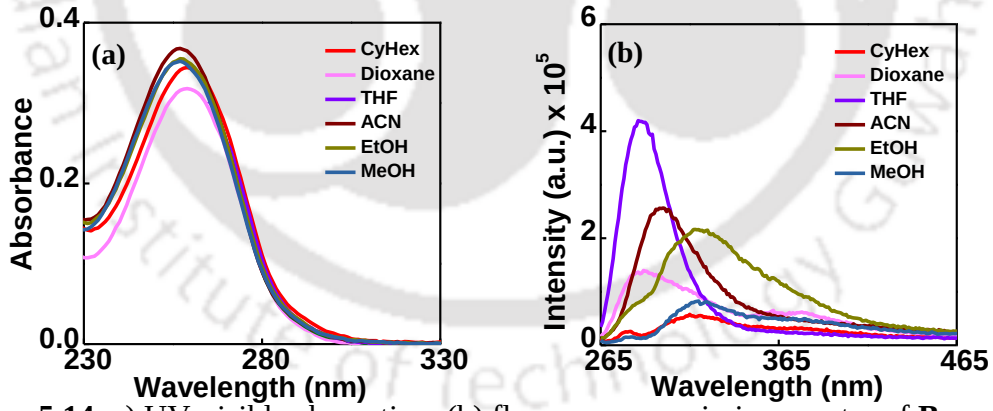

Figure 5.14. a) UV-visible absorption, (b) fluorescence emission spectra of **Benzyl-4-phenoxyphenyl-6-triazolylpenicillanate** in various organic solvents. Excitation wavelength was the λ_{max}^{abs} in each solvent and the concentration of each β-lactam was 10 μM.

Table 5.3. Summary of photophysical properties of β-lactam **5.78** (**Benzyl-4-phenoxyphenyl-6-triazolylpenicillanate**).

Entry →	**5.78 (Benzyl-4-phenoxyphenyl-6-triazolylpenicillanate)**						
Solvents →	**CyHex**	**Diox.**	**EtOAc**	**THF**	**DMF**	**ACN**	**MeOH**
λ_{max}^{abs} **(nm)**	258	259	257	262	279	257	257
$\varepsilon_{max\ X}\ 10^3$	33.7	31.2	29.9	30.8	9.6	36.7	35
λ_{max}^{fl} **(nm)**	318	286	383	288	287	298	320
Φ_f	0.0003	0.0006	0.0003	0.001	0.0005	0.001	0.0004

The β-lactam **5.79** (**Benzyl 4-methoxy-2-methylphenyl-6-triazolylpenicillanate**) containing 4-methoxy-2-methylphenyl donor aromatic unit showed broad absorption band at around 250 nm with 7 nm blue shift from nonpolar hexane to polar protic MeOH solvent. Upon excitation at UV maxima of β-lactam **5.79**, it showed two bands in almost every solvent. The first band appears at around 320 nm which is less intense in nonpolar solvents and more intense in polar solvents like ethanol. Another emission band appears at around 380 nm, with a quenched but red shifted (30 nm) fluorescence emission as the polarity of the solvent increases from nonpolar hexane to polar acetonitrile solvent. Quantum yield also followed the same trend as steady state fluorescence in β-lactam **5.79** (**Figure 5.15, Table 5.4**).

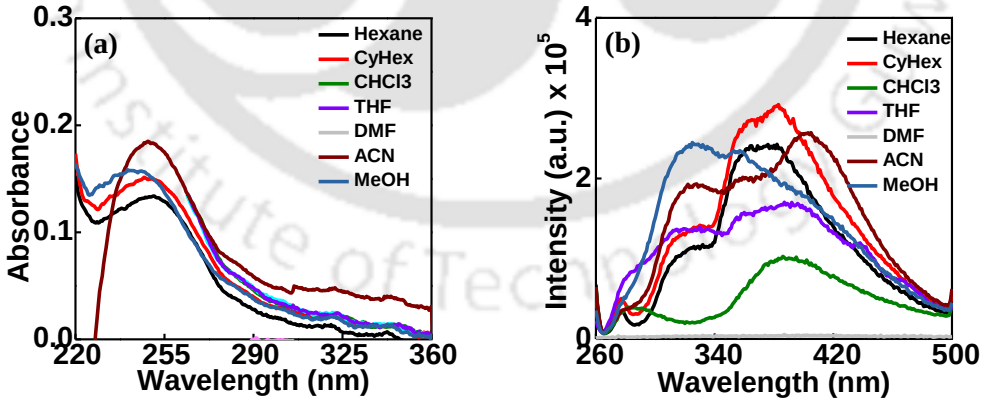

Figure 5.15. (a) UV-visible absorption, (b) fluorescence emission spectra of **Benzyl 4-methoxy-2-methylphenyl-6-triazolylpenicillanate** in various organic solvents. Excitation wavelength was the λ_{max}^{abs} in each solvent and the concentration of each β-lactams was 10 µM.

Table 5.4. Summary of photophysical properties of β-lactam **5.79** (**Benzyl 4-methoxy-2-methylphenyl-6-triazolylpenicillanate**)

Entry →	**5.79 (Benzyl 4-methoxy-2-methylphenyl-6-triazolylpenicillanate)**							
Solvents →	**CyHex**	**Diox.**	**$CHCl_3$**	**EtOAc**	**THF**	**DMF**	**ACN**	**MeOH**
λ_{max}^{abs} **(nm)**	247	--	248	257	245	269	249	243
ε_{max} x 10^3	15	--	15	15	18	9.6	18.6	16
λ_{max}^{fl} **(nm)**	382	292	389	382	387	394	402	355
Φ_f	0.025	0.003	0.006	0.0004	0.009	0.0004	0.025	0.023

The β-lactam compound **5.80** (**Benzyl-3,5-dimethoxy-phenyl-6-triazolyl penicillanate**) containing 3, 5-dimethoxy donor aromatic unit shows broad absorption band at around 290 nm with almost no solvatochromicity or change in absorbance in all organic solvents tested. When excited at its absorption maxima, it showed a strong emission band around 325 nm with 42 nm red shift from nonpolar cyclohexane to polar and protic MeOH solvent. The emission band also shows highest intensity in polar solvents like acetonitrile and ethanol. Quantum yield also follows the same sequence as steady state fluorescence in β-lactam **5.80** (**Figure 5.16, Table 5.5**).

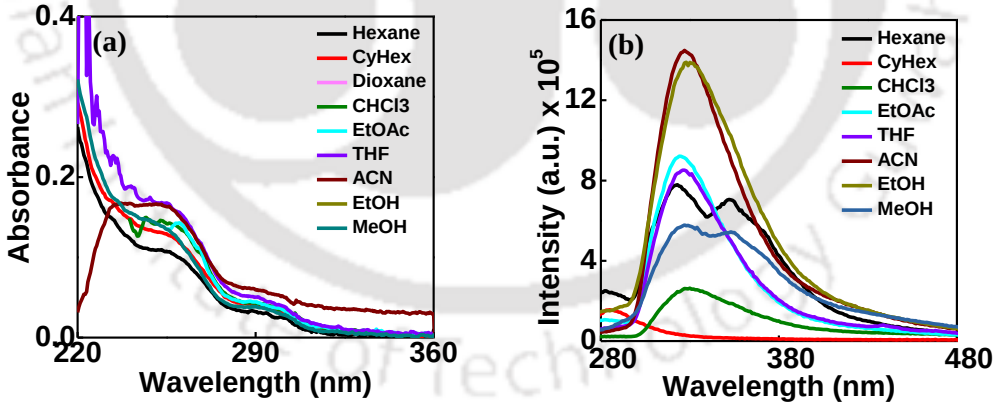

Figure 5.16. (a) UV-visible absorption, (b) fluorescence emission spectra of **Benzyl 3,5-dimethoxy-phenyl-6-triazolylpenicillanate** in various organic solvents. Excitation wavelength was the λ_{max}^{abs} in each solvent and the concentration of each β-lactams was 10 μM.

Table 5.5. Summary of photophysical properties of β-lactam **5.80** (**Benzyl 3, 5 - dimethoxy-phenyl-6-triazolyl penicillanate**).

Entry →	**5.80 (Benzyl 4-methoxy-2-methylphenyl-6-triazolylpenicillanate)**							
Solvents →	**CyHex**	**Diox.**	**$CHCl_3$**	**EtOAc**	**THF**	**DMF**	**ACN**	**MeOH**
λ_{max}^{abs} **(nm)**	290	295	290	290	290	290	290	290
$\varepsilon_{max} \times 10^3$	4.21	0.38	4.31	4.43	5.04	3.59	5.93	3.83
λ_{max}^{fl} **(nm)**	285	323	328	325	325	325	327	327
Φ_f	0.005	0.05	0.02	0.04	0.04	0.001	0.068	0.04

The β-lactam compound **5.81** (**Benzyl-6-methoxynapthalyl-6-triazolyl penicillanate**) containing 6-methoxynapthyl donor aromatic unit showed a characteristic structured absorption band of 6- methoxynaphthalene at around 290 and 300 nm with no solvatochromicity in all organic solvents tested. When excited at its absorption maximum, it exhibited a strong emission band at around 365 nm with 5 nm red shift from nonpolar hexane to polar acetonitrile solvent. Quantum yield also follows the same sequence as steady state fluorescence in β-lactam **5.81**(**Figure 5.17, Table 5.6**).

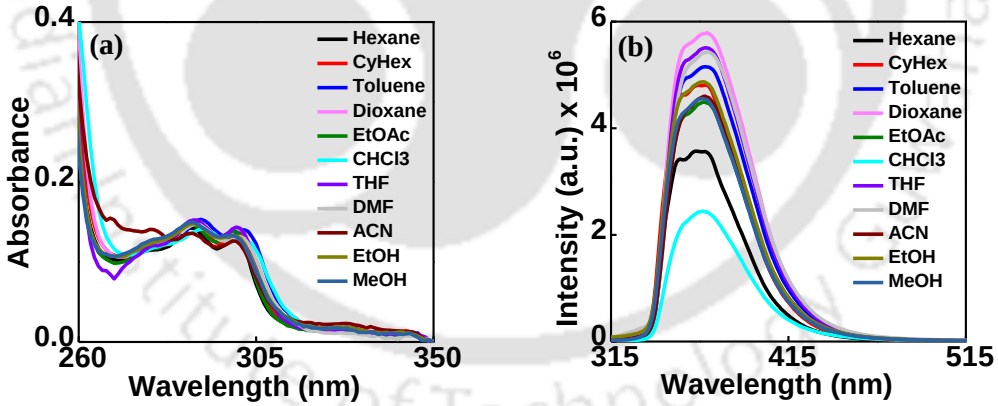

Figure 5.17. (a) UV-visible absorption, (b) fluorescence emission spectra of **Benzyl-6-methoxynapthalyl-6-triazolylpenicillanate** in various organic solvents. Excitation wavelength was the λ_{max}^{abs} in each solvent and the concentration of each β-lactams was 10 μM.

Table 5.6. Summary of photophysical properties of β-lactam **5.81** (**Benzyl-6-methoxynapthalyl-6-triazolylpenicillanate**).

Entry →	**5.81 (Benzyl-6-methoxynapthalyl-6-triazolylpenicillanate)**							
Solvents →	**CyHex**	**Diox.**	**$CHCl_3$**	**EtOAc**	**THF**	**DMF**	**ACN**	**MeOH**
λ_{max}^{abs} **(nm)**	300	300	301	300	300	300	300	300
ε_{max} x 10^3	13.75	14.05	13.79	12.66	14.36	13.13	12.59	13.13
λ_{max}^{fl} **(nm)**	363	368	367	368	368	368	368	366
Φ_f	0.33	0.42	0.16	0.31	0.39	0.39	0.32	0.31

The β-lactam compound **5.82** (**Benzyl 9-phenanthrenyl -6-triazolylpenicillanate**) containing 9-phenanthrene donor aromatic unit showed two structureless broad absorption band at around 255 and 300 nm with 3 nm blue shift from nonpolar toluene to polar protic MeOH solvent. Excitation on its absorption maximum a less structured band of phenanthrene at around 380 nm with almost no solvatochromicity was observed which experienced high intensity in dioxane and DMF and low intensity in high polar solvent like EtOH and MeOH. Quantum yield also followed the same sequence as steady state fluorescence in β-lactam **5.82** (**Figure 5.18, Table 5.7**).

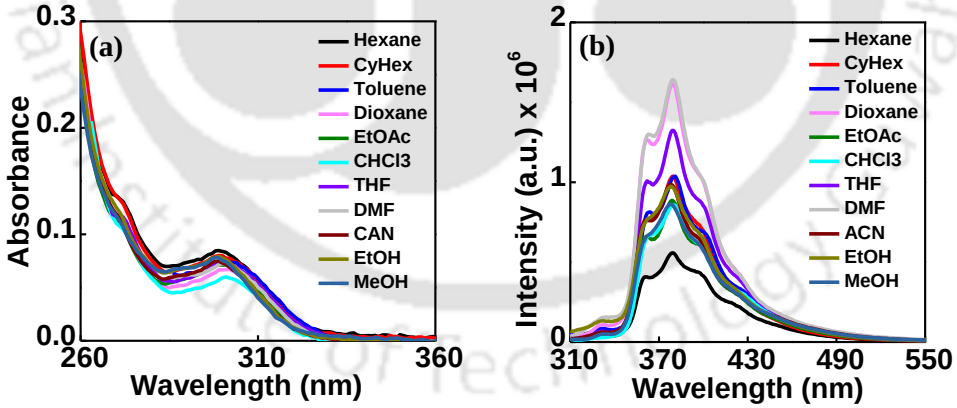

Figure 5.18. (a) UV-visible absorption, (b) fluorescence emission spectra of **Benzyl 1-phenanthrenyl -6-triazolylpenicillanate** in various organic solvents. Excitation wavelength was the λ_{max}^{abs} in each solvent and the concentration of each β-lactam was 10 μM.

Table 5.7. Summary of photophysical properties of β-lactam **5.82** (**Benzyl 1-phenanthrenyl -6-triazolylpenicillanate**).

Entry →	**5.82 (Benzyl 9-phenanthrenyl -6-triazolylpenicillanate)**							
Solvents →	**CyHex**	**Diox**	**$CHCl_3$**	**EtOAc**	**THF**	**DMF**	**ACN**	**MeOH**
λ_{max}^{abs} **(nm)**	299	300	300	299	300	300	298	298
ε_{max} **X** 10^3	8.01	6.66	7.14	5.72	7.24	7.17	7.46	7.77
λ_{max}^{fl} **(nm)**	379	379	380	379	379	379	378	378
Φ_f	0.055	0.083	0.0503	0.048	0.069	0.086	0.055	0.05

The 1-pyrene donor aromatic unit containing β-lactam **5.83** (**Benzyl 1-pyrenyl -6-triazolylpenicillanate**) showed a structure-less broad absorption band at around 348 nm with 4 nm blue shift from nonpolar dioxane to polar protic MeOH solvent. The disappearance of structured band of pyrene might be due to electronic coupling of π-electronic cloud of pyrene with triazole unit. Excitation at absorption maximum of compound **5.83** gave a less structured emission of pyrene with very little solvatochromicity and highest intensity in DMSO but less intensity in polar solvents like EtOH and MeOH. Quantum yield also followed the same trend as steady state fluorescence in β-lactam **5.83** (**Figure 5.19, Table 5.8**).

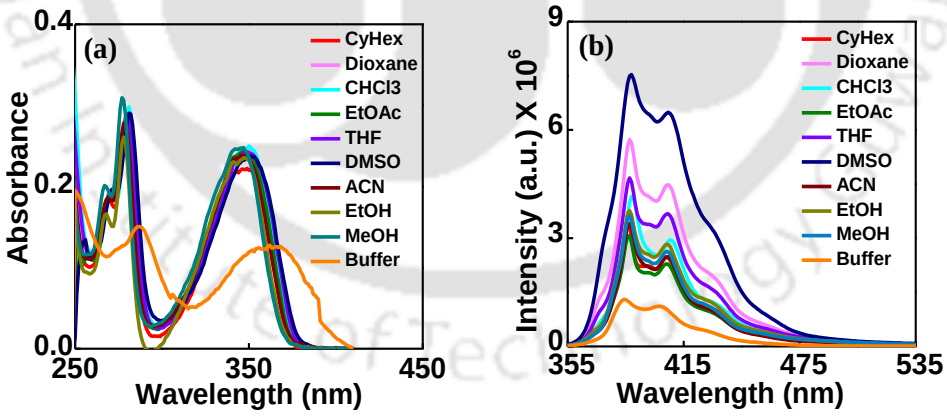

Figure 5.19. (a) UV-visible absorption, (b) fluorescence emission spectra of **Benzyl 1-pyrenyl-6-triazolylpenicillanate** in various organic solvents. Excitation wavelength was the λ_{max}^{abs} in each solvent and the concentration of each β-lactam was 10 μM.

Table 5.8. Summary of photophysical properties of β-lactam **5.83** (**Benzyl 1-pyrenyl -6-triazolylpenicillanate**).

Entry →	**5.83 (Benzyl 1-pyrenyl -6-triazolylpenicillanate)**							
Solvents →	**CyHex**	**Diox**	**$CHCl_3$**	**EtOAc**	**THF**	**DMF**	**ACN**	**MeOH**
λ_{max}^{abs} **(nm)**	348	346	347	350	346	347	344	346
ε_{max} x 10^3	24.35	24.28	23.99	23.31	23.74	23.54	24.42	22.07
λ_{max}^{fl} **(nm)**	406	406	406	407	406	406	406	406
Φ_f	0.44	0.22	0.35	0.67	0.23	0.27	0.25	0.23

The β-lactam compound **5.84** (**Benzyl 3-Perylenyl-6-triazolylpenicillanate**) containing perylene donor aromatic unit showed a structured absorption of perylene at around 452 nm in nonpolar solvents like hexane and cyclohexane and was blue shifted about 6 nm from nonpolar toluene to polar protic MeOH solvent. The absorbance value of perylene in compound **5.84** appears in quite higher wavelength (402, 425, 452 nm in cyclohexane) than the normal perylene (386, 408, 435 nm in cyclohexane). This might be due to the redistribution of electronic charge from electron rich triazole moiety to electron deficient perylene. When excited at the absorbance maximum of perylene in β-lactam **5.84** the emission band also appeared at longer wavelength (467, 497, 535 nm in cyclohexane) than perylene (435, 463, 497 nm in cyclohexane).[2] The emission spectra showed a red shift about 8 nm as the polarity of the solvent increases (from nonpolar hexane to polar DMF solvent). Quantum yield also followed the same trend as steady state fluorescence in β-lactam **5.84** (**Figure 5.20, Table 5.9**).

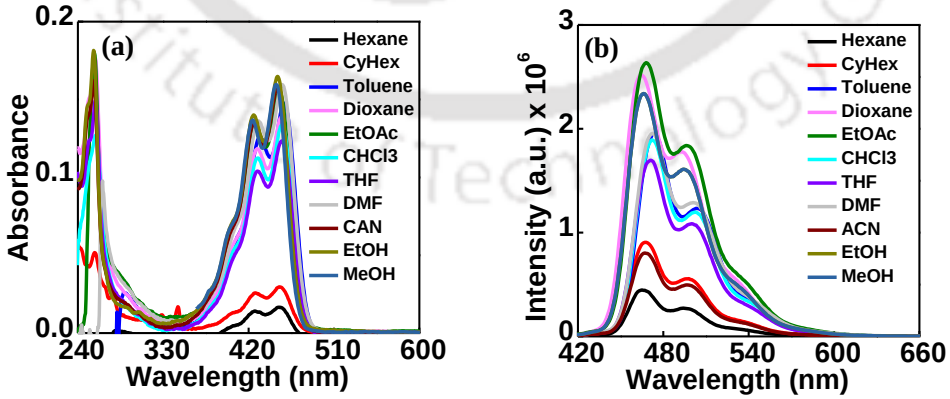

Figure 5.20. (a) UV-visible absorption, (b) fluorescence emission spectra of **Benzyl 3-Perelenyl-6-triazolylpenicillanate** in various organic solvents. Excitation

wavelength was the λ_{max}^{abs} in each solvent and the concentration of each β-lactams was 10 µM.

Table 5.9. Summary of photophysical properties of β-lactam **5.84** (**Benzyl 3-Perynyl-6-triazolylpenicillanate**).

Entry →	**5.84 (Benzyl 3-Perynyl-6-triazolylpenicillanate)**							
Solvents →	**CyHex**	**Diox.**	**$CHCl_3$**	**EtOAc**	**THF**	**DMF**	**ACN**	**MeOH**
λ_{max}^{abs} **(nm)**	452	454	455	452	455	455	450	449
ε_{max} **X** 10^3	2.9	13.3	15.4	12.6	11.8	15.1	15.7	15.7
λ_{max}^{fl} **(nm)**	467	464	471	467	471	473	467	466
Φ_f	0.25	0.8	0.84	0.50	0.61	0.59	0.23	0.74

The compound 4-fluoro-2-methylphenyl acceptor aromatic unit containing β-lactam **5.85** (**Benzyl 4**-fluoro-**2-methylphenyl-6-triazolylpenicillanate**) showed a structure-less broad absorption band at around 245 nm with almost no solvatochromicity in all organic solvent tested. **Excitation** at its absorption maximum it showed very low intense emission at 245 nm which experienced a 34 nm blue shift from nonpolar hexane to polar THF solvent. Quantum yield also followed the same trend as steady state fluorescence in β-lactam **5.85** (**Figure 5.21, Table 5.10**).

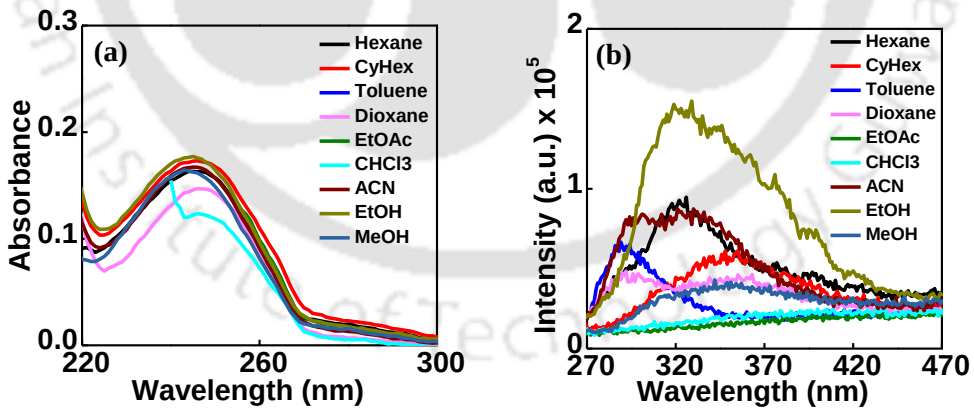

Figure 5.21. (a) UV-visible absorption, (b) fluorescence emission spectra of **Benzyl 4-fluoro-2-methylphenyl-6-triazolylpenicillanate** in various organic solvents. Excitation wavelength was the λ_{max}^{abs} in each solvent and the concentration of each β-lactam was 10 µM.

Table 5.10. Summary of photophysical properties of β-lactam **5.85** (**Benzyl 4-fluoro-2-methylphenyl-6-triazolylpenicillanate**).

Entry →	**5.85 (Benzyl 4-fluoro-2-methylphenyl-6-triazolylpenicillanate)**							
Solvents →	**CyHex**	**Diox.**	**$CHCl_3$**	**EtOAc**	**THF**	**DMF**	**ACN**	**MeOH**
λ_{max}^{abs} **(nm)**	245	245	245	245	245	245	245	245
ε_{max} x 10^3	17	15	12	13	5.3	14	16.7	16.3
λ_{max}^{fl} **(nm)**	347	354	382	360	288	287	328	348
Φ_f	0.014	0.013	0.006	0.008	0.006	0.007	0.018	0.012

The 4-benzonitrile acceptor aromatic unit containing β-lactam **5.86** (**Benzyl 4-benzonitrile-6-triazolylpenicillanate**) showed a structureless absorption band at around 269 nm with no solvatochromicity in all organic solvents tested. When excited at its absorption maximum a strong and broad emission band at 290 nm was observed which became red shifted about 40 nm in polar protic solvent MeOH. Emission band showed an increase in intensity from nonpolar to polar solvent with appearance of an extra band at 290 nm in DMF solvent. Quantum yield also followed the same trend as steady state fluorescence in β-lactam **5.86** (**Figure 5.22, Table 5.11**).

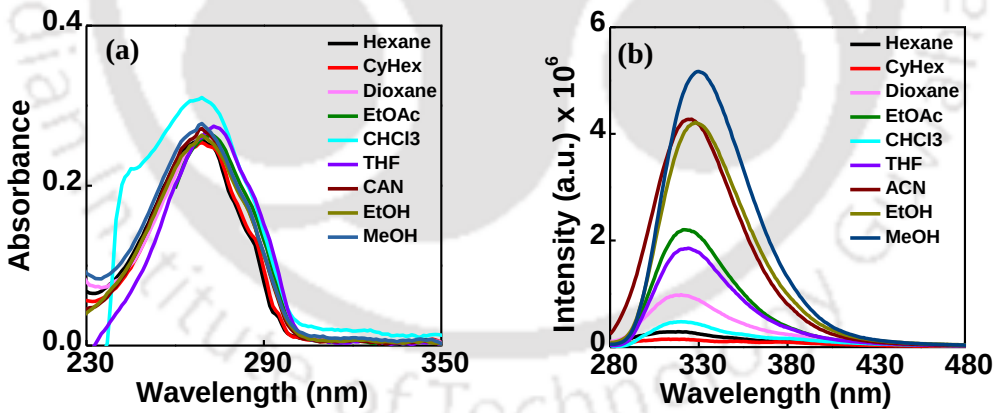

Figure 5.22. (a) UV-visible absorption, (b) fluorescence emission spectra of **Benzyl 4-benzonitrile-6-triazolylpenicillanate** in various organic solvents. Excitation wavelength was the λ_{max}^{abs} in each solvent and the concentration of each β-lactam was 10 μM.

Table 5.11. Summary of photophysical properties of β-lactam **5.86** (**Benzyl 4-benzonitrile-6-triazolylpenicillanate**).

Entry →	**5.86 (Benzyl 4-benzonitrile-6-triazolylpenicillanate)**							
Solvents →	**CyHex**	**Diox.**	**$CHCl_3$**	**EtOAc**	**THF**	**DMF**	**ACN**	**MeOH**
λ_{max}^{abs} **(nm)**	269	270	268	271	271	279	268	268
ε_{max} **x** 10^3	25.4	26.3	31.0	25.8	26.1	19.9	27.1	27.8
λ_{max}^{fl} **(nm)**	374	319	320	322	324	290	325	330
Φ_f	0.007	0.029	0.016	0.056	0.048	0.031	0.117	0.139

The β-lactam compound **5.87** (**Benzyl 4-benzaldehyde -6-triazolylpenicillanate**) containing 4-benzaldehyde acceptor aromatic unit showed two structureless broad absorption bands at around 210 and 287 nm with 6 nm blue shift from nonpolar hexane to polar acetonitrile solvent. Excitation at its absorption maximum a broad band at around 318 nm in hexane which became red shifted about 48 nm in THF solvent was observed. Emission band showed highest intensity and quantum yield in EtOH solvent. Quantum yield also followed the same trend as steady state fluorescence in β-lactam **5.87** (**Figure 5.23, Table 5.12**).

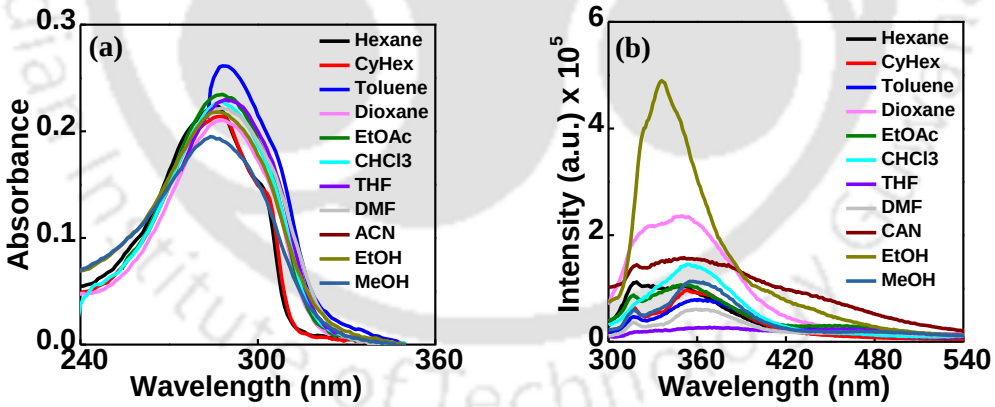

Figure 5.23. (a) UV-visible absorption, (b) fluorescence emission spectra of **Benzyl 4-benzaldehyde-6-triazolylpenicillanate** in various organic solvents. Excitation wavelength was the λ_{max}^{abs} in each solvent and the concentration of each β-lactam was 10 μM.

Table 5.12. Summary of photophysical properties of β-lactam **5.87** (**Benzyl 4-benzaldehyde -6-triazolylpenicillanate**).

Entry →	**5.87 (Benzyl 4-benzaldehyde-6-triazolylpenicillanate)**							
Solvents →	**CyHex**	**Diox.**	**$CHCl_3$**	**EtOAc**	**THF**	**DMF**	**ACN**	**MeOH**
λ_{max}^{abs} **(nm)**	287	287	287	287	288	289	279	284
$\varepsilon_{max}\ x\ 10^3$	20.9	20.3	22.8	22.01	21.6	21.34	22.8	19.35
λ_{max}^{fl} **(nm)**	359	346	355	350	366	316	353	357
Φ_f	0.003	0.009	0.005	0.005	0.002	0.003	0.009	0.004

5.4.3. Study of Chemical Cleavage of Triazolyl β-Lactams 5.81 and 5.83 Using Fluorescence Spectroscopy

After getting all the β-lactams in pure form we chose two fluorescent β-lactams, **5.81** (**^{TMNap}β-Lac^{Do}**) and **5.83** (**^{TPy}β-Lac^{Do}**) to examine the change in fluorescence photophysical property upon chemical cleavage of β-lactam ring by a nucleophilic amine. In case of β-lactam **5.81** we used benzyl amine to test the feasibility of conceptual cleavage which underwent smoothly at room temperature in absence of any base in dry dichloromethane (**Scheme 5.7**). Next, the same reaction was carried out in dry THF solvent in presence of Et_3N at 80-85 ^oC using aminomethyl pyrene as a pro-fluorescent nucleophile envisioning that in the ring-opened form the triazolyl methoxynaphthalene (**TMNap**) and the aminomethylpyrene (**AMePy**) would show photophysical interaction property and expectedly we would observe a FRET emission from aminomethylpyrene (**AMePy**) upon excitation at **TMNap** as well as an exciplex emission either via FRET or via direct excitation at FRET acceptor, **AMePy** (**Figure 5.9**). On the other hand, in the second example of β-lactam **5.83**, we expected an excimer formation/ground state complexation in the ring-opened form between the triazolylpyrene (**TPy**) and the aminomethylpyrene (**AMePy**) which would ultimately lead to the generation of excimer emission upon excitation at 350 nm (**Figure 5.9**). Though this study took help of amino nucleophile for cleavage, attaching a fluorophore at the carboxyl end and opening the β-lactam ring with enzyme's hydroxyl/amine or any organic hydroxyl/amine nucleophile would expectedly afford the similar optical response which is our future target. This system thus might help in designing such system to use in real enzymatic assay. The synthesis and the structures of all the ring-opened β-lactams are depicted in **Scheme 5.7**.

At first, we measured the spectroscopic properties of individual ring opened compounds (**5.95, 5.96** and **5.97**) in various organic solvents and then compared that with their corresponding β-lactams, **5.81** and **5.83**. Thus, in β-lactam **5.81** when ring opening was carried out using benzyl amine the ultimate ring opened product **5.95** shows a structured absorption band of 6-methoxynaphthalene unit at around 290 and 300 nm with no solvatochromicity in all organic solvents tested. When excited at its absorption maxima it shows strong emission band at around 365 nm in hexane and cyclohexane and is red shifted about 6 nm in polar and protic MeOH with high intensity in polar solvents. Quantum yield also follows the same sequence as steady state fluorescence for compound **5.95** (**Figure 5.24, Table 5.13**).

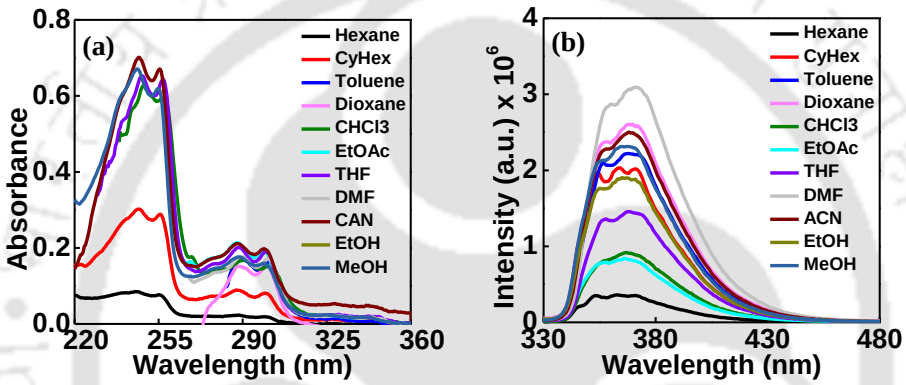

Figure 5.24. a) UV-visible absorption, (b) fluorescence emission spectra of ring opened compound **5.95** in various organic solvents. Excitation wavelength was the λ_{max}^{abs} in each solvent and the concentration of each sample solution was 10 µM.

Table 5.13. Summary of photophysical properties of compound **5.95.**

Entry →	**Ring opened Compound 5.95**							
Solvents →	**CyHex**	**Diox**	**$CHCl_3$**	**EtOAc**	**THF**	**DMF**	**ACN**	**MeOH**
λ_{max}^{abs} **(nm)**	299	300	300	299	300	300	299	300
ε_{max} x 10^3	8.02	15.3	15.1	18.7	18.9	16.98	19.4	15.6
λ_{max}^{fl} **(nm)**	371	370	367	366	368	370	368	365
Φ_f	0.24	0.31	0.11	0.10	0.17	0.37	0.29	0.27

The ring opened compound **5.96** shows a structured band of pyrene (due to presence of Pyren-1-Amine) at around 342 nm and a structured band of methoxynaphthalene (due to presence of triazolyl 6-Methoxynaphthalene unit) at

around at 300 nm. The absorption spectra showed 4 nm blue shift from cyclohexane to polar protic MeOH solvent.

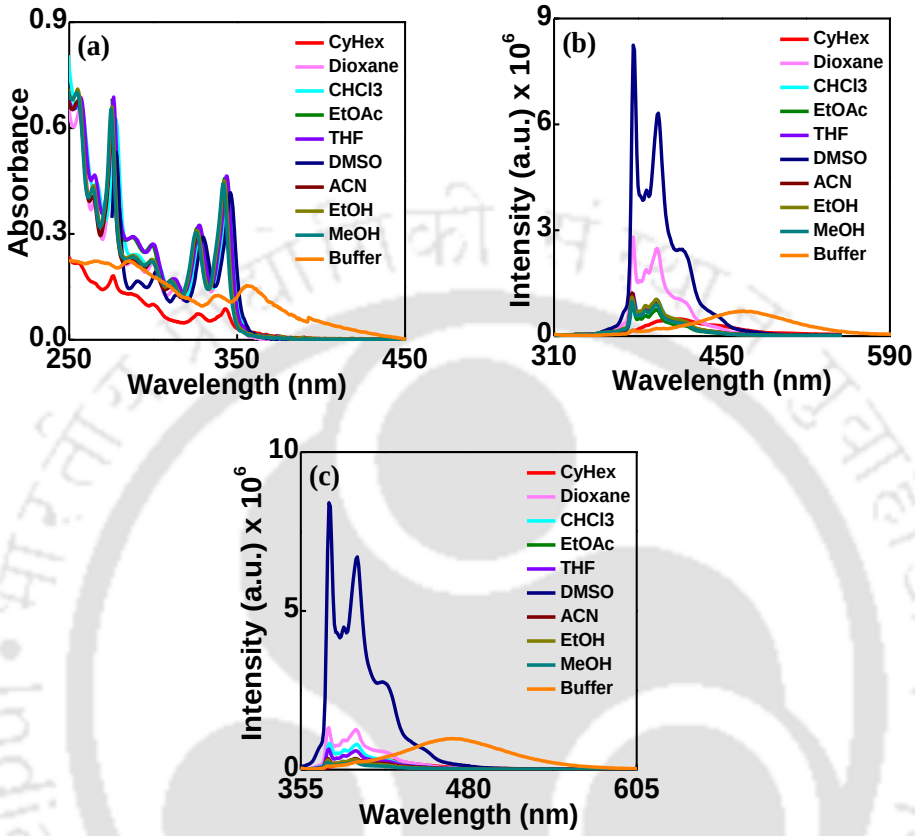

Figure 5.25. (a) UV-visible absorption, (b) fluorescence emission spectra at $\lambda_{ex} \approx 300$ nm and (c) fluorescence emission spectra at $\lambda_{ex} \approx 350$ nm of ring opened compound **5.96** in various organic solvents. Excitation wavelength was the λ_{max}^{abs} in each solvent and the concentration of each sample solution was 10 μM.

When the ring opened compound **5.96** was excited at 342 nm where absorbance of pyrene is high, **5.96** shows a structured emission of pyrene with very high intensity in DMSO solvent and when it was excited at 300 nm where absorbance of methoxynaphthalene is highest but absorbance of pyrene is negligible, **5.96** shows a very high intensity of pyrene and negligible intensity of methoxynaphthalene unit. This may be due to Förster resonance energy transfer. Quantum yield also follows the same sequence as steady state fluorescence for compound **5.96** (**Figure 5.25, Table 5.14**).

Table 5.14. Summary of photophysical properties of compound **5.96.**

Entry →	**Ring opened Compound 5.96**							
Solvents →	**CyHex**	**Diox.**	**$CHCl_3$**	**EtOAc**	**DMSO**	**ACN**	**MeOH**	**Buffer**
λ_{max}^{abs} **(nm)**	342	343	345	342	346	342	341	357
$\varepsilon_{max} \times 10^3$	7	41	42	29	39	24	21	16
λ_{max}^{fl} **(nm)**	395	395	395	395	396	395	395	397
Φ_f	0.06	0.13	0.06	0.05	0.32	0.06	0.05	0.02

The ring opened compound **5.97** shows a structured band of pyrene (due to presence of Pyren-1-Amine) at around 342 nm and an unstructured band of pyrene (due to presence of triazolyl pyrene unit) at around at 351 nm. The absorption spectra show almost no solvatochromicity or change in absorbance in all organic solvents tested. When excited at its absorption maxima it shows a less structured band of pyrene at 405 nm which shows no solvatochromicity and with an extra band appears at 475 nm in THF and buffer solvent. This is possibly due to excimer formation/ground state complexation in the ring-opened form between the triazolylpyrene (**TPy**) and the aminomethylpyrene (**AMePy**). Quantum yield also follows the same sequence as steady state fluorescence for compound **5.97** (**Figure 5.26, Table 5.15**).

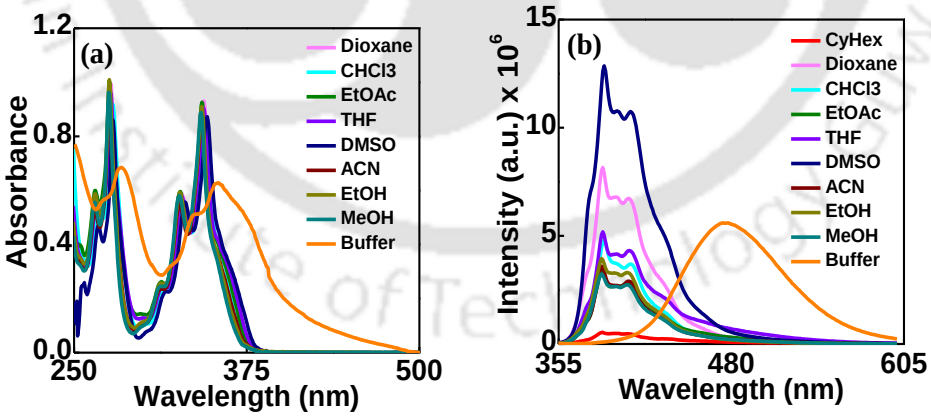

Figure 5.26. (a) UV-visible absorption, (b) fluorescence emission spectra of ring opened compound **5.97** in various organic solvents at $\lambda_{ex} \approx 350$ nm. Excitation wavelength was the λ_{max}^{abs} in each solvent and the concentration of each sample solution was 10 μM.

Table 5.15. Summary of photophysical properties of compound **5.97.**

Entry →	**Ring opened Compound 5.97**							
Solvents →	**Diox.**	**$CHCl_3$**	**EtOAc**	**THF**	**DMSO**	**ACN**	**MeOH**	**Buffer**
λ_{max}^{abs} **(nm)**	344	345	342	344	346	342	341	351
$\varepsilon_{max} \times 10^3$	93	82	85	90	76	75	73	13
λ_{max}^{fl} **(nm)**	405	406	405	475	407	405	405	475
Φ_f	0.40	0.23	0.18	0.31	0.67	0.17	0.17	0.21

To test our concept of fluorescence detection of ring-opened status and to discriminate fluorescent β-lactams, we next, studied and compare the photophysical property of the starting β-lactam **5.81** and **5.83** with their corresponding ring opened form, **5.96** and **5.97** respectively, in various solvents and in aqueous phosphate buffer (pH 7.4).

Next, a comparasion of photophysical properties between β-lactams and theirs corresponding ring opened forms were compared to test our hypothesis of FRET and dual path to exciplex emission in **5.96** (ring opened form of β-lactam **5.81**) and excimer emission in **5.97** (ring opened form of β-lactam **5.83**). At first, we studied the β-lactam probe **5.81** via FRET/exciplex emission. Thus, we compared the photophysical properties of the starting β-lactam **5.81** and the corresponding ring opened form, **5.96** in MeOH and in aqueous phosphate buffer (pH 7.4) to validate our concept of dual door entry to exciplex emission in the ring-opened form **5.96** after cleavage of β-lactam **5.81** upon reaction with pyrenylmethyl amine. Thus, the UV-visible absorption spectra of ring opened β-lactam **5.96** displayed the characteristic structured bands of both **TMNap** at 288, 300 nm and of **AMePy** at 327, 345 nm (**Figure 5.17** and **5.19**). Upon excitation at **TMNap** absorption band (λ_{ex} = 300 nm) the ring opened form **5.96** displayed structured emission at around 387, 407 nm characteristic of **AMePy** along with a negligible emission at 364 nm characteristic of **TMNap** emission (**Figure 5.25**). This observation reflected a possible FRET emission from **AMePy** acting as an acceptor upon excitation at **TMNap** acting as a donor chromophore which is also indicated from an overlap of absorption spectrum of **AMePy** and an emission spectrum of **TMNap**. A closer look at emission intensity of ring–un-opened β-lactam **5.81**, profluorescent nucleophile, pyrenylmethyl amine and the ring-opened form **5.96** revealed a drastic enhancement of acceptor (**AMePy**) emission intensity (by 3.5 times) out of a tremendously decreased emission intensity of donor (**TMNap**, by 7 times) evidencing the FRET process (**Figure 27a**) which was also supported from a time resolved fluorescence study (**Figure 27b**). Where the

decrease in donor life time (**TMNap**; λ_{ex} = 290 nm, λ_{em} = 365 nm) from 7.10 (in β-lactam **5.81**) to 3.91 ns (in ring opened β-lactam **5.96**) and increase in acceptor life time (**AMePy**; λ_{ex} = 290 nm, λ_{em} = 405 nm) from 14.60 ns (in **AMePy**) to 22.02 ns (in ring opened β-lactam **5.96**) was observe in MeOH solvent (**Figure 27b, Table 5.16**). The phenomena of FRET occurred in all solvents including THF and Methanol. Calculated FRET efficiency in MeOH solvent is 86.5 % from steady state fluorescence spectra and 44.7 % from fluorescence life time measurement.

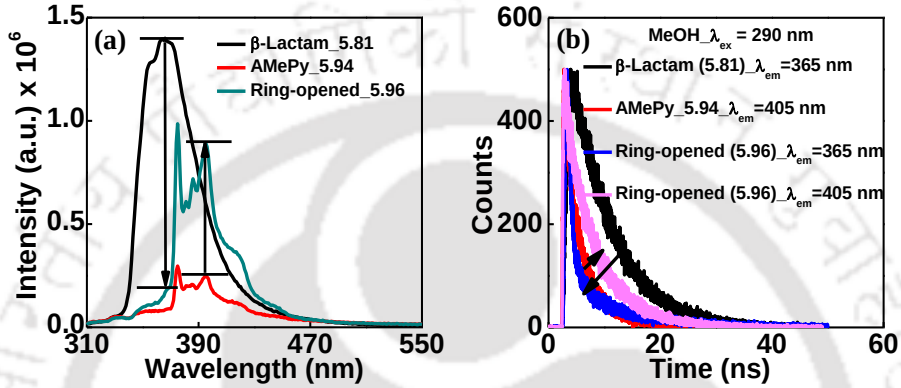

Figure 5.27. (a) Steady state fluorescence (λ_{ex} = 300 nm) and (b) time resolve fluorescence (λ_{ex} = 290) of β-lactam **5.81**, nucleophile **5.94** and ring-opened form **5.96** showing FRET in MeOH solvent. [10 µM each].

However, we did not observe any other extra band which we expected to come as an exciplex emission in any of the organic solvent. Interestingly, an extra, long-wavelength emission band appeared at 468 nm along with the appearance of pyrene monomer emission bands at 387, 407 nm while performing the study in phosphate buffer validating our concept of exciplex emission via FRET (**Figure 28a**). The exciplex band (λ_{ex} = 290 nm, λ_{em} = 468 nm) having life time 28.76 ns (**Figure 28a, Table 5.16**) in aqueous phosphate buffer (pH 7.4).

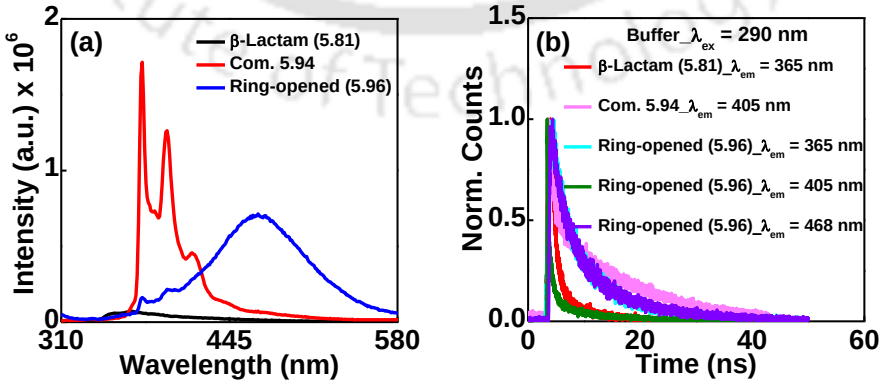

Figure 5.28. (a) Steady state fluorescence (λ_{ex} = 300 nm) and (b) time resolve fluorescence (λ_{ex} = 290) of β-lactam **5.81**, nucleophile **5.94** and ring-opened form **5.96** showing FRET in aqueous phosphate buffer (pH 7.4) solvent [10 µM each].

That the band at 468 nm is an exciplex was evident from a decreased intensity while measuring at various temperatures (**Figure 5.29**). As we observed the exciplex band in buffer we next excited the FRET acceptor **AMePy** at 350 nm and again we observed pyrenyl monomer emission as well as an exciplex emission.

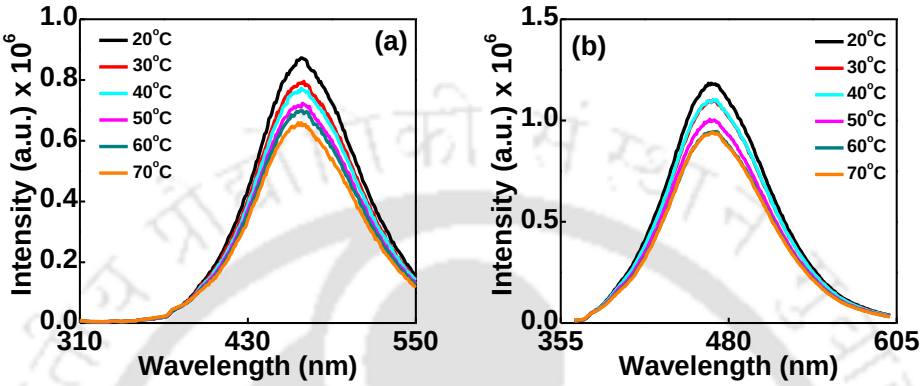

Figure 5.29. Variable temperature fluorescence spectra of β-lactam ring-opened compound **5.96** (a) λ_{ex} = 300 nm and (b) λ_{ex} = 355 nm in buffer, pH 7.4, 10 μM, r.t.

Therefore, Both the process either via FRET upon excitation at FRET donor (**TMNap**) or via direct excitation at FRET acceptor (**AMePy**) led to an exciplex emission in ring-opened form (**5.96**) after β-lactam (**5.81**) ring cleavage by a profluorescent nucleophile, pyrenylmethylamine. The ring-opened form of **5.81** having **TMNap-AMePy** pair showed exciplex emission which is a reflection of our conceptual expectation and came out to be due to π- π stacking interaction between the **TMNap** and **AMePy** units which was supported from 2D NMR (**Figure 5.40**). Inspection of the optimized geometry, TDDFT calculated electronic state and the orbitals involved in the HOMO-LUMO excitation revealed that the HOMO is mainly composed of the orbitals from aminomethylpyrene (**AMePy**) while the LUMO is almost entirely composed of **TMNap** orbitals. Thus, the exciplex formation is dominated mainly by π- π stacking interaction as well as by electrostatic contribution in the excited state.

On the other hand the UV-visible absorption spectra of β-lactam **5.83** displayed unstructured long wavelength absorption band at 348 nm corresponding to triazolylpyrene (**TPy**), the ring opened form **5.97** displayed pyrenyl vibronic absorption along with an appearance of a new band at about 364 nm which experienced blue shift with decreased absorption as the polarity of the solvent increases from THF to Methanol (354 nm) (**Figure 5.26a**). The UV-visible spectra suggested the electronic coupling between triazole and pyrene π-cloud in β-lactam **5.83** while the structured band for ring-opened form indicated a possible π-π stacking

interaction between the **TPy** and aminomethyl pyrenyl (**AMePy**) units. Therefore this study brought the idea that following the UV-visible spectra one can monitor the progress of cleavage of the β-lactam ring. In phosphate buffer the absorption spectra of β-lactam **5.83** showed structureless weak absorption at 349 nm while it was also weak with less vibronic character at 354 nm in case of ring-opened form (**Figure 5.26a**). Upon excitation at **TPy** absorption band (350 nm) the β-lactam **5.83** displayed structured emission at around 387, 407 nm characteristic of **TPy** emission with decreased intensity of both the bands as solvent polarity increases from THF to methanol (**Figure 5.26b**). In buffer the intensity was again very low which may be due to polar solvent solute interaction. However, the ring-opened form, **5.97** exhibited similar pattern and trend of intensity of the emission in all solvents with an appearance of extra weak band at 397 nm characteristic of aminomethylpyrene (**AMePy**) (**Figure 5.30**). More interestingly, the ring-opened form with **TPy-AMePy** pair showed only a structureless emission band at 475 nm characteristic of pyrene excimer/dimer (**Figure 5.30**). This phenomenon is supported by time resolved fluorescence study (**Figure 5.30b, Table 5.17**). The excimer band (λ_{ex} = 336 nm, λ_{em} = 475 nm) having life time 24.74 ns in aqueous phosphate buffer (pH 7.4) and 14.9 ns in THF solvent (**Table 5.17**). Both the excimer emission (λ_{ex} = 350 nm) and dimer emission (λ_{ex} = 354-364 nm) lies in the same wavelength and intensity. This may be due to π-π stacking interaction between two pyrenyl units of **TPy-AMePy** pair. This strategy can clearly distinguish between cleaved and non-cleaved state of a fluorescent β-lactam which can be utilized for assaying β-lactam susceptibility toward enzymatic cleavage via fluorescence with a suitably designed fluorescent β-lactam.

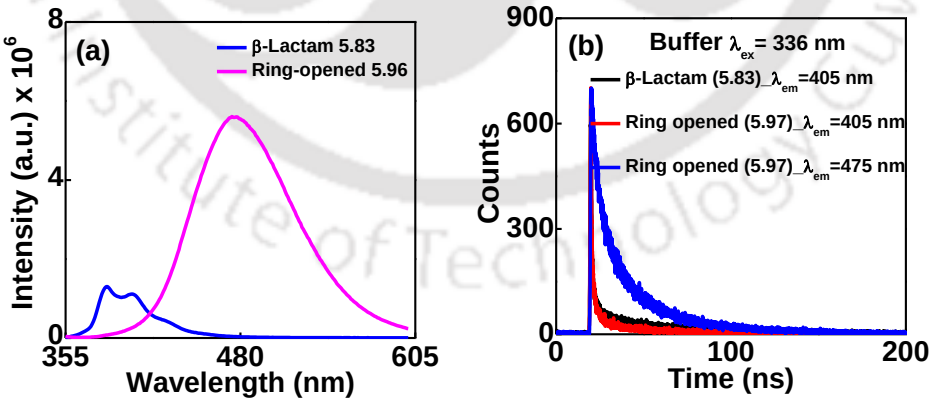

Figure 5.30. (a) Steady state fluorescence (λ_{ex} = 350 nm) and (b) time resolve fluorescence decay of β-lactam **5.83** and its ring-opened form **5.97** showing clear discrimination [10 μM in phosphate buffer pH 7.4].

Table 5.16: Summary table of fluorescence lifetimes of **Compound 5.81, Compound 5.94** and **Compound 5.96** at λ_{ex} **= 290 nm**

Entry	**Solvent**	Φ_f	**λ [nm]**	τ_1 **[ns]**	τ_2 **[ns]**	$\langle\tau\rangle$ **[ns]**	k_f **[$10^8 s^{-1}$]**	k_{nr} **[$10^8 s^{-1}$]**	χ^2
5.81	**MeOH**	0.31	365	7.10 (100%)	---	7.10	0.044	0.097	0.96
	Buffer	0.04		0.44 (55%)	4.56 (45%)	2.41	0.020	0.400	1.01
5.94	**MeOH**	0.03	405	14.60 (100%)	---	14.60	0.002	0.070	0.94
5.96	**MeOH**	0.003	365	0.55 (54%)	7.70 (46 %)	3.91	0.001	0.250	1.05
	Buffer	0.01		1.44 (20%)	7.78 (80%)	6.59	0.002	0.150	1.03
5.96	**MeOH**	0.05	405	22.02 (100%)	---	22.02	0.002	0.040	0.92
	Buffer	0.03		7.423 (46%)	34.20 (54%)	21.75	0.001	0.046	1.07
	Buffer	0.12	468	8.77 (22%)	34.54 (78%)	28.76	0.004	0.030	1.1

For lifetimes of the fluorescent β-lactams and ringopened compounds λ_{ex} = 290 nm, Concentration of each fluorescent β-lactams and ringopened compounds = 10 μM, $\langle\tau\rangle$, k_f, and k_{nr} are weighted means from the biexponential fits: $\langle\tau\rangle = 1/(\alpha_1/\tau_1 + \alpha_2/\tau_2)$, $k_f = \Phi_f/\langle\tau\rangle$, and $k_{nr} = (1-\Phi_f)/\langle\tau\rangle$.

Table 5.17: Summary table of fluorescence lifetimes of the **Comp. 5.83, 5.97 at λ_{ex} = 336 nm**

Entry	Solvents	Φ_f	λ_{em} [nm]	τ_1 [ns]	τ_2 [ns]	$\langle\tau\rangle$ [ns]	k_f [$10^8 s^{-1}$]	k_{nr} [$10^8 s^{-1}$]	χ^2
5.83	**ACN**	0.23	405	2.74 (10 %)	14.91 (90 %)	13.70	0.017	0.06	1.02
	MeOH	0.25		5.62 (13 %)	17.76 (87 %)	16.2	0.015	0.05	1.02
	THF	0.35		7.035 (16 %)	22.69 (84 %)	20.2	0.017	0.03	0.99
	Buffer	0.02		2.498 (41 %)	44.78 (59 %)	26.7	0.007	0.04	1.04
Comp. 5.97	**ACN**	0.17	405	2.945 (3 %)	16.08 (97 %)	15.70	0.01	0.05	1.00
	MeOH	0.17		9.123 (4 %)	19.0 (96 %)	18.60	0.01	0.04	1.03
	THF	0.31		8.425 (8 %)	23.05 (91 %)	21.80	0.01	0.03	1.05
	Buffer	0.21		2.287 (29 %)	26.41 (71 %)	19.30	0.01	0.04	0.99
Comp. 5.97	**THF**	0.31	475	5.59 (41 %)	21.11 (59 %)	14.90	0.02	0.05	1.00
	Buffer	0.21		7.07 (26 %)	30.82 (74 %)	24.74	0.01	0.03	1.04

For lifetimes of the fluorescent β-lactams and ringopened compounds λ_{ex} = 336 nm, Concentration of each fluorescent β-lactams and ringopened compounds = 10 μM, $\langle\tau\rangle$, k_f, and k_{nr} are weighted means from the biexponential fits: $\langle\tau\rangle = 1/(\alpha_1/\tau_1 + \alpha_2/\tau_2)$, $k_f = \Phi_f/\langle\tau\rangle$, and $k_{nr} = (1 - \Phi_f)/\langle\tau\rangle$.

5.5. Conclusion

In conclusion we have synthesized a newly designed triazolyl donor-acceptor chromophore decorated fluorescent penicilines, which marked a novel class of unnatural fluorescent β-lactams. Out of 12 β-lactams two were tested for their chemical cleavage with fluorescent nucleophile. They generate new fluorescence property in the ring-opened form. We have established the dual path to exciplex and excimer emission respectively, after clevage of two decorated β-lactams. This is the first report of design of a fluorescent β-lactam with a predicted photophysical properties after ring cleavage. Therefore, our strategy can discriminate between the β-lactam and its cleavage state via a clearly distinct fluorescence signal. The investigation on the change in photophysical property upon chemical cleavage of β-lactam ring can be treated as a model to study the kinetics of β-lactam susceptibility toward chemical cleavage.

5.6. Experimental Section

5.6.1. General (Materials and Methods)

All reactions were carried out under nitrogen atmosphere using flame-dried glassware. Organic extracts were dried over anhydrous sodium sulfate. Solvents were removed in a rotary evaporator under reduced pressure. Silica gel (60- 120 mesh) was used for the column chromatography. Reactions were monitored by TLC on silica gel 60 F254 (0.25). ^{1}H NMR spectra were recorded either at 400 MHz or at 600 MHz and ^{13}C NMR spectra were recorded either at 100 MHz or at 150 MHz (mentioned accordingly). Coupling constants (*J* value) were reported in hertz (Hz). The chemical shifts were shown in ppm downfield form tetramethyl silane, using residual chloroform (δ = 7.26 in ^{1}H NMR, δ = 77.23 in ^{13}C NMR), DMSO (δ = 2.5 in ^{1}H NMR, δ = 39.5 in ^{13}C NMR), as an internal standard. Mass spectra were recorded with a HR mass spectrometer and data analyzed by using built-in software. IR spectra were recorded in KBr on a FT-IR spectrometer.

All 2D NMR Experiments were carried out on 600 MHz spectrometer at room temperature using 7 - 10 mM concentration in $CHCl_3$ solvent. Spectra were acquired with 2048 x 256 in both dimension (F2 and F1) and other parameters are given below.

NOESY: Free induction decay (FID) with NS = 8 and DS =16, relaxation delay (D1) 2s, mixing time (D8) 0.6s, acquisition time (AQ) 0.085s, spectral width (SWH) 12019 Hz.

General procedure for [3+2] cyclo-addition reaction: The benzyl (+) 6-amino penicillanate was taken in dry THF and degassed for 5 min under nitrogen atmosphere. After adding alkyne (1.1 equivalent) degassing was continued for the next 5 min. Then, 1 mol % CuI was added. Then 1.2 equivalent DIPEA was added and reaction mixture was degassed and allowed to proceed for 4-5 h at room temperature. After total consumption of the starting azide, the reaction mixture was diluted with EtOAc and work up is done with EtOAc and NH_4Cl solution. The organic layer was washed with brine, dried over Na_2SO_4.The title (+) 6-triazolylpenicillanates were separated by column chromatography and characterized.

5.6.2. Synthesis of benzyl protected 6-azidopenicillin via azide transfer reaction

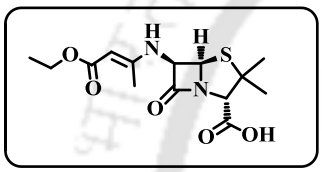

Synthesis of (2S,5R,6R)-6-(((E)-4-ethoxy-4-oxobut-2-en-2-yl)amino)-penicillanic acid (5.70): To a suspension of 6-aminopenicillanic acid (800 mg, 3.7 mmol) in dry DCM, triethyl amine (1.24 ml, 8.88 mmol) is added and the reaction mixture is stirred until the solution becomes colorless. Then EAA (0.56 ml, 4.44 mmol) is added drop wise till 5 minutes to the reaction mixture. The reaction mixture is then left is stirring condition for 3 hours. Completion of reaction is monitored by TLC (Solvent system = PE : EtOAc = 2:1, R_f = 0.4). After that the reaction mixture is dried in high vacuum. The excess TEA and EAA is evaporated out in this way. The crude gummy material is used for next step without further purification. ^{1}H NMR ($CDCl_3$, 400 MHz) δ 1.23 (3H, t, J = 6.8 Hz), 1.55 (3H, s), 1.59 (3H, s), 1.96 (3H, s), 3.40 (3H, s), 4.04-4.07 (2H, q, J = 6.0, 6.8 Hz), 4.32 (1H, s), 5.02 (1H, d, J = 5.2 Hz), 5.59 (1H, d, J = 3.6 Hz), 8.95 (1H, d, J = 8.8 Hz); ^{13}C NMR ($CDCl_3$; 100 MHz) δ 20.3, 26.9, 30.2, 33.1, 61.5, 62.5, 64.4, 67.7, 72.4, 158.5, 167.2, 169.9, 172.6; HRMS calcd. for $C_{14}H_{20}N_2O_5S$ [M - H]$^-$ 327.1020, found 327.1049.

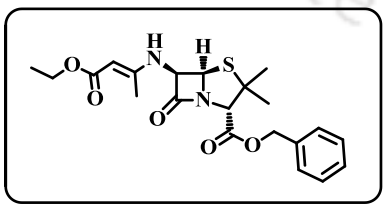

Synthesis of (2S,5R,6R)-6-(((E)-4-ethoxy-4-oxobut-2-en-2-yl)amino)-penicillanic acid benzyl ester (5.71): To a solution of **5.70** (1210 mg, 3.7 mmol) in dry DMF, K_2CO_3 (768 mg, 5.5 mmol) and KI (924 mg, 5.5 mmol) was added and then Benzyl Bromide (0.66 ml, 5.5 mmol) was added dropwise maintaining the temperature at 0^{o}C. The mixture was then stirred at room temperature for 18 h. After total consumption of the starting material (monitored by TLC, Solvent system = PE : EtOAc = 10:1, R_f = 0.4), the reaction mixture was diluted with EtOAc. Combined organic layer was washed with water, brine, and dried over Na_2SO_4 and concentrate in high vacuum. The crude material was used for next step without further purification.

Synthesis of PTSA salt of penicillanic acid benzyl ester (**5.72**)**:** The crude material of compound **5.71** was diluted with EtOAc and then PTSA (924 mg, 5.5 mmol dissolved in 10 ml EtOAc) is added into it. The mixture is then stirred at 0^{o}C. Within 10 minutes the white ppt of PTSA salt of Benzyl protected (+)6-APA **5.72** was obtained. Stirring was continued for another 15 minutes and the mixture was filtered. Title compound **5.72** was isolated in pure form as residue.

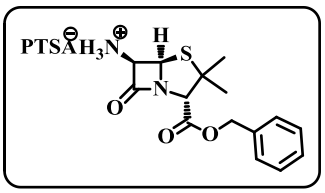

Synthesis of 6-amino penicillanic acid benzyl ester (**5.73**)**:** The suspension of PTSA salt of Benzyl protected (+)6-APA **5.72** in EtOAc was washed with $NaHCO_3$ solution. The combined organic layer was evaporated and dried over Na_2SO_4 and concentrates under high vacuum. Thus title compound **5.73** was isolated in pure form (monitored by TLC, Solvent system = PE : EtOAc = 2:1, R_f = 0.3) as colorless gel (946 mg, Yield 83.5% from (+) 6 APA). IR (KBr): 3337, 2965, 1782, 1737, 1667, 1498, 1200, 753 cm^{-1}; ^{1}H NMR ($CDCl_3$; 400 MHz) δ 1.36 (3H, s), 1.55 (3H, s), 4.37 (1H, s), 4.49 (1H, d, J = 4.4 Hz), 5.59 (1H, d, J = 3.6 Hz), 8.95 (1H, d, J = 8.8 Hz); ^{13}C NMR ($CDCl_3$; 100 MHz) δ 26.9, 27.9, 59.4, 59.7, 60.5, 67.0, 67.5, 68.9, 73.5, 128.9, 129.0, 129.4, 135.3, 165.4, 169.5; +APCI-MS calcd. for $C_{15}H_{19}N_2O_3S$ $[M + H]^+$ 307.1, found 307.0.

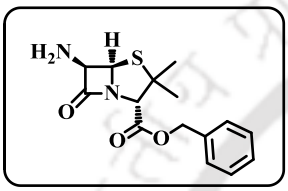

Synthesis of 6-azido penicillanic acid benzyl ester (**5.74**)**:** To a solution of pure benzyl-6-aminopenicillanate (430 mg, 1.4 mmol) in anhydrous toluene (5 mL) triflyl azide solution was added (2.97 mmol) in dry toluene, and Et_3N (0.3 mL, 2.1 mmol). The reaction was then stirred at room temperature for 2-3 h. Completion of the reaction was monitored by TLC (Solvent system = PE : EtOAc = 10:1, R_f = 0.3). After that the reaction mixture was diluted with EtOAc (10 mL) and washed with 1 (N) HCl (20 mL), water, and saturated brine. The organic layer was then dried over Na_2SO_4 and concentrated in vacuum. The title compound **5.74** was isolated by column chromatography (Si-gel, PE:EA = 10:1) in pure form as colorless gel (270 mg, Yield 59 %). IR (KBr) 3437, 2926, **2115**, 1784, 1741, 1630, 1385, 1196, 695 cm^{-1}; ^{1}H NMR ($CDCl_3$; 400 MHz) δ 1.41 (3H, s), 1.64 (3H, s), 4.51 (1H, s), 4.92 (1H, d, J = 4.0 Hz), 5.19 (2H, s), 5.48 (1H, d, J = 4.0 Hz), 7.37 (5H, s); ^{13}C NMR ($CDCl_3$; 100 MHz) δ 26.8, 31.8, 64.8, 66.8, 67.8, 67.9, 70.4, 128.9, 134.7, 167.7, 170.3; HRMS calcd. for $C_{15}H_{17}N_4O_3S$ $[M + H]+$ 333.1016, found 333.1085.

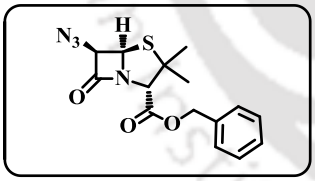

5.6.3. Synthesis of Triazolyl Penicillanates

Synthesis of benzyl-2,4,5-trimethylphenyl-6-triazolylpenicillanate (5.76):

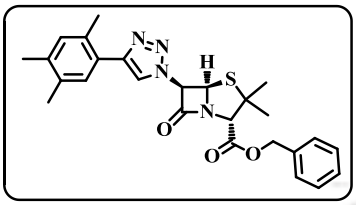

Using general procedure, starting from 40 mg (0.12 mmol) of benzyl-6-azidopenicillanate **5.74** and 19.06 mg (0.132 mmol) of 1-ethynyl-2,4,5-trimethylbenzene, 37 mg (0.078 mmol) of the title compound **5.76** was isolated within 4.5 h as a colourless gummy material. Completion of the reaction was monitored by TLC (Solvent system = PE : EtOAc = 2:1, R_f = 0.45). Purification was done by column chromatography (Si-gel, PE:EA = 2:1). Yield 75 %, IR (KBr) 2964, 2924, 1789, 1744, 1455, 1201, 1027, 749 cm^{-1}; ^1H NMR ($CDCl_3$, 600 MHz) δ 1.44 (3H, s), 1.68 (3H, s), 2.27 (3H, s), 2.27 (3H, s), 2.39 (3H, s), 4.68 (1H, s), 5.20-5.25 (2H, q, *J* = 8.4, 12 Hz), 5.62 (1H, d, *J* = 1.2 Hz), 5.89 (1H, d, *J* = 1.2 Hz), 7.05 (1H, s), 7.35-7.38 (5H, m), 7.53 (1H, s), 7.75 (1H, s); ^{13}C NMR ($CDCl_3$, 150 MHz) δ 19.3, 19.6, 20.9, 25.8, 34.1, 65.1, 67.9, 69.8, 70.0, 73.6, 120.7, 126.6, 128.9, 128.98, 129.1, 130.1, 132.5, 133.0, 134.5, 134.7, 137.2, 148.3, 165.0, 166.9; HRMS calcd. for $C_{26}H_{29}N_4O_3S$ $[M + H]^+$ 477.1955, found 477.1955.

Synthesis of benzyl-4-methoxyphenyl-6-triazolylpenicillanate (5.77):

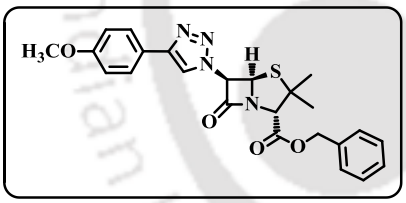

Using general procedure, starting from 40 mg (0.12 mmol) of benzyl-6-azidopenicillanate **5.74** and 17.4 mg (0.132 mmol) of 1-ethynyl-4-m ethoxybenzene, 42 mg (0.091 mmol) of the title compound **5.77** was isolated within 5 h as white solid material. Completion of the reaction was monitored by TLC (Solvent system = PE : EtOAc = 2:1, R_f = 0.4). Purification was done by column chromatography (Si-gel, PE:EA = 2:1). Yield 65 %. mp 165-168 ^oC. IR (KBr) 3452, 2974, 1784, 1733, 1309, 1184, 1204, 746 cm^{-1}; ^1H NMR ($CDCl_3$; 600 MHz) δ 1.44 (3H, s), 1.67 (3H, s), 3.85 (3H, s), 4.67 (1H, s), 5.198-5.26 (2H, q, *J* = 11.4, 12 Hz), 5.58 (1H, d, *J* = 1.2), 5.88 (1H, d, *J* = 1.2), 6.96 (2H, d, *J* = 6.6 Hz), 7.37–7.39 (5H, m), 7.75 (2H, d, *J* = 6.6 Hz), 7.83 (1H, s); ^{13}C NMR ($CDCl_3$; 150 MHz) *δ* 25.8, 34.0, 55.5, 65.2, 67.9, 69.8, 70.0, 73.6, 114.6, 118.1, 122.7, 127.5, 128.9, 129.0, 129.1, 134.8, 148.8, 160.2, 164.9, 166.9; HRMS calcd. for $C_{24}H_{25}N_4O_4S$ $[M + H]^+$ 465.1591, found 465.1591.

Synthesis of benzyl-4-phenoxyphenyl-6-triazolylpenicillanate (5.78):

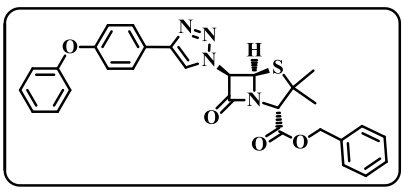

Using general procedure, starting from 40 mg (0.12 mmol) of benzyl-6-azidopenicillanate **5.74** and 25.6 mg (0.132 mmol) of 1-ethynyl-4-phenoxybenzene, 42 mg (0.091 mmol) of the title compound **5.78** was isolated within 5 h as yellowish gummy material.

Completion of the reaction was monitored by TLC (Solvent system = PE : EtOAc = 2:1, R_f = 0.4). Purification was done by column chromatography (Si-gel, PE:EA = 2:1). Yield 69 %, IR (KBr) 3347, 2976, 1667, 1552, 1166, 1054, 855, 726 cm^{-1}; ^1H NMR ($CDCl_3$, 400 MHz) δ 1.44 (3H, s), 1.67 (3H, s), 4.68 (1H, s), 5.18-5.26 (2H, q, *J* = 5.6, 12.4 Hz), 5.59 (1H, s), 5.88 (1H, s), 7.05–7.07 (4H, m), 7.13 (1H, t, *J* = 6.8 Hz), 7.34–7.38 (7H, m), 7.78 (2H, d, *J* = 8.0 Hz), 7.87 (1H, s); ^{13}C NMR ($CDCl_3$, 100 MHz) *δ* 25.8. 27.8, 34.0, 65.1, 67.9, 69.8, 69.9, 73.6, 118.5, 119.2, 119.4, 123.8, 124.9, 127.6, 128.9, 128.9, 129.1, 130.0, 134.7, 148.4, 156.9, 157.9, 164.9, 166.9; HRMS calcd. for $C_{29}H_{27}N_4O_4S$ $[M + H]^+$ 527.1748, found 527.1748.

Synthesis of benzyl-4-methoxy-2-methylphenyl-6-triazolylpenicillanate (5.79): Using general procedure, starting from 40 mg (0.12 mmol) of benzyl-6-azidopenicillanate **5.74** and 19.3 mg (0.132 mmol) of 1-ethynyl-4-methoxy-2-methylbenzene, 34 mg (0.071 mmol) of the title compound **5.79** was isolated within 4.5 h as yellowish gummy material. Completion of the reaction was monitored by TLC (Solvent system = PE : EtOAc = 2:1, R_f = 0.4). Purification was done by column chromatography (Si-gel, PE:EA = 2:1). Yield 62 %. IR (KBr) 2963, 2922, 1787, 1743, 1609, 1454, 1034, 745 cm^{-1}; ^1H NMR ($CDCl_3$, 400 MHz) δ 1.44 (3H, s), 1.67 (3H, s), 2.43 (3H, s), 3.83 (3H, s), 4.68 (1H, s), 5.18-5.26 (2H, q, *J* = 4.8, 12 Hz), 5.62 (1H, s), 5.89 (1H, s), 6.81 (2H, s), 7.37 (5H, s), 7.65 (1H, d, *J* = 8.0 Hz), 7.72 (1H, s); ^{13}C NMR ($CDCl_3$, 100 MHz) δ 21.7, 25.7, 34.1, 55.4, 65.1, 67.8, 69.8, 69.9, 73.5, 111.7, 116.5, 120.5, 122.1, 128.9, 128.93, 129.0, 130.5, 134.7, 137.5, 148.0, 159.8, 164.9, 166.8; HRMS calcd. for $C_{25}H_{27}N_4O_4S$ $[M + H]^+$ 479.1748, found 479.1747.

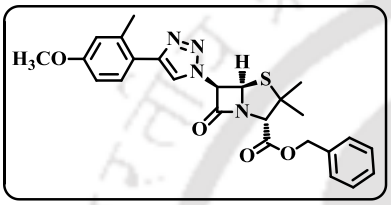

Synthesis of benzyl-3,5-dimethoxy-phenyl-6-triazolylpenicillanate (5.80): Using general procedure, starting from 40 mg (0.12 mmol) of benzyl-6-azidopenicillanate **5.74** and 21.4 mg (0.132 mmol) of 1-ethynyl-3,5-dimethoxybenzene, 36 mg (0.0728 mmol) of the title compound **5.80** was isolated within 4 h as yellowish gummy material. Completion of the reaction was monitored by TLC (Solvent system = PE : EtOAc = 2:1, R_f = 0.36). Purification was done by column chromatography (Si-gel, PE:EA = 2:1). Yield 67 %. IR (KBr) 3349, 2927, 1785, 1741, 1633, 1458, 1029, 805 cm^{-1}; ^1H NMR ($CDCl_3$, 400 MHz) δ 1.43 (3H, s), 1.66 (3H, s), 3.83 6H, s), 4.61 (1H, s), 5.18-5.25 (2H, q, *J* = 5.6, 12 Hz), 5.52 (1H, s), 5.82 (1H, s), 6.39 (1H, s), 6.92 (2H, s), 7.31 (5H, s), 7.84 (1H, s); ^{13}C NMR ($CDCl_3$, 100 MHz) δ 25.8, 33.9, 55.7, 65.1, 67.9, 69.8, 69.9, 73.5, 101.3, 104.0, 119.3, 128.9,

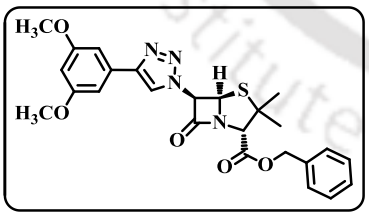

128.94, 129.1, 131.7, 134.7, 148.7, 161.4, 164.8, 166.9; HRMS calcd. for $C_{25}H_{27}N_4O_5S$ $[M + H]^+$ 495.1697, found 495.1706.

Synthesis of benzyl-6-methoxynapthalyl-6-triazolylpenicillanate (**5.81**)**:** Using

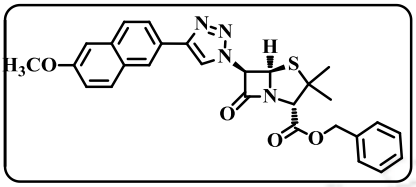

general procedure, starting from 40 mg (0.12 mmol) of benzyl-6-azidopenicillanate **5.74** and 24.02 mg (0.132 mmol) of 1- ethynyl-5-methoxynaphthalene, 39 mg (0.076 mmol) of the title compound **5.81** was isolated within 4 h as yellowish white solid material. Completion of the reaction was monitored by TLC (Solvent system = PE : EtOAc = 2:1, R_f = 0.4). Purification was done by column chromatography (Si-gel, PE:EA = 2:1). Yield 72 %, mp 190-193 ^oC, IR (KBr) 3131, 2966, 1787, 1739, 1206, 1035, 905, 749 cm^{-1}; ^1H NMR ($CDCl_3$, 400 MHz) δ 1.44 (3H, s), 1.67 (3H, s), 3.93 (3H, s), 4.69 (1H, s), 5.19-5.26 (2H, q, J = 4.8, 12.8 Hz), 5.62 (1H, s), 5.93 (1H, s), 7.14–7.18 (2H, m), 7.38 (5H, s), 7.77-7.80 (2H, m), 7.86-7.88 (1H, m), 7.99 (1H, s), 8.26 (1H, s); ^{13}C NMR ($CDCl_3$, 100 MHz) δ 25.8, 34.0, 55.5, 65.2, 67.9, 69.9, 70.0, 73.6, 106.1, 118.9, 119.6, 124.5, 124.9, 127.7, 128.9, 128.97, 129.1, 129.97, 134.8, 149.0, 158.3, 164.9, 166.9; HRMS calcd. for $C_{28}H_{27}N_4O_4S$ $[M + H]^+$ 515.1748, found 515.1746.

Synthesis of benzyl-9-phenanthrenyl-6-triazolylpenicillanate (**5.82**)**:** Using

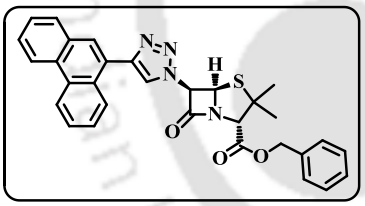

general procedure, starting from 40 mg (0.12 mmol) of benzyl-6-azidopenicillanate **5.74** and 26.6 mg (0.132 mmol) of 9-ethynylphenanthrene, 36 mg (0.0674 mmol) of the title compound **5.82** was isolated within 5 h as yellowish white solid material. Completion of the reaction was monitored by TLC (Solvent system = PE : EtOAc = 2:1, R_f = 0.42). Purification was done by column chromatography (Si-gel, PE:EA = 2:1). Yield 65 %, mp 155-158 ^oC IR (KBr) 3458, 2967, 1787, 1743, 1488, 1237,751, 693 cm^{-1}; ^1H NMR ($CDCl_3$, 600 MHz) δ 1.47 (3H, s), 1.70 (3H, s), 4.72 (1H, s), 5.23 (2H, q, J = 12.0 Hz), 5.72 (1H, d, J = 1.5 Hz), 5.99 (1H, d, J = 1.5 Hz), 7.32 – 7.43 (5H, m), 7.58 – 7.66 (2H, m), 7.68 – 7.73 (2H, m), 7.83 – 7.88 (1H, m), 7.91 – 7.95 (1H, m), 8.03 (1H, s), 8.33 (1H, d, J = 8.1 Hz), 8.73 (1H, dd, J = 15.9, 8.3 Hz), 8.78 (1H, d, J = 8.2 Hz); ^{13}C NMR ($CDCl_3$, 150 MHz) δ 25.8, 29.9, 34.1, 65.2, 67.9, 69.9, 70.1, 73.7, 122.3, 122.8, 123.3, 126.3, 127.1, 127.2, 127.3, 127.6, 128.9, 128.99, 129.0, 129.1, 129.2, 130.9, 147.9, 151.7, 164.8, 166.9, HRMS calcd. for $C_{31}H_{27}N_4O_3S$ $[M+H]^+$ 535.1798, found 535.1775.

Synthesis of benzyl-1-pyrenyl-6-triazolylpenicillanate (**5.83**)**:** Using general

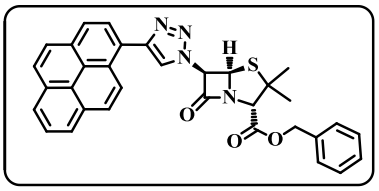

procedure, starting from 40 mg (0.12 mmol) of benzyl-6-azidopenicillanate **5.74** and 28.5 mg (0.132 mmol) of 1-ethynylpyrene, 33 mg (0.0591 mmol) of the title compound **5.83** was isolated within 5 h as light yellow

solid material. Completion of the reaction was monitored by TLC (Solvent system = PE : EtOAc = 2:1, R_f = 0.4). Purification was done by column chromatography (Si-gel, PE:EA = 2:1). Yield 53 %, mp 105-107 ^oC, IR (KBr) 2924, 2853, 1786, 1743, 1635, 1204, 731 cm^{-1}; ^1H NMR ($CDCl_3$, 600 MHz) δ 1.47 (3H, s), 1.72 (3H, s), 4.73 (1H, s), 5.21-5.27 (2H, q, *J* = 13.2, 12 Hz), 5.75 (1H, s), 6.02 (1H, s), 7.35–7.41 (5H, m), 8.04 (1H, t, *J* = 7.2 Hz), 8.08-8.15 (4H, m), 8.21-8.23 (4H, m), 8.64 (1H, d, *J* = 7.2 Hz); ^{13}C NMR ($CDCl_3$, 150 MHz) δ 25.8, 29.9, 34.2, 65.2, 67.8, 69.7, 70.1, 73.7, 122.3, 124.5, 124.7, 124.9, 125.1, 125.2, 125.5, 125.8, 126.4, 127.5, 127.6, 128.3, 128.7, 128.9, 128.96, 129.0, 129.1, 131.1, 131.6, 131.8, 134.7, 148.6, 164.9, 166.9; HRMS calcd. for $C_{33}H_{27}N_4O_3S$ $[M+H]^+$ 559.1798, found 559.1779.

Synthesis of benzyl-3-perynyl-6-triazolylpenicillanate (**5.84**)**:** Using general procedure, starting from 40 mg (0.12 mmol) of benzyl-6-azidopenicillanate **5.74** and 36.7 mg (0.132 mmol) of perylene alkyne, 47 mg (0.078 mmol) of the title compound **5.84** was isolated within 8 h as bwown solid material. Completion of the reaction was monitored by TLC (Solvent system = PE : EtOAc = 2:1, R_f = 0.5). Purification was done by column chromatography (Si-gel, PE:EA = 2:1). Yield 45 %, mp 150-155 ^oC, IR (KBr) 3453, 2923, 2852, 1788, 1742, 1641, 1182, 805, 762 cm^{-1}; ^1H NMR ($CDCl_3$, 400 MHz) δ 1.47 (3H, s), 1.71 (3H, s), 4.72 (1H, s), 5.199-5.28 (2H, q, *J* = 19.2, 7.2 Hz), 5.71 (1H, s), 5.98 (1H, s), 7.38 (5H, s), 7.48–7.59 (3H, m), 7.66-7.69 (2H, m), 7.75-7.73 (1H, m), 7.96 (1H, d, *J* = 8 Hz), 8.01 (1H, s), 8.07-8.22 (4H, m); ^{13}C NMR ($CDCl_3$, 100 MHz) *δ* 23.4, 31.2, 53.2, 62.1, 65.2, 67.1, 67.9, 70.4, 112.9, 118.77, 119.3, 120.2, 121.4, 123.6, 125.3, 125.8, 126.2, 126.7, 126.8, 128.4, 128.7, 130.4, 132.5, 133.5, 143.6, 153.9, 163.8, 165.2; HRMS calcd. for $C_{37}H_{29}N_4O_3S$ $[M + H]^+$ 609.1955, found 609.1958.

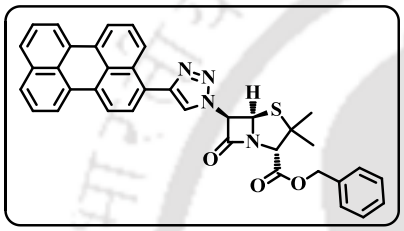

Synthesis of benzyl-4-fluoro-2-methylphenyl-6-triazolylpenicillanate (**5.85**)**:** Using general procedure, starting from 40 mg (0.12 mmol) of benzyl-6-azidopenicillanate **5.74** and 17.7 mg (0.132 mmol) of 1-ethynyl-2-fluoro-4-methylbenzene, 33 mg (0.0708 mmol) of the title compound **5.85** was isolated within 4 h as brownish gummy material. Completion of the reaction was monitored by TLC (Solvent system = PE : EtOAc = 2:1, R_f = 0.4). Purification was done by column chromatography (Si-gel, PE:EA = 2:1). Yield 59 %, IR (KBr) 3457, 2927, 1788, 1742, 1494, 1206, 1031, 805 cm-1; ^1H NMR ($CDCl_3$, 400 MHz) *δ* 1.43 (3H, s), 1.66 (3H, s), 2.31 (3H, s), 4.68 (1H, s), 5.18-5.25 (2H, q, *J* = 4.0, 12 Hz), 5.58 (1H, s), 5.88 (1H, s), 7.05 (1H, t, *J* = 9.2 Hz), 7.37 (5H, s), 7.57 (1H, bs), 7.68 (1H, d *J* = 6.8),

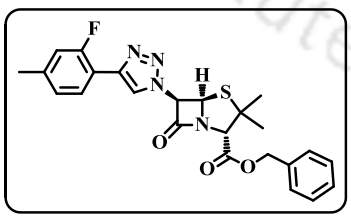

7.87 (1H, s); ^{13}C NMR ($CDCl_3$, 100 MHz) δ 25.8, 34.0, 65.2, 67.9, 69.8, 69.9, 73.5,115.6, 115.8, 118.7, 125.1, 125.2, 128.9, 128.95, 129.1, 129.3, 129.31, 134.7, 148.1, 164.8, 166.9; HRMS calcd. for $C_{24}H_{24}FN_4O_3S$ $[M + H]^+$ 467.1548, found 467.1554.

Synthesis of benzyl-4-benzonitrile-6-triazolylpenicillanate (5.86): Using

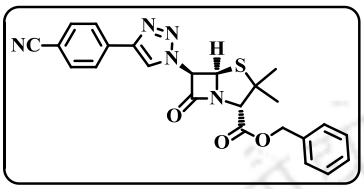

general procedure, starting from 40 mg (0.12 mmol) of benzyl-6-azidopenicillanate **5.74** and 16.8 mg (0.132 mmol) of 4-ethynylbenzonitrile, 38 mg (0.083 mmol) of the title compound **5.86** was isolated within 3.5 h as yellowish white solid material. Completion of the reaction was monitored by TLC (Solvent system = PE : EtOAc = 2:1, R_f = 0.4). Purification was done by column chromatography (Si-gel, PE:EA = 2:1). Yield 65 %, mp 165-167 ^{o}C, IR (KBr) 3347, 2976, 1667, 1552, 1166, 1054, 855, 726 cm^{-1}; ^{1}H NMR ($CDCl_3$, 600 MHz) δ 1.44 (3H, s), 1.67 (3H, s), 4.68 (1H, s), 5.22 (2H, q, *J* = 12.0 Hz), 5.61 (1H, d, *J* = 1.6 Hz), 5.89 (1H, d, *J* = 1.6 Hz), 7.38 – 7.38 (5H, m), 7.72 (2H, d, *J* = 7.7 Hz), 7.94 (2H, d, *J* = 8.0 Hz), 8.04 (1H, s); ^{13}C NMR (151 MHz, $CDCl_3$) δ 25.8, 34.0, 65.3, 67.9, 69.8, 73.5, 112.2, 118.8, 120.3, 126.5, 128.9, 128.97, 129.1,132.4, 133.0, 134.4, 134.7, 146.9, 164.4, 166.8; HRMS calcd. for $C_{24}H_{22}N_5O_3S$ $[M + H]^+$ 460.1438, found 460.1438.

Synthesis of benzyl-4-benzaldehyde -6-triazolylpenicillanate (5.87): Using

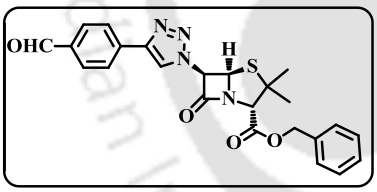

general procedure, starting from 40 mg (0.12 mmol) of benzyl-6-azidopenicillanate **5.74** and 17.7 mg (0.132 mmol) of 4-ethynylbenzaldehyde, 33 mg (0.0708 mmol) of the title compound **5.87** was isolated within 4 h as brownish gummy material. Completion of the reaction was monitored by TLC (Solvent system = PE : EtOAc = 2:1, R_f = 0.35). Purification was done by column chromatography (Si-gel, PE:EA = 2:1). Yield 69 %, IR (KBr) 2924, 1787, 1744, 1610, 1207,835cm^{-1}. ^{1}H NMR ($CDCl_3$, 600 MHz) δ 1.45 (3H, s), 1.68 (3H, s), 4.69 (1H, s), 5.20-5.26 (2H, q, *J* = 6.6, 12 Hz), 5.62 (1H, s), 5.91 (1H, s), 7.36–7.38 (5H, m), 7.95 (2H, d, *J* = 7.8 Hz), 8.01 (2H, d, *J* = 8.4 Hz), 8.05 (1H, s), 10.04 (1H, s), ^{13}C NMR ($CDCl_3$, 150 MHz) δ 25.8, 34.0, 65.3, 68.0, 69.9, 69.91, 73.6, 120.3, 126.5, 128.9, 129.0, 129.1, 130.6, 134.7, 135.7, 136.4, 147.5, 164.5, 166.8, 191.8, HRM calcd. for $C_{24}H_{23}N_4O_4S$ $[M+H]^+$ 463.1435, found 463.1439.

Synthesis of pyren-1-ylmethanamine (5.94): Starting from 1-Pyrene

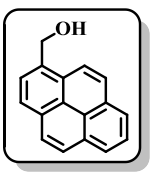

carboxaldehyde **5.90** (500 mg, 2.2 mmol) in dry MeOH then $NaBH_4$ (123 mg, 3.3 mmol) was added portion wise into it at 0^{o}C. The reaction mixture was stirred at room temperature for 30 min and then refluxed for 8 h under N_2 atmosphere. After completion of the reaction the reaction mixture was diluted with 5% HCl which causes the formation

of a white precipitate. The reaction mixture was extracted with EtOAc 3 times. The EtOAc layer was washed with brine, passed over Na_2SO_4 and finally dried to get the solid product (yield = 89 %). This crude material was used for the next step without further purification. ^{1}H NMR ($CDCl_3$, 600 MHz) δ 5.40 (2H, d, J = 9 Hz), 8.00-8.11 (4H, m), 8.15-8.23 (4H, m), 8.37-8.40 (1H, t, J = 9 Hz); ^{13}C NMR ($CDCl_3$, 150 MHz) δ 63.1, 123.2, 124.8, 124.9, 125.0, 125.3, 126.1, 127.4, 127.5, 127.8, 128.8, 130.9, 134.2.

Prepared pyren-1-ylmethanol **5.91** (500 mg, 2.155 mmol) was taken in a dry CH_2Cl_2. Mesyl chloride (0.255 ml, 3.23 mmol) and triethyl amine (0.45 ml, 3.23 mmol) were added to the reaction mixture at 0 ^{o}C. The reaction mixture was stirred at 0 ^{o}C till the starting material was vanished (monitored by TLC, Solvent system = PE : EtOAc = 5:1, R_f = 0.4). Then the reaction mixture was diluted with DCM, washed with water and dried over Na_2SO_4 and concentrates in high vacuum. The pure compound **5.92** was then isolated by column chromatography (si-gel, PE:EA = 5:1) as a white solid (590 mg, Yield 88%) and utilized immediately for the next step without further characterization.

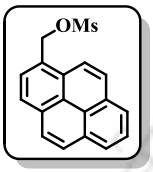

To a solution of the pyren-1-ylmethyl methanesulfonate **5.92** (590 mg, 1.903 mmol) in dry DMF (7 ml), NaN_3 (185 mg, 2.855 mmol) was added and stirrer for 18 h at 50 ^{o}C. Completion of the reaction was monitored by TLC (Solvent system = PE : EtOAc = 10:1, R_f = 0.3). Work up was done with EtOAc and water (20 ml each). The organic layer was washed with brine solution, dried over Na_2SO_4 and concentrated under high vacuum. The azide compound **5.93** was isolated by column chromatography (si-gel, PE:EA = 10:1) in pure form as yellowish white solid (400 mg, Yield 81.5%). IR (KBr) 3042, **2101**, 1603, 1233, 834, 706 cm^{-1}; ^{1}H NMR ($CDCl_3$, 600 MHz) δ 5.02 (2H, d, J = 4.2 Hz), 7.95-7.97 (1H, m), 8.02-8.09 (3H, m), 8.14 – 8.19 (2H, m) 8.21-8.23 (2H, m), 8.24 – 8.26 (1H, m); ^{13}C NMR ($CDCl_3$, 150 MHz) δ 53.3, 122.8, 124.8, 125.2, 125.7, 125.8, 126.4, 127.5, 127.6, 128.1, 128.4, 128.6, 129.4, 130.9, 131.4, 132.0.

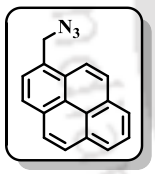

To a solution of the 1-(azidomethyl)pyrene **5.93** in methanol (350 mg, 1.36 mmol) Pd/C is added and to it hydrogen gas balloon was set and stir the reaction mixture for about 4 hours. Completion of the reaction was monitored by TLC. The reaction mixture was then filtered; filtrate is evaporated to afford the title compound **5.94** with quantitative yield. IR (KBr) 3039, 2922, **1601**, 844, 709 cm^{-1}; ^{1}H NMR ($CDCl_3$, 600 MHz) δ 4.80 (2H, s), 8.08-8.13 (2H, m), 8.16 (2H, d, J = 7.8 Hz), 8.26-8.30 (4H, m), 8.37 (1H, d, J = 8.4 Hz); ^{13}C NMR ($CDCl_3$, 150 MHz), δ 41.6, 13.4, 125.4, 125.8, 126.1, 126.8, 127.1, 127.6, 128.4, 128.8, 129.4, 129.8, 130.2, 131.6, 132.3, 132.9.

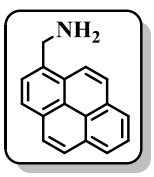

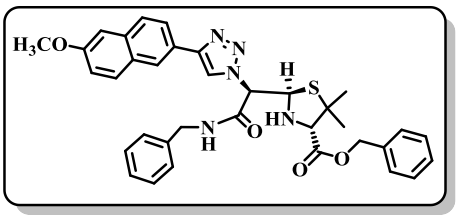

Synthesis of (2R,4S)-benzyl 2-((R)-2-(benzylamino)-1-(4-(6-methoxy naphthalen-2-yl)-1H-1,2,3-triazol-1-yl)-2-oxoethyl)-5,5-di methyl thiazo lidine-4-carboxylate (5.95): To a solution of the compound **5.81** in dry DCM (50 mg, 0.097 mmol) benzyl amine (52.2 mg, 0.487 mmol) is added and degass to create N_2 atmosphere then stir the reaction mixture at room temperature for 6 hours. Completion of the reaction was monitored by TLC (Solvent system = PE : EtOAc = 2:1, R_f = 0.3). The solvent DCM was then evaporated and the title compound **5.95** was isolated in pure form through coloumn chromatography (Hex:EA=2:1) as white solid. Yield 75 %, mp 127-130 ^oC, IR (KBr) 3336, 2961, 1721, 1670, 1549, 1453, 1277, 1209, 1029, 857, 697 cm^{-1}; ^1H NMR ($CDCl_3$, 600 MHz) δ 1.11 (3H, s), 1.45 (3H, s), 3.73 (1H, s), 3.80 (1H, d, *J* = 3.3 Hz), 3.93 (3H, s), 4.43 (1H, dd, *J* = 15.0, 5.7 Hz), 4.51 (1H, dd, *J* = 15.0, 5.9 Hz), 5.09 (1H, d, *J* = 12.0 Hz), 5.22 (1H, d, *J* = 12.0 Hz), 5.33 (1H, d, *J* = 8.5 Hz), 5.51 (1H, d, *J* = 8.5 Hz), 7.17 – 7.11 (2H, m), 7.20 – 7.28 (5H, m), 7.35 – 7.31 (5H, m), 7.39 (1H, t, *J* = 5.5 Hz), 7.75 (2H, dd, *J* = 8.4, 6.1 Hz), 7.89 – 7.83 (1H, m), 8.20 (1H, s), 8.23 (1H, s); ^{13}C NMR ($CDCl_3$, 150 MHz) δ 27.1, 27.2, 44.1, 55.5, 60.1, 67.5, 67.6, 69.4, 72.4, 106.0, 119.4, 120.4, 124.6, 124.7, 125.8, 127.5, 127.8, 127.9, 128.9, 129.0, 129.2, 129.9, 134.6, 135.0, 137.5, 148.3, 158.2, 166.4, 168.9; HRMS calcd. for $C_{35}H_{36}N_5O_4S$ $[M + H]^+$ 622.2483, found 622.2485.

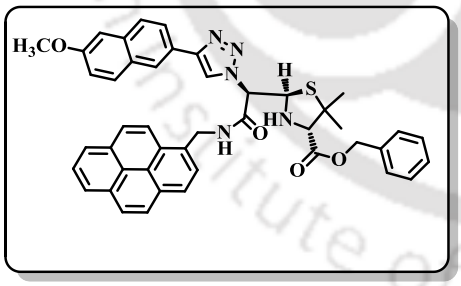

Synthesis of (2R,4S)-benzyl 2-((R)-1-(4-(6-methoxynaphthalen-2-yl)-1H-1,2,3-triazol-1-yl)-2-oxo-2-((pyren-1-ylmethyl) amino)ethyl)-5,5-dimethylthiazolidine-4-carboxylate (5.96): To a solution of the compound **5.81** in dry THF (200 mg, 1.1 mmol) pyren-1-ylmethanamine **5.94** and Et_3N (5 equivalent) was added then degass to create N_2 atmosphere then stir the reaction mixture for 8 hours at 70^{o}C-80^{o}C. Completion of the reaction was monitored by TLC (Solvent system = PE : EtOAc = 2:1, R_f = 0.25). The solvent THF was then evaporated and the title compound **5.96** was isolated in pure form through coloumn chromatography (Hex:EA=2:1) as white solid. Yield 65 %, mp 210-212 ^oC, IR (KBr) 3327, 2925, 1737, 1663, 1611, 1453, 1211, 1030, 846 cm^{-1}; ^1H NMR ($CDCl_3$, 600 MHz) δ 1.03 (3H, s), 1.32 (3H, s), 3.63 (1H, d, *J* = 12.1 Hz), 3.82 – 3.75 (1H, m), 3.93 (3H, s), 4.86 (1H, d, *J* = 12 Hz), 5.04 (1H, dd, *J* = 14.8, 5.4 Hz), 5.10 (1H, d, *J* = 12 Hz), 5.14 (1H, dd, *J* = 14.7, 5.5 Hz), 5.32 (1H, d, *J* = 8.5 Hz), 5.52 (1H, t, *J* = 8.3 Hz), 7.06 – 7.13 (2H, m), 7.17 (2H, d, *J* = 6.4 Hz), 7.23-7.29 (3H, m), 7.49 (1H, t, *J* = 5.3 Hz), 7.67 (2H, t, *J* = 8.8 Hz), 7.80 (1H, d, *J* = 8.3 Hz), 7.88 (1H, d,

J = 7.7 Hz), 7.96 (2H, dd, *J* = 8.2, 6.3 Hz), 8.02 (2H, dd, *J* = 8.6, 4.6 Hz), 8.00 (1H, s), 8.09 (2H, m), 8.11 (1H, d, *J* = 2.9 Hz), 8.13 – 8.18 (1H, m), 8.22 (1H, s); ^{13}C NMR ($CDCl_3$, 150 MHz) *δ* 27.0, 42.6, 55.5, 60.1, 67.4, 67.5, 69.5, 72.3, 106.0, 119.4, 120.4, 122.3, 124.6, 124.7, 124.8, 125.0, 125.2, 125.6, 125.7, 126.3, 127.4, 127.5, 127.8, 128.6, 128.8, 128.9, 129.1, 129.6, 130.2, 130.9, 131.4, 134.6, 134.9, 148.3, 158.1, 166.1, 168.8; HRMS calcd. for $C_{45}H_{40}N_5O_4S$ $[M + H]^+$ 746.2796, found 746.2793.

Synthesis of (2R,4S)-benzyl 5,5-dimethyl-2-((R)-2-oxo-1-(4-(pyren-1-yl)-1H-1,2,3-triazol-1-yl)-2-((pyren-1-ylmethyl)amino) ethyl) thiazo lidine-4-carboxylate (5.97): To a solution of the compound **5.83** in dry THF (200 mg, 1.1 mmol) pyren-1-ylmethanamine **5.94** and Et_3N (5 equivalent) was added then degass to create N_2 atmosphere then stir the reaction mixture for 9 hours at 70°C-80°C. Completion of the reaction was monitored by TLC (Solvent system = PE : EtOAc = 2:1, R_f = 0.3). The solvent THF was then evaporated and the title compound **5.97** was isolated through coloumn chromatography (Hex:EA=2:1) as light yellow solid. Yield 62 %, mp 150-152 °C, IR (KBr) 3445, 2924, 1737, 1662, 1453, 1185, 845 cm^{-1}. ^{1}H NMR (DMSO, 600 MHz) *δ* 1.11 (3H, s), 1.45 (3H, s), 3.89 (1H, s), 4.10 (1H, bs), 5.00 – 4.92 (2H, m), 5.05 (1H, d, *J* = 11.8 Hz), 5.21 (1H, dd, *J* = 14.8, 5.5 Hz), 5.60 (2H, s), 7.08 (2H, d, *J* = 7.0 Hz), 7.14 – 7.20 (3H, m), 7.95 - 8.10 (11H, m), 8.12-8.19 (6H, m), 8.41(1H, s), 8.61 (1H d, *J* = 9.3 Hz), 9.10 (1H, s); ^{13}C NMR (DMSO, 150 MHz) *δ* 27.0, 42.6, 55.5, 60.1, 67.4, 67.5, 69.4, 72.3, 82.9, 105.9, 119.4, 120.4, 122.8, 124.6, 124.7, 124.8, 125.0, 125.2, 125.6, 125.7, 126.3, 127.3, 127.4, 127.5, 127.8, 128.6, 128.8, 128.9, 129.1, 129.9, 130.2, 130.9, 131.4, 134.6, 134.9, 148.3, 158.1, 166.1, 168.8; HRMS calcd. for $C_{50}H_{40}N_5O_3S$ $[M + H]^+$ 790.2846, found 790.2803.

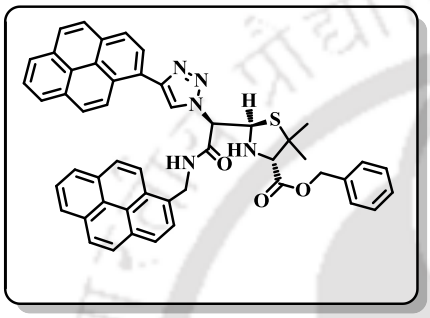

5.7. Photophysical Studies of the Synthesized β-Lactams.

UV-visible measurements: The UV–visible spectra of all final compounds (10 µM) were measured in different solvents using a UV-Visible spectrophotometer (**SHIMADZU**, **UV-2550**) with a cell of 1 cm path length. The measurements were done in absorbance mode. The sample solutions absorbance values were measured in the wavelength range of 200–700 nm. All the sample solutions were prepared freshly just before doing the experiment.

The fluctuations in solvent absorption/experimental error, encountered in some spectra may be due to absorption by air during operating the instrument. Poor

solubility of our synthesized compounds is also a factor regarding this issue. Hence we have corrected the solvent cutoff from all the spectra.

Fluorescence experiments: All the sample solutions for fluorescence measurements (**HORIBA Scientific**, **Fluoromax-4**) were also prepared freshly just before doing the experiment. Fluorescence spectra were obtained using a fluorescence spectrophotometer at 25 °C using 1 cm path length cell. The wavelengths for excitation in all the cases were set at the absorption maxima of each sample in each solvent. The emission spectra were measured in the wavelength regime of 300–700 nm with an integration time of 0.2 sec. From 2.0 ml 500 μM stock solution, 2 ml of 10 μM concentration of solution was used for fluorescence experiment in 1 ml cell. Fluorescence emissions were recorded by exciting the sample solutions at their absorption maxima. Steady-state fluorescence emission spectra were recorded at room temperature as an average of five scans using an excitation slit of 3.0 nm, emission slit 3.0 nm, and scan speed of 120 nm/min. Using quinine sulphate as a reference, the fluorescence quantum yields (Φ_f) were determined with the known Φ_f (0.55) in 0.1 molar solution in sulphuric acid. Following equation was used to calculate the quantum yield,

$$\Phi_S = \Phi_R \frac{Fl_S^{Area}}{Fl_R^{Area}} \frac{Abs_R}{Abs_S} \frac{n_S^2}{n_R^2}$$

where, Φ_R is the quantum yield of standard reference, Fl_S^{Area} (sample) and Fl_R^{Area} (reference) are the integrated emission peak areas, Abs_S (sample) and Abs_R (reference) are the absorbances at the excitation wavelength, and n_S (sample) and n_R (reference) are the refractive indices of the solutions.

A time resolved fluorescence spectrophotometer (*Eddinburg Instruments FSP920*) was utilized to perform fluorescence lifetime experiments. Working condition was maintained at 25^{o}C and results were recorded at an excitation wavelength of 290 nm LED and 375 nm laser using a cuvette having path length 1 cm. To analyze the lifetime data time correlated single photon counting (TCSPC) method was used and analysis was done using a software package with range 205 – 4000 channels.

Error analysis in spectroscopic studies: All the photophysical experiments were done four times. The experimental standard errors (SE, Equation 2) were calculated based on their individual standard deviations (SD, Equation 1) for four consecutive run for the same experiment under same experimental condition.

$$SD = \sqrt{\sum_{i=1}^{n} \frac{1}{n-1} (x - \overline{x})^2}$$

……Equation 1

where SD is standard deviation, *x* is individual data points, $\bar{x}$ is the mean value of the experiments and n is the total number of observations.

The standard error (*SE*) was measured by sample standard deviation obtained divided by the square root of number of observations

$$SE = \frac{SD}{\sqrt{n}} \quad \text{.....Equation 2}$$

The experimental errors in wavelength for both the UV-Visible and fluorescence measurement were found to be in the range of 1-2 nm. Error in Quantum yield calculation lies in the range of 8-10%. The experimental error for lifetime measurement lies between ± 0.5 ns range.

5.8. Some Selected Spectra

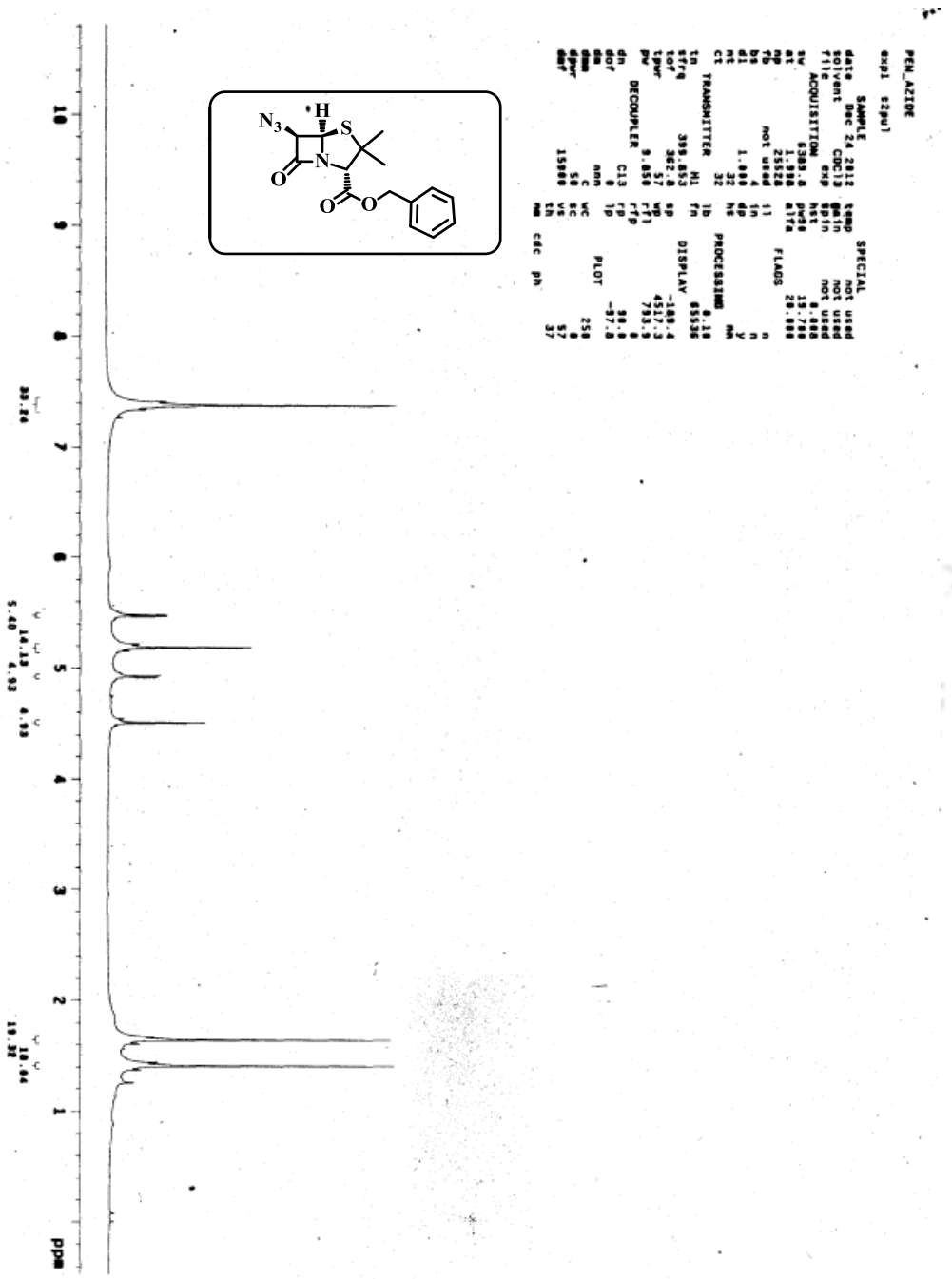

Figure 5.31. ^{1}H Spectra of synthesized compound **azido penicillin** (**5.74**)

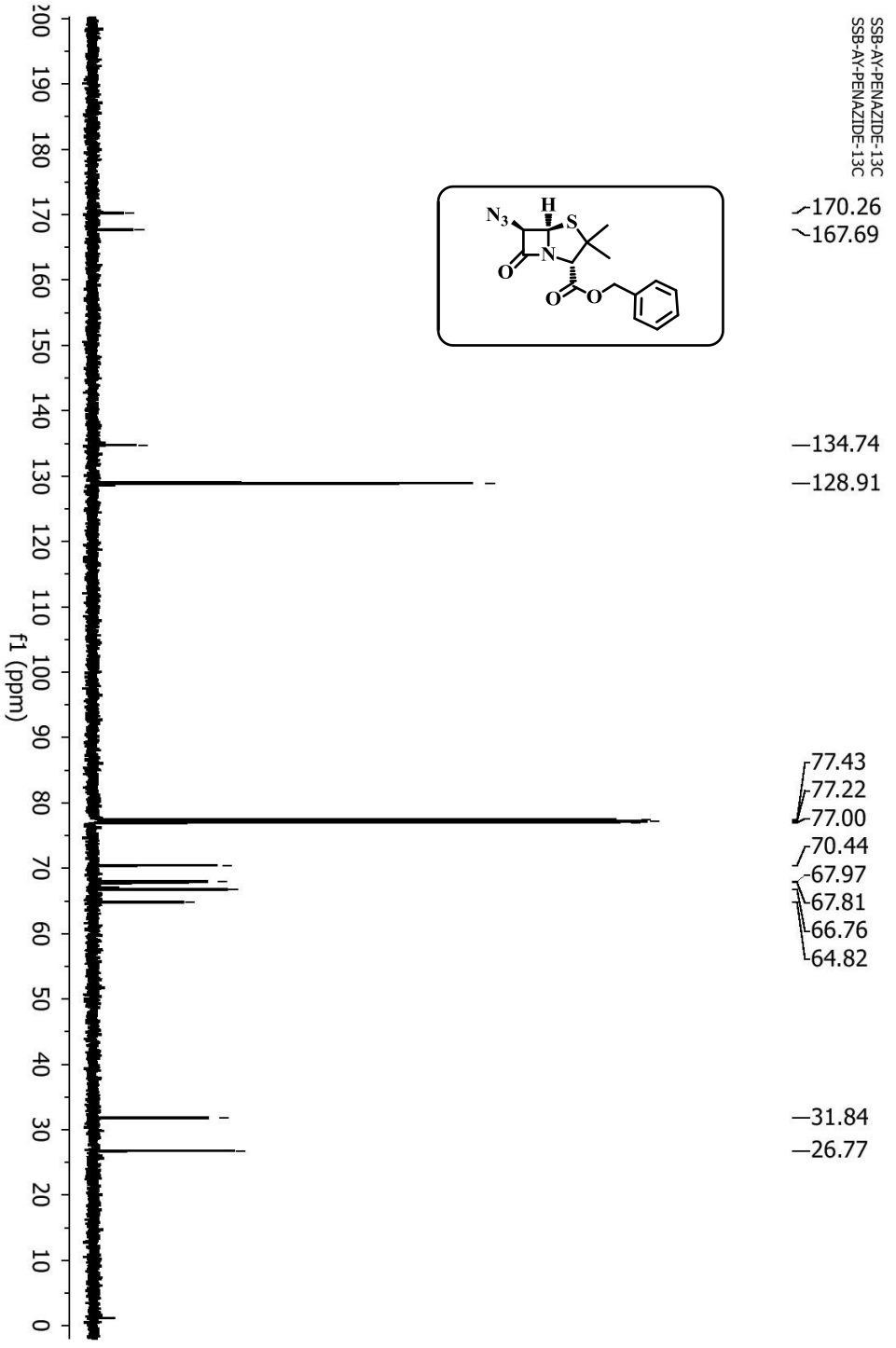

Figure 5.32. ^{13}C Spectra of synthesized compound **azido penicillin 5.74**

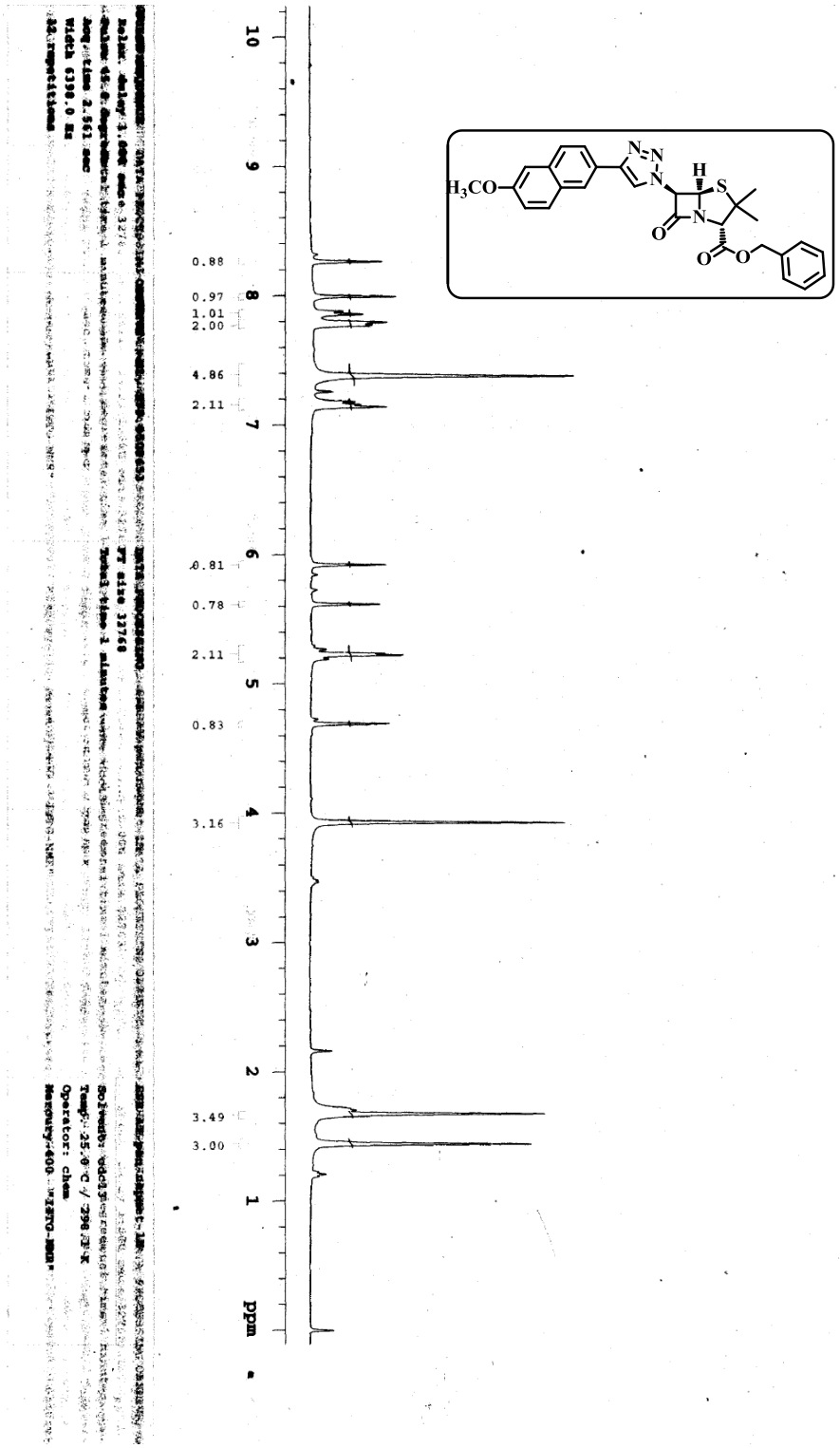

Figure 5.33. ^{1}H Spectra of synthesized compound **5.81** (**benzyl-6-methoxy napthalyl-6-triazolylpenicillanate**)

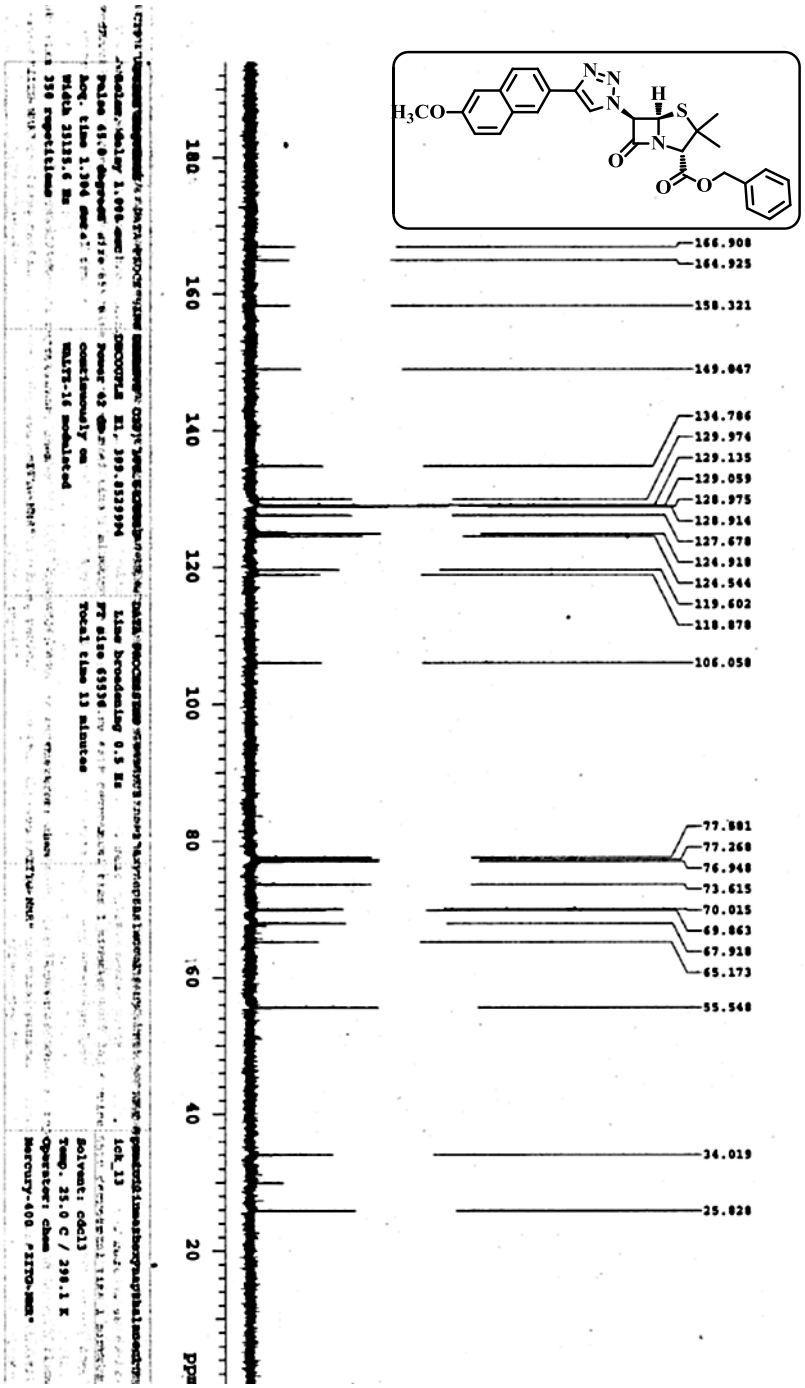

Figure 5.34. ^{13}C Spectra of synthesized compound **5.81** (**benzyl-6-methoxynapthalyl-6-triazolylpenicillanate**)

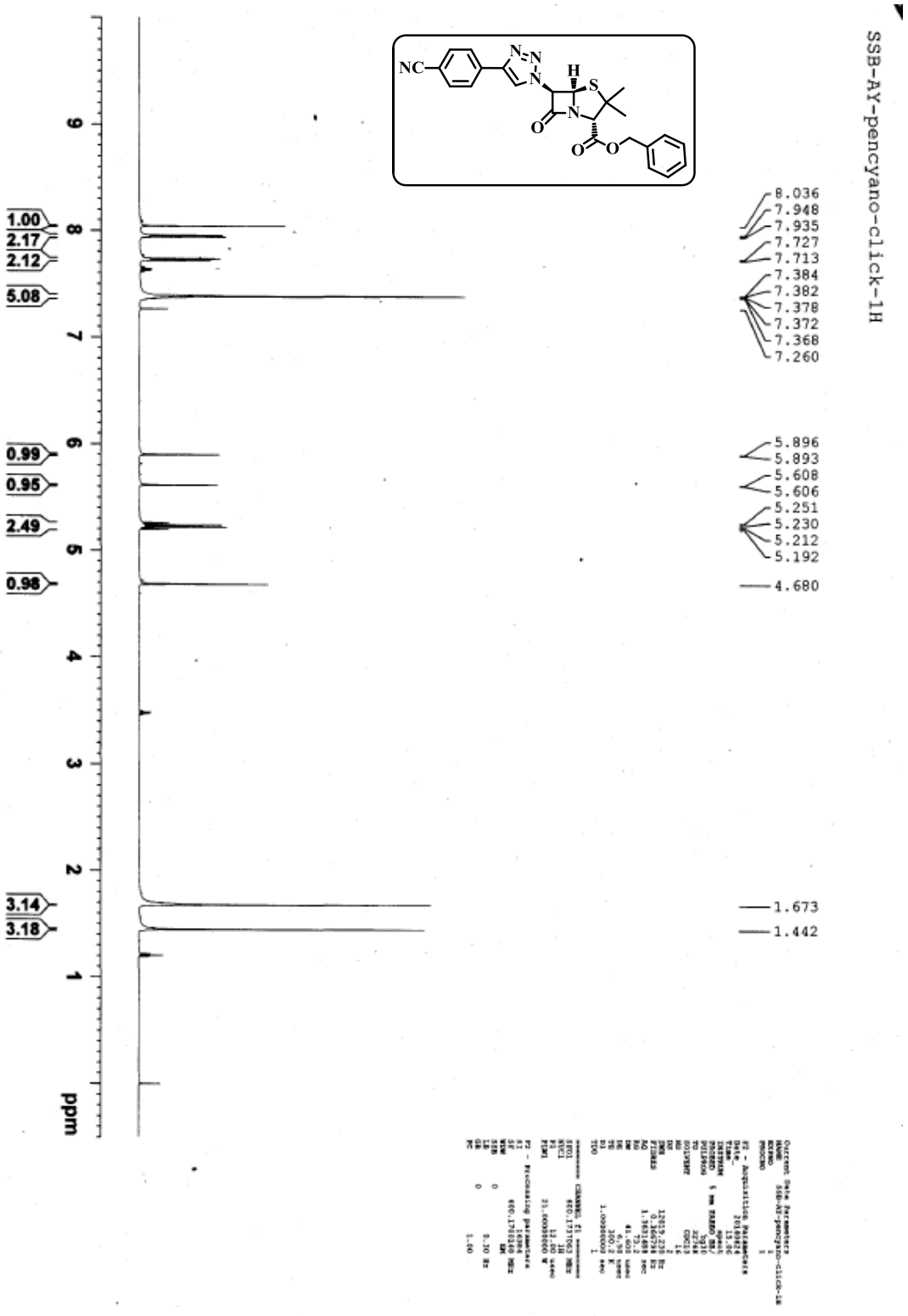

Figure 5.35. ^{1}H Spectra of synthesized compound **5.86** (**benzyl 4-benzonitrile-6-triazolylpenicillanate**)

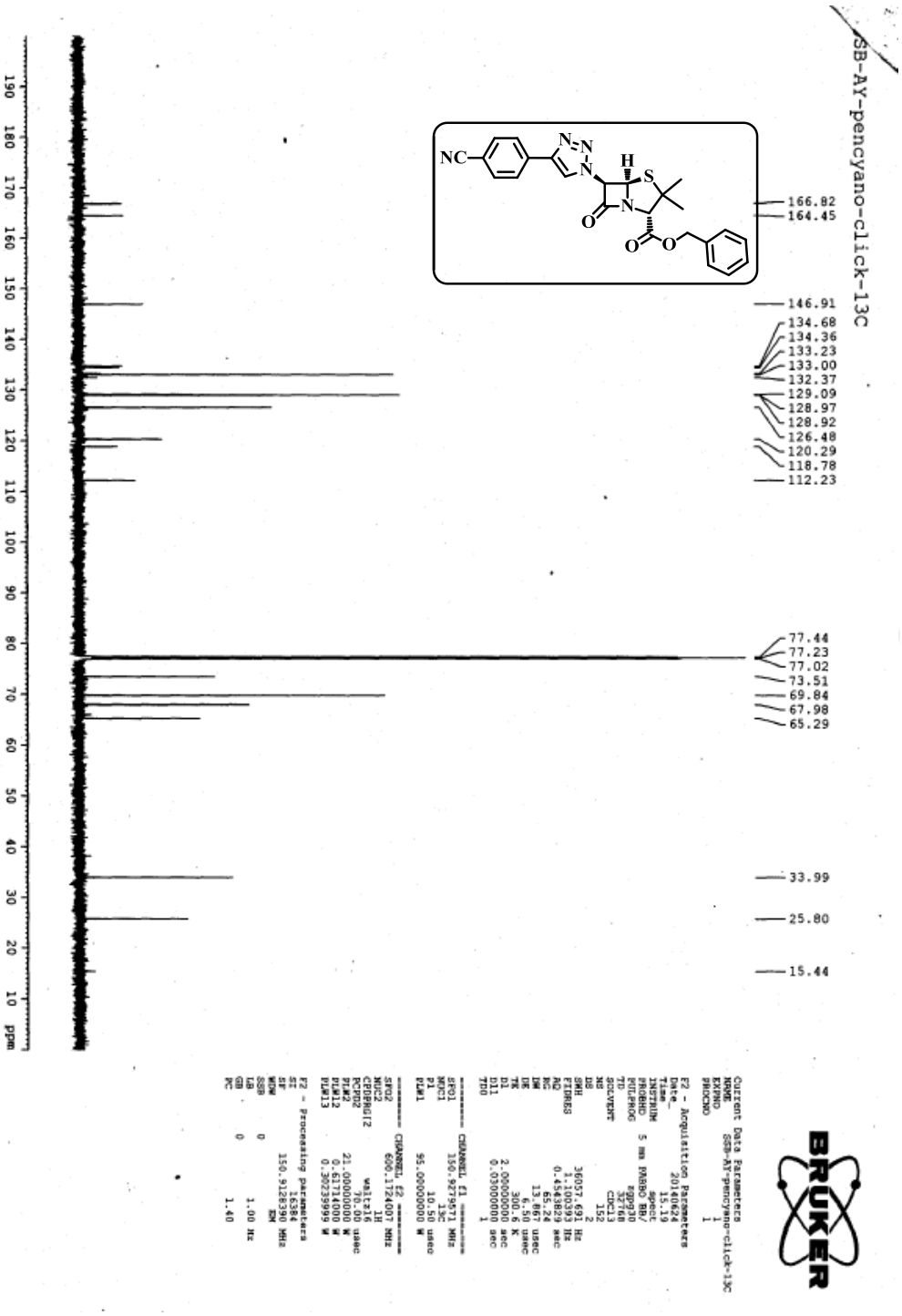

Figure 5.36. ^{13}C Spectra of synthesized compound **5.86** (**benzyl 4-benzonitrile-6-triazolylpenicillanate**)

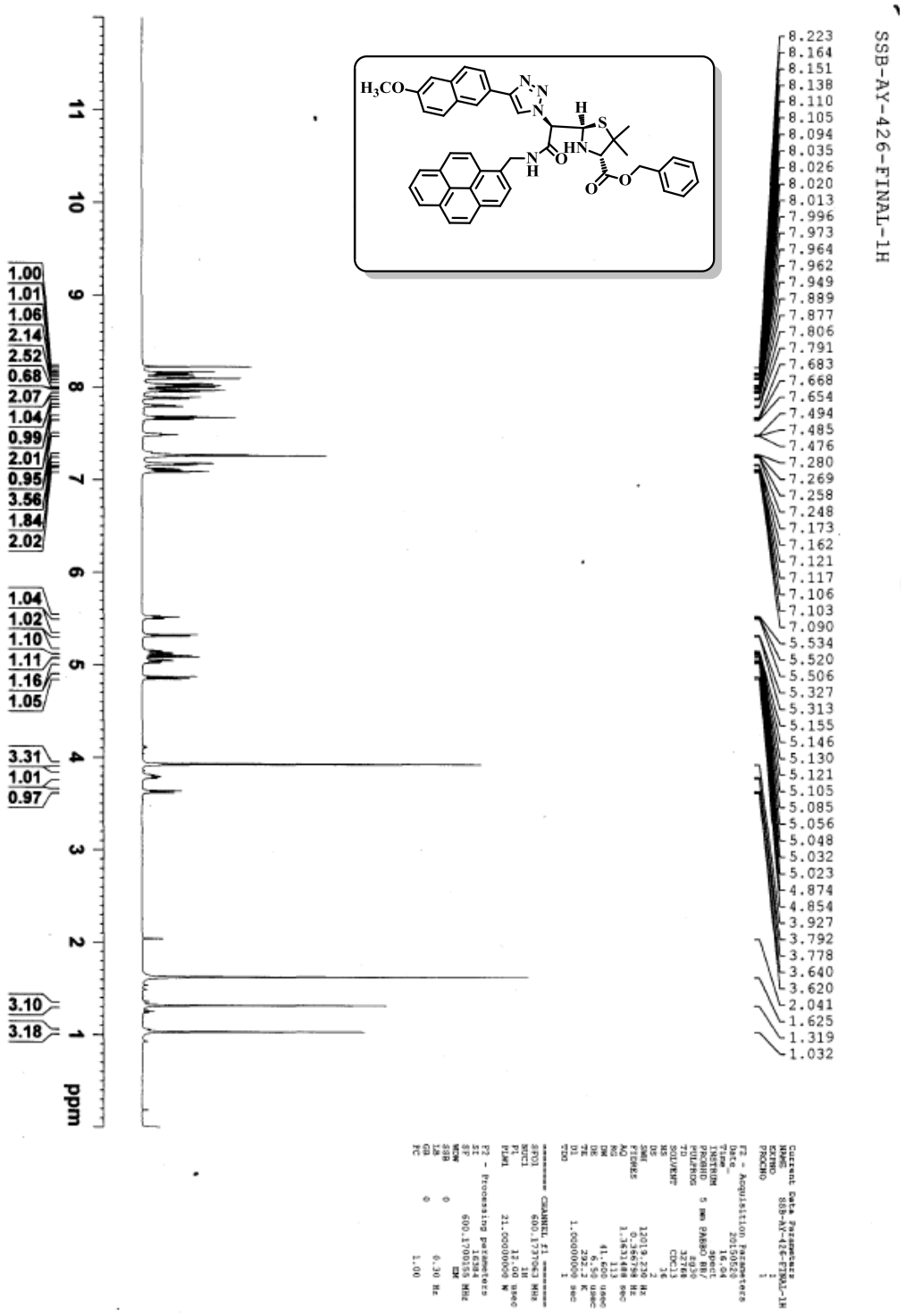

Figure 5.37. ^{1}H Spectra of synthesized compound compound **5.96**

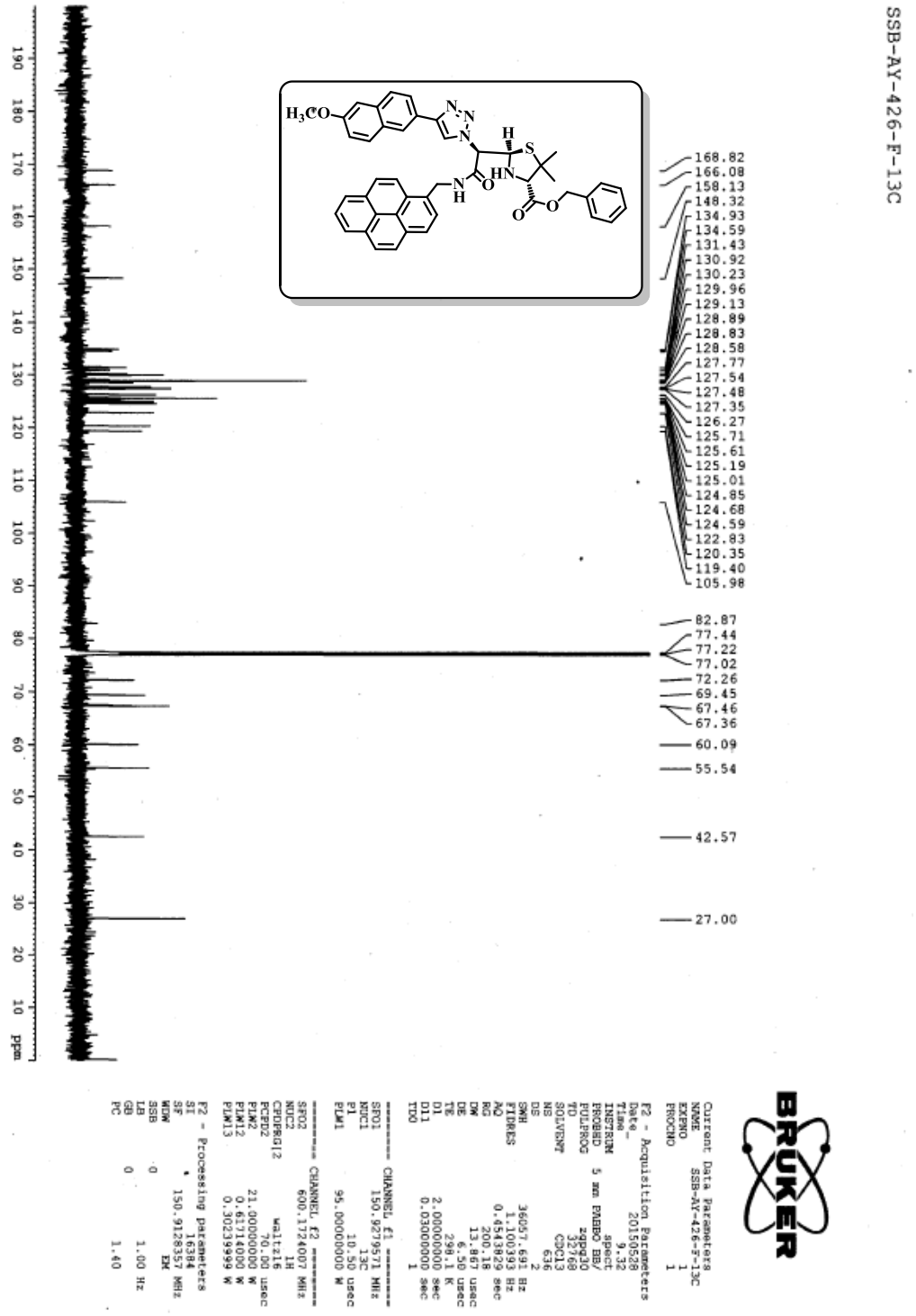

Figure 5.38. ^{13}C Spectra of synthesized compound compound **5.96**

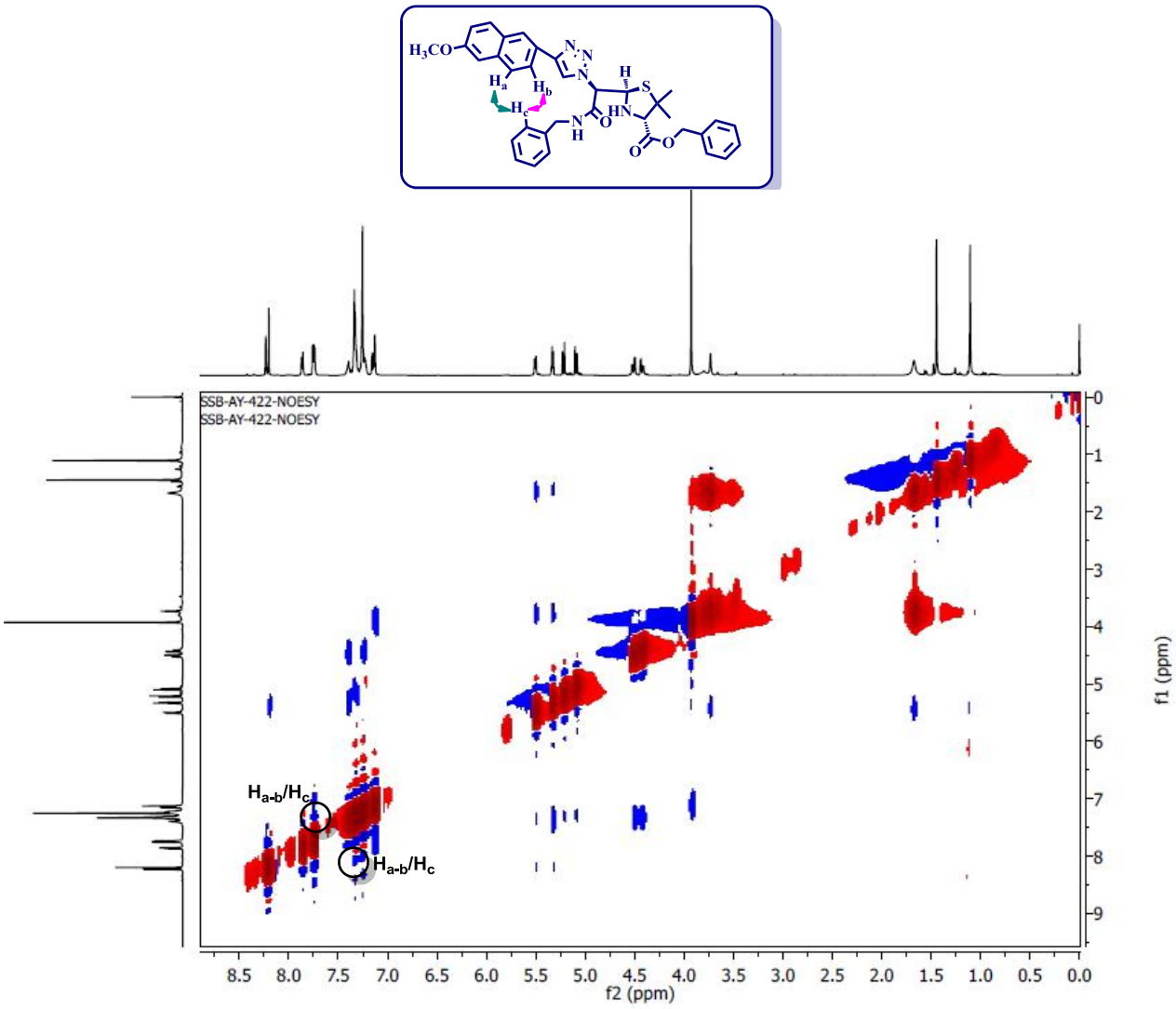

Figure 5.39. NOSEY spectra of ring open compound **5.95.**

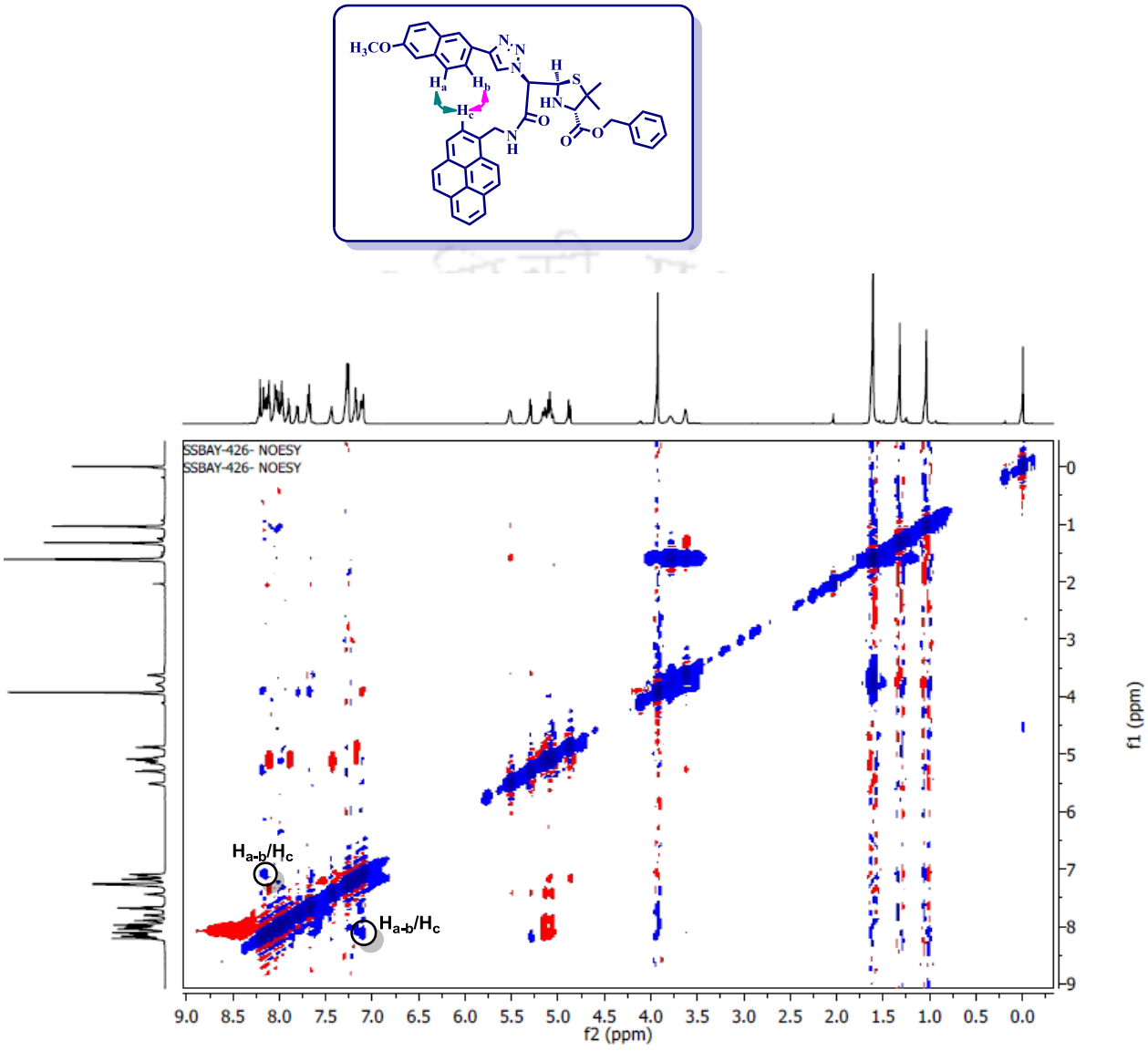

Figure 5.40. NOSEY spectra of ring open compound **5.96.**

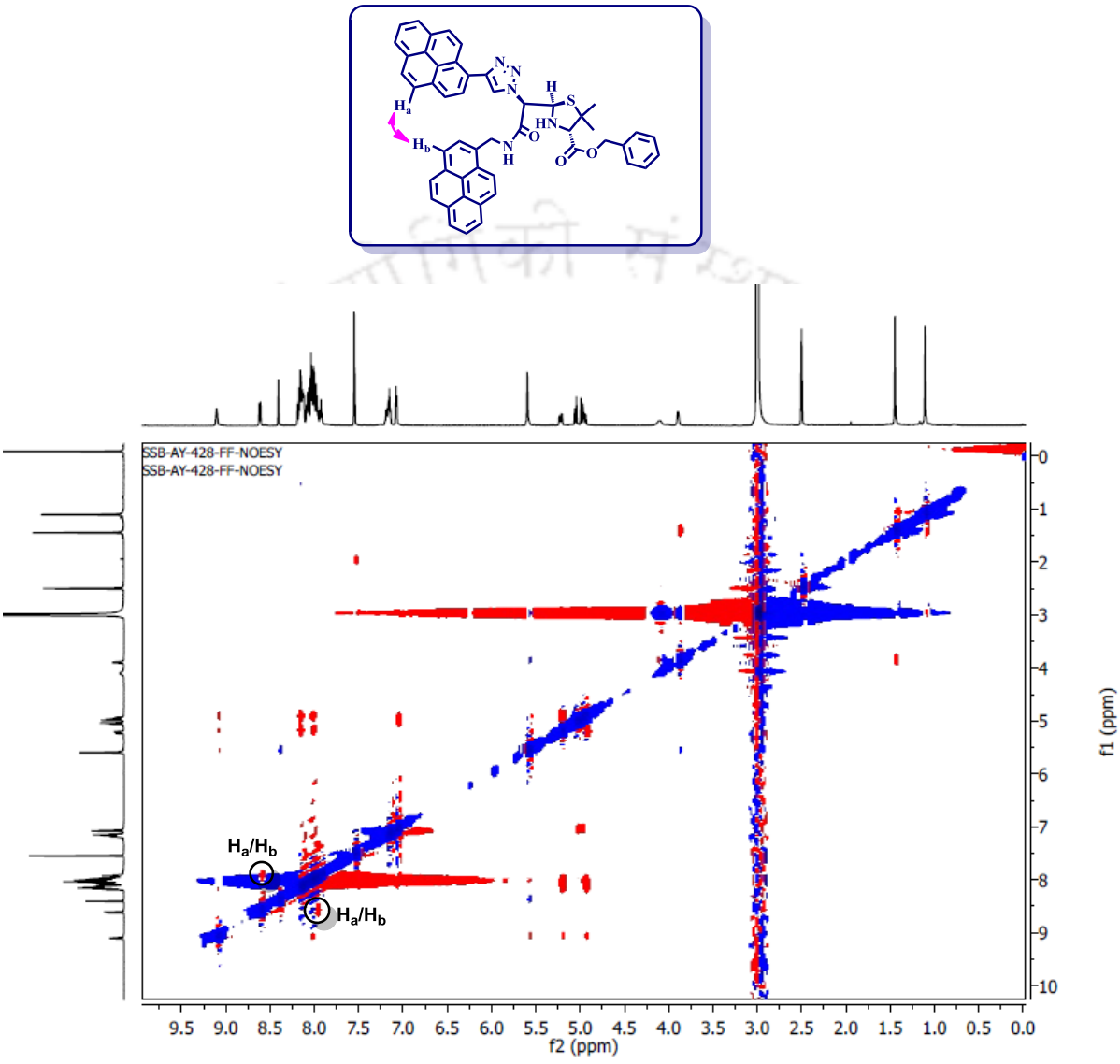

Figure 5.41. NOSEY spectra of ring open compound **5.97.**

5.9. References

1. Lee, M.; Hesek, D.; Suvorov, M.; Lee, W.; Vakulenko, S.; Mobashery, S. *J. Am. Chem. Soc.* **2003**, *125*, 16322.
2. Hwu, J. R.; Tsay, S.-C.; Hakimelahi, S. *J. Med. Chem.* **1998**, *41*, 4681.
3. Wittmann, S.; Schnabelrauch, M.; Scherlitz-Hofmann, I.; Mollmann, U.; Ankel-Fuchs, D.; Heinisch, L. *Bioorg. Med. Chem.* **2002**, *10*, 1659.
4. Heinze-Krauss, I.; Angehrn, P.; Charnas, R. L.; Gubernator, K.; Gutknecht, E.-M.; Hubschwerlen, C.; Kania, M.; Oefner, C.; Page, M. G. P.; Sogabe, S.; Specklin, J.-L.; Winkler, F. *J. Med. Chem.* **1998**, *41*, 3961.
5. Buynak, J. D.; Vogeti, L.; Doppalapudi, V. R.; Solomon, G. M.; Chen, H. *Bioorg. Med. Chem. Lett.* **2002**, *12*, 1663.
6. Leopold, I. H. *Invest. Ophthalmol.* **1964**, *5*, 504.
7. Broccolo, F.; Gianfranco, C.; Caltabiano, G.; Cocuzza, C. E. A.; Fortuna, C. G.; Galletti, P.; Giacomini,D.; Musumarra, G.; Musumeci, R.; Quintavalla, A**.** *J. Med. Chem.* **2006,** *49*, 2804.
8. Fisher, J. F.; Meroueh, S. O.; Mobashery, S. *Chem. Rev.* **2005**, *105*, 395.
9. Bush, K.; Macielag, M.; Weidner-Wells, M. *Curr. Opin. Microbiol.* **2004**, *7*, 466.
10. Dalhoff, A.; Thomson, C. J. *Chemotherapy* **2003**, *49*, 105.
11. Josephine, H. R.; Kumar, I.; Pratt, R. F. *J. Am. Chem. Soc.* **2004**, *126*, 8122.
12. Buynak, J. D. *Curr. Med. Chem.* **2004**, *1*, 1951.
13. Durkheimer, W. *Adv. Drug Res.* **1988**, *17*, 62.
14. Cohen, N. C. *J. Med. Chem.*, **1983**, *26*, 259.
15. Sheehan, J. C.; Henery-Logan, K. R. *J. Am. Chem. Soc.* **1959**, *81*, 3089.
16. Deshpande, A. D.; Baheti, K. G.; Chatterjee, N. R. *Current Science*, **2004**, 87, 1684.
17. (a) Lovell, J.F.; Liu, T.W.B.; Chen, J.; Zheng, G. *Chem. Rev.* **2010**, *110*, 2839. (b) Zheng, X.; Sallum, U.W.; Verma, S.; Athar, H.; Evans, C.L.; Hasan, T. *Angew. Chem. Int. Ed.* **2009**, *48*, 2148.
18. Celli, J.P.; Spring, B.Q.; Rizvi, I.; Evans, C.L.; Samkoe, K.S.; Verma, S.; Pogue, B.W.; Hasan, T. *Chem. Rev.* **2010**, *110*, 2795.
19. Gao, H.Z.; Yang, K.W.; Wu, X.L.; Liu, J.Y.; Feng, L.; Xiao, J.M.; Zhou, L.S.; Jia, C.; Shi, Z. *Bioconjug. Chem.* **2011**, *22*, 2217.
20. Xiao, J. M.; Feng, L.; Zhou, L. S.; Gao, H. Z.; Zhang, Y. L.; Yang, K. W. *Eur. J. Med. Chem.* **2013**, *59*, 150.
21. Chan, P. H.; So, P. K.; Ma, D. L.; Zhao, Y.; Lai, T. S.; Chung, W. H.; Chan, K. C.; Yiu, K. F.; Chan, H. W.; Siu, F. M.; Tsang, C. W.; Leung, Y. C.; Wong, K. Y. *J. Am. Chem. Soc.* **2008**, *130*, 6351.
22. Gao, W.; Xing , B.; Tsien , R. Y.; Rao, J. *J. Am. Chem. Soc.* **2003**, *125*, 11146.

23. Schneider, C. H.; De week, A. L. *Proc. Natl. Acad. Sci.* **1965**, *208*, 57.
24. Hou, J. P.; Poole, J. W. *J. Pharm. Sci*., **1971**, *60*, 503.
25. Blaha, J. M. *J. Pharm. Sci*. **1976**, *65*, 1165.
26. Styring, P.; Chong, S. S. F.; *Tetrahedron Lett.* **2006**, *47*, 1737.
27. Liu, C. J.; Dutta, D.; Mitscher, L. Chin. *Chem. Lett.* **2015**, *26*, 113.
28. Sapsford, K.E.; Berti, L.; Medintz, I.L. *Angew. Chem. Int. Ed.* **2006**, *45*, 4562.
29. Brun, M.A.; Tan, K.T.; Nakata, E.; Hinner, M.J.; Johnsson, K. *J. Am. Chem. Soc.* **2009**, *131*, 5873.
30. Sakaguchi, R.; Endoh, T.; Yamamoto, S.; Tainaka, K.; Sugimoto, K.; Fujieda, N.; Kiyonaka, S.; Mori, Y.; Morii, T. A. *Bioorg. Med. Chem.* **2009**, *17*, 7381.
31. Dwyer, M.A.; Hellinga, H.W. *Curr. Opin. Struct. Biol.* **2004**, *14*, 495.

Major findings and the future outlook of the present investigations described in this dissertation have been summarized below:

This Thesis has a total of five chapters out of which the first chapter is a literature review about the β-hairpin and β-sheet peptidomimetics. This review chapter contains a critical survey of conformationally constrained small molecular scaffold as inducer of particular secondary structure in a peptide, such as β-hairpin and β-sheet peptidomimetics. Second chapter includes uracil-di-aza-amino acid **(U^rAA)** as a new family of molecular scaffold with ability to induce β-hairpin structure with H-bonded β-sheet conformation in a short peptide which is demostrated in two designed fluorescent pentapeptides. We established the dual mechanism of exciplex emission in ExcipFRET-peptide **2.61** containing donor-acceptor triazolyl unnatural fluorescent amino acids ^{TMnap}**Ala**^{Do} and ^{TPy}**Ala**^{Do} at N- and C- terminus respectively, forming a FRET pair. On the other hand fluorescent pentapeptide **Excim-peptide 2.64** with triazolyl fluorescent unnatural amino acid ^{TPy}**Ala**^{Do} at both the termini showed excimer emission in its β-sheet conformation. Both the peptides maintainning their predefined photophysics were found to interact with a model biomolecule BSA with fluorescence swith-on response. The exploration of sequence specific DNA binding event of **U^rAA** scaffold and study of interaction with other protein biomolecules is the future prospect of this work. Chapter **3** includes the synthesis of *ortho,meta*-aromatic amino acid scaffold ($^{o,m\text{-}Ar}$**TAA**). Its incorporation into trichromophoric fluorescent pentapeptide and study of photophysics established a sequential FRET process. Our designed *ortho-meta*-triazolo aromatic amino acid scaffold ($^{o,m\text{-}Ar}$**TAA**) was found to induce turn induced β-sheet structure of a short peptide. The fluorescent peptide in the turn induced β-sheet conformation was found to exhibit relay FRET process from scaffold to **TPy** to **TPer.** This newly designed fluorescent peptide (**3.79**) might find wider applications as sensor in chemistry and biology for studying peptide–protein/peptide–DNA interactions. The peptide **3.79** was also used for studying interaction with BSA protein. Sensing of other specific proteins and DNA with this probe is future focus of this work. Chapter **4** describes the synthesis of triazolo aliphatic amino acids with different spacer length, incorporation into fluorescent pentapeptide containing triazolyl methoxynaphthalene (^{TMnap}**Ala**^{Do}) and triazolyl pyrene (^{TPy}**Ala**^{Do}) amino acids at the two termini and their conformational analysis. The study on the spacer length dependent FRET event in these designed peptides is the main concern of this chapter. With increase in chain length of the molecular scaffold the extent of flexibility increases that allowed to enhance the extent of FRET. Distance dependent FRET in a peptide is a new concept and would have potential application in designing fluorescent peptide probe for studying protein-peptide probe in future.

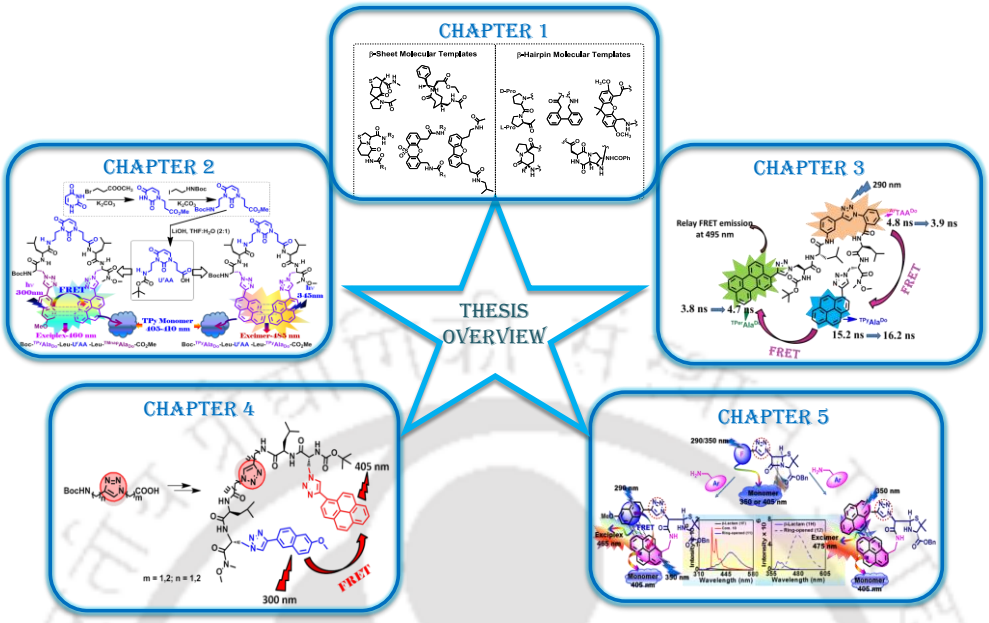

Chapter **5** includes the synthesis of fluorescent triazolyl β-lactams and fluorimetric sensing of chemical cleavage of β-lactam ring. The cleavage of the β-lactam ring of two selected out of twelve synthesised fluorescent triazolylpenicilines, (^{TMNap}**β-Lac**^{Do} and ^{TPy}**β-Lac**^{Do}) with aminomethylpyrene (**AMePy**) as fluoroscent nucleophile was found to be signaled via the generation of FRET/exciplex and excimer emission respectively. We have synthesized a newly designed triazolyl donor-acceptor chromophore decorated fluorescent penicilines, which marked a novel class of unnatural fluorescent β-lactams. We established the dual path to exciplex and excimer emission respectively, after clevage of two decorated β-lactams. The investigation on the change in photophysical property upon chemical cleavage of β- lactam ring can be treated as a model to study the kinetics of β-lactam susceptibility toward chemical cleavage.